FCTUC DEPARTAMENTO DE ENGENHARIA CIVIL
FACULDADE DE CIÊNCIAS E TECNOLOGIA
UNIVERSIDADE DE COIMBRA

FIRE RESISTANCE OF STEEL AND COMPOSITE STEEL-CONCRETE COLUMNS

Thesis presented in fulfilment of the requirements for the degree of Doctor of Philosophy in Civil Engineering

Author
António José Pedroso de Moura Correia

Supervisor
João Paulo Correia Rodrigues

Coimbra, July, 2011

…”Põe tudo o que és na mais pequena coisa que faças”…

F. Pessoa

…”Put everything you are in the smallest thing you make”…

ACKNOWLEDGEMENTS

First of all, I would like to thank the Department of Civil Engineering, of the University of Coimbra for the excellent conditions I had to carry out this work. Not only for the experimental tests, performed within the frame of the research project REEQ/499/2001, but also for the computer facilities used for the numerical simulations.

To the Portuguese Foundation for Science and Technology, I would like to acknowledge the Ph.D. scholarship SFRH/BD/21939/2005, and the research project FIRECOLUMN-PTDC/ECM/65696/2006.

To the Portuguese enterprises TRIA, METALOCARDOSO S.A. and A. COSTA CABRAL S.A. for their technical support and assistance in the development of the fire tests.

To Professor Valdir Pignatta e Silva, I express my sincere gratitude for the warm welcome I have received in 2007, in the University of São Paulo, in Brazil, and for all the valuable teachings I have received from him, about fire research.

To Professor Manfred Korzen, I thank for receiving me in BAM, in Berlin, in 2008, and his effort in allowing me to perform four fire resistance tests in columns.

To all of the employees of the Department of Civil Engineering, University of Coimbra, Nuno Almeida, David Rodrigues, Ricardo Oliveira, and the technical staff of the laboratory, in particular Luis Gaspar and Filipe Cruz, I acknowledge their support and availability for giving me all the conditions I needed to accomplish this work.

To all my colleagues within the Fire Research Group of Coimbra University, Adérito Alves, Tiago Pires, Bruno Fonseca and Alberto Martins, my gratitude for their measureless help in this work.

A special word of appreciation to Pedro Barata, for his personal effort in the final arrangements of this manuscript.Thank you Barata, for putting my work in first place, despite of the tight schedule of your own.

To my colleague Fernando Teixeira Gomes, I thank the patience in teaching me so many things about steel structures, and to make me see quite interesting things about fire in steel structures.

To my friend Luis Laím, I could not thank, because the words are not enough to express my gratitude. Thank you for pushing me to work, when I was tired. Luis, I will never forget your support and encouragement, when I had a retinal detachment, and lost the vision in my right eye. Thank you, Luis, for making me believe that I could finish this work. From the bottom of my heart, I thank you for doing my work, when I could not open my eyes.

To my supervisor, João Paulo Rodrigues, I thank the excellent supervision of this thesis, but also, for always being there for me, helping me to make difficult decisions, and to solve all the problems, technical, scientific and institutional problems. To you, João Paulo, I owe my scientific career, but most of all, I thank you for believing that I could do this job.

To my sons Zé Pedro and Gonçalo, I thank for always demanding more and more from me, my attention, my presence, my help, and for making worth the very high price I have paid for this thesis. Please, forgive me for my absence in your lives, in a great part of your childhood.

To my wife Maria, I thank for always being by my side, and all the patience and support during this time.

RESUMO

O fogo é uma acção extrema a que uma estrutura pode ser sujeita, e portanto deve ser dimensionada para lhe resistir. Os Eurocódigos estruturais disponibilizam métodos de cálculo para permitirem garantir às estruturas a resistência ao fogo adequada.

O objectivo deste trabalho foi estudar pilares de aço e mistos aço-betão em edifícios, em situação de incêndio. A influência de diversos parâmetros, tais como o contacto com as paredes de tijolo, a rigidez da estrutura circundante, o nível de carregamento, e a esbelteza do pilar, foram alvo de um estudo paramétrico realizado experimental e numericamente no presente trabalho. Resultados dos ensaios experimentais foram comparados com os estudos numéricos reproduzindo as condições usadas nos ensaios experimentais, com a finalidade de fornecer dados valiosos para o desenvolvimento ou melhoria de métodos de dimensionamento de pilares em situação de incêndio. O principal objectivo foi reproduzir, tanto quanto possível, em laboratório, as condições a que opilar está sujeito, num edifício real em incêndio.

O programa experimental comportou a realização de ensaios em pilares de aço de secção H embebidos em paredes, pilares de aço e mistos aço-betão parcialmente preenchidos com betão com dilatação térmica restringida. Os ensaios experimentais referenciados foram realizados na Universidade de Coimbra. Os resultados foram comparados com os de ensaios realizados no Bundesanstaltfür Material-forschungund- prüfung (BAM), em Berlim, Alemanha.

A modelação numérica dos ensaios foi realizada utilizando os programas de computador de elementos finitos SUPERTEMPCALC e ABAQUS. Foi realizada uma análise geométrica e material não-linear. Foi feita uma modelação numérica minuciosa tendo sido obtida uma boa concordância entre os resultados experimentais e numéricos, tanto em termos de temperaturas, forças de restrição e deformada dos pilares.

Para os pilares de aço embebidos nas paredes, o estudo incidiu sobre a influência das paredes na distribuição de temperaturas ao longo da secção dos pilares. Os pilares embebidos em paredes, comportam-se de maneira diferente em situação de incêndio, devido ao gradiente térmico, e à restrição.

Para os pilares de aço isolados, a principal conclusão foi sobre a influência real da restrição à dilatação, considerada simultaneamente com a restrição à rotação. Concluiu-se que estas duas rigidezes têm um efeito contrário na resistência ao fogo dos pilares. O parâmetro que maior influencia teve na resistência ao fogo dos pilares foi o nível de carregamento.

Para os pilares mistos aço-betão, a principal conclusão foi que a restrição à dilatação só influencia a resistência ao fogo para níveis de carregamento baixos.

Os principais resultados deste trabalho de investigação, foram a proposta de métodos para a avaliação da evolução da temperatura na secção transversal de pilares com aquecimento diferencial em contacto com as paredes, diagramas de interacção Esforço Axial – Momento Flector, para pilares com aquecimento diferencial, bem como propostas para o cálculo da temperatura crítica e resistência ao fogo de pilares de aço.

PALAVRAS CHAVE

fogo, pilar, aço, misto, restrição, experimental, numérico

ABSTRACT

Fire is an extreme action, to which a structure may be submitted, and therefore, must be designed to resist. The Eurocodes provide methods for the design of structures, to ensure the required fire resistance.

The purpose of this work was to study steel and composite steel-concrete columns in buildings, under fire situation. The influence of several parameters such as the contact with brick walls, the stiffness of the surrounding structure, the load level, and the slenderness of the columns, were the target of the parametric study carried out in the present research. Results of the experimental tests were compared with numerical studies reproducing the conditions used in the tests, with the purpose of providing valuable data for the development or improvement of analytical designing methods. The main goal was to reproduce as much as possible, in the laboratory, the conditions to which the column is subject to, in a real building.

The experimental programme was composed of tests on steel H columns embedded on walls, bare steel H columns with restrained thermal elongation and composite steel-concrete partially encased H columns with restrained thermal elongation.The experimental tests performed at the University of Coimbra, were then compared with tests performed at the Federal Institute for Materials Research and Testing, in Berlin.

The numerical modelling of the tests was performed using the finite element computer programs SUPERTEMPCALC and ABAQUS. A geometrical and material non-linear analysis was performed. A very accurate modelling of the experimental tests was done, with a very good agreement between experimental and numerical results, both in terms of temperatures, forces and deformed shapes of the columns.

For the steel columns embedded on walls, the study focused on the influence of the walls on the temperature distribution along the cross section of the columns. Columns embedded on walls, behave differently in fire situation, due to the thermal gradient, and the restraint.

For the steel bare columns, the main conclusion was about the real influence of the axial restraint considered simultaneously with the rotational restraint. It was concluded that these two stiffnesses have an opposite effect on the fire resistance of the columns. The parameter with greater influence of the fire resistance of the columns was the load level.

For the composite steel-concrete columns, the major conclusion was that the restraint to thermal elongation only affects the fire resistance of the columns for low load levels.

The major outcomes of this research, were proposals of methods for the assessment of the temperature evolution within the cross-section of unevenly heated steel columns in contact with walls, axial force – bending moment interaction diagrams for columns with differential heating, as well as proposals for the calculation of the critical temperatures and fire resistance of steel bare columns.

KEY WORDS

Fire, columns, steel, restraint, experimental, numerical

TABLE OF CONTENTS

FIGURE INDEX

TABLE INDEX

NOTATIONS

Latin upper case letters

A	area of the cross section
A_a	cross-sectional area of the structural steel
A_c	cross-sectional area of the concrete
A_C	cross-sectional area of the steel column
$A_{d(t)}$	design value of the accidental action resulting from the fire exposure
$A_{i,\theta}$	area of each element *i* the cross-section
A_m	surface area of the member per unit length
A_m/V	section factor for unprotected steel members
A_s	cross-sectional area of the steel reinforcement
A_t	total area of enclosure (walls, ceiling and floor, including openings
A_v	total area of vertical openings on all walls
C_c	specific heat of concrete
D	diameter of the fire
E	Young's modulus of steel at ambient temperature
E_a	modulus of elasticity of the structural steel at room temperature
$E_{a,\theta}$	characteristic value for the slope of the linear elastic range of the stress-strain relationship of structural steel at elevated temperatures.
E_c	effective modulus of elasticity of the concrete at room temperature
E_{cm}	secant modulus of elasticity of the concrete at room temperature
$E_{c.sec;\theta}$	characteristic value for the secant modulus of concrete in the fire situation
$E_{fi,d}$	design value of fire action
E_g	internal energy of gas
E_s	modulus of elasticity of the steel reinforcement at room temperature
$E_{s,\theta}$	characteristic value for the slope of the linear elastic range of the stress-strain relationship of reinforcing steel at elevated temperatures.
$(EA)_{eff}$	effective axial stiffness of the column

$(EI)_{eff}$	effective flexural stiffness of the column
$(EI)_{fi,eff}$	effective flexural stiffness of a composite section
$G_{k,j}$	characteristic value of the permanent action ("dead load")
H	distance between the fire source and the ceiling
H	web length in contact with the wall
$I_{a,z}$	moment of inertia of the structural steel section for the relevant bending axis z
$I_{c,z}$	moment of inertia of the un-cracked concrete section for the relevant bending axis z
I_C	moment of inertia of the steel column around the weak axis
$I_{i,\theta}$	moment of inertia of the partially reduced part *i* of the cross-section for bending around the weak or strong axis
$I_{s,z}$	moment of inertia of the steel reinforcement section for the relevant bending axis z
K_3	reduction coefficient for the yield stress
$K_{A,C}$	axial stiffness of the column
$K_{A,S}$	axial stiffness of the surrounding structure
Ke	correction factor
K_{sh}	shadow effect factor
$K_{R,C}$	rotational stiffness of the column
$K_{R,S}$	rotational stiffness of the surrounding structure
L	length of the column
L_c	length of the column
L_{cr}	buckling length
L_h	Horizontal flame length
M_{Pxe}	bending moment about the geometric centroid
M	bending moment
M_k	restraining moment
M_{pl}	plastic bending moment
M_T	bending moment resulting from the thermal action.
$M_{y,fi,Ed}$	design plastic resistance moment in fire situation, around y axis

$M_{z,fi,Ed}$	design plastic resistance moment in fire situation, around z axis
N	axial force
N_{pl}	plastic axial force
$NE22$	nominal axial strains
$N_{b,fi,\theta,Rd}$	design resistance of a compression member with a uniform steel temperature θ_a
$N_{b,fi,t,Rd}$	design buckling resistance at time t of a compression member
$N_{cr,z}$	critical force for the relevant buckling mode
$N_{fi,cr}$	Euler buckling load or elastic critical load in the fire situation
$N_{fi,Ed}$	design value of the axial force in fire situation
$N_{fi,pl,R}$	design value of $N_{fi,pl,Rd}$ when factors $\gamma_{M,fi,a}$, $\gamma_{M,fi,s}$ and $\gamma_{M,fi,c}$ are taken as 1.0
$N_{fi,pl,Rd}$	design value of plastic resistance to axial compression in the fire situation
$N_{fi\ Rd}$	Buckling load of columns, in fire situation
$N_{pl,Rd}$	design value of plastic resistance of the composite section to compressive normal force
$N_{pl,Rk}$	characteristic value of the plastic resistance of the composite section to compressive normal force
N_{Rd}	design value of the buckling load of the columns at room temperature
$N_{Rd,20}$	design value of the buckling load of the columns at room temperature
P	axial force
P_0	initial applied load or serviceability load of the column
P_R	resultant of the axial stresses
Q	rate of heat release in fire situation
Q_c	convective part of the heat release rate
Q_H^*	non-dimensional rate of heat release in fire situation
$Q_{k,1}$	characteristic value of the main variable action
$Q_{k,i}$	characteristic value of the other variable actions
Q_{wall}	loss of energy to the enclosure surfaces
Q_{rad}	loss of energy by radiation through the openings
$R_{fi,t,d}$	design buckling resistance at time t

$S22$	axial stresses
T, θ	temperature
T_{cr}	critical temperature;
T_s	steel temperature
T_y	temperature gradient
T_{th}	thermocouple
$T_{furnace}$	temperatures of the furnace
T_{ISO834}	temperatures of the standard curve ISO 834
V	volume of the member per unit length
$W_{el,y}$	elastic section modulus around y
$W_{el,z}$	elastic section modulus around z
$W_{pl,y}$	plastic section modulus around y
$W_{pl,z}$	plastic section modulus around z

Latin lower case letters

b	width of the cross section
b_f	flange width
$l_{c,z}$	buckling length of the column for the relevant bending axis
c	specific heat of boundary of enclosure
c_a	specific heat of steel
c^{mod}	stiffness of the surrounding environment
d	displacement
e	eccentricity of the loading
f	measured force
f^{mod}	model force
f_{ayk}	characteristic value of the yield strength of the structural steel at room temperature
f_{cd}	design value of the yield strength of the steel at room temperature

f_{ck}	characteristic value of the compressive strength of the concrete at room temperature
f_{sd}	design value of the yield strength of the reinforcing steel at room temperature
f_{syd}	design value of the yield strength of the steel at room temperature
f_{syk}	characteristic value of the yield strength of the steel reinforcement at room temperature
f_y	yield stress of steel at ambient temperature.
f_{yd}	design value of the yield strength of the steel at room temperature
γ_{GA}	partial safety factor for permanent actions in the accidental situation
h	height of the cross section
h_{eq}	equivalent height of the openings
$\dot{h}_{net}$	net heat flow per unit area
$\dot{h}_{net,c}$	net convective heat flux per unit surface area
$\dot{h}_{net,d}$	design value of the density of heat flow per unit area
$\dot{h}_{net,r}$	net radiative heat flux per unit surface area
h_w	web length
i	radius of gyration
$k_{ct}(\theta)$	reduction factor for the tensile strength of concrete
$k_{E,\theta}$	reduction factor for the slope of linear elastic range at the steel temperature θ_a reached at time t
$k_{p,\theta}$	reduction factor of the yield point of structural steel giving the proportional limit at temperature θ_a reached at time t
$k_{y,\theta}$	reduction factor for effective yield strength at the steel temperature θ_a reached at time t
k_r	Stiffness of a rotational spring
l_e	length of the element
l_{fi}	buckling length in fire situation
l_θ	buckling length in fire situation
m	combustion factor
$\dot{m}$	gas mass rate

$\dot{m}_{fi}$	rate of pyrolysis products generated
$\dot{m}_{in}$	rate of gas mass coming in through the openings
$\dot{m}_{out}$	rate of gas mass going out through the openings
$q_{f,d}$	design value of fire load density related to the surface area A_f of the floor
$q_{f,k}$	characteristic value of fire load density per unit floor area
$q_{t,d}$	design value of the fire load density related to the total surface area A_f of the enclosure
r	horizontal distance between the vertical axis of the fire and the point along the ceiling where the thermal flux is calculated
t	time
t_b	wall thickness
t_{cr}	critical time
t_f	flange thickness
$t_{fi,d}$	design value of the fire resistance
$t_{fi,requ}$	required fire resistance
t_{hw}	thermocouple in the walls
t_{lim}	time dependent on the speed of fire spreading depending on the occupation of the fire compartment
t_w	web thickness
u	displacement
u^{therm}	thermal displacement
u^{mech}	mechanical displacement
w	wall
x	is the position where the imperfection is calculated
y	non-dimensional parameter
$y_{1,1}$;$y_{2,1}$	combination factors for actions
z	height along the flame axis
z'	Vertical position of the virtual heat source

Greek upper case letters

Δt	time interval

Δ_a unit mass of steel

Φ configuration factor

θ_3^{STC} temperature in zone 3 obtained with the STC numerical simulations.

θ_3^{EC3} temperature in zone 3 obtained with the simplified calculation method for temperature evaluation on steel elements proposed in EN1993-1-2.

Greek lower case letters

α imperfection factor, thermal elongation coefficient

α_A non-dimensional axial restraint ratio of the column

α_c coefficient of heat transfer by convection

β_R non-dimensional rotational restraint ratio of the column

$\beta_{M,y}$ Equivalent uniform moment factor about y axis

$\beta_{M,z}$ Equivalent uniform moment factor about z axis

δ displacement

δ_n factor taking into account the different active fire fighting measures (sprinkler, detection, automatic alarm transmission, firemen, …).

δ_{q1} factor taking into account the fire activation risk due to the size of the compartment

δ_{q2} factor taking into account the fire activation risk due to the type of occupancy

ε emissivity of material

$\varepsilon_{cu,\theta}$ concrete strain corresponding to $f_{c,\theta}$

ε_E equivalent strains

ε_f emissivity of the fire

ε_φ contraction strain

ε_m surface emissivity of the member

ε_t true strain

ε_{total} total strain

$\varepsilon_{thermal}$ thermal Strain

$\varepsilon_{mechanical}$	mechanical strain
φ	curvature
$\gamma_{M,fi}$	partial safety factor of the steel profile in fire design
$\gamma_{M,fi,a}$	partial safety factor of the steel profile in fire design
$\gamma_{M,fi,c}$	partial safety factor of the concrete in fire design
$\gamma_{M,fi,s}$	partial safety factor of the reinforcing bars in fire design
χ	reduction factor for the relevant buckling mode
χ_{fi}	reduction factor for flexural buckling in the fire situation
$\chi_{fi,pl,Rd}$	is the design value of the plastic resistance to axial compression in fire situation
$\chi_{y,fi}$	reduction factor for flexural buckling in the fire situation, around y axis
$\chi_{z,fi}$	reduction factor for flexural buckling in the fire situation, around z axis
$\chi_{min,fi}$	minimum reduction factor for flexural buckling in the fire situation
λ	slenderness of the steel column
λ	thermal conductivity
$\overline{\lambda}$	relative slenderness of a column
$\overline{\lambda}_z$	relative slenderness of the column related to the weak axis
$\overline{\lambda_\theta}$	non-dimensional slenderness ratio at elevated temperatures
$\lambda_{y,\theta}$	non-dimensional slenderness ratio at elevated temperatures, around y axis
$\lambda_{z,\theta}$	non-dimensional slenderness ratio at elevated temperatures, around z axis
μ_o	degree of utilization
$\varphi_{I,\theta}$	reduction coefficient depending on the effect of thermal stresses
ϕ	curvature
σ	Stephan Boltzmann constant, stress
σ_n	nominal stress
σ_{sy}	yield stress of steel
$\theta_{a,cr}$	critical temperature of the steel
$\theta_{a,max}$	maximum steel temperature
θ_{crit}	critical temperature

θ_d	design value of material temperature
$\theta_{cr,d}$	design value of the material critical temperature
θ_g	gas temperature in the vicinity of the element or in the fire compartment
θ_m	surface temperature of the element
θ_r	effective radiation temperature of the fire environment
ρ	density of boundary of enclosure

ABBREVIATIONS

ABAQUS	Finite element computer programme
ADC	Analog digital converter
AFMFIC	Factory Mutual Fire Insurance Companies
BAM	Bundesanstalt fur Materialforschung und -prufung
BRE	Building Research Establishment
CAST3M	Finite element computer programme
CFD	Computational Fluid Dynamics
CHS	Concrete-filled circular hollow section
CSC	Composite steel column
CTICM	Centre Technique Industriel de la Construction Métallique
DAC	Digital analog converter
DTU	Document Technique Unifié
E	Embedded
EC	Eurocode
FCTUC	Faculdade de Ciências e Tecnologia da Universidade de Coimbra
FE	Finite Element
FEMFAN2D	Finite element computer programme
FINEFIRE	Finite element computer programme
FIRTO	Fire Insurers Research and Testing Organisation

HSS	Hollow steel section
iBMB	Institut fur Baustoffe Massivbau und Brandschutz, in Braunschweig
ISO	International Standard Organization
LVDT	Linear Variable Displacement Transducer
PID	Analog Controler
SHS	Square concrete filled hollow section
SIF	“Structures in Fire” Conference
STC	SuperTempCalc
SOSMEF	Software for the analysis of steel beams and columns subjected to high temperatures
ZWAN	Computer programme

1 INTRODUCTION

1.1 Overview

During the last decades, remarkable progress has been made in understanding not only the parameters which influence the development of building fires, but also the behaviour of fire exposed structural materials and structures. In particular, for steel structures, this progress has resulted in the production of very detailed rules for the design and calculation of structural behaviour and load bearing capacity in fire.

Nevertheless, it must be admitted that up to now the greater part of the research effort in relation to the fire behaviour of steel structures has been confined to the two aspects mentioned above, although in recent years it has become obvious that, whatever progress may have been made in a better assessment of the role played by compartmentation and structural fire behaviour, the answer to the problem of the fire safety of building is still incomplete.

Not only steel, but all material structural elements lose strength due to a degradation of the mechanical resistance with the increase of temperature. Because of some aspects such as temperature gradients and instability effects under high temperatures, it is not appropriate to apply the same strength reductions to structural members as they are applied to the material itself. Thus, further studies on the fire resistance of structural elements under thermal gradients are needed.

Steel construction is becoming more and more used in buildings, all over the world. The use of pre-fabricated elements is very useful and advantageous, for it can reduce substantially the construction time, and consequently the global cost. Also, it must be pointed out the sustainability of constructional materials, taking into account the life period of a building and the re-use of the construction remains in the end of its life period.

However, it must not be forgotten the poor behaviour of structural materials under the conditions of exposure to fire. It is well known that all materials, but particularly steel suffers a great reduction of yield stress and Young's modulus, under the effect of high temperatures. This is a very detrimental topic in the decision of using steel in construction. In fact, a bare steel structural element, cannot withstand more than a few minutes under a fire event. Moreover, a structural steel element, suffers a great increase of internal stresses, due to the restraint it is submitted when inserted in a real building. The influence of the restraint to thermal elongation on steel columns is not yet accurately known.

1.2 Purpose and Scope of this Research

The purpose of this work is to study the behaviour of steel and composite steel-concrete columns in buildings subjected to fire. Several parameters are related, and have a major influence on the fire behaviour of columns in buildings. The contact with brick walls, the stiffness of the surrounding structure, the load level, the slenderness of the columns, are the target of the parametric study carried out in the present study, both in isolated columns and columns embedded on walls. Three sets of experimental tests, to be compared with numerical studies reproducing the conditions used in the tests, were performed, with the purpose of provide valuable data for the development or improvement of analytical designing methods. The main goal was to reproduce as much as possible, in the laboratory, the conditions to which the column is subject in a real building.

1.2.1 Columns embedded on walls

The fire behaviour of steel structures has been traditionally regarded as being dominated by the degradation of mechanical properties under the action of elevated temperatures, mainly the yield stress and the Young's modulus.

Most of the columns in real buildings are in contact with walls. Thus, in case of fire, the thermal action may act only on one side of the wall, leading to a differential heating, and consequently a thermal bowing, giving rise to differential strains, in different zones of the cross sections. The fire behaviour of steel columns embedded on the masonry walls is substantially different from the one observed in isolated columns. The contact with the walls have on one hand a beneficial effect reducing the temperatures and, on the other hand, a detrimental effect since this differential heating may lead to large thermal gradients. These differences in the temperature within the cross-section may lead to the arising of unfavourable efforts in the structure, such as bending moments, which may lead to sudden failure of the columns. The effect of differential heating causes a thermal bowing, which must be evaluated by an accurate quantification of temperature distribution in the steel. The structural behaviour of the columns, is strongly dependent on second order effects. This is a very important phenomenon because it may lead to a significant reduction in the fire resistance of columns.

In this research work, an evaluation of the effects of a differential thermal action on the structural behaviour of steel columns was performed, in order to assess whether the walls have a beneficial or detrimental effect on the mechanical resistance of steel columns under elevated temperatures, and consequently in the fire resistance.

The EN 1991-1-2 (2002), states that the indirect actions on structures should be considered for structural analysis. As indirect actions, amongst others, considers the thermal gradients through the cross-sections of structural elements, and the differential thermal expansion. Although the concept of section factor may be used for each component of the profile, in general, the EN 1993-1-2 (2005) provides only a formula for calculating the evolution of temperature profiles in steel cross-sections, considering a uniform distribution of temperatures.

1.2.2 Steel columns

The influence of restraint to thermal elongation on the fire resistance of steel columns has been studied in the recent years. It is known that the restraint to thermal elongation may reduce the critical temperature and thus the fire resistance of steel columns.

The EN 1991-1-2 (2002) states that a structural fire design analysis should take into account, amongst others, the calculation of the mechanical behaviour of the structure exposed to fire. This mechanical behaviour must take into account not only the direct actions but also indirect fire actions. As indirect actions, the restraining to thermal elongation is important, particularly in columns in buildings of several storeys, because this restraint leads to an increase of the axial load. However, EN 1993-1-2 (2005) provides a formulation for calculating the critical temperature of a steel column, not taking into account the effect of the restraining to the thermal elongation promoted by the surrounding structure.

Several studies on this issue, involving numerical and experimental tests, have reached the conclusion that the higher the stiffness of the surrounding structure, the lower the fire resistance of the column. However, it was already concluded by Bennets (Bennets et al. 1989) that the axial restraint has no such negative influence as is generally considered. Moreover, most of the studies on this issue have only considered the axial restraint, but not the rotational restraint appropriately. Thus, the aim of studying this issue is to ascertain the real influence of a surrounding structure in the column behaviour under fire, considering both axial and rotational restraint.

1.2.3 Composite steel-concrete columns

A third part of this research work is composed of a set of tests on composite steel-concrete columns with restrained thermal elongation, under fire. On the contrary to steel columns, few experimental studies on the behaviour of composite partially encased steel-concrete columns under fire conditions have been performed up to now, taking into account the restraint to thermal elongation of the column. The main purpose of research on this type of columns, is to

provide data of a great deal of experimental tests to assess the fire resistance of partially encased steel columns with restrained thermal elongation, considering not only the axial but also the rotational stiffness of the surrounding structure on the behaviour of these columns in buildings.

1.3 Organization of the thesis

The thesis is organised in eight chapters. In the following paragraphs, a brief description of the contents of each is presented:

Chapter 1 – Introduction
Chapter 1 is an introduction to the research work presented in this thesis.

Chapter 2 – State-of-the-art
In Chapter 2 a brief review of the State-of-the-art is presented, concerning the fire behaviour of steel and also composite steel-concrete columns in buildings. The motivation for this work is also mentioned in this chapter.

Chapter 3 – Fire design of steel and composite steel-concrete columns according to Eurocodes
Chapter 3 presents the general procedure for fire design of steel and composite steel-concrete columns, according to Eurocodes 3 and 4. The definition of the thermal actions and the nominal and parametric fire curves are also described. The thermal and mechanical properties of steel and concrete are also mentioned. The calculation of temperatures in compartment fires and structural elements is described. The thermal bowing is presented as a phenomenon capable of playing a detrimental role in the structural behaviour of a column under high temperature actions.

Chapter 4 – Fire resistance tests on columns with restrained thermal elongation
Chapter 4 describes in detail the experimental programme of the fire resistance tests performed in the Department of Civil Engineering of the University of Coimbra. Three sets of experimental tests were carried out, on the research in the scope of this thesis and are presented in this chapter. The first set on steel columns embedded on walls with differential heating, the second set on steel columns, and the third on composite steel-concrete columns with restraint to thermal elongation subjected to fire.

Chapter 5 – Fire Resistance Tests on columns using an hybrid system

Chapter 5 presents several fire resistance tests on steel and composite steel-concrete columns, performed in the Bundesanstalt fur Materialforschung und –prufung, in Berlin, Germany. In this Laboratory, the columns are tested with restraint to thermal elongation provided by a sophisticated system, in which the stiffness of the surrounding structure is simulated by hydraulic jacks, servo-controled by computers. The technique used on this system, makes it possible to have only one element of the building structure inside the furnace, while computers simulate the behaviour of the remaining structural system. An interface node interconnects the element inside the furnace with the simulated system. The movements of the interface node are performed by several hydraulic jacks, while the computers are solving, in an iterative process, the equations of the equilibrium of forces and displacements between the element in the furnace and the simulated system. The system was conceived to study thermal restraint and subsequent restraining forces.

The main purpose of these tests was to assess the influence of the frame effect on the fire resistance tests performed in the University of Coimbra. The system used in BAM has the capacity if testing columns within a large range of values of stiffness of the surrounding structure, allowing a comparison with the results obtained in FCTUC. It was also possible to evaluate the capacity of the computers to perform the calculations, accompanying the development of the test inside the furnace.

Chapter 6 – Numerical simulations of steel and partially encased steel-concrete columns exposed to fire

In chapter 6, a numerical study on the fire behaviour of columns in buildings is presented. Not only all the experimental tests but several other cases were simulated using the finite element code ABAQUS. The influence of several parameters such as the temperature gradients along the cross section, the thickness of the walls, the orientation of the web of the steel profile in relation to the walls, the temperature gradients along the length of the columns, the load ratio, the slenderness of the columns and the stiffness of the surrounding structure were target of this study.

Chapter 7 – Proposal of simplified calculation methods for the temperature evolution and fire design of steel columns

Chapter 7 deals with the structural behaviour of a column under fire conditions, from an analytical point of view. A detailed discussion of the numerical and experimental results is held, and proposals for calculation methods are presented, for several of the studied situations. A method for the assessment of temperatures within the cross section of H sections of steel columns embedded on walls is to be presented. Based on the EN 1993-1-2(2005) formulation, a method for the calculation of temperatures in the exposed and unexposed flanges and webs

of the profile are presented, both for columns with the web parallel and perpendicular to the surface of the walls.

Moreover, new Axial Force – Bending Moment diagrams for the design of steel columns subjected to thermal gradients are presented, for the two orientations analyzed in this study.

Concerning the bare steel columns, a method is presented for the calculation of critical temperatures and critical times of steel columns, with restrained thermal elongation. Depending on the load level and the slenderness of the column, the methods derived on this study, allow the calculation of the fire resistance of this type of columns.

Chapter 8 – Conclusions and future work

Conclusions and future works are presented in Chapter 8. A great deal of conclusions was possible to draw, concerning the different kind of tests on the steel columns, isolated or embedded on walls and also on partially encased steel-concrete columns subjected to fire. The main conclusion on the set of tests in columns embedded on walls was the perception of the thermal bowing behaviour of these columns and the inversion of bending moments during the fire. This phenomenon is provoked by the thermal gradients developed within the cross section of the H profile. The influence of the temperature distribution on the columns is strongly dependent on the orientation of the web in relation to the wall surface, and on the thickness of the wall. Concerning the bare steel and composite steel and concrete columns, the main conclusions concerned the beneficial influence of the rotational restraint provided by the surrounding structure to the columns. The major outcome of this research concerns the real influence of axial and rotational restraints of the surrounding structure, on the fire behaviour of a column inserted on a frame.

2 STATE-OF-THE-ART

2.1 Research on steel columns embedded on walls

2.1.1 Experimental research

In 1988, Wainman and Kirby (Wainman et al., 1988) published a Compendium of the UK Standard Fire Test Data – Unprotected Structural Steel, jointly sponsored by the British Steel Corporation and the Building Research Establishment. This work was prepared with the purpose of providing data for researchers in the study of fire resistance of steel structures particularly in the development of accurate calculation methods, for the determination of high temperature performance and fire resistant design. Amongst other structural elements, they have presented results of fire resistance tests on columns blocked in webs exposed to fire on four sides, as well as columns embedded on walls. The tests on columns on walls consisted of universal columns built into a cavity wall construction, so that either one flange or a flange + part of the web from each section, was exposed to the fire. These tests were carried out at FIRTO, in Borehamwood, in 1982.

a) b)

Figure 2.1 – Views of fire tests on columns embedded on walls, carried out at FIRTO a) the exposed wall surface after testing b) the unexposed wall surface after testing

Measurements of temperatures in several points of the web and flanges, in different heights of the columns were presented, as well as vertical displacements and lateral deflections.

The results of the fire tests on six steel columns embedded on walls, all of them placed with the web perpendicular to the wall surface, showed that columns in this situation present great horizontal deflections at mid-span while the vertical displacements on top are negligible.

In 1988, Cooke and Morgan (Cooke et at., 1988b) have published a BRE Information Paper, on thermal bowing in fire and how it affects building design. The phenomenon of thermal bowing was already known, but little data is available on the magnitude of thermal bowing in a building on fire. Cooke has developed a simple theory of unrestrained thermal bowing which presented in his PhD Thesis, in 1988.

In the paper published by the Fire Research Station (FRS), also in 1988 (Cooke, 1988a), he presents both experimental and theoretical data, and suggests how the data can be used in the design of buildings to reduce the detrimental effect of thermal bowing. Concerning the thermal bowing of steel structures, it is stated that pin ended I-section steel columns first bow towards the heat source, straighten out and fail by bowing in the reverse direction. The influence of different parameters such as the length/thickness ratio of walls, the load level, the concrete type and the hydrocarbon fire curve for slabs was studied. The main recommendations drawn from this work were that the following design factors will help alleviate thermal bowing problems:

- choosing a material with a low coefficient of thermal expansion;
- reducing the temperature difference and increasing the distance between exposed and unexposed surfaces;
- transforming a member from a cantilever to a simply supported member wherever possible as the mid-span deflection is a quarter of the deflection of a member with a free end;
- providing edge support.

2.1.2 Numerical research

Burgess and Najjar, developed in 1994, (Burgess et al., 1994) an analytical approach based on simple “Perry-Robertson” principles to investigate the behaviour of steel columns in fire condition. This theory was used to predict approximately the failure temperatures of these members, and to provide a qualitative description of the behaviour, allowing the parameters which affect columns in fire to be separated out and their influences to be studied. The Perry approach was tested against analytical and test results. In this theory, failure is defined by the

first occurrence of material yield. Their study was aimed at developing a three-dimensional finite element model which could analyze sub-frames. It aimed to represent any particular structural and fire situation as accurately as possible, particularly thermal gradients across the section. In this study, they concluded that temperature gradient raised the hot flange failure temperatures which is in line with observations from the test results. They have noticed for H-sections, the lack of significant destabilization by the temperature gradient tends to be confirmed by the finite element study. Thermal bowing deflections do not appear very detrimental to the survival of columns if the gradients are relative to major axis. Minor axis gradients have shown much more severe effects in finite element studies.

Rotter and Usmani presented in the first International Workshop "Structures in Fire", in 2000 (Rotter et al., 2000), a study on the fundamental principles of structural behavior under uniform and differential thermal effects. It is pointed out by the authors that framed structures of the type tested at Cardington, posse enormous reserves of strength through adopting large displacement configurations, and that thermally induced forces and displacements, not material degradation, governs the response in fire. This study was based upon the analysis of the response of single structural elements under a combination of thermal actions and end restraints representing the surrounding structure. The paper describes in detail the most fundamental relationship that governs the behavior of structures when subjected to thermal effects. The most important factor that determines a real structural response to heating is the manner in which it responds to the unavoidable thermal strains induced in its members through heating. If the structure has insufficient end translational restraint to thermal elongation, the considerable strains are taken up in expansive displacements, producing a displacement-dominated response. Thermal gradients induce curvature, leads to bowing of a member whose ends are free to rotate, again producing large displacements (deflections). Curvature strains induced by the thermal gradient in members whose ends are rotationally restrained can lead to large hogging (negative) bending moments throughout the length of the member without deflection.

A detailed analysis of a beam axially and rotationally restrained with end restraints perfectly rigid as well as only finite restraints as offered by real structures to the structural elements.
Thermal bowing is described to occur on structural elements exposed to fire only on one side, which expands much more than the cool side. The key conclusion drawn from the discussion is that *…thermal strains will be manifested as displacements if they are unrestrained or as stresses if they are restrained through counteracting mechanical strains generated by restraining forces…* In 2004 Real et al. (Vila Real et al., 2004) published a numerical study on the behavior of steel beam-columns subjected to fire and a combination of axial force and bending moments, on bare steel elements. They have used the geometrical and material non-

linear finite element program SAFIR established in the University of Liège for the analysis of structures submitted to fire, to determine the resistance of a beam-column at elevated temperatures using the material properties of Eurocode 3, part 1-2 (EN 1993-1-2-2005). The numerical results have been compared with those obtained with Eurocode 3. They compared the non-dimensional bending resistance of a simply supported beam under equal end moments from two Eurocode proposals (1995 version (EN 1993-1-2-1995) and 2002 version (EN 1993-1-2-2002)) against the numerical results obtained for a range of uniform temperatures from 400 to 700ºC, for various levels of non-dimensional slenderness. Although the numerical study presented was limited to a single section size (IPE200) and steel class (S235), a previous parametric study for different steel sections and steel grades performed for lateral-torsional buckling of steel beams subjected to fire highlighted no qualitative changes, thus justifying the extrapolation of these results. Analogously, the influence of temperature gradients across the web and flanges, also studied in the context of the lateral-torsional buckling behaviour of steel beams was chosen to have negligible effect on the resistance of beams and was disregarded in this study. The new proposal is generally on the safe side when compared to numerical results, as would be expected from a simple calculation model. This is not systematically the case, especially for short members submitted mainly to axial forces. The main conclusion of this work was that the more recent version of Eurocode (EN 1993-1-2-2002) provides better results than the previous one, and a perfect fit to the numerical results.

In 2006, Garlock et al. (Garlock et al., 2006b) presented a study on the combined axial load and moment capacity of fire-exposed beam-columns with thermal gradients in which they have compared the capacity of members with temperature gradients to those with uniform temperature profiles. The beam-columns model used in the study were wide-flange steel sections that are part of a high-rise moment-resisting steel building. They have considered the effects of plate thickness, section depth, and the direction of bending (i.e. strong *vs* weak axis) on the *P-M* capacity envelope. The results show that members that experience uneven heating, such as perimeter columns or beams carrying a floor slab, will develop a thermal gradient through their depth. This thermal gradient may have a significant effect on the capacity of beam-columns, and evaluations that are made assuming a uniform temperature through the section may lead to overestimations of the true strength of the section. If the temperatures are high enough to reduce the yield strength, the resulting thermal gradient will shift the position of the resultant axial force, induce additional bending moments and alter the P-M capacity envelope. Depending on the combination of applied loading, the *P-M* capacity envelope that is calculated based on uniform temperature through the section (as usual) may provide aconservative or un-conservative estimate of the true capacity, which considers temperature gradient.

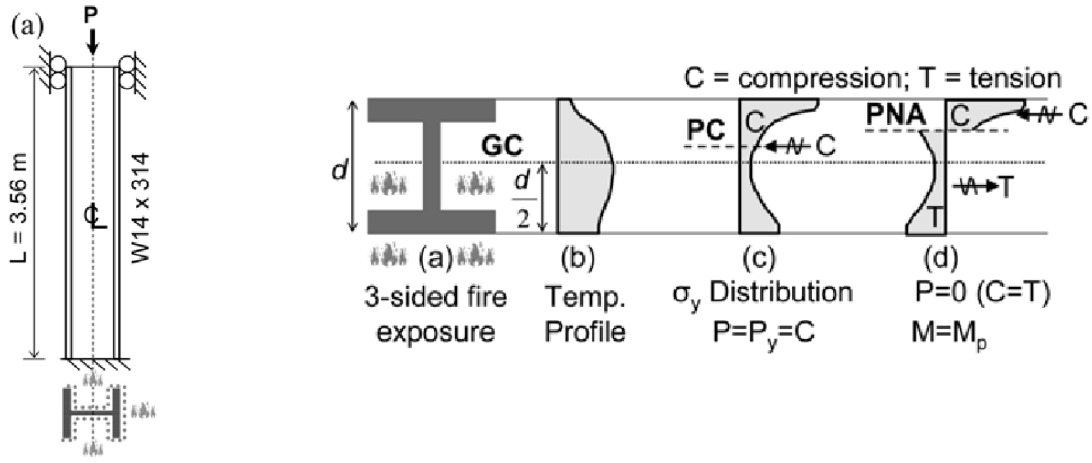

a) b)

Figure 2.2 –a) model of the column in study b) Stress profiles based on the section and temperature profiles provided, describing the plastic centroid PC and plastic neutral axis PNA (Garlock et al., 2007a).

Tsalikis presented in 2009, (Tsalikis et al., 2009) a study on Steel Beam-Columns under thermal Gradient – Combined axial-bending capacity of steel double-T cross-sections subjected to non-uniform temperature distributions. In their work, they investigated the way that a thermal gradient on a cross-section of a steel-beam member affects its mechanical strength. They have developed a theoretical approach based on numerical simulations performed with a finite element code named CAST3M. They have observed that the thermal gradient alters the capacity of the cross-section. The main conclusions of their work were that the region of safe operation of the cross-section presents under the presence of thermal gradient a differentiation in shape that is not accounted for by the present regulatory framework, and have pointed out that there is a great need for extensive parametric research to obtain N-M interaction safety regions for commonly used structural steel cross sections.

In 2010, another work on this issue was presented by Knobloch (Knobloch et al., 2010), in SIF conference. He has performed a numerical analysis of the cross-sectional capacity of structural steel members in fire. It describes a comprehensive research project on the cross-sectional capacity and the overall structural behavior of steel members in fire, performed at ETH, in Zurich. He has analyzed the cross-sectional capacity of steel sections subjected to combined axial compression and biaxial bending moments at elevated temperatures, considering full section yielding and local buckling effects. The results of the parametric study using finite element approach were presented as temperature-dependent normalized N-M interaction curves and compared to results using elastic plastic formulae. The main

conclusion of the work was that the interaction formulae for beam-columns in fire could be limited to the cross-sectional capacity for short beam-columns without member buckling effects.

In 2011, Tsalikis et al. (Tsalikis et al, 2011) presented a study on the elastic buckling of steel columns under thermal gradient. They have studied the behaviour of steel pin-ended columns under thermal gradients. Initially, they examinated separately, the effect of thermal gradient on the shift of the elastic neutral axis and then, added the thermal bowing of the member to investigate the combined behaviour. They have used two different approaches for the problem. At the first approach, the beam-column equation was applied in order the effect of the shift of the centroid to be studied. Results showed that the maximum allowable stresses are not far from the Euler buckling curves for the maximum temperature of the cross section. The eccentricity that arises from the shift of the centroid cannot be studied independently. The shift of the centroid should be always smaller than the lateral deflection of the column in order the equation to comply with the initial assumptions. Buckling curves approach the EC3 curve for the maximum temperature as thermal gradient raises. For small slopes of thermal gradients, buckling curves coincide with Euler curve. Furthermore, finite element analysis verifies the validity of the simple approach, for a specific thermal gradient. On the contrary, the analysis of the finite element model with the application of the elastoplastic material laws, as proposed by Eurocode, gave more conservative results. This difference arises from the initial overestimation of the yield stress in the bilinear laws that applied to the elastic model. The principles presented in this study constitute a step towards generating the analytical tools necessary for use. With the appropriate determination of bilinear stress-strain laws and the addition of the other phenomena that govern a column even at ambient temperatures, this method can be used safely for the prediction of lower-bounds on the elastic buckling of medium and high slenderness columns.

Thermal bowing

Columns are usually in real buildings embedded on walls, so they are exposed to fire only from the inside of the compartment. This is the most usual case in practice.

The failure temperatures of columns with non-uniform temperature distribution can be higher or lower than those with uniform temperature, depending on the temperature difference, column section depth, boundary conditions and column height.Thermal bowing is a phenomenon which is characterized by the appearance of stresses and forces, due to a temperature gradient along the cross section of the structural element, causing a deformed shape similar to an arc. The differential heating causes redistribution of bending moments.

The outside steel part of the profile remains cold for a long period of time, its yield strength is not reduced and the axial force produces compressive stresses, so that the change of the moment sign can be accommodated. The yield strength is reduced because of the high temperatures, so they start to yield very soon. Failure occurs, where the bending moment and the fire cause the same effect.

The axial load is applied through the centroid of the cross-section. Bending moment is generated due to the shift of the centroid. Resultant bending moment about the axis perpendicular to the temperature gradient is a result of the shift of the centroid and thermal bowing. At the column ends, the centroid of the section shifts towards the cold side, thus putting the hot side in compression and the cold side in tensile. At the column centre, due to thermal bowing, the column moves towards the fire (hot side), thus the cold side is in compression and the hot side in tensile.

In 2001, Usmani et al. (Usmani et. al, 2001) presented the fundamental principles of the structural behaviour of steel structural elements under thermal effects. The most fundamental relationship that governs the behaviour of structures when subjected to thermal effects is:

$$\varepsilon_{total} = \varepsilon_{thermal} + \varepsilon_{mechanical} \tag{2.1}$$

with

$$\varepsilon_{mechanical} \rightarrow \sigma \text{ and } \varepsilon_{total} \rightarrow \delta \tag{2.2}$$

The arrows mean that the mechanical strains lead to stresses and the total strains lead to displacements.
The total strains govern the deformed shape of the structure δ, through kinematic or compatibility considerations. By contrast, the stress state in the structure σ (elastic or plastic) depends only on the mechanical strains.

Pure axial expansion or pure thermal bowing results from

$$\varepsilon_{\text{total}} = \varepsilon_{\text{thermal}} \text{ and } \varepsilon_{total} \rightarrow \delta \tag{2.3}$$

By contrast, where the thermal strains are fully restrained without external loads, thermal stresses and plastification resulted from

$$0 = \varepsilon_{thermal} + \varepsilon_{mechanical} \text{ with } \varepsilon_{mechanical} \rightarrow \sigma \tag{2.4}$$

The single most important factor that determines a real structure response to heating is the manner in which it responds to the unavoidable thermal strains induced in its members

through heating. These strains take the form of thermal expansion to an increased length (under an average centroidal temperature rise) and curvature (induced by a temperature gradient through the section depth). If the structure has insufficient end translational restraint to thermal expansion, the considerable strains are taken up in expansive displacements, producing a displacement-dominated response. Thermal gradients induce curvature, leading to bowing of a member whose ends are free to rotate, again producing large displacements (deflections).

Members whose ends are restrained against translation produce opposing mechanical strains to thermal expansion strains and therefore large compressive stresses. Curvature strains induced by the thermal gradient in members whose ends are rotationally restrained can lead to large hogging (negative) bending moments throughout the length of the member without deflection. The effect of induced curvature in members whose ends are rotationally unrestrained, but translationally restrained, is to produce tensile.

Therefore for the same deflection in a structural member a large variety of stress states can exist; large compressions where restrained thermal expansion is dominant; very low stresses where the expansion and bowing effects balance each other; in cases where thermal bowing dominates, tensile occurs in laterally restrained and rotationally unrestrained members, while large hogging moments occur in rotationally restrained members. A fast burning fire that reaches flashover and high temperatures quickly and then dies off can, produce high thermal gradients (hot steel and relatively cold concrete) but lower mean temperatures. By contrast, a slow fire that reaches only modest temperatures but burns for a long time cools, produce considerably higher mean temperatures and lower thermal gradients.

Most situations in real structures under fire have a complex mix of mechanical strains due to applied loading and mechanical strains due to restrained thermal elongation. These lead to combined mechanical strains which often far exceed the yield strain values, resulting in extensive plastification. The deflections of the structure, by contrast, depend only on the total strains, so these may be quite small where high restraint exists, but they are associated with extensive plastic strains. Alternatively, where less restraint exists, larger deflections may develop, but with a lesser demand for plastic straining and so less destruction of the stiffness properties of the materials. These relationships, which indicate that larger deflections may reduce material damage and correspond to higher stiffness, or that restraint may lead to smaller deflections with lower stiffness, can produce structural situations which appear to be quite counterintuitive if viewed from a conventional (ambient) structural engineering perspective.

Thermal bowing causes the heated surfaces to expand much more than the outer surfaces inducing bending in the member.

Relationships can be derived for thermal bowing analogous to the one derived earlier for thermal expansion. Assuming the structural element simply suported, the following relationships can be derived:
The thermal gradient (T_y) over the depth is, considering a simple linear variation of temperature

$$T_y = \frac{T_2 - T_1}{d} \tag{2.5}$$

A uniform curvature (ϕ) is induced along the length as a result of the thermal gradient,

$$\phi = \alpha T_y \tag{2.6}$$

Due to the curvature of the element, the distance between the ends of the element will reduce. If this reduction is interpreted as a contraction strain (not literally) ε_φ is defined by

$$\varepsilon\phi = 1 - \frac{sin\frac{l_e\phi}{2}}{\frac{l_e\phi}{2}} \tag{2.7}$$

Considering the same structural element, but restrained, if a uniform thermal gradient T_y is applied to this element, the result (in the absence of any average rise in temperature, *i.e.* mean temperature remaining constant) is a thermally induced tensile in the element and corresponding reactions at the support (opposite the pure thermal expansion case discussed earlier). This is clearly caused by the restraint to end translation against the contraction strain (ε_φ) induced by the thermal gradient.

Considering a fixed ended element (by adding end rotational restraints) subjected to a uniform temperature gradient through its depth. Recalling that a uniform curvature $\varphi=\alpha T_y$ exists in a simply supported element subjected to gradient T_y. If that element is rotationally restrained, moments cancels out the thermal curvature and therefore the fixed ended beam remains "straight" with a constant moment $M=EI\varphi$ along its length.

From the above discussion, it is clear that the effect of boundary restraints is crucial in determining the response of structural members to thermal actions. The key conclusion to be drawn is that, thermal strains will be manifested as displacements if they are unrestrained or as stresses if they are restrained through counteracting mechanical strains generated by restraining forces.

For lateral restraint, perfect rotational restraint is also not very easily achieved in real structures (other than for symmetric loading on members over continuous supports, without any hinges from strength degradation). Considering an element restrained rotationally at the ends by rotational springs of stiffness k_r, the restraining moment in the springs as a result of a uniform thermal gradient T_y can be found to be,

$$M_k = \frac{EI\alpha T_y}{\left(1 + \frac{2EI}{k_r l_e}\right)} \tag{2.8}$$

This equation implies that if the rotational restraint stiffness is equal to the rotational stiffness of the element itself (EI/l_e) then the moment will be about a third of a built-in support moment.

2.2 Research on steel columns

2.2.1 Experimental research

Bauschinger seems to have been the first one to carry out fire resistance tests on steel columns (Aasen, 1985). Between 1885 and 1887, fire resistance tests on columns placed horizontally, were carried out. The results showed that cast iron columns had higher fire resistance than the wrought and mild steel columns.

Knublauch et al, reported in 1974, a series of twenty three fire resistance tests on steel columns with box shaped insulation made of vermiculite plates (Aasen, 1985). The tests were carried out at the Bundesanstalt fur Materialforschung und prüfung (BAM), in Berlin, Germany. The columns were tested without restraint to thermal elongation and subjected to an axial loading that was kept constant during the test. Columns with different type of cross-sections and of the same length were tested. In the tests only 80% of the column's length was heated. The main conclusion of the tests was that 95% of the columns had a critical temperature above 500ºC.

In the same laboratory, in 1977, Stanke reported fourteen fire resistance tests on steel columns with restrained thermal elongation (Aasen, 1985). In these tests, it was observed for the first time, that the column's restraining forces increased rapidly up to a maximum and then started to diminish gradually crossing the axis of the initial applied load for a certain temperature and time. This behavior is typical of columns with restrained thermal elongation.

Janss and Minne, reported in 1981 (Janss et al., 1981), a series of twenty nine fire resistance tests on steel columns, carried out at the University of Ghent, in Belgium. A series of eleven HEA and HEB columns with a slenderness ratio of 25 and a series of eighteen HEA, HEB and

IPE columns with slenderness ratios between 25 and 102, were carried out. The columns were tested in the vertical position and clamped in special end fixtures intended to provide a perfect rotational restraint at both ends. The load applied to the column was kept constant during the tests and no axial restraint was imposed. The whole length of the column was inside the furnace. Most of the columns were insulated and only two columns were unprotected. The critical temperatures varied in the first series between 444 and 610ºC and in the second series between 250 and 616ºC.

Olesen in 1980 reported the results of a series of twenty four fire resistance tests carried out at the University of Aalborg, in Denmark, on steel columns without axial thermal restraint. Hinged columns with different lengths were tested. The columns were tested in the horizontal position, subjected to a constant compressive applied loading and were connected outside the furnace to a restraining frame (Aasen, 1985).

Aribert and Randriantsara, in the early 80´s (Aribert et al., 1980, 1983), have also performed a series of fire resistance tests on steel columns, at the University of Rennes, in France. They were carried out thirty-three tests on non-insulated pin-ended columns with the same length and cross-section. The main conclusions of these tests were that the creep starts to influence the strength of the steel columns at around 450ºC. At 600ºC, the columns strength was significantly reduced.

Hoffend, between 1977 and 1983, performed a complete test program on steel columns subjected to fire. The main parameters investigated in these tests were: the slenderness of the column, the load level, the buckling axis, the load eccentricity, hinged and built in support conditions, the existence of thermal gradients along the column, the heating rate and the degree of axial restraint. These tests were performed at iBMB – Institut fur Baustoffe Massivbau und Brandschutz, in Braunschweig, Germany. The main conclusions of these studies were that the critical temperature was slightly higher for slender than for stocky columns; the load level has more influence on the critical temperature of less slender columns; the load eccentricity had a higher effect on diminishing the critical temperature for slender than for stocky columns. The thermal gradients in height had a minor effect on the strength of hinged columns.

In 1985, Aasen (Aasen, 1985) reported the results of eighteen fire resistance tests performed at the Norwegian Institute of Technology, Trondheim, Norway. Twelve pin-ended columns with free thermal elongation, four columns with end moment restraint and free axial thermal elongation and two pin-ended columns with axial restraint, were tested. The columns were made of IPE 160 cross-sections with lengths of 3.1, 2.21, 1.75 and 1.7m, which corresponded

to slenderness values about the weak axis of 169, 120, 95 and 92. The results of the tests showed, for the unrestrained columns, that the higher applied load levels led to smaller fire resistance, the initial out-of-straightness and the accidental eccentricities of the columns reduced the fire resistance and the slenderness of the columns and the heating rate affected slightly the column's strength. For the rotationally restrained columns, it was concluded that the beam to column connections change the columns behavior reducing the lateral deflections and smoothing the buckling failure, the columns with intermediate slenderness values showed flexural-torsional buckling mode of failure. For the axially restrained columns, the higher applied load levels led that the maximum restraining forces were reached earlier and the fire resistance was lower; the initial geometrical imperfections change the shape of the restraining forces curve and lateral deflections.

Burgess et al. (Burgess et al., 1992) presented a very complete study in 1992 on the influence of several parameters on the failure of steel columns in case of fire. This study was composed of a series of numerical simulations using a finite strip method, including non-linear material characteristics as functions of time temperature. The parameters studied were: the influence of slenderness, the effect of stress-strain relationships, the effect of residual stress levels, the influence of local buckling and the behaviour of blocked-in-web columns. Simulations were performed for pin-ended columns with no initial geometric imperfections, either as out-of-straightness or as load eccentricities. The temperature distribution was uniform throughout the length, and symmetric over the cross-section. Except for the case of blocked-in-web columns, the temperature over the cross-section was uniform. The method admitted all possible buckling modes and took account of the non-linear stress-strain characteristics of the steel as a function of the temperature. They concluded that the critical stresses, and consequently the buckling strength, diminish uniformly as a function of the temperature and with increasing residual stresses. They concluded also that the web in blocked-in-web columns is much protected from radiant and convective heat during fire. The fire resistance of this type of column is higher than that of normal steel columns without protection.In 1998, Ali et al. (Ali et al., 1988) presented a study on the effect of the axial restraint on the fire resistance of steel columns, carried out at the University of Ulster, in England. They were reported thirty seven fire resistance tests on pin-ended steel columns. Columns were made with UC and UB profiles, had 1.8m tall, slenderness values of 49, 75 and 98, and load levels of 0, 0.2, 0.4 and 0.6. The main conclusions of this work were that the critical temperature and consequently the fire resistance of the columns reduced with the increasing of the axial restraint. The magnitude of additional restraining forces generated decreased with increasing load level. The failure of stocky was smoother than of slender columns. Some of the slender columns exhibited sudden instability.

In 2000, Rodrigues et al. (Rodrigues et al., 2000) published the results of a large series of fire resistance tests on small steel elements with restrained thermal elongation. The specimens were steel bars of cross-sections 50mm x 5mm, 50mm x 8mm, 50mm x 12mm and 50 x 20mm, corresponding to slenderness values of 319, 199, 133 and 80, respectively. The parameters tested were beyond the slenderness of the elements, the axial stiffness of the surrounding structure, the load eccentricity and the end-support conditions. The main conclusion of this work was that the restraint to thermal elongation of centrally compressed elements can lead to reductions on the critical temperature up to 300ºC, especially on pin-ended elements.

In 2001, Ali and O´Connor (Ali et al., 2001) presented a study on the structural performance of rotationally restrained steel columns in fire, carried out at the University of Ulster, in England. The experimental set-up was similar to the one of the previous study, with some changes on the end-supports of the test columns, in order to simulate a rotational restraint. They were reported ten fire resistance tests on steel columns under two values of rotational restraint 0.18 and 0.93 and one value of axial restraint of approximately 0.29. Columns were made with 127x76UB13 profiles and had 1.8m tall. They were tested under the load levels of 0, 0.2, 0.4, 0.6 and 0.8. The main conclusions of this work were that the increasing of the rotational restraint had a minor effect on the value of the generated restraining forces nevertheless the critical temperatures were increased for the same load level. The rotationally restrained columns didn't present sudden buckling.

In 2003, Wang and Davies (Wang et al., 2003a) published an experimental study on non-sway loaded and rotationally restrained steel columns under fire conditions, performed at the University of Manchester, in England. In this work the interactions between a column and its adjacent members in a complete structure were analysed. Each test assembly consisted of a column with two beams connected to its web. The column was tested in a fire resistance furnace in the horizontal position. Both test column and adjacent beams were loaded with different combinations of loading in order to produce different bending moments on the column. For each series of tests, the parameters investigated were the total column load and the distribution of the adjacent beam loads. The total column load was the sum of the loads applied on the column and the two beams.

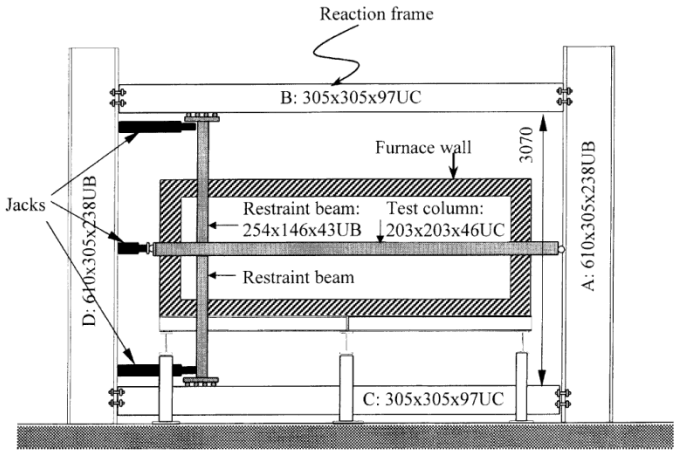

Figure 2.3 - Test set up (Wang et al., 2003a).

Three levels of total column load, representing about 30, 50 and 70% of the column compressive strength at room temperature, were applied. Two beam-to-column connections were tested; one using fine plate and the other using extended end plate connections. The main conclusions were that the column's failure temperature was dependent of the total applied load with a minimum influence of the type of connection and the initially applied bending moments. The bending moments in the test columns undergo complex changes under fire conditions. Moreover, better agreements between the test and calculated results are reached when column bending moments are ignored and its length ratio is considered equal to 0.7.

In 2005, Yang et al. (Yang et al., 2005) performed, in the National Kaohsiung First University of Science and Technology, in Taiwan, a series of fire resistance tests on box and H fire-resistant steel stub columns. The main purpose of this study was to investigate the structural behaviour of the columns under fire load; examine the deterioration of the strength of the columns at different temperature levels and evaluate the effect of the width-to-thickness ratios of the cross-sections on the ultimate strength of the columns at elevated temperatures. Based on this study, it was concluded that the ultimate loads of the columns decrease with the increasing of the width-to-thickness ratios and the temperature. However the effect of the width-to-thickness ratio in the ultimate strength is smaller for high temperatures. It was also observed that the effect of the width-to-thickness on the ultimate strength is more marked for the box than for the H columns.

Yang in collaboration with other authors presented in 2006 two other studies (Yang et al., 2006a, 2006b) and in 2009 one study (Yang et al., 2009) on the behaviour of H steel columns at elevated temperatures. The objective of this study was to study the influence of the width

to-thickness, the slenderness ratios and the residual stresses on the ultimate strength of the steel columns at elevated temperatures. Based on this study, it was concluded that for the temperature of 500ºC, the column retains more than 70% of its ambient temperature strength if the slenderness ratio is less than 50. However, in the case of the temperature exceeds 500ºC, or when the slenderness ratio is greater than 50, column strength reduces significantly. In order to avoid brittle behaviour of steel columns in fire, it is suggested to adopt 500ºC as the critical temperature and 50 as the slenderness ratio for the steel columns. Residual stresses were found to release during the fire test and their influence on columns strength could be neglected.

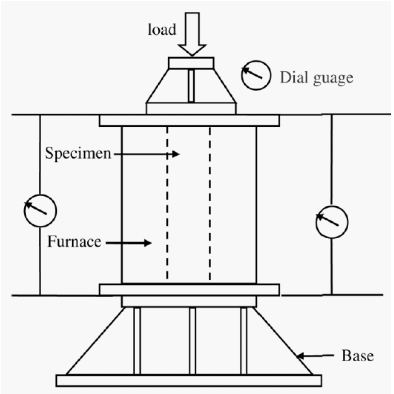

Figure 2.4 - Test set up (Yang et al., 2006a)

In 2007, Tan et al. (Tan et al., 2007) presented the results of several fire resistance tests on axially restrained unprotected steel columns, carried out at the Nanyang Technological University, Singapore. The objective of these tests was to determine the influence of the columns initial imperfections and the axial restraint level on their failure times and temperatures. All columns had an effective length of 1.74m, and slenderness ratios in relation to the weak axis of 45, 55, 81, and 97. The columns were pin-ended and were tested in the horizontal position. Axial restraint was provided by a simply supported transversal steel beam placed at the column end. The test results show that axial restraints as well as initial imperfections reduce the failure times and temperatures of axially-loaded steel columns. By contrast, bearing friction in columns supports increases the column failure times.

In 2010, Guo-Qiang Li et al. (Li et al, 2010) reported the results of two fire resistance tests on axially and rotationally restrained steel columns with different axial restraint stiffness. Axial and rotational restraints were applied by a restraint beam. It was observed, the already known, that the axial restraint reduced the buckling temperature of restrained columns. The effects of axial restraint to the failure temperature depended on the load ratio and axial restraint stiffness ratio.

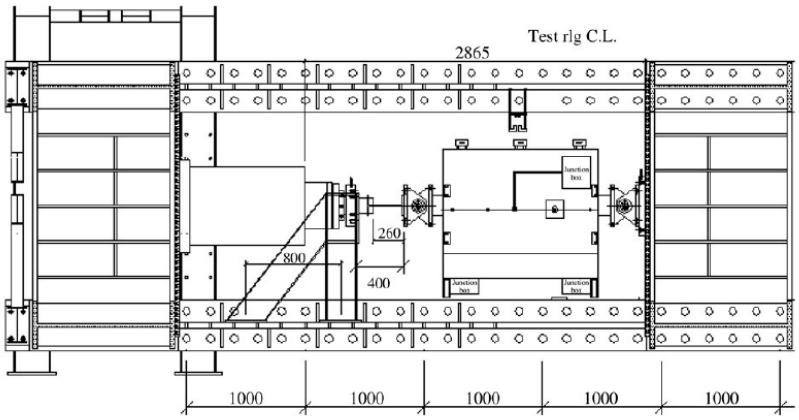

Figure 2.5 - Experimental set-up (Tan et al., 2007)

2.2.2 Numerical research

Bauschinger, in 1887, recommended the Rankine-Gordon formula as basis for the design of fire exposed columns made of wrought iron and cast-iron. This formula has been improved later by Toh et al. (Toh et al., 2000) and then by Huang and Tan (Huang and Tan, 2003a, b). A simple Rankine approach was used to compute the column failure times, which gave good predictions in comparison with the test results. So it can be used in the computation of steel column failure times/temperatures. The Rankine principle allows determining separately the strength and the stability of a steel column at a particular temperature.

Some numerical simulations to study the influence of the boundary conditions on the behaviour of heated steel columns were performed in 1972 and 1973 by Culver (Culver, 1972), Culver et al. (Culver et al., 1973) and Ossenbruggen et al. (Ossenbruggen et al., 1973). Various buckling curves were established depending on the following parameters: steel sections, different types of end conditions and thermal gradients either along the column or across the cross sections.

In 1981, Janss and Minne (Janss and Minne, 1981/82) described a simple design method for steel columns under concentric and eccentric loading in fire. The method adopted the European buckling curves for the design of steel elements at room temperature as the basic design curves for steel columns in fire, modified to take into account the temperature effects on the steel properties.

In 1982, a Document Technique Unifié (DTU) published by the Centre Technique Industriel de la Construction Métallique (CTICM), presenting a calculation method for the prediction of the fire behaviour of steel structures (DTU, 1982). A new calculation process for the critical temperature of steel elements with restrained thermal elongation was described for the first time.

In 1992, Burgess et al. (Burgess et al., 1992) presented a complete numerical study on the influence of several parameters on the failure of steel columns in fire: the influence of slenderness, the effects of stress-strain relationships, the effect of residual stress levels, the influence of local buckling and the behaviour of blocked-in-web columns. Simulations were performed for pin-ended columns. Slenderness was identified as the parameter having the most influence on the critical temperature of steel columns, and columns with high and small slenderness behave better in fire situations than those with intermediate slenderness values.

In the same year, Jeyarupalingan and Virdi (Jeyarupalingan and Virdi, 1992) presented a new method for the analysis of steel beams and columns subjected to high temperatures. This method was implemented into the software SOSMEF. The resulting program allowed: the cross-section to vary along the length of the member, non-linear variations of temperature in the three dimensions, non-linear stress-strain temperature relationships and the use of more than one material in composite elements.

In 1995, Pow and Bennetts (Pow and Bennetts, 1995a,b) described a general numerical method to calculate the non-linear behaviour of load-bearing members under elevated temperature conditions. The method took into account, among other things, the combined actions of axial and biaxial bending, external restraints and temperature variation over the cross-section and along the member.

Also in 1995, Cabrita Neves (Neves, 1995) performed a theoretical study using the computer programme ZWAN to analyse the behaviour of steel columns with restrained thermal elongation. Neves introduced the idea that the critical temperature should correspond to the instant when the restraining forces reach again the initial applied load. He concluded that for columns with a centred load, the critical temperature, and consequently the fire resistance, decreases as the stiffness of the structure increases; fire resistance is highest in cases of null stiffness, no axial restraint. For columns with an eccentric load, the critical temperature is independent of the stiffness of the structure. The explanation for the fact that the fire resistance did not depend upon the stiffness of the structure, may be related to the way on how the eccentricity was applied, or the calculation of the applied load.

Also in 1995, Franssen (Franssen, 1995) presented a simple model for the calculation of the fire resistance of axially-loaded members according to Eurocode 3. Using a non-linear computer code to determine the buckling load of axially-loaded members according to the hypotheses of Eurocode 3, Part 1.2 EN 1993-1-2 (1995). Different yield strengths, buckling axes, ultimate temperatures, lengths and 339 different steel H-sections were considered. A new proposal has been made, that ensures a conservative result when compared to the general model. An analytical formula was given for ultimate temperatures beyond 400ºC. It was verified that the analytical proposal is safer than the general model in 95% of the cases for unprotected sections submitted to the ISO heating.

In 1997, Wang (Wang, 1997a-b) studied different aspects of the structural continuity, notably improved column rotational restraint and increased compressive load in column due to axial restraint to column thermal expansion. A parametric analytical study was performed using three different methods to investigate the effects of structural continuity on column critical temperature and fire protection thickness.

Then, in 1999, Valente and Neves (Valente and Neves, 1999) published a new work on this subject studying the influence of various parameters on the fire resistance of steel columns with axial and rotational restraints, using the finite element program FINEFIRE. When rotational restraint was considered, the restraining forces and the fire resistance were greater for higher grades of rotational restraint.

Also in 2000, Franssen (Franssen, 2000b) studied the failure temperature of a system comprising a restrained column submitted to fire, introducing the principles of the arc-length technique, extending its application to extend a numerical simulation beyond the moment of local failures in case of fire. This technique is applied to the case of restrained columns and it is shown how it is possible to obtain a safe estimation of the critical temperature of the column leading to the failure of the structure, even if the degree of restraint applied to the column is unknown. He concluded that the column temperature leading to the failure of the structure can be estimated by modeling the heated column as totally restrained, which suppresses the necessity to evaluate the degree of restraint provided by the rest of the structure on the column. Because the load level in the unheated columns before the fire is usually less than their ultimate load bearing capacity, the failure of the structure will occur when the heated column supports less load than the initial load it supported before the fire. This makes the axial restraint a much less severe phenomenon than it has sometimes been imagined. In some cases, it could indeed be a positive phenomenon, provided the local failure of a column is accepted and only the failure of the complete structure has to be prevented.

In 2001, Ali and O'Connor (Ali et al., 2001) presented the outcomes of a parametric experimental investigation on the performance of rotationally restrained steel columns in fire. This work was based on an experimental programme performed at the Fire Research Center. Their work included a comparison with the behavior of a steel column previously tested in fire under axial restraint only. They have also presented a method for estimating the effective length of fixed end (partially fixity) columns tested under fire. The main conclusion of their work was that adding rotational restraint had a relatively minor effect on the value of generated restraint forces but failure temperatures were greatly increased under the same load.

In 2004, Huang and Tan (Huang et al, 2004) studied the effects of external bending moments and heating schemes on the responses of thermally restrained steel columns. They investigated the developments of column internal forces as well as cross-sectional stresses and strains for heated columns subjected to both external axial load and two moments acting on the opposite ends. They concluded that external moments can significantly reduce the critical temperature of pin-ended columns, while they have very limited effect on rotationally restrained steel columns due to the moment restoring effect. They also studied the effects of both rapid and slow heating schemes on the column critical temperature. Creep was found to dominate the column behaviour beyond 450ºC, and under a slower heating rate.

A great number of studies on this issue was performed by these authors, providing a great contribution on the knowledge of the fire resistance of thermally restrained steel columns.

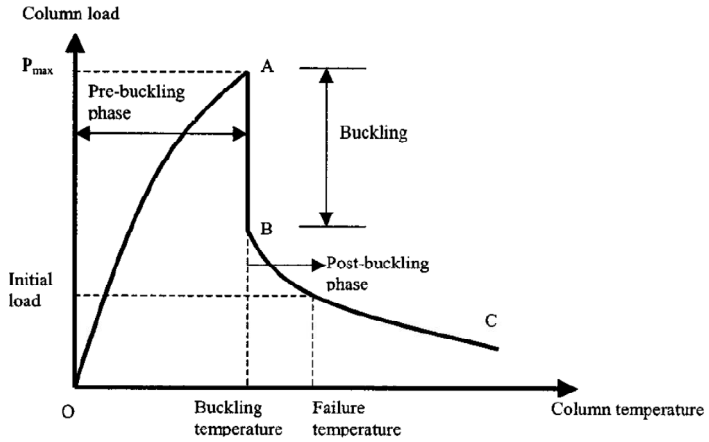

Figure 2.6 – Load-temperature relationship of na axially restrained steel column (Wang et al, 2004).

Also in 2004, Wang et al. (Wang et al, 2004) presented a theoretical study on the postbuckling behaviour of axially restrained and axially loaded steel columns under fire conditions. It was

investigated the effects on the column failure temperature by various factors, including the restraint stiffness during the column loading (expansion) and unloading (contraction) phases, column slenderness and the initial applied column load ratio. Results of this study indicate that the column failure temperature can be much higher than that of the column at first buckling and the higher the column slenderness, the larger the difference between temperatures of column failure and first buckling.
In 2007, Huang and Tan (Huang et al., 2007a, 2007b) modelled experimental tests using the finite element program FEMFAN2D, considering both material and geometrical nonlinearities. The objective was to propose a numerical approach to take into account the secondary effects: proposal of a method to model the axial restraint and unavoidable boundary friction effects; validation against experimental tests; examination of the effects of load eccentricity, boundary friction and different steel material models at elevated temperatures.
Axial and rotational restraints were modelled by, respectively, an axial and a rotational spring. Analytical models were proposed.

From the evolution of the internal axial force P in function of the time, it was showed an increase of P at the beginning of heating, due to the thermal expansion, following by a reduction of P, due to the mechanical contraction. In some cases, a short plateau was showed before a rapid decrease of P. This was due to the restoring effect of friction at the column ends that retarded or delayed column buckling.
Good agreement was shown between the test results and the finite element predictions. The effects of load eccentricity, boundary friction and steel material models on structural responses were shown to substantially affect the column behaviour at elevated temperatures.

In 2008, Tan and Yuan (Tan et al., 2008) studied the buckling of elastically restrained steel columns under longitudinal non-uniform temperature distribution. The objective of the work was to derive closed-form solutions to enable engineers to quickly ascertain the column stability under a non-uniform temperature distribution, without recourse to finite element modelling.

Also in 2008, Chen and Young (Chen et al., 2008) studied the behaviour and design of high strength steel columns at elevated temperatures using finite element analysis. In this study, equations predicting the yield strength and elastic modulus of high strength steel and mild steel at elevated temperatures were proposed. In addition, stress-strain curve model for high strength steel columns over a range of column lengths for various temperatures. The nonlinear finite element model was verified against experimental results of columns at room and elevated temperatures. Two series of box and I-section columns were studied using the finite element analysis to investigate the strength and behaviour of high strength steel columns at

elevated temperatures. Both fix-ended stub columns and pin-ended slender columns were considered. The column strengths predicted from the finite element analysis were compared with the design strengths predicted using the American, European and Australian specifications for hot-rolled steel columns at elevated temperatures. The main conclusion of their study was that the European Code predictions are slightly more conservative than the American Specification and the direct strength method predictions.

In 2010, Wang et al. (Wang et al., 2010) performed in the Shandon University, in China, a parametric study on the behaviour and design of restrained steel columns in fire. The parameters under study were the axial load, the axial restraint stiffness and the column slenderness. The main conclusions were: the axial restraint causes a reduction in the failure temperature of the restrained column. However, when the axial restraint stiffness ratio is greater than a certain value, no further reduction occurs; the difference between failure and buckling temperatures of a restrained column is great for columns with great axial restraint stiffness, or great slenderness, or small load ratio; an increase in the column axial load ratio causes or bending moment ratio causes both the column buckling and failure temperatures to decrease; with an increase in the column end moment ratio, the failure temperature decreases.

Also in 2010, Cai et al. (Cai et al., 2010) published a study on thermal buckling of rotationally restrained steel columns. They studied the buckling of columns in different thermal loading cases and proposed analytical solution to predict the critical temperature for elastic buckling. Two elastic rotational springs at the column ends were used to model the restraints which are provided by the adjacent structural members. Based on non-linear strain-displacement relationship, both the equilibrium and buckling equations were obtained. The results showed that the proposed analytical solution can be used to predict the critical temperature for elastic buckling. The thermal gradient plays a positive role in improving the stability of columns. Furthermore, the effect of thermal gradients decreases while increasing the rotational restraint stiffness and decreasing the slenderness ratios of columns. Moreover, they concluded that rotational restraints can significantly affect the column elastic buckling loads. The main conclusion of their work is that increasing the rotational stiffness of thermal restraints will increase the critical temperature.

2.3 Research on composite steel-concrete columns

2.3.1 Experimental research

There are very few results of fire resistance tests on encased and partially encased steel columns, especially when with restraining to thermal elongation.

Between 1917 and 1919 an extensive programme of tests on columns under fire event was developed, by the Associated Factory Mutual Fire Insurance Companies, The National Board of Fire Underwriters, Bureau of Standards, Department of Commerce, in Chicago (AFMFIC, 1917-1919).This experimental investigation on the fire resistance of columns, consisted on experimental tests to obtain information on which proper requirements for different types of columns could be based. The columns were tested under a constant load during the test. A gas-fired furnace applied the thermal action. Fire and water tests were also performed. In these tests, the column was loaded and exposed to fire for a predetermined period, at the end of which the furnace doors were opened and a hose stream applied to the heated column.

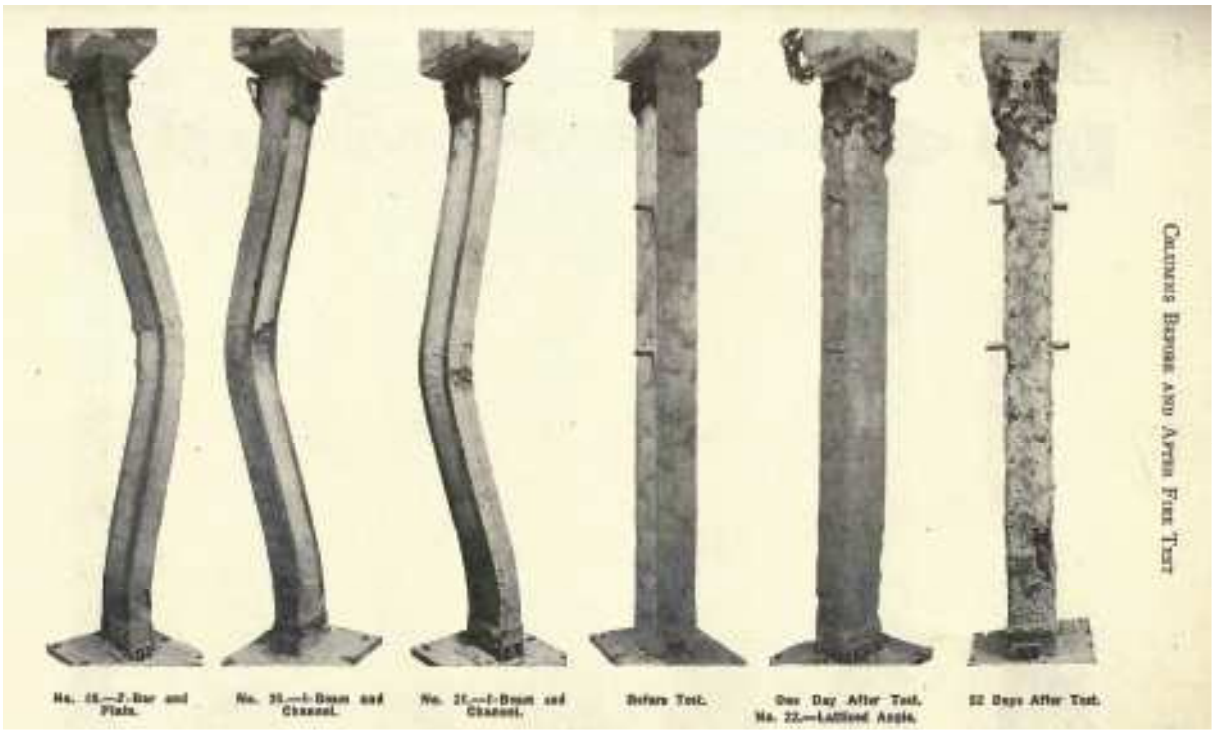

Figure 2.7 - Tests on composite columns, carried out in Chicago, (AFMFIC, 1917-1919).

The purpose of this investigation was to ascertain: the ultimate resistance against fire of protected and unprotected columns as used in the interior of buildings; their resistance against impact and sudden cooling from hose streams when in highly heated condition. This investigation was undertaken to obtain information on which proper requirements for the more general types of columns and protective coverings can be based. Several sets of tests were performed on loaded columns, one of them comprising tests wherein the metal was partly protected by filling the reentrant portions or interior of columns with concrete. Figure 2.7 depicts the columns 2.74 meters tall, partly protected by concrete, under test. Different types of aggregates were used. The results obtained comprised the temperature

variation over the cross section and the length of the columns, the deformation, and the time to failure.

In 1964, Malhotra and Stevens (Malhotra et al., 1964) presented results of fourteen fire resistance tests on encased steel stanchions, submitted to different load ratios, between 0.27 to 0.36. They have analyzed the effects of concrete cover, the concrete type, the load eccentricity on the fire resistance of the column, and also the limited heating on the column residual strength. The results show that the concrete cover has a significant effect on the fire resistance, and the lightweight concrete has higher fire resistance compared to normal gravel concrete which has more spalling. Given the fact that the load level is known to play a very important role in the fire resistance of columns, the validity of the results was not totally proved, once the range of load level adopted was very narrow.

In 1990, Lie and Chabot (Lie et al., 1990) tested five circular hollow steel columns, filled with concrete, and have proposed a mathematical model to predict the temperature distribution within the cross section and also the structural response under fire event. The heat transfer analysis is based on a division of the circular section into annular elements, while gas temperature around the section was considered uniform. The effect of moisture in the concrete was considered, by assuming that when an element within the cross section reaches the temperature of 100ºC or above, all the heating to that element drives out moisture until it is dry. This mathematical model was later applied to composite steel-concrete columns with rectangular cross-section and circular composite columns with fiber-reinforced concrete.

In 1996, Lie and Kodur (Lie et al., 1996) investigated the fire resistance of fiber-reinforced concrete filled hollow sections. They have investigated the influence in the fire resistance of several parameters such as the diameter of the column, the steel profile wall thickness, the axial load ratio, the percentage of steel reinforcement, the concrete cover thickness and the aggregate type. They concluded that the main parameters influencing the fire resistance are the external diameter of the column, the load ratio and the concrete strength. However, all of the columns were subjected to the same axial load, so the effect of the load level on the fire resistance of the columns was not properly evaluated.

In 2002, Han et al. (Han et al., 2002) carried out six fire resistance tests on small-sized concrete filled rectangular hollow section (RHS) columns. The goal was to assess the residual strength after exposure to the ISO 834 fire curve. They have proposed a formula to calculate the column residual strength. The formula takes into account the fire duration, the cross section perimeter and the slenderness ratio, and is used to calculate the column residual

strength index. A similar formula was proposed for concrete-filled circular hollow section (CHS) columns.

In 2003, Han et al. (Han et al., 2003) published the results of eleven fire resistance tests on concrete filled hollow SHS and RHS columns subjected to the ISO 834 fire curve. They tested columns with and without fire protection. The main purpose of the study were to report a series of fire resistance tests on composite columns with square and rectangular sections; to analyze the influence of several parameters such as the fire duration, cross-sectional dimension, slenderness ratio, load eccentricity ratio, strength of steel and concrete on the residual strength index; and to develop formulas for the calculation of the fire resistance and fire protection thickness of this type of columns. They have concluded that because of the infill of concrete, the SHS and RHS columns behaved in a relatively ductile manner, and that the fire protection thickness for these columns can be reduced about 25% to 70% of that for bare steel columns. Formulas for the calculation of fire resistance and fire protection were presented.

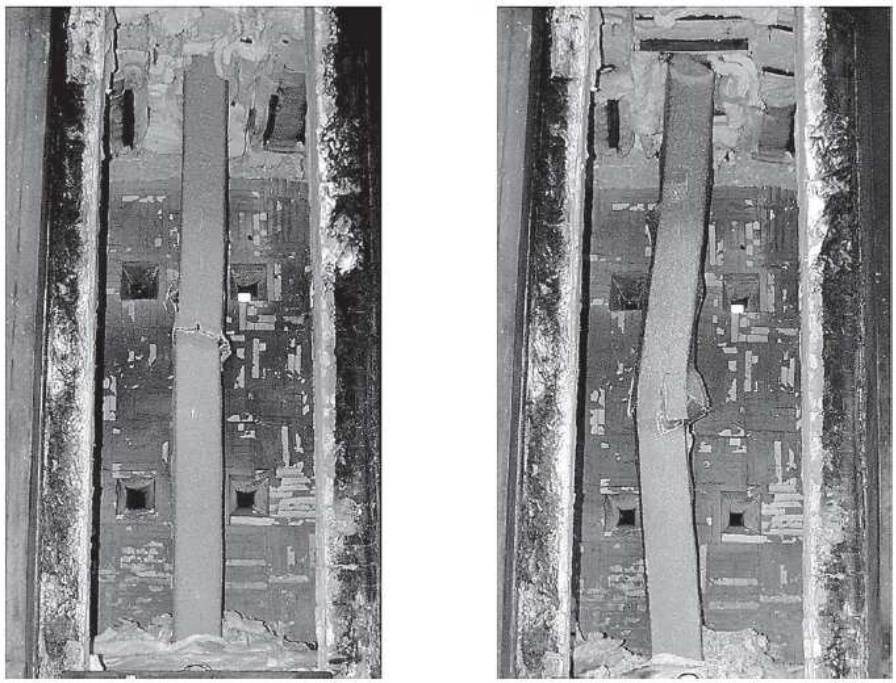

Figure 2.8 – Typical failure mode of the tested RHS columns, of tests performed by Han (Han et al., 2003)

Also in 2003, Wang and Davies (Wang et. al., 2003) performed an experimental study of the fire performance of non-sway loaded concrete-filled tubular steel column assemblies with extended end plate connections. The objective of the study was to investigate the effects of rotational restraint on column bending moments and column effective lengths. Two series of column assemblies have been tested at the University of Manchester. From the results, it was

found that the position of local buckling of the steel tube has direct influence on the effective length of a concrete filled column. The effective length of these columns with a pin end maybe taken as the distance from the largest local buckle of the steel tube to the pin end. The design column bending moment may be taken as the unbalanced beam load acting eccentrically from the column centerline.

In 2005, Han et al. (Han et al., 2005) presented a new series of compression and bending tests, carried out on concrete filled steel tubes after exposure to the ISO 834 standard fire. The main purpose of this work was to assess the post-fire behavior of this type of columns. Four stub columns under axial compression were tested. A previously developed mechanics model that can predict the load-deformation behavior of concrete filled HSS (hollow steel sections) stub columns has been used to predict the test results. Formulas for the calculation of the residual compressive capacity after exposure to fire were presented. They concluded that the concrete filled steel SHS and RHS stub columns behave in a ductile manner, due to the "composite action" of the steel tube and the concrete core. The previously developed mathematical model by Han et al showed good agreement with test results.

In 2006, Han et al. (Han et al., 2006) presented a new series of compression and bending tests carried out on concrete filled steel tubes after exposure to the ISO 834 standard fire [9]. The main purpose of this work was to assess the post-fire behavior of columns and beams. A mechanical model, previously developed by the authors, that can predict the load-deformation behavior of concrete filled hollow stub columns after exposure to the ISO 834 fire has been used to predict the columns test results. The agreement in the results was quite good. They concluded that the concrete filled steel SHS and RHS stub columns behave in a ductile manner in fire due to the "composite action" of the steel tube and the concrete core. The authors previously developed mathematical model showed good agreement with test results.

In 2007, Huang et al. (Huang et al., 2007a, 2007b) published a study about the effects of the axial restraint on the behavior of composite columns subjected to fire. In this research work they have tested four unprotected real-sized axially-restrained encased I-section composite columns. All columns were 3.54m tall and were subjected to an axial load ratio of 0.7. A specific heating curve with two ascending phases was adopted. Different degrees of axial restraint were investigated. They concluded that the axial restraint markedly reduces the column fire resistance since it increases the internal axial force. All columns failed in flexural buckling mode. Also, it was observed that during heating all specimens underwent concrete spalling, which was responsible for a great reduction of the column fire resistance. A comparison with the fire resistance calculated by Eurocode 4 part 1.2 showed that the predictions of that document are very conservative.

All of the mentioned experimental tests reported in these studies were carried out with either pin-ended or built in columns. Real boundary conditions of a column are not pin-ended nor built-in. In fact columns when inserted in a real structure are not only submitted to an axial but also to a rotational restraint. This fact has not been considered in most of the studies carried out up to now. The axial restraint is known to have a detrimental effect on the fire resistance of the columns while the rotational restraint to have a beneficial effect.

2.3.2 Numerical research

In 2002, Breccolotti et al. (Breccolotti et al., 2002) presented a simplified methodology of analysis for evaluating the ultimate bearing capacity of steel and concrete composite columns in fire, taking into account also the second order effects. The main parameters which govern the fire performance of columns were reviewed in order to deduce simplified design tools. They have studied different typologies of composite columns: columns built with steel profiles totally embedded in concrete ("concrete encased profiles"), columns built filling with concrete the space between the flanges of the steel profiles ("partially encased profiles") and columns built filling with concrete hollow steel profiles ("concrete filled profiles"). They have proposed a simplified procedure for the assessment of safety of steel and concrete composite columns under fire. It allows avoiding the task of evaluating the thermal field induced by the fire into the columns at the design duration of exposure. The proposed procedure is based on the definition of a suitable non-dimensional thermal damage law. It can be used to evaluate the Mu-Nu interaction domain at the ultimate limit state at any time during the development of the fire, simply multiplying by it the interaction domain evaluated at "cold" conditions. The thermal damage laws have been calibrated by fitting the results of an extensive parametric analysis carried out considering the most widely used sections of steel profiles and type of composite columns.

In 2006, Wang et al. (Wang et. al., 2006) presented a design concept called the residual area method to calculate the equivalent thickness of concrete for temperature analysis of concrete-encased I-sections in fire. The steel temperature response of concrete-encased I-sections subjected to fire is characterized by three temperature variables. The proposed method makes use of the EC3 provisions to formulate the temperature response of each representative point along the steel profile using a 1D heat transfer model. The results demonstrate that the residual area method is intrinsic to the geometric configurations (cross sections) of concrete-encased I-sections, but independent of heating conditions. The proposed method has been further verified by three series of specimens, and the predictions are compared against the results obtained from finite element analysis.

In 2007 and 2008, Huang et al. (Huang et al., 2007a, 2007b, 2008) presented a numerical study on the fire resistance of embedded I-section composite columns. The objective was to examine the effects of cross-sectional dimension and load level on column fire resistance. Four groups of columns, consisting of square cross-section were used. The columns were subjected to axial compression forces and four-side uniform heating. Four load levels were studied: 0.2, 0.3, 0.4 and 0.5. These load levels were a percentage of the design load capacity at ambient temperature, calculated according to Eurocode 4. They concluded that under high load levels, columns with small cross-sections fail to meet the fire resistance as suggested by EN 1994-1-2 (2005). The authors state very clearly in this work that their study was limited to pin-ended columns, where boundary conditions have been oversimplified. An actual column within a building normally experiences limited axial and rotational restraints at its ends. Some studies have shown that the boundary restraints play a key role in the structural behaviour as well as fire resistance.

In 2010, Ellobody et al. (Ellobody et al., 2010) presented a nonlinear 3-D finite element model for investigating the behavior of concrete encased steel columns at elevated temperatures. The composite columns were pin-ended, axially loaded, having different load ratios during fire. The nonlinear material properties of steel, concrete, longitudinal and transverse reinforcement bars, as well as the effect of concrete confinement at ambient and elevated temperatures were taken into account. They have concluded that the fire resistance of the columns generally increases with the decrease in the column slenderness ratio, as well as the increase in the structural steel ratio. It was also shown that the time-axial displacement relationship is considerably affected by the coarse aggregate. Calculating the fire resistance with EN 1994-1-2 (2005), it was observed that Eurocode is conservative for all studied cases, except for the columns with a load ratio of 0.5 as well as columns having a slenderness ratio of 0.69 and a load ratio of 0.4.

Also in 2010, Espinos et al. (Espinos et al., 2010) presented an advanced model for predicting the fire response of CHS columns. In this work, a nonlinear finite element three-dimensional model was presented and validated in order to study the behaviour of axially loaded of the mentioned type of columns exposed to fire. A realistic sequentially coupled nonlinear thermal-stress analysis was conducted for a series of columns. The model was validated by comparing the simulation results with fire resistance tests. By means of this model, an extensive sensitivity analysis was performed over a wide range of aspects concerning the finite element modeling of the problem. Based on this analysis, several modeling recommendations were presented. The validated numerical model was employed to study and discuss the Eurocode 4 part 1-2 simple calculation model. The numerical model showed good agreement with the tests both quantitative and qualitative. This research proved that Eurocode

4 simple calculation model may lead to unsafe results when working with columns with relative slenderness values over 0.4 and in general for pinned-pinned columns under concentric axial load.

3. FIRE DESIGN OF STEEL AND COMPOSITE STEEL-CONCRETE COLUMNS ACCORDING TO EUROCODES

3.1. Mechanical Actions

3.1.1. Introduction

The analytical determination of the fire resistance of load bearing structural elements as an alternative to testing has always implicit the uncertainty of the thermal action and mechanical loads to consider, in a real fire.
Due to high costs, a full scale fire resistance test is usually limited to one test specimen. For this reason, a great amount of research is performed on single elements and sub-frames.

An analytical determination of the load bearing capacity of the structural element is based on the characteristic value of the material strength. This gives an analytically determined fire resistance which is lower than the corresponding value derived from a standard fire resistance test.

The action of fires on structures of buildings is characterized by scenarios of actions which are not always easy to determine. The EN 1991-1-2(2002) presents methods for their determination.

Regarding mechanical actions, it is commonly agreed that the probability of the combined occurrence of a fire in a building and an extremely high level of mechanical loads is very small. In fact, the load level to be used to check the fire resistance of elements refers to other safety factors than those used for normal design of buildings. The general equation proposed to calculate the relevant effects of actions is:

$$\Sigma g_{GA} \,.\, G_{k,j} + \Psi_{1,1} \,.\, Q_{k,1} + \Sigma \Psi_{2,1} \,.\, Q_{k,i} + \Sigma A_{d(t)} \qquad (3.1)$$

where:
$G_{k,j}$ = characteristic value of the permanent action (“dead load”)
$Q_{k,1}$ = characteristic value of the main variable action
$Q_{k,i}$ = characteristic value of the other variable actions
γ_{GA} = partial safety factor for permanent actions in the accidental situation;
$\Psi_{1,1}$; $\Psi_{2,1}$ = combination factors for buildings according to EN 1991-1-1 (2005)
$A_{d(t)}$ = design value of the accidental action resulting from the fire exposure

This accidental action is represented by:

- the temperature effect on the material properties;

- the indirect thermal actions created either by deformations and expansions caused by the temperature increase in the structural elements, where as a consequence internal forces and moments may be initiated, P-δ effect included, either by thermal gradients in the cross-sections leading to internal stresses.

3.1.2. Verification Methods

According to EN 1992-1-2 (2004), EN 1993-1-2 (2005) and EN 1994-1-2 (2005), three types of design methods can be used to assess the mechanical behaviour of structures under fire conditions:

- Simple calculation method based on predefined tabulated data, applicable only to concrete and composite steel-concrete structures;
- Simple calculation models. This type of design method can be divided into two different groups: the critical temperature method and simple mechanical models developed for structural member analysis.
- Advanced calculation models. These models may be applied to all types of structures, and they are based on finite element or finite difference methods.

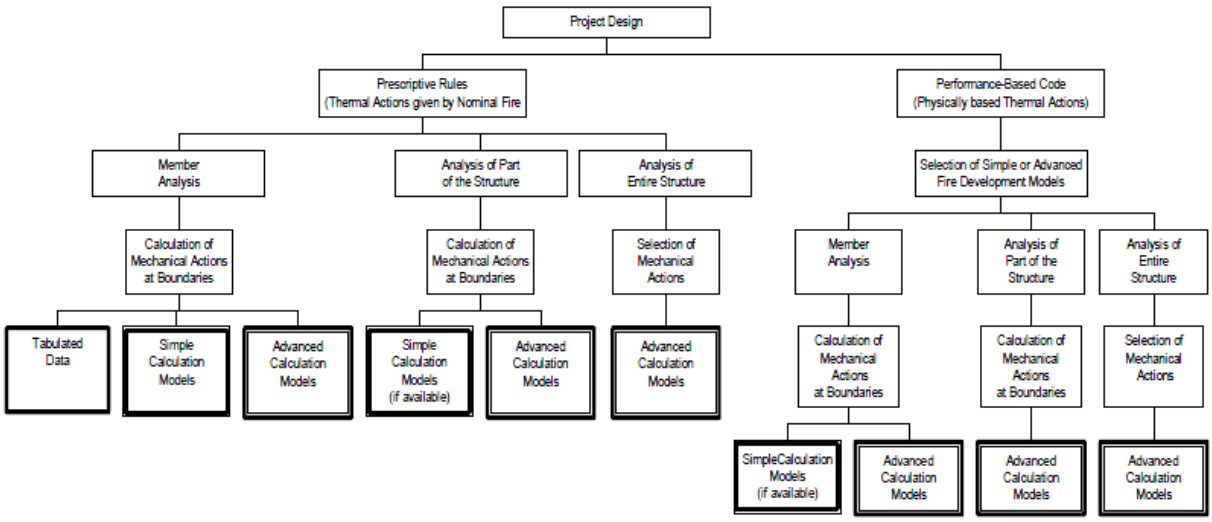

Figure 3.1– Design flowchart, EN 1992-1-2 (2004), EN 1993-1-2 (2005) and EN 1994-1-2 (2005)

The structural analysis for fire situation may be carried out performing a member analysis, an analysis of parts of the structure or a global structural analysis.

3.1.2.1. Resistance Domain

Considering an analysis in the resistance domain, it should be verified that, during the relevant duration of fire exposure *t*:

$E_{fi,d} \leq R_{fi,d,t}$ (3.2)

where:

$E_{fi,d}$ is the design effect of action for fire situation, determined in accordance with EN 1991-1-2 (2002), including the effects of thermal expansion and deformations;

$R_{fi,d,t}$ is the corresponding design resistance in fire situation.

3.1.2.2. Time Domain

Verification of the fire resistance may also be done in the time domain. In this case:

$t_{fi,d} \geq t_{fi,requ}$ (3.3)

where:

$t_{fi,d}$ is the design value of the fire resistance

$t_{fi,requ}$ is the required fire resistance time

3.1.2.3. Temperature Domain

Verification of the fire resistance may also be carried out in the temperature domain. In this case:

$\theta_d \leq \theta_{cr,d}$ (3.4)

where:

θ_d is the design value of the material temperature

$\theta_{cr,d}$ is the design value of the material critical temperature

Except when considering deformation criteria or when stability phenomena have to be taken into account, the critical temperature $\theta_{a,cr}$ of a carbon steel, of the steel grades S235, S275 and S355, at time t for a uniform temperature distribution in a member may be determined for any degree of utilization μ_0 at time t=0 using:

$$\theta_{a,cr} = 39{,}19 \ln\left[\frac{1}{0{,}9674\mu_0^{3{,}833}} - 1\right] + 482 \quad (ºC) \tag{3.5}$$

In this formula, μ_0 should not be taken less than 0,013, and values of $\theta_{a,cr}$ are given in EN 1993-1-2 (1995).

3.1.3. Indirect Actions

Imposed and constrained expansions and deformations caused by temperature changes due to fire exposure result in effects of actions, i.e., forces and moments, which should be considered in the structural analysis.

As indirect actions, the EN 1991-1-2 (2002) considers:

- constrained thermal expansion of the members themselves, i.e., columns in multi-storey frame structures with stiff walls;
- differing thermal expansion within statistically indeterminate members, i.e., continuous floor slabs;
- thermal gradients within cross-sections giving internal stresses;
- thermal expansion of adjacent members, i.e. displacement of a column head due to the expanding floor slab, or expansion of suspended cables;
- thermal expansion of members affecting other members outside the fire compartment.

The indirect fire actions should be determined on the basis of the design values of the thermal and mechanical material properties in function of the temperature, for the relevant fire exposure.

3.2. Thermal actions

3.2.1. Introduction

Traditional methods for determining the fire performance of elements in building construction involve conducting a fire resistance test. For structural elements, these are carried out on beams and columns at accredited fire laboratories. The furnace heating conditions are specified in accordance with the European standard EN 1363-1 (1999). The most common of these for testing components in buildings is referred to as the standard ISO 834 fire curve (EN 1991-1-2 (2002)).

Increasing knowledge on the natural fire behaviour is now beginning to have an impact on the manner in which structural stability is analyzed, being necessary for the full compartment contents to be engulfed by the flames. This condition is called flashover. Flashover occurs when sustained flaming from combustibles reach the ceiling and the temperature of the hot gas layer is between 550ºC and 600ºC. The heat release rate will then increase rapidly until it reaches a maximum value for the enclosure. For simplified design, it may be assumed that when flashover occurs, the rate of heat release instantaneously increases to the maximum

value set by the available air. This is the second of three stages in a natural fire, the first and third stage being the growth and decay phases respectively.

Growth rate of a fire in the pre-flashover stage can be determined by considering the item first ignited, the flame spread, the potential for fire spread from item to item, the potential for fire spread from ceiling and the effect of suppression systems. When flashover occurs, the behaviour of a fire in a compartment depends on a number of factors, such as the fire load density and the ventilation. Temperature distribution in compartment fires can be analyzed using zone models. Where it is assumed that the whole compartment is burning at the same time, and attains the same temperature throughout, this is referred to as a single zone model. Two zone models exist in which the height of the compartment is separated into two gaseous layers each with their own temperature, such as CFAST, OZONE and ARGOS.

In Eurocode 1 Part 1.2 (2002) single zone post flashover fires can be described using parametric expressions that describe the entire heating and cooling cycle. These consider the fire load, ventilation characteristics, compartment geometry, and thermal properties of the surrounding walls floor and ceiling.

Computational fluid dynamics (CFD) may be used to analyse fires in which there are no boundaries to the gaseous state. This type of analysis is widely adopted in very large compartment or enclosures.

Concerning thermal actions, a distinction is made in EN 1991-1-2 (2002), between nominal fires and parametric fires. They take into account the main parameters which influence the growth and development of fires. In this respect, the temperature-time curve and subsequently the heat flux vary when the size of the building or the amount or kind of fire load varies.

With respect to the thermal actions, they are defined in terms of a heat flux density incident on the surface of the element. These actions are composed of two terms one due to radiation and another due to convection.

For the characterization of thermal actions the gas temperature in the vicinity of the element exposed to fire should be determined. This temperature can be calculated from nominal fire curves or by models of natural fires. Nominal fire curves contained in EN 1991-1-2(2002) are the standard fire curve, the external fire curve and the hydrocarbon fire curve. With regard to natural fire models, they are divided into simplified calculation models (parametric fire curves

and localized fire models) and advanced calculation models (one zone models; two-zone models and computational fluid dynamics models (CFD)).

To be able to evaluate the heat release during a fire in a given space, it is necessary to account for the existing fire load, i.e. a study of the products that are likely to feed the combustion. Once the fire load known, one can predict how it will evolve the fire particularly in what concerns the lifting of the gas temperature.

3.2.2. Thermal Actions

According to EN1991-1-2 (2002), the thermal actions are defined in terms of density of heat that focuses on the border of the element, containing two parts, one due to convection and another due to radiation. So the design value of the density of heat flow per unit area is given by:

$$\dot{h}_{net,d} = \dot{h}_{net,c} + \dot{h}_{net,r} \quad [W/m^2] \quad (3.6)$$

The net convective heat flux component is determined by the expression:

$$\dot{h}_{net,c} = \alpha_c \cdot (\theta_g - \theta_m) \quad [W/m2] \quad (3.7)$$

where

α_c – is the coefficient of heat transfer by convection [W/m^{2}K];

θ_g – is the gas temperature in the vicinity of the fire exposed member [°C];

θ_m – is the surface temperature of the member [°C].

In the unexposed faces of separating members, the net heat flux is determined using equation (3.6), α_c = 4 W/m^{2}K. This coefficient should be taken α_c = 9 W/m^{2}K when considering it contains the effect of heat transfer by radiation.
The net radiative heat flux component per unit surface area is calculated by:

$$\dot{h}_{net,r} = \Phi \cdot \varepsilon_f \cdot \varepsilon_m \cdot \sigma \cdot \left[(\theta_r + 273)^4 - (\theta_m + 273)^4 \right] \quad [W/m^2] \quad (3.8)$$

where;

Φ – is the configuration factor;
ε_m – is the surface emissivity of the member;
ε_f – is the emissivity of the fire;
σ – is the Stephan Boltzmann constant (=5.67x10^{-8} W/m^{2}K^4);
θ_r – is the effective radiation temperature of the fire environment [°C];
θ_m – is the surface temperature of the member [°C].

The values of the emissivity of the element and the fire must be chosen by the designer as the case, and may be taken in ordinary situations, $\varepsilon_m = 0.7$ for steel, $\varepsilon_m = 0.8$ for stainless steel and $\varepsilon_f = 1.0$. Normally, the fire parts of the Eurocodes give the values of the emissivity for the different materials.

The configuration factor (Φ) is a geometric parameter that takes into account the size and relative position between the emission source and the sensing element. In making $\Phi = 1$ is considered that all the energy that is released in the form of radiation covers the exposed element, which is not a very realistic situation. For the radiation temperature in the vicinity of the element, the temperature of the gas surrounding it can be taken.

As a fire progresses and the fire load is being consumed, the density of heat flow that addresses the various elements will vary. Except for the temperatures and the gases in the compartment, all other parameters can be considered constant.

3.2.3. Nominal Fire Curves

The evolution of temperatures inside the compartment can be determined from the so-called nominal fire curves. “Nominal fires” are conventional fires which can be expressed by a simple formula and which are assumed to be identical whatever is the size or the design of the building. Nominal fires are mainly the standard fire ISO 834, the hydrocarbon fire and the external fire (used only for external walls). They have to be used in order to prove that an element has the required level of fire resistance to fulfil national or other requirements expressed in terms of fire rating related to one of these nominal fires.

- ***Standard temperature-time curve***

The standard fire curve is the best known and most widely used method of estimating temperatures in compartment fires. It assumes that the temperature in a fire compartment is uniform and that it increases indefinitely according to a logarithmic relationship with time. The standard fire curve has been incorporated into a great number of design standards

worldwide. In EN 1991-1-2 (2002), the gas temperature θ in ºC, at time t in minutes, is given by expression 3.9.
This form of temperature-time relationship was originally derived from measurements of tests taken early in the 20th century, and has been shown to have only a very limited similarity to the temperatures in real compartment fires. This curve is suitable for cellulosic materials.

$$\theta_g = 20 + 345 \cdot \log_{10}(8 \cdot t + 1) \quad [°C] \quad (3.9)$$

where

θ_g – is the gas temperature in the fire compartment [°C];

t – is the time [min].

The standard fire curve ISO 834, is used in the experimental furnace tests in order to determine the fire resistance of structural elements. Although with limited physical reality, the merit of using this curve, was and still is, to standardize the thermal processes used in the furnace tests, allowing the comparison of experimental results of fire resistance achieved in laboratories of various countries. When using this curve to determine the evolution of temperatures within the compartment, should be used for the coefficient of heat transfer by convection the value α_c = 25 W/m^{2}K in calculating the density of heat flow.

- ***External fire curve***

This curve is to be used for the outside surface of walls which are exposed to fire from different parts of the façade.

$$\theta_g = 660 \cdot (1 - 0{,}687 \cdot e^{-0{,}32 \cdot t} - 0{,}313 \cdot e^{-3{,}8 \cdot t}) + 20 \quad [°C] \quad (3.10)$$

where

θ_g – is the gas temperature near the member [°C];

t – is the time [min].

This curve is applied when the elements are not in direct contact with fire, and temperature for the same instant of time less than that determined for the standard fire curve.
Also, in this case, for the coefficient of heat transfer by convection must be taken α_c = 25 W/m^{2}K.

- ***Hydrocarbon curve***

Although the standard curve has been used for many years, it soon became apparent that the burning rates for certain materials such as petrol, gas and chemicals were well in excess of the rate at which for instance, timber would burn. Therefore, there was a need for an alternative exposure for the purpose of carrying out tests on structures and materials used within the petrochemical industry, and thus the hydrocarbon curve was developed. This curve is applicable where small petroleum fires might occur, i.e., car fuel, tanks, petrol or oil tankers, certain chemical tankers, etc.

$$\theta_g = 1080 \cdot (1 - 0{,}325 \cdot e^{-0{,}167 \cdot t} - 0{,}675 \cdot e^{-2{,}5 \cdot t}) + 20 \quad [°C] \quad (3.11)$$

where

θ_g – is the gas temperature in the fire compartment [°C];

t – is the time [min].

This curve is more severe than other previously presented as evidenced in Figure 3.2. In this case, for the coefficient of heat transfer by convection must be taken the value α_c = 50 W/m^{2}K.

- ***RABT ZTV curve***

The RABT curve was developed in Germany. In this curve, the temperature rise is very rapid up to 1200ºC, within 5 minutes. The duration of the 1200ºC exposure is shorter than other curves with the temperature drop off starting to occur at 30 minutes for car fires. The failure criteria for specimens exposed to the RABT-ZTV time/temperature curve is that the temperature of the reinforcement should not exceed 300ºC. There is no requirement for a maximum interface temperature. This curve is applicable to fires in tunnels.

- ***RWS (Rijkswaterstaat) curve***

The RWS curve was developed by the Rijkswaterstaat, Ministry of Transport in Netherlands. This curve is based on the assumption that in a worst case scenario, a 50m^{3}fuel, oil or petrol tanker fire with a fire load of 300MW could occur, lasting up to 120 minutes. The RWS curve simulates the initial rapid growth of a fire using a petroleum tanker as the source, and the gradual drop in temperatures to be expected as the fuel load is burnt off. The failure criteria for specimens exposed to RWS time/temperature curve is that the temperature of the interface between the concrete and the fire protective lining should not exceed 380ºC and the temperature on the reinforcement should not exceed 250ºC. This curve is also applicable to tunnels.

The nominal temperature-time curves here described are depicted in the following graph.

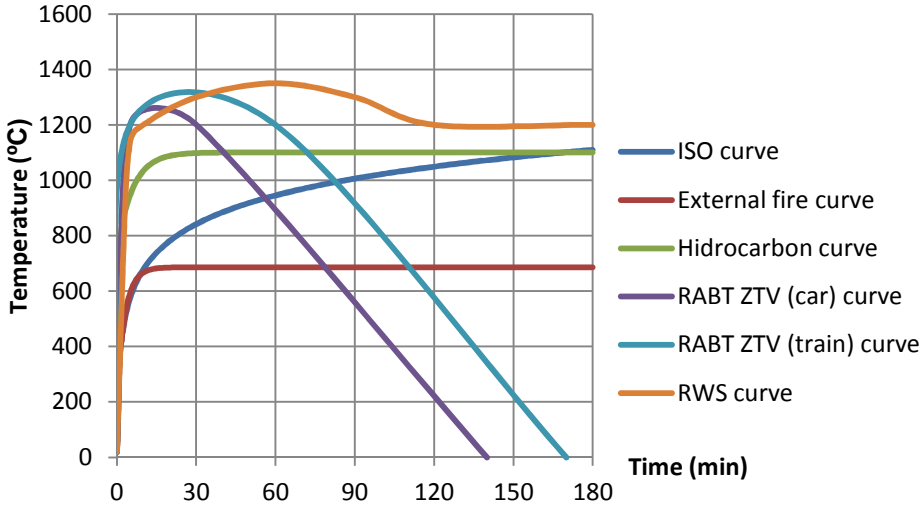

Figure 3.2 – Nominal temperature-time curves

3.2.4. Natural Fire Models

3.2.4.1. Simplified Fire Models

The simple fire models are based on specific physical parameters that, in spite of obtaining satisfactory results, have some limitations in its application. The temperature is determined from a compartment fire model or models of localized fire, which depend among other parameters, of the fire load and characteristics of the compartment on fire. Assuming a uniform distribution of temperature in the compartment, a model of fire compartment should be used. If we assume a non-uniform distribution of temperatures, a localized fire model should be used.

The value of fire load can be calculated accurately, taking into account the distribution of combustible material in the floor surface of the compartment and also the variation with time of the quantity of material. However the EN 1991-1-2 (2002) presents a method for determining its approximate value. The design value of the fire load density is given by:

$$q_{f,d} = q_{f,k} \cdot m \cdot \delta_{q1} \cdot \delta_{q2} \cdot \delta_n \qquad [\text{MJ/m}^2] \qquad (3.12)$$

where

m – is the combustion factor;
δ_{q1} – is a factor taking into account the fire activation risk due to the size of the compartment;
δ_{q2} – is a factor taking into account the fire activation risk due to the type of occupancy;
$\delta_n = \prod_{i=1}^{10} \delta_{ni}$ – is a factor taking into account the different active fire fighting measures (sprinkler, smoke detection, automatic alarm transmission, firemen, …).
$q_{f,k}$ – is the characteristic fire load density per unit floor area [MJ/m^2].

When using the simplified fire methods, for the coefficient of heat transfer by convection should be taken the value α_c = 35 W/m^{2}K.

3.2.4.1.1. Compartment Fires

In compartment fire models, the gas temperature depends among other parameters, of the density of fire load and ventilation conditions. In EN 1991-1-2 (2002) two methods are presented, the parametric fire curves for inner elements and a method for the evaluation ofemperatures in the exterior elements surrounding the fire compartment. A method for calculating the thermal actions on external elements to the compartment fire is proposed. Due to the current features of the construction methods, this method is rarely used.

The heat flow through radiation incident on any external element should encompass the flow of radiation due to components which are inside the combustion chamber and emitting energy in the form of radiation through the openings (windows) and a portion due to radiation emitted by the flames coming out by the openings.

The method allows determining:

- the maximum temperature in the fire compartment;
- the size and flame temperature in the openings;
- parameters of radiation and convection.

This method considers steady state conditions for various parameters and is valid only for fire loads $q_{f,d}$ in excess of 200 MJ/m^2.

- ***Parametric Fires***

"Parametric fires" is a general term used to cover fire evolution more in line with real fires expected to occur in buildings. The parametric curves are distinguished by the cooling phase.

These curves are intended to translate more appropriately the real fires in view of the main parameters that influence the extent and development of the fires. These curves depend on certain parameters such as:

- the fire load density (the higher the fire load, the longer the fire duration - this issue of density may arise not only in terms of duration but also intensity of fire);
- the ventilation conditions, mainly dependent on the geometry, size and distribution of openings in the compartment (large ventilation openings lead to faster fires but also more severe);
- the properties of the walls surrounding the fire compartment (here a balance must be done taking into account the heat stored and transmitted through these walls - walls that absorb energy limit the temperature of the fire).

Parametric fire curves are valid for fire compartments up to 500 m^2 of floor area, with no openings in the roof, for a maximum depth-height of the compartment of 4m based on the assumption that the fire load of the compartment is completely burnt out.
The parametric curves have a heating phase followed by a cooling phase. The heating phase is given by:

$$\theta_g = 20 + 1325 \cdot (1 - 0{,}324 \cdot e^{-0{,}2 \cdot t^*} - 0{,}204 \cdot e^{-1{,}7 \cdot t^*} - 0{,}472 \cdot e^{-19 \cdot t^*}) \quad [°C] \qquad (3.13)$$

where:

θ_g – is the gas temperature in the fire compartment[°C];

t^* $= t \cdot \Gamma$ [h];

t – time [h];

Γ $= \dfrac{(O/b)^2}{(0{,}04/1160)^2}$;

b $= \sqrt{\rho \cdot c \cdot \lambda}$, factor b [$J/m^2s^{1/2}K$] – with the following limits: $100 \le b \le 2200$;

ρ – density of boundary of enclosure [kg/m^3];

c – specific heat of boundary of enclosure [J/kg K];

λ – thermal conductivity of boundary of enclosure [W/mK];

O $= \dfrac{A_v \cdot \sqrt{h_{eq}}}{A_t}$, opening factor [$m^{1/2}$];

A_v – total area of vertical openings on all walls [m^2];

h_{eq} – weighted average of window heights on all walls [m];

A_t – total area of enclosure (walls, ceiling and floor, including openings[m^2].

in case of $\Gamma = 1$ equation (3.13) approximates the standard temperature-time curve ISO 834. The maximum temperature $\theta_{\max}$ in the heating phase happens for $t^* = t^*_{\max}$

For the heating curve (3.13) approaches the curve of standard fire ISO 834. The maximum temperature in the heating phase occurs for

$$t^*_{max} = t_{max} \cdot \Gamma \quad [h] \quad (3.14)$$

$$t_{max} = max\left[\left(\frac{0{,}2 \times 10^{-3} \cdot q_{t,d}}{O}\right); t_{lim}\right] \quad [h] \quad (3.15)$$

where

$q_{t,d}$ – Is the design value of the fire load density related to the total surface area A_f of the enclosure whereby $q_{t,d} = q_{f,d} \cdot \frac{A_f}{A_t}$ [MJ/m^2],: the following limits should be observed $50 \le q_{t,d} \le 1000$ MJ/m^2;

$q_{f,d}$ – is the design value of the fire load density related to the surface area A_f of the floor [MJ/m^2];

t_{lim} – time dependent on the speed of fire spreading (slow - 25min, medium - 20min or fast - 15min), depending on the occupation of the fire compartment [h];

The time t_{max} corresponding to the maximum temperature is given by t_{lim} the case of fires controlled by the fire load. In other cases t_{max} is given by $(0{,}2 \times 10^{-3} \cdot q_{t,d} / O)$ and the fire is said to be controlled by ventilation.

When $t_{max} = t_{lim}$, $t*$ must be replaced by:

$$t^* = t \cdot \Gamma_{lim} \quad [h] \quad (3.16)$$

with

$$\Gamma_{lim} = \frac{(O_{lim} / b)^2}{(0{,}04 / 1160)^2} \quad (3.17)$$

$$O_{lim} = \frac{0{,}1 \times 10^{-3} \cdot q_{t,d}}{t_{lim}} \tag{3.18}$$

if ($O > 0{,}04$ and $q_{t,d} < 75$ and $b > 1160$), Γ_{lim} has to be multiplied by k :

$$k = 1 + \left(\frac{O - 0{,}04}{0{,}04}\right) \cdot \left(\frac{q_{t,d} - 75}{75}\right) \cdot \left(\frac{1160 - b}{1160}\right) \tag{3.19}$$

In the cooling phase, the time-temperature curves are given by:

$$\theta_g = \theta_{max} - 625 \cdot (t^* - t^*_{max} \cdot x) \text{ if } t^*_{max} \le 0{,}5 \quad [°C] \tag{3.20}$$

$$\theta_g = \theta_{max} - 250 \cdot (3 - t^*_{max} \cdot x) \cdot (t^* - t^*_{max} \cdot x) \text{ if } 0{,}5 < t^*_{max} \le 2 \quad [°C] \tag{3.21}$$

$$\theta_g = \theta_{max} - 250 \cdot (t^* - t^*_{max} \cdot x) \text{ if } t^*_{max} \ge 2 \quad [°C] \tag{3.22}$$

where

$$x = 1 \quad \text{if } t_{max} > t_{lim}$$

$$x = \frac{t_{lim} \cdot \Gamma}{t^*_{max}} \quad \text{if } t_{max} = t_{lim}$$

with

$$t^*_{max} = \frac{0{,}2 \times 10^{-3} \cdot q_{t,d}}{O} \cdot \Gamma \tag{3.23}$$

3.2.4.1.2. Localized Fires

When it is unlikely the occurrence of flashover in the fire compartment the thermal actions should be considered located on the elements. The EN 1991-1-2 (2002) presents a method to calculate thermal actions on localized fires. There are some differences regarding the relative height of the flame to the ceiling, taking into account if the flame does not clash or ceiling of the compartment.

The heat flux on localized fires that focuses on the structural elements must be calculated with expression (3.6) taking into account the factor of general configuration.

The expressions given below are only valid for the following conditions:
• the diameter of the fire is limited to $D \le 10$ m;
• the rate of heat loss in the fire is limited to $Q \le 50$ MW.

The height L_f of the flame of a localized fire (see Figure 3.3) is given by:

$$L_f = -1.02 \times D + 0.0148 \times Q^{2/5} \quad \text{[m]} \quad (3.24)$$

When the flame does not reach the ceiling of the compartment ($L_f < h$) or in case of fire in open air, the temperature $\theta_{(z)}$ of the plume along the vertical flame axis can be calculated by:

$$\theta_{(z)} = 20 + 0{,}25 \cdot Q_c^{2/3} \cdot (z - z_0)^{-5/3} \quad \leq 900 \quad \text{[°C]} \quad (3.25)$$

where

D – is the diameter of the fire [m];
Q – Is the rate of heat release of the fire [W];
Q_c – is the convective part of the rate of heat release[W], $Q_c = 0{,}8 \cdot Q$ by default;
z – is the height along the flame axis [m];
H – is the distance between the fire source and the ceiling [m].

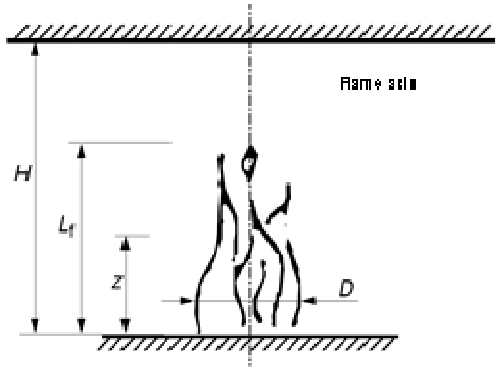

Figure 3.3 – Localized fire – Flame not reaching the ceiling.

The virtual origin z_0 of the axis is given by:

$$z_0 = -1{,}02 \cdot D + 0{,}00524 \cdot Q^{2/5} \quad \text{[m]} \quad (3.26)$$

When the flame is impacting the ceiling ($L_f \geq H$; see Figure 3.4) the heat flux $\dot{h}$ [W/m^2] received by the fire exposed unit surface area at the level of the ceiling is given by:

$$\dot{h} = 100000 \quad \text{if } y \leq 0{,}30 \quad (3.27)$$

$$\dot{h} = 136300 - 121000 \cdot y \quad \text{if } 0{,}30 < y \le 1{,}0$$

$$\dot{h} = 15000 \cdot y^{-3{,}7} \quad \text{if } y > 1{,}0$$

where: $y = \dfrac{r + H + z'}{L_h + H + z'}$, non-dimensional parameter

r – is the horizontal distance between the vertical axis of the fire and the point along the ceiling where the thermal flux is calculated [m];

H – Is the distance between the fire source and the ceiling [m].

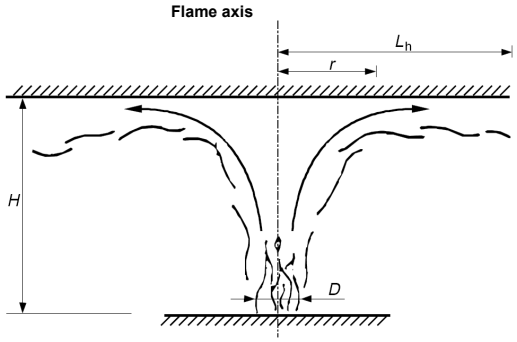

Figure 3.4 – Localised fire – Flame reaching the ceiling.

The horizontal flame length L_h is given by the following expression:

$$L_h = (2{,}9 \cdot H \cdot (Q_H^*)^{0{,}33}) - H \quad \text{[m]} \qquad (3.28)$$

The non-dimensional rate of heat release Q_H^* is given by:

$$Q_H^* = \frac{Q}{1{,}11 \times 10^6 \cdot H^{2{,}5}} \qquad (3.29)$$

The vertical position of the virtual heat source z' [m] is given by:

$$z' = 2{,}4 \cdot D \cdot (Q_D^{*2/5} - Q_D^{*2/3}) \quad \text{when } Q_D^* < 1{,}0$$

$$z' = 2{,}4 \cdot D \cdot (1{,}0 - Q_D^{*2/5}) \quad \text{when } Q_D^* \ge 1{,}0 \qquad (3.30)$$

where:

$$Q_D^* = \frac{Q}{1{,}11 \times 10^6 \cdot D^{2{,}5}} \qquad (3.31)$$

The net radiative heat flux per unit surface area "$\dot{h}_{net}$" received by the ceiling is given by:

$$\dot{h}_{net} = \dot{h} - \alpha_c \cdot (\theta_m - 20) - \Phi \cdot \varepsilon_m \cdot \varepsilon_f \cdot \sigma \cdot [(\theta_m + 273)^4 - 293^4] \quad [\mathrm{W/m^2}] \qquad (3.32)$$

where the various coefficients depend on expressions (3.7), (3.8) and (3.27)

In case of separate localized fires, the expression (3.27) can be used to determine the different individual heat fluxes $\dot{h}_1$, $\dot{h}_2$, ... received by the fire exposed unit surface area at the level of the ceiling. The total heat flow can be calculated by:

$$\dot{h}_{tot} = \dot{h}_1 + \dot{h}_2 + \ldots \qquad \leq 100000 \qquad [\mathrm{W/m^2}] \qquad (3.33)$$

3.2.4.2. Advanced Fire Models

The advanced calculation methods for thermal actions to which the elements are subject to the development of a fire, represent in a more accurately way the associated phenomena. However, the application of this method shows the difficulty for most of the designers of structures, and it is necessary to have some knowledge on energy and mass transfer. The calculation methods available normally include an iterative procedure, because small variations of the parameters produce variations in all others. It is important in this process, the application of conservation laws of mass and energy, among others.
To calculate the fire load density, as well as the rate of heat release, the principles are used as previously reported.

According to EN 1991-1-2 (2002) one of the following models should be used:

- One-zone models - it is assumed a uniform distribution of temperature in the compartment, varying only with time.
- Two-zone models- it is assumed that an upper layer thickness will vary with time and temperature, as well as a lower layer with uniform lower temperature.
- Computer models of fluid dynamics (CFD) - give the evolution of temperature in the compartment, depending on the time and space.

3.2.4.2.1. One-Zone Models

A one-zone model can be applied to post-flashover conditions. The temperature, density, internal energy and gas pressure in the compartment are assumed homogeneous. The temperature can be calculated by considering:

• the resolution of equations of mass and energy conservation;
  • the exchange of mass between the internal gas, the external gas (through openings) and the fire pyrolysis rate;
  • the energy exchange between the fire, the internal gas, the walls and openings.

The ideal gas law considered is:

$$P_{int} = \rho_g \cdot R \cdot T_g \qquad [N/m^2] \qquad (3.34)$$

The mass balance of the compartment gases is written as:

$$\frac{dm}{dt} = \dot{m}_{in} - \dot{m}_{out} + \dot{m}_{fi} \qquad [kg/s] \qquad (3.35)$$

where:

$\frac{dm}{m}$ – is the rate of change of gas mass in the fire compartment;

$\dot{m}_{out}$ – is the rate of gas mass going out through the openings;

$\dot{m}_{in}$ – is the rate of gas mass coming in through the openings;

$\dot{m}_{fi}$ – is the rate of pyrolysis products generated

The rate of change of gas mass and the rate of pyrolysis may be neglected, thus

$$\dot{m}_{in} = \dot{m}_{out} \qquad [kg/s] \qquad (3.36)$$

These mass flows may be calculated based on static pressure due to density differences between air at ambient and high temperatures, respectively.

The energy balance of the gases in the fire compartment may be taken as:

$$\frac{dE_g}{dt} = Q - Q_{out} + Q_{in} - Q_{wall} - Q_{rad} \qquad [W] \qquad (3.37)$$

where:

E_g – is the internal energy of gas [J];

Q – is the rate of heat release of the fire [W];

$Q_{out} = \dot{m}_{out} \cdot c \cdot T_f$

$Q_{in} = \dot{m}_{in} \cdot c \cdot T_{amb}$

$Q_{wall} = (A_t - A_{h,v}) \cdot \dot{h}_{net}$, is the loss of energy to the enclosure surfaces

$Q_{rad} = A_{h,v} \cdot \sigma \cdot T_f^4$, is the loss of energy by radiation through the openings

with:

c – is the specific heat [J/kg K];

$\dot{h}_{net}$ – is given by expression (3.6);

$\dot{m}$ – is the gas mass rate [kg/s];

T – is the temperature [K].

3.2.4.2.2. Two-Zone Models

The two-zone models are based on the assumption of accumulation of combustion products in a layer below the ceiling with a horizontal interface. These models take advantage of the laws of physical sciences, supplemented by some empirical knowledge, and have the core idea of the decomposition spaces, for the purpose of simulating the development and fire spread in two distinct zones: one, higher, corresponding to the part where the smoke and toxic gases accumulate, the other below, where the temperature is lower. Its main limitations are related to the failure to consider three-dimensional effects, and non-consideration of local values.

In these models, in systems of natural ventilation, the gas flow rates and speed of the flows are calculated assuming that the pressure at the site only varies with the height from the ground. Under forced ventilation, when the extraction and insufflation flow is known or it is articulated with the model of another fire, in which the modelling of the vents is performed. For the chemical reactions, these models rely on the exploration of balance, usually assuming that these reactions are instantaneous and complete and that the mixture in the presence of the elements is very fast, using more or less empirical correlations. For the pressure fields that are established during a fire, their evaluation is based on the law of fluid statics to represent a vertical field of pressures in the considered areas.

The conservation of momentum is treated based on the Navier-Stokes equations, although they are not explicitly introduced in these models, being used in general, Bernoulli's law, which is a simplified form of those equations for the calculation of the flow through the openings, while the determination of the flow of the flame semi-empirical expressions are used. Regarding the effect of turbulence seen by the flow of fresh air, it is represented by empirical coefficients. Finally, in these models is considered that the media obey the ideal gas law, and whether or not containing solid or liquid particles, thermal equilibrium is considered. At the top layer, uniform characteristics of the gas can be assumed. The variations of mass, energy and chemical properties of substances can be calculated between these different areas. In a given fire compartment with a fire load evenly distributed, the two-zone model can be developed as a fire zone in the following situations:

- if the gas temperature obtained in the upper layer is greater than 500°C;

- if the top layer grow up to 80% of the height of the compartment.

3.2.4.2.3. Computational Fluid Dynamic Models (CFD)

The field models are based on equations that describe the phenomena of combustion and heat transfer, in which the initial conditions are needed in advance. In these models, the compartment is divided into a finite number of elements, to each one the energy balance is made, obtaining as a result, in particular, the values of temperature, velocity and pressure. These equations represent the mathematical statements of the conservation laws of physics:

- The mass of a fluid is conserved;
- The rate of change of momentum equals the sum of the forces on a fluid particle (Newton´s second Law);
- The rate of change of energy is equal to the sum of the rate of heat increase and the rate of work done on a fluid particle (first law of thermodynamics)

For any of the presented models, the coefficient of heat transfer by convection should be $\alpha_c = 35$ [W/m^2], if no more precise information is available.

3.2.5. Calculation of temperatures in steel elements (EN 1993-1-2)

Simplified methods for a calculation of the temperature of fire exposed steel structural elements are, as a rule, based on the assumption of a uniformly distributed temperature over the cross section and along the structure at each time of fire exposure. In certain types of steel structures a considerable temperature variation arises over the cross section as well as in the longitudinal direction during a fire resistance test. A simplified calculation method, which neglects this influence, gives a further underestimation of the fire resistance in relation to the corresponding result obtained in a fire resistance test.
Thus, alternative methods of correction are desirable for obtaining better agreement between the analytical and experimental approaches. One of these methods is developed further to a design basis that can be applied easily in practice.

The heating rate of a steel element has great effect on its fire resistance. A massive section will heat up slowly (and thus normally have a higher fire resistance) than a slender section. The influence of the massiveness of the profile is considered in EN 1993-1-2 (2005) by the "Section Factor" (Figure 3.5).

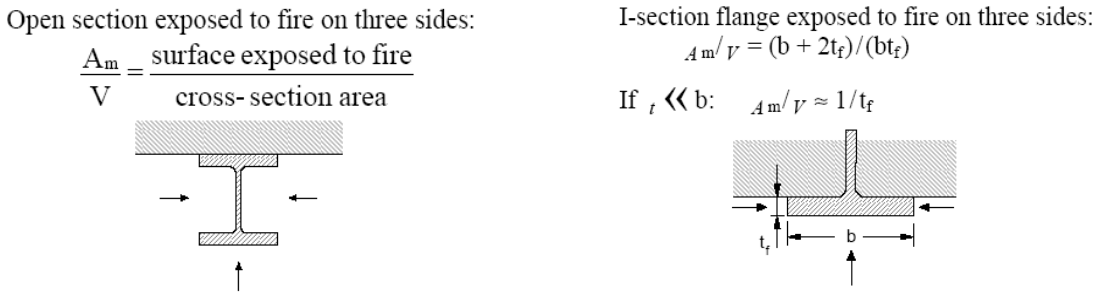

Figure 3.5 – Section factors according to EN 1993-1-2 (2005)

$$\text{Section factor} = \frac{A_m}{V} \tag{3.38}$$

where:

A_m is the lateral surface area of the steel profile exposed to fire (m^2)

V is the volume of the element exposed to fire (m).

For an equivalent uniform temperature distribution in the cross-section, the increase of temperature in an unprotected steel member during a time interval is determined by the following expression, from EN1993-1-2 (2005):

$$\Delta\theta_{a,t} = k_{sh} \cdot \frac{A_m / V}{c_a \cdot \rho_a} \cdot h_{net,d} \cdot \Delta t \tag{3.39}$$

where:

K_{sh} - is the correction factor for the shadow effect

A_m/V - is the section factor for unprotected steel members

c_a - is the specific heat of steel (J/Kg.K)

$h_{net,d}$ - is the design value of the net heat flux (W/m^2)

Δt - is the time interval (seconds)

Δ_a - is the unit mass of steel (Kg/m^3)

For I-sections under nominal fire actions the correction factor for the shadow effect may be determined from:

$$K_{sh} = 0.9 \left[\frac{A_m}{V} \right]_b \Big/ \left[\frac{A_m}{V} \right] \tag{3.40}$$

where $\left[\frac{A_m}{V} \right]_b$ is box value of the section factor.

In all other cases:

$$K_{sh} = \left[\frac{A_m}{V}\right]_b \Big/ \left[\frac{A_m}{V}\right] \tag{3.41}$$

For cross sections with a convex shape fully engulfed in fire, the shadow effect does not play role and consequently the correction factor k_{sh} may be considered equal to unity. The shadow effect is due to the radiation interchange between surface areas during heat transfer. The quantification of the shadow effect is possible by using a configuration factor Φ. This factor is the ratio between the radiative heat that reaches a given receiving surface and the total radiative heat leaving another surface. Its value depends on the size of the radiating surface, on the distance from the radiating surface to the receiving surface and on their relative orientation. Methods for calculating the configuration factor are given in EN 1993-1-2 (2005).

3.3. Material properties

3.3.1. Thermal Properties

In the following sections, some thermal properties of steel and concrete are presented.

3.3.1.1. Steel

The thermal elongation $\Delta l/l$, and the specific heat of steel c_a, are defined in EN 1993-1-2 (2005), according to the following graphs.

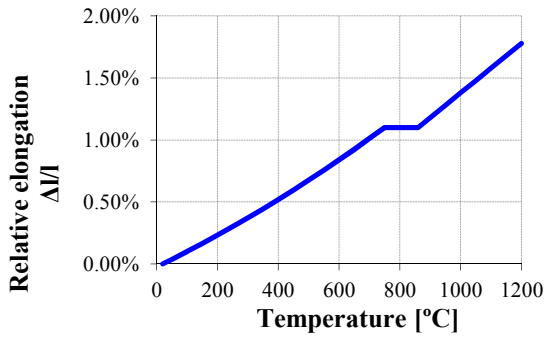

Figure 3.6 – Relative elongation of carbon steel function of the temperature, EN 1993-1-2 (2005)

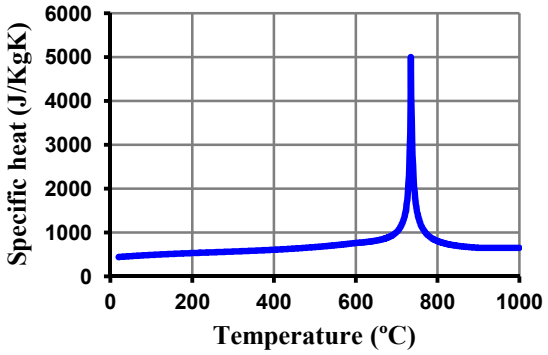

Figure 3.7 – Specific heat of carbon steel as a function of the temperature, EN 1993-1-2 (2005)

The thermal conductivity of carbon steel λ_a, as a function of temperature is illustrated in Figure 3.8.

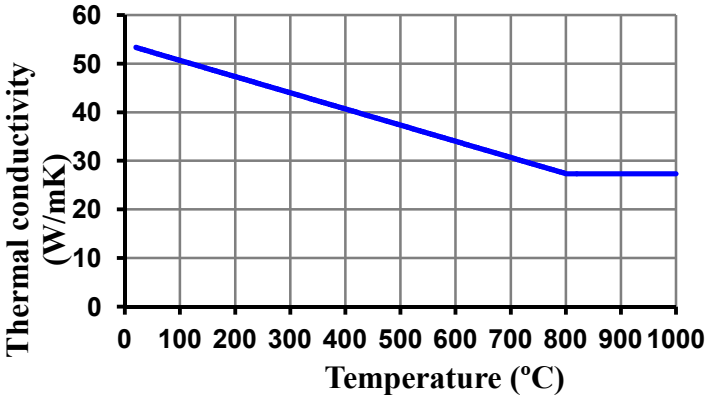

Figure 3.8 – Thermal conductivity of carbon steel as function of temperature, EN 1993-1-2 (2005)

3.3.1.2. Concrete

Such as steel, when subjected to uniform temperature, concrete expands or contracts, in function of the thermal differential which is subject. According to EN 1992-1-2 (2004), concrete thermal elongation varies with the temperature, depending on the type of aggregates in its composition.

This parameter has a particular interest in the study of elements with the thermal constraint influencing the values of the restraining forces that are generated during heating.

Where the moisture content is not considered explicitly in the calculation method, the function may be modelled by a constant value.

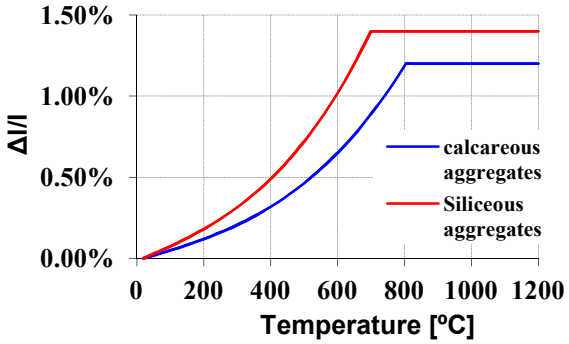

Figure 3.9 – Thermal elongation of calcareous and siliceous aggregates as a function of temperature, EN 1992-1-2 (2004)

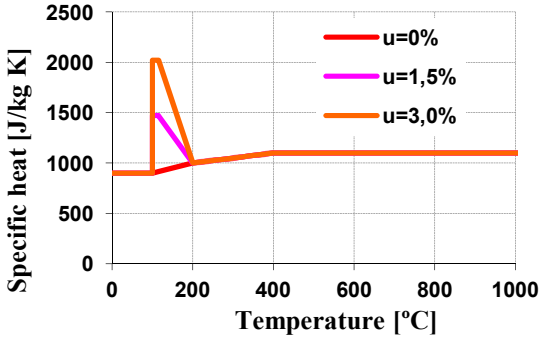

Figure 3.10 – Specific heat of concrete as a function of temperature, EN 1992-1-2 (2004)

The specific heat of concrete, C_c, can be defined as the energy required to raise one Celsius or Kelvin degree the temperature of a unit mass of concrete, without change of state, to a defined temperature (Figure 3.10).

The thermal conductivity of concrete as a function of the temperature, according to EN 1992-1-2 (2004), is depicted in figure 3.11.

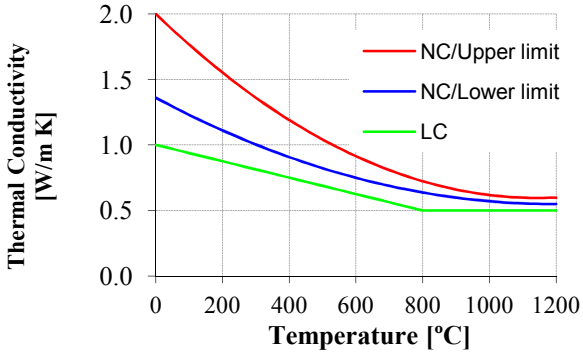

Figure 3.11 – Thermal conductivity of concrete as a function of the temperature, EN 1992-1-2 (2004)

3.3.2. Mechanical Properties

3.3.2.1. Steel

The stress-strain relationship given in figure 3.12, should be used to determine the strength of structural elements of steel in tensile, in compression, bending and shear. In this graph, four distinct zones can be observed. In the first zone Hook law is valid limited by the proportional limit stress. The second zone is defined by an elliptic curve, limited by the yield stress, corresponding to the beginning of yield. In the third zone, stress is constant and equals the yield stress, corresponding to the plastic zone. The last zone is characterized by a linear decrease of the yield stress.

Reduction factors of the stress-strain relationship are illustrated in figure 3.13. For intermediate values of temperature, a linear interpolation can be used.

- effective yield strength relative to yield strength at 20 ºC $k_{y,\theta} = f_{y,\theta} / f_y$ (3.42)
- proportional limit relative to yield strength at 20 ºC $k_{p,\theta} = f_{p,\theta} / f_y$ (3.43)
- slope of linear elastic range relative to slope at 20 ºC $k_{E,\theta} = E_{a,\theta} / E_a$ (3.44)

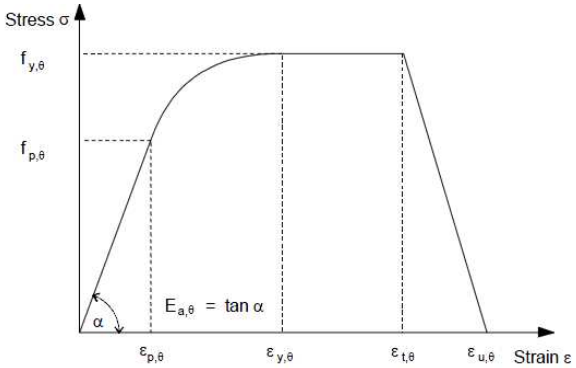

Figure 3.12 – Stress-Strain relationship for carbon steel at elevated temperatures, EN 1993-1-2 (2005)

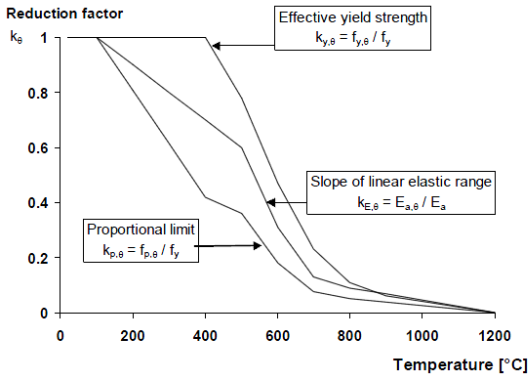

Figure 3.13 – Reduction factors for the stress-strain relationship of carbon steel at elevated temperatures, EN 1993-1-2 (2005)

In figure 3.13, it can be observed that, reduction factor $k_{y,\theta}$, suffers a sudden decrease, beginning from temperature 400ºC. The proportional limit, relative to yield strength is reduced by the factor $k_{p,\theta}$, and it can be observed that it decreases suddenly from 100 ºC. Young's modulus is reduced by the reduction factor $k_{E,\theta}$. This factor also suffers a reduction from 100ºC since it is related to the proportional limit stress.

The following table defines the shape of the stress-strain relationship for carbon steel, at elevated temperatures, as defined in EN 1993-1-2 (2005).

Strain range, ε	Stress, $\sigma(\theta)$	Tangent modulus
$\varepsilon \le \varepsilon_{sp,\theta}$	$\varepsilon \cdot E_{s,\theta}$	$E_{s,\theta}$
$\varepsilon_{sp,\theta} < \varepsilon \le \varepsilon_{sy,\theta}$	$f_{sp,\theta} - c + (b/a)\left[a^2 - (\varepsilon_{sy,\theta} - \varepsilon)^2\right]^{0,5}$	$\frac{b(\varepsilon_{sy,\theta} - \varepsilon)}{a\left[a^2 - (\varepsilon - \varepsilon_{sy,\theta})^2\right]^{0,5}}$
$\varepsilon_{sy,\theta} < \varepsilon \le \varepsilon_{st,\theta}$	$f_{sy,\theta}$	0
$\varepsilon_{st,\theta} < \varepsilon \le \varepsilon_{su,\theta}$	$f_{sy,\theta}\left[1 - (\varepsilon - \varepsilon_{st,\theta})/(\varepsilon_{su,\theta} - \varepsilon_{st,\theta})\right]$	--
$\varepsilon = \varepsilon_{su,\theta}$	0,00	--
Parameters	$\varepsilon_{sp,\theta} = f_{sp,\theta} / E_{s,\theta}$ $\quad \varepsilon_{sy,\theta} = 0,02$ $\quad \varepsilon_{st,\theta} = 0,15$ $\quad \varepsilon_{su,\theta} = 0,20$	
Functions	$a^2 = (\varepsilon_{sy,\theta} - \varepsilon_{sp,\theta})(\varepsilon_{sy,\theta} - \varepsilon_{sp,\theta} + c / E_{s,\theta})$ $b^2 = c(\varepsilon_{sy,\theta} - \varepsilon_{sp,\theta})E_{s,\theta} + c^2$ $c = \frac{(f_{sy,\theta} - f_{sp,\theta})^2}{(\varepsilon_{sy,\theta} - \varepsilon_{sp,\theta})E_{s,\theta} - 2(f_{sy,\theta} - f_{sp,\theta})}$	

Table 3.1 – Stress-strain relationship for carbon steel at elevated temperatures EN 1993-1-2 (2005)

3.3.2.2. Concrete

The stress-strain relationship for the one-dimensional self-compacting concrete as a function of temperature is defined in EN 1992-1-2 (2004) (Figure 3.14).

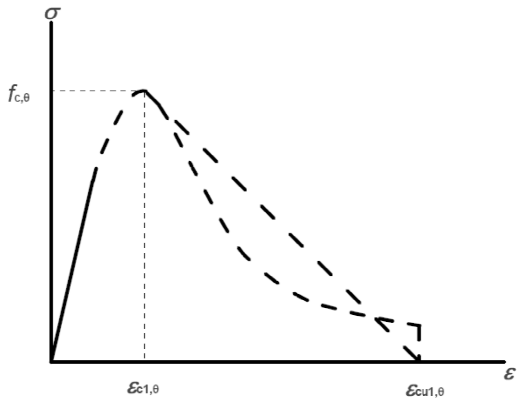

Figure 3.14 – Stress-strain relationship for concrete, EN 1992-1-2 (2004)

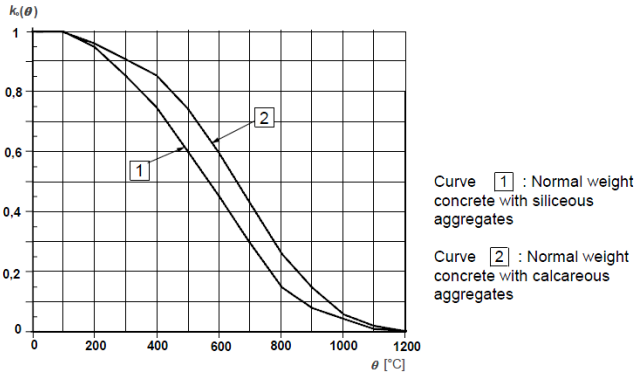

Figure 3.15 – Coefficient for decrease of characteristic strength of concrete, EN1992-1-2 (2004)

The EN 1992-1-2 (2004) allows the consideration of a conservative approach ignoring the tensile strength of concrete. In simplified or advanced calculation methods, the tensile strength of concrete should be affected by a reduction factor $k_c(\theta)$ as a function of the temperature. It is considered that up to 100ºC the concrete keeps the tensile strength at ambient temperature then decreasing to zero at 600ºC.

3.4. Fire Design of Columns

3.4.1. Steel Columns

The design buckling resistance $N_{b,fi,t,Rd}$ at time t of a compression member with class 1, class 2 or class 3 cross-section with a uniform temperature θ_a should be determined from:

$$N_{b,fi,t,Rd} = \chi_{fi} A k_{y,\theta} f_y / \gamma_{M,fi} \quad (3.45)$$

where

χ_{fi} – is the reduction factor for flexural buckling in the fire design situation;

$k_{y,\theta}$ - is the reduction factor for the yield strength of steel at the steel temperature θ_a reached at time t.

The value of χ_{fi} should be taken as the lesser of the values of $\chi_{y,fi}$ and $\chi_{z,fi}$ determined according to:

$$\chi_{fi} = \frac{1}{\phi_\theta + \sqrt{\phi_\theta^2 - \lambda_\theta^2}} \tag{3.46}$$

with

$$\phi_\theta = \frac{1}{2}\left[1 + \alpha\lambda_\theta + \lambda_\theta^2\right] \tag{3.47}$$

and the imperfection factor given by:

$$\alpha = 0,65\sqrt{235/f_y} \tag{3.48}$$

The non-dimensional slenderness λ_θ for the temperature θ_a is given by

$$\lambda_\theta = \lambda\sqrt{k_{y,\theta}/k_{E,\theta}} \tag{3.49}$$

where:

$k_{y,\theta}$ - is the reduction factor for the yield strength of the steel at temperature θ_a reached at time t;

$k_{E,\theta}$ - is the reduction factor for the slope of the linear elastic range at the steel temperature θ_a reached at time t;

The non-dimensional slenderness $\bar{\lambda}$ is given by

$$\bar{\lambda} = \frac{\lambda}{\lambda_1} \tag{3.50}$$

reached at time t;

in which λ is the slenderness of the element, given in this case in function of the buckling length in fire situation, by

$$\lambda = \frac{l_{fi}}{i} \tag{3.51}$$

in which i is the gyration radius of the cross section, and λ_1 is given by

$$\lambda_1 = \pi\sqrt{\frac{E}{f_y}} = 93,9\varepsilon \tag{3.52}$$

with

$$\varepsilon = \sqrt{\frac{235}{f_y}} \tag{3.53}$$

in which

E – is the Young modulus at ambient temperature;

f_y – is the yield strength at ambient temperature.

The buckling length l_{fi} of a column for the fire design situation should be determined as for normal temperature design. However, in a braced frame the buckling length l_{fi} of a column may be determined by considering it as fixed in direction at continuous or semi-continuous connections to the column lengths in the fire compartments above and below, provided that the fire resistance of the building components that separate these fire compartments is not less than the fire resistance of the column.

In the case of a braced frame in which each storey comprises a separate fire compartment with sufficient fire resistance, in an intermediate storey, the buckling length l_{fi} of a continuous column may be taken as $l_{fi} = 0{,}5.L$ and in the top storey the buckling length may be taken as $l_{fi} = 0{,}7.L$, where L is the system length in the relevant storey.

When designing using nominal fire exposure, the design resistance $N_{b,fi,t,Rd}$, at time t, of a compression member with a non-uniform temperature distribution may be taken as equal to the design resistance $N_{b,fi,\theta,Rd}$ of a compression member with a uniform steel temperature θ_a equal to the maximum steel temperature $\theta_{a,max}$ reached at time t.

For members with class 4 cross-sections it may be assumed that the load-bearing function of a steel element is maintained after a time t, if the steel temperature θ_a at all cross-sections is not more than θ_{crit}. The value of θ_{crit} may be obtained in the National Annex of each EU country or a conservative value of 350ºC may be used.

For members with class 1, 2 or 3 cross-sections subject to combined bending and axial compression, the design buckling resistance $R_{fi,t,d}$ at time t, should be verified by satisfying the following expressions:

$$\frac{\mathrm{N_{fi,Ed}}}{\chi_{\mathrm{min,fi}} A k_{y,\theta} \dfrac{f_y}{\gamma_{M,fi}}} + \frac{k_y M_{\mathrm{y,fi,Ed}}}{W_{pl,y} k_{y,\theta} \dfrac{f_y}{\gamma_{M,fi}}} + \frac{k_z M_{\mathrm{z,fi,Ed}}}{W_{pl,z} k_{y,\theta} \dfrac{f_y}{\gamma_{M,fi}}} \le 1 \tag{3.54}$$

$$\frac{\mathrm{N_{fi,Ed}}}{\chi_{\mathrm{z,fi}} A k_{y,\theta} \dfrac{f_y}{\gamma_{M,fi}}} + \frac{k_{LT} M_{\mathrm{y,fi,Ed}}}{W_{LT,fi} W_{el,y} \dfrac{f_y}{\gamma_{M,fi}}} + \frac{k_z M_{\mathrm{z,fi,Ed}}}{W_{el,z} k_{y,\theta} \dfrac{f_y}{\gamma_{M,fi}}} \le 1 \tag{3.55}$$

$$k_{LT} = 1 - \frac{\mu_{LT} N_{fi,Ed}}{\chi_{z,fi} A k_{y,\theta} \frac{f_y}{\gamma_{M,fi}}} \leq 1 \tag{3.56}$$

$$\mu_{LT} = 0.15 \lambda_{z,\theta} \beta_{M,LT} - 0.15 \leq 0.9 \tag{3.57}$$

$$k_y = 1 - \frac{\mu_y N_{fi,Ed}}{\chi_{y,fi} A k_{y,\theta} \frac{f_y}{\gamma_{M,fi}}} \leq 3 \tag{3.58}$$

$$\mu_y = (1.2\beta_{M,y} - 3)\lambda_{y,\theta} + 0.44\beta_{M,y} - 0.29 \leq 0.8 \tag{3.59}$$

$$k_z = 1 - \frac{\mu_z N_{fi,Ed}}{\chi_{z,fi} A k_{y,\theta} \frac{f_y}{\gamma_{M,fi}}} \leq 3 \tag{3.60}$$

$$\mu_z = (2\beta_{M,z} - 5)\lambda_{z,\theta} + 0.44\beta_{M,z} - 0.29 \leq 0.8 \tag{3.61}$$

and $\lambda_{z,\theta} \leq 1.1$

3.4.2. Composite Steel-Concrete Columns

The simple calculation models may only be used in columns inserted in braced frames. In this case the design value in fire situation, of the resistance of composite columns in axial compression (buckling load) shall be obtained from:

$$N_{fi,Rd} = \chi N_{fi,Pl,Rd} \tag{3.62}$$

where :χ is the reduction coefficient for buckling curve c, depending on the non-dimensional slenderness ratio $\overline{\lambda_\theta}$;

$N_{fi,pl,Rd}$ is the design value of the plastic resistance to axial compression in fire situation.

The design value of the plastic resistance to axial compression in fire situation is given by:

$$\sum_j \left(A_{a,\theta} f_{a\max,\theta} \right) / \gamma_{M,fi,a} + \sum_k \left(A_{s,\theta} f_{s\max,\theta} \right) / \gamma_{M,fi,s} + \sum_m \left(A_{c,\theta} f_{c,\theta} \right) / \gamma_{M,fi,c} \tag{3.63}$$

where:

$A_{i,\theta}$ is the area of each element i the cross-section;

The effective flexural stiffness is calculated as

$$(EI)_{fi,eff} = \sum_j \left(\varphi_{a,\theta} E_{a,\theta} I_{a,\theta}\right) + \sum_k \left(\varphi_{s,\theta} E_{s,\theta} I_{s,\theta}\right) + \sum_m \left(\varphi_{c,\theta} E_{c,sec,\theta} I_{c,\theta}\right) \quad (3.64)$$

where:

$I_{i,\theta}$ is the second moment of area, of the partially reduced part i of the cross-section for bending around the weak or strong axis,

$\varphi_{I,\theta}$ is the reduction coefficient depending on the effect of thermal stresses.

$E_{a,\theta}$ is the characteristic value for the slope of the linear elastic range of the stress-strain relationship of structural steel at elevated temperatures.

$E_{s,\theta}$ is the characteristic value for the slope of the linear elastic range of the stress-strain relationship of reinforcing steel at elevated temperatures.

$E_{c.sec,\theta}$ is the characteristic value for the secant modulus of concrete in the fire situation, given by $f_{c,\theta}$ divided by $\varepsilon_{cu,\theta}$.

The Euler buckling load or elastic critical load in fire situation is as follows

$$N_{fi,cr} = \pi^2 (EI)_{fi,eff} / l_\theta^{\,2} \quad (3.65)$$

where:

l_θ is the buckling length of the column in fire situation.

The non-dimensional slenderness ratio is given by

$$\overline{\lambda_\theta} = \sqrt{N_{fi,pl,R} / N_{fi,cr}} \quad (3.66)$$

where

$N_{fi,pl,R}$ is the value of $N_{fi,pl,Rd}$ when the factors $\gamma_{M,fi,a}$, $\gamma_{M,fi,s}$ and $\gamma_{M,fi,c}$ are taken as 1.0.

For the determination of the buckling length l_θ of columns, the rules of EN 1994-1-1(2003) apply, with the exception given hereafter.

A column at the level under consideration, fully connected to the column above and below, may be considered as completely built-in at such connections, provided the resistance to fire of the building elements, which separate the levels under consideration, is at least equal to the fire resistance of the column.

In the case of a steel frame, for which each of the stories may be considered as a fire compartment with sufficient fire resistance, the buckling length of a column on an

intermediate storey subject to fire l_θ equals 0.5 times the system length L. For a column on the top floor, the buckling length in fire situation l_θ equals 0.7 times the system length L.

These calculation models may only be applied in the following conditions:

		buckling length l_θ	≤	13.5 b
230mm	≤	height of cross section h	≤	1100mm
230mm	≤	width of cross section b	≤	500mm
1%	≤	percentage of reinforcing steel	≤	6%
		standard fire resistance	≤	120min

4. FIRE RESISTANCE TESTS ON COLUMNS WITH RESTRAINED THERMAL ELONGATION

4.1. Introduction

The fire resistance of a steel column is strongly influenced by the conditions in which it is inserted in the building. Beyond other parameters the contact of the column with the building walls has a great influence on its behaviour in fire. The walls, on one hand, have a favourable influence on the fire resistance of the steel columns because they protect a large part of its lateral surface from heating, but on the other hand, they will have an unfavourable influence because they lead to differential heating of the cross-section. The design methods considered in EN 1993-1-2 (2005) do not take into account this fact and the fire resistance is determined as if the heating was uniform.

In this chapter, several aspects concerning the experimental program carried out for the development of this work are described.

The experimental work was performed with the main goal to study the behaviour of steel columns embedded in walls with restrained thermal elongation under fire conditions. A parametric study was performed, to study the evolution of temperatures on these elements and to analyze different parameters such as: a) thickness of the wall; b) orientation of the web in relation to the wall; c) slenderness of the column.

4.2. Experimental setup

4.2.1. Tests on columns embedded on walls

Figure 4.1 shows the test set-up, which was specially conceived and constructed in the Laboratory of Testing Materials and Structures of the Faculty of Sciences and Technology of University of Coimbra, for testing loaded columns with restrained thermal elongation.

The system comprises a restraining steel frame of variable stiffness with the function of simulating the stiffness of the surrounding structure to the column subjected to fire. The use of a three-dimensional restraining frame allowed taking into account not only the axial but also the rotational stiffness such as observed in a real structure. The restraining frame was composed by four columns, two upper beams and two lower beams, placed orthogonally. The beams of this frame were steel profiles HEA200, grade S355. The connections between these

structural elements were performed with M24 bolts, grade 8.8., except the connections between the columns and upper beams where threaded rods M27, grade 8.8, were used. The connections between columns and lower beams were formed by four M24 bolts with nuts of the same diameter. Special attention should be devoted to the detail of the connection between the columns and upper beams. These connections were designed to allow adjustment of the position of the upper beams, with a total appliance of the load on the columns to be tested. Thus, the connections were formed by four threaded rods M27 with about 250mm in length, rigidly connected to the flanges of the upper beams.

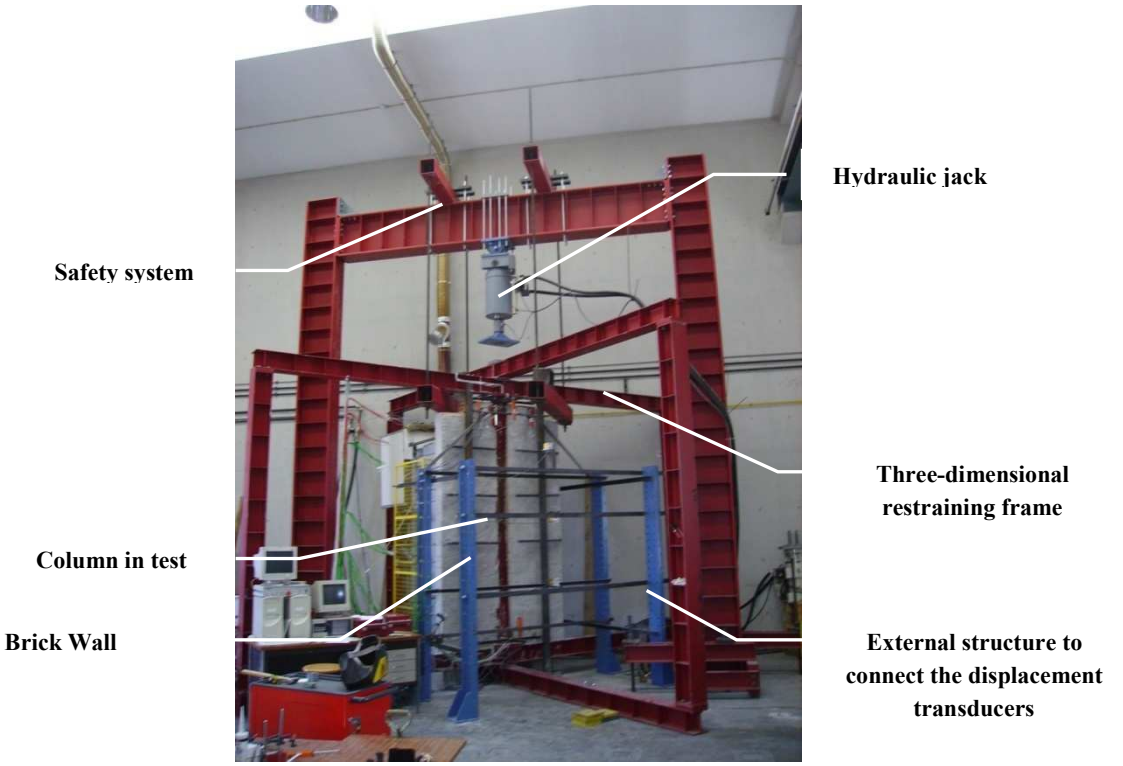

Figure 4.1 - Experimental set-up

A reaction frame was used to place the hydraulic jack in position to apply the load during the fire resistance tests. This frame was composed by two HEB500 (steel grade S355) columns 6.5m long, and an HEB600 (steel grade S355) beam 4.5m long. This frame was fixed to the laboratory slab using Diwidag bars, 36mm of diameter. This frame was also provided by a safety system, used to prevent destruction of the testing set-up when the sudden collapse of the test columns occurred. This system was composed of four tubular square profiles, two over the beam of the reaction frame, and the other two under the beams of the restraining frame. Four Diwidag bars, 36mm of diameter kept the two tubular profiles in position, with a gap of 35mm to the beams of the reaction frame, preventing bigger displacements downwards of the top of the column.

The load was applied by a hydraulic jack of 1MN. This load simulated the serviceability load of the column when part of a real structure. The hydraulic jack was placed in the two-dimensional reaction frame.

The thermal action was applied by a gas fired furnace following approximately the standard ISO 834 fire curve (Figure 4.2 a)). This furnace is composed of one chamber, placed on one side of the column and adjacent walls with dimensions of 1.2m x 1.2m x 2.1m.
The thermal action acted only on one side of the element, in such a way to permit the analysis of the thermal gradient throughout the wall and cross-section of the column. In Figure 4.2a), three holes for placing three thermocoulples, 2mm width, can be seen in the right end side of the furnace.

a) b)

Figure 4.2 – a) Test furnace b) Column in the restraining frame after test.

The steel columns were placed in the centre of the frame (Figure 4.2 b). The specimen was connected to the restraining frame by a steel plate of 30mm thickness with four M24 bolts.

Three displacement transducers in the top and other three in the base of the column were placed, in orthogonal axes, for measuring the axial displacement and rotations of the column (Figure 4.3a)). The lateral deflections of the tested column were also measured in three levels by displacement transducers (Figure 4.3b)).

a) b)

Figure 4.3 - Displacement transducers a) at bottom of the column b) at top of the column

4.2.2. Tests on columns not embedded on walls

Figure 4.4 shows the other experimental system which was constructed in the Laboratory of Testing Materials and Structures of the University of Coimbra for fire resistance tests on building columns with restrained thermal elongation, and Figure 4.5 presents a scheme of the same experimental system.

Figure 4.4 – General view of the test set-up

The conception of the system is very similar to the one described previously. Two main differences should be pointed out: the columns and beams of the restraining frame were made of HEB300 steel profiles, steel grade 355, and a special device for the measurement of the restraining forces generated during the tests was placed between the specimen and the upper beams of the frame. Figure 4.5 represents a detailed scheme of the set-up, in which all the components are labelled. The system comprises a restraining steel frame of variable stiffness (1) with the function of simulating the stiffness of the surrounding structure to the column subjected to fire.

The connections between these structural elements were performed with M24 bolts, grade 8.8, except the connections between the columns and upper beams (2) where threaded rods M27, grade 8.8, were used. Different hole positions in the flanges of the beams of the restraining frame, allowed the assembly of the columns in different positions, leading to different spans

of the beams that corresponded to different values of the stiffness of the surrounding structure. The tested values of the axial stiffness were 13, 45 and 128kN/mm.

The hydraulic jack of 3MN (3) was controlled by a load cell of 1MN (4). It was fixed in the reaction frame (5) provided with a safety system (6).

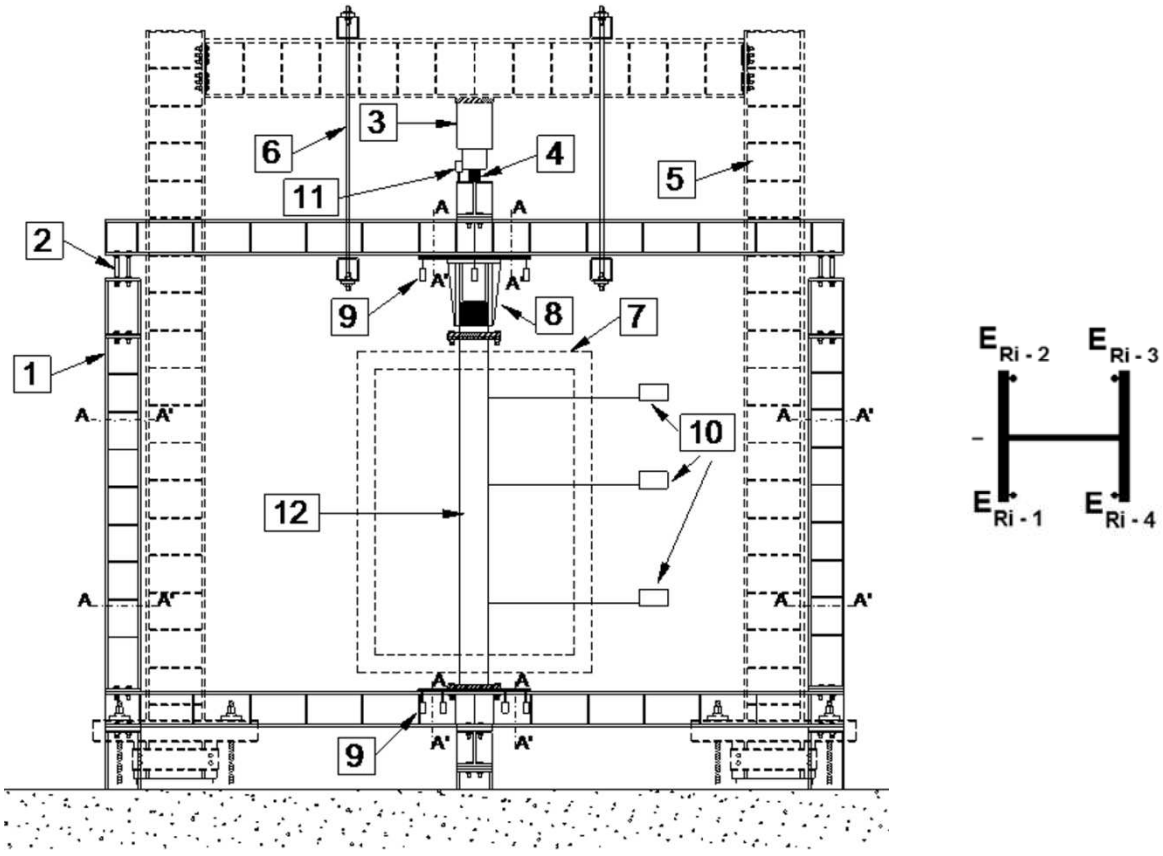

a) b)

Figure 4.5 – Scheme of the test set-up a) general view b) position of strain gauges

Four Linear Variable Displacement Transducers (LVDT) on bottom and three on top of the test columns (9) were used. The LVDT's were orthogonally arranged allowing the measurement of all deformation planes of the ends of the test columns and consequently their rotations.

The lateral displacements of the column were measured by wire displacement transducers placed in two orthogonal directions, at 0.81m, 1.81m and 2.49m height in relation to the column base (10). Furthermore, an extra displacement transducer was placed in the centre of

the 3D restraining frame, near the point of application of the load, to confirm the axial displacements of the test columns (11).
The test column (12) was placed in the centre of the restraining frame and was properly fitted to it, in each end plate, with four steel bolts M24, class 8.8.

Strain gauges were used to measure de strains on the columns and beams of the three-dimensional restraining frame, in order to confirm indirectly the restraining forces generated in the test columns and have the strains in different points of this structure (sections AA' of Figure 4.5). In each of this section four strain gauges type TML FLA-6-11 were placed in the flanges, 10mm from the edge of the flange.

The device to measure the restraining forces generated in the test columns during the fire resistance tests due to the thermal restraint provided by the surrounding structure (8) is depicted in Figure 4.6.

This device was built to allow accurate measurement and record of the restraining forces generated by the surrounding structure, during the heating process. It consists of a hollow and stiff cylinder, rigidly connected to an upper beam, above the specimen. On top of the specimen, a massive cylinder was rigidly connected. The lateral surface of this cylinder was Teflon lined. This special material has the particularity of a very low friction coefficient. This massive cylinder was placed inside the hollow cylinder, and the load cell, capable of measuring forces up to 3000kN, was placed between the massive cylinder and the end plate of the hollow cylinder. The thermal forces during the fire resistance tests were this way accurately measured.

a) b) c)

Figure 4.6 – Device for measuring thermal forces a) inner cylinder Teflon lined b) outer hollow cylinder c) placing of the device in the frame centre

This device was conceived for the fire tests in steel and composite isolated columns, but was also used in some of the tests on steel columns embedded on walls.

The thermal action was applied by a modular electric furnace (7) following approximately the standard ISO 834 fire curve (ISO 834, 1975). This furnace is composed of modules 1m height and one module 0.5m height, placed on top of each others forming a free chamber around the column 1.5m x 1.5m x 2.5m (Figure 4.7). In each module, the temperature sensors were positioned at mid-height.

a) b)

Figure 4.7 - Vertical modular furnace

Seven Linear Variable Displacement Transducers (LVDT) were used to measure the columns rotations on bottom and top (9). Special bars with plates in the ends were welded to the bottom and top end plates of the columns, in order to allow the measurement of rotations of the column extremities.

Six wire displacement transducers were used to monitor the displacements of the columns in the weak and strong axis, three in each plane (10).

Another displacement transducer was placed on top of the upper beam of the restraining frame, in order to measure the vertical displacement on the column (11).

Figures 4.8 a) and b) and Figure 4.9 a) and b) depict the position of the displacement transducers on bottom and top of the column, as well as the wire displacement transducers along the height of the column, to monitor the rotations and lateral deflections during the fire tests.

a) b)

Figure 4.8 - Displacement transducers a) on bottom of the column b) on top of the column

a) b)

Figure 4.9 - Displacement transducers along the height of the column

All the mentioned values were measured and recorded, using a datalogger TML TDS-530 and three additional boxes, two of model SSW-50D and one IHW-50G. This system is able of acquiring 180 channels of different measurements, along the time of the test.

4.3. Test columns

The experimental programme involved the fabrication of test models in which steel columns embedded on walls, steel and composite steel-concrete columns were considered, all of them instrumented with thermocouples to measure the temperatures.

4.3.1. Columns embedded on walls

The specimens of columns embedded on walls were composed by steel profiles HEA 160 and HEA 200 grade 355, totally or partially embedded on walls, with the web parallel or perpendicular to the wall surface. The thick walls were approximately the same width of the

steel profile cross-section width, as well as thin wall, and the thin walls were approximately ¾ of the width of the profile cross-section.

In each specimen 30 type k thermocouples (chromel-alumel) were used, six thermocouples in each section, five different sections along the height of the column. The five sections considered along the height of the column are depicted in figure 4.10 a).

Thermocouples were also inserted in the walls to measure the temperatures on it (figure 4.10b)).

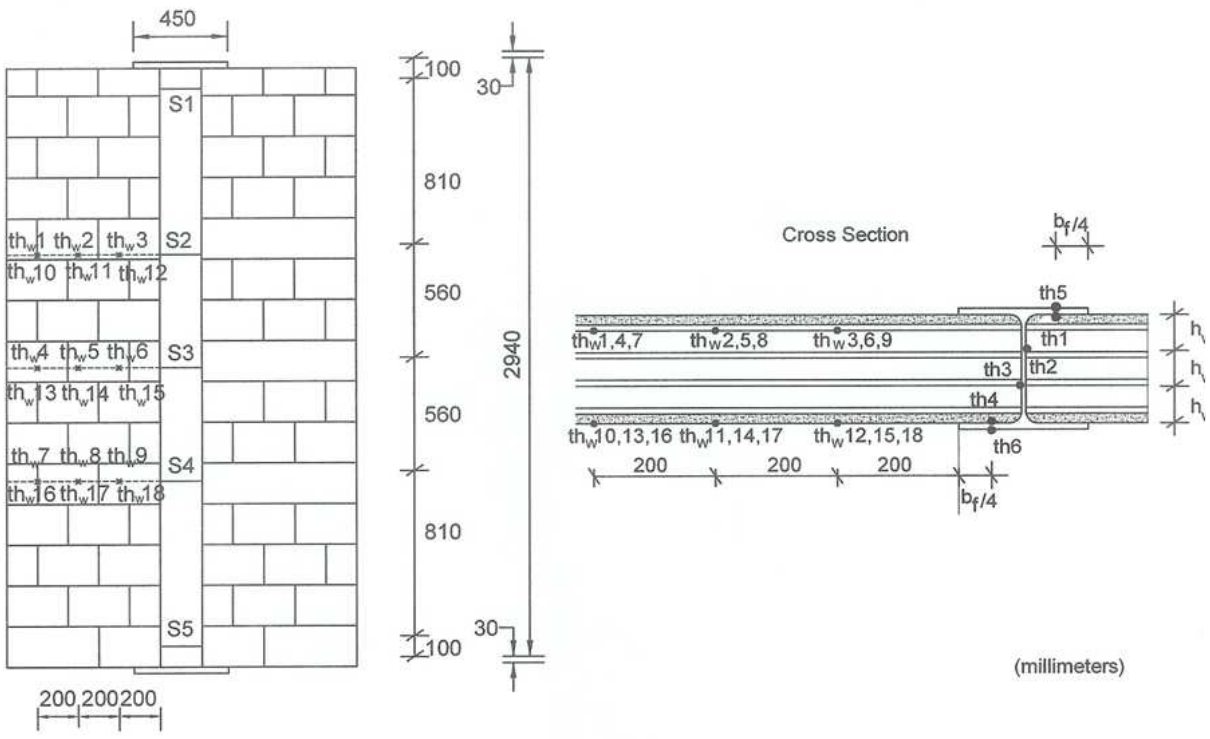

a) b)

Figure 4.10 – Specimens with thermocouples in the column and in the wall a) front view b) view-cut

For this set of tests, both loaded and unloaded columns, also restrained were tested.

4.3.2. Steel bare columns

The following figure shows the geometrical dimensions of the specimens used in the tests, with the definition of the 5 sections where the temperatures were measured. The length of the columns was 3.00m, including the end plates, which were 30mm thick.

These end plates were square 450 x 450 mm, with 4 holes for bolts M24, to perform a semi-rigid connection between the columns to be tested and the upper and lower beams of the 3D restraining frame.

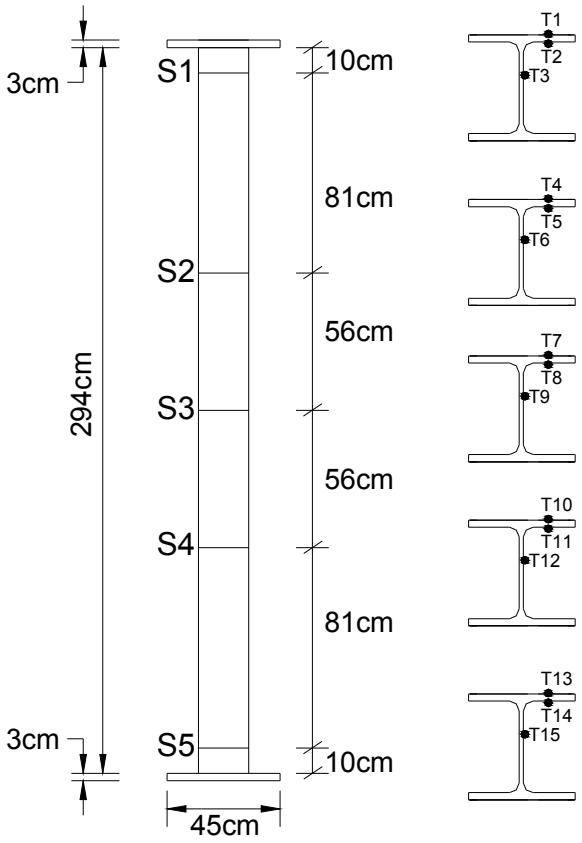

a) b)

Figure 4.11 – Steel specimens with position of the thermocouples a) View and definition of measuring sections b) Cross section geometry with position of thermocouples

The specimens used in the tests were HEA 160 and HEA 200 bare steel columns, 3m height, steel grade 355. All the columns were instrumented with three type K thermocouples per section in 5 sections along the height of the column (fig. 4.11 a) and b)). All the columns were subjected to a constant compressive load to simulate the serviceability load of the column when inserted in a real building structure. This load was 70 and 30% of the design value of the buckling resistance at room temperature calculated according to EN 1993-1-1 (2005).

4.3.3. Composite steel-concrete columns

The study was extended to composite steel-concrete columns partially encased in buildings. The geometry of the composite steel-concrete columns is depicted in the following figure.

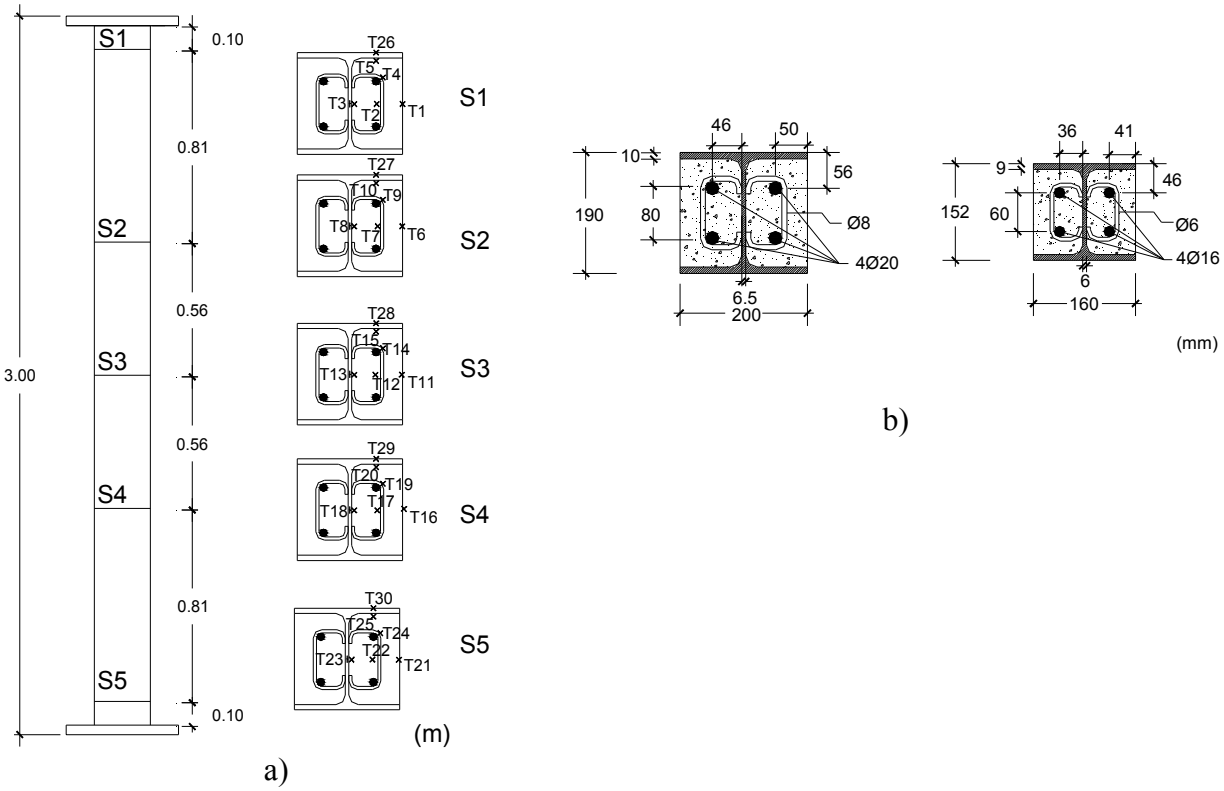

Figure 4.12 – Composite steel-concrete columns a) View and position of thermocouples b) Cross section geometry of CSC200 and CSC200

The steel profiles used were HEA160 and HEA200. Steel grade was S355 and C25/30 class of concrete was used in all specimens. Longitudinal rebars 20mm diameter and 8mm diameter stirrups were used in the HEA200 profiles, while for HEA160 columns rebars 16mm diameter and stirrups 6mm diameter were adopted. The study performed for the composite columns was similar to the one performed for steel bare columns.

The same two levels of load were considered: 70% and 30% of the design value of the buckling load of columns, at room temperature.

4.4. Test programme

In the following sections, the experimental test programme for the several types of columns is presented.

4.4.1. Columns embedded on walls

Steel profiles with two different cross sections, two different orientations, web perpendicular and parallel to the furnace opening, and two different wall thicknesses were tested. The tested

columns where HEA160 and HEA200, steel class S355 and the walls made of bricks with different thicknesses. The bricks were layed using ordinary cement mortar.

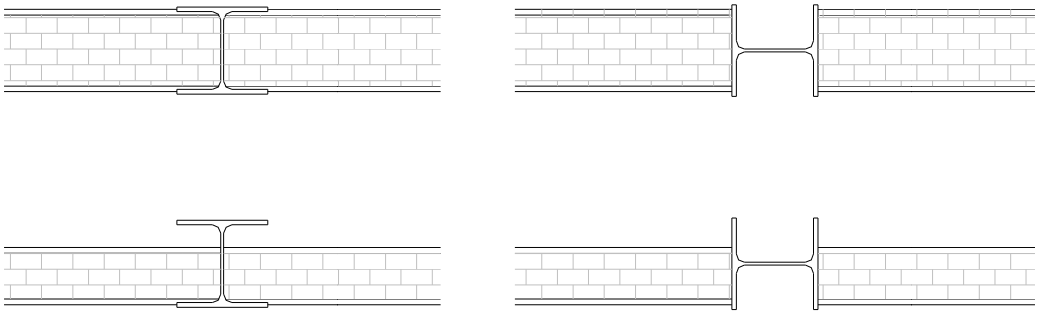

Figure 4.13 – Specimens embedded on walls

Two brick walls were built, one on each side of the column (fig. 4.13). The specimens were instrumented with thermocouples type k (chromel-alumel) to measure the temperatures in different points of the cross-section and walls.

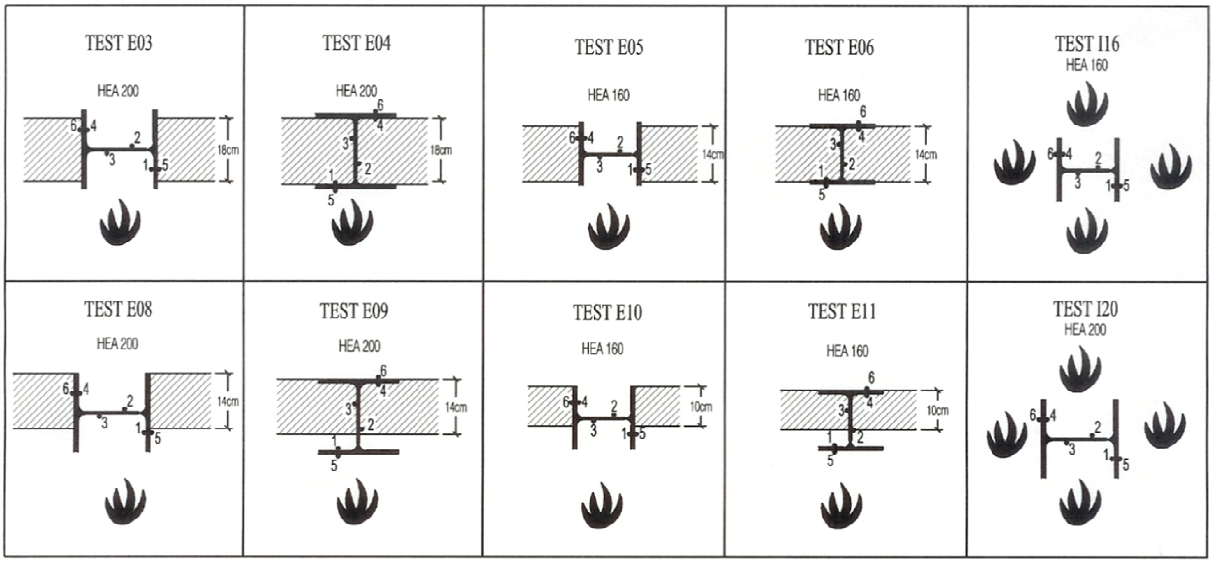

Figure 4.14 – Cases study and position of the thermocouples

In this series, sixteen tests were performed (table 4.1). Eight tests were performed without loading. The tests with loading were performed with an applied load of 70% of the design value of the buckling load at ambient temperature, $N_{Rd,20}$.
The columns in some of the tests were subjected to the application of a constant vertical load. This load intended to simulate the serviceability load of a column when inserted in the structure of a building.

Table 4.1 – Test plan for steel columns embedded on walls

Test Number	Steel Profile	Orientation of web to furnace	Wall width (mm)	Load (kN) (% of $N_{Rd,20}$)	Stiffness (kN/mm)
E01	HEA 160	parallel	140	704 (70% $N_{Rd,20}$)	7
E02	HEA 160	perpendicular	140	704 (70% $N_{Rd,20}$)	7
E03	HEA 200	parallel	180	-	7
E04	HEA 200	perpendicular	180	-	7
E05	HEA 160	parallel	140	-	7
E06	HEA 160	perpendicular	140	-	7
E07	HEA 160	parallel	140	621 (70% $N_{Rd,20}$)	7
E08	HEA 200	parallel	140	-	7
E09	HEA 200	perpendicular	140	-	7
E10	HEA 160	parallel	100	-	7
E11	HEA 160	perpendicular	100	-	7
E12	HEA 160	parallel	100	621 (70% $N_{Rd,20}$)	7
E13	HEA 160	perpendicular	100	704 (70% $N_{Rd,20}$)	7
E14	HEA 160	parallel	100	1088 (70% $N_{Rd,20}$)	7
I16	HEA 160	No walls	-	704 (70% $N_{Rd,20}$)	13
I20	HEA 200	No walls	-	1088 (70% $N_{Rd,20}$)	13

The columns embedded on walls, were tested all with the same stiffness of the surrounding structure, because for this set of tests, this parameter was not under analysis, except in tests I16 and I20, because they were performed in another restraining frame.

The tests in this table, with an applied load, were performed without the special device with the load cell, except test E07, in which the device was used. In this case, the load was calculated with a length of 3.6 meters. This is the reason why the loads in this table are different from the ones in table 4.2. Test E07 is the only one with an equal value of load as in table 4.2

4.4.2. Steel bare columns

This research investigated the effect of several parameters on the performance of steel bare columns in buildings. A detailed table referring to the experimental test carried out is presented.

In this table, twelve tests were carried out with centered load, and two with eccentricity. In these cases, the column was fixed to the restraining frame with special steel plates with holes, in such a way that the specimen had an eccentricity of 20cm, first in one axis, and then in two axis. The loads applied in these tests were calculated with the interaction formulae of EN 1993-1-1 (2005), at ambient temperature.

Table 4.2 – Test plan for steel isolated columns

Test Reference	Axial Restraint Ratio α_A	Rotational Restraint Ratio β_R	λ	Load (kN) (% of $N_{Rd,20}$)	Stiffness (kN/mm) $K_{A,S}$	Eccentricity
HEA200-K13-L70	0.035	1.290	50.6	999,8 (70%)	13	Centered
HEA200-K13-L70-E2	0.035	1.290	50.6	224 (70%)	13	Two axis
HEA200-K13-L70-E1	0.035	1.290	50.6	570 (70%)	13	One axis
HEA160-K13-L70	0.048	2.801	63.3	621 (70%)	13	Centered
HEA200-K13-L30	0.035	1.290	50.6	428 (30%)	13	Centered
HEA160-K13-L30	0.048	2.801	63.3	266 (30%)	13	Centered
HEA160-K45-L70	0.166	3.262	63.3	621 (70%)	45	Centered
HEA160-K45-L30	0.166	3.262	63.3	266 (30%)	45	Centered
HEA200-K45-L70	0.119	1.503	50.6	999,8(70%)	45	Centered
HEA200-K45-L30	0.119	1.503	50.6	266 (30%)	45	Centered
HEA200-K128-L30	0.341	2.097	50.6	428 (30%)	128	Centered
HEA160-K128-L30	0.473	4.551	63.3	266 (30%)	128	Centered
HEA200-K128-L70	0.341	2.097	50.6	999,8 (70%)	128	Centered
HEA160-K128-L70	0.473	4.551	63.3	621 (70%)	128	Centered

The first column indicates the specimen reference. Thus, as an example, reference HEA200-K13-L70 indicates that the steel profile of the cross-section of the specimen is an HEA200, tested with the stiffness of the surrounding structure of 13 kN/mm (K) and a load level of 70% of the design value of the buckling load at room temperature (L). E1 indicates the test was carried out with an eccentricity of 200mm from the weak axis of the column and E2 eccentricity of 200mm from the strong and weak axis of the column in two orthogonal directions.

It should be pointed out that the slenderness of the columns was calculated considering the length of the testing column, including the device in the top of it, used to measure the restraining forces, *i.e.*, 3.6m, and a buckling length of 0.7*l*.

The non-dimensional axial restraint ratio α_A of the columns is defined by a relation between the axial stiffness of the surrounding structure $K_{A,S}$ and the elastic axial stiffness of the column $K_{A,C}$:

$$\alpha_A = \frac{K_{A,S}}{K_{A,C}} \tag{4.1}$$

where:

$$K_{A,C} = \frac{A_C . E_C}{L_C} \tag{4.2}$$

The axial stiffness of the structure $K_{A,S}$ was calculated both experimentally and numerically . A special test, where the column was replaced by an hydraulic jack, was also carried out to determine the axial stiffness of the restraining frame. The hydraulic jack applied a force that made to move away the upper beams in relation to the lower beams of the restraining frame. In this test were constantly measured the applied force and the resulting displacements of the restraining frame.

The non-dimensional rotational restraint ratio β_R is defined by the relation between the structure rotational stiffness $K_{R,S}$ and the elastic rotational stiffness of the column $K_{R,C}$:

$$\beta_R = \frac{K_{R,S}}{K_{R,C}} \tag{4.3}$$

where

$$K_{R,C} = \frac{4.E_C.I_C}{L_C} \tag{4.4}$$

The rotational stiffness of the structure $K_{R,S}$ was determined numerically with ABAQUS, considering the whole experimental system. The values of the rotational stiffnesses are presented in chapter 6, in Table 6.3.

The parameters involved in the tests were:

a) Load level: Two load levels were considered: 70 and 30% of the design value of the buckling load of the column at room temperature;
b) Axial restraint: Three values of the stiffness of the surrounding structure: 13, 45 and 128 kN/mm.
c) Three values for the axial restraint α_A= 0.048, 0.166 and 0.473 for the column HEA160 and three values α_A= 0.035, 0.119 and 0.341 for the column HEA200. The axial restraint level α_A is defined by a relation between the structure stiffness $K_{A,S}$, and the column axial stiffness $K_{A,C}$:
d) Two slenderness values for the columns; 50.6 for the HEA200 and 63.3 for the HEA160.
e) Eccentricities of the axial load: Three different situations were studied. Twelve tests were performed with a centered load, one test with eccentricity in one direction and one test with eccentricity in two orthogonal directions.

4.4.3. Composite steel-concrete columns

The study was extended to composite steel-concrete columns partially encased in buildings. The test plan is presented in Table 4.3.

Table 4.3 – Test plan for composite steel-concrete partially encased columns

Test Number	Steel Profille	α_A	β_R	$\overline{\lambda}_z$	Load(kN) (% of $N_{Rd,20}$)	Stiffness (kN/mm)	Reinforcement
CSC160-K128-L30	HEA 160	0.242	2.437	1.1	(273)30%	128	4 bars – 16mm Stirrups 6mm //0.15m
CSC160-K128-L70	HEA 160	0.242	2.437	1.1	(637)70%	128	4 bars – 16mm Stirrups 6mm //0.15m
CSC200-K128-L30	HEA 200	0.163	1.048	0.87	(514)30%	128	4 bars – 20mm Stirrups 8mm //0.15m
CSC200-K128-L70	HEA 200	0.163	1.048	0.87	(1199)70%	128	4 bars – 20mm Stirrups 8mm //0.15m
CSC160-K45-L30	HEA 160	0.085	1.747	1.1	(273)30%	45	4 bars – 16mm Stirrups 6mm //0.15m
CSC160-K45-L70	HEA 160	0.085	1.747	1.1	(637)70%	45	4 bars – 16mm Stirrups 6mm //0.15m
CSC200-K45-L30	HEA 200	0.057	0.751	0.87	(514)30%	45	4 bars – 20mm Stirrups 8mm //0.15m
CSC200-K45-L70	HEA 200	0.057	0.751	0.87	(1199)70%	45	4 bars – 20mm Stirrups 8mm //0.15m
CSC160-K13-L30	HEA 160	0.025	1.500	1.1	(273)30%	13	4 bars – 16mm Stirrups 6mm //0.15m
CSC160-K13-L70	HEA 160	0.025	1.500	1.1	(637)70%	13	4 bars – 16mm Stirrups 6mm //0.15m
CSC200-K13-L30	HEA 200	0.017	0.645	0.87	(514)30%	13	4 bars – 20mm Stirrups 8mm //0.15m
CSC200-K13-L70	HEA 200	0.017	0.645	0.87	(1199)70%	13	4 bars – 20mm Stirrups 8mm //0.15m

Twelve full-scale composite steel-concrete columns were tested. Experimental tests were performed to determine the mechanical properties of the steel and the concrete at room temperature. Results of these properties are presented in Appendix A. Longitudinal rebars 20mm diameter and 8mm diameter stirrups were used in the HEA200 profiles, while for HEA160 columns rebars 16mm diameter and stirrups 6mm diameter were adopted.

The study performed for the composite columns was similar to the one performed for steel bare columns:

The same two levels of load were considered: 70% and 30% of the buckling load of the column at room temperature. The same three levels of restraint provided by the surrounding structure were used: 13, 45 and 128 kN/mm. These values of stiffness of the structure, led to the following values of relative axial stiffness α_A: 0.025, 0.085 and 0.242 with column CSC160 and 0.017, 0.057 and 0.163 with column CSC200. The axial restraint level α_A is defined by a relation between the structure stiffness $K_{A,S}$, and the column axial stiffness $K_{A,C}$, as defined in expressions 4.1 and 4.2.

Two different non-dimensional slenderness of the columns were obtained with HEA 200 and HEA160: 0.87 for column CSC200 and 1.1 for column CSC160.

4.5. Test procedure

4.5.1. Columns embedded on walls

Walls on both sides of the columns were built. The following figures depict the construction of the test model of the columns embedded on walls. Figure 4.15 a) and b) show the two brick walls being built. In figure 4.15 c), both walls are finished with plaster in both sides.

The furnace applies the thermal action following the standard ISO 834 fire curve on one side of the specimen (column and walls). The columns and walls were instrumented with type K thermocouples.

a) b) c)

Figure 4.15 – a) Construction of the test model b) Column embedded on a wall c) Lateral view of the experimental system.

The temperatures inside the furnace were measured by shielded probe thermocouples, 2mm diameter type K in the first tests and were later changed to plate thermometers in the last tests. In both cases, they were positioned at heights 0.5m, 1.0m, and 1.5m from the bottom. This change was due to the fact that a small delay in the heating of the furnace was observed in the first tests and so the decision was taken to change the thermocouples that controlled the furnace.

a) b) c)

Figure 4.16 – a) Front view of the test model, b) Lateral view of the wall, c) Front view of the experimental system after test.

4.5.2. Steel bare columns

The mechanical load applied in the experimental tests was a vertical compressive load on the column, more specifically in the node connecting the upper beams. This constant load in the test system was applied using a hydraulic jack. This mechanical load aims to simulate the serviceability load acting in a column of the structure of a real building.

The application of the load in a column inserted in a frame is difficult because, if the upper beams are rigidly connected to the columns, the applied load would be partially distributed to the peripheral columns. Moreover, the bending of the columns would interfere in the restraint provided to the column. In order to avoid this, the connections between the upper beams and peripheral columns was performed with threaded rods, whose nuts were unscrewed, before the appliance of the load. Then, with the hydraulic jack, the load was applied increasingly, up to the desired value of the serviceability load. The upper beams vertical displacement downwards was allowed freely. Once the desired value was reached, the nuts were screwed to provide full connection between the upper beams extremities and the peripheral columns. After this process, the load applied by the hydraulic jack was totally directed to the column to be tested. At this moment, the thermal action was now applied.

In order to eliminate the thermal inertia of the furnace, a pre-heat was provided before the beginning of each test. Thus, instead of 20ºC, the temperatures of the furnace starts at about 120ºC, leading to a much closer heating curve to the ISO 834 fire curve.

4.5.3. Composite steel-concrete columns

The test procedure was the same as described in section 4.5.2 for steel bare columns.

4.6. Results

4.6.1. Columns Embedded on Walls

4.6.1.1. Temperatures in the Columns

The following graphs depict the evolution of temperatures in the flanges and web of the steel profiles, obtained experimentally in the fire resistance tests of unloaded columns. In these graphs, it can be clearly observed that great thermal gradients will develop during the fire tests and that after 60 minutes of test, the temperature difference between the exposed and unexposed part of the steel cross section is important, mainly in the cases of the web orientation perpendicular to the wall surface. With a thick wall, and the orientation of the web perpendicular to the wall, the thermal gradient along the web direction is about 550ºC, after 60 minutes (Figure 4.17). With a thin wall and the same orientation, the thermal gradient is about 700ºC (Figure 4.18).

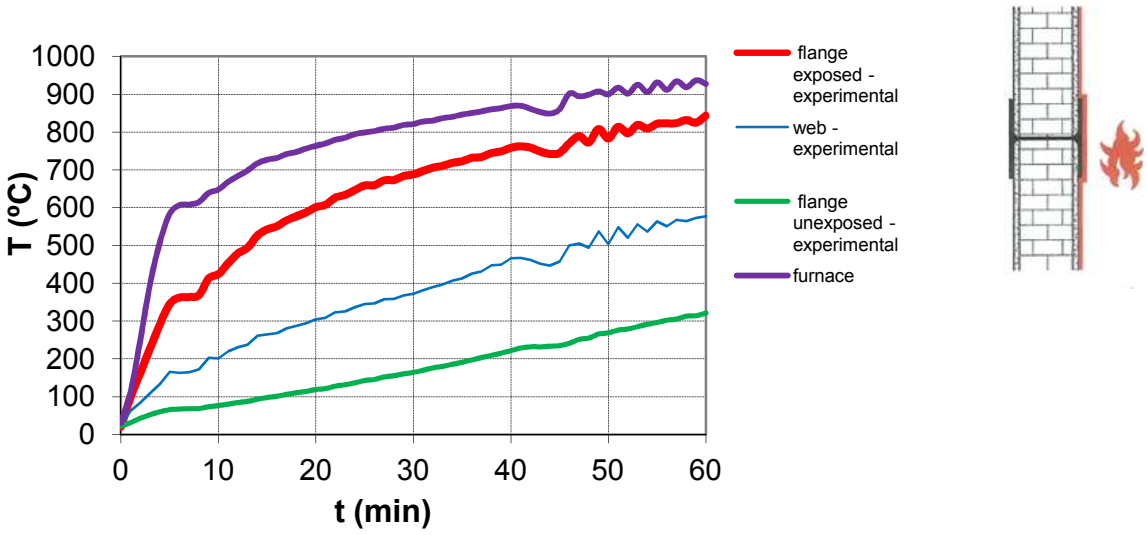

Figure 4.17 – HEA160 steel profile with the web perpendicular to the wall and a thick wall (test E06)

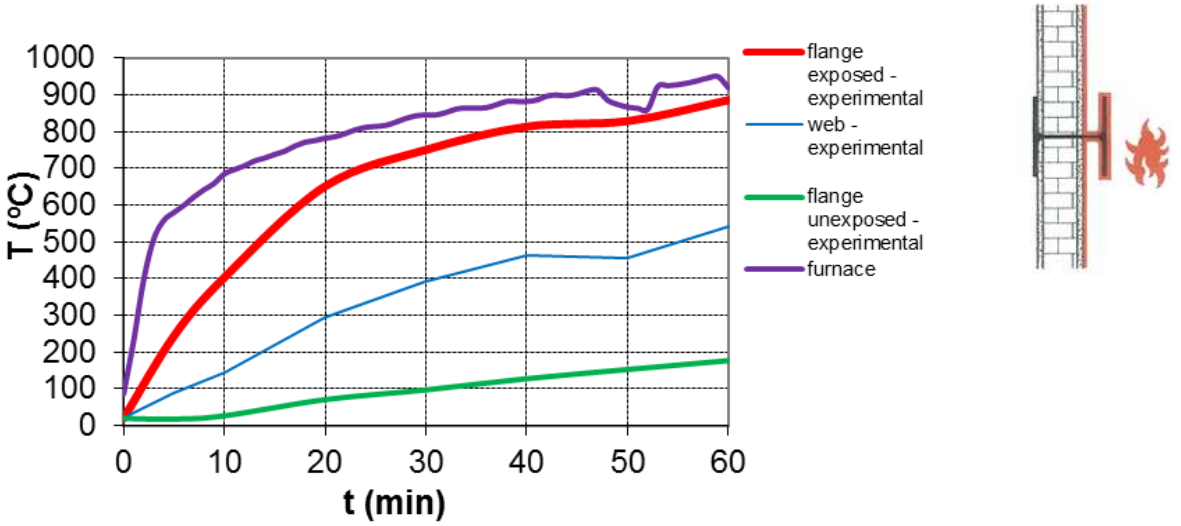

Figure 4.18 – HEA200 steel profile with the web perpendicular to the wall and a thin wall (test E09)

With a thin wall and the web parallel to the wall, the thermal gradient is about 500ºC (Figure 4.19). With a thick wall, and the same orientation, the thermal gradient along the web direction is about 400ºC, after 60 minutes (Figure 4.20).

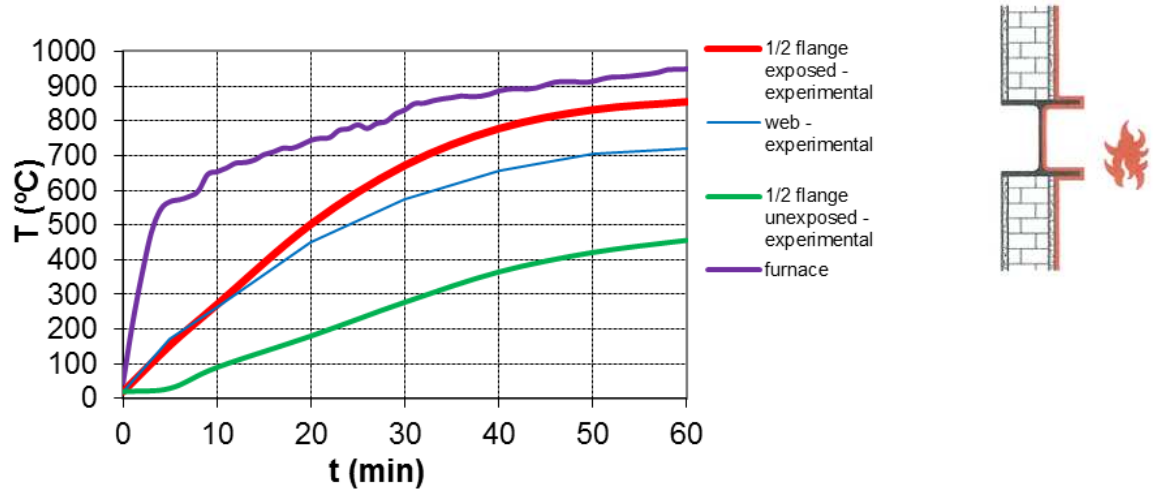

Figure 4.19 – HEA200 steel profile with the web parallel to the wall and a thin wall (test E08)

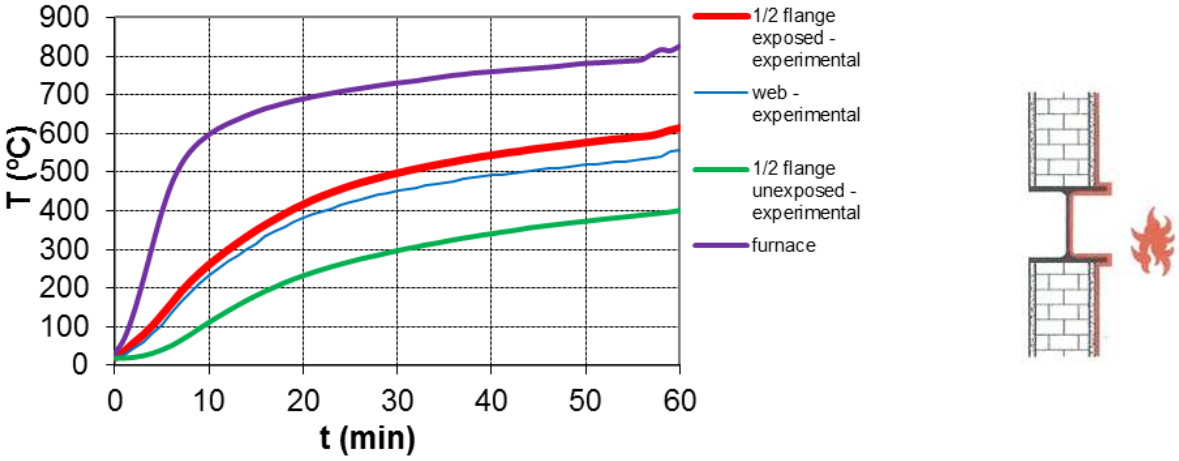

Figure 4.20 – HEA160 steel profile with the web parallel to the wall and a thick wall (test E10)

These results show that the contact with walls, provide the steel profile an important insulation, reducing the temperatures in the unexposed side, leading to huge thermal gradients which are responsible for the appearance of additional axial forces and bending moments.

4.6.1.2. Axial and Lateral Displacements

Figures 4.21 a) and b) depict the axial displacement and the lateral deflections in the plane perpendicular to the walls, of the test column E11, HEA 160 steel profile, with the web perpendicular to the wall and walls 100mm thick.

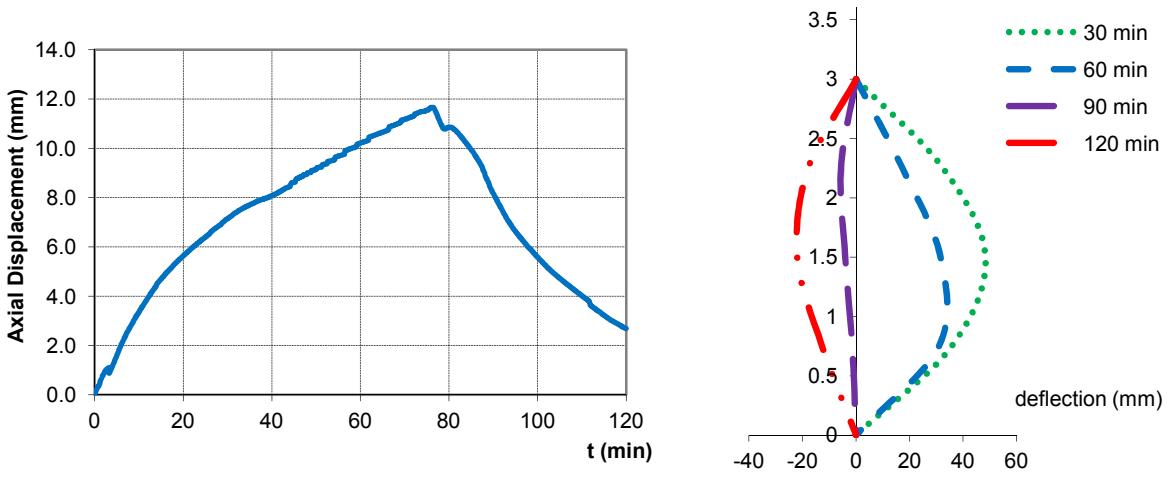

a) Axial displacement b) lateral deflection

Figure 4.21 – Axial displacement and lateral deflections in the plane perpendicular to the walls, of the test column E11, HEA 160 steel profile, with the web perpendicular to the wall and walls 100mm thick.

The test E11 was performed without mechanical load, and this is the reason why it was possible to test it for 120 minutes. Even without load, the columns was inserted in the restraining frame, submitted to a certain restraint, which lead to a reduction of the axial displacement.

Moreover, it is possible to observe the inversion on the column deflection, firstly moving towards the hot side and then moving in the opposite direction, towards the cold side (in graph of figure 4.21 b), the fire is in the right side).

4.6.1.3. Restraining Forces

Figure 4.22 presents the evolution of restraining forces versus mean steel temperature of the columns, for tests E07 and test E12. It is observed that the decreasing of restraining forces after the maximum is quite gentle. Also, it was concluded that the thicker walls provide a greater insulation to the steel profile, giving as result a lower increase of the restraining forces and higher fire resistance.

It may also be observed that in columns embedded on walls, the maximum restraining forces are very low, between 2 and 4%, when compared with the bare steel columns (See Figures 4.29, 4.30 and 4.31).

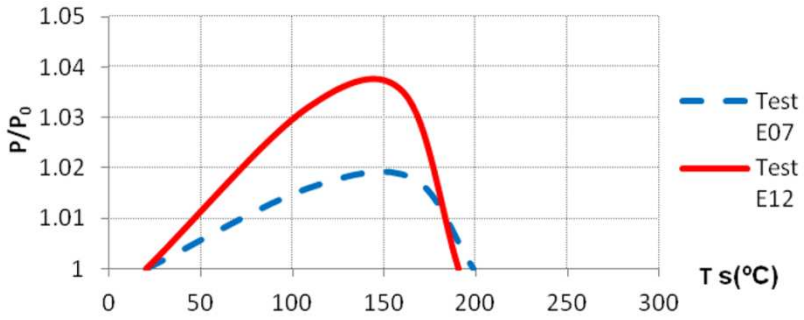

Figure 4.22 - Restraining forces on columns embedded on walls as a function of columns mean steel temperature

4.6.2. Steel Bare Columns

4.6.2.1. Temperatures in the Columns

Figure 4.23 presents the evolution of the furnace and steel column temperatures in function of the time for test reference HEA160-K13-L70. In order to reduce the initial thermal inertia of

the furnace, a pre-heat was provided before the beginning of each test. Thus, instead of 20ºC, the furnace temperature curve starts in some cases at about 150ºC. In the first instants of the test, the furnace temperature is bellow the set point temperature, defined by the programmed ISO 834 heating curve, reaching it eight minutes after the test started. As expected, the evolution of temperature on the steel of the test column is slower than the furnace temperature. This temperature was determined defining the mean temperatures in the five sections defined for the measurement of temperatures, and considering the influence length of each section, to obtain a mean temperature in the whole length of the column.

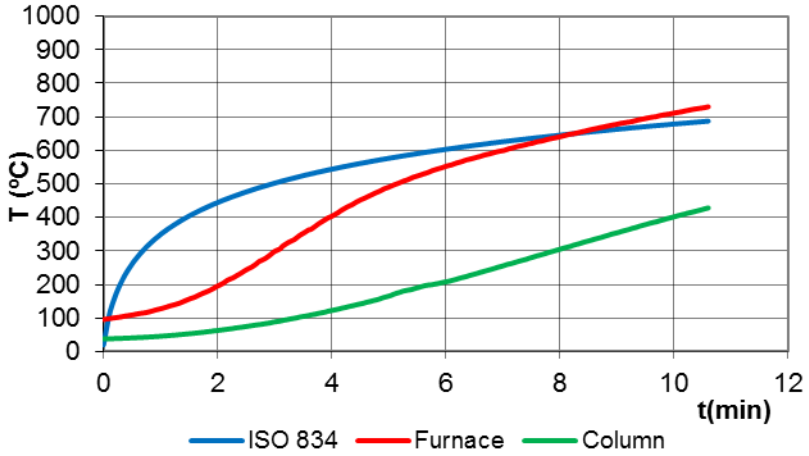

Figure 4.23 – Distribution of temperature in test HEA160-K13-L70

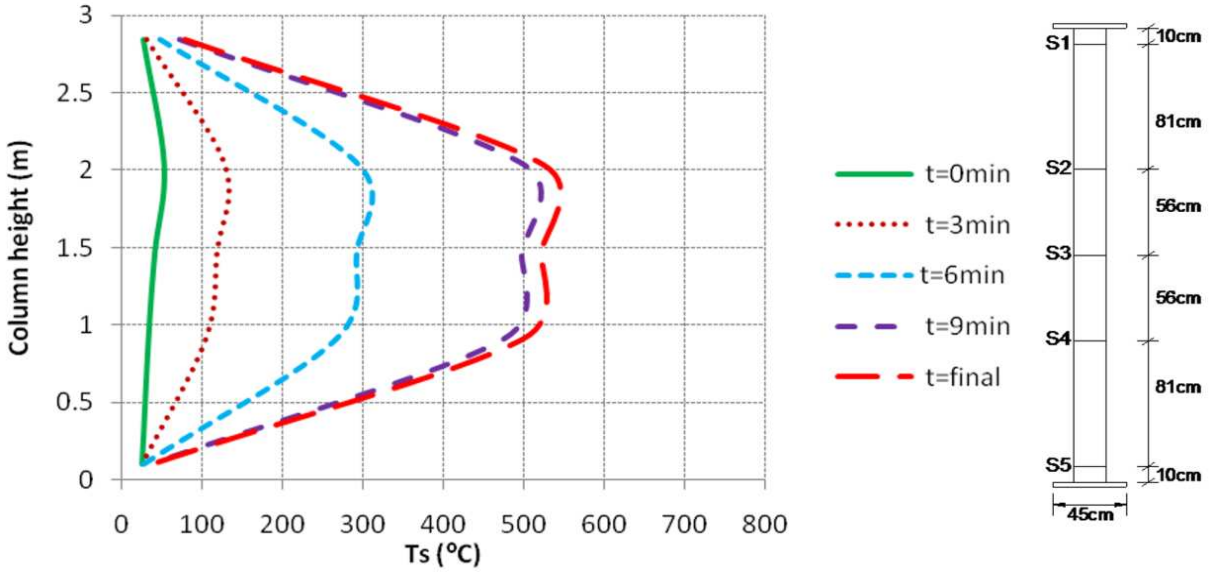

Figure 4.24 -Temperatures along the height of the column in test HEA160-K13-L70.

Figure 4.24 presents the evolution of temperatures along the height of the test column HEA160-K13-L70, for different instants of time, up to the final instant. The distribution of temperatures, presents great thermal gradients, in the direction of the columns end supports. This is explained by the fact that the extremities were not directly exposed to the heating during the test, since they were outside the furnace. It is observed that between sections S2 to S4, which are inside the furnace, the temperature is quite uniform.

4.6.2.2. Axial and Lateral Displacements

Figures 4.25, 4.26 and 4.27 show the evolution of the axial displacements in the test columns as a function of the mean steel temperature, for stiffness of the surrounding structure of 13, 45 and 128 kN/mm, respectively. The dashed curves stand for the lower load level (30%) and the continuous curves stand for the higher load level (70%) tests. The red lines represent the HEA 200 profile, while the blue lines represent the HEA 160 steel section. The shape of the curves is very similar for the two tested cross sections.

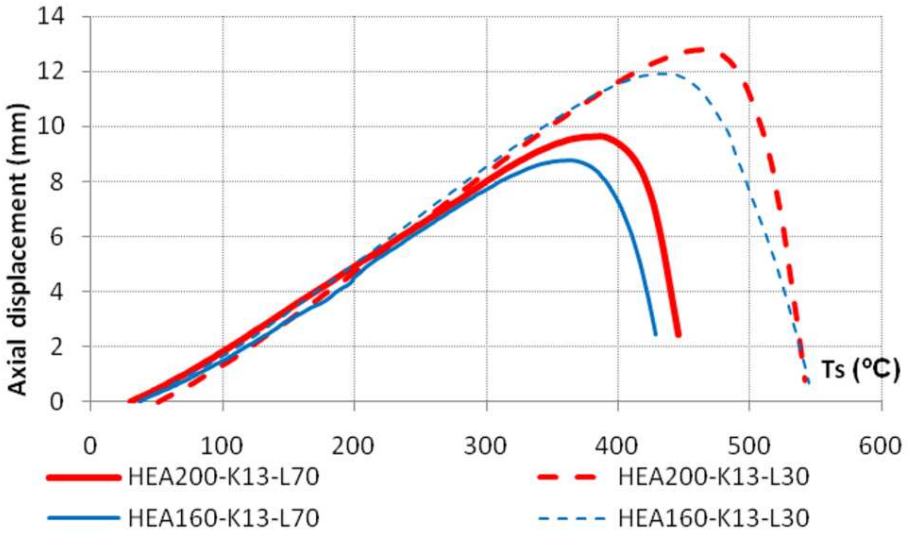

Figure 4.25 - Axial displacements - $K_{A,S}$ =13 kN/mm.

The lower load level leads to higher axial displacements, and also larger critical temperatures. The difference of displacements in the test columns, between the two load levels, is nearly 3.5mm, 2.5mm and 1.5mm for the cases of a stiffness of the surrounding structure of 13, 45 and 128kN/mm respectively.

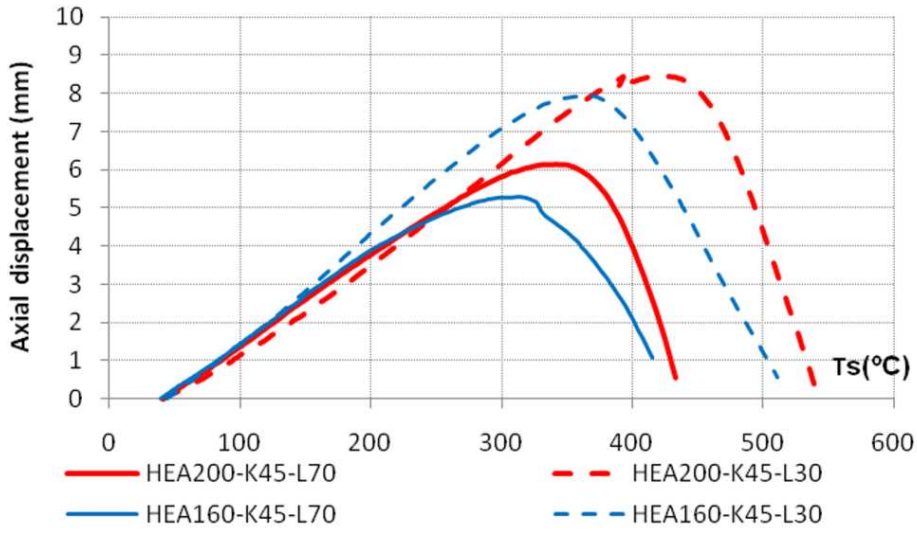

Figure 4.26 - Axial displacements - $K_{A,S}$ =45 kN/mm.

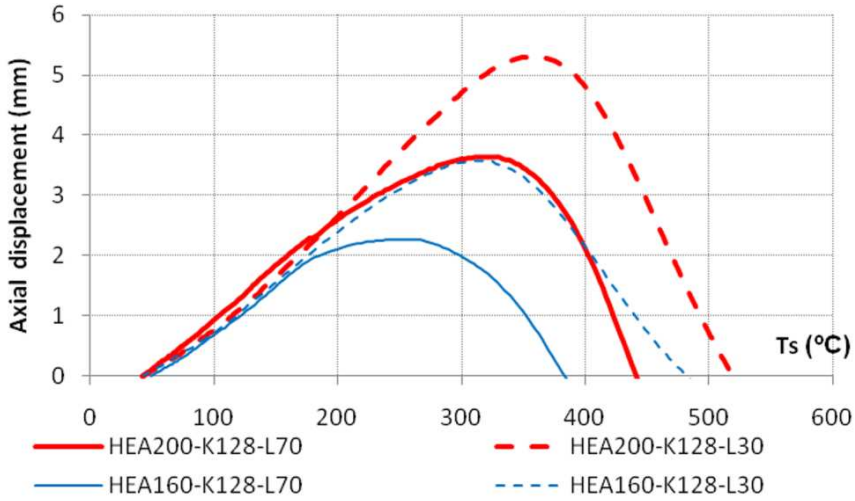

Figure 4.27 - Axial displacements - $K_{A,S}$ =128 kN/mm.

Comparing these figures, it can be observed that the higher stiffness leads to smaller values of the axial displacements. Moreover, the higher the load level, the lower the axial displacements and the critical temperatures.

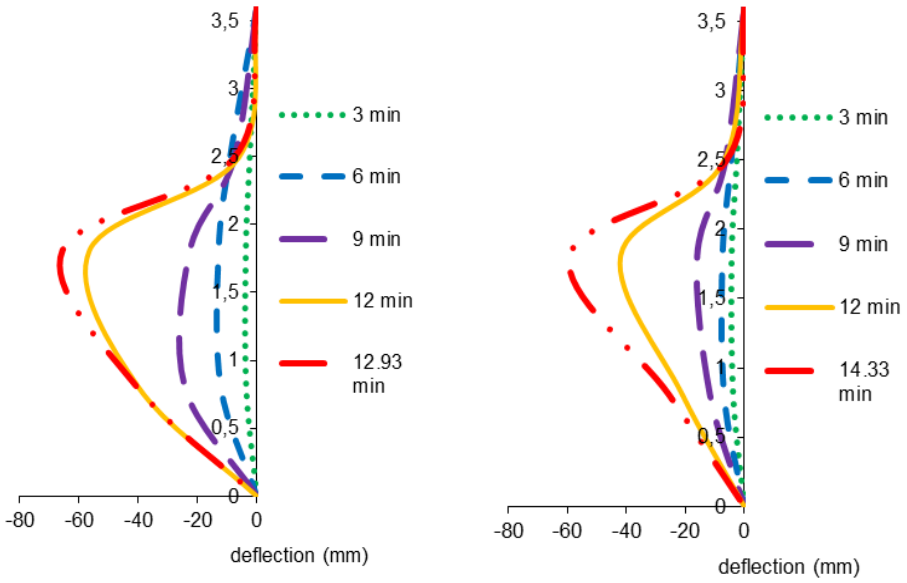

a) HEA160-K128-L30 b) HEA200-K128-L0.3

Figure 4.28 - Lateral deflections around minor axis of the test columns.

Figure 4.28 shows the lateral deflections observed around minor axis in the test columns HEA160-K128-L0.3 and HEA200-K128-L0.3. As expected, larger lateral deflections were observed in the HEA 160 profile. Results of lateral deflections of the other tests are presented in Appendix F.

4.6.2.3. Restraining Forces

Figures 4.29, 4.30 and 4.31 show the evolution of the restraining forces in the test columns as a function of the mean steel temperature, for the axial stiffness of the surrounding structure of 13, 45 and 128 kN/mm, respectively. The restraining forces are presented in a non-dimensional form, in relation to the value of the initial applied load.

The critical temperature is defined in these tests as the time when the restraining forces, after increasing and reaching a peak, decreases reaching again the value of the initial applied load.

The value of the maximum restraining forces is strongly influenced by the stiffness of the surrounding structure. Higher values of the stiffness led to higher values of the restraining forces. The restraining forces, for the load level of 70%, are around 1.2, 1.4 and 1.6 times while for the load level of 30%, are around 1.5, 2.2 and 2.7 times the initial applied load, respectively for the stiffness of 13, 45 and 128 kN/m.

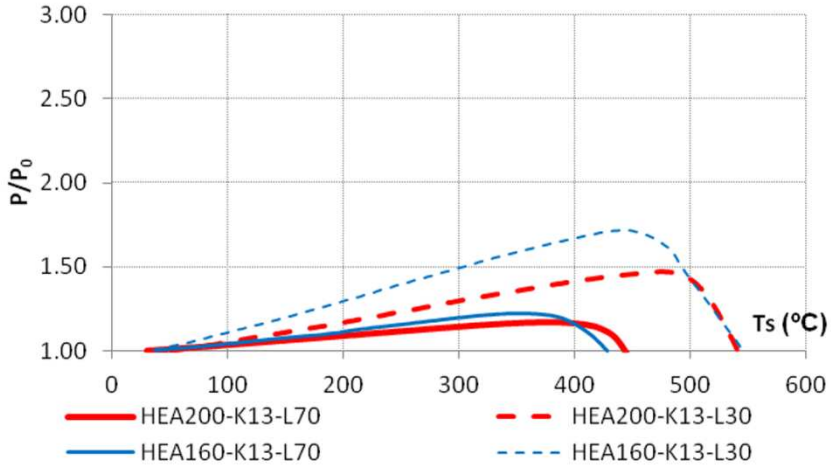

Figure 4.29 – Restraining forces - $K_{A,S}$ =13 kN/mm.

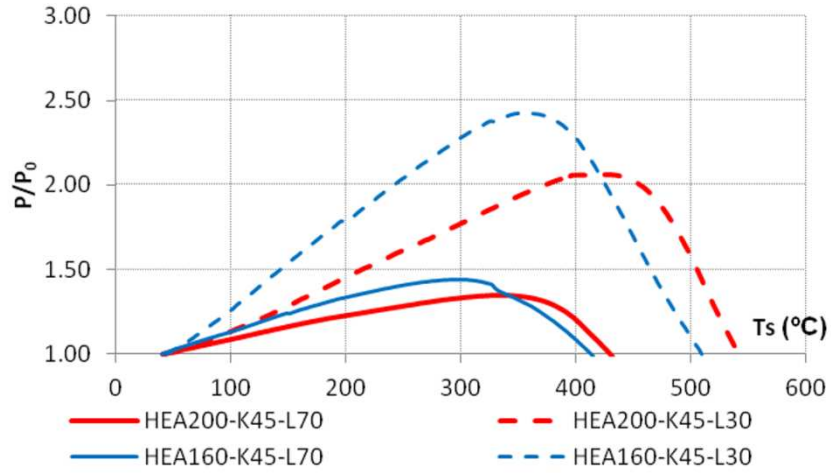

Figure 4.30 – Restraining forces - $K_{A,S}$ =45 kN/mm

The load level influences the value of the maximum restraining forces. Higher load levels lead to smaller values of the restraining forces. The critical temperatures of the test columns were also smaller for the higher load levels. When the load level increases from 30 to 70% the critical temperature reduces around 100ºC.

Comparing figures 4.29, 4.30 and 4.31, it can be observed that the stiffness of the surrounding structure did not influence the critical temperatures of the test columns. In this experimental set-up, associated to an increase of the axial stiffness is an increase of the rotational stiffness which provides an opposite effect to the first one on the column behavior in fire case. The increasing of the axial stiffness lead to a reduction, while the increasing of the rotational stiffness lead to an increase of the critical temperature of the test columns.

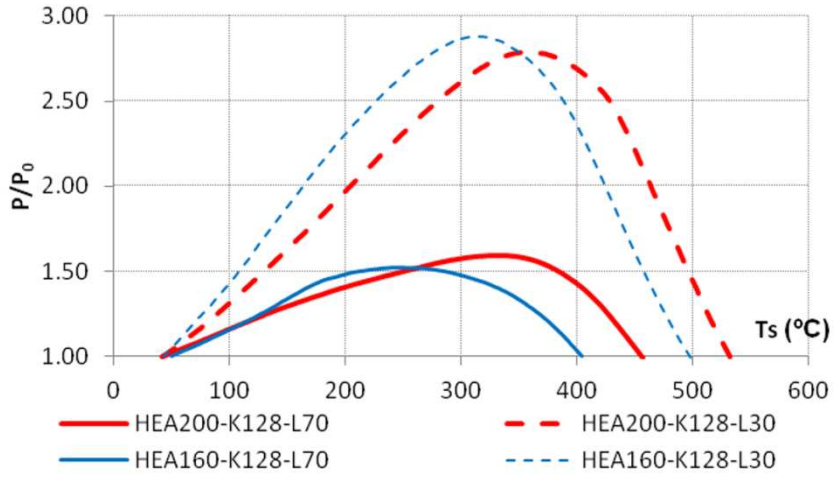

Figure 4.31 – Restraining forces - $K_{A,S}$ =128 kN/mm

Figure 4.32 presents the influence of the eccentricity of the loading on the columns behavior. They are compared the restraining forces for columns tested with loading centered, eccentric in the direction of the minor axis and eccentric in the two principal directions of the cross-section, for a stiffness of the surrounding structure of 13 kN/mm. It can be observed that the critical temperature is influenced by the eccentricity of the loading. The column with eccentric loading in the two principal directions, lead to higher values of the critical temperatures, followed by the one with eccentricity of the loading in direction of the minor axis and the one with centered loading.

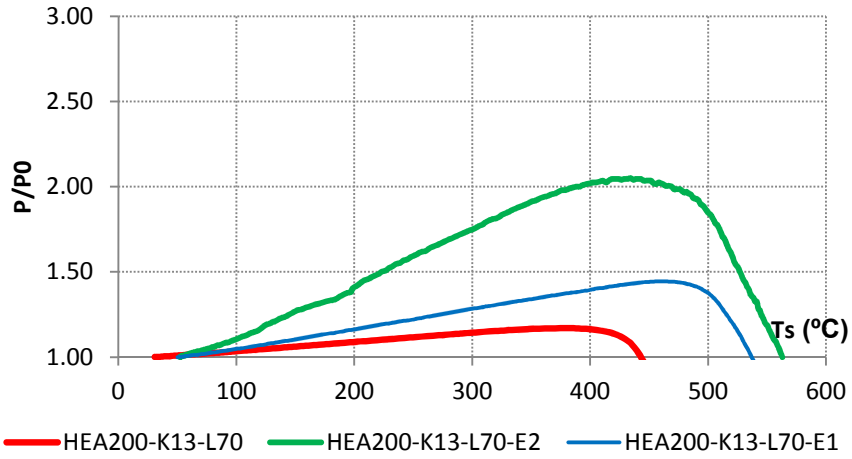

Figure 4.32 – Influence of the loading eccentricity on the restraining forces - $K_{A,S}$ =13 kN/mm.

Concerning the restraining forces in relation to the initial value of the applied loading, they increase more in the column with eccentric loading in the two directions than in the one with eccentric loading in one direction or even centered.

The columns tested with eccentric loading presented also higher critical temperatures than the ones tested with centered loading. This is due to the fact that the initial applied load was lower for the columns with eccentric than the ones with centered loading. The EN 1993-1-1 (2005) methods for determining the buckling load at room temperature of columns with bending and axial force, give very low values of the load. This may be the explanation for this different behaviour of centered and eccentric loaded columns.

4.6.2.4. Rotations

Figures 4.33, 4.34 and 4.35 depicts the evolution of the rotations at the base and top of the test columns as a function of the mean steel temperature, for the tested values of stiffness of the surrounding structure (13, 45 and 128 kN/mm).

The depicted values were obtained from the linear displacements measured with the three LVDT's on the top end plate of the column, and the four LVDT's on bottom. Considering the exact locations of the linear displacement measures, the angle was obtained in miliRads.

The rotations were very similar on the bottom and top of the columns, in all tests.

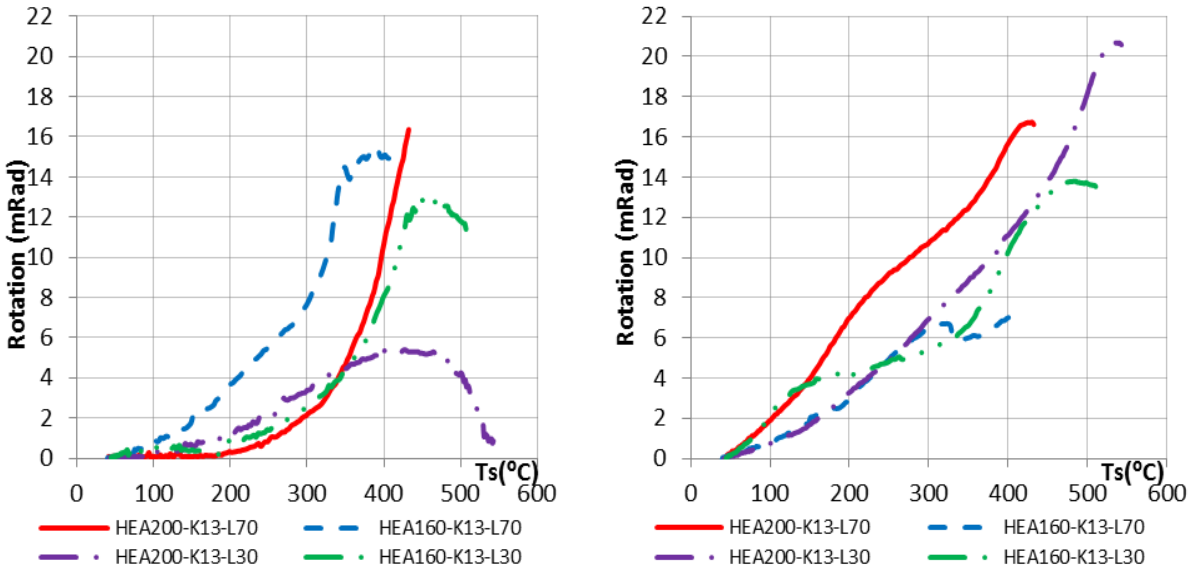

a) b)

Figure 4.33 – Rotations - $K_{A,S}$ =13 kN/mm a) on top b) at the base

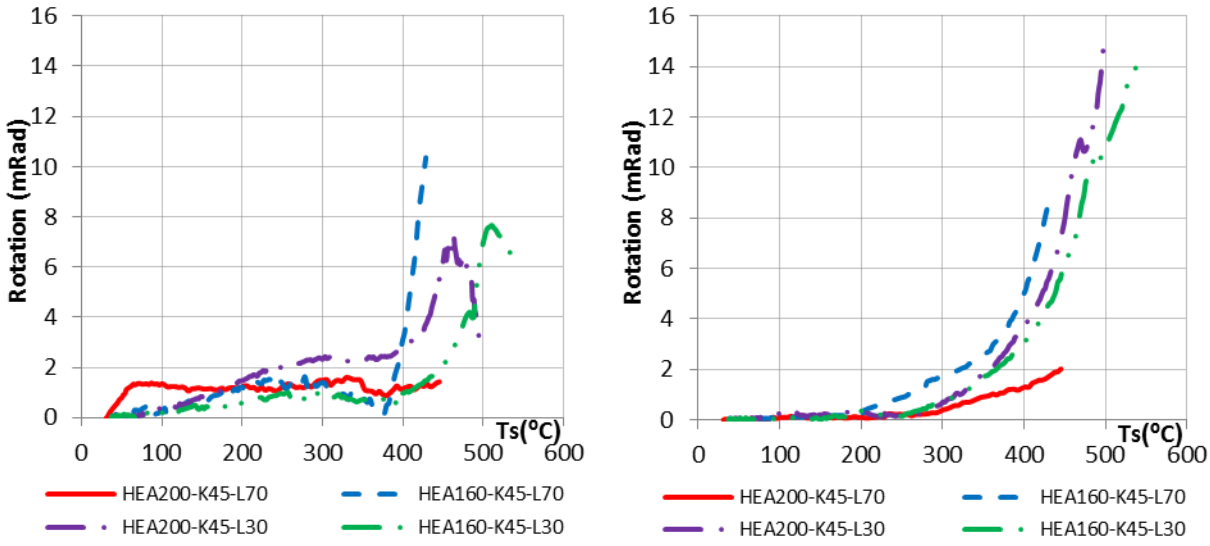

a) b)

Figure 4.34 – Rotations - $K_{A,S}$ =45 kN/mm a) on top b) at the base

In terms of rotations at the base and top of the columns, the influence of the load level was observed in an inversion of rotation in some tests, for the lower load level (30%).

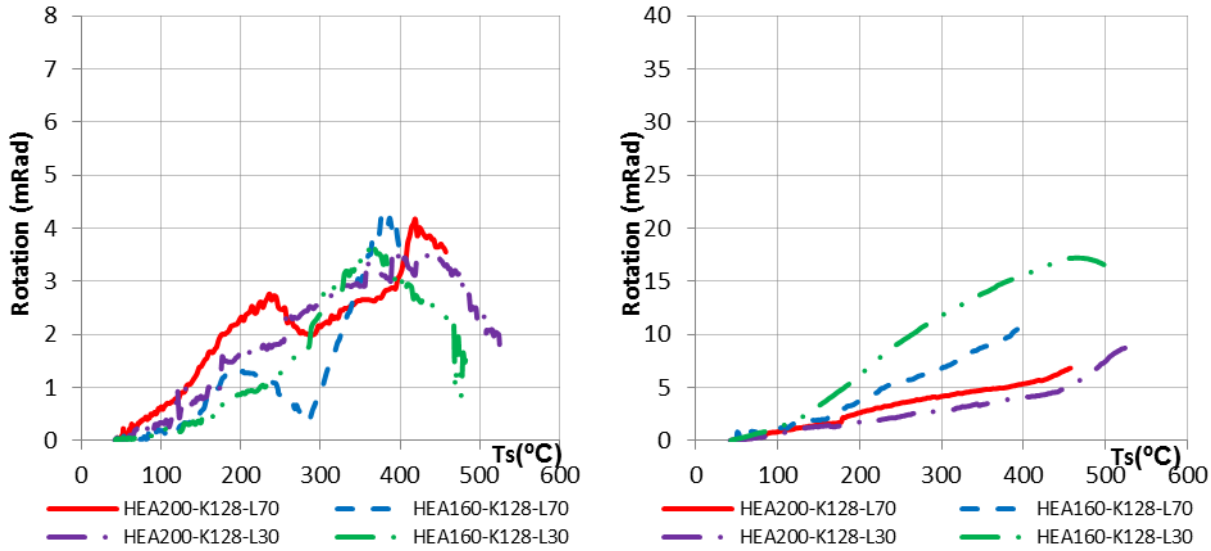

a) b)

Figure 4.35 – Rotations - $K_{A,S}$ =128 kN/mm a) on top b) at the base

In general, the rotations were higher in tests with lower stiffness of the surrounding structure. In fact, with exception of test HEA160-K128-L30, rotations in tests with the higher stiffness of surrounding structure were negligible.

4.6.3. Composite Steel-Concrete Columns

4.6.3.1. Temperatures in the Columns

In Figure 4.36 the evolution of temperatures in the furnace and specimen, for test CSS160-K13-L30, at its mid-height, is represented. It can be observed an acceptable agreement between the heating curve of the furnace and the ISO 834 fire curve. It can also be observed a great thermal gradient from the surface to the interior of the concrete (thermocouples $T_{28,}$ T_{12} and T_{13}). The thermocouple T_{13} is placed in the web of the steel profile, showing a great thermal gradient between the flanges T_{15}. Thermocouple T_{14} gives the temperature in the reinforcement bars, which is very low.

It is quite interesting to observe that from the first 30 minutes of test, the difference between the gas furnace temperature and the mean temperature of the steel profile remains practically constant, equal to 400ºC.

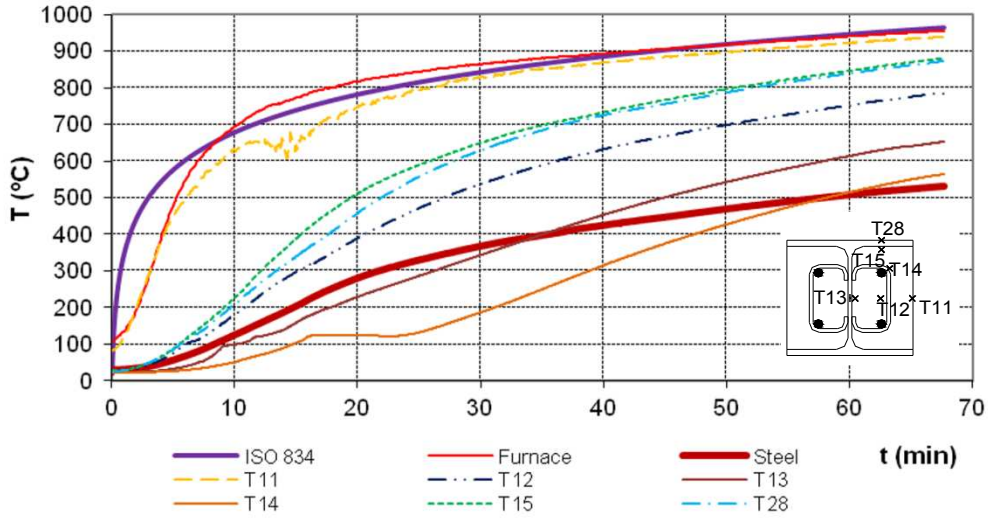

Figure 4.36 – Evolution of temperatures in the cross-section of test column CSC160-K13-L0.3 and furnace

Figure 4.36 shows the evolution of the mean temperatures in the cross sections of the column, in the vertical direction of the test columns, for different instants of time, during the test.

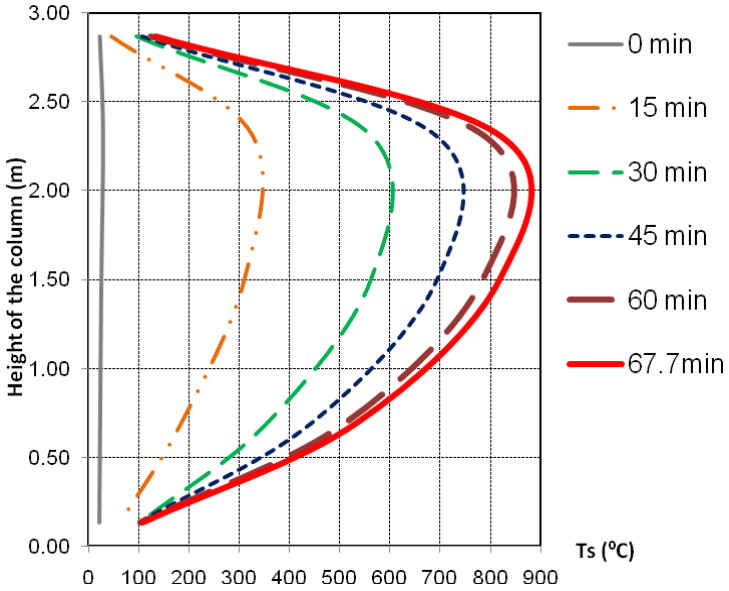

Figure 4.37 – Evolution of mean temperatures in the vertical direction of the test column CSC160-K13-L0.3

The graph of figure 4.37 was obtained plotting the mean temperatures in sections S1 to S5 of the steel profile. This mean temperature was calculated with temperatures of thermocouples T_{15} and T_{28} in the flange, and T_{13} in the web. The temperature in the flanges was considered uniform, and in the web was considered a linear variation from the center to the flanges. The mean value in the cross section was obtained multiplying the temperature of the flanges by its area, plus the temperature of the web multiplied by its area, then divided by the total area of the steel profile cross-section. It should be mentioned that 0.25m on bottom and top of the column were not directly exposed to the heating of the furnace, these parts are in zones of the furnace covers. A great thermal gradient was observed, 200ºC after 15 minutes of test and 450ºC in the end of the test.

4.6.3.2. Axial and Lateral Displacements

Figures 4.38 a) and 4.38 b) show the lateral deflections observed around minor axis in the test columns CSC160-K128-L0.3 and CSC200-K128-L0.3. At first sight the fact that column CSC160 with a higher slenderness value of 1.09 suffers lower lateral deflections than column CSC200 with a slenderness value of 0.87, may seem abnormal. This fact may be explained by the higher value of the non-dimensional rotational stiffness of column CSC160, 2.44, while for column CSC200 is 1.05.

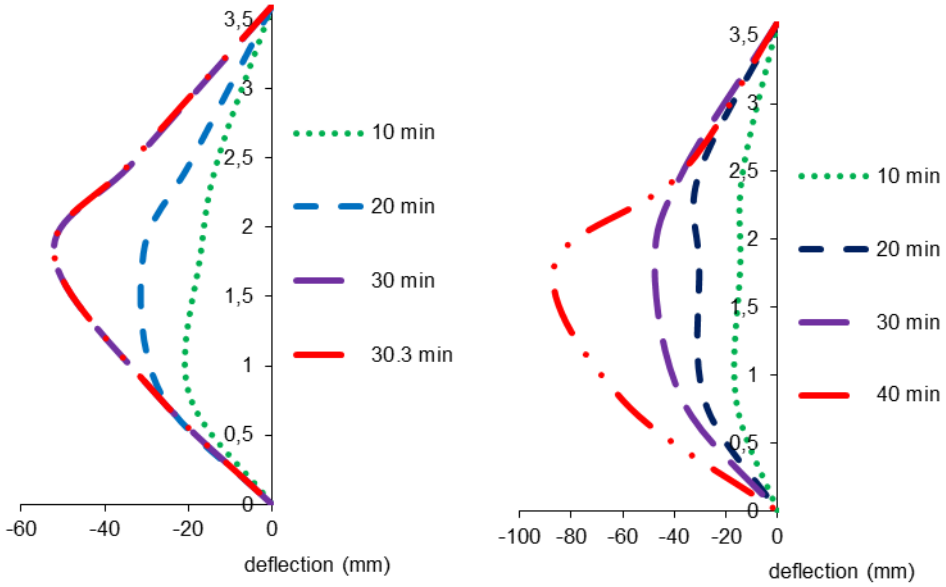

a) CSC160-K128-L0.3 b) CSC200-K128-L0.3

Figure 4.38 - Lateral deflections around minor axis of the test columns.

Figures 4.39 to 4.41 present the evolution of the axial displacement of the columns for the different cases studied. The displacements are plotted versus time. In figure 4.39, for the axial stiffness of the surrounding structure of 128 kN/mm, it can be observed that the lower load level 0.3 lead to higher axial displacements and higher the critical temperatures of the specimens. The agreement between the two cross-sections for two load levels tested was quite good. The difference on the axial displacements between the two load levels tested were 1mm for the test columns CSC200 and 0.5mm for the test columns CSC160.

In Figure 4.40, for the axial stiffness of 45kN/mm, a great difference in the critical temperatures and development of the axial displacement is observed for the two cross-sections tested for each load level. The increase of the load level from 0.3 to 0.7 leads to a reduction in the axial displacement of 3.5mm for the test columns CSC200 and 2mm for the test columns CSC160.

For the axial restraint of 13kN/mm the higher the load level, the smaller are the axial displacements and the critical temperatures. The shape of the curves change between the two load levels tested. In test columns CSC200 the increase of the load level form 0.3 to 0.7 leads to a reduction in axial displacement of 4mm, while for columns CSC160, the same variation of load level leads to a reduction of axial displacement of 2mm. The fact that increasing the load ratio from 0.3 to 0.7 leads to lower reduction in axial displacements in columns CSC160 may be strange. It was expectable that columns CSC160 would suffer a greater reduction in

the axial displacement than columns CSC200. This may be explained by the fact that the non-dimensional axial restraint is higher for columns CSC160 than for columns CSC200.

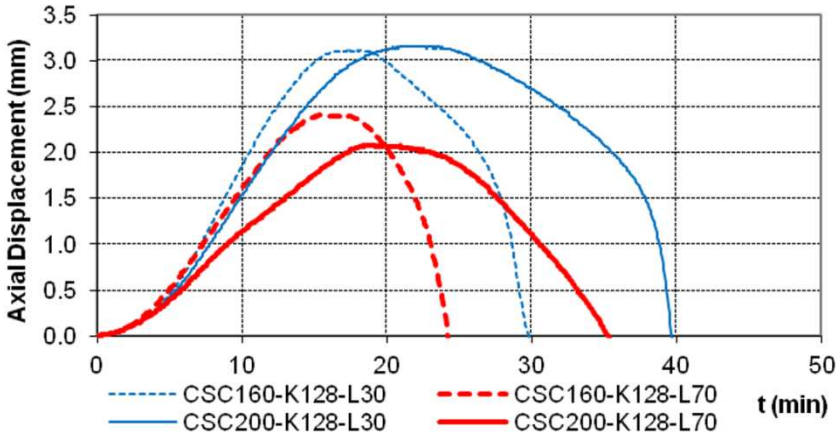

Figure 4.39 - Axial displacements, $K_{A,S}$ =128kN/mm.

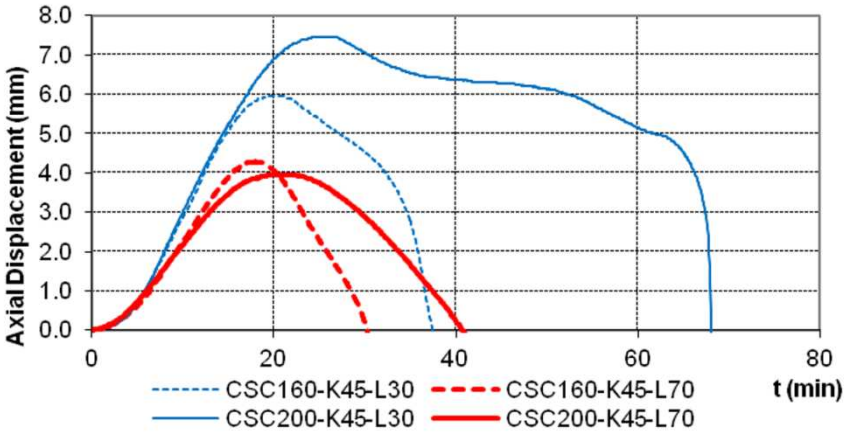

Figure 4.40 - Axial displacements, $K_{A,S}$ =45kN/mm.

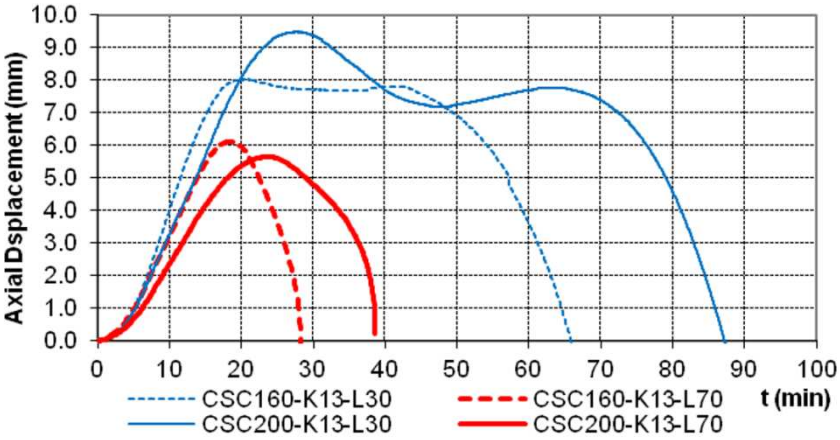

Figure 4.41 - Axial displacements, $K_{A,S}$ =13kN/mm.

4.6.3.3. Restraining Forces

The evolution of the restraining forces, in function of the mean steel temperature of the columns, is depicted in Figures 4.42 to 4.44. A typical behavior is observed in the columns tested: a gentle increase of the restraining forces followed by a sudden decay. In these graphs the critical temperature is defined as the instant in which the axial forces reach again the value of the initial applied forces, i.e., $P/P_0=1$.

In the following figures it can be observed that higher is the load level the smaller is the critical temperatures. Also higher slenderness values lead to lower critical temperatures.
In Figure 4.42, the behaviour of test columns CSC160 and CSC200 is depicted, for the two load levels used, and for a stiffness of surrounding structure of 128 kN/mm. Increasing the load level from 0.3 to 0.7 leads to a reduction in critical temperature of about 100ºC, and a reduction in the maximum of axial restraining forces of about 60% for test column CSS160. For test column CSC200, the same increase in load level provokes a reduction on the critical temperature of 50ºC and a reduction in the maximum axial restraining forces of 35%.
In Figure 4.43, the same type of columns were tested, but with a stiffness of surrounding structure of 45kN/mm. For the test column CSC160, the mentioned increase of load ratio provokes a reduction on the critical temperature of about 50ºC and a reduction in the maximum axial restraining forces of 80%. For test column CSC200, the same increase of load ratio leads to a reduction of 100ºC in the critical temperature and 40% in the maximum axial restraining forces.

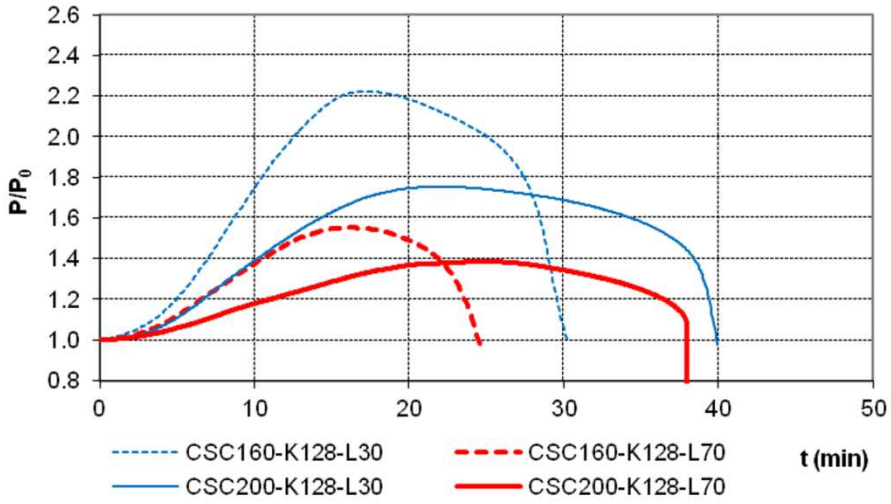

Figure 4.42 - Restraining Forces, $K_{A,S}$ =128kN/mm.

In Figure 4.44, the same analysis can be made, for columns tested with the stiffness of surrounding structure of 13kN/mm. For test column CSC160, the increase of load level from 0.3 to 0.7 provokes a reduction of the critical temperature of about 100ºC and a reduction in

the maximum axial restraining forces of 20%. For tests column CSC200, the same increase of load level leads to a reduction of about 175ºC in the critical temperature and 15% in the maximum axial restraining forces.

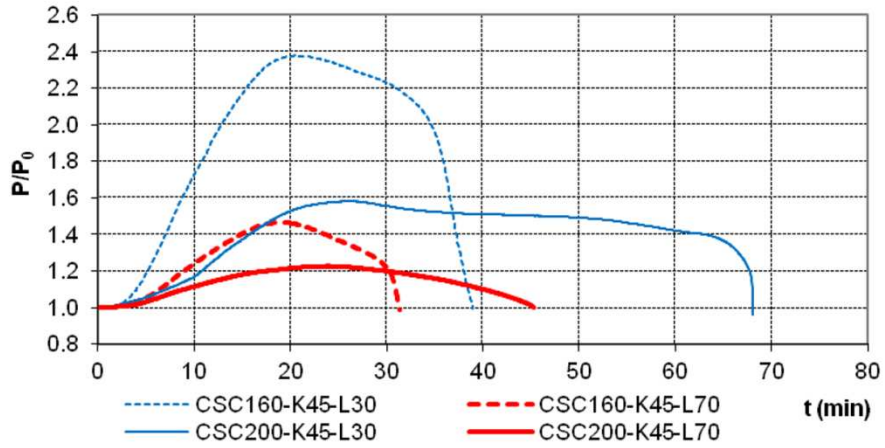

Figure 4.43 - Restraining Forces, $K_{A,S}$ = 45kN/mm.

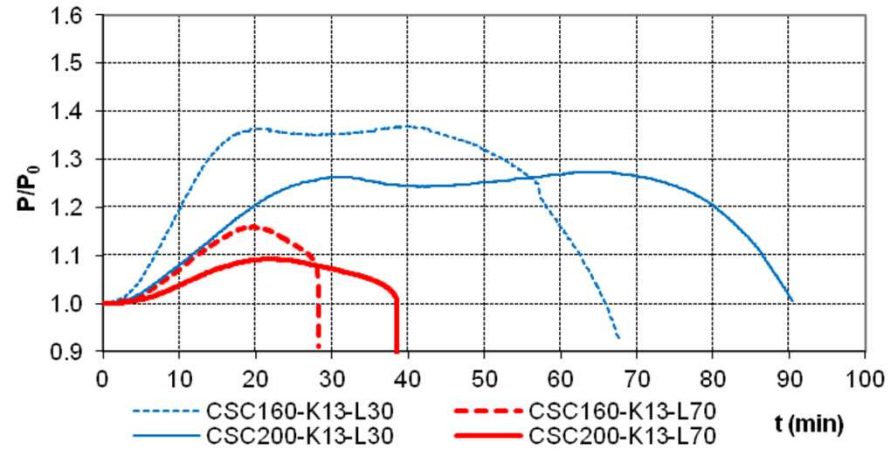

Figure 4.44 - Restraining Forces, $K_{A,S}$ = 13kN/mm.

4.6.3.4. Rotations

Figures 4.45, 4.46 and 4.47 show the evolution of the rotations at the base and top of the test columns as a function of the mean steel temperature, for the tested values of stiffness of the surrounding structure (13, 45 and 128 kN/mm).

These values were obtained using the same calculation process as described for the steel columns.

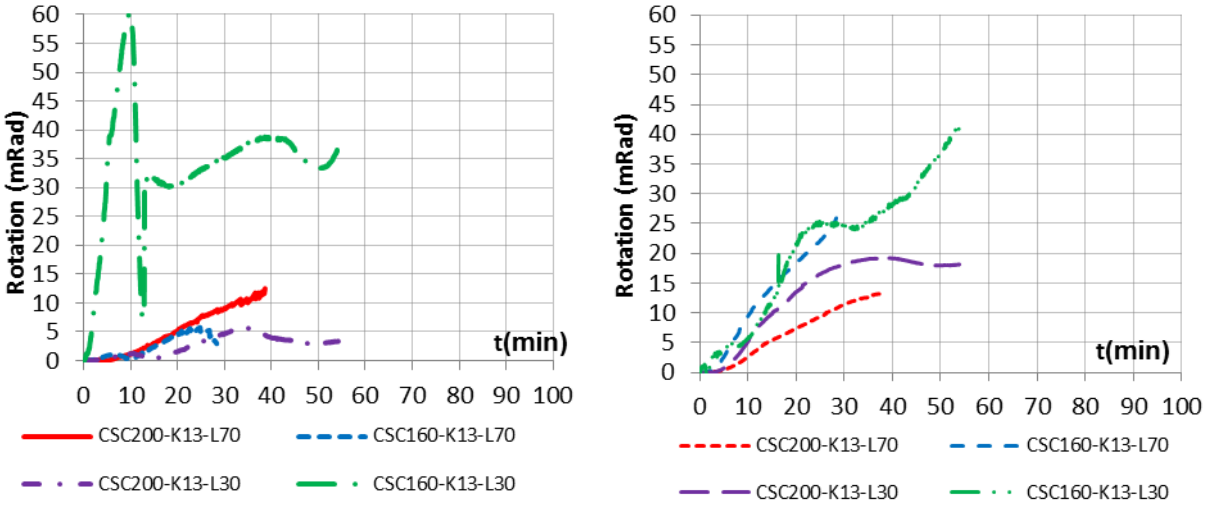

a) b)

Figure 4.45 – Rotations - $K_{A,S}$ =13 kN/mm a) on top b) at the base

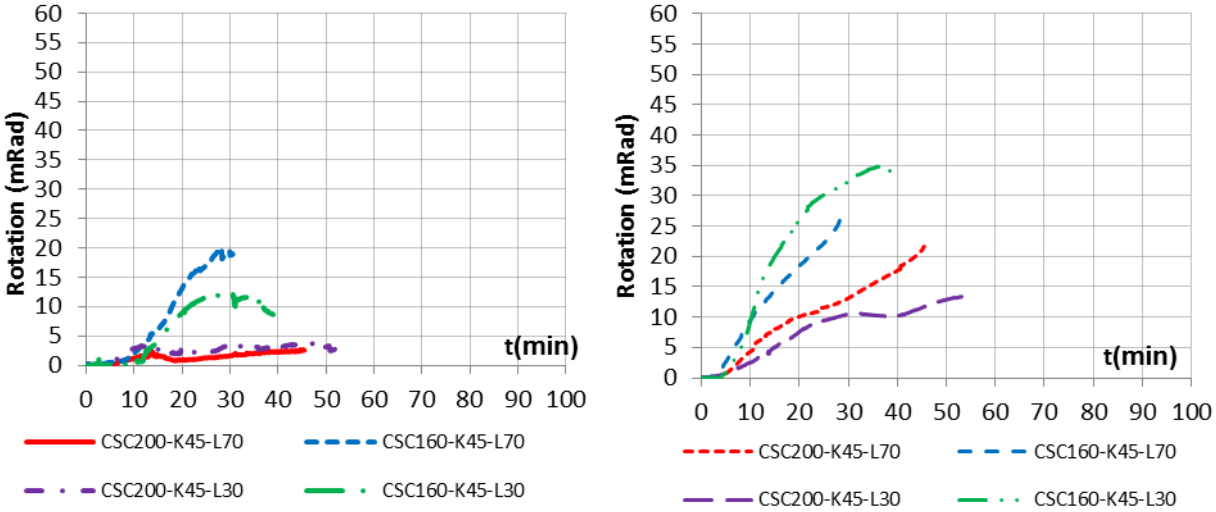

a) b)

Figure 4.46 – Rotations - $K_{A,S}$ =45 kN/mm a) on top b) at the base

In terms of rotations at the base and top of the columns, the influence of the load level was observed in an inversion of rotation in some tests, for the lower load level (30%).

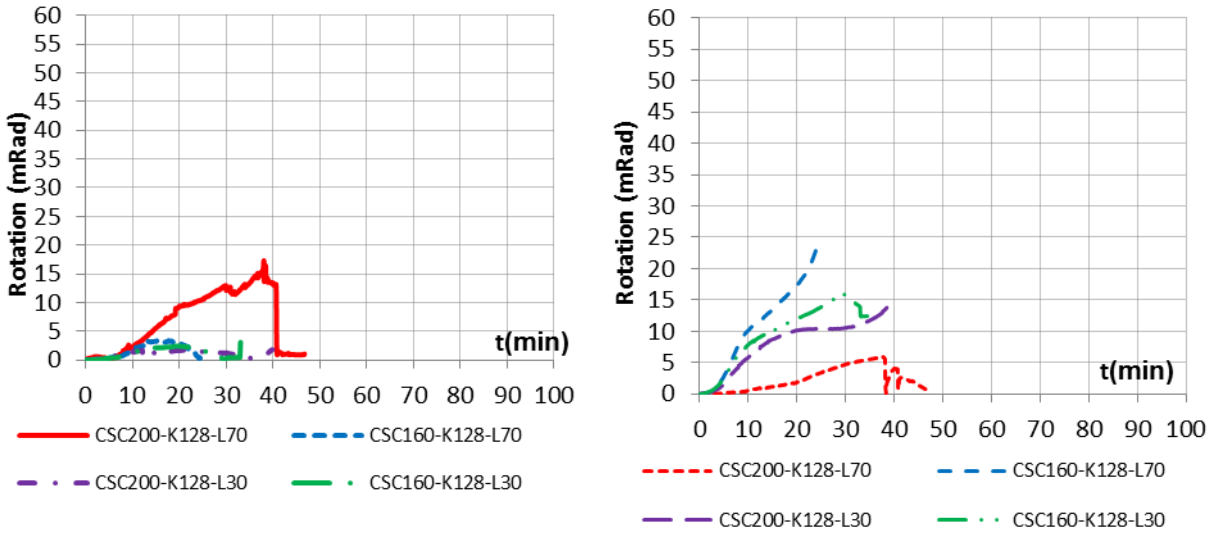

a) b)

Figure 4.47 – Rotations - $K_{A,S}$ =128 kN/mm a) on top b) at the base

In general, the rotations were higher in tests with lower stiffness of the surrounding structure. In fact, with exception of test CSC160-K128-L30, rotations in tests with the higher stiffness of surrounding structure were negligible.

4.7. Comparison of Steel Columns Embedded on Walls, Bare Steel Columns and Composite Steel-Concrete Columns

4.7.1 Comparison of temperatures

In the following graphs, a comparison between the temperatures observed in steel columns embedded on walls, bare steel columns and composite columns is presented. Both the distributions of temperature along the axis of the columns and within the cross sections is depicted.

In Figure 4.48, a comparison can be made between the mean temperatures in the steel profile can be made. In Figure 4.48 a), for a steel column embedded on wall, very low temperatures are observed during the test. After 9 minutes of test, the mean temperature in the cross-section does not exceed 200 ºC. In Figure 4.48 b) and 4.48 c), respectively for steel bare columns and partially encased steel-concrete columns, it is observed a very similar temperature profile in both cases. The main difference is the duration of the test. In the bare column, the critical time was 10.6 minutes, while in the composite column, the critical time was 30.3 minutes.

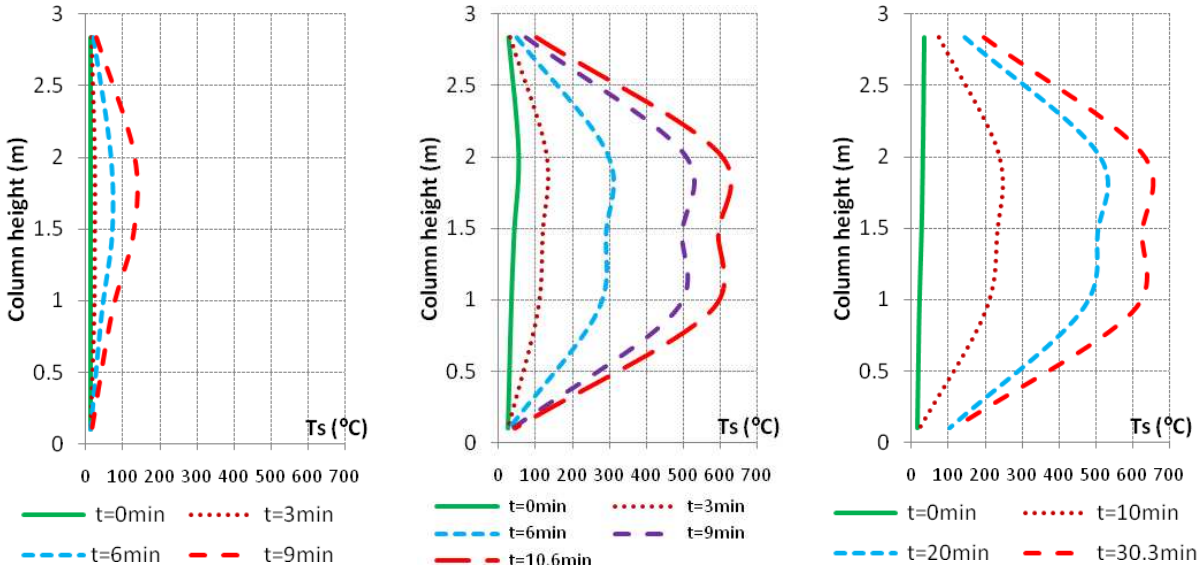

a) b) c)

Figure 4.48 – Temperatures along the height of the columns a) Steel column embedded on walls E07 b) Bare steel column HEA160-K13-L70 c) Composite column CSC160-128-L30

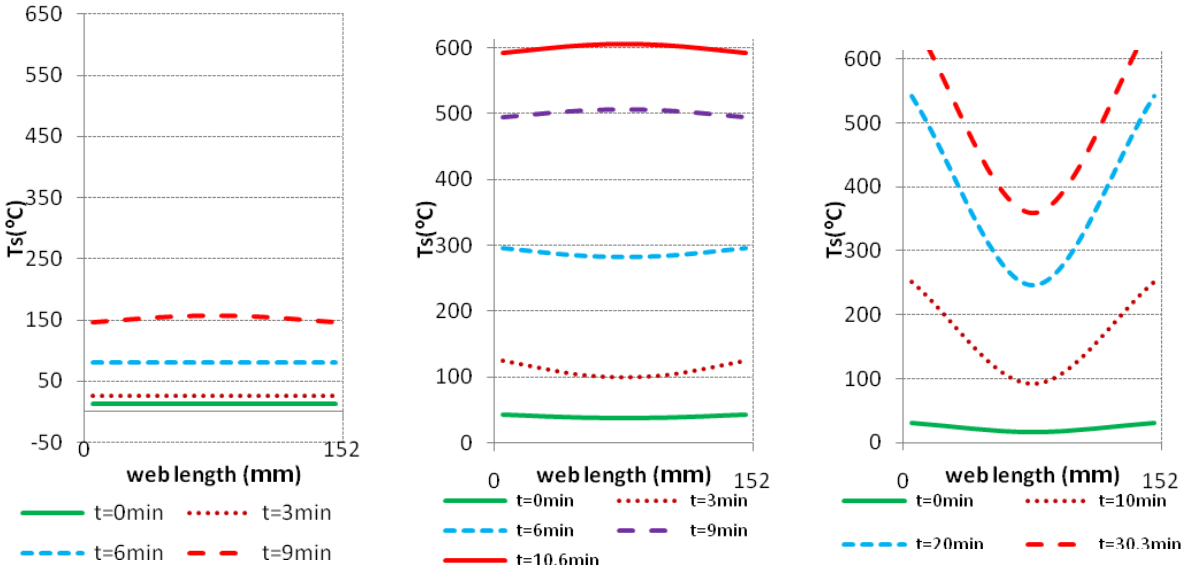

a) b) c)

Figure 4.49 – Temperatures within the web length a) Steel column embedded on walls E07 b) Bare steel column HEA160-K13-L70 c) Composite column CSC160-128-L30

In figure 4.49 a) a uniform distribution of temperatures was observed. This is due to the fact that test E07 was performed with the web parallel to the wall. This test was performed with load. The contact with the wall is observed in the very low temperatures attained. In figure 4.49 b), nearly the same temperature profile was observed, but with higher temperatures, due to the fact that it is a bare column. In Figure 4.49c), a variation of temperatures from the

flanges to the centre of the web is observed, due to the contact with the concrete between flanges.

It can be observed that both the contact with the walls and the presence of concrete between flanges is very effective in reducing the temperatures.

4.7.2 Comparison of restraining forces

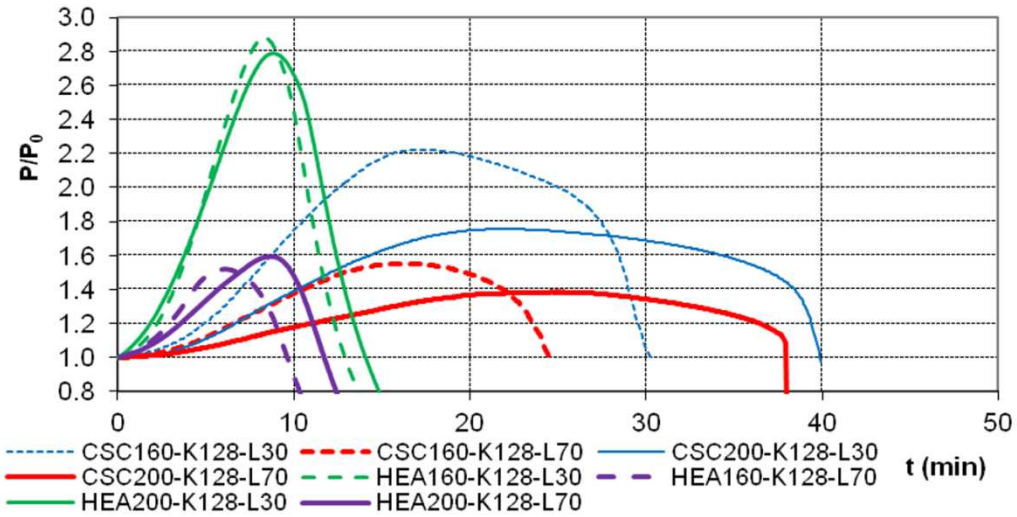

Figure 4.50– Comparison of the evolution of the restraining forces for composite and steel bare columns, $K_{A,S}$ = 13kN/mm

In figure 4.50, a comparison between bare steel columns and the composite columns is presented, in the time domain.

The influence of the concrete is obvious, providing greater fire resistances, and lower increases of the restrsining forces.

4.7.3 Comparison of vertical displacements

In figure 4.51, the same comparison between bare steel columns and the composite columns is presented, concerning the axial displacements. The conclusions are nearly the same.

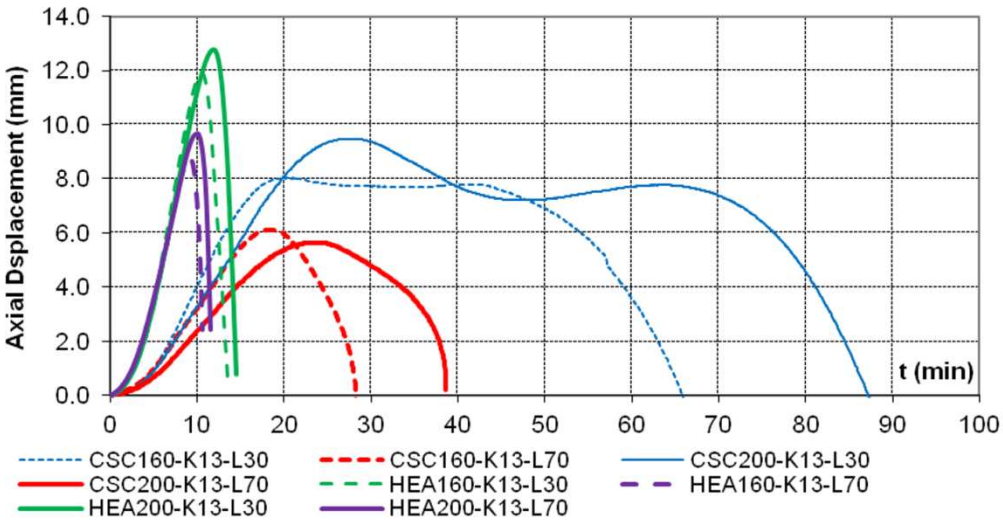

Figure 4.51 – Comparison of the evolution of the vertical displacements for composite and steel bare columns, $K_{A,S}$ = 13kN/mm

4.8. Columns after test

4.8.1. Columns Embedded on Walls

The steel columns embedded on walls had a differential heating characterized by greater temperatures on the exposed side, leading to huge thermal gradients within the cross-section. This difference of temperatures leads to a greater thermal expansion of the heated zone of the steel profile.

Due to the restraint provided by the surrounding structure to the column, the thermal elongation was transformed in stresses, which being greater on the hot side, lead to a different mode of failure.

The thermal bowing is a phenomenon in which the differential thermal action leads to an inversion of the deflection in the structural element, from one to the other side. Figure 4.52 presents column E13, after test. This column has suffered at first, a deflection towards the side of the fire, and afterwards a deflection towards the opposite side, outside of the fire. It can also be observed in this figure that the walls prevented the column to bend around minor axis.

Thermal bowing is most likely to happen in steel columns with the web perpendicular to the wall surface, but it was also observed in case of the steel profile placed with the web parallel to the wall surface, as long as the upper beams are strong enough to withstand the applied load (see Figure 4.54).

Figure 4.52 - Column E13 after test - web perpendicular to wall – wall thickness 100mm - HEA 160

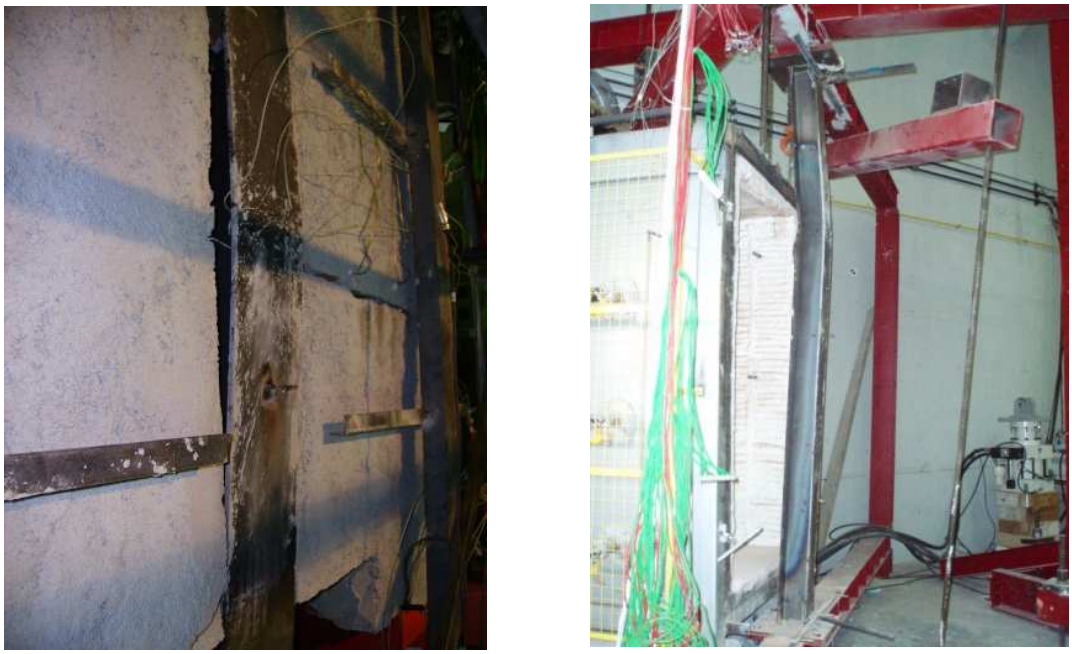

a) b)

Figure 4.53 - Column E02 after test - web perpendicular to wall – wall thickness 140mm - HEA 160

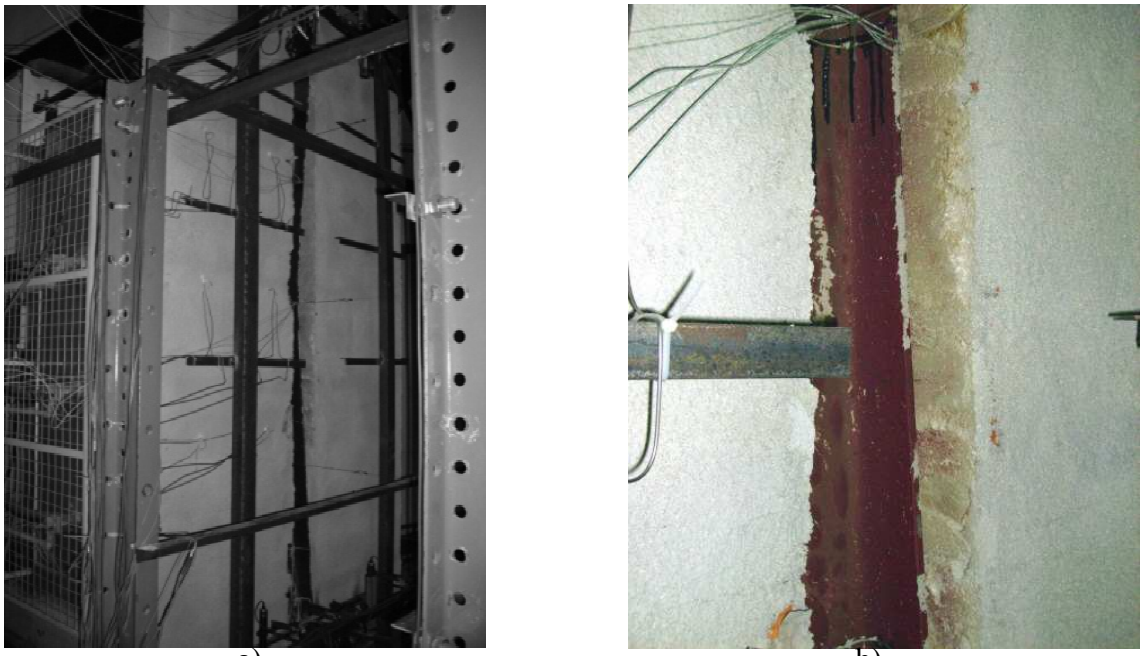

a) b)

Figure 4.54 - Column E01 during and after test - web parallel to wall – wall thickness 140mm - HEA 160

The differential heating provoked a redistribution of bending moments, moving the column from one to the other side, following the corresponding lateral deflections of the column.

In figure 4.53, column E02 after test is observed. A HEA160, with the web perpendicular to the wall surface, is tested. The wall is 140mm thick, about the same column width. In this case, the thermal gradient provoked the same effect as in test E02, leading to buckling in the plane of the wall. The wall plays an important role in preventing the sudden failure of the column.

In figure 4.54, column E01 after test is observed. This specimen is an HEA160, with the web parallel to the wall, which was 140mm thick. In this case, the same behaviour of deflection towards the fire, and then to the opposite side was observed.

4.8.2. Steel Columns

Figures 4.55 to 4.57 show the failure modes of the steel bare columns.

The failure modes of the steel columns were mainly due to instability by global buckling (Figure 4.55a)) and in some cases local buckling also occurred (Figure 4.55b)).

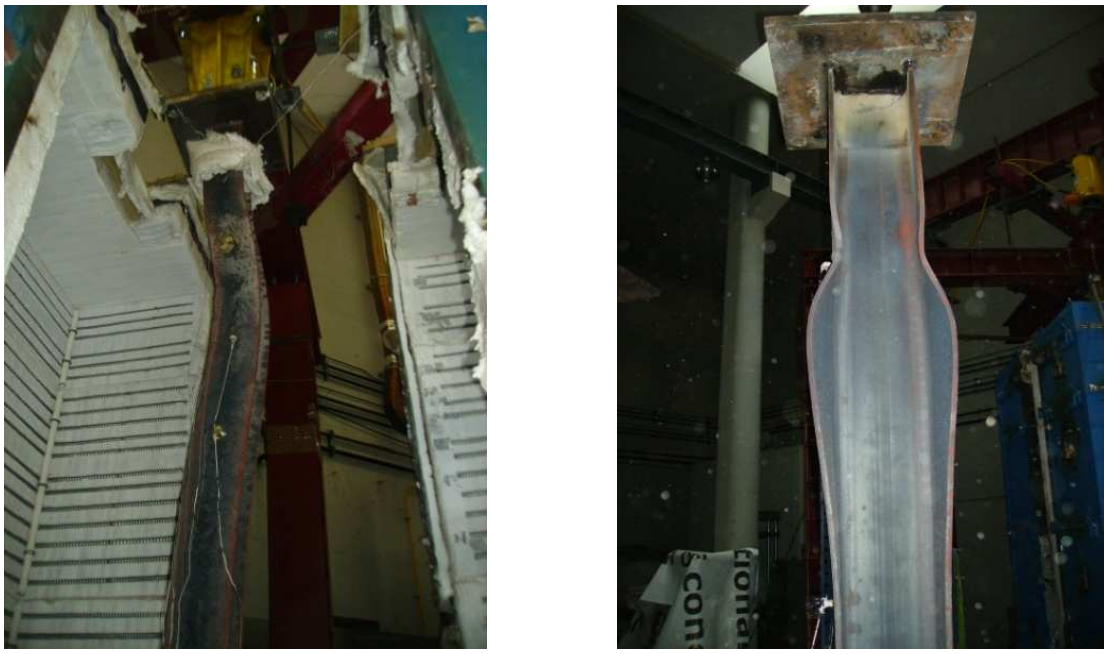

a) b)

Figure 4.55 - Failure modes of the columns after test SC160-K45-L70 b) SC200-K128-L30

Local buckling was mainly observed in the HEA200 steel columns. In the tests of these columns, both local and global buckling was observed (Figure 4.56 a) and b)).

a) b)

Figure 4.56 - Failure modes of column SC200-K13-L70 after test a) global failure b) local failure

In the HEA160 columns, in most of the columns, only global buckling was observed.

a) b)

Figure 4.57 - Failure modes of column SC200-K13-L70-E2 after test a) global buckling b) local buckling

Local buckling is dependent on the width-to-thickness ratio of the steel plates. The width-to-thickness for columns HEA200 was 20, while for columns HEA160 was 17.8. This failure mode may be justified by the small thickness of the flanges of the HEA steel profiles and might have not occurred if HEM or HEB steel profiles had been used in the columns, leading to lower values of the width-to-thickness ratio (between 6.95 and 13).

Global buckling is justified by the higher slenderness ratio of the tested columns and it is characterized by a drop reduction in the columns strength. In fact, it was observed in the tests that the failure mode changes from local to global buckling when the slenderness ratio changes from 50 to 60. Regardless of the stiffness of surrounding structure, columns HEA200 (slenderness ratio=50.6) failed with local and global buckling and columns HEA160 (slenderness ratio=63.3) failed by global buckling. A slenderness of 50 is thought to define for these columns the border between the inelastic and elastic buckling range.

4.8.3. Composite Steel-Concrete Columns

Figures 4.58 to 4.59 show a representative view of the composite columns after the fire tests. All the tested specimens were observed to fail by global buckling. In these columns regardless the load level, type of cross section, and stiffness of surrounding structure, only global buckling was observed. The absence of local buckling can be explained by the presence of the concrete between flanges. This concrete is beneficial, not only in providing thermal insulation, but also in preventing local buckling of the flanges.

a) b)

Figure 4.58 - Columns after test a) column of test CSC200-K128-L30 b) column CSC160-K13-L30

a) b)

Figure 4.59 - Columns after test a) CSC200-K13-L70 b) CSC160-K13-L70

a) b)

Figure 4.60 - Columns after test a) column CSC200-K13-L70 b) column CSC160-K13-L70

In Figure 4.60, the detachment of the concrete between flanges is observed. It is also observed that no spalling occurred. Only the detachment due to large displacements and deformations.

a) b)

Figure 4.61 Detachment of concrete on the columns subjected to fire a) column CSC200-K13-L70 b) column CSC160-K13-L70

4.9. Sinopsis

The main conclusions regarding steel columns embedded on walls are related to thermal bowing. Columns in contact with walls under a fire event, are submitted to a huge thermal gradient which is responsible for an inversion of displacements and bending moments from the heated to the unheated side of the column. The columns in this case, seem to suffer bending, instead of buckling. The walls have a favorable effect in preventing local buckling of column flanges and in case of columns with the web perpendicular to the wall, prevent buckling around minor axis, providing an increase on fire resistance.

For cases with the web parallel to the wall surface, it was concluded that the walls play an important role in reducing the temperatures on the unexposed half of the flanges and also in the web. While for cases with the web perpendicular to the wall surface, a quite interesting result was observed, in the unexposed face of the flange the temperatures were slightly higher with the thicker wall. On the contrary on the exposed flange the temperatures were higher for the thinner walls.

The behaviour of a steel column subjected to fire is known to be dependent from its interaction with the building surrounding structure. In particular, the restraint to thermal elongation is an important factor which has a great influence on the column fire behaviour. This influence may be considered in two parts: an axial restraint, which provides a detrimental effect on the columns fire behaviour, and a rotational restraint, which provides a beneficial effect on the columns, in case of fire.

In the Laboratory of Testing Materials and Structures of the University of Coimbra, an experimental set-up was conceived and constructed, to perform fire resistance tests on columns with restrained thermal elongation. In this experimental facility, a full-scale three-dimensional restraining frame was used to simulate the adjacent structure to the column in fire. A mechanical load as well as a thermal load were applied using an hydraulic jack and an electrical furnace, to simulate the real conditions experimented by the columns in real buildings under fire.

This study, presents the results of a series of experimental tests on the effects of the restraint of the surrounding structure on the fire resistance of bare steel and composite steel-concrete columns, inserted in buildings. The purpose of these tests is to evaluate the influence of the load level, the stiffness of the surrounding structure, the slenderness of the column, and the rotational restraint on the column extremities on its fire resistance.

The purpose of this work was also to provide quality experimental data on the behaviour of a restrained column in fire, and to evaluate the influence of the mentioned parameters on the fire resistance of the columns, in particular with a strong rotational restraining.

5 FIRE RESISTANCE TESTS ON COLUMNS USING AN HYBRID SYSTEM

5.1 Introduction

The fire parts of the Eurocodes, allow the designer the possibility of using analytical and numerical methods in order to guarantee the adequate fire resistance of the structures, apart from the expensive experimental tests. Both advanced calculation methods and single elements or parts of structures are allowed. In a single element analysis, the mechanical action of the surrounding structure in which the structural element is inserted, is considered as "indirect fire action". However, the Eurocodes allow the designers to neglect these actions, in the case of a single element analysis, subjected to the normalized fire.

Experimental tests and numerical studies carried out in the past, by other researchers, in steel columns with restrained thermal elongation, have pointed out that the fire resistance in these elements can be significantly reduced, due to this restraint to thermal elongation. However, this has not been observed in the experimental part of this thesis.

A set of tests was performed in the Federal Institute for Materials Research and Testing (BAM), in Berlin, in Germany, in steel and composite steel-concrete columns under fire conditions. This chapter describes the experimental set-up of the Laboratory, the set of fire resistance tests carried out, and a comparison with the tests carried out at the University of Coimbra (FCTUC), in Portugal.

In classical fire resistance tests, building elements are considered as stand alone elements. In a real fire however, each building element is interacting with adjacent elements. This behaviour is also supported by numerical calculations. Additionally, there is a current international trend for a change in the design procedure from Descriptive Methods to Performance Based Design. This will require the development of special experimental techniques in order to run a fire resistance tests in a more realistic manner and to get a set of continuously acquired data representing the mechanical boundary conditions and temperature field of the specimen during the test.

A great effort is being put in the development of three-dimensional experimental set-ups in both Institutions, in order to perform experimental tests on load-bearing elements, under fire situation, reproducing as much as possible the conditions to which the columns are submitted in real buildings.

In the BAM laboratory the stiffness of the surrounding structure is performed using the so-called substructuring method. Due to this concept, the entire building is divided in two parts, which are connected through a special hardware-software interface. One part is represented by the column, under test in a special furnace, whereas the remaining building environment is simulated in-line by a computer model.

5.2 The Substructuring Method

In contrast to real fires, in classical fire resistance tests building elements are considered as stand-alone elements without interaction with the surrounding building. In order to run a fire test in a more realistic way, the development of special experimental techniques is required. As a contribution to overcome the situation the application of the substructuring method, a special hybrid method has been adopted to fire engineering. The next paragraphs give a presentation of the concept including a short description of utilized system components (Korzen et al., 2006)

Due to the concept of hybrid substructuring (Figure 5.1), the entire building is decomposed in two parts: one part is represented by the building element under test, i.e. the column specimen, whereas the remaining building environment is simulated by an analytical or numerical model. Fire Engineering is characterized by static loadings and generally a nonlinear thermo-inelastic behaviour of the simulated substructure. On the other hand, the communication between the experimental and simulated substructure is of the same type: forces and moments at the boundaries of the specimen, i.e., at the upper and lower bearing of the column, are measured and utilized for the computation of the corresponding displacements and angles, which are sent to the specimen in order to keep the entire building in mechanical equilibrium with its prescribed overall boundary conditions.

The substructuring method plays an important role at the *BAM* column furnace (Figure 5.1). Mechanical and thermal actions are applied through this device to the specimen under test. Whereas the thermal set point is a known to be function of time for the mean gas temperature before starting the test, the mechanical set point has to be calculated online during a fire test in substructuring mode.

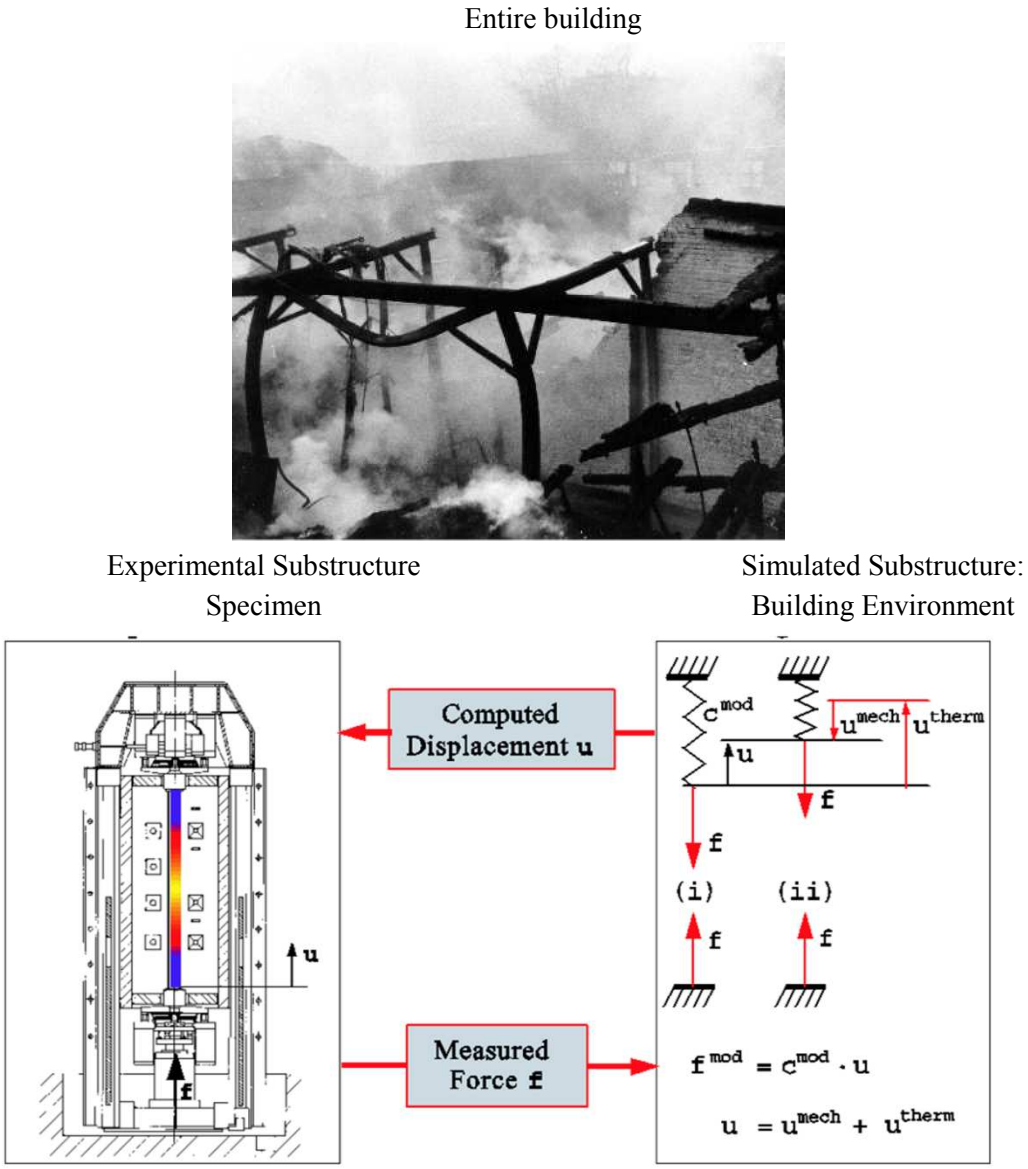

Figure 5.1– Substructuring method – basic idea, (Korzen et al., 1999)

5.3 Experimental Set-up

The mechanical loading of the columns can be achieved by six analog servo-hidraulic control loops representing two rotation degrees of freedom perpendicular to each other for bending at the upper and lower bearing as well as one channel for bottom axial and one for top horizontal loading.

One of these channels with its substructuring supplement is presented in more detail in Figure 5.2. In substructuring mode the PID analog controller is running in displacement control, i.e.

it reads displacement values from a displacement transducer, compares it with the target values and gives a corresponding signal via the servo valve to the hydraulic actuator (inner loop). The necessary displacement target values are generated from measured displacement values, which can be helpful for supplementary on and offline analysis, are sent via an analog digital converter (ADC) to the PC, (Korzen et al., 1999)

It is bi-directionally connected with another PC, which operates as a simulation and supervision computer. New displacement values are calculated on this machine. Additionally it represents the necessary user interface, e.g. for changing experimental parameters during the test. Both activities, i.e. simulation and supervision, do not disturb the continuously running target generating process (outer loop), which enters via a digital analog converter (DAC) the inner loop. This concept represents a strong and necessary improvement in comparison with earlier approaches. A reliable communication between the servo-hydraulic system and the computer, as it is e.g. performed by the inner and outer loop, is the heart of the substructuring method (Korzen et al., 1999).

From the control algorithm point of view the principle is very simple: it is composed by three basic steps, i.e. a) Read measured forces and moments, b) Compute target displacements (via the Substructuring Model) and c) Impose target displacements are characterizing the substructuring method in fire engineering. It belongs to the class of hybrid methods, which represents the state-of-the-art in experimental mechanics.

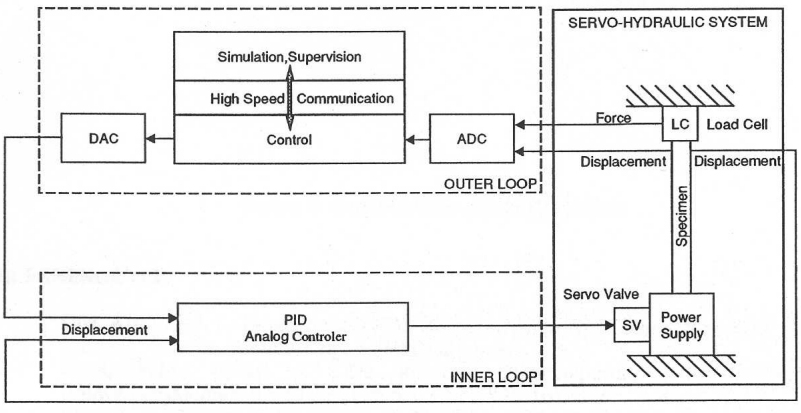

Figure 5.2– Inner and outer loop of one control channel, (Korzen et al., 1999)

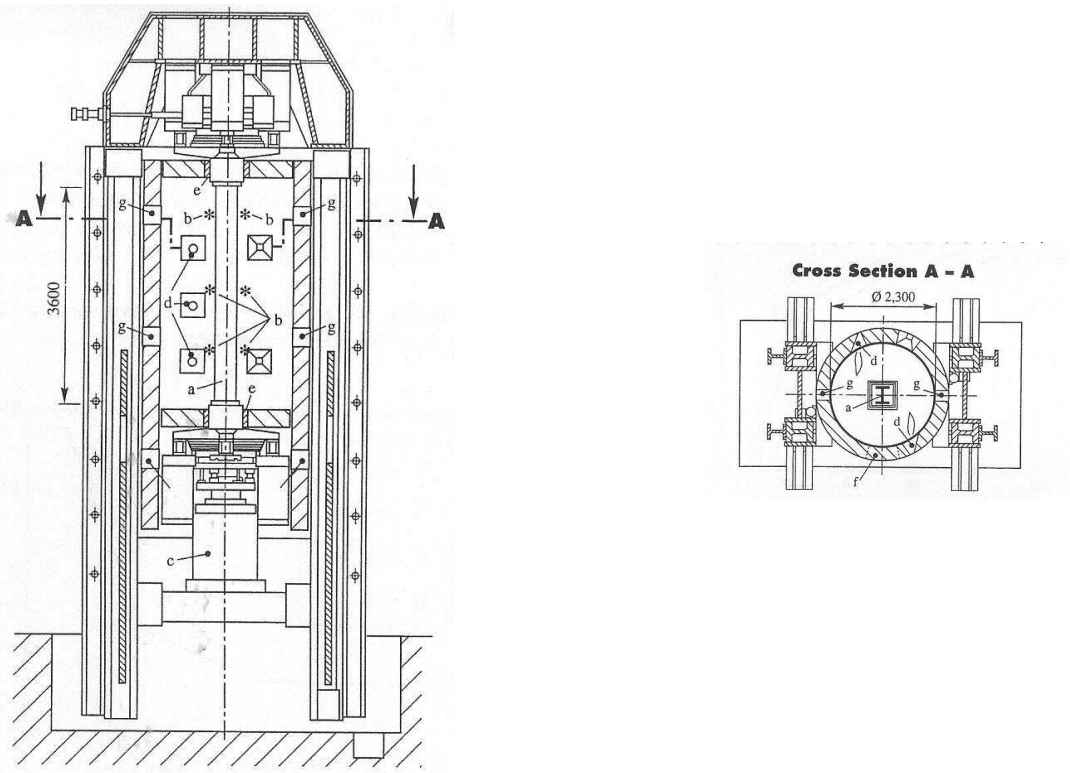

Figure 5.3 – Simplified vertical and horizontal sectional drawings of furnace a) specimen b) thermocouples c) hydraulic jack d) oil burners e) mineral fiber seal f) furnace door g) smoke vents, (Pan et al., 1997)

The technique used on these systems, makes it possible to have only one element of the building structure inside the furnace, while computers simulate the behaviour of the remaining structural system. An interface node interconnects the element inside the furnace with the simulated system. The movements of the interface node are performed by several hydraulic jacks, while the computers are solving, in an iterative process, the equations of the equilibrium of forces and displacements between the element in the furnace and the simulated system.

The system has been developed for future use with standard and natural fire tests, and structural systems composed of all relevant construction materials. It may be used to study the behaviour of steel columns in a fire situation as a part of a building structure. Thermal restraint and subsequent restraining forces can be studied with this technique.

Whereas the thermal set point is a known function of time for the mean gas temperature, which is realized through six oil burners, before starting the test, the mechanical set point has to be calculated online during a fire test in substructuring mode. Six electro-hydraulic control channels equipped with displacement and force sensors are available to influence the mechanical boundary conditions, i.e. two bending rotations each at top and bottom, one axial

displacement at the bottom and one horizontal displacement at the top. During a substructuring test, forces and moments at the boundaries of the specimen, i.e. at the upper and lower bearings of the column, are measured and utilized for the computation of the corresponding displacements and angles, which are sent to the specimen in order to keep the entire building in mechanical equilibrium with its prescribed overall boundary conditions. This closed loop for only one channel in substructuring mode is displayed in Figure 5.2. According to the free body diagram in this figure, the experiment is driven by the thermal displacement, which is diminished by the mechanical displacement u^{mech} due to the stiffness c^{mod} of the surrounding environment resulting in a compressive force on the column under test. The function of the control loop is to change the (total) displacement u by moving the position of the electro-hydraulic axial cylinder in such a way that the model force f^{mod} is equal to the measured force f .

Figure 5.4 shows two different views of the laboratory.

Figure 5.4 – General view of the laboratory

The laboratory is provided with three furnaces: one for testing loaded columns, another for testing slabs and beams, also with loads, and the third furnace for testing walls and other compartmentation material.

Figure 5.5 shows the vertical furnace used to test columns with load and restraint to thermal elongation. The hydraulic jacks are placed under the column, and the axial force is provided by a restraint frame placed on top of the set-up.

a) b)

Figure 5.5 – View of the vertical furnace for testing columns

Figure 5.6 depicts details of the hydraulic jack and hydraulic circuit to apply the loads and simulate the surrounding structure.

a) b) c)

Figure 5.6 – Hydraulic system for applying loads and simulating the stiffness

Figure 5.7 shows several views of the control rooms of the equipment to control the furnace, the hidraulic system, recording dataloggers and video cameras.

a) b) c)

Figure 5.7 – View of the control room of the laboratory

5.4 Test Programme and Specimens

In BAM fire resistance tests the specimens were HEA140 and HEB180 for the steel columns and HEA200 for the composite columns, 3.56m height. The steel grade of the steel columns was S235 and the composite S355 and concrete C25/30.

The following table presents the experimental programme carried out at BAM Laboratory. Two steel columns, with similar values of slenderness to the columns tested in FCTUC were tested, submitted to the same level of load, *i.e.,* 70% of the buckling load at room temperature. Column HEB180 was tested to compare with the column HEA200, and column HEA140 was compared with column HEA160. The composite columns were partially encased steel composite columns, with concrete between the flanges. Two columns were tested, both HEA200 steel profiles, with the same load level, 70% of the buckling load. For all tests, the stiffness of the surrounding structure was adopted within the range of values of the experimental ser-up used in FCTUC, *i.e,* between 13 and 128 kN/mm.

Table 5.1 – Test programme on steel and composite steel-concrete columns carried out in BAM Laboratory.

Reference	**BAM-SC180-K69.5-L70**	**BAM-SC140-K47_L70**	**BAM-CSC200-K59-L70**	**BAM-CSC200-K11-L70**
Section	HEB180	HEA140	HEA200	HEA200
Stiffness $K_{A,S}$ (kN/mm)	69.5	47	59	11
Load Level	70%	70%	70%	70%
Initial Load	1052	492	1199.71	1202.78

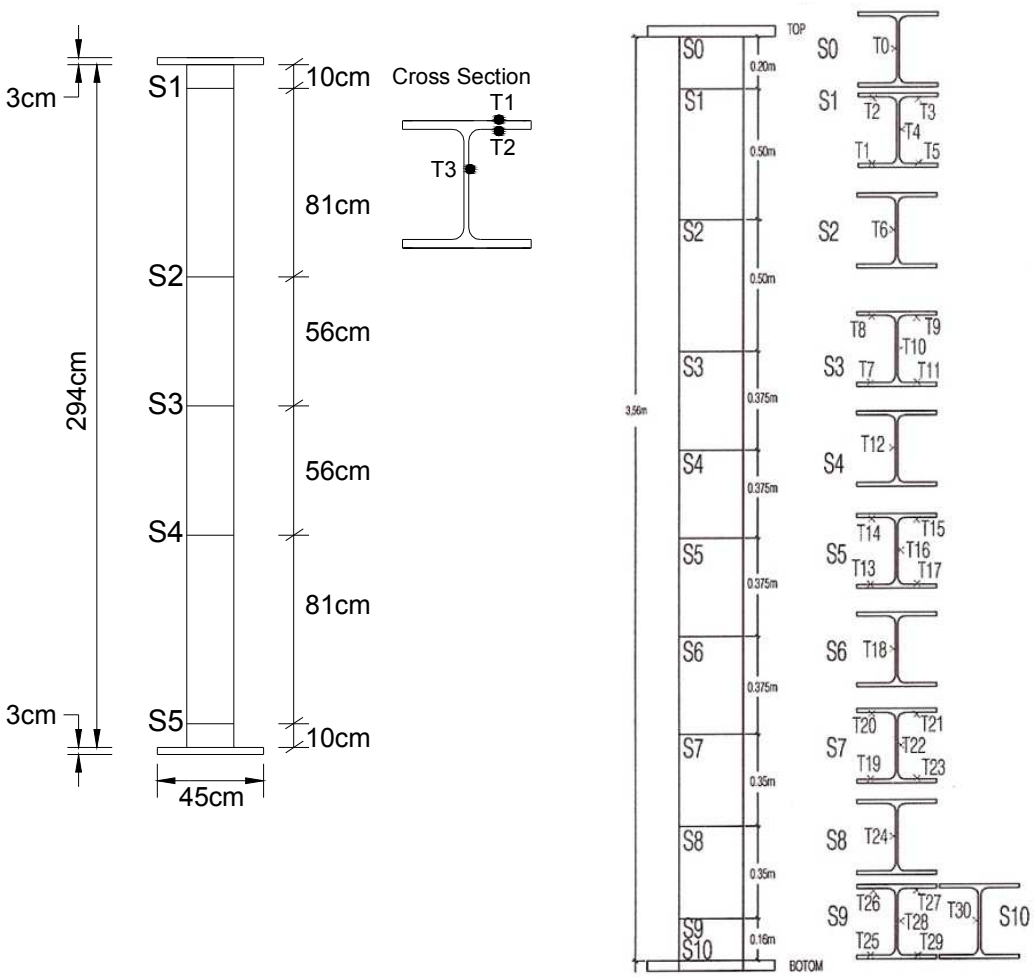

a) b)

Figure 5.8 – Steel specimens with position of thermocouples a) FCTUC columns b) BAM columns

The specimens were fitted with thermocouples type k (chromo-alumel) to measure the temperatures in different points of the cross-section. In the steel columns, 11 sections along the height of the column were considered, and the number of thermocouples varied between 1 and 5, in adjacent sections, with a total of 30 thermocouples per column. In the composite columns, 5 different sections were considered, with 7 thermocouples, with a total of 35 thermocouples per column.

The height of the columns in BAM tests was adopted 3.56m, which is very close to the column length of the columns in FCTUC tests, considering the columns 3m height, with the device for measuring the axial forces, which was 0.62m height.

The FCTUC and BAM test columns are composite columns made of partially encased steel sections (Figures 5.9 a) and b)). The steel grade of the testing columns was S355 and the concrete C25/30.

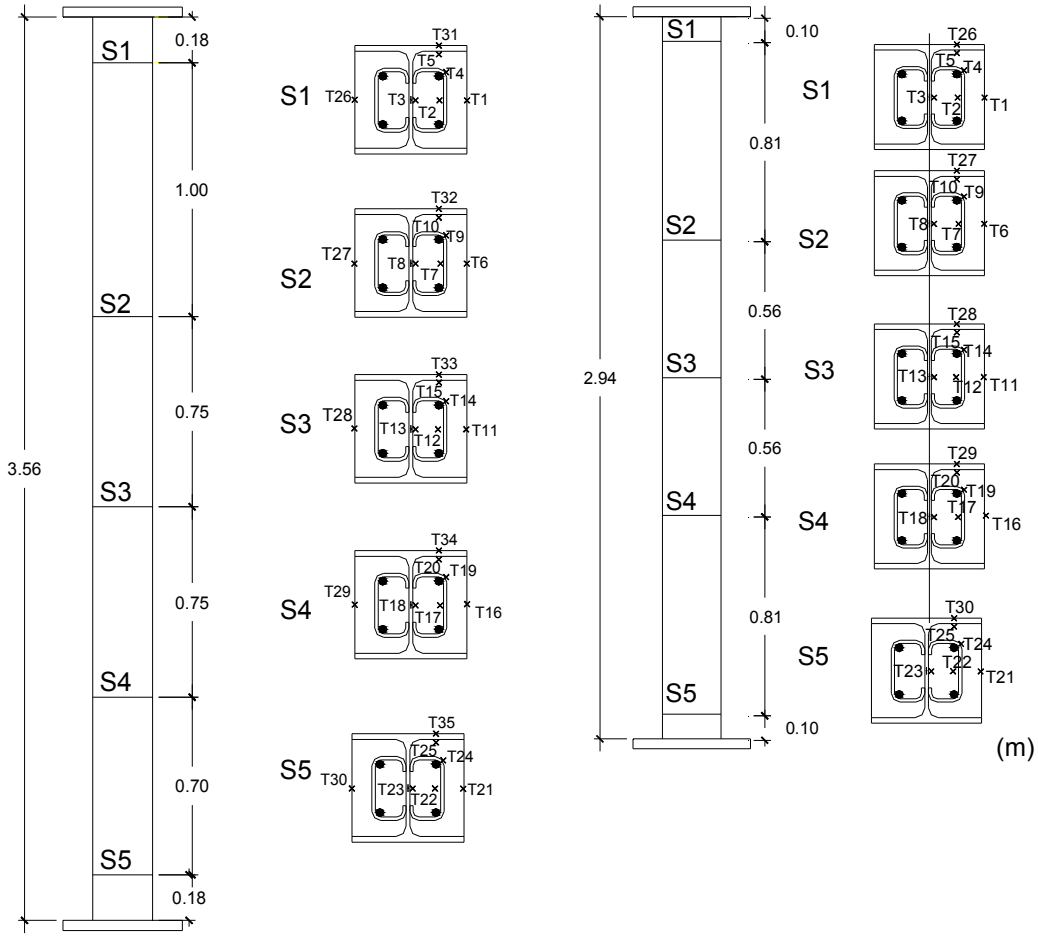

a) b)

Figure 5.9 - Composite steel-concrete columns a) BAM columns b) FCTUC columns

5.5 Test procedure

In figure 5.10 two views of the preparation of a composite column are shown. The thermocouples inside the concrete were placed before the concreting, and the thermocouples in the outer face of the steel flanges were placed after concreting, with a welding machine.

a) b)

Figure 5.10 – Preparation of the composite column of test BAM-CSC200-K11-L70

a) b)

Figure 5.11 – Preparation of specimen of test BAM-SC140-K47-L70

In figure 5.11, the steel specimen is prepared with all the thermocouples, and is placed inside the furnace. The bottom and top plates of the columns are carefully insulated, with ceramic wool.

The test procedure used in these tests was very simple. The columns instrumented with the thermocouples were placed inside the furnace. The thermocouples were connected to the datalogger, for the acquisition and record of the data. Once inside the furnace, the column was fixed on bottom with threaded rods and nuts, to the hydraulic jacks of the test set-up. In figure 5.11b), it can be observed that the furnace is controlled by plate thermometers.
The door of the furnace was closed, and the mechanical load was applied and kept constant. The value of the mechanical load and the axial stiffness of the surrounding structure was

programmed in the system. Then, the thermal action was applied following the standard ISO 834 fire curve (ISO 834, 1975).

a) b) c)

Figure 5.12 – Views of placing the specimen inside the furnace

Figure 5.12 shows one column being inserted in the furnace with a special crane, in such a way to transport it safely in the vertical position.

5.6 Results

5.6.1 Steel Columns

In this chapter, graphs with the evolution of restraining forces and vertical displacements in the experimental tests, and plots of the evolution of temperatures of the four tests carried out at BAM laboratory are presented.

Figures 5.13 and 5.14 present the results of test BAM-SC180-K69.5-L70. Figures 5.13 a) and b) depict the evolution of axial force and vertical displacements in the column. Figure 5.14 depicts the evolution of temperatures in thermocouples of section at mid-height of the column along the time.

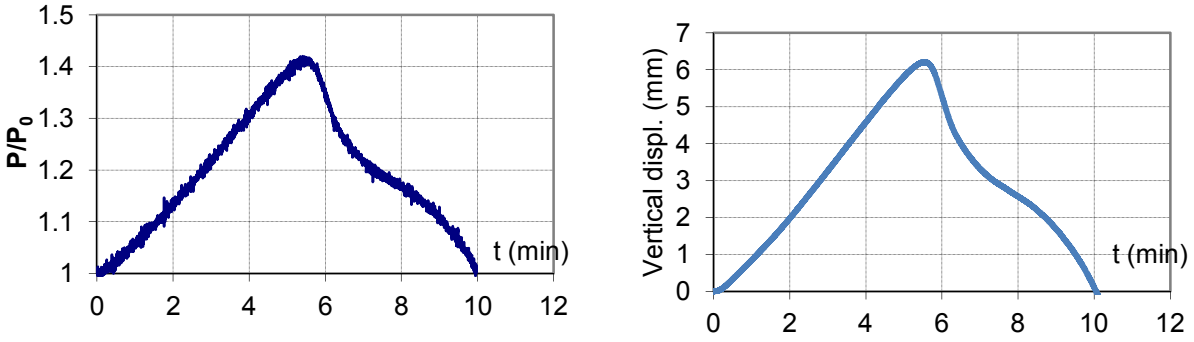

a) b)

Figure 5.13 – Restraining force and vertical displacements in column of test BAM-SC180-K69.5-L70

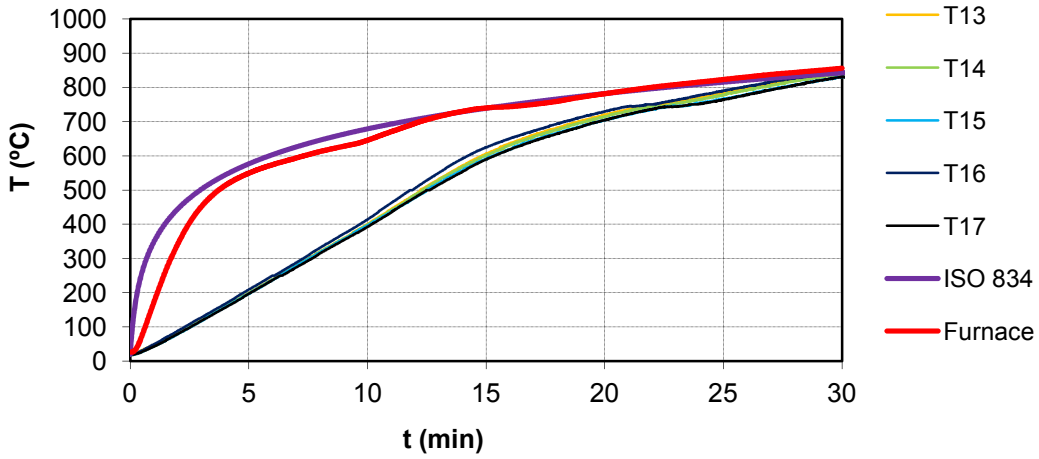

Figure 5.14 – Temperatures in thermocouples of section S3 of column of test BAM-SC180-K69.5-L70

The graphs in Figures 5.15 and 5.16 depict the results of test BAM-SC140-K47-L70, in terms of restraining forces, vertical displacements and temperatures.

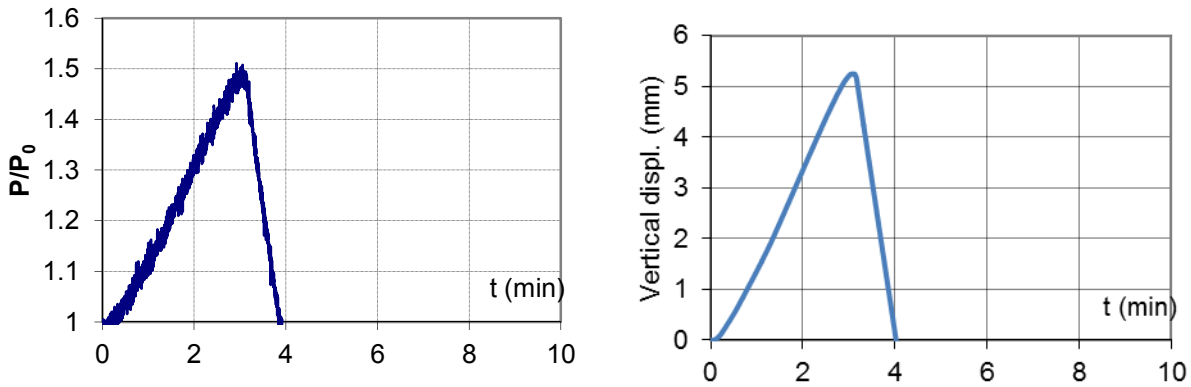

a) b)

Figure 5.15 – Restraining force and vertical displacements for test BAM-SC140-K47-L70

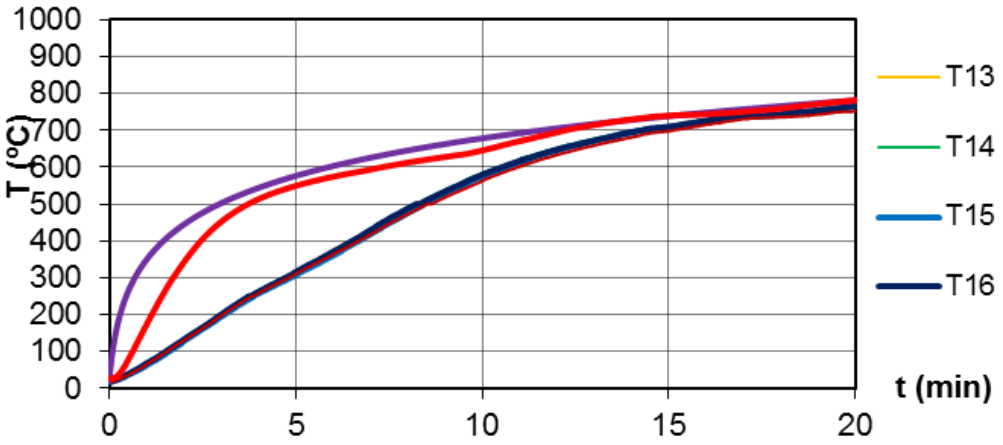

Figure 5.16 – Temperatures in column of test BAM-SC140-K47-L70

The evolution of temperatures was quite different in the two tests. After 5 minutes of test, with the standard curve ISO 834, HEA140 profile had about 300ºC while HEB180 had about 200ºC, while inside the furnace the gas temperature had 600ºC. The fire resistance was therefore very different. For column HEB180 column it was about 10 minutes, while for column HEA140 it was 4 minutes, for the same load level.

5.6.2 Composite Steel-Concrete Columns

The results of the composite columns are now presented. Results of test BAM-CSC200-K59-L70 are in Figures 5.17 and 5.18.

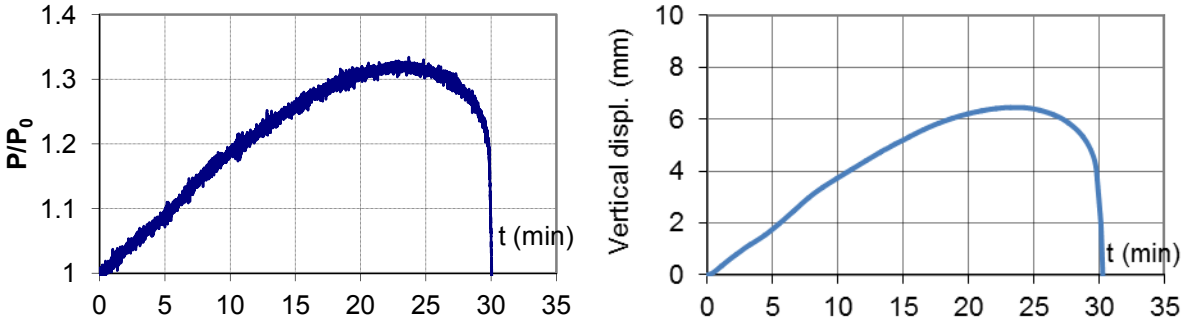

a) b)

Figure 5.17 – Restraining force and vertical displacements for test BAM-CSC200-K59-L70

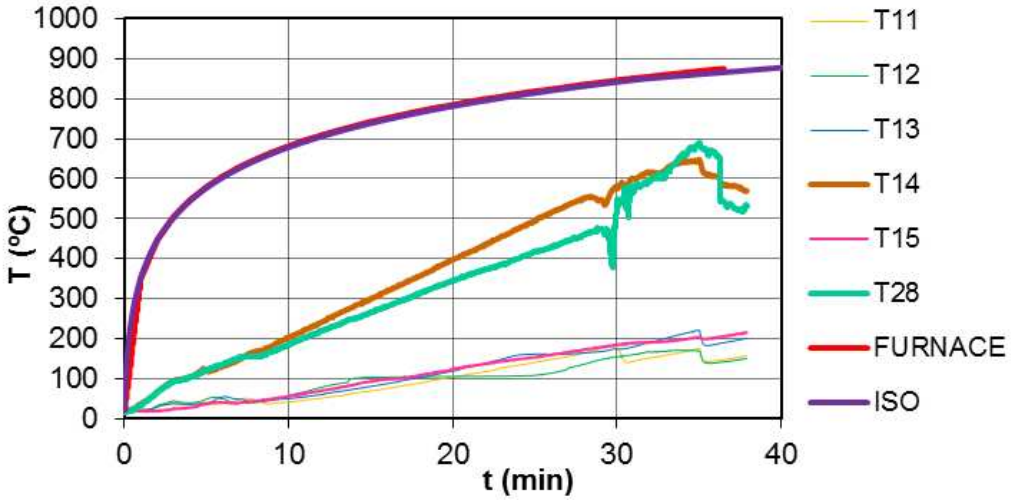

Figure 5.18 – Temperature evolution in column of test BAM-CSC200-K59-L70

Results of test BAM-CSC200-K11-L70 are depicted in Figures 5.19 and 5.20.

It can be observed that the higher restraint provoked a slightly lower fire resistance, 30 minutes against 35 minutes for the column tested with lower restraint. The vertical displacement was higher with the lower restraint, as expected, and the higher increase of axial force was observed with higher value of restraint to thermal elongation.

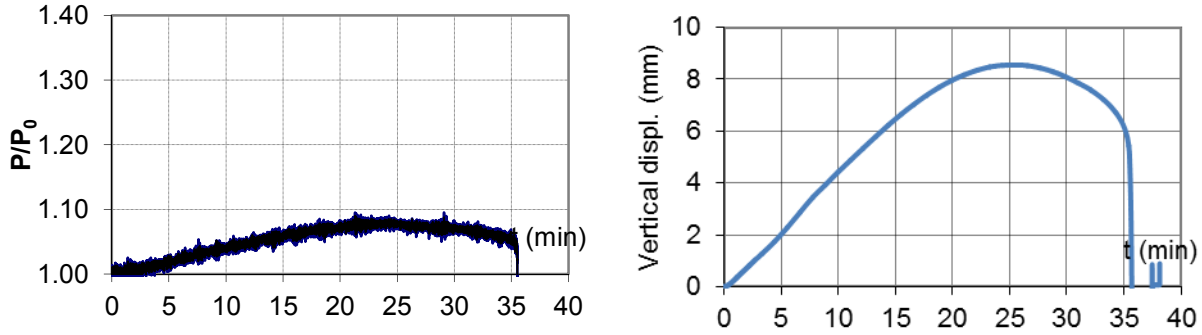

Figure 5.19 – Evolution of axial force and axial displacements of column BAM-CSC200-K11-L70 during test

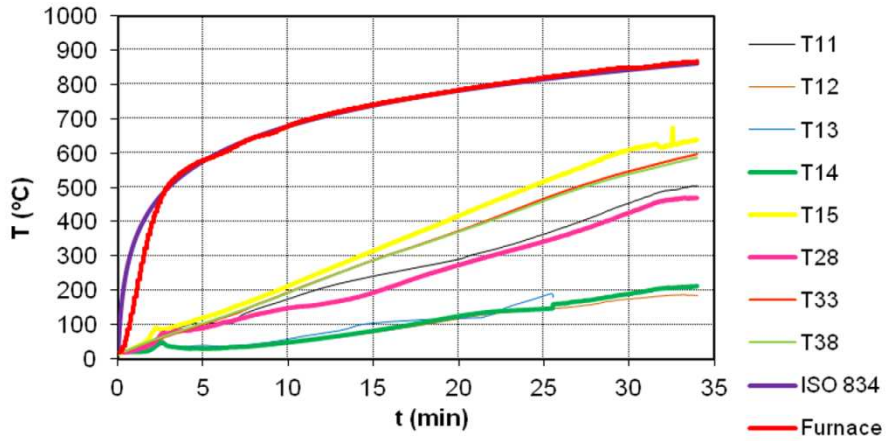

Figure 5.20 – Evolution of temperatures in thermocouples of section 3 of specimen BAM-CSC200-K11-L70

5.7 Comparison of Results FCTUC *vs* BAM Tests

5.7.1 Steel Columns

Tables 5.2 and 5.3 present a description of the tests on steel bare columns and the corresponding steel bare columns tested at FCTUC, to allow the comparison of the tests performed at BAM with the ones performed at FCTUC.

Figure 5.21 presents the evolution of the restraining forces related to the initial load in function of time for tests on steel columns HEA200 (in FCTUC) and HEB180 (in BAM).

Table 5.2– Comparison of experimental tests on steel columns

Reference	BAM-SC180-K69.5-L70	HEA200-K13-L70	HEA200-K45-L70	HEA200-K128-L70
Section	HEB180	HEA200	HEA200	HEA200
Load Level	70%	70%	70%	70%
Initial Load	1052	999.8	999.8	999.8
Stiffness $K_{A,S}$ (kN/mm)	69.5	13	45	128
Stiffness $K_{A,C}$ (kN/mm)	385.20	376.81	376.81	376.81
$\alpha_A = K_{A,S} / K_{A,C}$	0.180	0.035	0.119	0.341

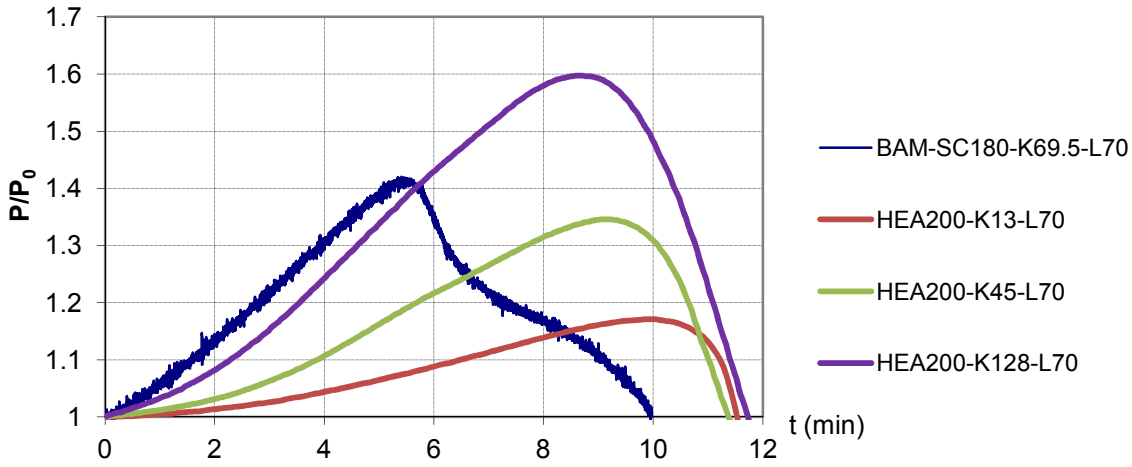

Figure 5.21 – Evolution of axial forces in tests with load level 70%, comparison between FCTUC tests in specimen HEA200 and BAM test with HEB180, with different stiffnesses of the surrounding structure

In this graph it is observed that the critical time of the tests in FCTUC is almost the same, i.e., 11.5 minutes, regardless of the value of the restraint provided by the surrounding structure. The fire resistance of the column tested in BAM was lower, i.e., about 10 minutes, due to the fact that the furnace in BAM laboratory is very effective in following the standard curve, and also the columns in this furnace are totally placed inside the furnace, while in FCTUC furnace the extremities of the columns are not heated. The major influence of the degree of restraint is in the value of the maximum increase of axial force. The higher value of P/P_0 observed was 1.6 of the initial value for the stiffness of the surrounding structure 128kN/mm, while the lower value was 1.17 for the stiffness of surrounding structure 13kN/mm. Quite interesting to observe is the decay phase of the graphs, very abrupt in the FCTUC tests and very steep in the BAM test. The reason for this is the fact that in FCTUC set-up, the surrounding structure is

provided by a real 3D frame, while in BAM, the surrounding structure is artificially provided by a system in which displacements and forces are computed to simulate a desired value of restraint.

Results of test BAM-SC140-K47-L70 are in Figure 5.22, comparing with the similar tests performed in FCTUC with a HEA160 steel profile, with stiffnesses of 13, 45 and 128kN/mm.

Table 5.3 – Comparison of experimental tests on steel columns

Reference	**BAM-SC140-K47-L70**	**HEA160-K13-L70**	**HEA160-K45-L70**	**HEA160-K128-L70**
Section	HEA140	HEA160	HEA160	HEA160
Load Level	70%	70%	70%	70%
Initial Load	492	621	621	621
Stiffness $K_{A,S}$ (kN/mm)	47	13	45	128
Stiffness $K_{A,C}$ (kN/mm)	185.22	271.39	271.39	271.39
$\alpha_A = K_{A,S} / K_{A,C}$	0.254	0.048	0.166	0.473

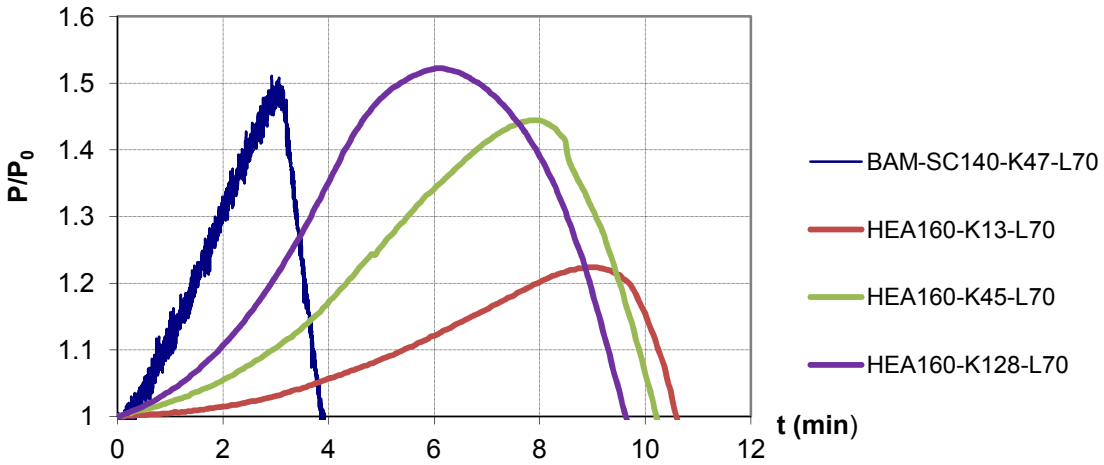

Figure 5.22 – Evolution of axial forces in tests with load level 70%, comparison between FCTUC tests in specimen HEA160 and BAM test with HEA140, with different stiffnesses of the surrounding structure

The fire resistance for the column in BAM laboratory is much lower due to the higher effectiveness in the heating process. In these columns, the slenderness is greater than in the FCTUC tests, so this aspect has a major influence. In this case, the fire resistance of 10 minutes in the tests of FCTUC, is very different from the 4 minutes observed in BAM tests. In these tests, the decay phase is more similar in the tests in both Laboratories (Korzen et al., 2009).

5.7.2 Composite Steel-Concrete Columns

A great deal of data was gathered from the tests carried out with both systems, however, only some of these results will be compared and presented in this thesis.

One of the main correlation parameters identified was the non-dimensional stiffness ratio α_K, defined as the ratio between the axial stiffness K_{AS} of the external system (external restraining frame in the case of the FCTUC tests, virtual structure in the case of the BAM tests) and the axial stiffness $K_{A,C}$ of the tested composite columns, i.e.

Table 5.4 summarizes the values of the parameters used in the tests.

Table 5.4 – Comparison of experimental tests on composite steel-concrete columns

Reference	**BAM-CSC200-K11-L70**	**BAM-CSC200-K59-L70**	**CSC200-K13-L70**	**CSC200-K45-L70**	**CSC200-K128-L70**
Section	HEA200	HEA200	HEA200	HEA200	HEA200
Length (mm)	3560	3560	2940	2940	2940
Load Level	70%	70%	70%	70%	70%
Initial Load	1202.78	1199.71	1185	1185	1185
Relative Slenderness $\overline{\lambda}_z$	0.856	0.856	0.856	0.856	0.856
Stiffness $K_{A,S}$ (kN/mm)	11	59	13	45	128
Stiffness $K_{A,C}$ (kN/mm)	664.7	664.7	788.8	788.8	788.8
$\alpha_A = K_{A,S} / K_{A,C}$	0.016	0.089	0.016	0.057	0.162

The relative slenderness $\overline{\lambda}_z$ around minor axis is given by:

$$\overline{\lambda} = \sqrt{\frac{N_{pl,Rk}}{N_{cr}}} \tag{5.1}$$

where $N_{pl,Rk}$ is the characteristic value of the plastic resistance to compression, given by the following expression,

$$N_{pl,Rk} = A_a.f_{ayk} + 0.85A_c.f_{ck} + A_s.f_{syk} \quad (5.2)$$

and $N_{cr,z}$ is the critical force for the relevant buckling mode

$$N_{cr,z} = \frac{\pi^2.(EI)_{eff}}{l_{c,z}^2} \quad (5.3)$$

calculated with the effective flexural stiffness $(EI)_{eff}$, determined in accordance with the following formula:

$$(EI)_{eff} = E_a.I_{a,z} + E_s.I_{s,z} + 0.6.E_{cm}I_{c,z} \quad (5.4)$$

Four values for α_A were chosen: 0.016, 0.057 and 0.089 and 0.162. The average stiffness ratio α_A found in practice is between 0.05 and 0.1. The chosen values are in this range, except for α_A = 0.016 and α_A = 0.162, which were chosen to be extreme values, one very low and the other very high.

The temperature development in several points at mid-height of the specimens CSC200-K128-L70 and BAM-CSC200-K59-L70 as a function of time are visualized in Figures 5.23 and 5.24, respectively. Both diagrams show temperatures, mean furnace temperatures and target temperatures of the ISO 834 fire curve as a function of time. Due to differences between the heating systems, i.e. electrical heating at FCTUC and oil burners heating at BAM, the FCTUC furnace temperatures are a bit in delay with respect to the target furnace temperatures. This may be the reason that the temperature distribution of the specimen BAM-CSC200-K59-L70 was more uniform in comparison to the CSC200-K128-L70. The expected thermal gradients in depth in the cross-section are observed (thermocouples 11, 12 and 13) (Figures 5.23 and 5.24).

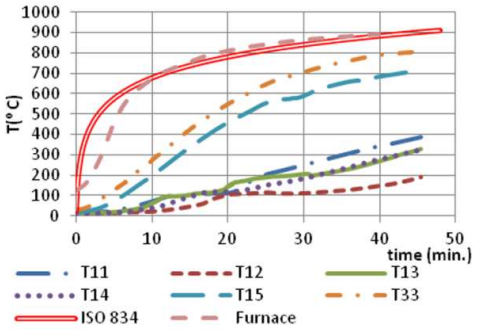

Figure 5.23 - Furnace and specimen (Section S3) temperatures of specimen CSC200-K128-L70

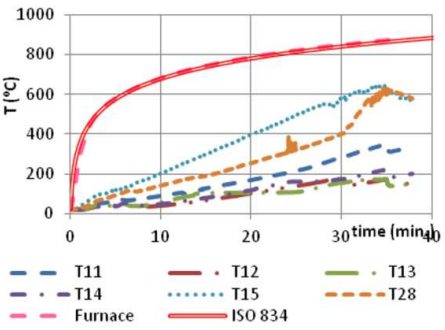

Figure 5.24 - Furnace and specimen (Section S3) temperatures of specimen BAM-CSC200-K59-L70

For the composite columns the expected thermal gradients in depth in the cross-section was observed (thermocouples 11, 12 and 13). However, the heating was quite uniform around the cross-section (thermocouples 33 and 38, 11 and 28 of BAM tests).

Figures 5.25 a) and b) present the evolution of temperatures in the vertical direction of columns BAM-CSC200-K59-L70 and CSC200-K128-L70, respectively. These temperatures were derived integrating the mean temperatures in the five cross sections of the steel along the height. The mean temperatures in each cross section were obtained calculating the temperatures in the flanges and in the web, and then calculating the weighted temperature of the section according to the surface areas of the web and flanges. It can be observed that in FCTUC tests there is a higher thermal gradient in the test columns in the direction of the supports than in BAM tests. This is due to the fact that the columns in FCTUC were tested with the ends connected outside the furnace, 0.25 m of each extremity of the columns were not directly exposed to the heating, and in BAM the columns were totally heated.

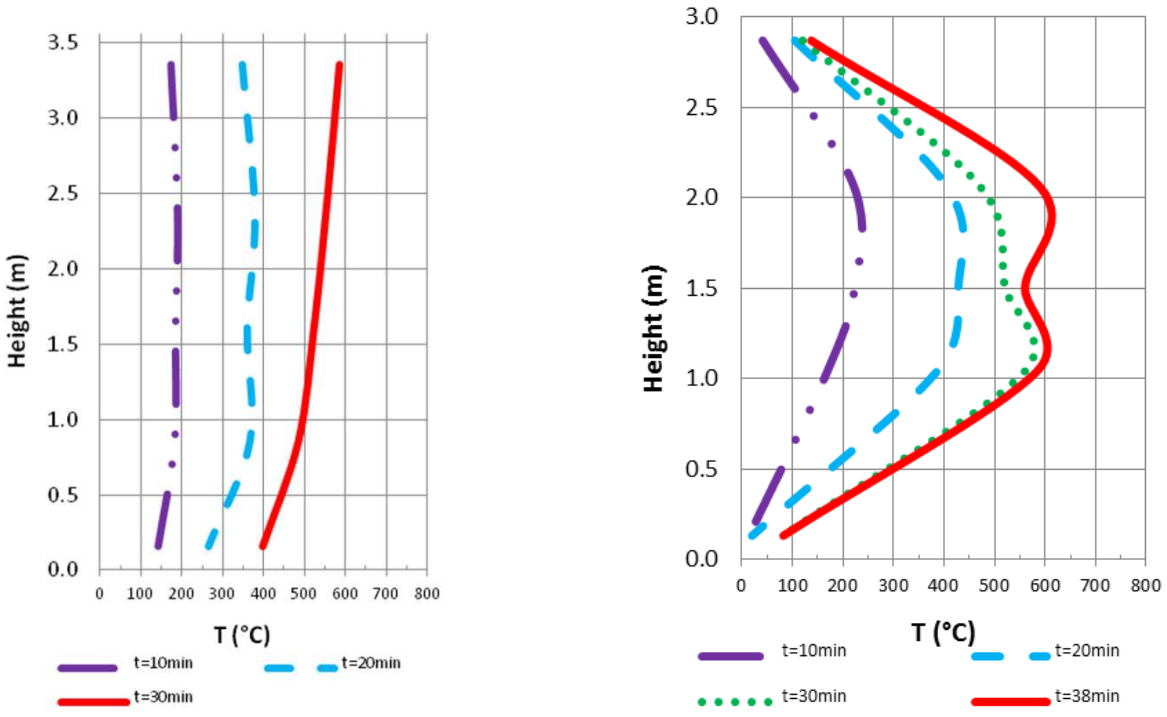

a) b)

Figure 5.25 – Thermal gradients in column´s height a) BAM-CSC200-K59-L70 b) CSC200-K128-L70

However, it is believed that the uniform temperature in the heated zone of test CSC200-K128-L70 has a greater extent, than the one showed in Figure 5.25. This is due to the fact that the instrumented sections were very close (1.12 meters), while the heated extension of the column was 2.5 meters. In fact, the instrumentation of the columns should consider placing

thermocouples between sections S1 and S2, and also between sections S4 and S5. This way, it would be verified that the low temperatures are only attained in the extremities of the column (0.5m in each extremity).

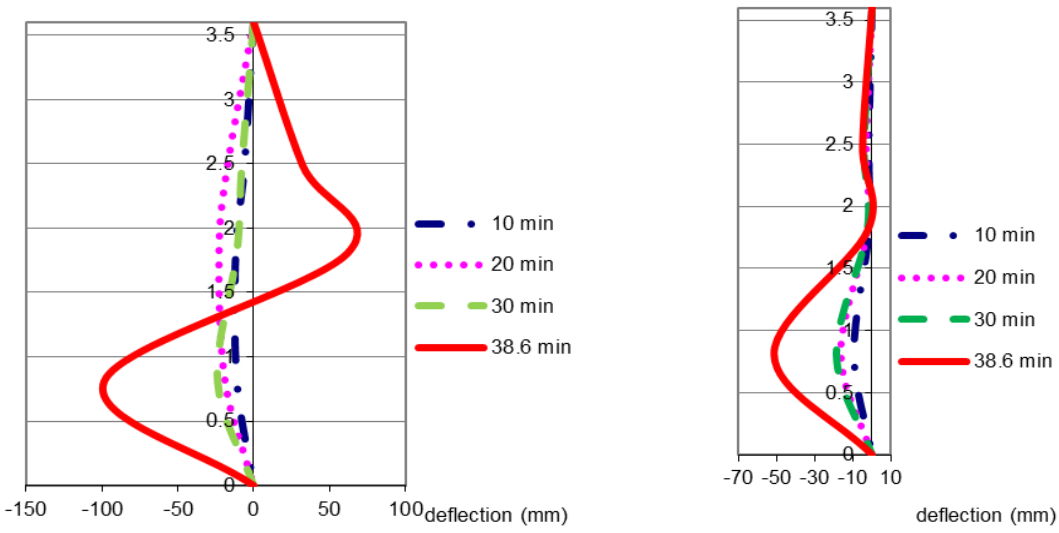

a) b)

Figure 5.26 – Lateral deflections in test CSC200-K128-L70 a) around minor axis a) around major axis

Figure 5.26 depicts the lateral deflections in test CSC200-K128-L70 around minor axis and around major axis. As expected, greater lateral deflections were observed around minor axis. It was observed that during the test, the deflections were very gentle, and in the end of the test, a sudden deflection was observed, leading to an inversion of the curvature of the deformed shape of the column.

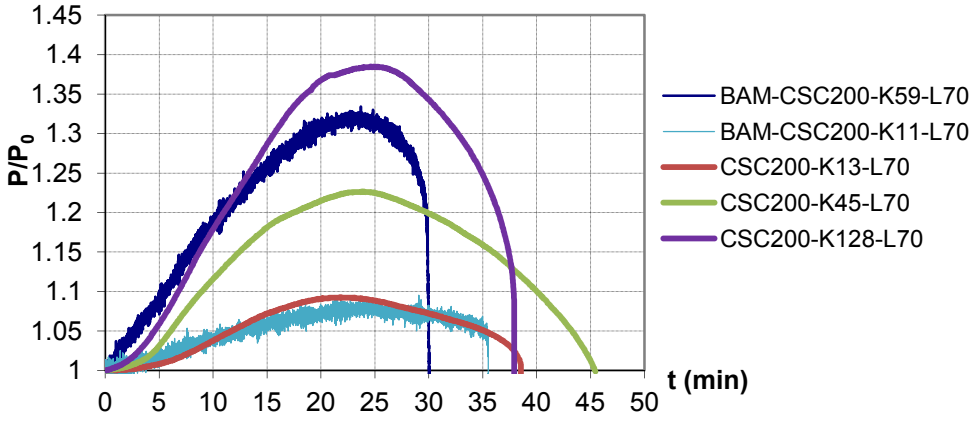

Figure 5.27 – Evolution of restraining forces in tests with load level 70%, and comparison between FCTUC tests in specimens CSC200 and BAM tests, with different stiffnesses of the surrounding structure

The graph in figure 5.27 depicts the evolution of axial force during the fire resistance tests in composite columns. The typical behaviour of a restrained column under fire is depicted for the studied cases. As the columns are heated they expand, thus inducing an initially-increasing restraining force P, which is plotted as a ratio to the constant initial applied load P_0. This expansion will lead to a vertical displacement, controlled by the stiffness of the structure. After reaching a peak, the axial force will decay due to the degradation of the mechanical properties of materials. It can be observed that the restraining forces were higher for the higher values of the non-dimensional axial restraint ratio. The instant of time when the restraining forces regain its initial value is here defined as the critical time. It is difficult to define a pattern of variation of the critical time of the columns in function of the non-dimensional axial restraint ratio for the different FCTUC tests. The difference in the critical times in the FCTUC tests is very small, because associated to an increase of the axial stiffness is an increase of the rotational stiffness. These two stiffnesses play roles in opposite directions. The increase of the axial stiffness reduces while the increase of the rotational stiffness increases the critical time. In BAM tests the increasing of the non-dimensional axial restraint ratio led to a reduction of the critical time of the columns because the two stiffnesses are applied independently. It is worth to mention that in BAM tests, the rotational restraint on top and bottom of the columns was total. The reason for this, is that the system was under development, and was not prepared for applying different values of rotational stiffness.

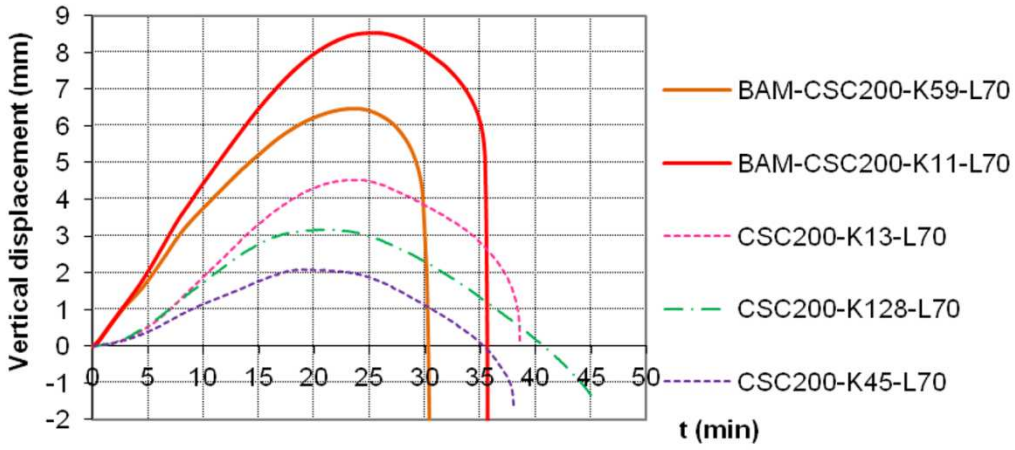

Figure 5.28 – Evolution of axial displacements in tests with load level 70%, and comparison between FCTUC tests in specimens CSC200 and BAM test, with different stiffnesses of the surrounding structure

Comparing for constant stiffness ratios the performance of the two experimental systems at FCTUC and BAM one can say that the BAM system produces smaller critical times. The main reason for this difference is given by the fact that according to Figures 5.25 a) and b) the

mean temperature in the BAM tests is at all times during the experiment higher than in the FCTUC tests. The influence of this behaviour is so strong that the critical time is shorter for test BAM-CSC200-K59-L70 with α_A =0.089 than for test CSC200-K128-L70 with α_A =0.162. The best correlation between FCTUC and BAM tests can be found for the smallest stiffness ratio, i.e. α_A = 0.016.

Figure 5.28 presents the evolution of the axial displacements as a function of the time. In accordance with higher mean temperatures at BAM and column lengths of 3.6 m and 3.0 m at BAM and FCTUC, respectively, larger axial displacements at BAM in comparison with FCUTC are quite natural. Assuming about 50% greater mean temperatures at BAM according to Figures 5.25 a) and b) and taking into account 20 % greater column lengths at BAM a ratio of about 80% higher axial displacements at BAM as presented in Figure 5.28 are quite reasonable based on a thermoelastic analysis with pure thermal expansion. These results would be a little bit modified taking account additionally the different restraining grades.

Figures 5.29 to 5.32 present the force-displacement diagrams for several cases studied. In the FCTUC tests it was observed a hysteresis phenomenon in the loading unloading process, which did not occur in BAM tests. This is probably due to the fact that in FCTUC, the restraint to thermal elongation is provided by a real restraining structure and in BAM is virtually simulated in a computer program and applied to the column by a set of servo-controlled hydraulic jacks.

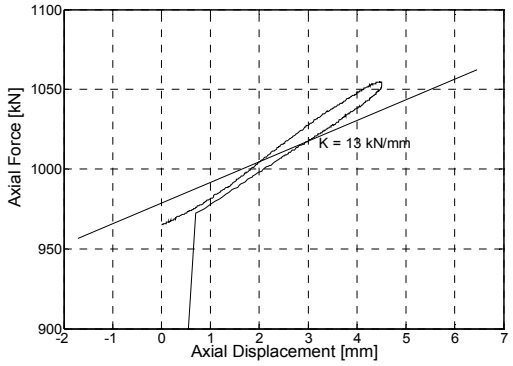

Figure 5.29 - Force-displacement diagram of specimen CSC200-K13-L70 (α_A = 0.016)

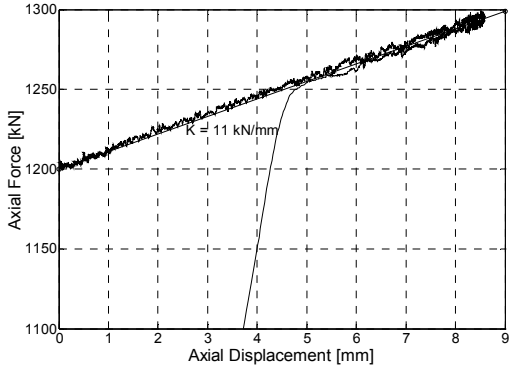

Figure 5.30 - Force-displacement diagram of specimen BAM-CSC200-K59-L70 (α_A = 0.016)

It is not possible to assess if any errors in the measurement of the vertical displacements or any small axial displacements experimented by the threaded rods were responsible for this hysteresis. However, it is expectable that this behaviour occurs in real structures due to a

change in the stiffness in the two phases (increasing and decreasing of the axial force in the column).

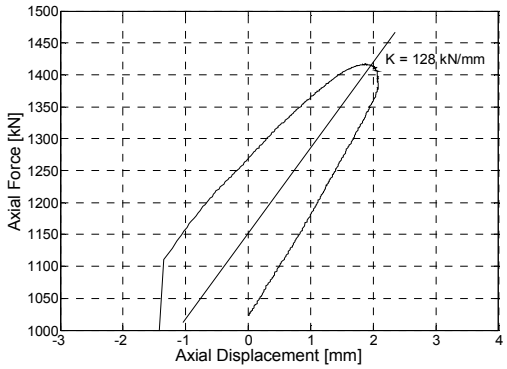

Figure 5.31 - Force-displacement diagram of specimen CSC200-K128-L70 (α_A = 0.162)

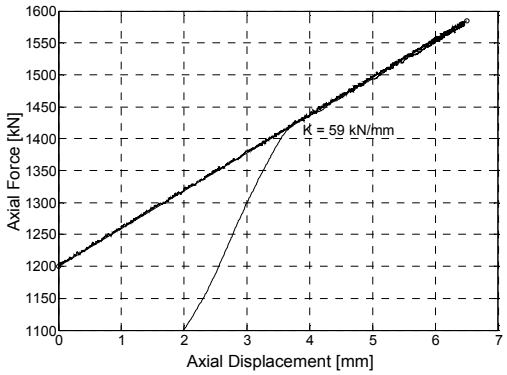

Figure 5.32 - Force-displacement diagram of specimen BAM-CSC200-K59-L70 (α_A = 0.089)

Another interesting remark that should be pointed out is that the columns in the BAM set-up were built-in while in the FCTUC set-up semi-rigidly connected. This fact, although it was not quantified, must have an influence in the fire resistance of the columns (Korzen et al., 2010).

5.8 Columns in and after Test

5.8.1 Steel Columns

In this chapter, photographs during and after the tests are presented. In BAM laboratory it was possible to record and make some photographs to observe the development of the deformed shape of the columns during the tests. Figures 5.33 and 5.34 refer to test B-SC180-K69.5-L70.

In Figure 5.33 it is possible to observe the influence of the built-in end conditions in this experimental set-up.

Figure 5.33 – Views of the column BAM-SC180-K69.5-L70 after test

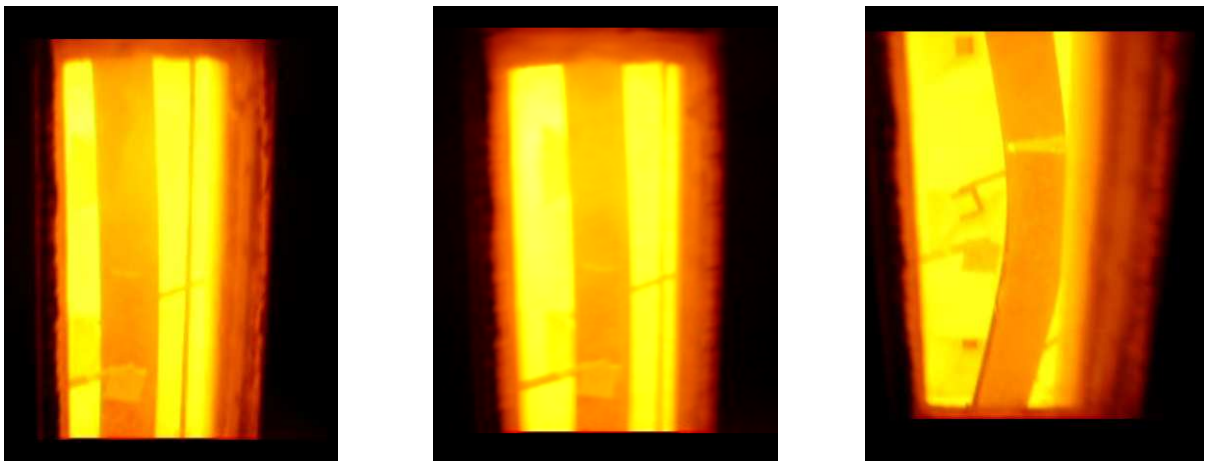

a) Time = 4:30 minutes b) Time = 7:20 minutes c) Time = 10:00 minutes

Figure 5.34 – Evolution of the deformed shape of column in test BAM-SC180-K69.5-L70, during the test

Figures 5.35 and 5.36 show views of the column of test BAM-SC140-K47-L70 before during and after test.

Figure 5.35 – Views of column of test BAM-SC140-K47-L70 before and after test

a) Time = 2:20 minutes b) Time = 4:00 minutes c) Time = 5:50 minutes

Figure 5.36 – Lateral deflection in test BAM-SC140-K47-L70 during test

Although it was not possible to measure the lateral deflections in this furnace, it was observed that buckling occurred with great displacements around minor axis and negligible displacements around major axis. In these tests, no local buckling of the flanges was observed.

In these photographs it is also possible to observe the plate thermometers which control the furnace.

5.8.2 Composite Steel-Concrete Columns

Photographs 5.37 a) and b) show the composite column of test BAM-CSC200-K59-L70 inside the furnace, before and after test.

a) b)

Figure 5.37 – Views of column of test BAM-CSC200-K59-L70, before and after test

Figures 5.38 a) and b) show the column during the test. It is observed that the buckling of the column occurs around minor axis, as expected. In Figures 5.39 it may be observed that no spalling occurred during the fire test. Detachment of some portions of surface concrete was observed, as well as the disconnection of the stirrups from the web. This phenomenon was observed only in the final stage of the test.

a) Time = 2:00 minutes b) Time = 30:30 minutes

Figure 5.38 – Lateral deflection in test BAM-CSC200-K59-L70, during the test

The same conclusions presented above are valid for the other composite column tested in BAM. Figures 5.39 and 5.40 show column of test BAM-CSC200-K11-L70 during and after test.

a) b) c)

Figure 5.39 – Views of the composite column of test BAM-CSC200-K59-L70, after test

a) Time = 2:00 minutes b) Time = 31:30 minutes c) Time = 36:30 minutes

Figure 5.40 – Photographs of column of test BAM-CSC200-K11-L70 during the test

In Figure 5.39, the detachment of the concrete from the steel profile is visible. Figure 5.40 a) and b) show the column inside the furnace, during the test, and Figure 4.40 c) shows the column after the furnace was shut down, and it can be observed the incandescent stage of the steel profile, due to the very high temperatures in this part of the column. In Figure 5.41, it is possible to observe the large lateral deflections experimented by the column BAM-CSC200-K11-L70 after test.

Figure 5.41 – View of the deformed shape of column BAM-CSC200-K11-L70 after test

Figures 5.42 to 5.46 depict the deformed shape of the columns after test. All the columns failed by global buckling. The concrete between the flanges of the steel profile prevented local buckling to occur.

The main difference observed in the specimens in the two experimental setups was the rotation on the extremities of the columns. In BAM tests, no rotation was observed due to the fact that the boundary conditions were full restraint to rotation. In FCTUC tests, a certain rotation angle was observed in the specimen's extremities. In all cases, greater rotation was observed on top, leading to asymmetric deformed shapes of the columns.

In almost all the tested columns the concrete between the flanges of the steel profile has detached, pull-out the stirrups that were welded to the web of steel profile. This phenomenon occurred, as could be observed in the BAM test, in the late stages of the test.

Figure 5.42 - BAM-CSC200-K11-L70

Figure 5.43 - CSC200-K45-L70

Figure 5.44 - CSC200-K13-L70

Figure 5.45 - BAM-CSC200-K59-L70

Figure 5.46 - CSC200-K128-L70

5.9 Sinopsis

The results of several column tests performed for thermal comparison of differently designed furnaces have been presented. It was the aim of this work to find out what kind of differences occur, and what significance they might have for standard fire testing. The main findings can be summarized as follows:

- First, the steel-temperature distribution in BAM Furnace is much more uniform along the height, than in the FCTUC furnace. Another reason for this problem is that the top and bottom ends of the columns in the FCTUC furnace are not heated. This fact is responsible for much lower temperatures in these parts of the columns.

- Considering the purpose of the tests, no great influence was observed due to the level of restraint to thermal elongation in the tests. The main difference was probably due to the fact that the rotational restraint was infinite in BAM tests, since the set-up in this laboratory is not prepared yet for simulating different values of rotational restraint. In FCTUC tests, the connection to the upper beams provided a real connection with a certain rotational stiffness, leading to the main differences observed in the tests, and documented in this analysis.

Concerning the comparison of the two test set-ups it can be said that they are similar leading to similar shapes of the curves for the restraining forces. The main difference observed in the experimental set-ups was the fact that the specimen in the BAM furnace is heated along its

whole length while in FCTUC furnace around 8% of the column length in each end is not heated. This fact has influence in the fire resistance, being smaller for the same testing conditions, in the BAM test set-up.

The influence of the surrounding structure has influence in the development of axial forces in the test columns. This can be observed in the results of the evolution of restraining forces in the five experimental tests presented in this work. With no exception, the higher the stiffness of the surrounding structure the higher the axial forces generated during the fire.

These fire resistance tests allowed to understand not only the real behaviour of steel and composite steel concrete columns in fire, but also to find out specific problems of the performance of both systems. As a main conclusion of this comparison it can be pointed out that the higher stiffness of the surrounding structure induces higher maximum values of restraining forces. Concerning the slenderness, for steel columns, the less slender columns presented higher fire resistance.

Concerning the critical times of the columns, in BAM tests, it was observed that the higher the non-dimensional axial restraint ratio α_A, the lower the critical time. In FCTUC tests, despite the result for the test column with the higher the non-dimensional axial restraint ratio α_A (0.162), it was observed that no influence of this parameter exists on the critical time.

6. NUMERICAL SIMULATIONS OF STEEL AND PARTIALLY ENCASED STEEL-CONCRETE COLUMNS EXPOSED TO FIRE

6.1. Introduction

The finite element method acts as a link between experimental studies and analytical models, enabling a better understanding of behavior and experimental control to obtain simplified methods.

The modeling of elements of composite steel-concrete columns, presents a high level of complexity to treat some local phenomena such as cracking of concrete, spalling, the local buckling, the characterization of the interaction between the surfaces of steel and concrete, and welded connection between the profile and stirrups.

In this study, a great number of numerical simulations on the fire resistance of steel columns, with the finite element code ABAQUS and SupertempCalc is presented. The first set of numerical simulations was performed with columns with the same geometry as the ones of the experimental tests carried out in order to calibrate and validate the finite element model. In this way, and once built the model, varying the different parameters, it was possible to evaluate the influence of each parameter on the overall behavior of the columns in fire.

6.2. Columns Embedded on Walls

6.2.1. Modelling with SupertempCalc

6.2.1.1. Introduction

At the initial stage of this part of the work, in order to assess the temperature evolution in steel columns in contact with wall, a “user-friendly” finite element 2D computer code SupertempCalc, was used. This is a very useful program, due to the simplicity of use at an early stage of a numerical analisys.

The computer software SupertempCalc, (Anderberg, Y., 1997), is a tool for thermal analysis of fire exposed structures. The three main parts that compose this software are:

- Graphical User Interface for pre-and postprocessing
- Tempcalc
- Fire design

The graphical user interface of STC version used in this work was a MATLAB-toolbox, compatible with MATLAB v.5.3. SupertempCalc is a 2-dimensional, fire-dedicated finite element program (Anderberg, 1997). The differential equation for 2-dimensional heat flow is derived from conservation of energy, describing the fact that total inflow per unit time equals the total outflow per unit time. The constitutive relation invoked is Fourier´s law of heat

conduction, which describes heat flow within the material. The spatial and time domains are discretized by the weighted residual approach. Boundary conditions implemented include convective and radiative heat flow and heat exchange within enclosures. 4-node rectangular and 3-node triangular finite elements are used. Thermal properties of materials are described as temperature dependent. The heat transfer system can be solved in rectangular, cylindrical or polar coordinate systems.

Numerical modeling with SupertempCalc is very simple. The first step is to define material properties and fire exposure. Geometry is defined using existing material definitions and boundary is defined using existing fire exposure definitions. Then the geometry is divided into a finite element mesh. Geometry, boundary and mesh can either be generated automatically for a number of predefined standard cases or be defined manually.

Mesh generation is the next step when geometries and boundaries have been defined. In this study, rectangular mesh generation was used. The resolution of the mesh is crucial for the accuracy of the calculations. The need for refinement is dependent on material properties and the gradients of applied exposures. After the calculation was carried out, the temperature fields at any time can be displayed.

In the following text, a brief description of the numerical formulation of the transient heat conduction used in Supertempcalc is given. The numerical approach is based on the concept of approximating continuous function by a discrete model, composed of a set of piecewise continuous functions, which are defined over a finite number of subdomains or elements. This approach is the Finite Element Method.

To maintain the properties of a discrete system, to a system of piecewise continuous functions, the method of weighted residuals will form the base of the finite element approximations. This implies that the residual (error) of the finite element approximation is given in a weighted integral formulation.

The heat flux is the total amount of heat that passes through a unit area of the boundary per unit time. The two-dimensional heat flow is described by a heat flux vector, which has the direction of the heat flow and its length expresses the heat per unit time that passes through a unit surface area (length) perpendicular to the direction of the flow. The differential equation that controls heat flow in two dimensions is derived by considering a two-dimensional body. To solve the balance equation, boundary conditions are requires. The boundary conditions used in Supertempcal, are of type natural (Neumann), essential (Dirichlet) and linear (Newton). The boundary conditions implemented for the thermal analysis are Gas Temperature and Enclocure.

As with the spatial domain, the method of weighted residuals forms the base for the finite element discretization of the time domain. As the time dimension is of an infinite extent, finite domains of time are dealt with. Calculations are repeated for subsequent domains with new initial conditions. The process leads thus to a step by step or recurrence calculation.

The Fire Design program consists of three applications, SBEAM, CBEAM and COMPRESS. SBEAM calculates the moment capacity of the fire exposed structural steel beams in the ultimate limit state. The plastic sagging bending moment capacity of a beam is calculated based on the tensile capacity at elevated temperatures in the lower part of the beam cross-section and similarly the compressive capacity in the upper part. CBEAM calculates the moment capacity of fire exposed tension reinforced concrete beams and slabs in the ultimate limit state. COMPRESS calculates the plastic yield compression resistance, the critical Euler buckling load and the design load of fire exposed structural steel, concrete and reinforcement composite members in the fire limit state. These applications were not used in this study.

6.2.1.2. Numerical Models

A set of five different steel cross-sections (HEA 120, HEA 160, HEA 200, HEA 240 and HEA 280) with the web parallel and perpendicular to the wall surface, with different wall thickness was modelled numerically (Table 6.1). The cases tested experimentally, are included on these.

Table 6.1– Numerical simulations - geometry of the models

HEA	h	b_f	t_f	t_w	Model 1		Model 2		Model 3		Model 4	Model 5
					t_b (mm)	H (mm)	t_b (mm)	H (mm)	t_b (mm)	H (mm)	t_b (mm)	t_b (mm)
120	114	120	8	5	98	98	70	62	70	70	100	70
160	152	160	9	6	140	134	100	91	100	100	140	100
200	190	200	10	6.5	180	170	140	130	140	140	180	140
240	230	240	12	7.5	230	230	140	128	140	140	180	140
280	270	280	13	8	-	-	180	167	180	180	180	180

The test cases were organized in 5 models as represented in Figure 6.1. The fire was considered act on one side as in the fire resistance tests.

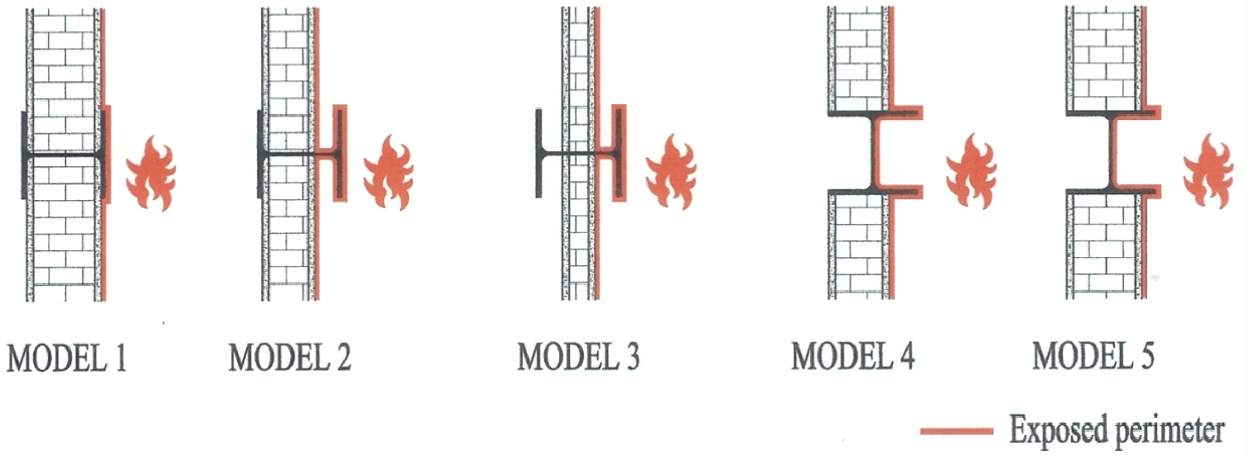

Figure 6.1– Studied Cases

6.2.1.3. Finite Elements, Mesh, Interactions, Thermal Action

The same materials and testing conditions as in the fire resistance tests were considered in the numerical simulations. The values of the thermal conductivity and specific heat variations in function of the temperature, as proposed in EN 1993-1-2 (2005) and EN 1994-1-2 (2005), were used for the steel and mortar. The mortar mass density, with an initial value of 2300 kg/m^3 was also considered varying in function of temperature. The moisture content of the mortar was 1.5%. The mass density for the steel was equal to 7850kg/m^3.

The thermal properties of the bricks were considered constant, since no specific values were found in function of the temperature. A thermal conductivity = 0.7 W / m °C, a specific heat = 840 J/kg °C and a capacitance (specific heat × density) = 1344000 J/m^3 °C, were considered. The mass density of the bricks was 1600 kg/m^3. These values were obtained from the Ozone computer program (Cadorin, 2003).

For steel, concrete and cladding a coefficient of heat transfer by convection α_c = 25 W/m^2°C and an emissivity coefficient ε = 0.9 were adopted for the exposed side of the elements. For the unexposed side of separating members, the net heat flux was considered with a coefficient of heat transfer by convection α_c = 9 W/m^2°C, assuming it contains the effect of heat transfer by radiation. These values were assumed, as referred in EN 1991-1-2 (2002). At this stage, no distinction was made between steel and concrete emissivity coefficients.

The models were meshed in finite square elements with 5mm (Figures 6.2 and 6.3).

Figures 6.2 and 6.3 show, for example, the temperature field for model HEA 200, after 30 and 60 minutes of fire exposure to the ISO 834 fire curve.

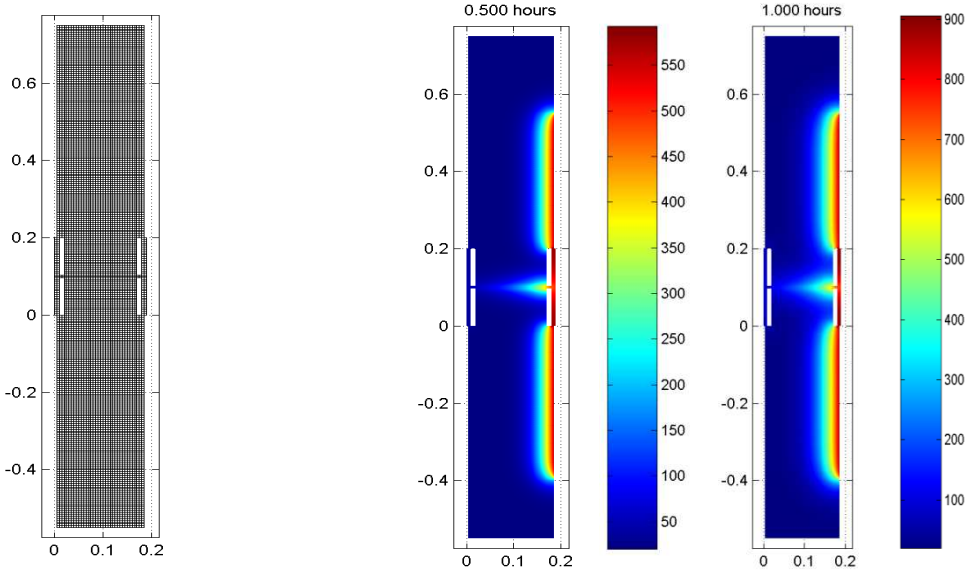

a) b)

Figure 6.2 – Example of results obtained with STC numerical analysis: (a) mesh distribution, (b) temperature field for model HEA 200, with the web perpendicular to the wall.

a)

b)

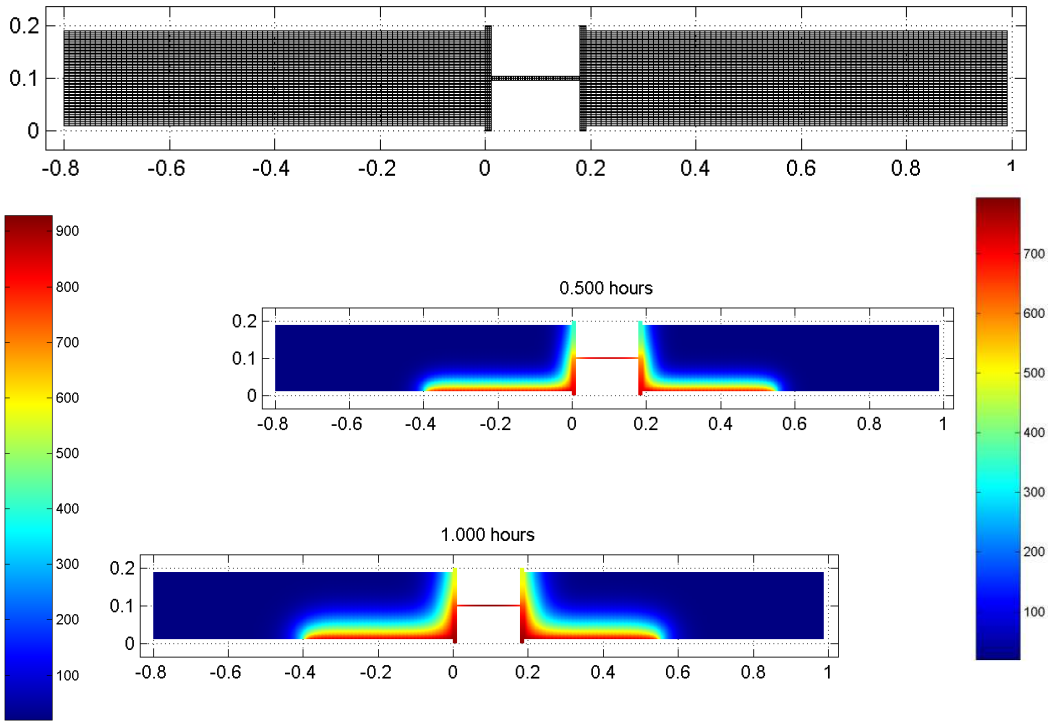

Figure 6.3 – Example of results obtained with STC numerical analysis: (a) mesh distribution, (b) temperature field for model HEA 200, with the web parallel to the wall.

It was possible to determine the temperature distribution in the models cross-section, for different times. These temperatures show the influence of the building walls on the heating of the steel cross-section of the columns. The zones of the walls and steel profiles directly exposed to fire present higher temperatures. A large thermal gradient along the steel cross-section was observed.

The comparison between experimental and numerical results obtained with SupertempCalc is presented in chapter 7.

6.2.2. Modelling with ABAQUS

6.2.2.1. Introduction

For the thermal and structural analysis of columns in fire, a computational modeling of the various problems studied was made with the finite element program ABAQUS (v. 6.7-1), available at the Department of Civil Engineering, University of Coimbra. This software general and versatile for application in various fields of Civil Engineering, consists of several modules, among which are the graphic modules (CAE pre-processor) and the main modules STANDARD and EXPLICIT, employed in this work (ABAQUS, 2005).
The preprocessor ABAQUS/CAE is a graphical interface that allows the user a quick and efficient definition of the geometry of the problem, allocation of the properties of different materials, application of loads and boundary conditions of the problem, selecting the number of steps sought in the analysis and finally, generation of finite element mesh corresponding to the body examined. An analysis of consistency and adequacy of the model thus generated can be made using special tools to ABAQUS / CAE for verifying various aspects of the partitions defined for the model geometry (modulo PART), mechanical properties of the materials involved (module PROPERTY), grouping the partitions (ASSEMBLY module) and the imposition of the sequence of steps of analysis (STEP module), and its nature - linear or nonlinear, definition of boundary conditions and loads (LOAD module), the mesh generation Finite element (module MESH) and finally obtain the input file (module JOB). After generation by the pre-processor file containing the data entry problem, which can in turn be further manipulated by the user to situations not adequately addressed by ABAQUS / CAE, you can then execute the simulation by the method of finite element models using ABAQUS / STANDARD and ABAQUS / EXPLICIT. The software also offers post-processor ABAQUS / VIEWER, operating on the output files, allows for interpretation of numerical results, procedures CFATF visualization and animation.

The various capabilities of ABAQUS allow complex engineering problems involving complex geometries, non-linear constitutive relations, the occurrence of large deformation, transient loads, interactions between materials (soil-structure, fluid-structure, ...) can be modeled numerically, even that the process of constructing an appropriate model is not a

simple task, because it involves a very large amount of parameters and option arising from the very high range of possible problems that can be modeled with ABAQUS.

6.2.2.2. Numerical Models

A numerical model was built with solid elements from the ABAQUS library of finite elements (Figure 6.4). The elements chosen for the columns were the C3D20RT while for the rest of the surrounding structure were the C3D8RT. The C3D8RT is a 8-node while the C3D20RT is a 20 node linear finite element with reduced integration, an hourglass control solid element and a first-order (linear) interpolation. These elements have one integration point, three degrees-of-freedom per node corresponding to translations and six stress components in each element output.

The finite element mesh was generated automatically by the ABAQUS program and the side of the finite elements was 30 mm in the specimen, walls and upper beams of the restraining frame and 100mm in the columns of the restraining frame.

The thermal and mechanical properties at high temperatures of the concrete were defined according to EN 1992-1-2 (2004) and of the steel according to EN1993-1-2(2005). For the bricks the properties were not considered varying with temperature due to a lack of data available in the literature. Values used in the software Ozone, from the University of Liège, were adopted (Cadorin, 2003).

The constitutive models from the Abaqus library options, chosen to represent the materials Eurocode properties were the “Concrete damaged plasticity” for concrete and “Plastic-Plasticity” for the steel. These models are described further in the text.

In order to perform a non-linear geometrical analysis the stress-strain curves of the materials were converted to the true stress-logarithmic strain law. Since steel and concrete are non-linearly temperature dependent, the material properties were used as defined in the Eurocode fire parts.

Based on a sensitivity analysis, calibrated with the temperatures obtained in the experimental tests, the following coefficients were adopted: on the un-exposed side, a convection coefficient of 4 $Wm^2/ºC$ and emissivity coefficients of 0.7 for the concrete and 0.8 for the steel, although they are different from the ones mentioned in EN 1991-1-2 (2002), and on the exposed side a convection coefficient of 25 $Wm^2/ºC$ and an emissivity of 0.7 were used for both materials.

Table 6.2 and Figure 4.14 (chapter 4), describe the studied cases in the numerical simulations and the correspondent fire resistance tests. The specimens were modeled with the same geometry and materials as used in the experimental tests. The reference "Exx" indicates the tests carried out on columns embedded on walls while the reference "Iyy" indicates the tests carried out on isolated bare steel columns.

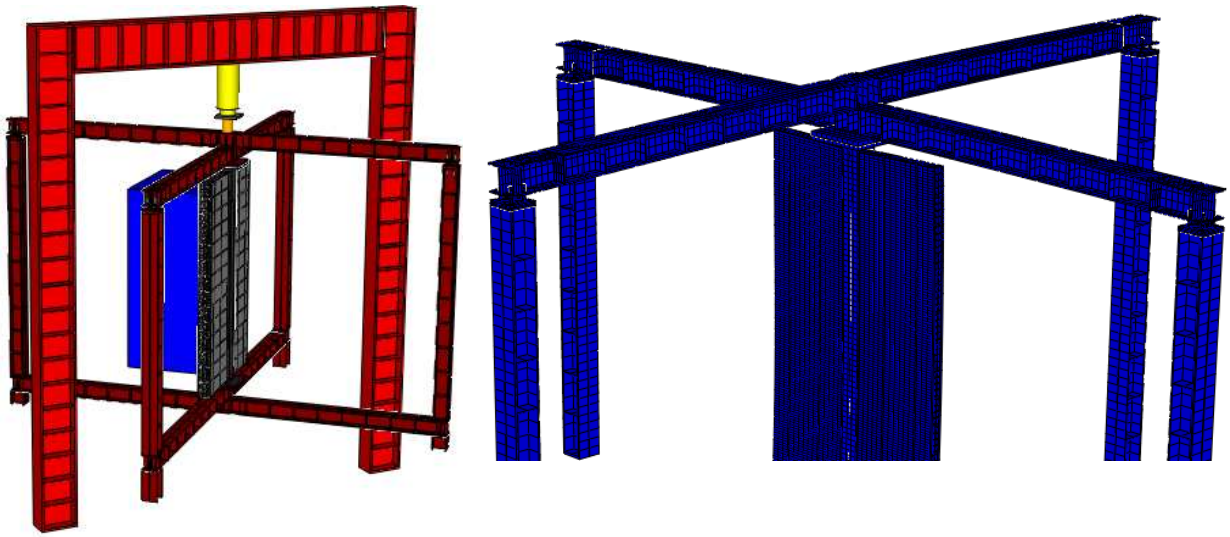

a) b)

Figure 6.4 - Three-dimensional model and finite element mesh for the fire resistance of steel columns embedded on walls.

Table 6.2 - Cases Study of steel columns embedded on walls

Test	Steel profile	Web in relation to the wall surface	Wall thickness (mm)	Serviceability load (kN)	Slenderness	Steel specimen
E03	HEA 200	parallel	180	1088	42.2	Specimen 10
E04	HEA 200	perpendicular	180	1088	42.2	Specimen 12
E05	HEA 160	parallel	140	704	52.8	Specimen 5
E06	HEA 160	perpendicular	140	704	52.8	Specimen 4
E07	HEA 160	parallel	140	704	-	Specimen 7
E08	HEA 200	parallel	140	1088	42.2	Specimen 6
E09	HEA 200	perpendicular	140	1088	42.2	Specimen 1
E10	HEA 160	parallel	100	704	52.8	Specimen 3
E11	HEA 160	perpendicular	100	704	52.8	Specimen 4
E12	HEA 160	parallel	100	704	-	Specimen 7
I16	HEA 160	No walls	-	704	52.8	Specimen 9
I20	HEA 200	No walls	-	1088	42.2	Specimen 6

Two different orientations of the profile in relation to the wall surface were considered: web parallel and perpendicular to the walls surface. The reason for this choice is that a different behaviour was expected, since in the two cases, bending occurred around the weak or strong axis of the cross sections.

In Table 6.2 the studied cases of steel columns embedded on walls, considered for the structural analysis of the fire behaviour of columns embedded on walls are again described.

In the following paragraphs, a brief description of the numerical modeling with the commercial program ABAQUS is presented. The process of modeling the structure, applying the mechanical loads and thermal actions is performed using different modules of the software.

"***Part Module"***

A part created using the Part module tools is called a native part and has a feature-based representation. A feature contains geometry information as well as a set of rules that govern the behaviour of the geometry. The Part module is used to create, edit and manage the parts in the current model. ABAQUS/CAE stores each part in the form of an ordered list of features. The parameters that define each feature combine to define the geometry of the part.

"Property Module"

The Property module is used to create and edit materials, define sections, assign sections, orientations, normals and tangents to parts, define general material data, mechanical material models and thermal material models.

"Assembly Module"

The Assembly module is used to create and modify the assembly. The model contains only one assembly, which is composed of instances of parts from the model. When one creates a part, it exists in its own coordinate system, independent of other parts in the model. In contrast, one can use the Assembly module to create instances of the parts and to position the instances relative to each other in a global coordinate system, thus creating the assembly. The positioning of part instances is performed by sequentially applying position constraints that align selected faces, edges or vertices or by applying simple translations and rotations.

An instance maintains its association with the original part. If the geometry of a part changes, ABAQUS/CAE automatically updates all instances of the part to reflect these changes. A model can contain many parts and a part can be instanced many times in the assembly; however, a model contains only one assembly. Loads, boundary conditions, predefined fields and meshes are applied to the assembly.

Figure 6.5 presents several details of the construction of the 3D-model, with a single column, several parts of the model and a view of the assembly process of the model.

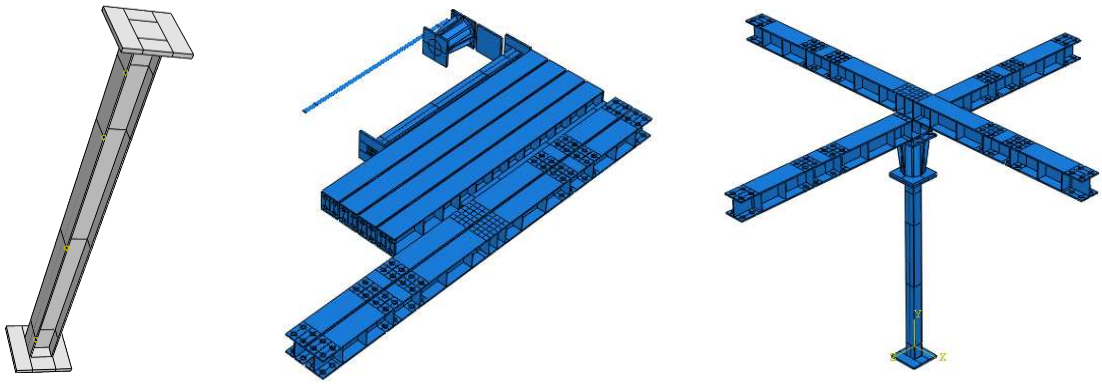

a) b) c)

Figure 6.6 – Construction of the 3D-model a) column b) several parts c) view of the assembly

"Step Module"

The step module can be used to create analysis steps, specify output requests and specify analysis controls. Within a model one can define a sequence of one or more analysis steps. The step sequence provides a convenient way to capture changes in the loading and boundary conditions of the model, changes in the way parts of the model interact with each other, the removal of addition of parts, and any other changes that may occur in the model during the course of the analysis. In addition, steps allow one to change the analysis procedure, the data output and various controls.

ABAQUS writes output from the analysis to the output database; one can specify the output by creating output requests that are propagated to subsequent analysis steps. An output request defines which variables will be output during an analysis step, from which region of the model they will be output, and at what rate they will be output.

When the first step is created, ABAQUS/CAE selects a default set of output variables corresponding to the step´s analysis procedure. By default, output is requested from every node or integration point, in the model and from default section points. In addition, ABAQUS/CAE selects the default rate at which the variables are written to the output database. One can edit these default output requests or create and edit new ones. Default output requests and output requests that were modified will be propagated to subsequent steps in the analysis.

"Interaction Module"

The interaction module can be used to define and manage several objects: mechanical and thermal interactions between regions of a model or between a region of a model and its surroundings, analysis constraints between regions of a model, assembly-level wire features, connector sections, and connector section assignments to model connectors, inertia (point mass, rotary inertia and heat capacitance) on regions of a model, cracks on regions of a model, springs and dashpots between two points of a model or between a point of a model and ground.

Interactions are step-dependent objects, which means that when we define them, we must indicate in which steps of the analysis they are active.

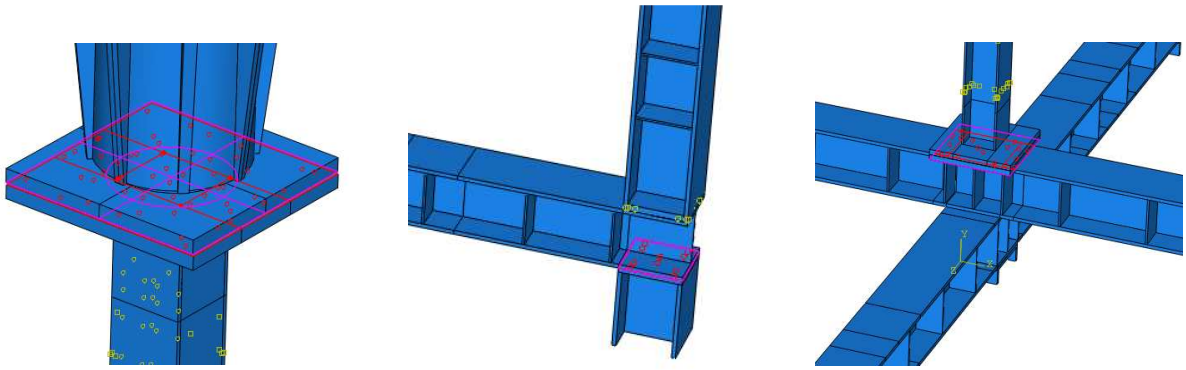

a) b)

Figure 6.7 – Details of the construction of the 3D-model - interaction between parts a) column-cilinder b) beam – column c) column – lower beams

"Load Module"

The load module is used to define and manage the loads, the boundary conditions, predefined fields and load cases. Prescribed conditions in ABAQUS/CAE are step-dependent objects, which means that we must specify the analysis steps in which they are active. We can use the load, boundary conditions and predefined field managers to view and manipulate the stepwise history of prescribed conditions. We can use the Amplitude toolset in the Load module to specify complicated time or frequency dependencies that can be applied to prescribed conditions.

"Mesh Module"

The Mesh module allows us to generate meshes on parts and assemblies created within ABAQUS/CAE. Various levels of automation and control are available so that we can create a mesh that meets the needs of our analysis. As with creating parts and assemblies, the process of assigning mesh attributes to the model – such as seeds, mesh techniques, and

element types – is feature based. As a result, we can modify the parameters that define a part or an assembly, and the mesh attributes that we specified within the Mesh module are regenerated automatically.

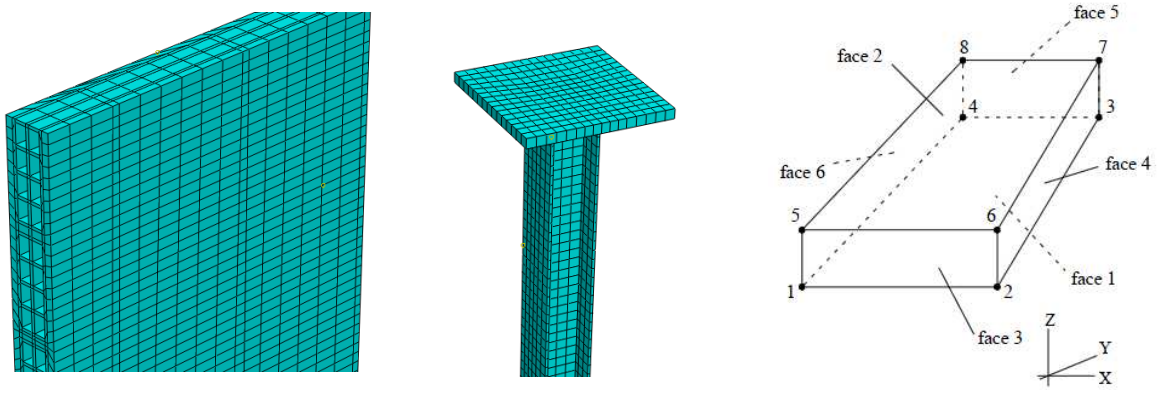

a) b) c)

Figure 6.8 – Finite element mesh in the parts of the FE model a) wall b) steel column c) detail of C3D8RT finite element

"Job Module"

The Job module is used to analyze the model. It allows us to create a job, and to submit it to ABAQUS/Standard or ABAQUS/Explicit, and to monitor its progress. It is also possible to create multiple models and jobs and run and monitor the jobs simultaneously.

If the model contains multiple steps, we do not have to analyze all of the steps in a single analysis job. Indeed, it is often desirable to run a complex analysis in stages. This allows us to examine the results and confirm that the analysis is performing as expected before continuing with the next stage. The restart files generated by an ABAQUS analysis, allows one to continue the analysis from a specified step.

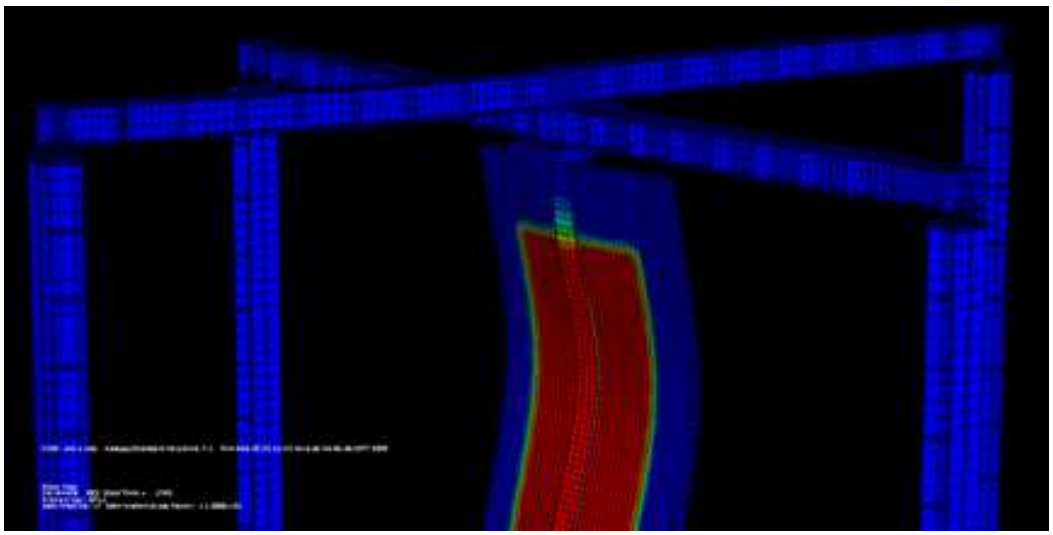

Figure 6.9 – Finite element models of steel columns embedded on walls with the web perpendicular to the wall surface.

6.2.2.3. Finite Elements, Mesh, Interactions, Thermal Action

Figures 6.9 a) to d) depict the numerical models used in the Finite Element Analysis of the fire behavior of steel columns embedded on walls.

Four different situations with two steel profiles HEA160 and HEA200 were considered. Two orientations of the web in relation to wall, parallel and perpendicular, and two thicknesses of the wall, one equal to the steel profile width (flange or web), and a lower thickness, close to ¾ of the steel profile width. The figures presented are a view-cut at mid-height of the column. It may be observed that the bricks and vertical and horizontal mortar layers between them were accurately modeled.

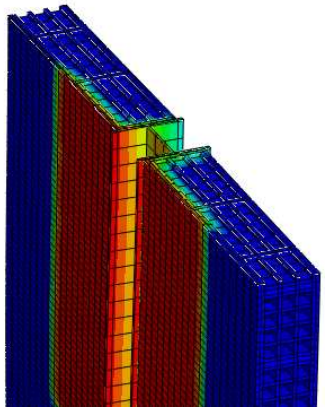

a) Test E03

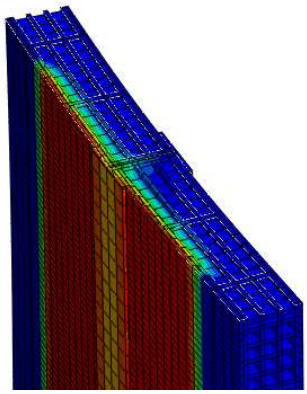

b) Test E04

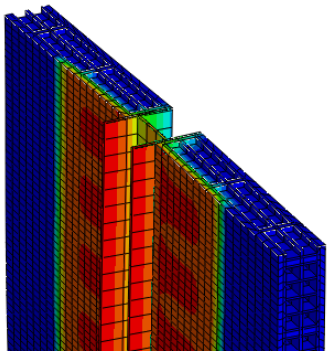

c) Test E08

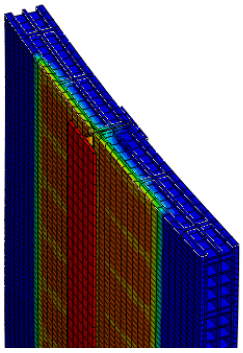

d) Test E09

Figure 6.10 – Finite element models of steel columns embedded on walls a) Test E03 b) Test E04 c) Test E08 d) Test E09

6.3. Steel and Composite Partially Encased Steel-Concrete Columns

6.3.1. Introduction

With the aim of proposing simplified calculation methods of steel and composite steel-concrete columns, taking into account the effect of the restraint to their thermal elongation, a numerical study was carried out with the finite element program ABAQUS, version 6.7. The results of numerical simulations were compared with the ones from fire resistance tests on steel columns with restrained thermal elongation. For the steel columns, a parametric analysis was performed with more than one hundred numerical simulations, to sustain an analytical proposal which was derived from this work.

6.3.2. Numerical Models

The fire resistance tests on steel columns used to calibrate the numerical study were carried out in the Laboratory. The experimental system which was specially conceived and constructed for fire resistance tests on building columns with restrained thermal elongation was already described in chapter 4, and was reproduced with great accuracy for the numerical simulations (Figure 6.10).

The restraining frame was modelled with the same geometry, dimensions, stiffeners, holes, and the special device for the measurement of the restraining forces, as the structure used in the tests, with great accuracy. The use of a three-dimensional frame allowed to take into account not only the axial stiffness but also the rotational stiffness, such as observed in a real structure.

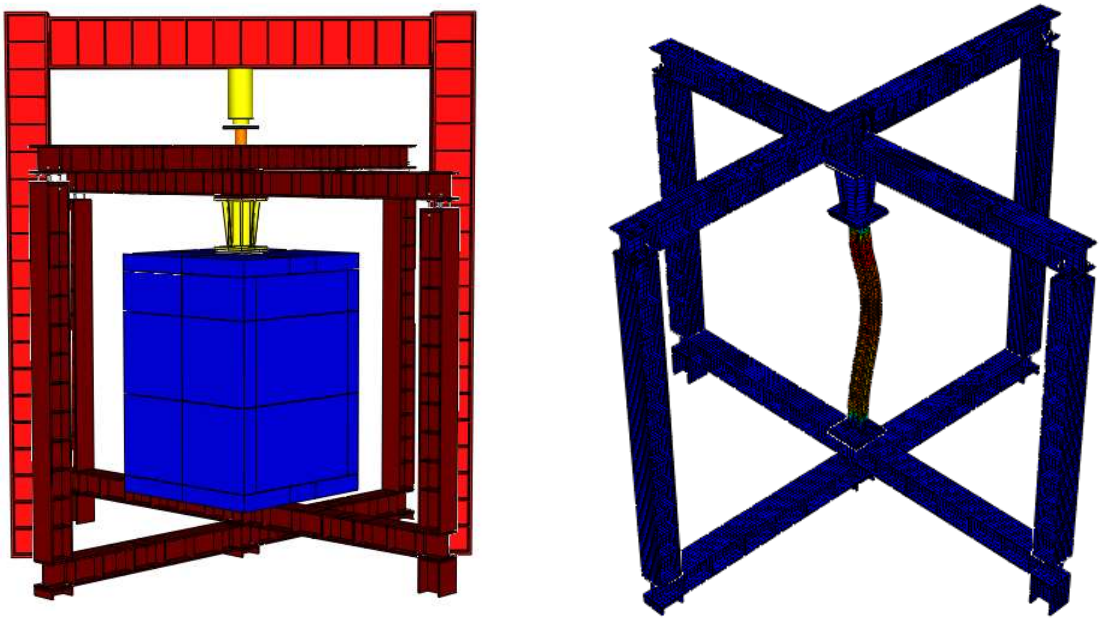

a) b)

Figure 6.11 – Numerical model a) whole model b) column and restraining frame

As already explained, the different values of stiffness of the surrounding structure were provided by positioning the peripheral columns of the restraining frame in different positions. The beams had holes in different positions, at different distances to the centre of the frame, providing different values of axial and rotational stiffness to the columns under test. This different configurations were also reproduced in the model. Figure 6.11 presents the simulated cases. With different values of the span, different values of axial and rotational stiffness were obtained.

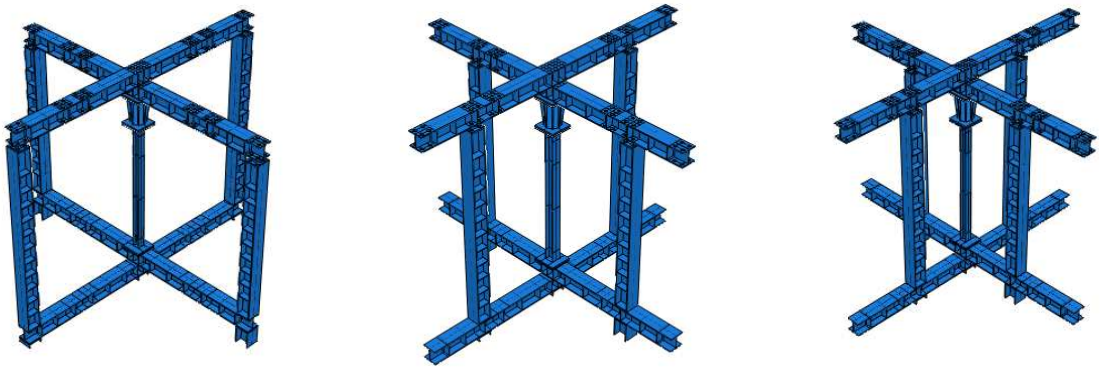

a) b) c)

Figure 6.12 – Test model of the 3D restraining frame for the different stiffness of the building surrounding structure tested

Table 6.3 presents the calculated values of the axial and rotational stiffness of the surrounding structure. The axial stiffness $K_{A,S}$ was calculated applying a force upwards, and measuring the displacement in the centre of the frame. The stiffness is the force to obtain a unitary displacement. These values were obtained both experimentally and numerically. The rotational stiffness $K_{R,S}$ was calculated applying a bending moment in the central node of the beams, and measuring the rotation. The stiffness is the bending moment which produces a unitary rotation. This value was calculated numerically, only in the plane of buckling of the columns. In all tests, experimental and numerical, the columns were placed with the same orientation of the web, and the buckling was always observed in the same plane, perpendicular to the web of the columns.

Table 6.3 – Surrounding structure axial and rotational stiffness

Case Simulated	**Span of the beams (m)**	$K_{A,S}$ **(kN/m)**	$K_{R,S}$ **(kN.m/rad)**
Figure 6.11 a)	3	13100	4827.5
Figure 6.11 b)	2	45000	5622
Figure 6.11 c)	1.5	128350	7844

6.3.2.1. Test plan

Table 6.4 presents the yield stresses of the steel columns obtained experimentally in steel coupons (see Appendix A). Twelve tests were used for the calibration of the numerical model. Two steel cross-sections, HEA200 and HEA160, two load levels *(L)*, 30% and 70% of $N_{Rd,20}$, and three values of the stiffness of surrounding structure ($K_{A,S}$), 13, 45 and 128 kN/mm

Table 6.4 – Test plan for isolated steel bare columns

Test reference	Steel Profile	Slenderness λ	Load (kN) *(LL)*	$K_{A,S}$ (kN/mm)	σ_{sy} (Mpa)
HEA200-K13-L70	HEA 200	50.6	1000 (70%)	13	364
HEA160-K13-L70	HEA 160	63.3	621 (70%)	13	399
HEA200-K13-L30	HEA 200	50.6	428 (30%)	13	375
HEA160-K13-L30	HEA 160	63.3	266 (30%)	13	399
HEA160-K45-L70	HEA 160	63.3	621 (70%)	45	399
HEA160-K45-L30	HEA 160	63.3	266 (30%)	45	385
HEA200-K45-L70	HEA 200	50.6	1000(70%)	45	360
HEA200-K45-L30	HEA 200	50.6	266 (30%)	45	364
HEA200-K128-L30	HEA 200	50.6	428 (30%)	128	412
HEA160-K128-L30	HEA 160	63.3	266 (30%)	128	395
HEA200-K128-L70	HEA 200	50.6	1000 (70%)	128	412
HEA160-K128-L70	HEA 160	63.3	621 (70%)	128	395

Table 6.5 – Test plan for composite steel-concrete columns

Test Reference	Steel Profile	$\overline{\lambda}_z$	Load (kN) (% of $N_{Rd,20}$)	$K_{A,S}$ (kN/mm)	Yield stress of steel coupon tests (Mpa)	Compressive resistance of concrete (Mpa)
CSC160-K128-L30	HEA 160	1.1	(273)30%	128	395.82	41.31
CSC160-K128-L70	HEA 160	1.1	(637)70%	128	394.43	41.31
CSC200-K128-L30	HEA 200	0.87	(514)30%	128	375.35	41.31
CSC200-K128-L70	HEA 200	0.87	(1199)70%	128	362.28	41.31
CSC160-K45-L30	HEA 160	1.1	(273)30%	45	395.26	41.31
CSC160-K45-L70	HEA 160	1.1	(637)70%	45	394.43	41.31
CSC200-K45-L30	HEA 200	0.87	(514)30%	45	425.37	42.15
CSC200-K45-L70	HEA 200	0.87	(1199)70%	45	360.36	38.59
CSC160-K13-L30	HEA 160	1.1	(273)30%	13	395.82	42.15
CSC160-K13-L70	HEA 160	1.1	(637)70%	13	395.82	42.15
CSC200-K13-L30	HEA 200	0.87	(514)30%	13	362.28	42.15
CSC200-K13-L70	HEA 200	0.87	(1199)70%	13	360.36	42.15

6.3.2.2. Numerical simulations

A thorough numerical simulation of the experimental tests described in the last section, as well as several other cases, with a geometrical and material non-linear analysis with imperfections, was carried out.

The numerical model used was generated with three-dimensioned solid elements C3D8RT and C3D20RT from the ABAQUS program library. The C3D8RT and C3D20RT are defined as hexahedral 8 node and 20 node linear brick with reduced integration, an hourglass control solid element and a first-order (linear) interpolation element, with 3 degrees of freedom per node, referring to translations in the 3 directions X, Y and Z (global coordinates). These finite elements have one integration point, three degrees-of-freedom per node, corresponding to translations and six stress components in each element output. The hourglass control was introduced in the element to suppress spurious modes.

The finite element mesh was generated automatically by the ABAQUS program and the size of finite element was approximate 30mm for the specimen and 50mm for the surrounding structure.

The structural analysis was coupled temperature-displacement type, in which thermal and mechanical responses are performed together.

The temperatures used in the numerical simulations for calibration the numerical models were the gas temperatures registered in the experimental tests. In the further numerical simulations, to provide data for the development of the simplified calculation methods for fire design of steel columns, the ISO 834 (ISO 834 (1975)) standard fire curve was used. Thermal action was thus applied in the gas in the vicinity of the surfaces of the structural elements. Radiation was considered with emissivity coefficient $\varepsilon=0.8$ for steel with "radiant to ambient" surfaces. Convection was considered with convection $\alpha_c=25W/m^2ºC$ with "surface film condition" surfaces. The thermal action in the tests for the calibrations of the model was considered with different temperatures at different heights according to the modules of the electrical furnace. Constraints between different parts of the model were considered tie constraint, with interfaces of master-slave type.

The nonlinear geometry parameter (*NLGEOM=ON) was set to deal with the geometric non-linear analysis, namely, with the large displacement analysis.

The mechanical properties of the steel at room temperature were determined experimentally in tensile tests in steel coupons (Appendix A). The thermal and mechanical properties of the steel at high temperatures considered were those given in EN 1993-1-2 (2005). In order to perform a non-linear geometrical analysis, the stress-strain curve was converted to a true-stress-logarithmic strain law. The nominal stress-nominal strain $\sigma_{nom} - \varepsilon_{nom}$ curve obtained from conventional coupon tests does not give a true indication of the deformation characteristics of a material at higher strain as it is based entirely on the original dimensions of the specimens. In fact, the dimensions of the material change continuously during coupon test. Therefore, nominal stress σ_{nom} and nominal strain ε_{nom} were converted to true stress σ_t and true strain ε_t using following equations:

$$\sigma_t = \sigma_{nom} (1 + \varepsilon_{nom}) \quad (6.1)$$

$$\varepsilon_t = \ln (1 + \varepsilon_{nom}) \quad (6.2)$$

ABAQUS considers the plastic behaviour of materials, defined with the true stress σ_t related to the plastic true strain ε_{nom}.

The thermal action was applied on the testing column, at different heights, in accordance with the data taken from the furnace. It was observed in the tests a great temperature gradient along the vertical direction, in the gas inside the furnace. In such a way to reproduce as faithfully as possible the test conditions, different gas temperatures were applied in the gas in the vicinity of the column at different heights, with the corresponding coefficients of radiation and convection. The column was partitioned into two parts 1m height, and one part 0.5m height, according to the furnace dimensions. The temperature used in the numerical simulations were the ones recorded in the tests, for each of the mentioned modules (Figures 6.12 a) to c)).

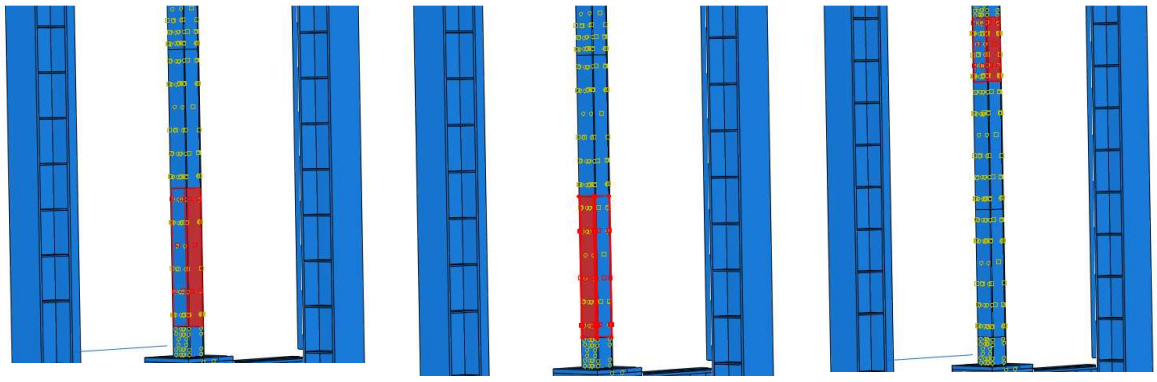

a) b) c)

Figure 6.13 – Thermal action on composite columns a) on concrete at the lower module b) on steel at the lower module c) on concrete at the upper module

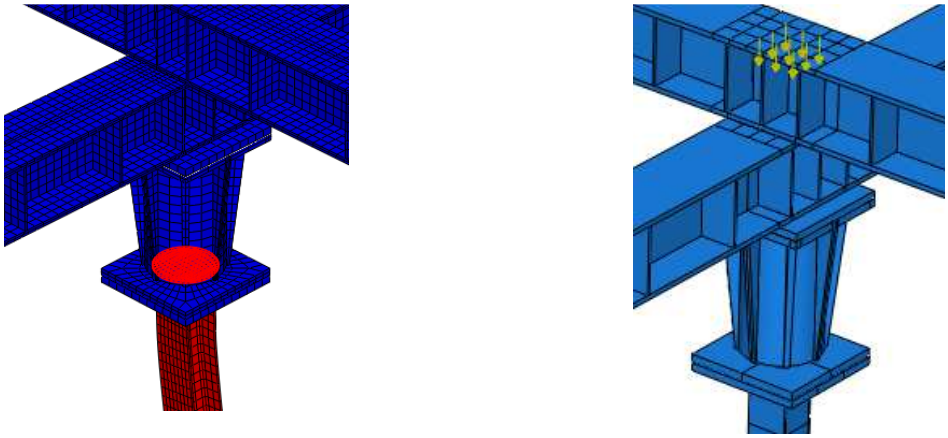

a) b)

Figure 6.14 – Details of the numerical modeling of the testing column a) finite elements considered in the cylinder for the calculations of axial force b) load applied at different points.

The axial forces developed during the tests were determined with the stresses in the finite elements of the cylinder on top of the column. This cylinder was modeled exactly as in the experimental tests and was used only in the numerical simulations to calibrate the model (Figures 6.13).

The load was applied on top of the upper beam, in several points, to prevent excessive deformation of the upper flange (Figures 6.13 b)).

Geometrical imperfections were considered as initial eccentricity of the load in relation to the column axis and bow out-of-straightness of L/1000 at mid-height of the column. This value was calculated according to the formula (Santiago, 2008):

$$y = \frac{L}{1000} sin\left(\frac{\pi.x}{L}\right) \tag{6.3}$$

in which:
L is the column span;
x is the position where the imperfection is calculated.

Eccentricities of L/1000 were also considered in the position of the column.

The test procedure used in the tests for totally transfer the initial applied load to the testing columns was reproduced in the numerical simulations using different time steps.

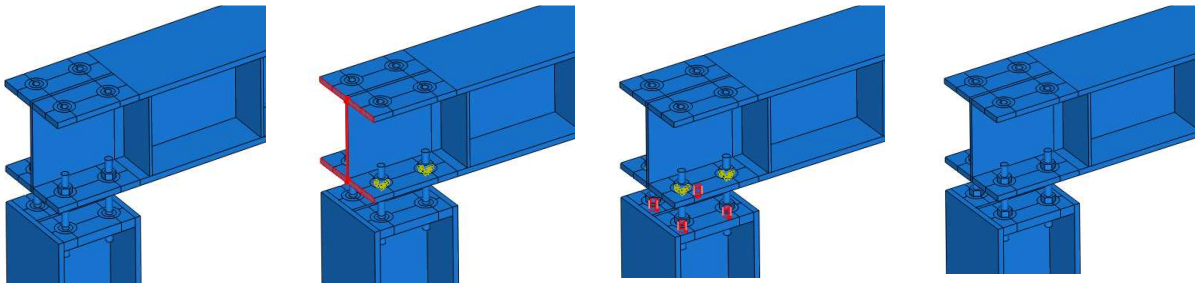

a) b) c) d)

Figure 6.15 – Procedure used in the numerical simulations to simulate the application of the initial applied load

In the first step no constraint between the upper beams and peripheral columns of the restraining frame (Figure 6.14 a)). The upper beams could descend in vertical movement of translation guided by a top constraint allowing only vertical displacement, as a slide (Figure 6.14 b)). This was necessary due to the fact that geometrical imperfections were considered as an initial eccentricity and out-of-straightness of the column axis. In the second step, considering a tie constraint between the threaded rods and the end plate of the columns, to simulate the screw of the nuts, the thermal load was applied (Figure 6.14 c) and d)). With this procedure, the initial load was exactly the load applied on top of the beams, in the center of the frame.

Table 6.6 – Plan of the parametric numerical study in bare steel columns

Test Reference	$K_{A,S}$ *(kN/mm)*	α_A	β_R	l_c *(m)*	λ	*Load Level L*	P_0 *(kN)*
K13-L30-λ35.1	13, 45, 128 and full restraint	0.03	1.08	2.5	35.1	30%	495.7
K13-L30- λ50.6		0.04	1.55	3.6	50.6		428.5
K13-L30- λ65.4		0.05	2.00	4.65	65.4		359.5
K13-L30- λ80.1		0.07	2.45	5.7	80.1		293.5
K13-L30- λ90		0.07	2.75	6.4	90		254.8
K45-L50- λ35.1		0.10	1.25	2.5	35.1	50%	826.1
K45-L50- λ50.6		0.14	1.80	3.6	50.6		714.2
K45-L50- λ65.4		0.19	2.33	4.65	65.4		599.1
K45-L50- λ80.1		0.23	2.86	5.7	80.1		489.1
K45-L50- λ90		0.26	3.21	6.4	90		424.6
K45-L70- λ35.1		0.28	1.75	2.5	35.1	70%	1156.6
K45-L70- λ50.6		0.41	2.52	3.6	50.6		998.8
K45-L70- λ65.4		0.53	3.25	4.65	65.4		838.8
K45-L70- λ80.1		0.65	3.98	5.7	80.1		684.8
K45-L70- λ90		0.73	4.47	6.4	90		594.5

Table 6.6 summarises the plan of the numerical simulations carried out. Sixty simulations were carried out on HEA200 cross-sections. To obtain the different values of slenderness, different lengths were considered, as presented in the previous table.

Moreover, numerical simulations were also carried out for the columns with the five different lengths here described, but considering a full constraint provided by the surrounding structure. In this table, the first column indicates the references of the tests that are similar to the ones used in the experimental tests. The reference K13-L30-λ35.1 indicates a column tested with an axial stiffness of the surrounding structure, a load level (L) of 30% and a slendernesss (λ) of 35.1.

It should also be pointed out that the modelling of the experimental set-up was performed at this stage without the device used to measure the restraining forces. This device was modelled and used only in the simulations of the experimental tests. For these simulations, the peripheral columns had to be modelled again with a smaller length, so that no gap between the specimen and restraining frame was observed. The slenderness of the columns was calculated considering the length of the column of 3.0m, and a buckling length of 0.7L.

The initial applied load P_0 is a percentage of the design value of the buckling load at room temperature calculated according EN 1993-1-1(2005).

The calibration of the numerical models was a process which consisted in testing several values of the emissivity coefficients for steel and for the flames, taking as reference the measured temperatures in the columns obtained in the experimental tests. The thermal action was applied in the gas in the vicinity of the steel specimen, and the convection and radiation performed by the coupled temperature-displacement analysis by ABAQUS. The adopted values for the emissivity were $\varepsilon_m=0.8$ for steel, $\varepsilon_m=0.7$ for concrete and $\varepsilon_f=0.8$ for the fire, and a convection coefficient factor of $\alpha_c=25 W/m^2 ºC$, leading to very close temperatures to the ones obtained experimentally.

The numerical modeling of the concrete columns was very similar to the one performed for the steel columns. The interaction with the surrounding structure, the test procedure and imperfections were considered exactly the same way. The main differences concerned the modeling of the concrete. The model used in these simulations was the “Concrete damaged plasticity”. This model uses concepts of isotropic damaged elasticity in combination with isotropic tensile and compressive plasticity to represent inelastic behaviour of concrete. It consists of a combination of non-associated multi-hardening plasticity and isotropic damaged elasticity to describe the irreversible damage that occurs during the fracturing process. This model is a continuum, plasticity based, damage model for concrete. It assumes that the main two failure mechanisms are tensile cracking and compressive crushing of the concrete

material. The evolution of the yield (or failure) surface is controlled by two hardening variables, linked to failure mechanisms under tension and compression loading, respectively.

The modeling of the reinforcement rebars was performed using solid elements, using the constitutive model "Plastic-plasticity", which is an elasto-plastic model available in Abaqus library. An attempt was made to use embedded elements, a type of finite element specially conceived for steel reinforcements of concrete, available in ABAQUS, but better results were obtained with solid elements.

The interface between the concrete and the steel elements was performed of type "tie" constraint. Some simulations were performed, allowing the detachment of the concrete from the steel, but better results were obtained with "tie" constraint.

6.4. Results

6.4.1. Columns Embedded on Walls

6.4.1.1. Temperatures

The temperatures in the experimental tests were measured in 6 points of 5 sections of the steel column. The temperatures at mid-height of the columns were compared with the ones obtained in numerical simulations for 60 minutes. In these figures, th_1 stands for the thinner walls, and th_2 stands for thicker walls.

In the case of the web parallel to the wall surface, the temperature in the flange not exposed to the fire (thermocouple 4), is higher in the case of the walls of smaller thicknesses (Figure 6.15 a) and 6.17 a)). For the HEA160, the difference is nearly 100ºC for the STC calculations and experimental tests while for the HEA200, the difference is nearly 75ºC for the STC calculations and experimental tests.

In the face of the web exposed to the fire, the temperatures are higher for the thin than for the thick walls (thermocouple 3), presenting a very small difference between STC simulations and the experimental tests (Figure 6.17 b)).

In the case of the web perpendicular to the wall surface, the temperature in the exposed flange (thermocouple 5) is also higher in the case of the thin wall than in the thick wall (Figure 6.16 a) and Figure 6.18 a)). For HEA160 the difference is approximately 50ºC in the STC simulations and nearly the same in the experimental tests. For HEA200 the difference is about 100ºC in both analyses.

Curiously in the flange not exposed the temperatures are higher for the thick wall (thermocouple 6), in the experimental tests. For HEA160 the difference is about 100ºC in the experimental test and for HEA200 they are very close in both analysis.

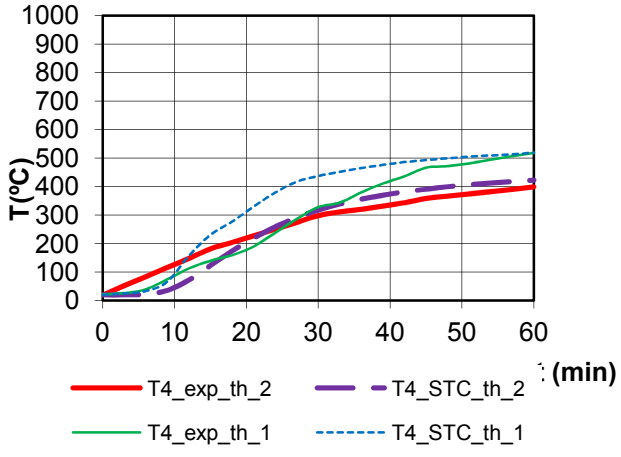

a) thermocouple T4 ;

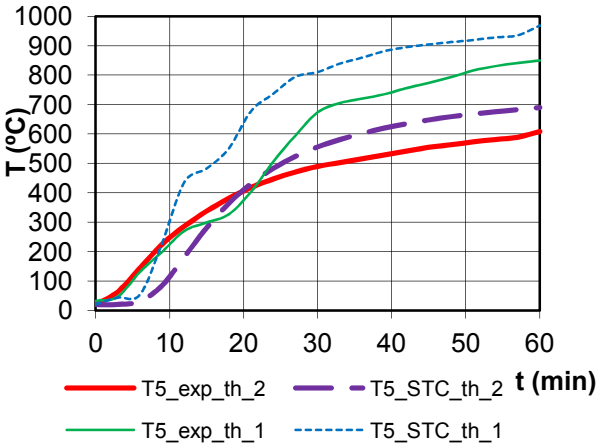

b) thermocouple T5

Figure 6.16 – Comparison between thick and thin wall, of temperatures vs time for HEA160 with the web parallel to the wall ;

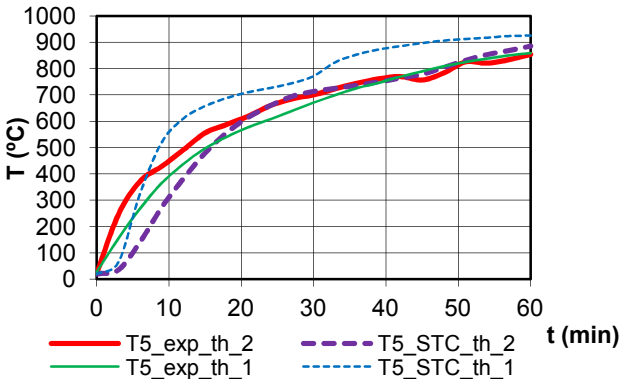

a) thermocouple T5 ;

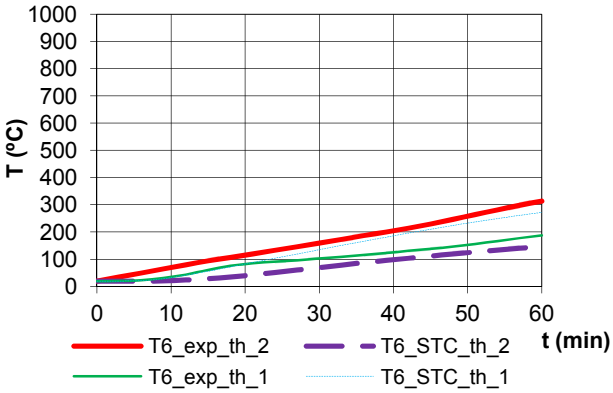

b) thermocouple T6

Figure 6.17 – Comparison between thick and thin wall, of temperatures vs time for HEA 160 with the web perpendicular to the wall ;

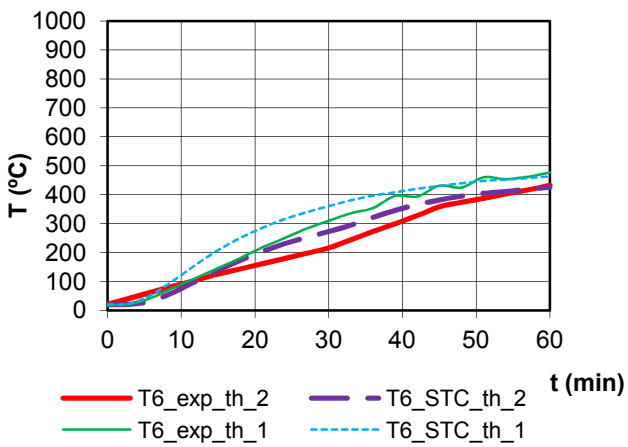

a) thermocouple T6 ;

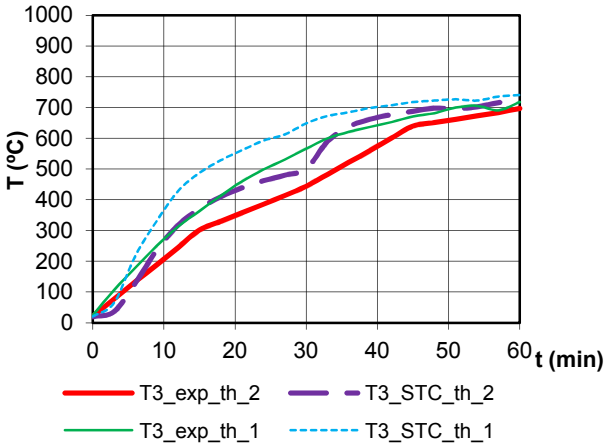

b) thermocouple T3

Figure 6.18 – Comparison between thick and thin wall, of temperatures vs time for HEA 200 with the web parallel to the wall ;

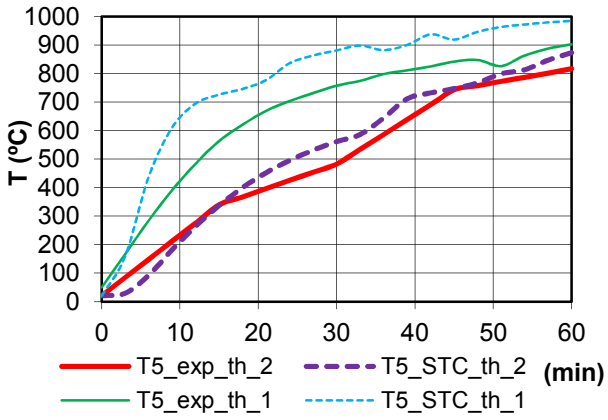

a) thermocouple T5 ;

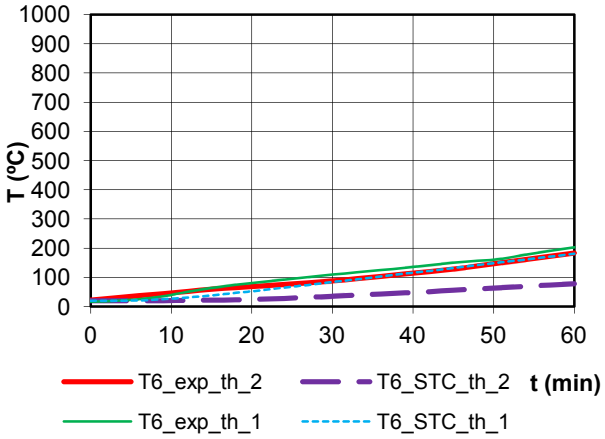

b) thermocouple T6

Figure 6.19 – Comparison between thick and thin wall, of temperatures vs time for HEA 200 with the web perpendicular do the wall;

In Figure 6.19, a comparison of the temperature distribution in the bare steel column, totally engulfed by the fire, with a column embedded on walls, is performed.

From Figure 6.19 b) it may be observed the great thermal gradient within the web in the case of the column embedded on the walls. If the column is totally engulfed in the fire, the temperatures in the flanges and web are nearly the same.

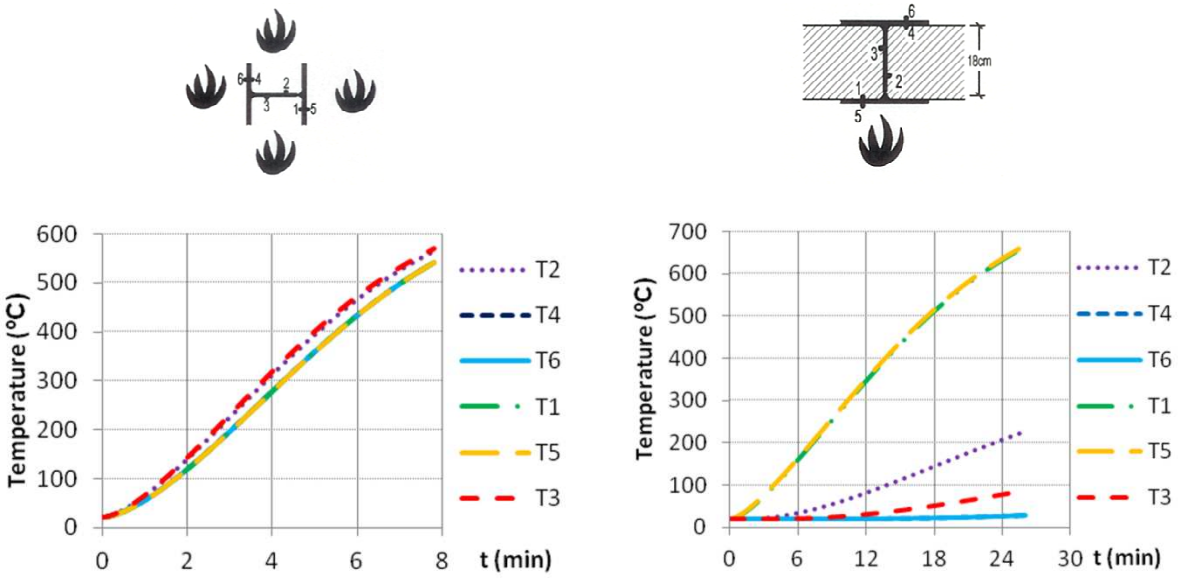

a) Bare steel column, in test I20 (isolated HEA200)

b) steel column totally embedded on walls in test E04 (HEA 200, thick wall, web perpendicular to the wall)

Figure 6.20 - Temperature evolution in the mid-height cross section

The following tables and figures depict in a more detailed way the great thermal gradients observed in the H steel profile cross section, both with the web perpendicular and parallel to the walls, for an HEA160 steel profile, with thick walls in both cases. The data in these tables is necessary for the development of the analytical analysis of these columns presented in the next chapter.

Table 6.7 – Temperatures in the exposed flange, web, unexposed flange and mean temperature for a steel column embedded on walls, with the web perpendicular to the wall (Test E11)

t(min)	Exposed flange	Web	Unexposed flange	Mean steel temperature
0.0	20	20	20	20
1.8	101	49	20	57.5
3.2	203	87	20	105
4.5	301	127	20	152
5.9	401	170	21	200
7.6	502	220	23	252
10	601	280	28	306
14.6	700	362	42	369
24	793	465	84	445

Both Table 6.7 and Figure 6.20 depict the evolution of the temperatures in the web, exposed and unexposed flanges, and the mean temperature in the steel profile, along the time, for the test E11, with the web perpendicular to the wall. It is clearly observed that the temperature in the unexposed flange reaches a maximum value of 84ºC, in the end of the test, despite of the mean value exceeds 400ºC.

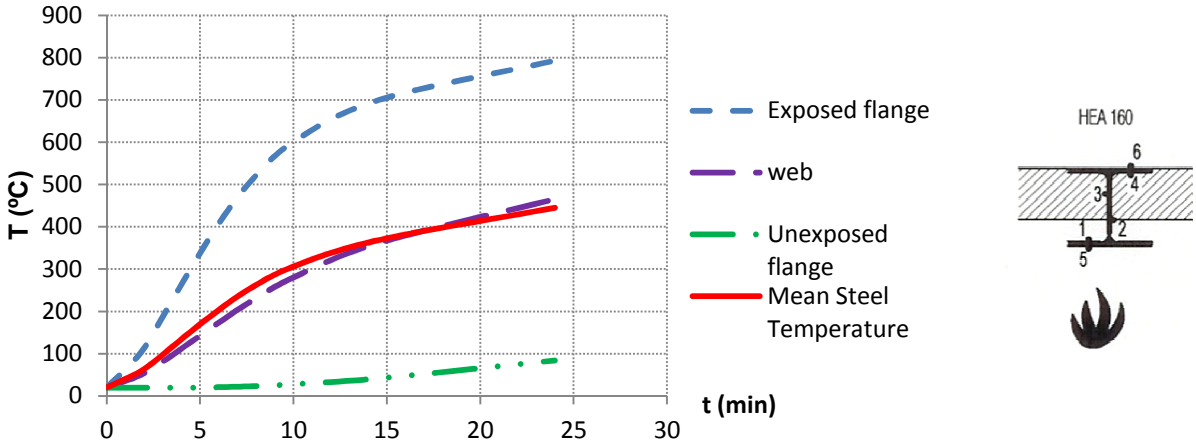

Figure 6.21 – Temperatures in the exposed flange, web, unexposed flange and mean temperature for a steel column embedded on walls, with the web perpendicular to the wall (Test E11)

Table 6.8 – Temperatures in the exposed half-flange, web, unexposed half-flange and mean temperature for a steel column embedded on walls, with the web parallel to the wall (Test E11)

t(min)	Exposed half-flange	Web	Unexposed half-flange	Mean steel temperature
0	20	20	20	20
2.25	101	80	37	71.8
4.16	200	159	72	141.9
6.1	300	244	119	218.4
8.3	400	329	174	297.8
11.1	500	417	245	383.9
15.5	600	513	333	478.5
16.3	614	526	347	492.2

Table 6.8 and Figure 6.21 present the temperatures in the exposed half-flange, web, unexposed half-flange and the mean temperature for a steel column embedded on walls, with the web parallel to the wall (Test E10). A lower thermal gradient is observed in this case, but still the temperature in the unexposed side is lower than 400ºC.

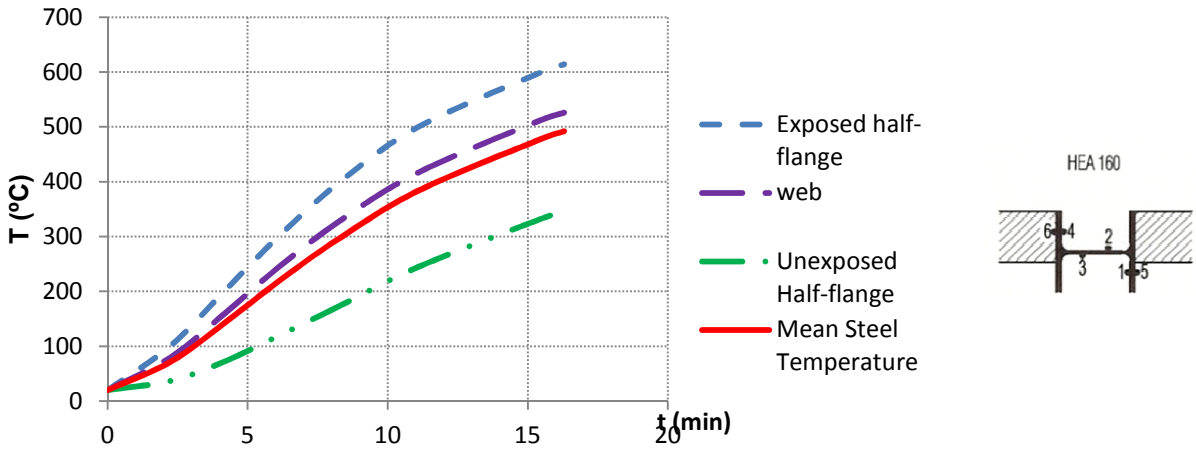

Figure 6.22– Temperatures in the exposed half-flange, web, unexposed half-flange and mean temperature for a steel column embedded on walls, with the web paralell to the wall (Test E10)

6.4.1.2. Restraining forces

Figure 6.22 presents the variation of the restraining forces for steel columns HEA200 and HEA160 embedded on walls and isolated in function of the time. The values are refered to the initial applied load. In these graphs, the reference Exx means column embedded on walls and Ixx means isolated columns. The fire resistance is here defined as the instant when the restraining forces after increasing and reaching a peak, equal again the initial applied load.

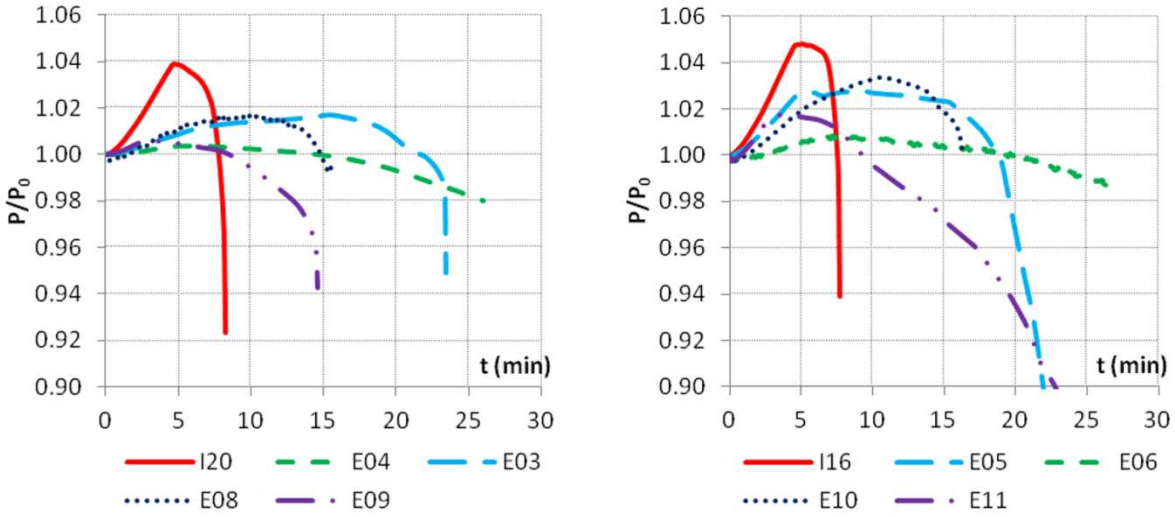

a) HEA 200 b) HEA 160

Figure 6.23 - Restraining forces in function of time

It can be clearlly observed in Figures 6.22 a) and b) that the steel columns embedded on walls attained higher fire resistances than the isolated ones. Also, it is observed that the variation of restraining forces was lower than in bare steel columns.

For the HEA200 columns, the embedding on walls, increase the fire resistance up to 21.4 minutes (test E03) instead of 8.3 minutes for bare steel column (test I20). Also, it is observed that the increasing of restraining forces can be as low as 0.4% for test E04, instead of 4% for the bare steel column (test I20), i.e., 10 times lower (Figure 6.22 a)).

For the HEA160 columns, a fire resistance of around 20 minutes was achieved for tests E05 and E06 for columns embedded on walls. In therms of restraining forces, the lowest value observed is 1% for test E06 (Figure 6.22 b)). This result was expected, once that both in tests E04 and E06, the steel profile was completely embedded on the walls.

Tests E11, E06, E09 and E04 on columns embedded on walls and with the web perpendicular to the wall surface provided lower restraining forces. Tests E04 and E06, where columns were completely embedded on walls, presented higher fire resistance, showing the beneficial effect of the walls on protecting the columns.

The behaviour in tests E05 and E10 are very similar to the test with the bare steel column (Figure 6.22 b)). The failure seem to occur by buckling due to an abrupt reduction in the axial displacements.

Tests E04 and E06 presented the most smooth evolution of restraining forces, once the columns are almost totally embeded on walls, except the outter surface of the flange.

The analysis of these graphs lead to the conclusion that the failure of steel columns embdded on walls is significantly different form the failure of bare steel columns. The criterion of considering the colapse as the instant when the axial force after increasing up to a maximum decays and reaches the initial value seems to be inadequate to the columns embedded on walls, due to the fact that in these cases failure is not so abrupt, and a great resistance is observed for a long period of time.

In Figure 6.23 both the axial displacements and the lateral deflections were very similar in tests E04 and E09.

This phenomenon known as “Thermal Bowing” was already described by other authors. The inversion of bending moments, accompanied with the inversion of deflections is

typical of a heated column with restraint to thermal elongation, submitted to a differential heating process (Figure 6.24).

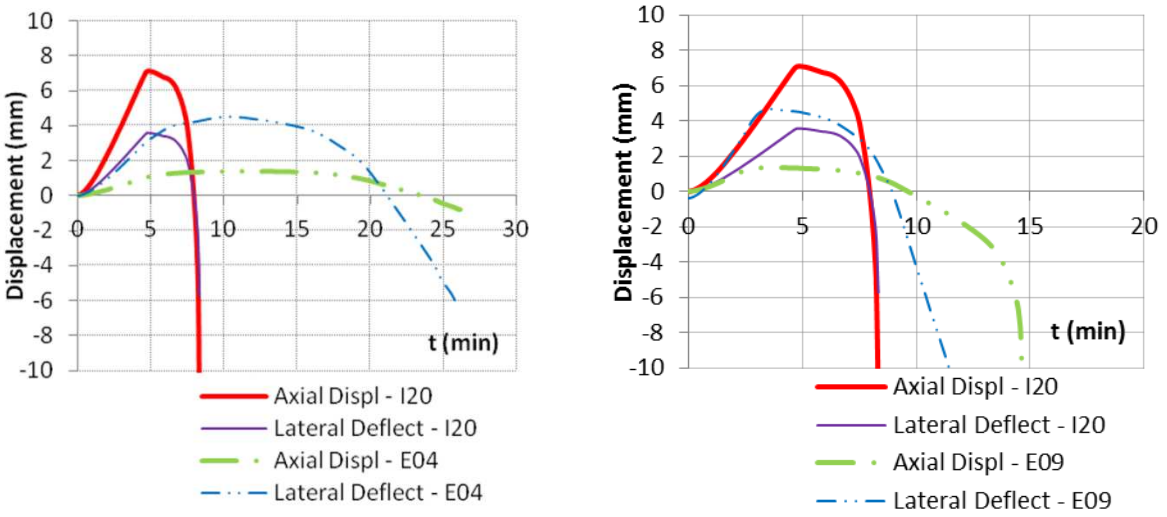

a) E04 (wall thicness=180mm) b) E09 (wall thicness=140mm)

Figure 6.24 - Axial displacements and lateral deflections for isolated and embedded on walls HEA200 steel columns - web perpendicullar to the wall surface

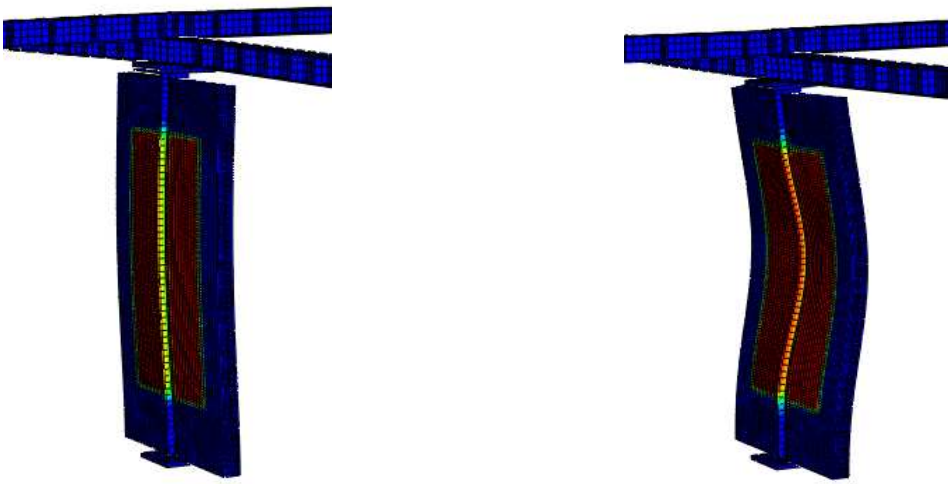

a) Test E11 – instant t=440s (scale factor=10) b) Test E11 – instant t=1445s (scale factor=5)

Figure 6.25 - Deformed shape of the columns, in test E11, HEA 160, web perpendicular to the wall, with thin wall.

Figure 6.25 shows the behaviour of an H steel column with a thermal gradient in the direction of the web (figure 6.25 a)) and in the direction of the flange (figure 6.25 b)). The sign convention for this analysis is such that positive moments produce tension in the right-hand

(cooler) face of the member, and positive axial forces correspond to tensile. Initially, the column will develop a bending moment in response to the thermal strains induced by the gradient because the column ends are fixed against rotation. Since the left flange is hotter than the right one, the left flange will undergo larger thermal strains and consequently greater thermal expansion. Due to the fact that the ends of the columns are restrained from rotating, the left flange becomes compressed and the right flange will experience tensile. This reaction creates a positive bending moment according to our sign convention. This "thermal" moment is referred to as M_T. Before the increasing temperatures affect the steel material properties, ther position of the Effective Centroid coincides with the Geometrical Centroid. When the temperatures in the section have increased, so that the Young's modulus and the yield stress have reduced, the Effective Centroid begins to migrate towards the cooler flange, due to the fact that the cross-section is from this moment on, composed of a material with non-uniform yield stress. The resultant of the axial stresses P_R in the section must equal the applied load P to maintain equilibrium. The position of P_R (which is located at the Effective Centroid) moves according to the change in the section´s material properties. The movement of P_R generates an additional moment about the Geometric Centroid M_{Pxe}, that is equal to P times the distance "e" from the Geometrical Centroid to the new position of the Effective Centroid. M_{Pxe} is opposite in direction to M_T, so it is obvious that at some interval of time, during the heating process, the total moment will reverse its direction, and then reverse its sign when M_{Pxe} becomes larger than M_T. This behaviour of steel columns unevenly heated was firstly described in detail, by Garlock and Quiel (Garlock et al., 2007a).

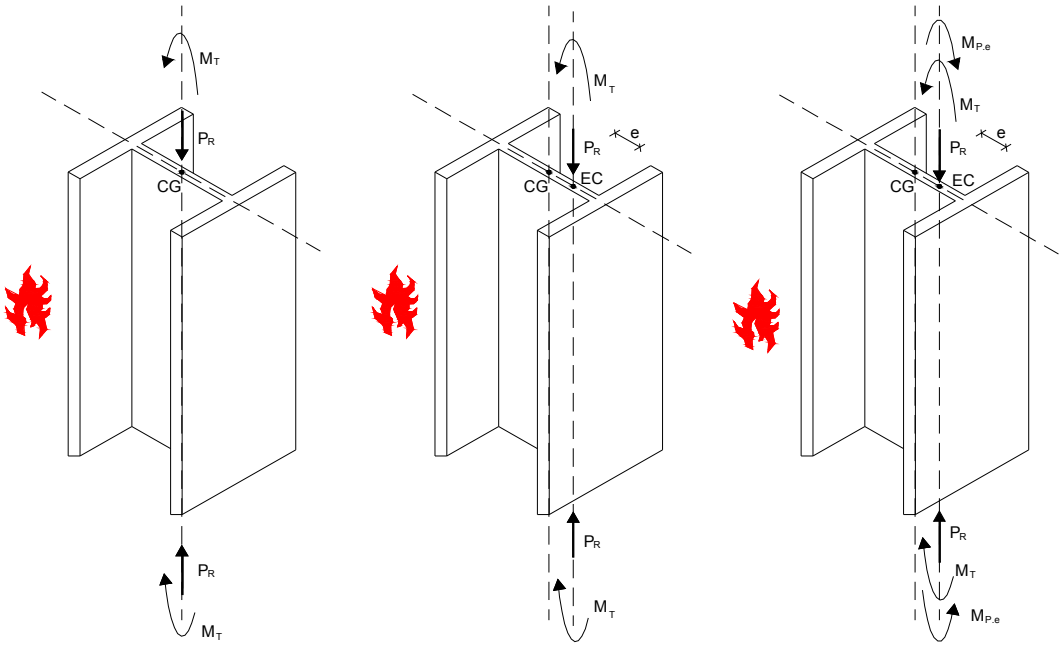

a)

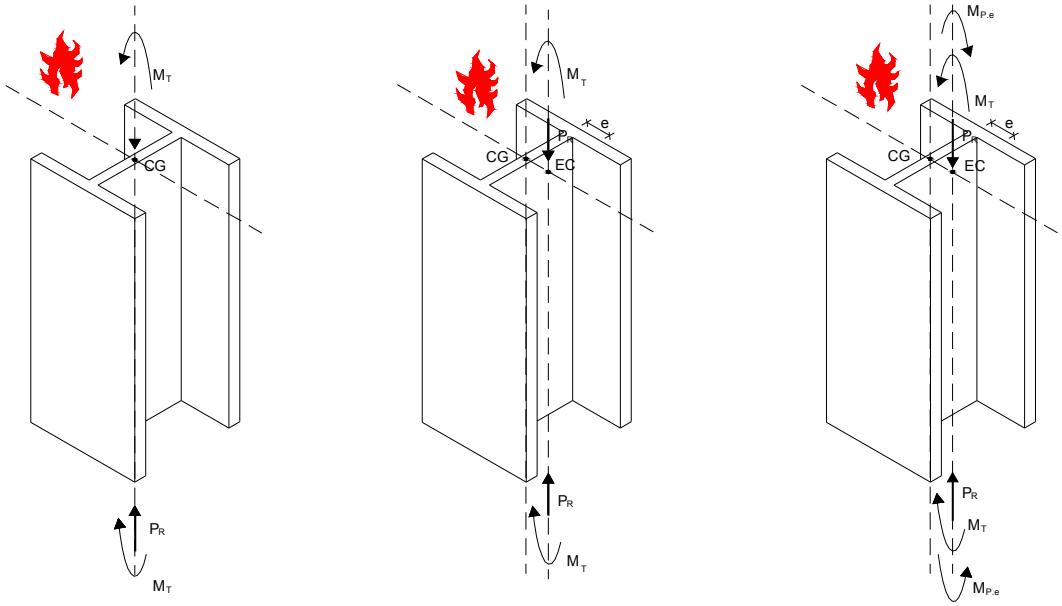

b)

Figure 6.26 – Behaviour of an unevenly heated column with the shift of the efective centroid during the fire event a) gradient along the web b) gradient along the flange

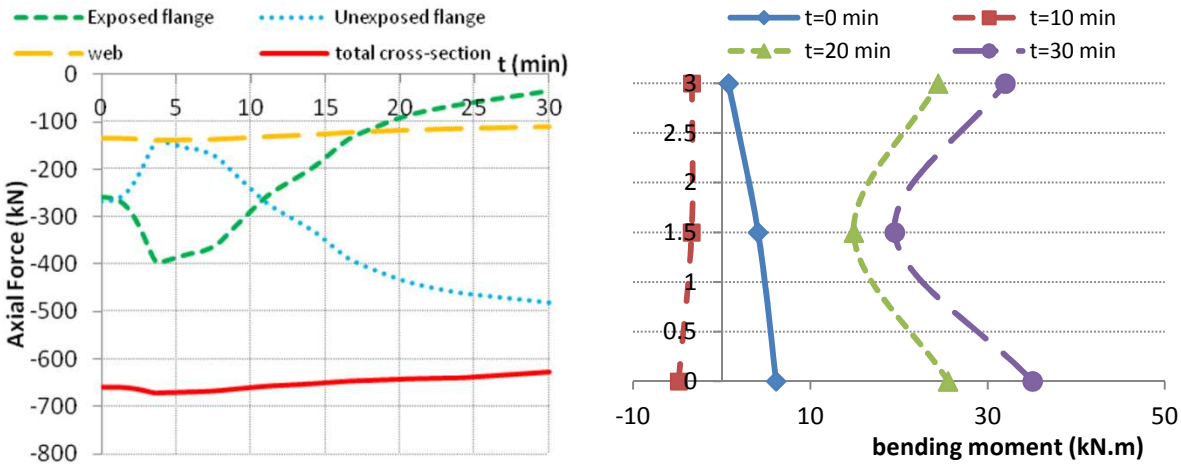

a) b)

Figure 6.27 – Evolution of axial force and bending moments during a fire event in a steel column in contact with walls, obtained in the numerical simulation of test E11

Figure 6.26 a) depicts the variation of the axial force in the flanges, in the web and the total section, on top of the column. It can be observed that the flanges alternate with each other the resistance to the axial force. In the beginning of the test, the axial force increases in the exposed flange and reduces in the unexposed one (in absolute value). After 4 minutes, there is an inversion on this behaviour, and the axial force reduces in the exposed flange and increases

in the unexposed one. The contribution of the web is very small. In the total cross-section, a slight reduction of the axial force is observed during the test. Figure 6.26 b) depicts the inversion of bending moments along the column length, during the time of the test.

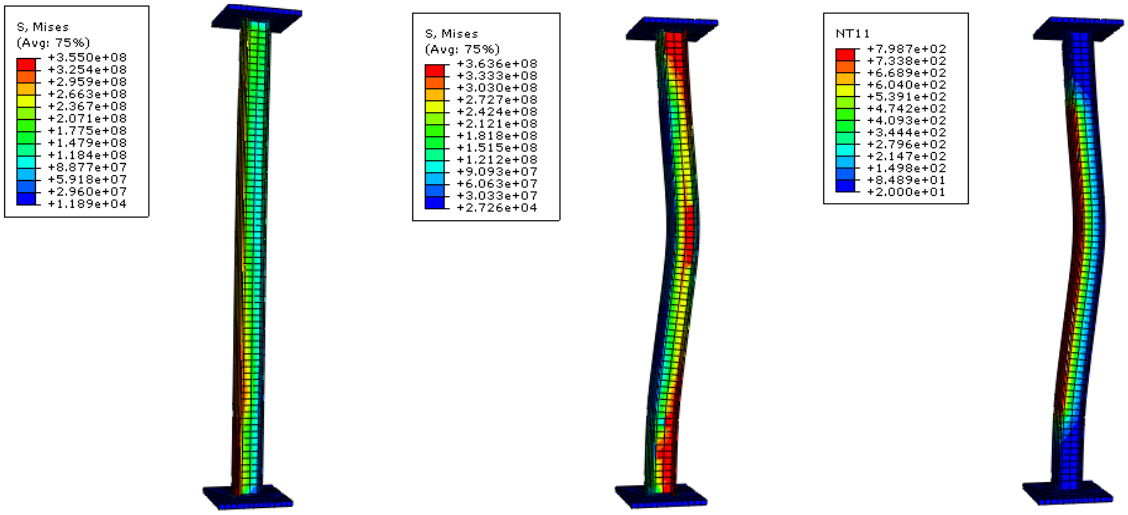

a) b) c)

Figure 6.28 – Evolution of Von Misses stresses and nodal temperatures in a fire test with HEA 160 with the web perpendicullar to the wall E11 a) Von Misses stresses for t=240s (instant of inversion) b) Von Misses stresses for t=1440s c) nodal temperatures for t=1440s

Figure 6.27 a) and b) depict the distribution of Von Misses stresses in the instant of inversion of bending moments (t=4 minutes) and in the end of the test (t=24 minutes) for test E11. It can be observed that yield stress is achieved after 4 minutes of test in the exposed flange, and then again after 24 minutes of test, achieved and overcome in the web and unexposed flange on top, bottom and mid-height of the column, although only a small part of the profile achieved high temperatures (about 800ºC).

Figures 6.28 a) to c) show the behaviour of column E11 during the fire event. A detailed analysis of the temperature evolution, and axial principal stresses and axial strains is performed, in five sections along the height of the column. Analysis of column behavior of test E11 show a similar behavior to test E09 (the same case with the HEA200 steel profile). In these figures, the heat source is on the right side.

The yield stresses in compression on bottom of the heated flange of the column are reached at time 228s, and the nominal strains reach ε_{nom} =0.0025 in the heated border of the flanges (phase 1). Great bending moments will be observed in the extremities of the column, and tension is observed in the unheated extremities of the column. From this moment on, the column will invert its lateral deflection, and starts to bow to the other side, towards de cold side. By the time 555s, it will be again in the initial position and moving on towards the cold side. At this instant, temperatures in the steel column have reached 590ºC and the nominal

strains reach the maximum value of ε_{nom} =0.0077 (phase 2). The increasing of the temperature will lead to an increase of the bowing towards the cold side. At the time 1134s, yield stress in compression is overcome (355MPa) in the web and in the heated flange of the column (phase 3). At this time, maximum temperature in the steel is 758ºC and equivalent strains ε_{nom} =0.02 at mid-height of the column, on the cold side (phase 3). From this instant on, the column will continue bending towards the unheated side, and plastification will occur on the unexposed flange and in a great extent of the web. This will occur at instant 1440s (24 minutes) from beginning, in which large lateral deflections are observed, and great speed of deformation (phase 4). Maximum temperature reached was 799 ºC and maximum nominal strain reaches ε_{nom} =0.076. Comparing this test with test E09, in which the difference is only the steel profile, which is an HEA200, as well as analyses of column behavior for the other described tests would lead to the same behaviour.

Test E11 - Temperatures

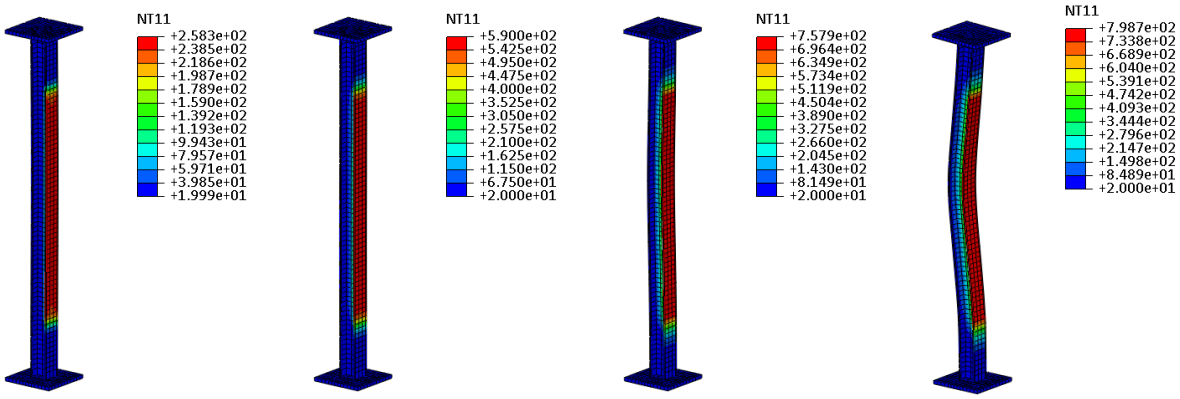

228s – 3.8min **555s – 9.25min** **1134s – 18.9min** **1440s – 24 min**

a)

Test E11 – axial stresses S22

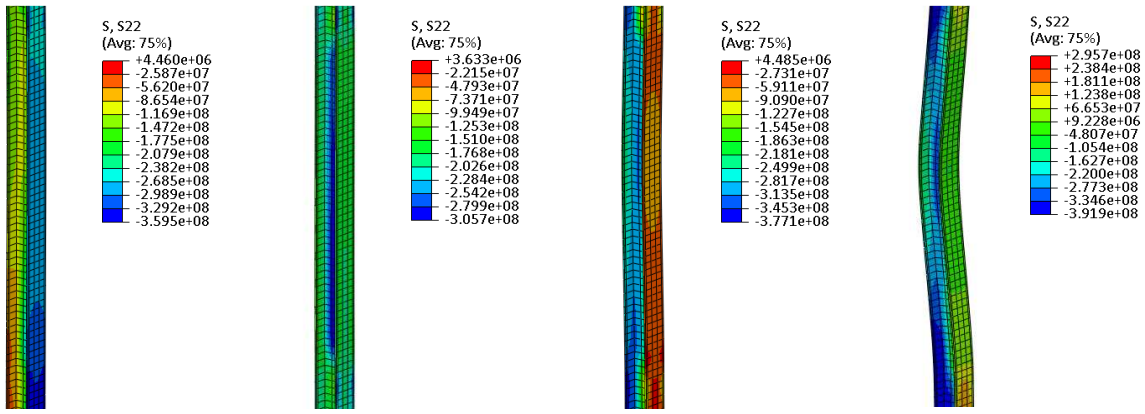

228s – 3.8min **555s – 9.25min** **1134s – 18.9min** **1440s – 24 min**

b)

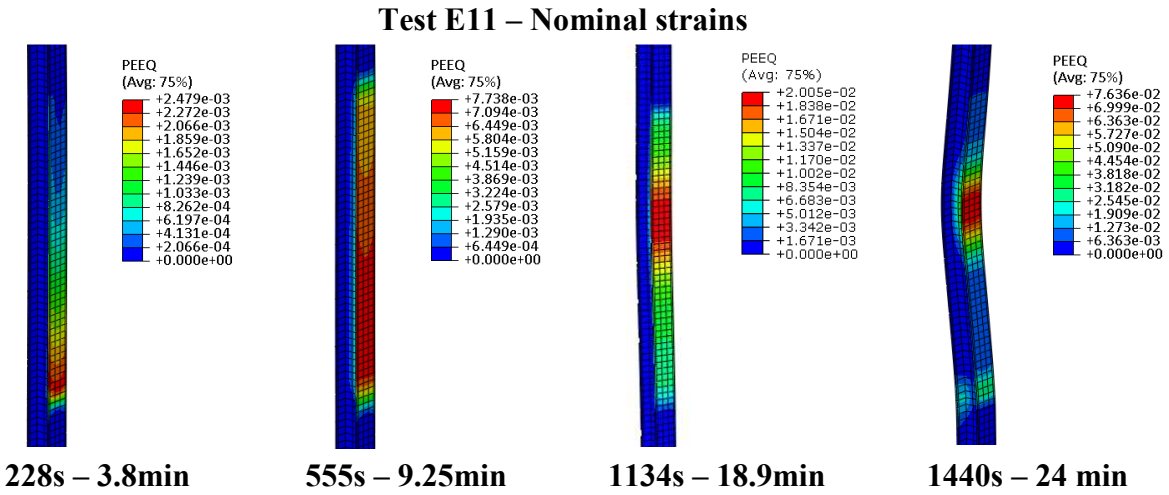

c)

Figure 6.29 – Behaviour of column E11 during the fire event a) temperatures b) axial stresses S22 c) axial strains

In the following lines, an analysis of the temperature dependent stress-strain behaviour of a steel column in contact with walls will be made.

The following graphs depict the evolution of temperatures, nominal strains and axial stress in five steel cross-sections, during the time of a fire test on a HEA160 column, with a thin wall (approximately ¾ of the web length) and the web perpendicular to the wall (Test E11). In all graphs, fire acts on the left side.

Figure 6.29 presents the temperatures, axial stresses and axial strains at the base section of the column during the fire. Despite of the low temperatures, yield stress is reached in the unheated side.

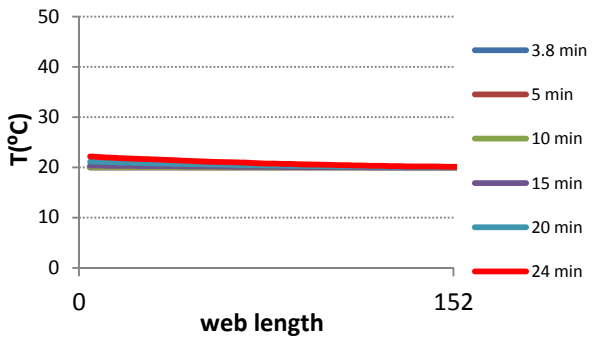

a)

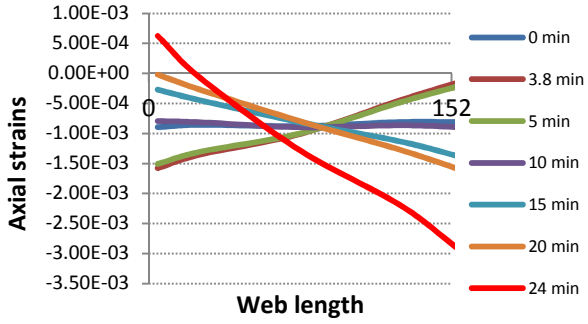

b)

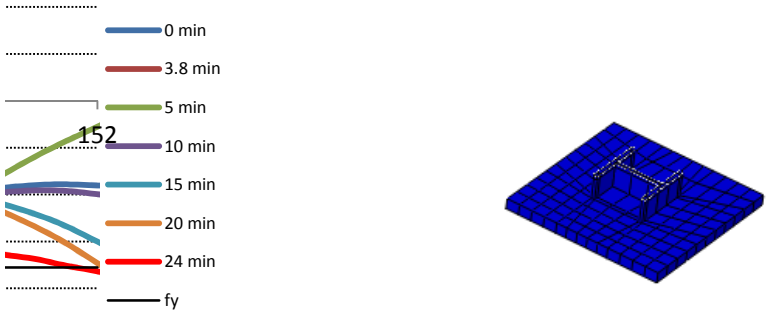

c)

Figure 6.30 – Behaviour of the base section of the column during the fire event a) temperatures b) nominal axial strains NE22 c) axial stresses S22

Figure 6.30 presents the temperatures, principal stresses and axial strains at the section, at 0.58m from the base of the column during the fire.

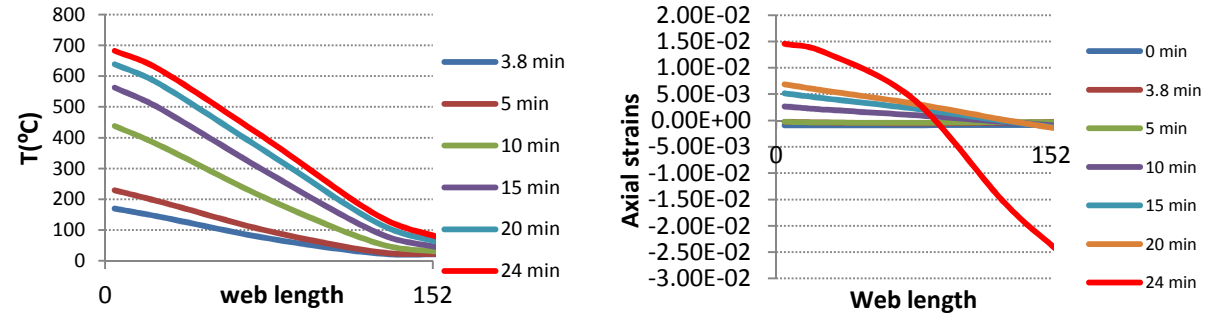

a) b)

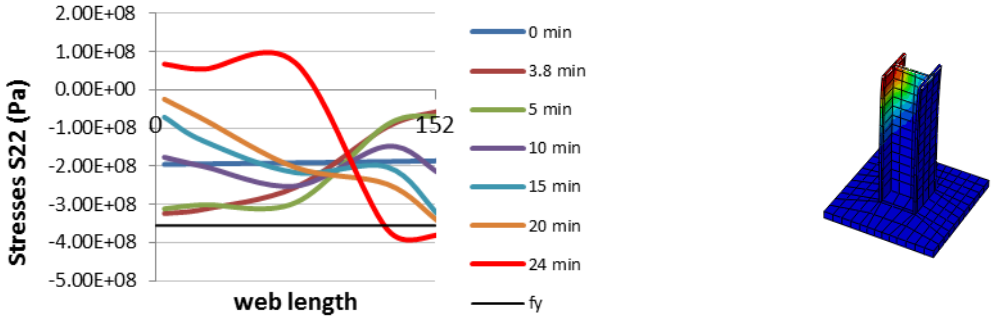

c)

Figure 6.31 – Behaviour of the section at 0.58m from the base of the column during fire a) temperatures b) nominal axial strains NE22 c) axial stresses S22

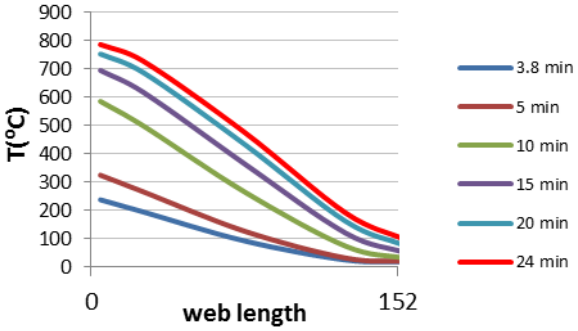

a)

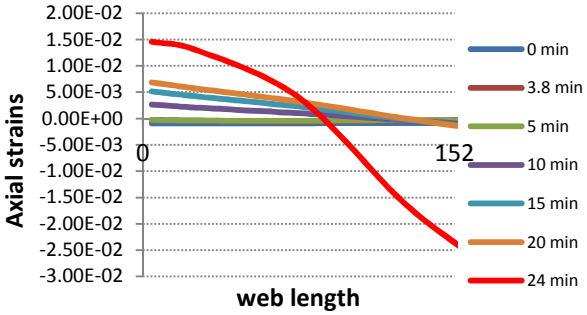

b)

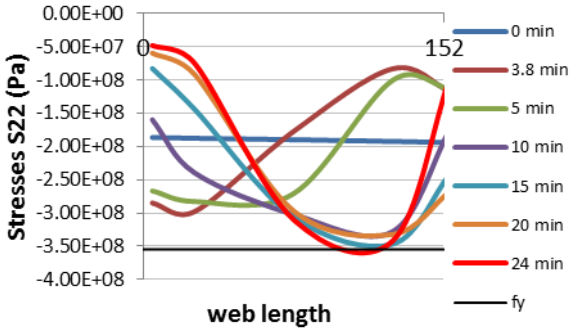

c)

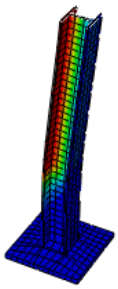

Figure 6.32 – Behaviour at mid-height (1.5m) section of the column during the fire event a) temperatures b) nominal axial strains NE22 c) axial stresses S22

Figure 6.31 depicts the behaviour at the mid-height section of the column.

Figure 6.32 presents the same results for a section at 2.42m from the base of the column, again in the borderline between the heated and unheated length of the column.

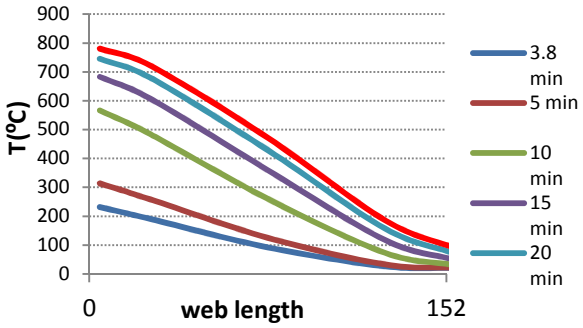

a)

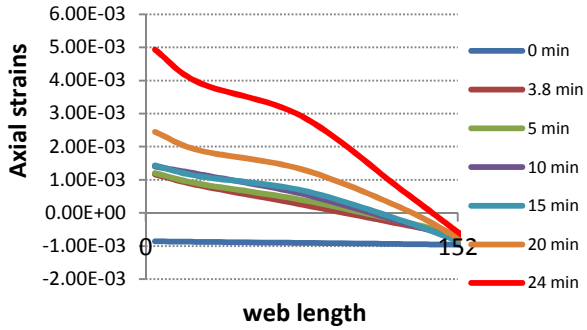

b)

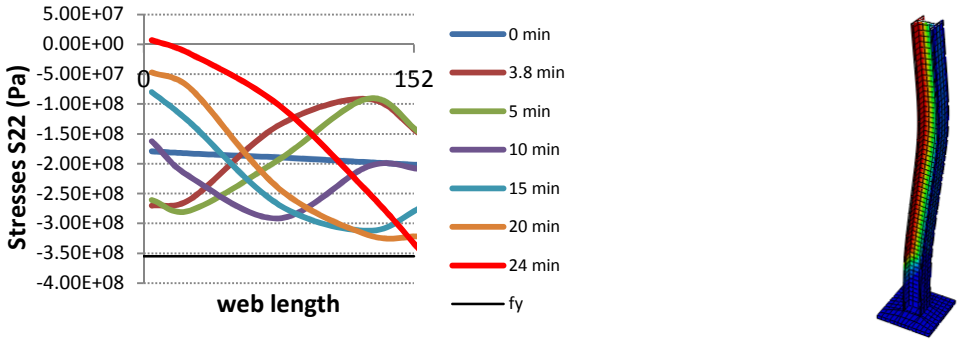

c)

Figure 6.33 – Behaviour of the section at 2.42m from the base section of the column during the fire a) temperatures b) nominal axial strains NE22 c) axial stresses S22

In figure 6.33, referring to the top section of the column, even though the temperature is uniform around 20ºC, plastification occurred in the unheated flange and a large extent of the web.

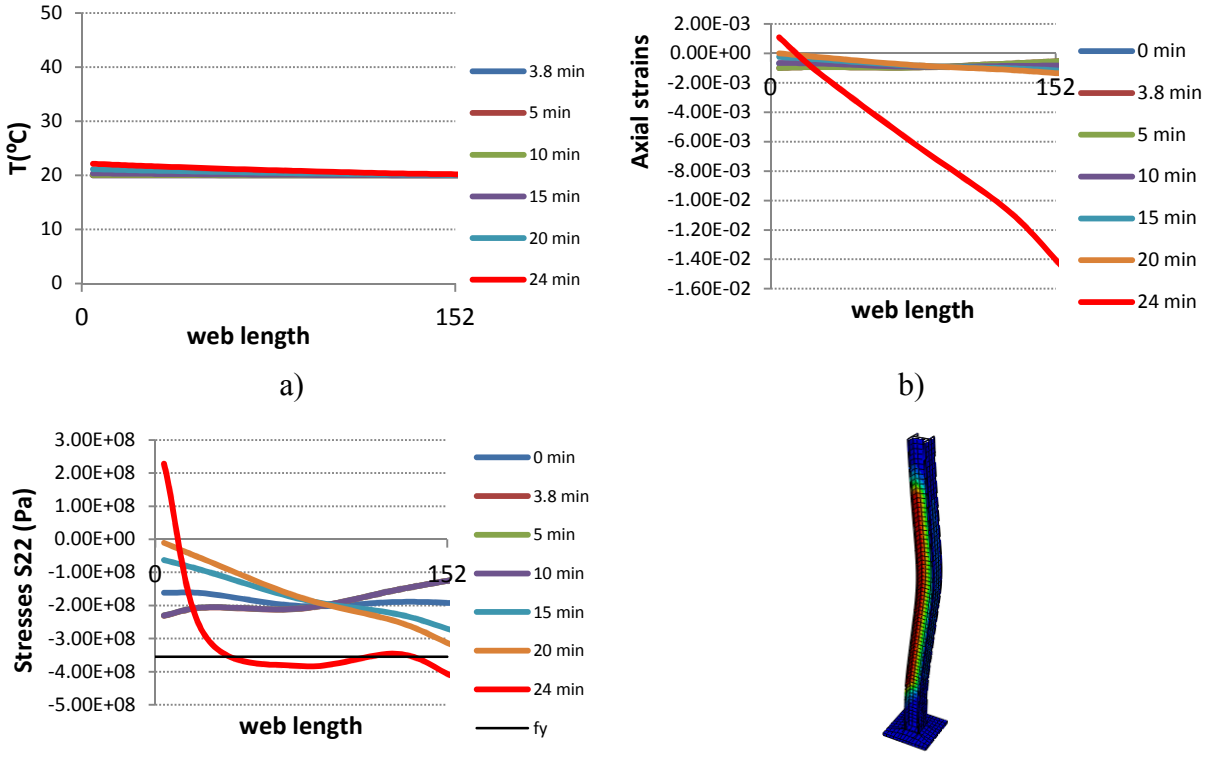

a)

b)

c)

Figure 6.34 – Behaviour of the top section of the column during the fire a) temperatures b) nominal axial strains NE22 c) axial stresses S22

With this analysis, it was possible to monitor in detail the behaviour of several sections, along the height of the column. Taking into account the efect of temperature, along the time, the

evolution of stresses and strains was represented along the direction of the web of the steel profile. It was possible to observe the inversion of axial stresses, in some sections from compression to tension, and sudden variation in the axial stresses, in sections with very low temperatures.

6.4.2. Steel Columns

In this section, results of the numerical simulations for the steel columns are presented.

The folowing figures depict the deformed shapes of the steel columns in the end of the simulation of the fire test. In Figure 6.34 a), it is possible to observe the local buckling of the flanges and web. In Figure 6.34 b), global buckling in the whole column is observed. This behaviour is quite similar to the one observed in the experimental tests. The boundary conditions were considered in the end plates of the columns of type tie constraint.

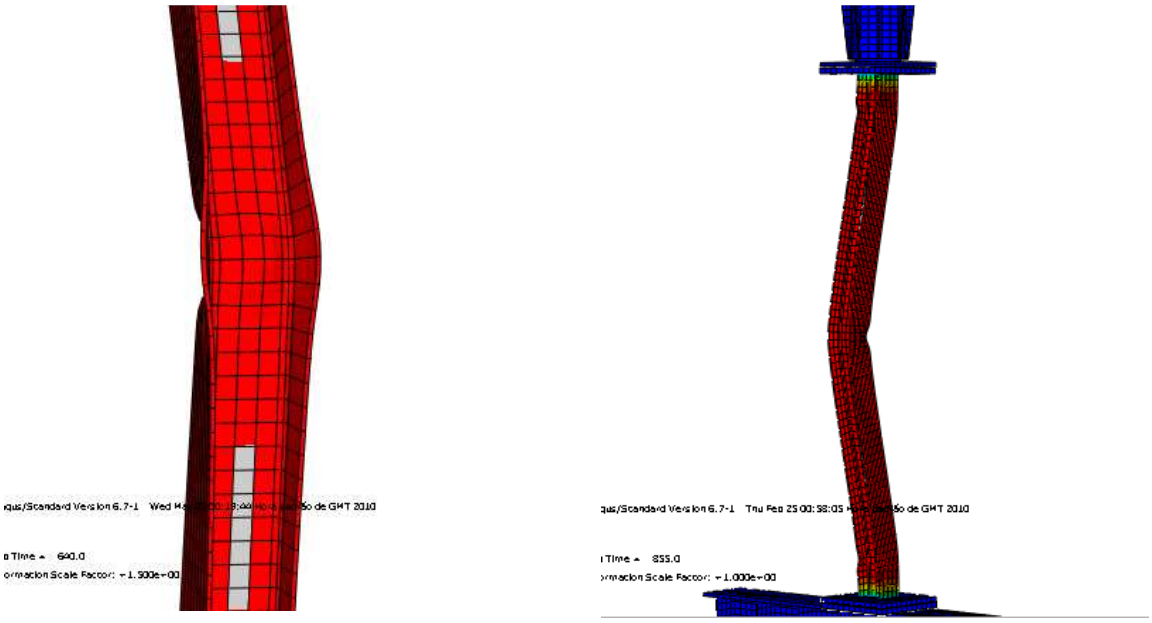

a) b)

Figure 6.35 – Deformed shape of the steel columns after test, obtained with the finite element modeling a) local buckling b) global buckling

Figure 6.35 shows the temperature distribution in the steel section, along the height of the column, in which is visible that at the ends of the column much lower temperatures were attained (sections S1 and S5) since they were out of the furnace. In each of these sections, the mean temperature was considered uniform temperature in the flanges, calculated with the data from the thermocouples in both faces, and a uniform temperature in the web, calculated with one thermocouple. In this figure, continuous lines stand for the mean temperatures obtained experimentally in the several sections, and dashed lines stand for the mean temperatures in the same sections, obtained numerically with ABAQUS.

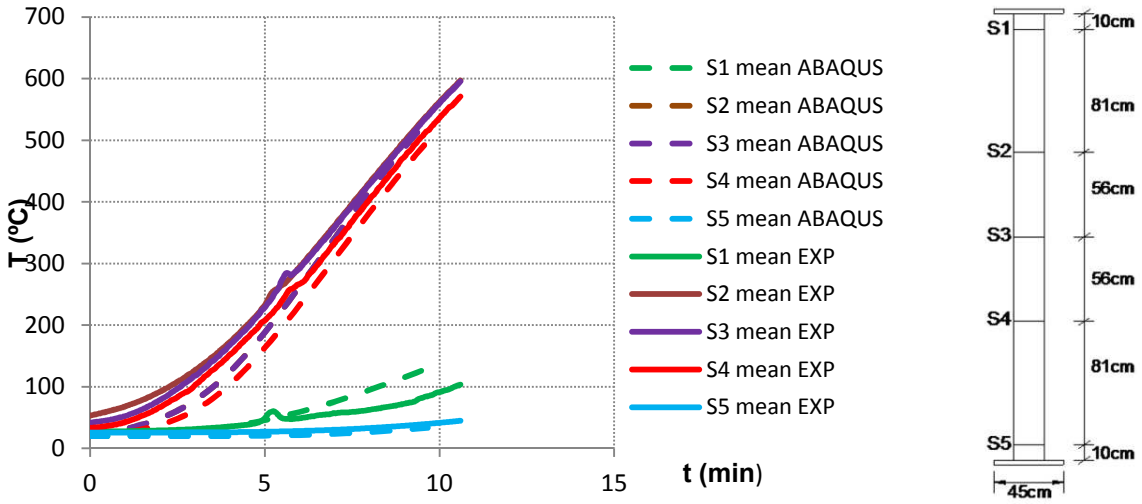

Figure 6.36 – Temperature distribution in a steel bare column during the fire

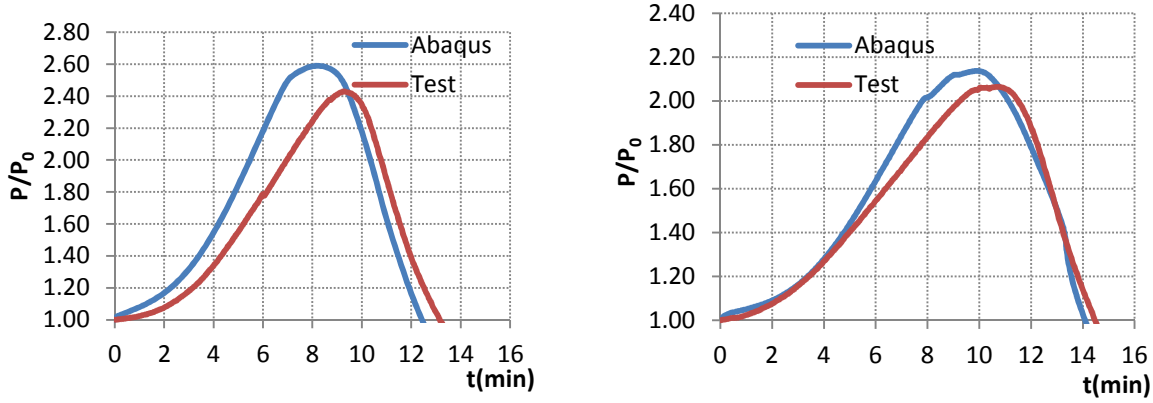

a) HEA 160-K45-L30

b) HEA 200-K45-L30

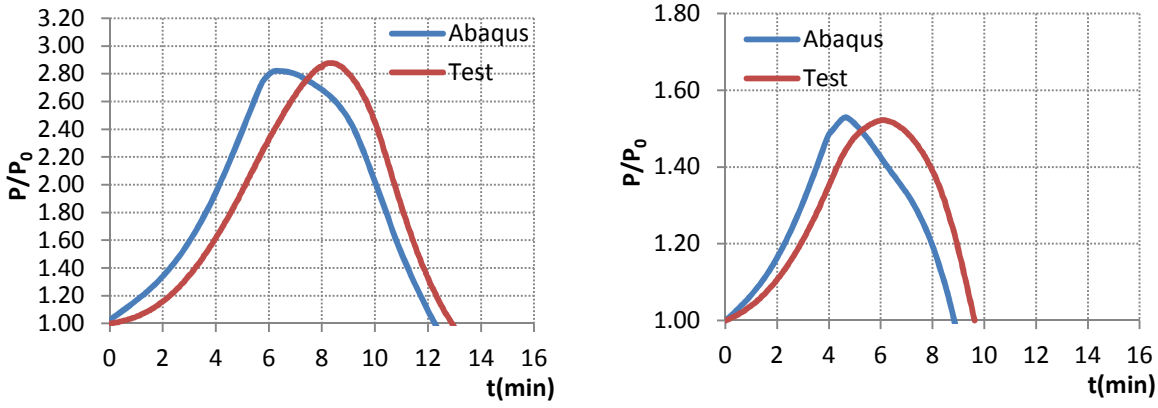

c) HEA 160-K128-L30

d) HEA 160-K128-L70

Figure 6.37 - Evolution of axial forces for experimental tests and numerical simulations

In Figure 6.36, the comparison of the evolution of restraining forces as a function of the time is presented. It can be observed a good agreement between the experimental tests and the numerical simulations. Only four cases are presented here, the other simulated cases are presented in appendix G.

Table 6.9 presents a comparison of critical times and temperatures for both the experimental tests and numerical simulations of these 12 tests, used for the calibration of the model. In the numerical simulations, the axial forces were calculated with the axial stresses on the top plate of the column. Critical temperatures were calculated as the mean value of the temperatures in the finite elements of the specimen, in the end of the test.

Table 6.9 – Comparison between the critical times and critical temperatures obtained experimentally and numerically for the steel columns used for calibration of the model

Test reference	**Steel Profile**	**t_{crit} experimental (min)**	**t_{crit} numerical (min)**	**T_{crit} experimental (ºC)**	**T_{crit} numetrical (ºC)**
HEA200-K13-L70	HEA 200	11.6	11.1	445	464
HEA160-K13-L70	HEA 160	10.6	8.5	428	453
HEA200-K13-L30	HEA 200	14.6	13.6	494	556
HEA160-K13-L30	HEA 160	13.6	12.9	545	560
HEA160-K45-L70	HEA 160	10.3	9.8	416	446
HEA160-K45-L30	HEA 160	13.2	12.4	511	556
HEA200-K45-L70	HEA 200	11.4	11.1	433	442
HEA200-K45-L30	HEA 200	14.6	14.1	543	541
HEA200-K128-L30	HEA 200	14.3	13.4	538	553
HEA160-K128-L30	HEA 160	12.9	12.3	499	549
HEA200-K128-L70	HEA 200	11.8	11.3	457	454
HEA160-K128-L70	HEA 160	9.6	10.1	404	437

The following graphs depict the evolution of the restraining forces during the numerical simulations for different load levels of columns with the axial stiffness of the surrounding structure equal to 45kN/mm.

It is clearly observed in each graph, that for low values of slenderness (between 35 to 50) the curves are more gentle, while for higher values (between 50 to 90) the graph assumes a defined peak. It is also observed that, for higher values of slenderness, greater values of maximum restraining forces are generated.

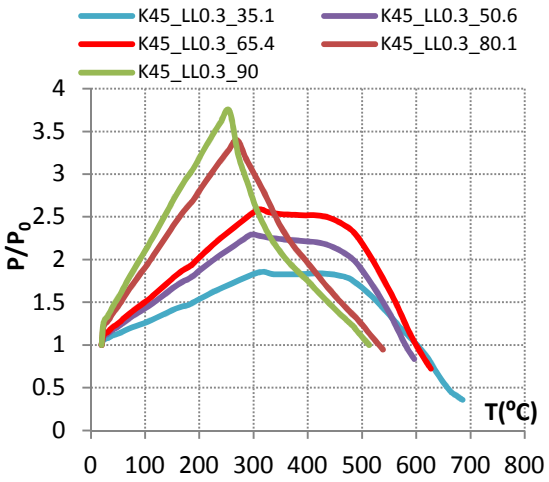

a) Load Level = 0.30

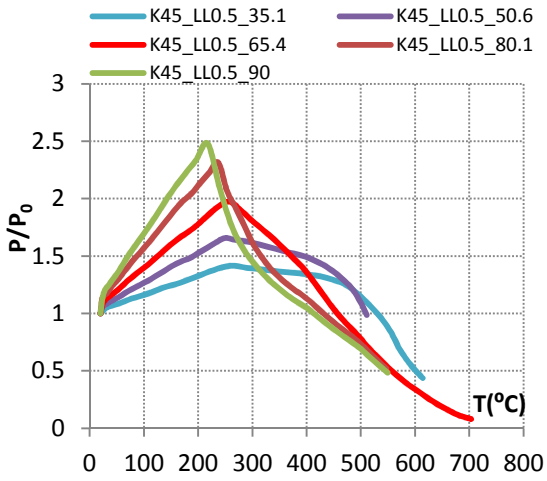

b) Load Level = 0.50

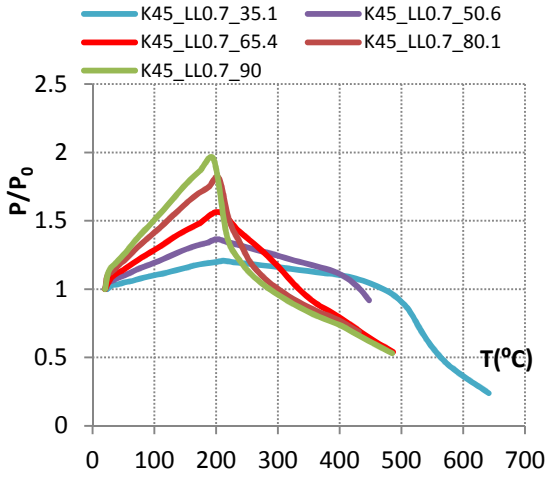

c) Load Level = 0.70

Figure 6.38 - Restraining forces P/P_0, for tests with stiffness of surrounding structure 45kN/mm, for different values of slenderness and load levels

In figure 6.37, the evolution of restraining forces P/P_0 is depicted, for different load levels, and for columns with different slendernesses. It may be observed that, in some cases, specially with very slender columns, the decay phase of the graphs is very gentle, which may mean that the post-buckling is a stage which should be evaluated, and that columns in a fire scenario may resist to a high percentage of the axial load for a longer period of time.

6.4.3. Partially Encased Steel Concrete Columns

The following figures show the analysis of temperature distributions in the end of the fire test simulation.

Figure 6.38 a) shows the temperature distribution in the concrete and steel, along the height of the column, in which is visible that at the ends of the column much lower temperatures were attained, since they were out of the furnace. Figure 6.38 b) presents a cut at mid-height of the column with the temperature distribution at the end of the test.

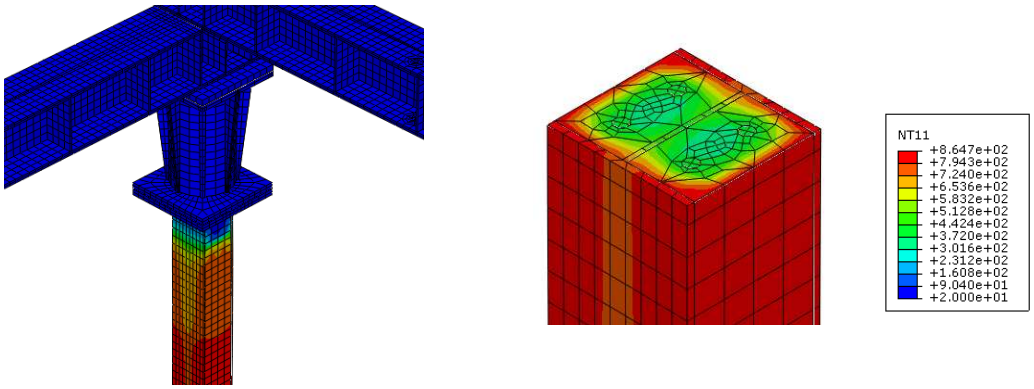

a) b)

Figure 6.39 - Analysis of the temperature distributions a) along the height of the column b) in the cross section

The heating curve used in the numerical simulations was the same used in the experimental tests. Figure 6.39 represents the evolution of the temperature at mid-height of the column in a fire resistance test with a composite column HEA160 with axial stiffness of the surrounding structure of 13kN/mm, and a load level equal to 30% of the buckling load at room temperature. We can observe an acceptable correlation between the heating curve ISO 834 and the furnace temperature curve. The thermocouple T11 on the concrete surface is very close to the furnace temperature. In the evolution of temperatures, it can also be observed a great temperature gradient inside the concrete (thermocouples T28, T12 and T13). The T13 thermocouple was placed in the web of the steel profile, showing the temperature difference to the flanges (thermocouple T15).

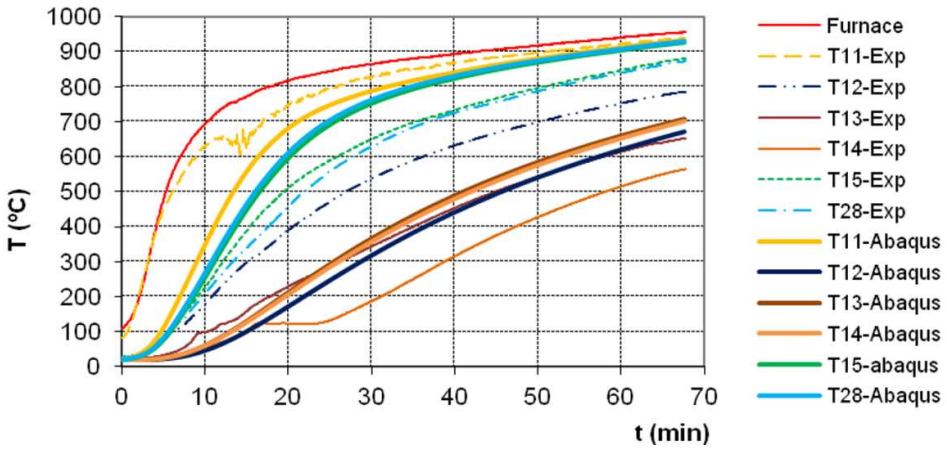

Figure 6.40 – Evolution of temperatures in the cross-section of a composite column

Thermocouple T14 gives the temperature in the longitudinal reinforcement of the column, which was very low. In general, the correlation between the experimental and numerical temperatures was good, except in this thermocouple in longitudinal reinforcement.

Figure 6.40 shows the comparison of the evolution of restraining forces as a function of time obtained in numerical simulations and experimental tests. These graphs represent the typical behavior of a real column inserted in a building structure, in which it is submitted to restraint to thermal elongation. Due to the effect of the thermal action, the axial force on the column begins to increase until it reaches a maximum value. After this maximum it begins to decline due to deterioration of mechanical properties of concrete and steel with temperature, reaching values lower than the initially applied load.

A good agreement may be observed between the results of the experimental tests and the numerical simulations.

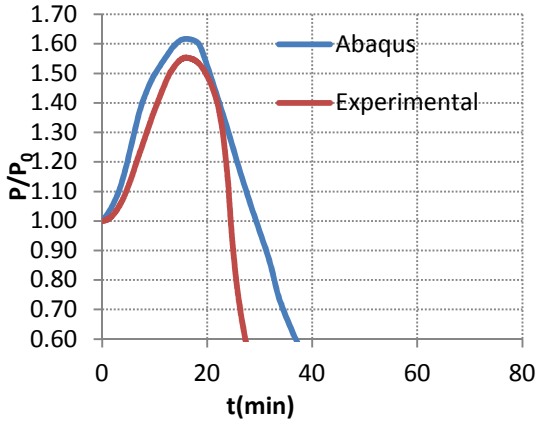

a) HEA160 – k=128kN/m – 70% N_{bRd}

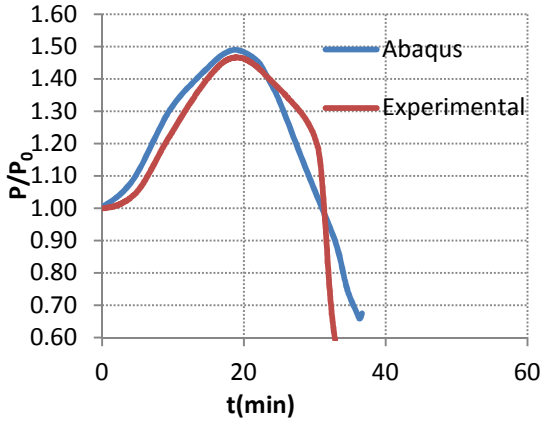

b) HEA160 – k=45kN/m – 70% N_{bRd}

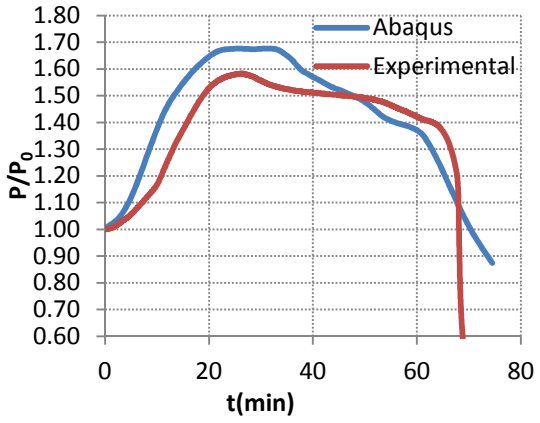

c) HEA200 – k=45kN/m – 30% N_{bRd}

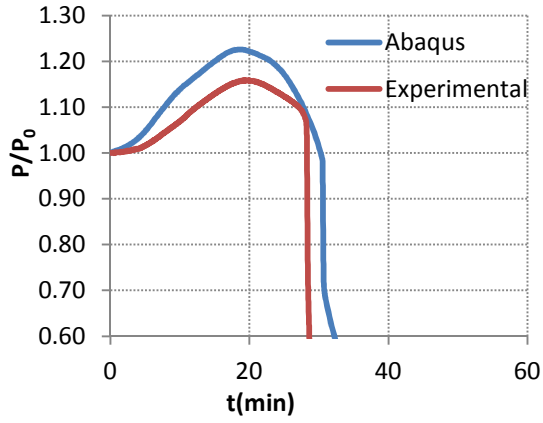

d) HEA160 – k=13kN/m – 70% N_{bRd}

Figure 6.41 – Comparison of the evolution of restraining forces as a function of time obtained in numerical simulations and experimental tests.

A comparison of the experimental and numerical restraining forces obtained in all tests of the composite columns is presented in Appendix G.

Table 6.10 – Comparison between the critical times obtained experimentally and numerically for the composite steel-concrete columns

Test Reference	Steel Profile	Load Level	Stiffness of the surrounding structure (kN/mm)	t_{crit} experimental (min)	t_{crit} numerical (min)
CSC160-K128-L30	HEA 160	30	128	30,3	40,6
CSC160-K128-L70	HEA 160	70	128	24,5	29,3
CSC200-K128-L30	HEA 200	30	128	39,9	48,7
CSC200-K128-L70	HEA 200	70	128	38	33
CSC160-K45-L30	HEA 160	30	45	39	48,6
CSC160-K45-L70	HEA 160	70	45	31,4	31
CSC200-K45-L30	HEA 200	30	45	68	70,3
CSC200-K45-L70	HEA 200	70	45	45,5	33,3
CSC160-K13-L30	HEA 160	30	13	67,7	53,3
CSC160-K13-L70	HEA 160	70	13	28,3	30,2
CSC200-K13-L30	HEA 200	30	13	90,6	72
CSC200-K13-L70	HEA 200	70	13	38,6	35,6

Table 6.10 compares the critical times obtained in the experimental and numerical simulations of tests on composite steel-concrete columns. Some discrepancies are observed in the critical times obtained experimentally and numerically, due to the difficulty in modeling the structural behaviour of concrete in fire situations.

6.5. Sinopsis

In this chapter the results of numerical simulations on the behaviour of steel and composite steel-concrete columns partially encased by concrete, as well as steel columns embedded on walls were presented.

Concerning the columns embedded on walls, both with a two-dimensional modeling (using SUPERTEMPCALC) and with a three-dimensional commercial programme (ABAQUS), good results were obtained in terms of temperatures. The modeling of the fire in this type of columns, with the purpose of a structural analysis, allowed a detailed explanation of the thermal bowing effect, in unevenly heated columns. For the studied cases, the contact with the walls, proved to have a favorable influence.

The major outcome of this numerical analysis is related to a better understanding of the "thermal bowing" phenomenon. The inversion of the bending moments and the formation of

plastic hinges on top, bottom and at mid-height of the column lead to a different failure mode than usually observed in columns. The failure of the columns embedded on walls is significantly different from the failure of bare steel columns. The criterion of considering the collapse as the instant of time when the axial force, after increasing and reaching up to a maximum decays to the initial value, seems to be inadequate to these columns. In fact, in these columns, the failure is not so abrupt, and a high value of structural resistance is observed for a long period of time. The failure of these columns is more like by bending than by buckling. A new criterion for the definition of column failure, and the fire resistance time is yet to be proposed and discussed in future research on this issue.

In terms of restraining forces, the columns embedded on walls, presented lower restraining forces than bare columns.

Concerning the steel and composite columns, the analysis was a geometric and material nonlinear analysis, with imperfections, modeling the steel and concrete materials, as well as the mechanical and thermal properties varying with temperature. The main conclusions of this study were the following:

- The tools of ABAQUS program for the application of thermal actions allow to simulate the phenomenon of heat transfer between air and structural elements with satisfactory results;

- The typical behavior of increase and subsequent decrease in axial force in columns heated with restraint to thermal elongation observed experimentally was also observed in the numerical model;

- The agreement between the critical times of fire resistance obtained experimentally and numerically was quite satisfactory;

- The model developed in this study has the potential to be used in developing parametric studies to obtain analytical formulae for simplified design or verification of the fire resistance of columns;

- The most important parameter in the reduction of the fire resistance of the columns was the load level;

- Based on the experimental tests and the numerical analyses, presented in this study, it may be concluded that the influence of the surrounding structure has not so important detrimental

influence on the fire resistance. This conclusion, that the influence of the surrounding structure may have a negligible influence on the fire resistance of a steel column in a real structure of a building was already stated by other authors Bennets (Bennets et al., 1989) and Franssen (Franssen, 2000).

7 PROPOSAL OF SIMPLIFIED CALCULATION METHODS FOR TEMPERATURE EVOLUTION AND FIRE DESIGN OF STEEL COLUMNS

7.1 Simplified Calculation Methods for Temperature Evolution on Steel Columns Embedded on Walls

7.1.1 Comparison of temperatures numerical simulations vs EN 1993-1-2

In chapter 3, in section 3.2.7, a detailed explanation was presented about the EN 1993-1-2 (2005) formulation for the calculation of temperatures in steel profile cross-sections. In this document, the section factors are presented for the common situations of protected and unprotected steel sections. However only one situation is stipulated for the case of steel elements partially embedded on walls.

In this chapter, the results of fire resistance tests performed in steel columns embedded on walls, and the numerical simulations carried out on a great number of situations will be used to develop simplified calculation methods for the assessment of the evolution of temperatures within the steel cross-sections.

The following graphs depict the evolution of temperatures in test E05, HEA160 profile, with the web parallel to the wall, and a thick wall.

As a final objective, the analysis of the accuracy of the method of EN 1993-1-2 (2005) for the determination of the evolution of temperatures on steel elements embedded on walls is presented.

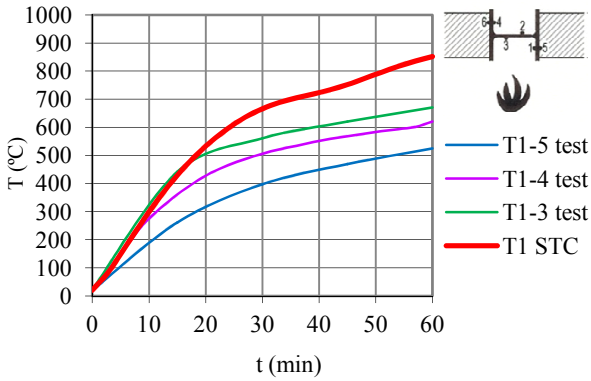

Figure 7.1 -Temperature in thermocouple 1- internal flange face exposed to fire – test E05

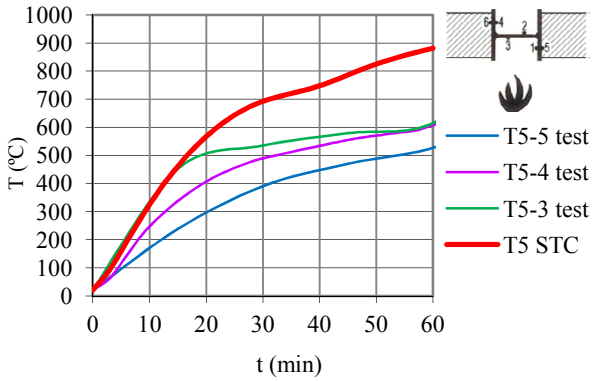

Figure 7.2 – Temperature in thermocouple 5 – in flange in contact with brick wall – test E05

As observed in the figures 7.1 and 7.2, the values for the temperatures calculated by STC are higher than the values obtained in the experimental tests. These differences are higher on the web and in the part of the steel profile outside the furnace. These differences may be explained because it was considered in the calculations an adiabatic surface in the external surface of the web of the steel profile, in contact with outside the furnace. This assumption considered due to the process of calculation of the program, is not totally correct. Another explanation might be due to the thermal properties of the brick walls considered in the calculations. Properties for this material varying in function of the temperature were not considered. Finally, another explanation could be the moisture content of the specimens in the tests that was maybe higher than the one considered in the STC calculations. A high moisture content, might have delayed the heating of the specimens and consequently the temperatures did not increase as much as expected.

Figure 7.3 depicts different approaches for the calculations of the area and the exposed perimeter of the cross-section, for the assessment of the temperatures evolution using EN 1993-1.2 (2005), for the case of the profile with the web parallel to the walls.

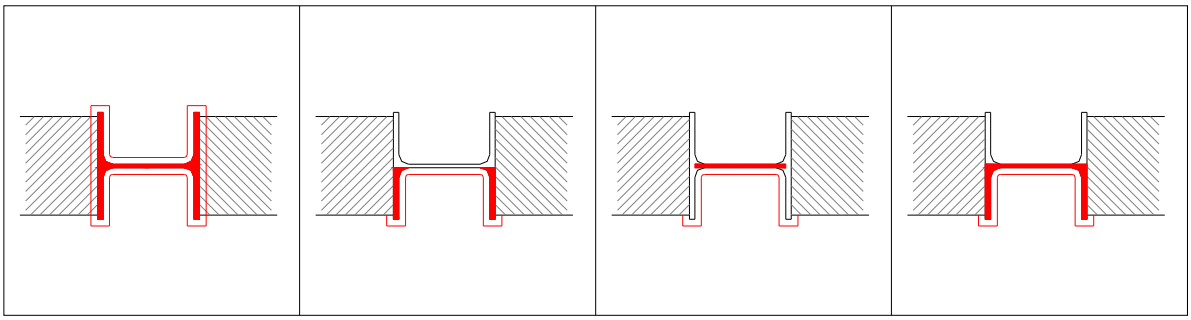

a) b) c) d)

Figure 7.3 –Comparison of the several approaches – test E05 a) Total section b) half flange c) web d) U section

The graphs in Figure 7.4 depict the evolution of temperatures in test E05, HEA160 profile, with the web parallel to the wall and a thick wall. In this graph, as well as in graph of Figure 7.10, no plateau is observed between 700ºC and 800ºC. This is due to the fact that, if a constant specific heat of 600 (J/KgK) is used, as suggested for simple calculation methods in the ENV version of the Eurocode 3 (1995), this plateaux does not exist (Franssen et al., 2010).

In Figure 7.4, several calculations performed with the simplified calculation method of EN 1993-1-2 (2005) for the evolution of temperatures in steel cross-sections, are compared with the experimental results and the STC analysis. In these calculations half of the flange was considered (half flange), the web (web), two half flanges and the web (U section) and the total

area of the cross-section (total section) (Figure 7.3). The section factors for these cases were: total section – $A_m/V = 228$, U section – $A_m/V = 59.5$, half flange – $A_m/V = 124$ the web – $A_m/V = 167$.

From figure 7.4 it is observed that there are no great differences in the evolution of temperatures when half of the flange is considered, or only the web or two halves of the flanges and the web. The consideration of the total section in the calculations performed with the simplified calculation method of EN1993-1-2 (2005) presents results similar to the ones of STC. The temperatures obtained in the experimental tests are slightly lower than the ones obtained in the calculations.

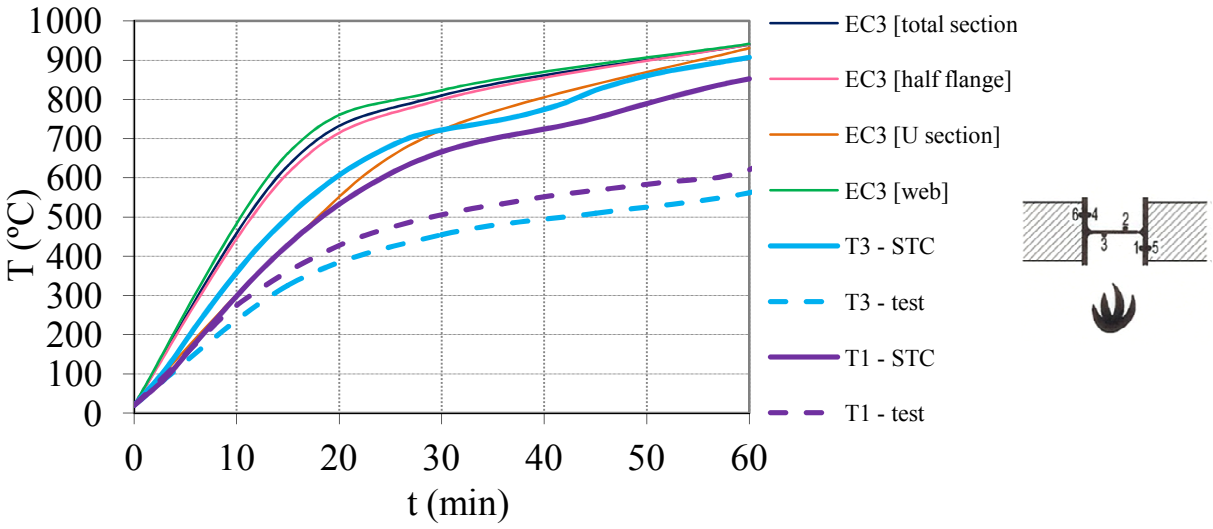

Figure 7.4 –Comparison of the several approaches for the calculation of temperatures (experiments, STC and EN1993-1-2 (2005)), thick wall, web parallel to the wall – test E05

Figures 7.5 to 7.7 present the comparison between the results of the experimental test E06, with a HEA160 profile, with the web perpendicular to the wall surface, in a thick wall, and the numerical simulations performed by STC. In figure 7.5, the temperatures in thermocouple 5, in the external face of the inner flange directly exposed to fire, obtained by STC are very close to the ones of the experimental test. In figures 7.6 and 7.7 the same is not observed, the temperatures of STC are lower than the ones of the test.

Figure 7.8 represents the variation of temperature in thermocouple T3 (web in contact with the wall) and thermocouple T6 (external face of outer flange) related to the temperature in thermocouple T5 (external face of the inner flange directly exposed to fire). From this figure

there can be observed a linear variation of the temperature from the inner flange to the outer flange of the column in test.

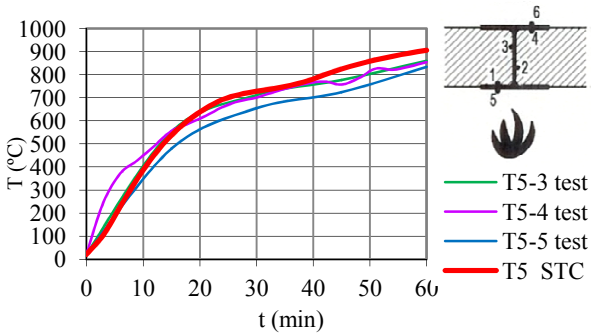

Figure 7.5 –Temperature in thermocouple 5 – external face of the inner flange - test E06

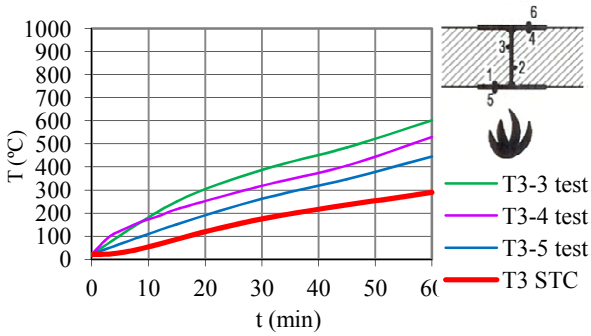

Figure 7.6 –Temperature in thermocouple 3 – in web in contact with the wall - test E06

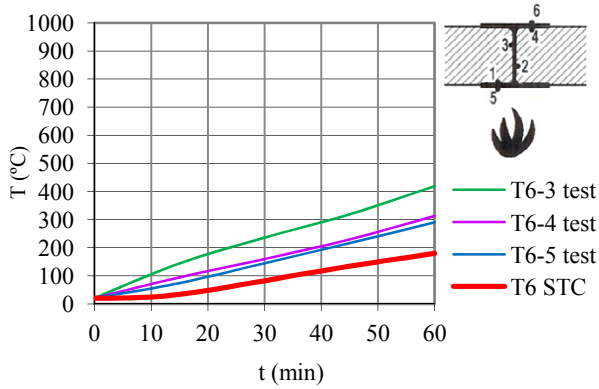

Figure 7.7 – Temperature in thermocouple 6 – external face of the outer flange - test E06

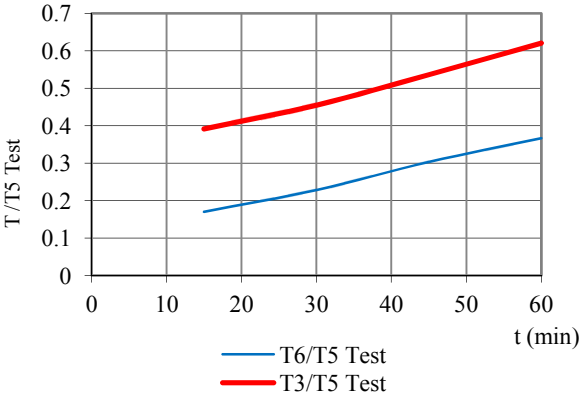

Figure 7.8 – Variation of temperature in thermocouple T3 and T6 related to temperature of thermocouple T5– test E06

As in the previous test, several calculations were performed using the simplified calculation method stipulated in EN 1993-1-2 (2005) for the evolution of temperatures in steel. The cases considered were the total section exposed to fire, the external face of the inner flange exposed to fire related to the area of the whole cross-section (1 face / total area), the external face of the inner flange exposed to fire related to the half area of the cross-section (1 face / half area), the external face of the flange exposed to fire related to the area of the flange (1 face / flange area).

Figure 7.9 depicts different approaches for the calculations of the area and the exposed perimeter of the cross-section, for the assessment of the temperatures evolution using EN 1993-1-2 (2005), for the case of the profile with the web perpendicular to the walls.

In figure 7.10, several calculations performed with the simplified calculation method of EN 1993-1-2 (2005) for the evolution of temperatures in steel cross-sections, are compared with the experimental results and the STC analysis. In these calculations, the total section was considered (total section), one face exposed and total section (1 face/total section), one face exposed and half section (1face/half section) and one face exposed and flange section (1face/ flange section).

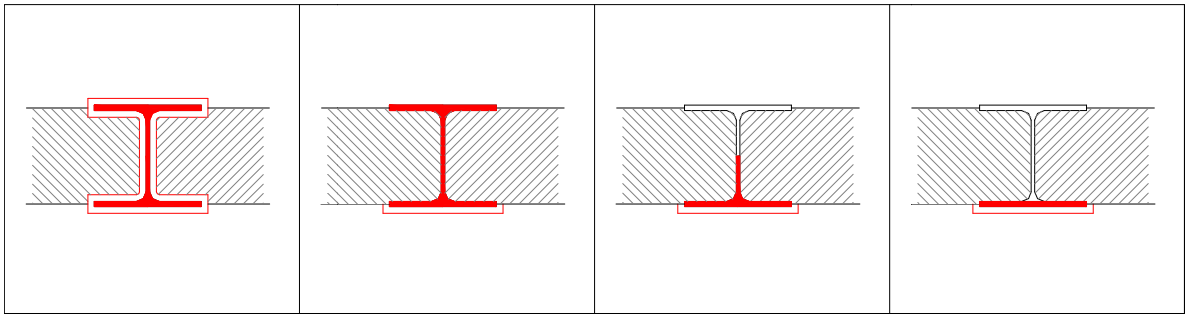

a) b) c) d)

Figure 7.9 –Comparison of the several approaches – test E06 a) Total section b) 1 face / total section c) 1 face / half section d) 1 face / flange section

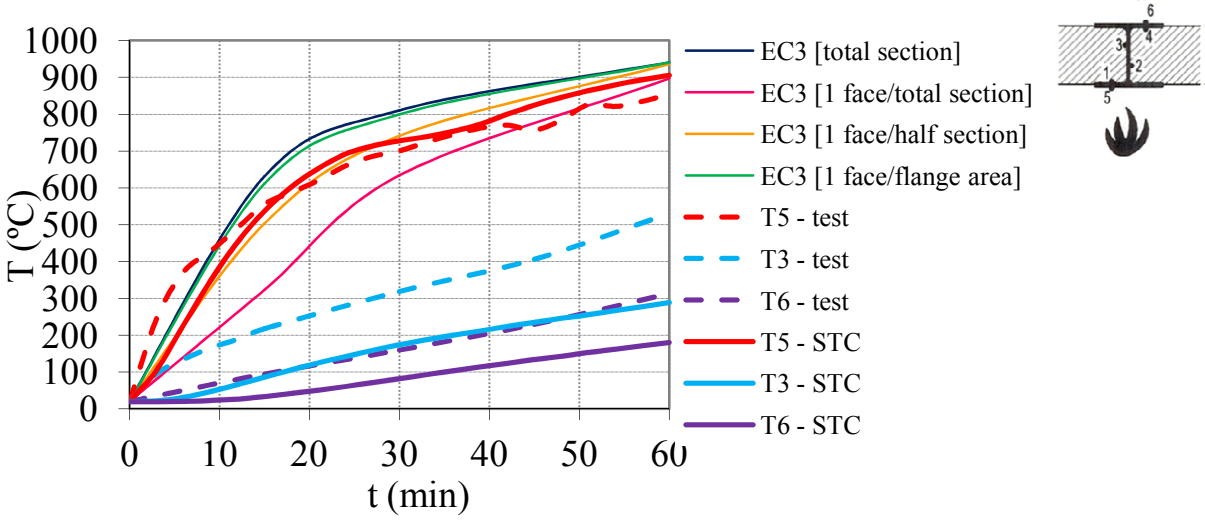

Figure 7.10 –Comparison of the several approaches for the calculation of temperatures (experiments, STC and EN1993-1-2 (2005)), thick wall, web perpendicular to the wall – test E06

In that case the section factors gave the following values: total section – A_m/V = 228, 1 face / total section – A_m/V = 39, 1 face / half section – A_m/V = 78 and 1 face / flange area – A_m/V = 123.

The same conclusions drawn for test E05 are true for test E06. The EN 1993-1-2 (2005) formulation for the section factor are not accurate for the cases of steel columns embedded on walls.

The graphs in figures 7.11 and 7.12 depict the evolution of temperatures in test E04, with a HEA200 profile, with the web perpendicular to the wall and a thick wall.

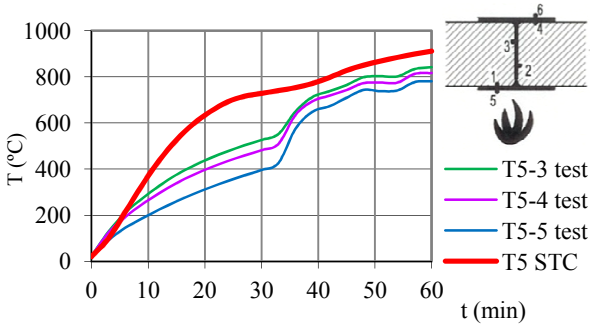

Figure 7.11 – Temperature in thermocouple 5 – external face of the inner flange - test E04

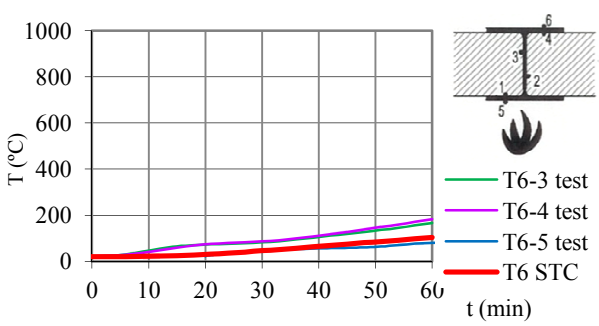

Figure 7.12 – Temperature in thermocouple 6 – external face of the outer flange - test E04

In this test a better correlation was verified between the experimental results and the results obtained in the numerical simulations by STC. This fact might be explained by the higher massivity of the steel profile in these tests (Figures 7.11 and 7.12).

Figure 7.11 illustrates a delay in the heating of the thermocouple T5 lasting 35 minutes. This difference was originated by a delay in the heating of the furnace that did not follow the ISO 834. After that instant the furnace was adjusted in order to follow the ISO 834 fire curve and the temperatures in thermocouple T5 increased following the temperature evolution given in the calculations of STC.

The evolution of temperatures in different points of the cross-section of the elements obtained in experimental tests were compared with the ones obtained from calculations performed with the finite element program SUPERTEMPCALC (STC) and with the simplified calculation method stipulated in EN 1993-1-2 (2005) for the determination of the temperature evolution in steel elements.

The main conclusion to be drawn from this work is that the temperature evolution obtained by STC and the method of EN 1993-1-2 (2005), are in general higher than the ones obtained in the tests. The differences are higher when the web is parallel to the wall surface and in the thermocouples placed in the external face not directly exposed to the fire. It can be said that the method of EN 1993-1-2 (2005) and the STC over estimates the temperatures in the cross

section of the steel column when the elements are embedded on walls, and so underestimates the real fire resistance of the element.

The numerical approach for the heating process considered in the calculations performed with STC, does not take into account the heat losses throughout the walls and the steel surfaces in contact with the air outside the furnace. This fact might explain certain differences between the temperatures obtained in the numerical simulations and the experimental results.

Quite interesting results were observed in this study for the case of specimen with web perpendicular to the wall surface, the temperatures in the flange exposed to the fire for the numerical simulations performed with STC, the method of EN 1993-1.2 (2005) and the experimental test, are very similar. In the web and the flange not exposed to the fire there are significant differences. A linear variation of the temperature across the section of the steel profile was observed.

From this study it is concluded that the section factor defined in EN 1993-1.2 (2005) for the case of steel sections embedded on walls is not appropriate. Studies in this area should be made in order to find a more representative section factor for these cases. In University of Coimbra further experimental tests and numeric simulations will continue in this area.

7.1.2 Proposal of a simplified calculation method for the temperature evolution

7.1.2.1 Parametric method

Four methodologies were developed for the assessment of temperatures in the cross section of steel columns embedded on walls:

- Method 1: web parallel to the fire – wall thickness and flange width similar (comparison between test E03 and E05)

- Method 2: web perpendicular to the fire – wall thickness and web height similar (comparison between test E04 and E06);

- Method 3: web parallel to the fire – wall thickness smaller than flange width (comparison between test E08 and E10);

- Method 4: web perpendicular to the fire – wall thickness smaller than web height (comparison between test E09 and E11);

The thick wall was used to simulate the cases in real buildings, where the thickness of the wall is nearly the same as the width of the column. Walls of 140mm thickness for HEA 160 columns and 180mm thickness for HEA 200 columns were used. The thin wall was used to

simulate cases where the wall is thinner than the column flange width. In these cases, the wall thickness is approximately ¾ of the flange width, and the fire is considered to act on the side where the steel cross section is not embedded on the wall. Walls of 100mm thickness for HEA 160 columns and 140mm thickness for HEA 200 columns were used. These thicknesses were considered depending on the commercial brick thicknesses available in the market.

In methods 1 and 3, the section was considered to be divided in 3 zones, in which the temperature is uniform, being the web, half-flange exposed to fire and the half-flange not exposed to fire. In methods 2 and 4, the section was considered to be composed by 3 zones, the flange exposed to fire, the web and the flange not exposed to fire.

In each zone, two temperature measuring points were used, one at each side of the zone, so that the average value of the temperature was considered at each instant of time.

The numerical analysis was carried out using the temperatures registered in the furnace in each experimental test. To eliminate some deviation of the furnace temperatures from the ISO 834 fire curve the obtained values of temperature with STC were multiplied by a correction factor.

$$f = \frac{T_{ISO834}}{T_{furnace}} \tag{7.1}$$

The temperatures obtained experimentally were used to calibrate and validate the results of the numerical analyses with STC. The calculations to obtain the reduction coefficients proposed in the following methods were performed using the results of the numerical analysis.

The results of the temperatures calculated with STC in each zone, were then compared with the ones obtained with the simplified calculation method presented in EN1993-1.2 (2005) for the exposed zone of the steel cross-section. This procedure allowed determining reduction factors for the temperatures in each of the 3 zones.

The section factors were calculated dividing the exposure perimeter by the exposed surface (Figure 7.13). The coefficient K_{sh} was considered in all cases, except case 2 and 4.

The temperatures in the experimental tests were measured at 6 points on 5 sections of the steel cross-section. These temperatures in the mid-height section of the HEA 200 columns were compared with the ones obtained in the numerical simulations (Figures 7.14 to 7.17).

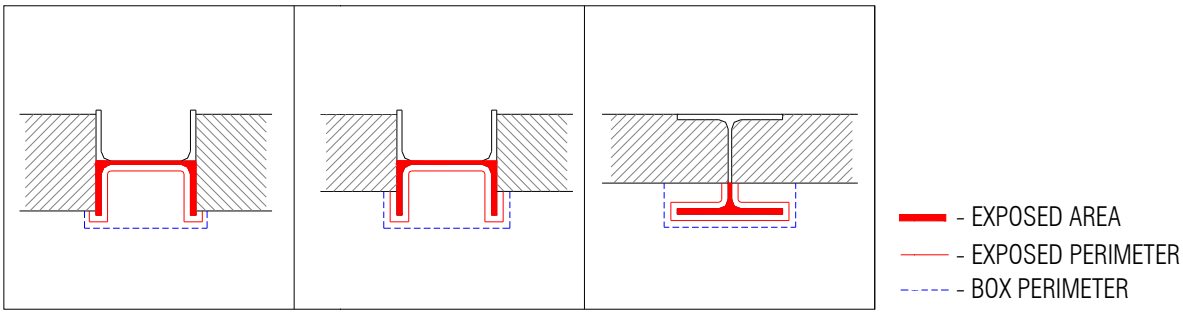

Figure 7.13 – Process of calculation of the section factor.

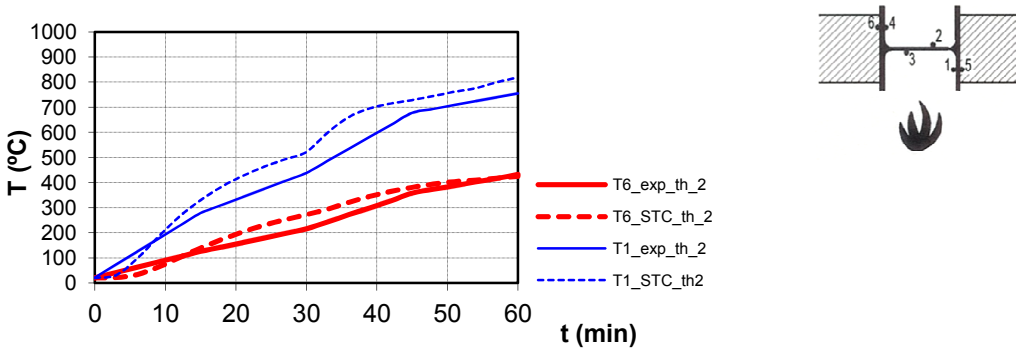

Figure 7.14 – Temperatures *vs* time - HEA200 - web parallel to the wall – thick wall - thermocouple T6 and T1 - test E03

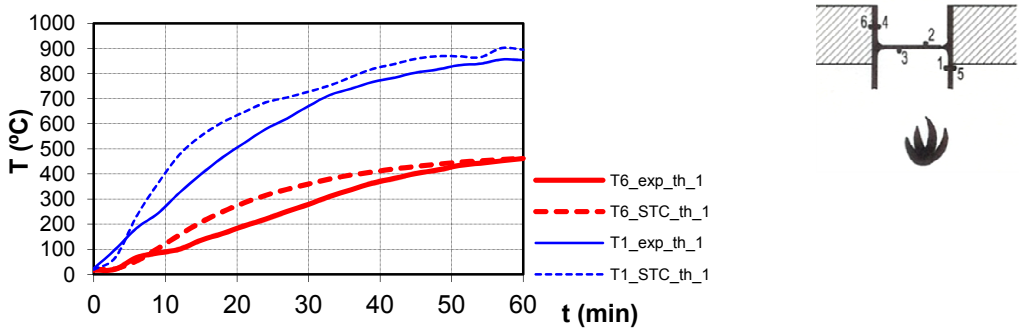

Figure 7.15 – Temperatures *vs* time - HEA200 - web parallel to the wall – thin wall thermocouple T6 and T1 – test E08

For the cases of the web perpendicular to the wall, a huge thermal gradient was observed along the height of the steel cross-section (between thermocouple 5 and 6), of about 700ºC for the thinner wall (test E09) and about 600ºC for the thicker wall (test E04), (Figures 7.16 and 7.17).

Also for the cases with the web parallel to the wall, a great difference of temperatures between the exposed and unexposed half-flanges was obtained, 400ºC for the thinner wall and 300ºC for the thicker wall (Figures 7.14 and 7.15).

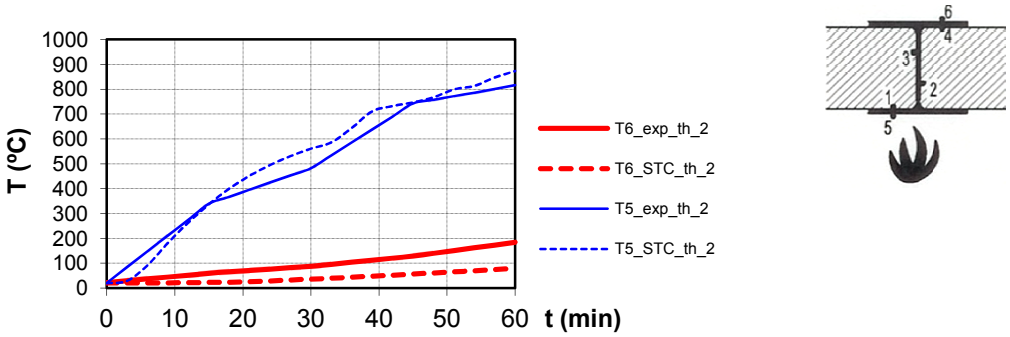

Figure 7.16 – Temperatures *vs* time - thermocouple T5 and T6 - HEA200 – thick wall - web perpendicular to the wall – test E04

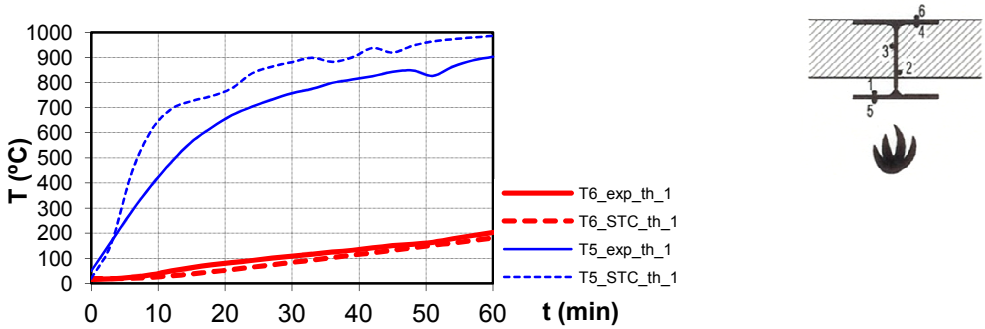

Figure 7.17 – Temperatures *vs* time - thermocouple T5 and T6 - HEA200 – thin wall - web perpendicular to the wall – test E09

Tables 7.1 to 7.4 present the reduction coefficients that should be multiplied by the temperatures calculated in the exposed zone of the steel cross-section, using the EN 1993-1-2 (2005) simplified calculation method, in order to obtain the temperatures in the other zones of the steel cross-section.

Table 7.1 - Method 1- web parallel – thick wall

Time (minutes)	Half-flange exposed	Web	Half-flange unexposed
10	0.71	0.87	0.27
20	0.80	0.83	0.39
30	0.81	0.76	0.44
40	0.84	0.78	0.46
50	0.87	0.78	0.49
60	0.87	0.77	0.49

Table 7.2 - Method 2- web perpendicular – thick wall

Time (minutes)	Flange exposed	Web	Half-flange unexposed
10	0.78	0.18	0.07
20	0.82	0.23	0.05
30	0.87	0.30	0.07
40	0.86	0.32	0.09
50	0.90	0.36	0.10
60	0.95	0.39	0.12

Table 7.3 – Method 3 – Web parallel – thin wall

Time (minutes)	Half-flange exposed	Web	Half-flange unexposed
10	0.98	0.84	0.30
20	0.85	0.73	0.39
30	0.88	0.77	0.44
40	0.93	0.78	0.48
50	0.95	0.78	0.50
60	0.95	0.78	0.50

Table 7.4 – Method 4 – web perpend. – thin walls

Time (minutes)	Flange exposed	Web	Half-flange unexposed
10	1.00	0.40	0.06
20	1.00	0.46	0.07
30	1.00	0.50	0.10
40	1.00	0.54	0.13
50	1.00	0.58	0.16
60	1.00	0.60	0.19

As expected, the flanges of the steel profile directly exposed to fire will be at high temperature than the unexposed ones. This will cause a higher expansion of the heated flange than the cooler one, inducing bending moments in the column cross-section. This effect is called thermal bowing and may be very important in bare steel columns in fire.

The EN 1993-1.2 (2005) formulation for the section factor can be used, although it was proven to be valid only for the exposed flange engulfed in fire (cases of wall thickness smaller than web height). In all other cases, the temperature in each zone of the cross-section can be calculated in function of the temperature of the exposed area. Several reduction factors were defined in such a way that multiplying the temperature of the exposed area of the steel profile by them, the temperature in the corresponding zone is obtained.

The methods presented in this work for the calculation of the temperatures in the different parts of the steel cross-section have potential to be used in a future formulation, in EN 1993-1.2 (2005), of the section factor of columns embedded on walls.

The assessment of temperatures in structural elements subjected to differential heating is essential to the development of analytical methods to predict buckling behavior of this type of columns.

7.1.2.2 Simplified method

The simplified calculation method proposed in this section for the temperature evaluation on steel columns embedded on walls is based on the various numerical simulations carried out with the STC computer program as described in section 3. Both steel columns with web perpendicular and parallel to the wall surface were considered in the following sections.

7.1.2.2.1 Steel column with web perpendicular to the wall

In this case, three models corresponding to three different thicknesses and positions of the wall (models 1, 2 and 3), were studied (Figure 7.18). The steel cross-section was divided in areas of the same temperature, where θ_3 is the temperature in the exposed part of the steel profile, θ_2 is the temperature in the part of the web in contact with the wall and θ_1 is the temperature in the unexposed part of the steel profile not in contact with the wall. These temperatures were determined with the STC numerical analysis.

The temperatures in parts 1 and 2 of the steel cross-section were then adjusted proportionally by multiplying them with a factor $\theta_3^{EC3}/\theta_3^{STC}$, where θ_3^{EC3} is the temperature in zone 3 determined with the simplified calculation method of EN 1993-1.2 (2005) for temperature evaluation in steel cross-sections engulfed in fire and θ_3^{STC} is the temperature in the same zone determined with the STC numerical analysis.

Figure 7.18 depicts the temperature zones for models 1, 2 and 3, for the case of the steel profile with the web perpendicular to the walls.

The temperatures adjusted for the different zones were used in an analytical study that allowed the proposal of the following formulae for the different models tested. For the three models, temperatures in zones 1 and 2 are calculated as a function of θ_3^{STC} and several other geometrical parameters of the cross section such as the thickness of the web profile t_w, the web

length in contact with the wall H and the height of the steel profile h, as a function of the time in minutes.

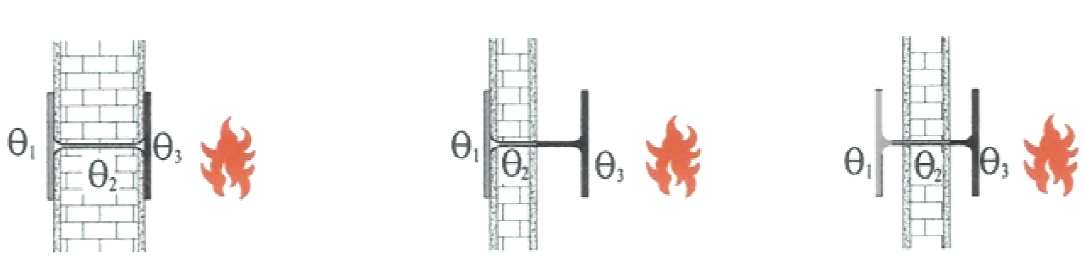

a) Model 1 b) Model 2 c) Model 3

Figure 7.18 - Temperature zones for models 1, 2 and 3 – steel profile with the web perpendicular to the wall surface.

Model 1:

$$\theta_2 = \theta_3^{EC3}\frac{0.7t^{0.3}}{t_w} \qquad \theta_1 = \theta_3^{EC3}\frac{9.5t^{0.6}}{Ht_w} \tag{7.2}$$

Model 2:

$$\theta_2 = \theta_3^{EC3}\frac{t^{0.3}}{1.7Ht_w/h} \qquad \theta_1 = \theta_3^{EC3}\frac{2t^{0.9}}{H^2t_w/h} \tag{7.3}$$

Model 3:

$$\theta_2 = \theta_3^{EC3}\frac{0.9t^{0.3}}{t_w} \qquad \theta_1 = \theta_3^{EC3}\frac{9.4t^{0.6}}{Ht_w} \tag{7.4}$$

In which t is the time in minutes, t_w is the thickness of the web profile, H is the web length in contact with the wall and h is the height of the steel profile, all in mm.

7.1.2.2.2 Steel column with web parallel to the wall

For the case of the steel profile with the web parallel to the wall surface two models were studied (Figure 7.19).

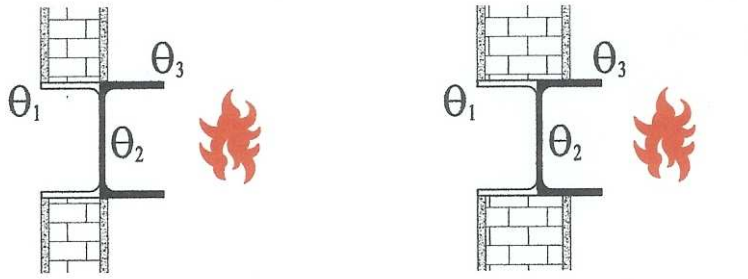

a) Model 4

b) Model 5

Figure 7.19 - Temperature zones for models 4 and 5 – profile with the web parallel to the wall surface.

The EN 1993-1-2 (2005) simplified calculation method for temperature evaluation in steel cross-sections engulfed in fire is not applicable in these cases because this elements geometry is not contemplated in that document. It is proposed that the temperature on the exposed part of the steel profile was determined using equation (7.5). This equation is valid both for the exposed half flange and web of the steel profile because the temperatures achieved were similar in both zones (7.6). The temperatures on these profile's zones are independent of their geometrical dimensions since the flange and the web have small thickness. In the unexposed half-flanges, the length in contact with the wall is important, so in these cases, the formula is dependent upon the flange width $b_{f,}$ in mm.

Models 4 and 5:

$$\theta_3 = -0{,}28t^2 + 30t + 55 \quad (7.5)$$

$$\theta_2 = \theta_3 \quad (7.6)$$

$$\theta_1 = \theta_3 - 1.35 \times bf \text{ (for 15min<t<60min)} \quad (7.7)$$

For the unexposed half flange, for times lower than 15 minutes, the temperature in the unexposed half-flanges can be assessed considering a linear variation between 20ºC and the calculated value for t=15 minutes.

7.1.2.2.3 Validation of the proposal

Many numerical simulations were carried out with STC computer program and the results for the temperatures were then compared with those registered in the experimental tests and calculated with the simplified calculation method proposed (proposal).

As an example, the temperatures obtained in the STC numerical simulations, for model 5 – HEA160 and model 2 – HEA160 (Figures 7.20 and 7.21) and for model 4 – HEA200 and model 2 – HEA200 (Figures 7.22 and 7.23) are compared with the ones obtained in the fire resistance tests.

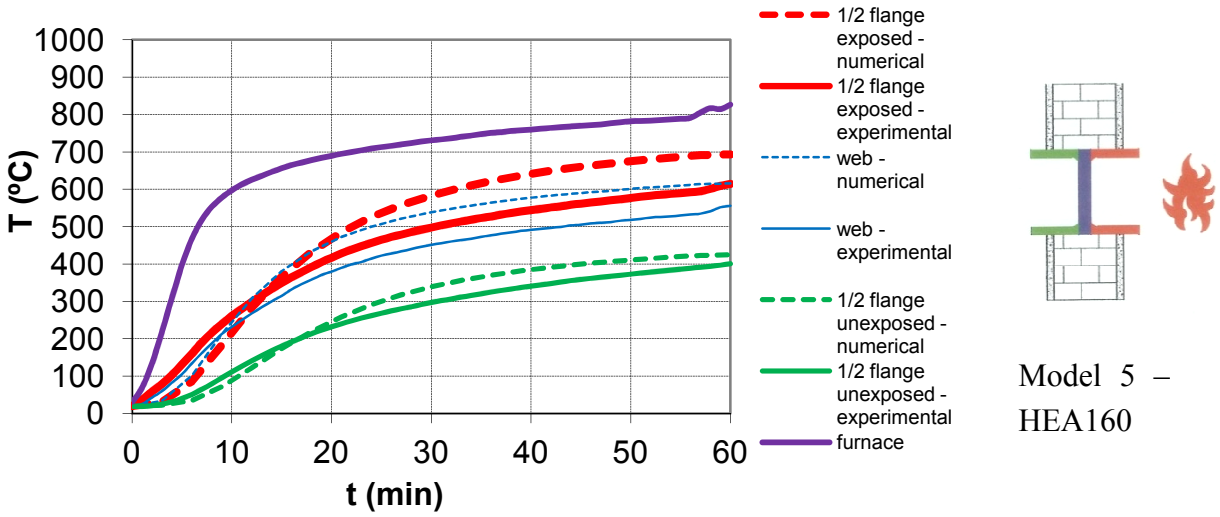

Figure 7.20 – Variation of the temperature with time for model 5 - HEA 160

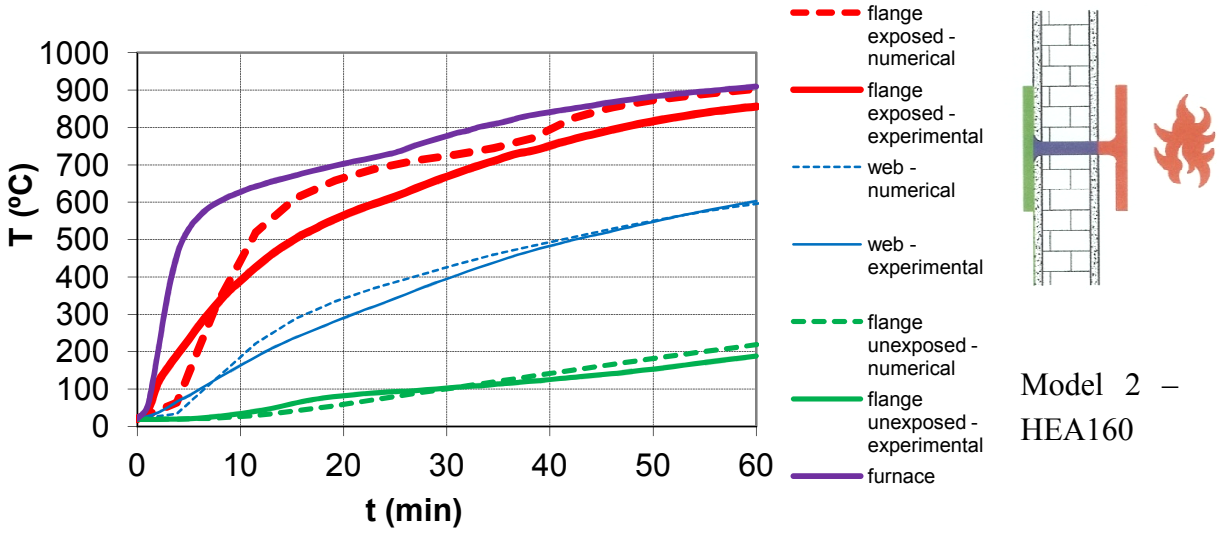

Figure 7.21 – Variation of the temperature with time for model 2 - HEA 160

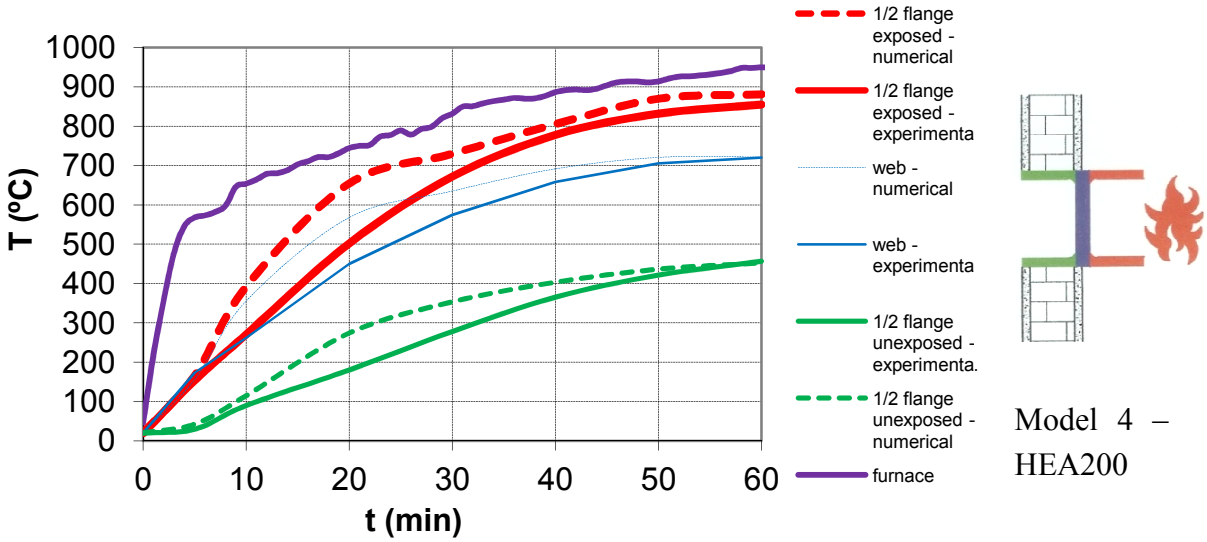

Figure 7.22 – Variation of the temperature with time for model 4 - HEA 200

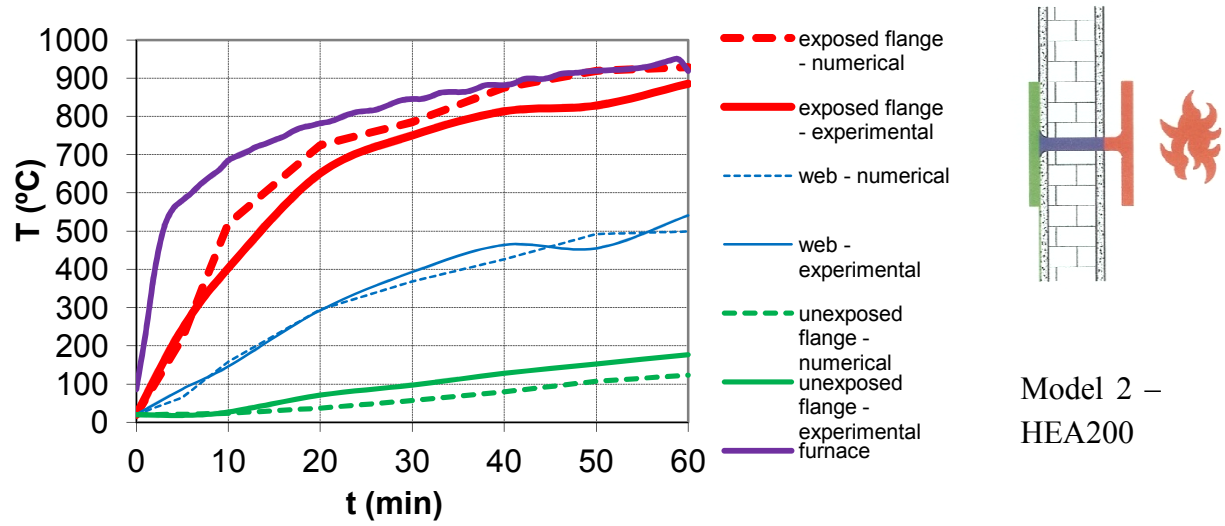

Figure 7.23 – Variation of the temperature with time for model 2 - HEA 200

These graphs show the influence of the building walls on the heating of the columns steel cross-sections because a high thermal gradient is observed between the exposed and unexposed parts. These thermal gradients are higher for the cases of the steel profile with web

perpendicular to the wall surface. After 60 min the temperature difference between the exposed and unexposed flange could be higher than 800ºC.

The temperatures measured experimentally and calculated in the numerical simulations with STC computer program were quite close indicating that the proposal is founded upon the correct base. The differences observed may arise from the thermal properties and parameters considered in the numerical simulations and the difficulty to consider all the parameters in play in the experimental tests.

The following graphs present a comparison between the results obtained with the STC numerical simulations and the proposal. The temperatures in the different zones of the steel cross-section for ten of the twenty four cases studied are presented (Figures 7.24 to 7.28).

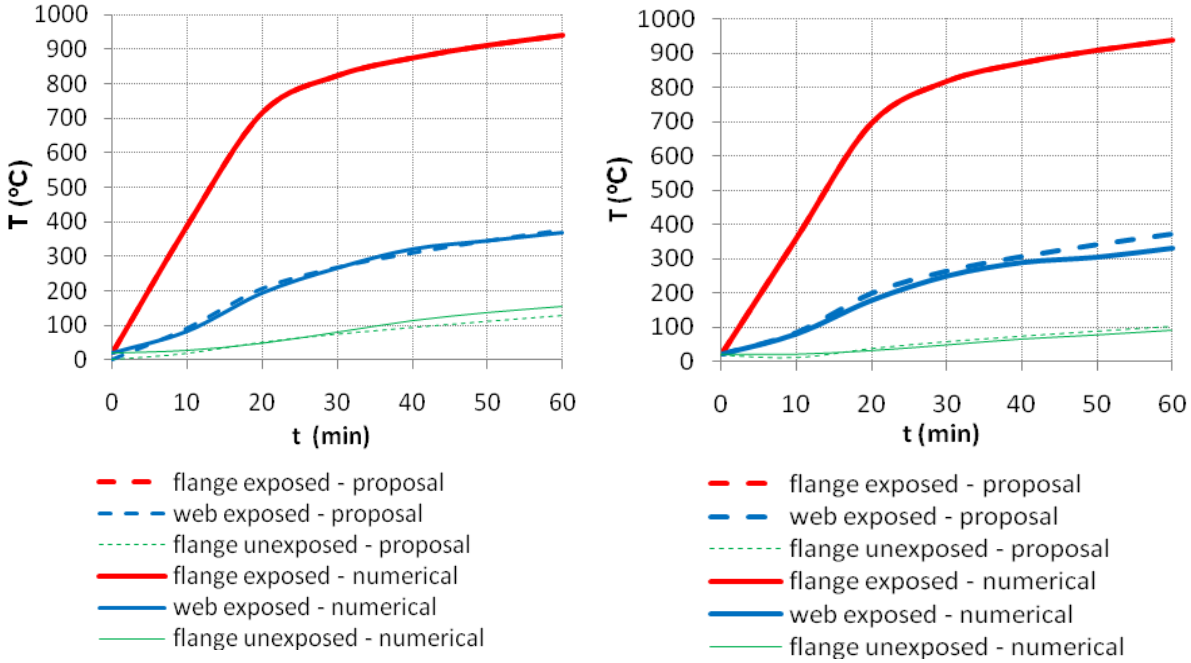

a)HEA 160 b) HEA 200

Figure 7.24 - Comparison between the STC numerical simulations and the proposal – Model 1.

In all graph, the red colour stands for the exposed part of the profile, the blue colour for the web and the green colour is for the unexposed part of the profile.

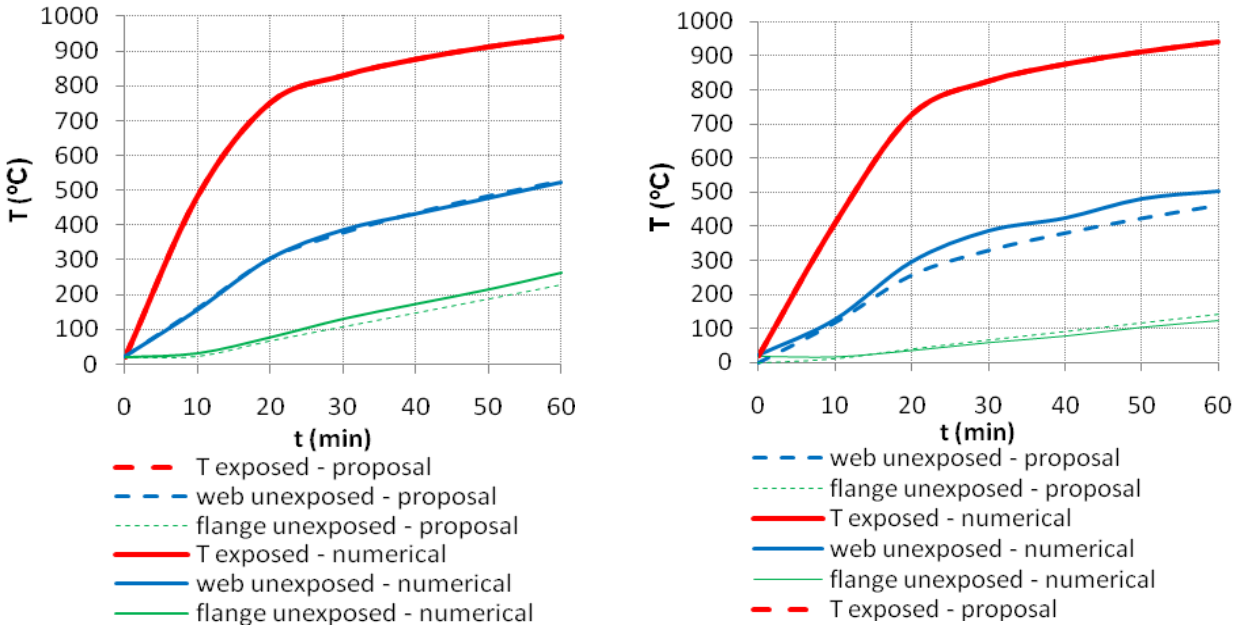

a)HEA 160 b)HEA 200

Figure 7.25 - Comparison between the STC numerical simulations and the proposal – Model 2

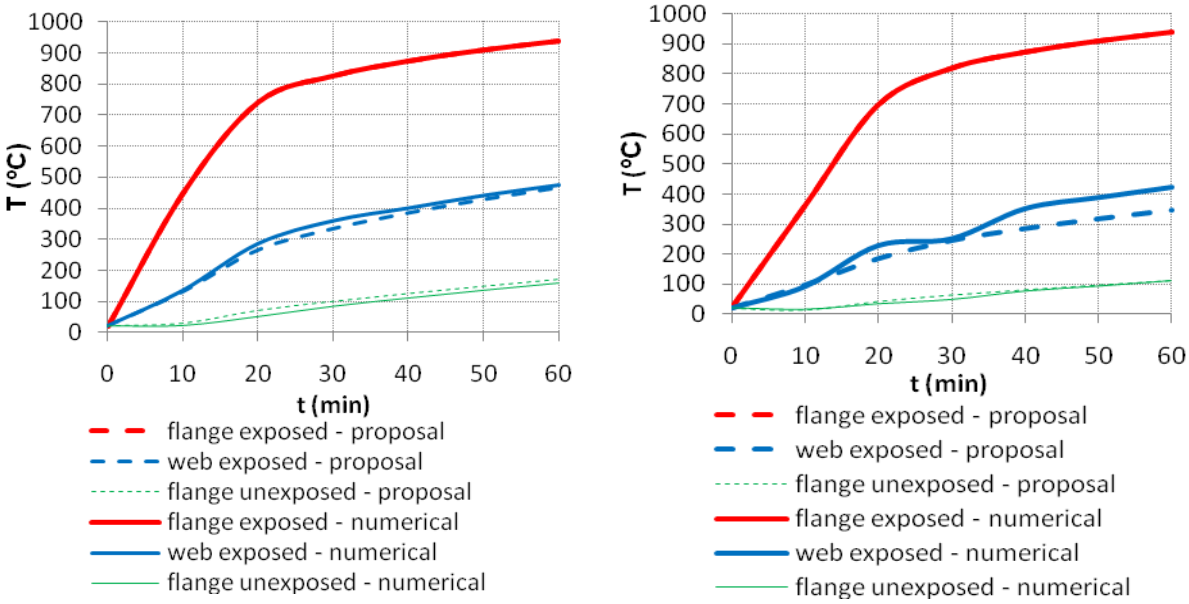

a)HEA 160 b)HEA 200

Figure 7.26 - Comparison between the STC numerical simulations and the proposal – Model 3.

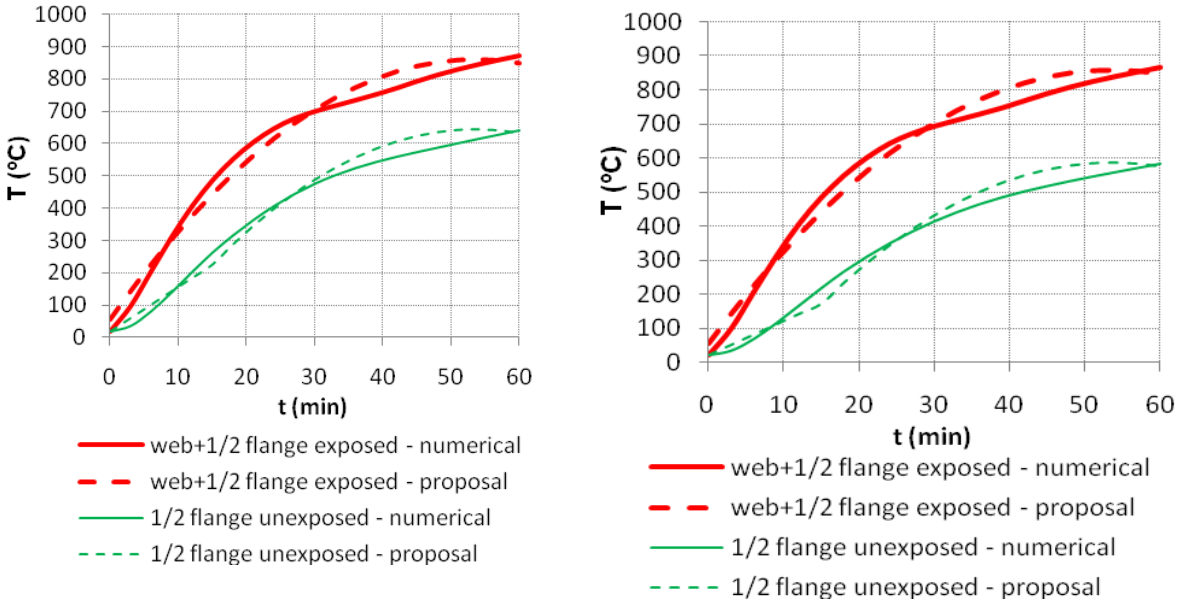

a) HEA160 b) HEA 200

Figure 7.27 - Comparison between the STC numerical simulations and the proposal – Model 4

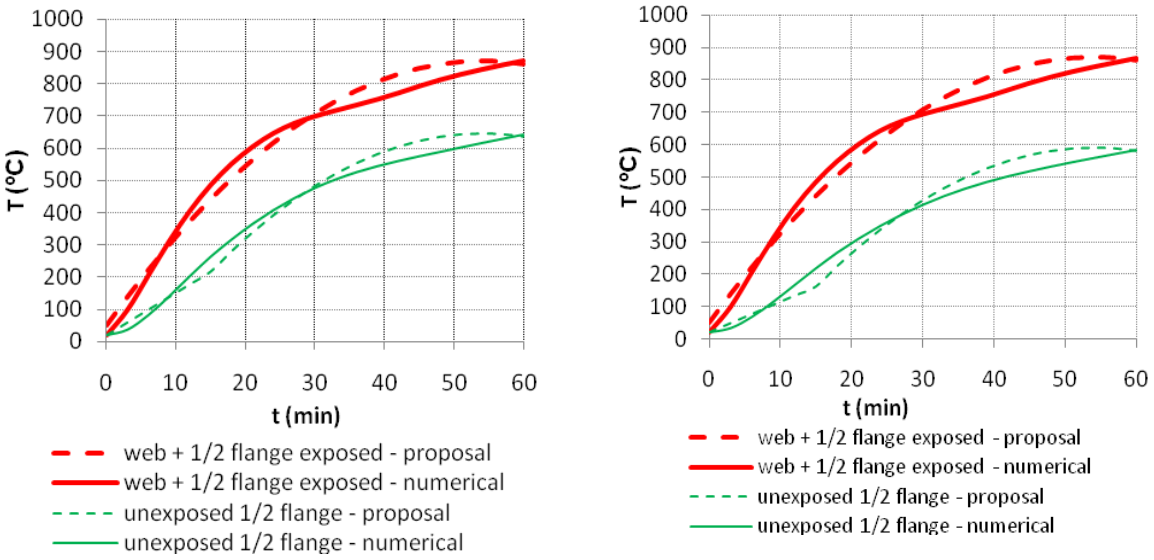

a) HEA160 b) HEA200

Figure 7.28 - Comparison between the STC numerical simulations and the proposal – Model 5.

Once again, the graphs demonstrate a high level of agreement between the temperatures determined with the STC numerical simulations and the proposal, showing its accuracy.

7.2 Proposal of Axial Force - Bending Moment Interaction Diagrams for Steel Columns

The analysis of the results presented in the previous chapters, allowed a better understanding of the fire behavior of a steel column in contact with walls. The inversion of bending moments, as well as the variation of stresses and strains in the flanges and along the web showed that the column in contact with the walls behaves as a beam-column, and fails by bending with compression. The discussion of this topic leads us to a comparison with the Eurocode formulation for structural elements subject to bending and compression at ambient temperature, and under high temperatures with a uniform distribution. Using this formulation, reduction factors for the yield stress of the steel were used according to the temperature of the steel, to derive the interaction diagrams for different uniform temperatures of the steel-cross section. Those curves are depicted in the following graphs, in dashed lines. Continuous lines are also plotted, representing different values of temperature of the exposed flange of the column. In the web and unexposed flange, temperatures were under 400ºC, thus no reduction of the yield stress was considered.

Figure 7.29 depicts the stress diagrams along the steel cross-section, considering an heating process with non-uniform temperature distribution. In this study, for the case of the orientation of the profile with the web perpendicular to the wall, the reduction of the yield stress was only considered in the heated flange. For the case of the profile with the web parallel to the wall the reduction of the yield stress was only considered in the heated half flange.

Figure 7.30 depicts the interaction diagrams axial force-bending moments for uniform temperature within the cross-section, equal to the temperature in the exposed flange (based on the Eurocode formulation), for the web perpendicular to the wall, considering uniform temperature in the cross section. Althought the Eurocode does not suggests the use in the whole steel profile of the temperatures attained in the heated part, in this analysis, this assumption is considered, hopefully as a conservative assumption.

In Figure 7.31, the axial force-bending moments diagrams of the Eurocode formulation are compared with the real resistance of the cross-section, considering the reduction of the strength in the heated portion of the profile, for the case of the web perpendicular to the wall.

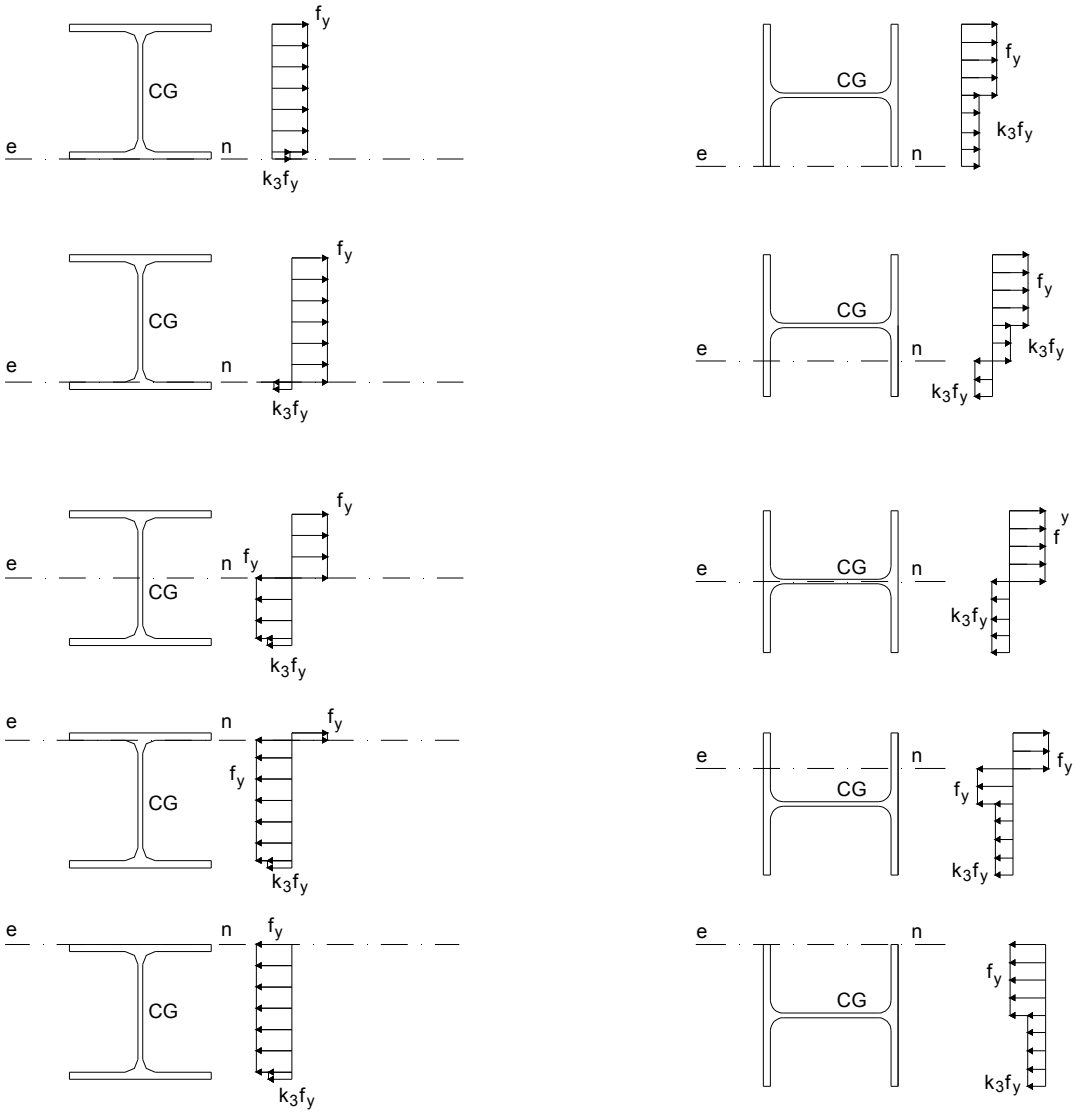

Figure 7.29 – Stress diagrams for non-uniform heated steel column with web perpendicular to the wall, and thick wall a) thermal gradient along the web b) thermal gradient along the flange

The continuous lines in Figure 7.31 stand for the envelope of values (Axial Force, Bending Moment), which represent the plastic limit state of the steel cross-section. These curves were obtained considering the neutral axis in several positions of the cross-sections, and considering the reduction of the yield stress of steel, in the exposed parts of the section, and the corresponding reduction factors for the stress-strain relationship of steel at elevated temperatures. Each point of the continuous curves represents a position of the neutral axis, and the corresponding values of the relation N/N_{pl} and M/M_{pl}.

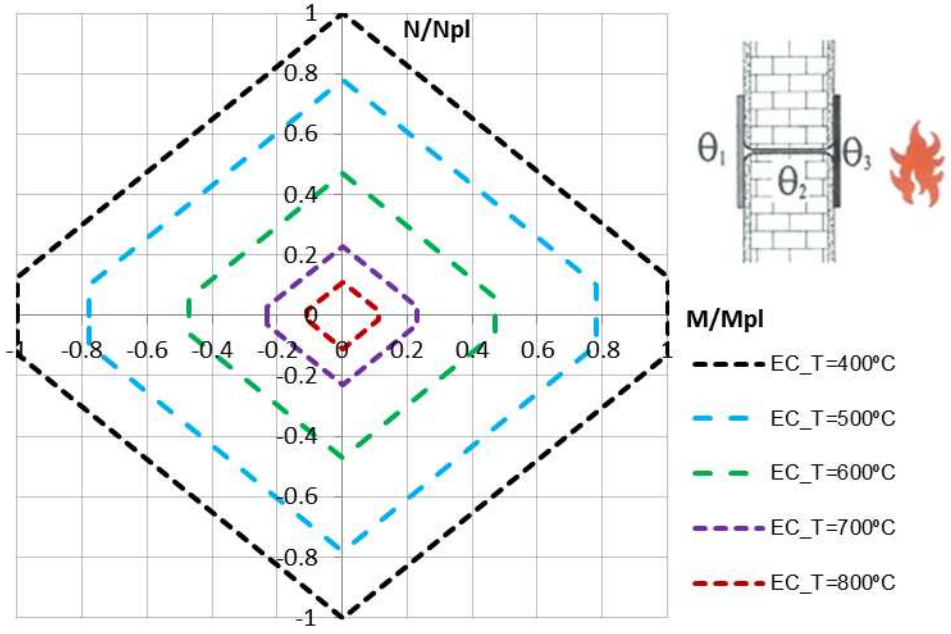

Figure 7.30 – Interaction diagrams axial force-bending moments for uniform temperature within the cross-section, equal to the temperature in the exposed flange (based on the Eurocode formulation), for the web perpendicular to the wall, considering uniform temperature in the cross section

It is observed that for high values of temperature considering uniform temperature within the section, equal to the temperature in the exposed flange, based on a great thermal conductivity of the steel, leads to very conservative curves, for the case of the H profile with the web perpendicular to the wall. Considering that dashed lines stand for EN 1993-1-2 (2005) based formulation with uniform temperature, and continuous lines stand for the real resistance of the section, with the thermal gradient, it may be observed that for temperatures above 700ºC, great reduction in the resistance of the section is implicit in the EN 1993-1-2 (2005) based formulation for high temperatures, while in reality, a thorough analysis show that above this value of temperature, the real reduction of resistance is not so great. This may be explained by the great difference in the mean temperature of the cross-section and the temperature in the exposed flange. A better proposal would be to consider the mean temperature of the steel cross-section, instead of a uniform temperature equal to the one observed in the exposed flange.

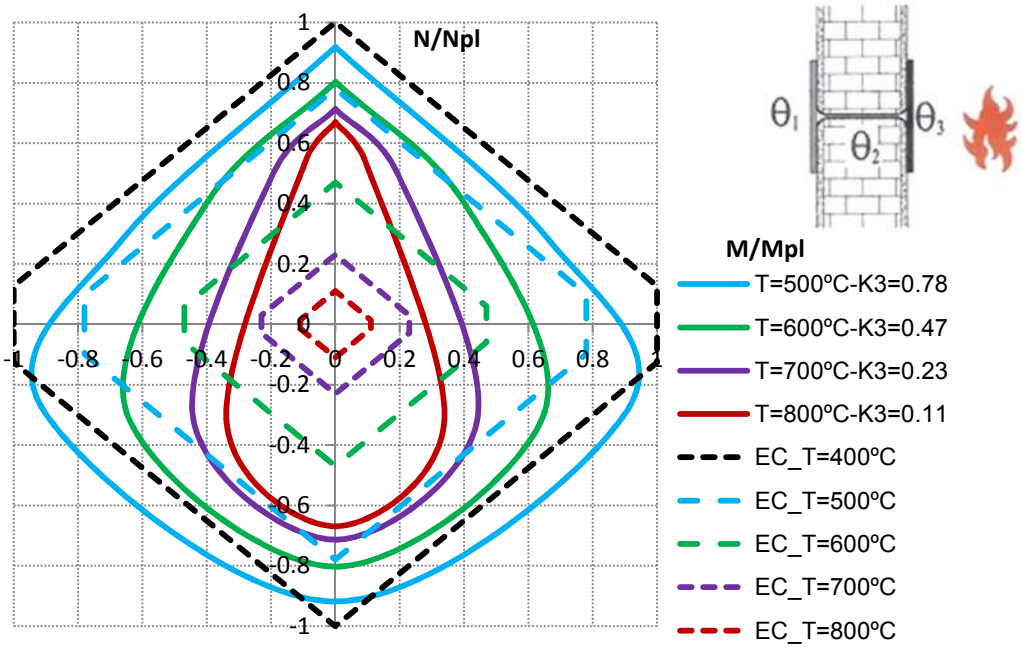

Figure 7.31 – Comparison of the interaction diagrams axial force-bending moment envelopes for uniform temperature within the cross-section, equal to the temperature in the exposed flange (based on the Eurocode formulation) and considering an unevenlly heated section, with thermal grandient in the web direction

The comparison of the interaction N-M diagrams considering uniform temperature within the cross-section and considering different temperatures in the flanges and in the web lead to the conclusion that the Eurocode formulation is very conservative. It can be observed that the envelopes obtained with uniform temperature (dashed lines) for all temperatures, are always inside the diagrams obtained with non-uniform temperatures. This fact allows us to conclude that for beam-columns with thermal gradients along the web direction, the assumption of uniform temperature within the cross-section equal to the maximum temperature in the exposed part of the profile, is very conservative.

Figure 7.32 depicts the interaction diagrams axial force-bending moments for uniform temperature within the cross-section, equal to the temperature in the exposed half-flange (based on the Eurocode formulation), for the web parallel to the wall, considering uniform temperature in the cross section.

In Figure 7.33, the envelopes of the axial force-bending moments diagrams of the Eurocode formulation are compared with the real resistance of the cross-section, considering the reduction of the strength in the heated portion of the profile, for the case of the web parallel to the wall.

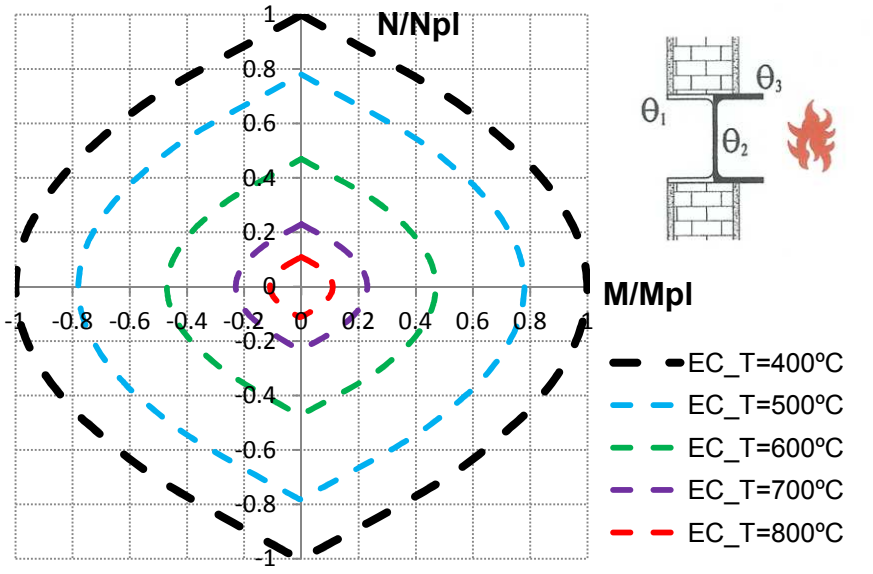

Figure 7.32 – Interaction diagrams axial force-bending moments for uniform temperature within the cross-section, equal to the temperature in the exposed half-flange (based on the Eurocode formulation), for the web parallel to the wall, considering uniform temperature in the cross section

For the case of the H profile with the web parallel to the wall, it is observed that considering uniform temperature within the section, equal to the temperature in the exposed half-flange, the envelope of the interaction diagrams N-M, is always inside the diagrams related to the real resistance of the section, giving thus conservative results. In figure 7.33 it may be observed that the continuous lines representing the real resistance of the cross-section are always outside the envelope defined by the EN 1993-1-2 (2005) approach, meaning that the Eurocode formulation is always safe.

The aim of this work was to explain in detail the phenomenon of thermal bowing in restrained steel H columns in contact with walls. A geometrical material non-linear analysis of the behavior of columns under the ISO 834 fire curve was carried-out to ascertain whether the phenomenon of thermal bowing in steel H columns in contact with walls is beneficial or detrimental for the column fire resistance. It was concluded that the contact with the walls is responsible for a great reduction in the temperatures in the cross-section, leading to greater fire resistances than the ones observed in the bare steel columns.

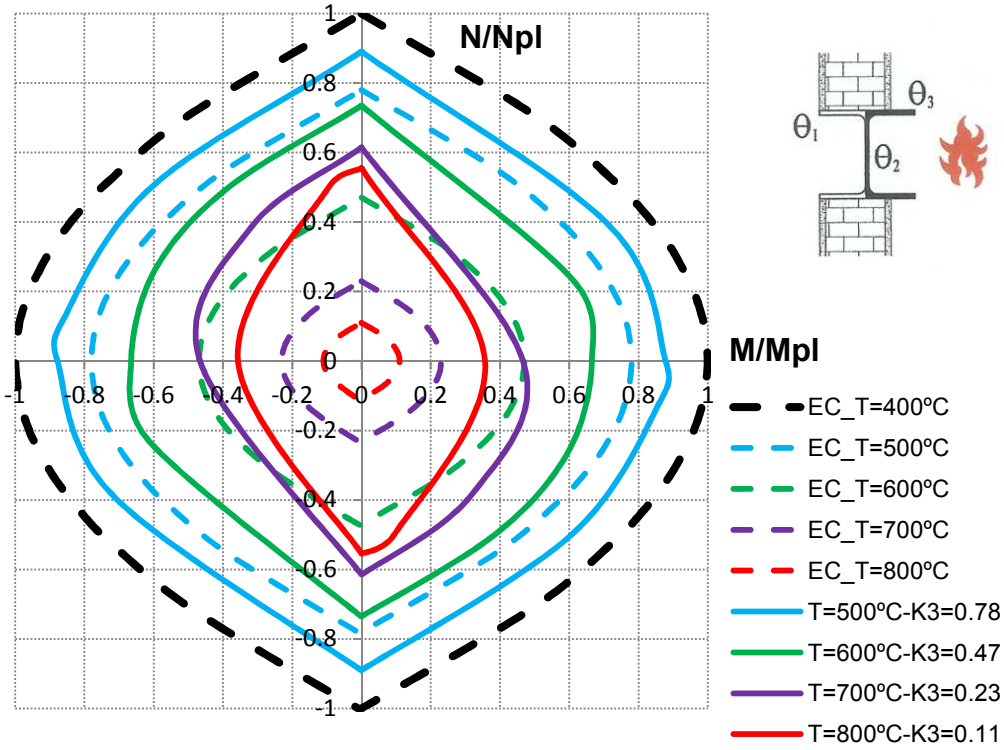

Figure 7.33 – Interaction diagrams axial force-bending moments for uniform temperature within the cross-section, equal to the mean temperature (based on the Eurocode formulation) and considering an unevenlly heated section, with thermal grandient in the flange direction

The detailed analysis of the finite element study allowed the understanding of the stress-strain state experimented by the several parts of the H profile, during the fire event. The inversion of bending moments was documented using a specific case, and the collapse mechanism observed with the formation of plastic hinges on bottom, top and mid-height of the column.

The first conclusion was that the failure of steel columns embedded on walls is significantly different form the failure of bare steel columns. The criterion of considering the colapse as the instant when the axial force after increasing up to a maximum decays and reaches the initial value seems to be inadequate to the columns embedded on walls, due to the fact that in these cases failure is not so abrupt, and a great resistance is observed for a long period of time. It was observed that these columns behave much more like beam-columns failing by bending, provoqued by “thermal bowing”, instead of columns failing by buckling.

The main conclusion of this work is that the use of EN 1993-1-2 (2005), for the design of steel-beam columns using plastic interaction diagrams axial force-bending moment with uniform temperature equal to the temperature attained in the exposed part of the steel profile, is always very conservative either with the column oriented with the web perpendicular to the wall, and with the web parallel to the walls.

7.3 Proposal of a Simplified Method for Fire Design of Steel Columns

Figures 7.34 and 7.35 present the variation of the critical temperatures and critical times as a function of the slenderness of the columns, for different load levels and different axial restraints. The critical temperature is defined as the mean steel temperature of the column when the restraining forces reach again the value of the initial applied load. The definition of critical time is similar however now in terms of time. The axial stiffness of the surrounding structure $K_{A,S}$ was used in this analysis, because the non-dimensional axial restraint ratio of the columns α_A is different for each column, and no comparison was possible.

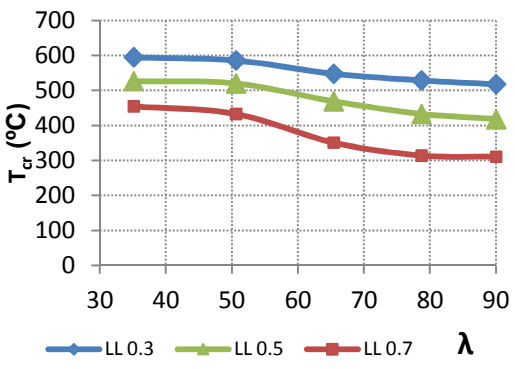

a) $K_{A,S}$ = 13kN/mm

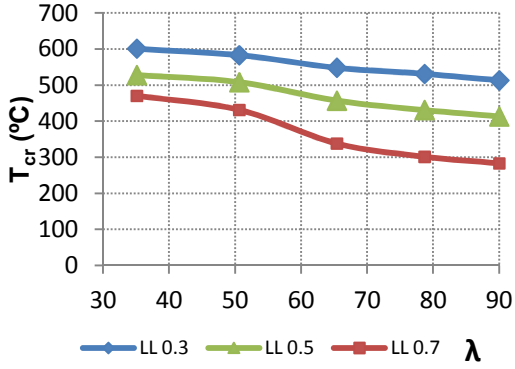

b) $K_{A,S}$ = 45kN/mm

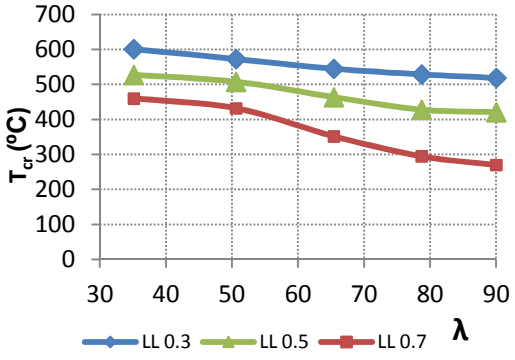

c) $K_{A,S}$ = 128kN/mm

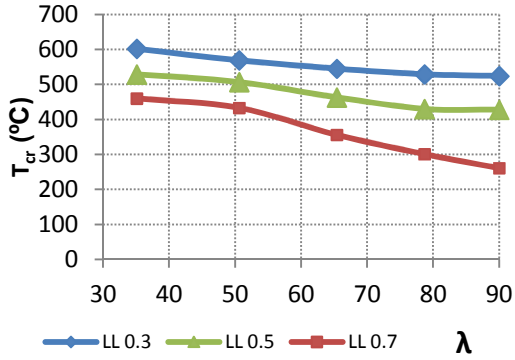

d) $K_{A,S} = \infty$

Figure 7.34 - Critical temperatures as a function of the slenderness for different axial stiffness of the surrounding structure

From Figure 7.34 a) to d), it is observed a reduction on the critical temperatures with the increasing of the slenderness of the columns. However, the reduction is more notorious for columns tested with the higher load level. The analysis of the four graphs, referring to different values of axial restraint, lead to the conclusion that the stiffness of the surrounding structure does not influence greatly the critical temperatures. Another interesting observation

is that for the slenderness between 35 and 50, the variation of the critical temperature with the slenderness seems to be linear (although only two values 35 and 50 were tested), while for values between 50 and 90, the variation is parabolic.

From Figure 7.35 a) to d), it can be said that the conclusions drawn for the critical temperatures are valid as well as for the critical times. The great influence of the load level in reducing the fire resistance of the columns is clearly evident. A large reduction in the critical times with the increase of the slenderness is also observed. It is also observed that there are no major differences in the results, for the several values of $K_{A,S}$, from 13 kN/mm to a fully restrained column.

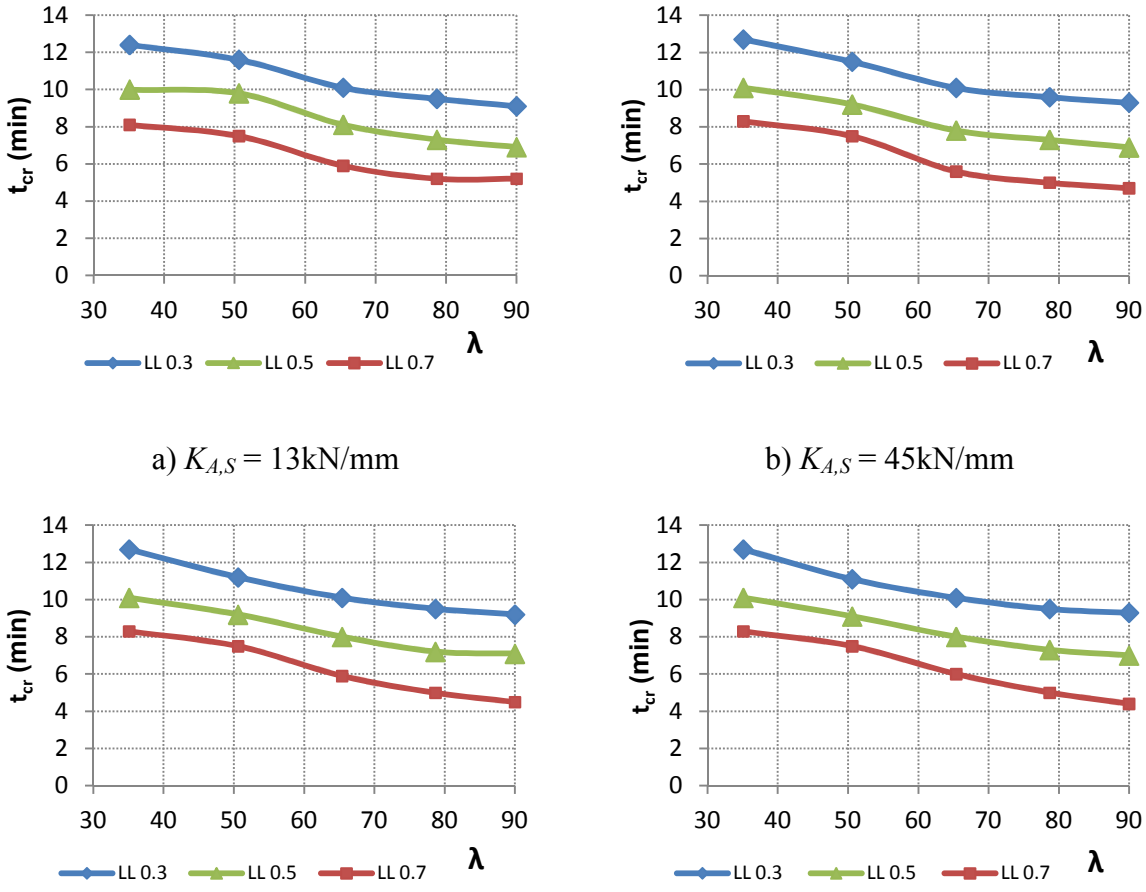

a) $K_{A,S}$ = 13kN/mm

b) $K_{A,S}$ = 45kN/mm

c) $K_{A,S}$ = 128kN/mm

d) $K_{A,S} = \infty$

Figure 7.35 – Critical times as a function of the slenderness for different axial stiffness of the surrounding structure

From figures 7.36 a) to d) it can be observed with no exception that lower load levels lead to higher restraining forces during the tests. Also, in all sets of tests, an increase of this peak was

observed for higher values of slenderness. As expected, the higher the restraint provoked by the surrounding structure, the greater the maximum $(P/P_0)_{max}$. For a total restraint $K_{A,S} = \infty$ and load level L=0.3, the axial force in the column can be 5 times greater than the initial value, *i.e.* the applied load. For this case, no experimental tests were carried out, only numerical simulations.

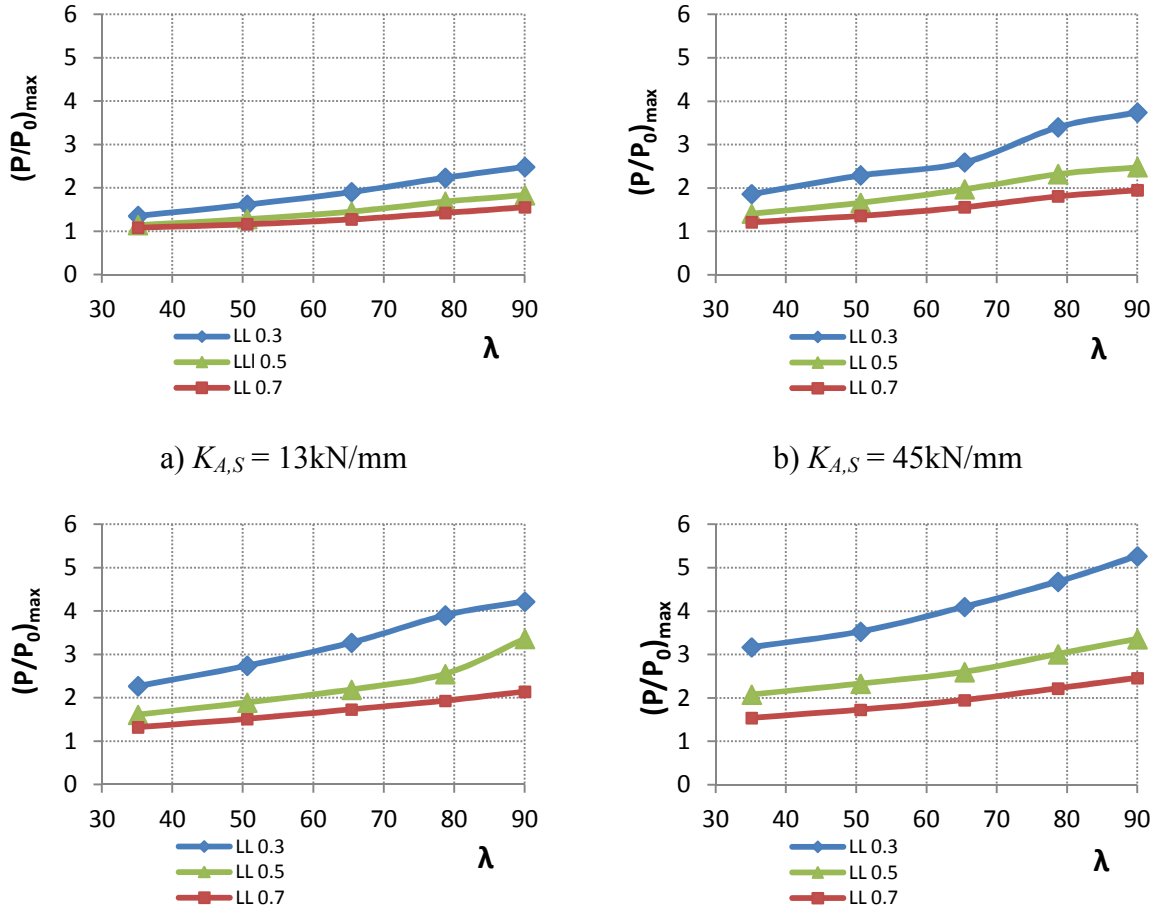

a) $K_{A,S}$ = 13kN/mm

b) $K_{A,S}$ = 45kN/mm

c) $K_{A,S}$ = 128kN/mm

d) $K_{A,S} = \infty$

Figure 7.36 - Maximum restraining forces as a function of the slenderness for different axial stiffness of the surrounding structure

Figure 7.37 a) to c) represents the critical temperatures in the steel columns, as a function of the non-dimensional axial restraint ratio for different load levels. The analysis of each graph, corresponding to a specific value of load level, leads to the conclusion that the critical temperatures decrease with the increase of the load level. Comparing the three graphs, it is concluded that the increase of the load level from 0.3 to 0.5, leads to a reduction of about 100ºC, and from 0.5 to 0.7 leads to a reduction in the critical temperature approximately of

the same value. The critical temperatures are independent of the non-dimensional restraint ratio.

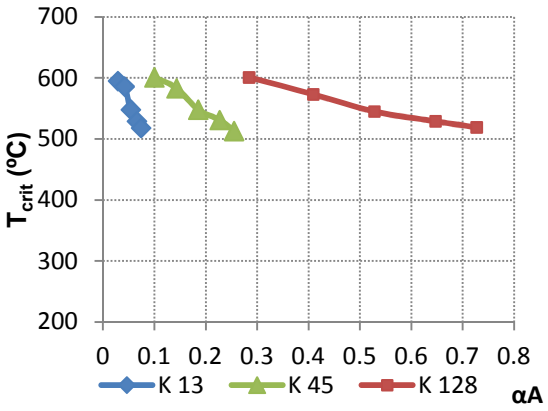

a) Load Level = 0.3

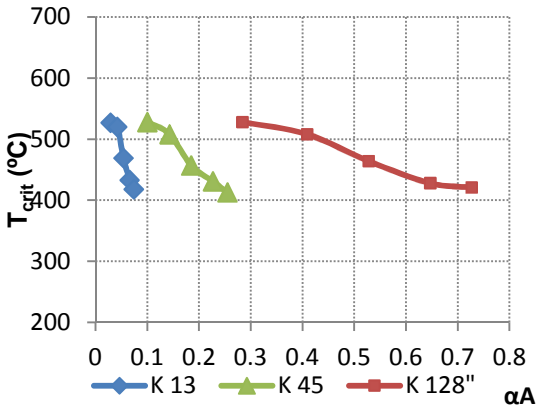

b) Load Level = 0.5

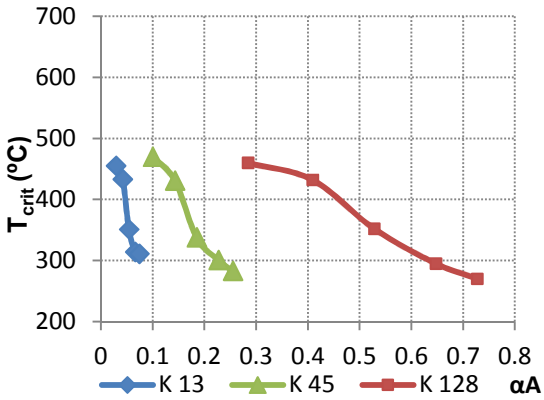

c) Load Level = 0.7

Figure 7.37 - Critical temperatures as a function of the non-dimensional axial restraint ratio for different axial stiffness of the surrounding structure and load levels

There is no continuity of the different lines in the graphs of Figure 7.37, bacause they correspond to tests with different stiffness of surrounding structure.

The graphs of Figure 7.38 present the results of the critical temperatures of the numerical simulations used to sustain the formulation of the proposal for HEA sections. In figure 7.38 a) the critical temperatures are plotted for different values of load level and stiffness of surrounding structure, as a function of the slenderness. In Figure 7.38 b) the critical times are presented, varying with the same variables. These graphs were the basis of the analytical proposals presented in this thesis.

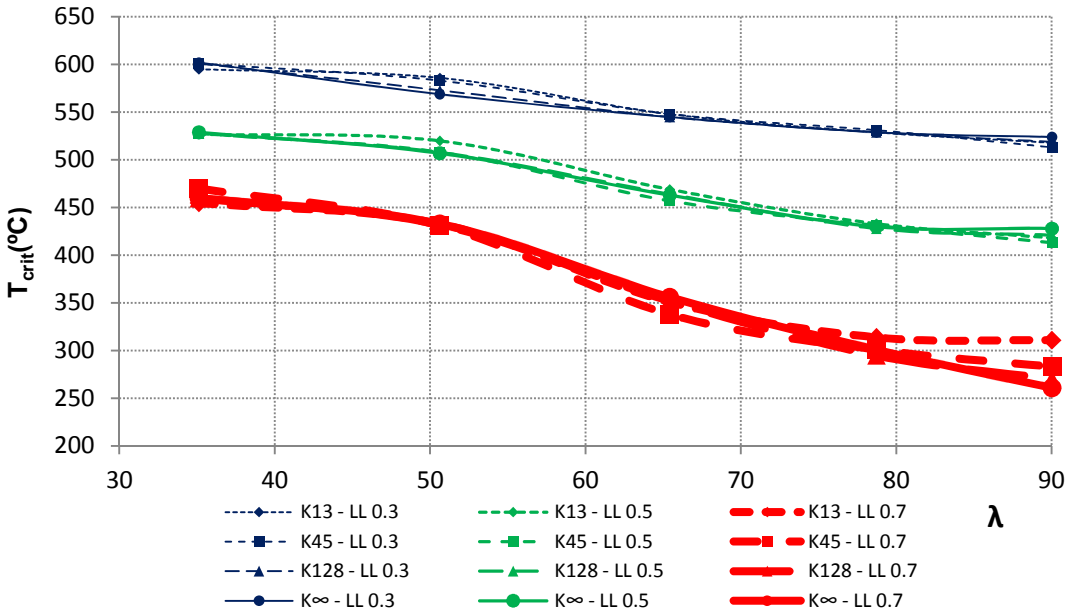

a)

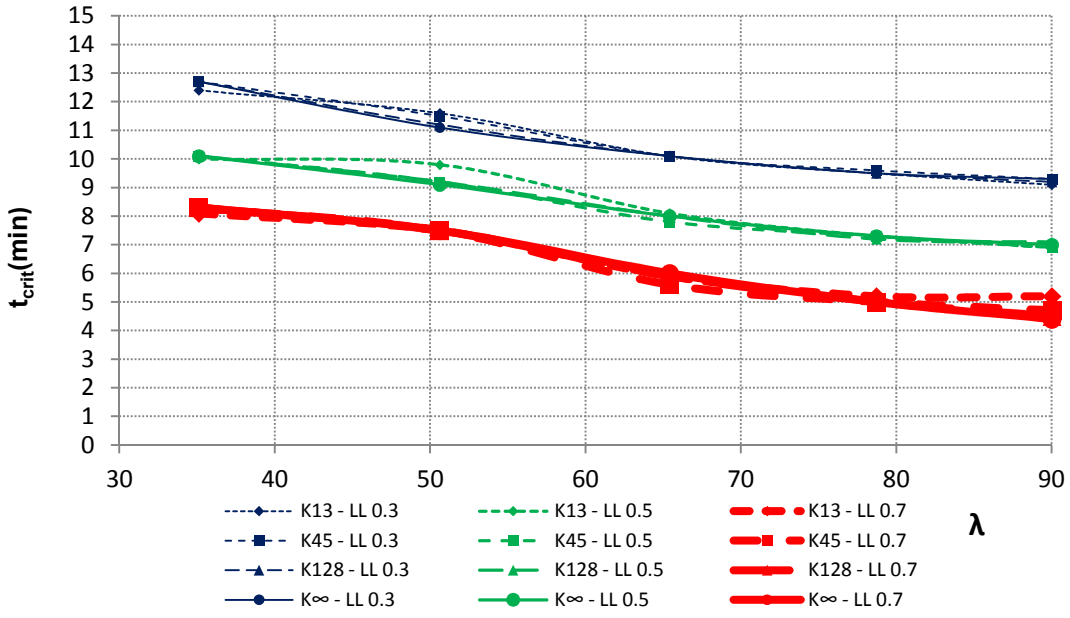

b)

Figure 7.38 - a) Critical temperatures for different values of load level and axial stiffness of surrounding structure as a function of the slenderness b) Critical times for different values of load level and axial stiffness of the surrounding structure as a function of the slenderness.

It can be observed from these graphs that the influence of the stiffness of the surrounding structure is only observed for a load level of 0.7, and slenderness of the column higher than 80.

The analysis of graphs in figures 7.38 a) and b) allowed the derivation of analytical formulae for the assessment of the critical temperatures and times for a wide range of load levels between 0.3 to 0.7 and slenderness values between 35 to 90, which are very realistic values in columns belonging to real buildings.

Quite interesting is to note that the variation of critical temperatures and times undergoes a linear variation from slenderness between 35 to 50, and a quadratic variation for slenderness between 50 to 90. The equations presented in table 7.5a) and b) reflect this behaviour, as well as the great influence of the load level, thus leading to different formulae for different load levels. The critical temperatures and critical times can be calculated, for different ranges of slenderness (between 35 and 50, or between 50 and 90), for load levels 0.3, 0.5 and 0.7.

Table 7.5 – Analytical formulae for the calculation of critical temperatures and times on steel columns a) for $35 < \lambda < 50$ b) for $50 < \lambda < 90$

Critical Temperatures	**Critical Times**
$35 < \lambda < 50$	
Load Level = 0.3	
$T_{cr} = 599 - 1.16(\lambda - 35.1)$ (7.8)	$t_{cr} = 12.6 - 0.077(\lambda - 35.1)$ (7.9)
Load Level = 0.5	
$T_{cr} = 528 - 1.03(\lambda - 35.1)$ (7.10)	$t_{cr} = 10.1 - 0.045(\lambda - 35.1)$ (7.11)
Load Level = 0.7	
$T_{cr} = 462 - 1.93(\lambda - 35.1)$ (7.12)	$t_{cr} = 8.2 - 0.045(\lambda - 35.1)$ (7.13)

a)

Critical Temperatures	**Critical Times**
$50 < \lambda < 90$	
Load Level = 0.3	
$T_{cr} = 0.025(\lambda - 50.6)^2 - 2.61(\lambda - 50.6) + 582$ (7.14)	$t_{cr} = 0.0012(\lambda - 50.6)^2 - 0.10(\lambda - 50.6) + 11.4$ (7.15)
Load Level = 0.5	
$T_{cr} = 0.035(\lambda - 50.6)^2 - 3.87(\lambda - 50.6) + 515$ (7.16)	$t_{cr} = 0.0013(\lambda - 50.6)^2 - 0.11(\lambda - 50.6) + 9.4$ (7.17)
Load Level = 0.7	
$T_{cr} = 0.066(\lambda - 50.6)^2 - 6.79(\lambda - 50.6) + 436$ (7.18)	$t_{cr} = 0.0014(\lambda - 50.6)^2 - 0.13(\lambda - 50.6) + 7.5$ (7.19)

b)

The proposed formulae were obtained for the best fit of the numerical data, with a linear regression for $35 < \lambda < 50$, and parabolic regression for $50 < \lambda < 90$.

The proposal here presented is only based on empiric results of a great number of numerical simulations. The concepts of flexural buckling, Euler critical load and section factors do not explicitly appear, but they were considered, once they were simulated in the models. This methods should only be used, as simple and quick calculation methods, to have an idea of the fire resistance of the columns. The proposal is only valid for bare steel columns. For columns with fire protection, further simulations would have to be performed.

The formulae here proposed were obtained with the same steel cross-section HEA200, varying the length, to obtain different values of slenderness. For the validation of the proposal to all HEA cross-sections, a set of 6 numerical simulations, using steel profiles HEA260, and HEA280, for 3 values of the load level, 30, 50 and 70% of the buckling load at room temperature were performed. It can be observed from table 7.6 that both critical temperatures and critical times show good agreement between the numerical analysis and the proposal.

Table 7.6 – Validation of the proposal for HEA sections

Steel Profile	Length (m)	Load (kN)	$K_{A,S}$ (kN/mm)	λ	Critical Temperature Numerical	Critical Temperature Proposal	Critical Time Numerical	Critical Time Proposal
HEA 260	6.0	1367 (70%)	45	64	369	354	6.9	6.0
HEA 260	6.0	976 (50%)	45	64	529	468	9.75	8.1
HEA 260	6.0	586 (30%)	45	64	562	550	11.8	10.2
HEA 280	4.5	1914 (70%)	45	45	434	443	8.4	7.8
HEA 280	4.5	1367 (50%)	45	45	515	518	10.5	9.7
HEA 280	4.5	820 (30%)	45	45	589	588	12.9	11.8

For the extension of the proposal to HEB and HEM cross-sections, a set of 15 numerical simulations, using steel profiles HEB200, 240, 300, 320, and HEM200, 3 values of the load level, 30, 50 and 70% of the buckling load at room temperature were performed.

For these tests, the critical temperatures as well as the critical times were calculated by the numerical modeling and the analytical proposal.

It can be observed in table 7.7 that the critical temperatures obtained by numerical simulation for HEB and HEM cross-sections are very close to the ones obtained by the proposed formulae, however, the critical times are different. The reason for this difference is the greater thickness of the flanges of these profiles. The proposed method can be used, due to the fact that the critical times obtained by the proposal are conservative, in relation to the ones

obtained by the numerical calculation. For HEB profiles, the critical times of the proposal should be increased by the factors 1.25 for load level 70%, 1.35 for load level 50% and 1.4 for load level 30%. For HEM profiles, the critical times of the proposal should be increased by a factor of 1.65, for any load level.

Table 7.7 – Extension of the proposal to HEB and HEM cross-sections

Steel Profile	Length (m)	Load (kN)	$K_{A,S}$ (kN/mm)	λ	Critical Temperature Numerical	Critical Temperature Proposal	Critical Time Numerical	Critical Time Proposal
HEB 200	3.3	1528 (70%)	128	45.6	459	441	9.9	7.7
HEB 200	3.3	1092 (50%)	128	45.6	529	517	12	9.6
HEB 200	3.3	655 (30%)	128	45.6	604	588	15	11.9
HEB 240	5.7	1647 (70%)	128	65.6	353	349	7.8	5.9
HEB 240	5.7	1176 (50%)	128	65.6	477	465	10.9	8.0
HEB 240	5.7	706 (30%)	128	65.6	564	548	13.6	10.2
HEB 300	3.6	3255 (70%)	128	33.2	432	467	10.4	8.3
HEB 300	3.6	2325 (50%)	128	33.2	519	531	14.5	10.2
HEB 300	3.6	1395 (30%)	128	33.2	624	602	17.6	12.8
HEB 320	8.5	2098 (70%)	45	78.6	232	297	5.8	5.0
HEB 320	8.5	1499 (50%)	45	78.6	421	434	10.1	7.3
HEB 320	8.5	899 (30%)	45	78.6	573	528	15.0	9.5
HEM 200	5.2	1949 (70%)	128	69	344	333	9.4	5.6
HEM 200	5.2	1392 (50%)	128	69	466	456	13.1	7.8
HEM 200	5.2	835 (30%)	128	69	557	542	16.5	10

Figure 7.39 depicts the comparison of the critical temperatures for HEB cross-sections obtained with the numerical simulations, with the critical temperatures obtained by the proposal derived for HEA cross-section.

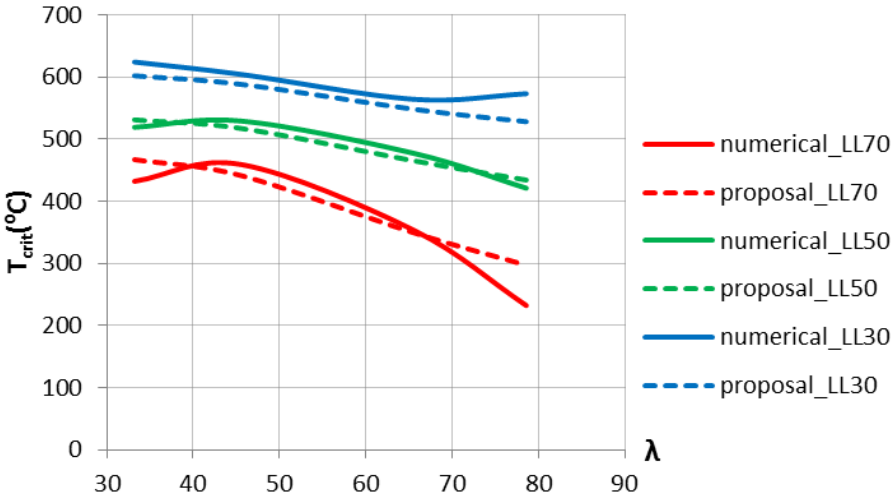

Figure 7.39 - Critical Temperatures for HEB sections, with different values of load level as a function of the slenderness obtained by numerical simulation with FE analysis and calculated by the proposed formulae derived with HEA profiles.

7.3.1 Comparison with the Eurocode

To conclude this study, a comparison of critical times and temperatures obtained with the numerical analysis performed with ABAQUS, the proposal of the present study and the EN1993-1-2 (2005) is presented.

For this comparison the values concerning the columns totally restrained were considered, due to the fact that the EN1993-1-2 (2005) formulation does not take into account this parameter. Moreover, the criterion used in this study is not the same as the one adopted by EN 1993-1-2 (2005). It is observed that the critical times and temperatures obtained by EN 1993-1-2 (2005) formulation are very similar to the ones observed in the numerical simulations with ABAQUS. For low values of slenderness, the results are very similar, but for high values of the slenderness, the EN 1993-1-2 (2005) gives slightly higher fire resistances than obtained in the numerical approach, and thus with the proposal.

Table 7.8 – Comparison of critical temperatures of steel columns totally restrained

Load Level	Load (kN)	Length (m)	Slenderness	PROPOSAL T_{cr}(ºC)	ABAQUS T_{cr}(ºC)	EN1993-1-2 T_{cr}(ºC)
30%	495.68	2.5	35.1	599	602	635
	428.49	3.6	50.6	582	569	625
	359.47	4.65	65.4	549	545	617
	293.48	5.6	78.7	528	529	614
	254.77	6.4	90	518	524	608
50%	826.14	2.5	35.1	528	529	557
	714.16	3.6	50.6	515	507	550
	599.11	4.65	65.4	465	463	544
	489.13	5.6	78.7	433	430	543
	424.61	6.4	90	417	428	537
70%	1156.59	2.5	35.1	462	460	490
	998.82	3.6	50.6	436	433	478
	838.75	4.65	65.4	350	356	464
	684.78	5.6	78.7	297	301	461
	594.46	6.4	90	271	261	438

Table 7.9 – Comparison of critical times of steel columns totally restrained

Load Level	Load (kN)	Length (m)	Slenderness	PROPOSAL t_{cr}(min)	ABAQUS t_{cr}(min)	EN1993-1-2 t_{cr}(min)
30%	495.68	2.5	35.1	12.6	12.7	11.6
	428.49	3.6	50.6	11.4	11.1	11.0
	359.47	4.65	65.4	10.2	10.1	10.8
	293.48	5.6	78.7	9.5	9.5	10.7
	254.77	6.4	90	9.3	9.3	10.6
50%	826.14	2.5	35.1	10.1	10.1	9.1
	714.16	3.6	50.6	9.4	9.1	8.9
	599.11	4.65	65.4	8.1	8.0	8.7
	489.13	5.6	78.7	7.3	7.3	8.7
	424.61	6.4	90	7.1	7.0	8.6
70%	1156.59	2.5	35.1	8.2	8.3	7.6
	998.82	3.6	50.6	7.5	7.5	7.3
	838.75	4.65	65.4	5.9	6.0	7.0
	684.78	5.6	78.7	5.0	5.0	7.0
	594.46	6.4	90	4.6	4.4	6.6

7.4 Sinopsis

A proposal of a simplified calculation method for the temperature evaluation in the different zones of H steel cross-sections embedded on walls was presented. The great number of columns in normal practice, is embedded on building walls. Formulae for the case of the web parallel and perpendicular to the wall surface were presented in this work. This study raised the issue of calculation of the temperatures in steel cross-sections of columns with thermal gradients, on the contrary to the EN 1993-1-2 (2005) formulations which considers uniform temperature distribution.

The high thermal gradient observed, in both cases of web perpendicular and parallel to the wall surface, leads usually to unfavourable forces and moments in the columns cross-sections. In fact, thermal bowing is provoked by the high thermal gradients in the cross-section of steel elements with restrained thermal elongation. The thermal restraint leads to differential strains in the heated and unheated zones of the steel profile which associated to the reduction of the Young's modulus and yield stress in function of the temperature, leads to an inversion of the bending moments in the column. The high bending moments generated in the cross-section

may lead to the premature failure of the steel columns, or on the contrary, delay this failure. In this study, no premature failure was observed.

The proposed simplified calculation methods for the assessment of temperatures in columns embedded on walls are valid for all steel cross-sections with dimensions proportional to the walls thicknesses, as in the studied cases. Other cases of proportionality between the steel profiles dimensions and the wall thicknesses have yet to be studied.

Another purpose of this work was the proposal of a new simplified calculation method for the design of steel columns with restrained thermal elongation. The parametric study carried out under this study focused on the influence of several parameters involved on the behavior of steel columns subjected to fire considering their interaction with the surrounding structure.

In this chapter, a parametric study was presented, for different values of slenderness ranging from 35 to 90, different values of load level, ranging 0.3 to 0.7, and different values of the stiffness of the surrounding structure, ranging from 13kN/mm to fully restrained.

As expected, the load level (or degree of utilization) was undoubtedly the most important parameter involved. Increasing the load level from 0.3 to 0.7, leads to a reduction of 150ºC in the critical temperatures for slenderness values between 35 and 50, and 250ºC for values of slenderness between 50 and 90, which correspond to a reduction on the critical time of approximately 4 minutes, regardless of the slenderness.

The slenderness of the column was also proven to have great influence on the critical temperatures and times. For the load level 0.3, increasing the slenderness from 35 to 90 lead to a reduction on the critical temperature of 75ºC, meaning 3.5 minutes. For the load level 0.7, the same variation on the slenderness of the column, leads to a reduction on the critical temperature of 175ºC, meaning 3.5 minutes.

The main conclusion of this research contradicts the general idea that in real structures, higher stiffness of the surrounding structure, leads to a reduction in the critical temperatures and fire resistance of the columns. This is because the restraint to thermal elongation of a column subjected to fire is composed by an axial and a rotational restraint. In fact, the detrimental effect of the axial restraint to thermal elongation is canceled by the beneficial effect of the rotational restraint provided by the structure. This fact leads to the conclusion that an analytical formulation for the assessment of the fire resistance of steel columns in buildings may neglect the restraint provided by the building. Acceptable results are obtained considering the columns fully axially restrained (Franssen, 2000). The conclusions presented are valid for the range of slenderness between 35 to 90, and load level between 0.3 to 0.7, with any value of restraining of the building structure.

8 CONCLUSIONS AND FUTURE WORK

8.1 Conclusions

8.1.1 Steel Columns Embedded on Walls

The main goals of this work were: a) better understanding of the failure of steel columns in contact with walls; b) evaluation of the thermal gradients developed within the cross section of a steel column embedded on walls; c) comparison of temperatures in steel columns in contact with walls, with the ones calculated by the Eurocode 3; d) better understanding the thermal bowing phenomenon in this structural elements; e) proposal for a new methodology for the assessment of temperatures in steel columns embedded on walls; f) conclude whether the contact with the walls have a favorable or detrimental influence on the structural behavior of the columns.

The assessment of temperatures in structural elements subjected to differential heating is essential to the development of analytical methods to predict buckling behaviour of this type of columns.

Concerning the assessment of the temperature evolution in the steel profiles, in the beginning of this study, a set of numerical simulation tests of the experimental tests was performed. The evolution of temperatures in different points of the cross-section of the elements obtained in experimental tests were compared with the ones obtained from calculations performed with the finite element program SUPER-TEMPCALC (STC) and with the simplified calculation method presented in EN 1993-1-2 (2005) for the determination of the temperature evolution in steel elements. The main conclusion drawn from this comparison was that the temperature evolution obtained by STC and the method of EN 1993-1-2 (2005), gives in general higher temperatures than the ones obtained in the tests. The differences are higher when the web is parallel to the wall surface and in the thermocouples placed in the external face of the web not directly exposed to fire. It can be said that the method of EN 1993-1-2 (2005) and the STC overestimate the temperatures in the cross section of the steel column when the elements are embedded on walls and so, eventually is conservative in the estimation of the real fire resistance of the element.

Quite interesting results were observed in this study for the case of specimen with web perpendicular to the wall surface, the temperatures in the flange exposed to the fire for the numerical simulations performed with STC, the method of EN 1993-1-2 (2005), and the experimental tests, were very similar. In the web and the flange not exposed to the fire there are significant differences.

From this study it was concluded that the section factor defined in EN 1993-1-2 (2005) for the case of steel sections embedded in walls is not appropriate. Studies on this issue were made in order to find a more representative definition of the section factor for these cases.

As expected, in steel columns embedded on walls, the flanges of the steel profile directly exposed to fire, are submitted to higher temperatures than the unexposed ones. This will cause a higher expansion of the heated flange than the cooler one, inducing bending moments in the column cross-section. This effect is called thermal bowing and may be very important in steel columns.

The EN 1993-1-2 (2005) formulation for the section factor can be used, although it was proven to be valid only for the exposed flange engulfed in fire. In all other cases, the temperature in each zone of the cross-section can be calculated in function of the temperature of the exposed area. Several reduction factors were in this study, defined in such a way that multiplying the temperature of the exposed area of the steel profile by them, the temperature in the corresponding zone is obtained.

The methods presented in this work for the calculation of the temperatures in the different parts of the steel cross-section have potential to be used in a future formulation, in EN 1993-1-2 (2005), of the section factor of columns embedded on walls.

The high thermal gradient observed, in both cases of web perpendicular and parallel to the wall surface, leads usually to unfavourable forces and moments in the columns cross-sections. In fact, thermal bowing is provoked by the high thermal gradients in the cross-section of steel elements with restrained thermal elongation. The thermal restraint leads to differential strains in the heated and unheated zones of the steel profile, which associated to the reduction of the Young's modulus and yield strength of the steel at high temperatures, leads to an inversion of the bending moments in the column..

Comparing the two orientations of the web, in relation to the wall, for cases with the web parallel to the wall surface it was concluded that the thicker wall plays an important role in reducing the temperatures on the unexposed half of the flange and also in the web. While for cases with the web perpendicular to the wall surface a quite interesting result was observed, in the unexposed face of the flange, the temperatures were slightly higher with the thicker wall. On the contrary on the exposed flange the temperatures were higher for the thinner walls.

Concerning the structural performance of steel columns in contact with walls, the cases studied in this work, showed that steel columns embedded on walls presented higher fire resistance than those totally engulfed in fire. This means that the beneficial effect of the insulation provided by the walls plays a major influence over the detrimental effect of the thermal gradients developed in the column cross-section.

In all situations under test, thermal bowing was observed, causing an inversion of lateral deflections from the hot to the cold side of the wall. This behaviour led to a failure mode more like bending, than buckling. Buckling was only observed in bare steel columns.

The slenderness of the columns did not influence strongly the fire resistance, due to the fact that only two similar values of slenderness were tested. However, it was observed that the higher the slenderness, the lower was the fire resistance.

The main parameter that influenced the behavior of the columns subjected to fire was the wall thickness: thinner walls provided lower fire resistances.

The walls were also effective in preventing the columns with the web perpendicular to the wall surface to fail around the minor axis. In these cases, the detrimental effect of the thermal bowing seems to be canceled by the fact that failure is forced to occur around the strong axis. Moreover, no local buckling was observed in the flanges due to the contact with the walls.

In experimental tests some detachment of the columns in relation to the walls was observed. This reduces the fire resistance of the columns. The problem was solved by welding some steel connectors to the columns, which enhanced the connection between the columns and the walls.

In the scope of this research, a proposal of a simplified calculation method for the temperature evaluation in the different zones of H steel cross-sections embedded in building walls was presented. The great number of columns in real buildings is embedded on the building walls. Formulae for the case of the web parallel and perpendicular to the wall surface were presented in this thesis. This study raised the issue of calculation of temperatures in steel cross-sections of columns with thermal gradients, on the contrary to the EN 1993-1-2 (2005) formulations which considers uniform temperature distribution. The proposed simplified calculation method is valid for all steel cross-sections with dimensions proportional to the walls thicknesses as in the cases studied. Other cases of proportionality between the steel profile dimensions and the wall thickness have to be studied.

In the future, similar studies for other types of steel cross-sections embedded on walls and in the corner of the walls will be carried out in order to propose new formulae for the temperature evaluation.

Concerning the design of steel columns in contact with wall, considering the uniform temperature stipulated by EN 1993-1-2 (2005), it was concluded that the formulation of this document is always conservative, than the consideration of the gradients with the real temperatures within the cross section. In fact, the interaction Axial Force – Bending Moment diagrams derived for this situation, is always outside the ones obtained from the EN 1993-1-2 (2005), using uniform elevated temperatures in the whole section, meaning that this document leads to conservative designs.

8.1.2 Bare Steel Columns

The main goals of this work concerning the fire resistance tests on steel bare columns were: a) design and build a full scale experimental set-up, to be used in fire resistance tests of columns of different shapes and materials b) obtain valuable data of experimental full scale fire tests on steel columns with restrained thermal elongation; c) evaluation of the real influence of the stiffness of the surrounding structure, considering simultaneously the axial and rotational restraint; d) develop and calibrate a finite element numerical model submitted to the mechanical and thermal loads of a column in a real building, submitted to fire; e) develop new simplified analytical methods for the design of steel columns under fire situation; f) compare the results of the numerical modeling with the EN 1993-1-2 (2005) calculation methods.

With this set of tests, a great amount of test results, concerning temperatures, axial displacements, lateral deflections, rotations and axial forces was obtained. The main conclusion of this work contradicts the general idea that in real structures higher stiffness lead to a reduction of the critical temperatures and fire resistance of the columns. Usually, in real buildings, increasing the axial restraint corresponds to an increase of the rotational restraint. While the first leads to a reduction, the second leads to an increase of the critical temperature and fire resistance of the columns. In these tests, the reduction in the critical temperatures with the increase of the stiffness of the surrounding structure was very small. The reduction was smaller than 50ºC for the HEA 160 columns and practically null for the HEA 200 columns.

The load level is an important parameter in the fire resistance of steel columns. Columns with higher load levels present lower critical temperatures and fire resistances. For the tested columns, increasing the load level from 30 to 70% of the design value of the buckling load at room temperature, a reduction of about 100ºC in the critical temperature was observed.

Concerning the eccentricity of the load, it was concluded that the EN 1993-1-2 (2005) formulation for the design of steel columns with combined bending and axial compression, is very conservative, leading to very low values of the load. It was observed in the tests that the higher the eccentricity of the load, the higher the critical temperature and the fire resistance of the column. This occurred due to the lower value of the load applied on the columns with eccentricity, during the test.

Columns with higher slenderness ratio present lower critical temperatures and fire resistance**.** The values of the slenderness of the tested columns were 50.6 and 63.3. These values are very realistic in steel buildings however too close. As expected, there is a reduction in the critical temperature with the increase of the slenderness. For the tested values, this reduction was not considerable.

It was possible to conceive a very thorough finite element numerical model, to reproduce the experimental fire resistance tests performed in the laboratory. The calibration of the model led to very satisfactory results comparing the experimental and numerical results.

A simplified method for the assessment of the critical times and temperatures on bare steel columns was developed and presented, taking into account the axial and rotational restraint.

The comparison of the fire resistance of steel columns in buildings, between the numerical approach and the EN 1993-1-2 (2005) formulation led to very similar results, although the failure criteria is different.

8.1.3 Composite Steel-Concrete Columns

Due to the fact that there are very few published results of experimental tests on the fire resistance of composite columns with embedded steel sections, the main aim of this work was to provide data, for researchers on this issue. In this thesis, the results of an experimental programme on composite steel-concrete columns with restrained thermal elongation under fire, was presented.

The main conclusion is that the concrete between the flanges provide a huge fire resistance, in comparison with the steel bare sections. This concrete is also important in preventing the local buckling of the flanges. The results here presented are suitable to be used in calibrating a finite element model to carry out a parametric study, varying the parameters involved in the

behavior of these columns, such as the relative slenderness of the column, the load level and the stiffness of the surrounding structure. Another interesting remark that should be pointed out, is that failure of all columns was by flexural buckling, and the detachment of the stirrups from the web was observed in all tests. One recommendation that can be made at this stage is that the fire resistance of these columns can be enhanced if holes would have been done in the web and only one stirrup, crossing the web was used, instead of two stirrups, one at each side, welded to the web.

The results of the test programme led to the following conclusions:

For the load level 0.3 there is a great influence of the stiffness of the surrounding structure on the critical times of the columns. The increase of the axial restraint leads to a reduction on the critical times. The same was not observed for the load level of 0.7, where practically no reduction on the critical times was observed. For the load level 0.7 the reduction in the critical times was negligible. In fact, for this load level, increasing the stiffness of the surrounding structure leads to a slight increase of the critical times. This is probably due to the fact that the rotational restraint plays an opposite influence than the axial restraint. The axial restraint is known to play a detrimental role, while the rotational restraint plays a beneficial role, and the two effects combined, lead to a negligible effect on the fire resistance of the column for high load levels. For the load level of 0.3 the axial restraint seem to have a greater importance than the rotational, and the effect of the interaction with the surrounding structure is important, leading to great reduction in the fire resistance.

The values of the relative slenderness of the tested columns were very similar. They are realistic values commonly used in real buildings. As expected, there is a reduction in the critical temperature with the increase of the slenderness. For the tested values, this reduction is not considerable.

8.2 Recommendations for Future Works

In the future, similar studies for other types of steel cross-sections embedded on walls and in the corner of the walls should be carried out in order to propose new formulae for the temperature evaluation. It will be very important to evaluate the thermal bowing in peripheral columns, i.e., with high initial bending moments. In this case, the thermal bowing may play a different role in the column behaviour.

It would be interesting to carry out more tests in loaded columns embedded on walls. The thermal behaviour of these columns was analyzed in this study, and the assessment of

temperatures is now very easy to carry out. However, the thermal bowing is still to be more understood in detail, so more experimental tests should be carried out, to analyze the inversion of bending moments and rotations on bottom and top of the column, in the connection with the upper and lower beams. On this issue, great influence is certainly the restraint to rotational displacements provided by the surrounding structure.

Concerning the steel columns, it is very important to test columns with restrained thermal elongation, with different insulating materials such as silicatum boards and gypsum boards, and other new materials to be developed, such as expanded clay concrete panels.

Fire tests on the buckling of steel columns, to assess the plastic load for each temperature would be of great interest.

Concerning the composite steel-concrete columns, a set of tests on encased steel-concrete columns should be carried out. A special attention should be devoted to the connection between the stirrups and the web of the steel profile, in such a way to prevent the detachment.

In partially encased steel-concrete columns, it must be developed a more accurate numerical model to simulate the interaction between the concrete and the steel flanges and web. This way, a parametric study based on a great number of numerical simulations should be done, and a simplified method of assessing the fire resistance of this type of columns could be proposed.

Circular composite steel-concrete columns of high slenderness should be target of further experimental and numerical studies, since EN 1994-1-2 (2005) is considered unsafe for these cases. Moreover, other steel sections such as I and H profiles inside the concrete core should be tested.

Moreover, new interaction axial force – bending moment diagrams could be developed for composite columns in contact with walls.

Concerning concrete columns, further research should be developed to study in detail the phenomenon of spalling and cracking of concrete at elevated temperatures. New thermo-mechanical models for concrete columns subject to high temperatures should also be studied.

Columns made of other materials such as timber and cold-formed steel with restraint to thermal elongation should also be target of experimental and numerical studies.

It would be interesting to evaluate the real effect of the rotational restraint, apart from the axial restraint, perhaps with tests without rotational restraint. Experimental tests should be carried out on columns, in experimental set-ups specially conceived for this purpose. Moreover, different values of the restraint to thermal elongation should be tested.

In conclusion, new simplified methods for fire design of all kinds of columns would be welcome to structural fire designers.

REFERENCES

Aasen, B. (1985). "An Experimental Study on Steel Columns Behaviour at Elevated Temperatures", Division of Steel Structures, Norwegian Institute of Technology, University of Trondheim, Trondheim, Norway.

ABAQUS. ABAQUS/standard version 6.7 user's manual: volumes I-III. Pawtucket, Rhode Island: Hibbit, Carlsson & Sorensson, Inc.; 2005

Ali, F. A., Shepherd P., Randall, M., Simms, I., Connor, D., Burgess, I. (1998). "The Effect Of Axial Restraint On The Fire Resistance Of Steel Columns", Journal of Constructional Steel Research, vol. 46, n. º 177, pp. 305-306.

Ali F. and O'Connor D. (2001). "Structural performance of rotationally restrained steel columns in fire". Fire Safety journal 36, 679-691.

Ali F., Nadjai A., Talamona D. (2004)."Effect of rotational restraint on performance of steel columns in fire". Journal of Applied Fire Science, vol. 13, Issue 1, 21-34.

Anderberg, Y. (1997), TCD 5.0 - User's Manual. Fire Safety Design, Lund.

Aragón, J., Rey, F., Chica, J. (2004). "DIFISEK - Software for fire design". Tese de Mestrado, LABEIN Technological Centre, Bilbao

Aribert J.M. and Randriantsara C. (1980) "Etude du flambement à des températures d'incendie - Action du fluage". Construction Métallique, No. 4.

Aribert J.M. and Randriantsara C. (1983) "Sur une modélisation du flambement des poteaux métalliques dans des conditions d'incendie". Third International Colloquium on Stability of Metal Structures, Preliminary Report, CTICM, Paris.

AFMFIC, Associated Factory Mutual Fire Insurance Companies, (1917-1919)). "Fire Tests of Building Columns", Chicago, Illinois,

Bennets, I. D., Moore, D. B., O'Meagher, A. J., Thomas, J. R., (1989), "Restraint of compression members in fire", B.H.P. Melbourne Research Lab. Report No. MRL/PSGS/89/002.

Bernardes, F. S. (2009) "Análise Termomecânica de pilares de aço e mistos de aço e betão em caso de incêndio", Dissertação de Mestrado na Especialidade de Estruturas, Departamento de Engenharia Civil, Faculdade de Ciências e Tecnologia da Universidade de Coimbra.

Breccolotti, M., D'Elia, P., Materazzi, A., Nigro, E. (2002) "Simplified Assessment of Steel and Concrete Composite Columns in the Event of Fire". Proceedings of the Third European Conference on Steel Structures, Coimbra, Portugal.

Burgess, I. W., Olawale, A. O., Plank, R. J. (1992). "Failure of Steel Columns in Fire", Fire Safety Journal, vol. 18, pp. 183-201.

Burgess I.W., Najjar S.R. (1994)."A Simple Approach to the Behaviour of Steel Columns in Fire". Journal of Constructional Steel Research 31, 115-134.

Cadorin, Jean-François, (2003) "Compartment Fire Models for Structural Engineering", PhD Thesis, Faculté de Sciences Appliqués, Université de Liège.

Cai, J., Feng, J., (2010) "Thermal buckling of rotationally restrained steel columns", Journal of Constructional Steel Research 66 (2010) 835-841.

Carvalho, L.T. (2008) "Modelação numérica do comportamento ao fogo de pilares de aço", Dissertação de Mestrado na Especialidade de Estruturas, Departamento de Engenharia Civil, Faculdade de Ciências e Tecnologia da Universidade de Coimbra.

Carvalho L.T., Rodrigues J.P.C., Gonçalves M.C., Correia A.M.(2009a)."Numerical simulation of steel columns in fire". Application of Structural Fire Engineering, Prague, Czech Republic.

Carvalho, L. T., Rodrigues, J.P., Correia, A. M. (2009b) "Avaliação numérica do comportamento ao fogo de pilares mistos parcialmente preenchidos com concreto*";*Congresso CMNE CILAMCE – Métodos Numéricos e Computacionais em Engenharia, Buzios, Brasil.

Chen, J., Young, B. (2008). "Design of high strength steel columns at elevated temperatures". Journal of Constructional Steel Research, Vol. 64, pp. 689–703.

Cooke, G. M. E., (1988a). "Thermal Bowing and how it affects the design of fire separating construction", Proceedings of the Interflamm'88, 230-236, London.

Cooke, G. M. E., Morgan, P. B. E.(1988b). "Thermal bowing in fire and how it affects building design", BRE Information Paper, Fire Research Station, IP21/88, Borehamwood

Correia A.M., Rodrigues J.P.C., Silva V.P. (2007)."Studies on the fire behaviour of steel columns embedded on walls". 11th International Conference on Fire Science and Engineering – Interflam, London.

Correia A.M., Rodrigues J.P.C., Silva V.P. (2009a)."Experimental research on the fire behaviour of steel columns embedded on walls". Application of Structural Fire Engineering, Prague, Czech Republic.

Correia, A. M., Rodrigues, J. P., Silva, V. P., Laim, L. (2009b). "Section factor and steel columns embedded in walls"*;* Nordic Steel – Construction Conference, Malmö, Sweden.

Correia, A. M.; Rodrigues, J. P., (2009c). *"*Análise experimental da resistência ao fogo de pilares de aço com dilatação térmica restringida"; VII Congresso CMM – Construção Metálica e Mista, Lisboa.

Correia, A. M.; Rodrigues, J. P., (2009d) "Comportamento termomecânico de pilares de aço inseridos em paredes em caso de incêndio"*;* VII Congresso CMM – Construção Metálica e Mista, Lisboa.

Correia, A.M., Rodrigues, J.P.C., Silva, V. P. (2009e) "Influence of Brick walls on the Temperature Distribution in Steel Columns in Fire", Acta Polytechnica – Journal of Advanced Engineering, vol.49 No.1/2009, ISSN 1210-2709.

Correia, A. M., Pires, T. A. C. and Rodrigues, J. P. C., (2010a). "Behaviour of Steel Columns subjected to Fire", Sixth International Seminar on Fire and Explosion Hazards, Leeds, UK.

Correia A. M., Rodrigues J.P.C. (2010b) "Buckling of Steel and Composite Steel and Concrete Columns in Case of fire"; SDSS'Rio 2010 STABILITY AND DUCTILITY OF STEEL STRUCTURES, Rio de Janeiro, Brazil.

Correia, A.M., Rodrigues, J.P.C., Silva, V. P.; (2010c). "Numerical Study on the Behavior of Steel Columns Embedded on Brick Walls Subjected to Fire"; International Symposium "SSCS 2010 - Steel Structures: Culture & Sustainability 2010", Istambul, Turkey.

Correia, A. M., Rodrigues, J.P.C., Silva V.P. (2010). "A Simplified Calculation Method for Temperature Evaluation of Steel Columns Embedded in Walls"*;* Fire and Materials, DOI:10.1002/fam.1063.

Correia, A. M., Rodrigues, J. P. C., (2010) "Fire Resistance of Partially Concrete Encased Steel Columns with Restrained Thermal Elongation"; Journal of Constructional Steel Research (doi:10.1016/j.jcsr.2010.12.002).

Correia, A. M., Rodrigues, J. P.C., "Fire Resistance of Steel Columns with Restrained Thermal Elongation"*;* Fire Safety Journal (Accepted February 2011)

Culver, C. G. (1972). "Steel Column Buckling Under Thermal Gradients", Journal of the Structural Division, American Society of Civil Engineers (ASCE), ST8, Vol. 98, pp. 1853-1865.

Culver, C. G., Aggarwal, V., Ossenbruggen, P. (1973). "Buckling of Steel Columns at Elevated Temperatures", Journal of the Structural Division, American Society of Civil Engineers (ASCE), ST4, Vol. 99, pp. 715-726.

Document Technique Unifié (DTU) (1982). « »Méthode de prévision par le calcul du comportement au feu des structures en acier », Construction Métallique No.3, France, pp. 39-79.

ECCS, (1978). "European Recommendations for Steel Construction". European Convention for Constructional Steelwork, The Construction Press, London.

ECCS (1985), "Design Manual on the European Recommendations for the Fire Safety of Steel Structures". ECCS Technical Note nº.35. Technical Commitee 3. European Commission for Constructional Steelwork, Brussels, Belgium.

ECCS (1988), "Calculation of the Fire Resistance of Centrally Loaded Composite Steel-Concrete Columns Exposed to the Standard Fire". ECCS Technical Note nº.55. Technical Commitee 3. European Commission for Constructional Steelwork, Brussels, Belgium.

ECCS (1995), "Fire Resistance of Steel Structures". ECCS Technical Note nº.89. Technical Commitee 3. European Commission for Constructional Steelwork, Brussels, Belgium.

ECCS (2001), "Model Code on Fire Engineering". ECCS Technical Note nº.111. Technical Commitee 3. European Commission for Constructional Steelwork, Brussels, Belgium.

Ellobody, E., Young, B., (2010). "Investigation of concrete encased steel composite columns at elevated temperatures, "Thin Walled Structures", 48 (2010) 597-608.

EN 10002-1 (1990), Materiais metálicos. Ensaio de tracção. Parte 1. Método de Ensaio à temperature ambiente. European Community. CEN, Brussels. (in portuguese)

EN 10002-2 (1991), Materiais metálicos. Ensaio de tracção. Parte 2. Verificação do sistema de medição da força da máquina de ensaio de tracção. European Community. CEN, Brussels. (in portuguese)

EN 10002-4 (1999), Materiais metálicos. Ensaio de tracção. Parte 4. Extensómetros electromecânicos. European Community. CEN, Brussels. (in portuguese)

EN 1363-1 (1999), Fire resistance tests – Part 1: General requirements. European Community. CEN, Brussels

EN 1363-2 (1999), Fire resistance tests – Part 2: Alternative and additional procedures. European Community. CEN, Brussels

EN 1990 (2002), "Eurocode 0: Eurocode – Basis of Structural Design. CEN, Brussels.

EN 1990-2 (2005), Execution of steel and aluminium structures – Part 2: Technical requirements for the execution of steel structures. European Community. CEN, Brussels.

EN 1991-1-1 (2005), Eurocode 1: Actions on Structures. Part 1.1: General rules and rules for buildings. European Community. CEN,Brussels.

EN 1991-1-2 (2002), Basis of Design and Actions on Structures – Part 1-2: Actions on Structures Exposed to Fire. European Community. CEN,Brussels.

EN 1992-1-1 (2004). "Eurocode 2: Design of concrete structures: Part 1.1: General rules and rules for buildings". CEN, Brussels.

EN 1992-1-2 (2004). "Eurocode 2: Design of concrete structures: Part 1.2: General rules – Structural fire design". CEN, Brussels.

EN 1993-1-1 (2005). "Eurocode 3 - Design of steel structures: Part 1.1: General rules and rules for buildings". CEN, Brussels.

EN 1994-1-1(2003) – "Eurocode 4 - Design of composite steel and concrete structures – Part 1-1: General – General rules and rules for buildings, European Community, Brussels, Belgium.

EN 1994-1-2 (2005). "Eurocode 4 – Design of composite steel and concrete structures: Part 1.2: General rules Structural fire design". CEN, Brussels.

EN 1993-1-2 (2002). "Eurocode 3 - Design of steel structures - Part 1.2: General rules - Structural fire design". CEN, Brussels.

EN 1993-1-2 (2005). "Eurocode 3 - Design of steel structures - Part 1.2: General rules - Structural fire design". CEN, Brussels.

Espinos, A., Romero, M., Hospitaler, A. (2010) "Advanced model for predicting the fire response of concrete filled tubular columns", Journal of Constructional Steel Research (2010), doi:10.1016/j.jcsr.2010.03.002

Franssen J.M., Dotreppe, J.-C. (1992). "Fire resistance of columns in steel frames". Fire Safety Journal, 19 (1992) 159-175.

Franssen J.M., Schleich J.B., Cajot L.G. (1995). "A simple Model for the Fire Resistance of Axially-loaded Members – Members According to Eurocode 3". Journal of Constructional Steel Research, Vol. 35, 49-69.

Franssen, J., Schleich, J., Cajot, L., Azpiazu, W. (1996). "A Simple Model for the Fire Resistance of Axially Loaded Members - Comparison with Experimental Results". J. Construct. Steel Research, Vol. 37, No. 3, pp. 175-204.

Franssen J.M., Talamona D., Kruppa J., Cajot L.C. (1998)."Stability of Steel Columns in case of Fire: Experimental Evaluation". Journal of Structural Engineering, Vol. 124, No. 2.

Franssen, J., Kodur, V., Mason, J. (2000a). "User's manual for SAFIR 2001: A computer program for analysis of structures submitted to the fire", University of Liège, Liège.

Franssen J.M. (2000b)"Failure temperature of a system comprising a restrained column submitted to fire". Fire Safety Journal 34, 191-207.

Franssen, J., Kodur, V., Mason, J. (2002a). "Elements of theory for SAFIR 2001 free: A computer program for analysis of structures submitted to the fire", University of Liège, Liège.

Franssen, J., Kodur, V., Mason, J. (2002b). "User's manual for SAFIR 2001 free: A computer program for analysis of structures submitted to the fire", University of Liège, Liège.

Franssen, J.M. (2006)."Calculation of temperature in fire-exposed bare steel structures: Comparison between ENV 1993-1-2 and EN 1993-1-2". Fire Safety Journal 41, 139-143.

Franssen, J.M., Vila Real, p., (2010) "Fire Design of Steel Structures". ECCS: Ernst & Sohn.

Garlock, M. E. M., Quiel, S. E., (2006a), "Mechanics of wide-flanged steel sections with thermal gradients due to fire exposure", Proc. 4th Int. Symp. on Steel Structures, (ISSS '06), Korean Society of Steel Construction (KSSC), 410-419.

Garlock, M. E. M., Quiel, S. E., (2006b), "Combined axial load and moment capacity of fire-exposed beam-columns with thermal gradients", Proc. 4th International Workshop for Structures in Fire (SIF '06), Vol. I, University of Aveiro, 187-198, Portugal.

Garlock, M. E. M., Quiel, S. E., (2007a), "Mechanics of wide-flanged steel sections that develop thermal gradients due to fire exposure", Steel Structures 7 (2007) 153-162.

Garlock, M. E. M., Quiel, S. E., (2007b), "The behaviour of steel perimeter columns in a high-rise building under fire" Engineering Journal, 44 (4), 359-372.

Garlock, M. E. M., Quiel, S. E., (2008), "Plastic Axial Load and Moment Interaction Curves for Fire-Exposed Steel Sections with Thermal Gradients", Journal of Structural Engineering, ASCE, DOI:10.1061/(ASCE)0733-9445(2008)134:6(873).

Ghojel, J. (2004), "Experimental and analytical technique for estimating interface thermal conductance in composite structural elements under simulated fire conditions", Experimental Thermal and Fluid Science 2004; 59:769-79.

Gomes, F., Costa, P., Rodrigues, J., Neves , I. (2007). "Buckling length of a steel column for fire design". Engineering Structures, Vol. 29, pp. 2497–2502.

Gonçalves, M., (2008). "Comportamento ao fogo de elementos estruturais de betão – análise numérica e metodologia". Tese de Doutoramento, Faculdade de Engenharia da Universidade do Porto, Porto.

Han L.H., Yang Y.F., Yang H., Huo J.S., (2002)."Residual strength of concrete-filled RHS columns after exposure to the ISO-834 standard fire", Thin-Walled Structures, 40:991-1012.

Han L.H., Yang Y.F., Yang H., Xu Lei., (2003)."An experimental study and calculation on the fire resistance of concrete-filled SHS and RHS columns", Journal of Constructional Steel Research, 59 (2003) 427-452.

Han L.H., Huo J.-S., Wang Y.C.(2005)."Compressive and flexural behaviour of concrete filled steel tubes after exposure to standard fire". Journal of Constructional Steel Research, 2005; 61:882-901.

Hozjan, T., Planinc, I., Saje, M., Srpcic, S., (2008). "Buckling of restrained steel columns due to fire conditions", Steel and Composite Structures, 2008; 8: 159-78.

Huang Z.F., Tan K.H. (2003a)."Analytical Fire Resistance of Axially Restrained Steel Columns". ASCE Journal of Structural Engineering, Vol. 129, No. 11, 1531-1537.

Huang Z.F., Tan K.H. (2003b) "Rankine approach for fire resistance of axially-and-flexurally restrained steel columns". Journal of Constructional Steel Research 59, 1553-1571.

Huang Z.F., Tan K.H. (2004)."Effects of external bending moments and heating schemes on the responses of thermally restrained steel columns". Engineering Structures 26, 769-780.

Huang Z.F., Tan K.H., Ting S.K. (2006)."Heating rate and boundary restraint effects on fire resistance of steel columns with creep". Engineering Structures 28, 805-817.

Huang, Z., Tan, K., Phng, G. (2007a). "Axial restraint effects on the fire resistance of composite columns encasing I-section steel". Journal of Constructional Steel Research, Vol. 63, pp. 437–447.

Huang Z.F., Tan K.H. (2007b)."Structural response of restrained steel columns at elevated temperatures. Part 2: FE simulation with focus on experimental secondary effects". Engineering Structures 29, 2036-2047.

Huang, Z., Tan, K. Toh, W. Phng, G. (2008). "Fire resistance of composite columns with embedded I-section steel—Effects of section size and load level". Journal of Constructional Steel Research, Vol. 64, pp. 312–325.

Iding, R., Nizamuddin, Z., Bresler, B. (1977). "A computer program for the Fire Response of Structures – Thermal – Three Dimension Version". University of California, Berkeley, USA.

ISO 834, (1975) "Fire Resistance Tests – Elements of Building Construction" International Organisation for Standardisation, Geneva, Switzerland

Janss, J. e Minne, R. (1981). "Buckling of Steel Columns in Fire Conditions", Fire Safety Journal, vol. 4, pp. 227-235.

Jeanes, D. C., (1985). "Computer Modelling the Fire Endurance of Floor Systems in Steel-Framed Buildings", American Society for Testing and Materials, pp. 223-238.

Jeyarupalingam, N., Virdi, K. S. (1992). "Steel Beams and Columns Exposed to Fire Hazard", Conference Structural Design for Hazardous Loads, pp. 429-438.

Kamikawa D., Hasemi Y., Wakamaty T., Kagiya K.(2002). "Experimental Flame Heat Transfer and Surface Temperature Correlations for a Steel Column Adjacent to and Surrouned by a pool fire". Proceedings of IFASS.

Kamikawa D., Hasemi Y., Wakamaty T., Kagiya K.(2004). "Prediction of the Thermal response of a metal column exposed to a localised fire". Proceedings of SiF'04, Third International Workshop Structures in Fire.

Kamikawa D. (2006)."Mechanical responses of a steel column exposed to a localised fire". SIF'06, Fourth International Workshop "Structures in Fire", Aveiro, Portugal, 244-253.

Kimura M, Ohta H, Kaneko H, Kodaira A, Fujinaka H. (1990). "Fire resistance of concrete-filled square steel tubular columns subjected to combined loads". Takenaka Tech. Res. Rep. 43, 47–54.

Klingsch W. and Neves I.C. (1980). "Restraint Effects in Steel Frames by Local Fire". International Seminar on Steel and Composite Columns under Fire Action, Delft, The Netherlands.

Knobloch, M., Fontana, M., Frangi, A., (2008)"Steel beam-columns subjected to fire", Steel Construction 1(2008), Issue 1, Ernst & Sohn.

Knobloch, M., Somaini, D., Pauli, J., Fontana, M. (2010) "Numerical Analysis of the Cross-Sectional Capacity of Structural Steel Members in Fire", Proc. of the 6th International Conference Structures in Fire, Michigan State University, USA

Kodur V. K. R. and Lie T.T. (1996). "Fire resistance of circular steel columns filled with fiber-reinforced concrete. Journal of Structural Engineering, American Society of Civil Engineers (ASCE), 122 (7):776-782.

Kodur, V., Garlock, M., Iwankiw, N. (2007) "Structures in Fire: State-of-the-Art, Research and Training Needs", National Workshop on Structures in Fire: State-of-the-art, Research and Training Needs, National Science Foundation, U. S. Department of Commerce, National Institute of Standards and Technology, USA

Korzen M., Magonette, G. & Buchet, P. (1999). "Mechanical Loading of Columns in Fire Tests by Means of the Substructuring Method", Zeitschrift fur Angewandte Mathematik und Mechanik, vol.79

Korzen M., Neves I.C., Rodrigues J.P.C., Valente J.C. (2006)."Behaviour in fire of thermally restrained compressed steel members experimental and numerical approach". Proceedings of the fourth International Workshop "Structures in Fire", SiF'06, Aveiro, Portugal, 273-286.

Korzen M., Rodrigues J.P.C., Correia A.M. (2009)."Thermal restraint effects on the fire resistance of steel and composite steel and concrete columns", Application of Structural Fire Engineering, Prague, Czech Republic.

Korzen M., Rodrigues J.P.C., Correia A.M. (2010). "Composite Columns Made of Partially encased Steel Sections Subjected to Fire", International Conference on Structures in Fire – SIF´10, Michigan, USA.

Laim, L.; Rodrigues, J. P., Correia, A. M.; (2009)."Fire resistance of a cold formed steel roof beam"; Nordic Steel – Construction Conference, Malmö, Sweden.

Lamont, Susan (2001). "The Behaviour of Multi-storey Composite Steel Framed Structures in Response to Compartment Fires". Tese, University of Edinburgh, Edinburgh.

Li, G.-Q., Wang, P., Wang. Y., (2010). "Behaviour and design of restrained steel column in fire: part 1. Fire Test", Journal of Constructional Steel Research 66 (2010) 1138-1147.

Lie T.T. and Chabot M.(1990)., "A method to predict the fire resistance of circular steel columns filled hollow steel columns. Journal of Fire Protection Engineering", 2 (4): 111-126.

Lie T.T. and Kodur V. K. R. (1996). "Fire resistance of circular steel columns filled with bar-reinforced concrete". Journal of Structural Engineering, American Society of Civil Engineers (ASCE), 122 (1): 30-36.

Malhotra H.L. and Stevens R.F.(1964) "Fire resistance of encased steel stanchions". Proceedings of the Institution of Civil Engineers - ICE; 27: 77-97.

Martins, A. (2008). "Resistência ao fogo de pilares de betão armado com dilatação térmica restringida", Dissertação de Mestrado em Engenharia Civil, na Especialidade de Estruturas, Departamento de Engenharia Civil, Faculdade de Ciências e Tecnologia da Universidade de Coimbra.

Mesquita, L. (2004). "Instabilidade termo-mecânica de vigas submetidas a temperaturas elevadas - Estudo numérico e experimental". Tese de Mestrado, Faculdade de Engenharia da Universidade do Porto, Porto.

Neves I.C. (1982) "The Column – Structure Interaction on the Behaviour of Steel Columns Under Local Fire, Ph.D. Thesis, Instituto Superior Técnico, Technical University of Lisbon, Lisbon, Portugal.

Neves, I. C. (1995). "The Critical Temperature of Steel Columns With Restrained Thermal Elongation", Fire Safety Journal, vol. 24, pp. 211-227.

Neves, I., Valente, J., Rodrigues, J. (2002). "Thermal restraint and fire resistance of columns". Fire Safety Journal, Vol. 37, pp. 753-771.

NP EN 10002-1-1990. "Materiais metálicos. Ensaio de tracção. Parte1. Método de Ensaio à temperature ambiente. Brussels (in Portuguese).

Olawale, A. 0. e Plank, R. J. (1998). "The collapse analysis of steel columns in fire using a finite strip method". International journal for numerical methods in engineering, Vol 26, pp. 2755-2764.

Ossenbruggen, P., Aggarwal, V., Culver, C. G. (1973). "Steel Column Failure Under Thermal Gradients", Journal of the Structural Division, American Society of Civil Engineers (ASCE), ST4, Vol. 99, pp. 727-739.

Pan, Z.-F., Schriever, R., Bock, H. M., Korzen, M., (1997). "Comparison of the temperature distribution in isolated steel columns tested in two furnaces" Fire Technology, vol. 33, nº.4, 316-335

Pires, T.A.C., Rodrigues, J.P.C., Silva, J.J.R., Correia A.M.; "Concrete Filled Steel Hollow Columns Subjected to Fire"; International Symposium "SSCS 2010 - Steel Structures: Culture & Sustainability 2010", Istambul.

Poh K.W. and Bennetts I.D. (1993)."Comparison of Test and Calculated Behaviour of Steel Columns at Elevated Temperatures". Rep. BHPR/PPA/R/93/024/SG011A, BHP Research and New Technology, Melbourne Research Laboratories, Melbourne, Australia, November.

Poh, K. W., Bennetts, I. D. (1995a). "Analysis of Structural Members Under Elevated Temperature Conditions", Journal of Structural Engineering, American Society of Civil Engineers (ASCE), No. 4, Vol. 121, pp. 664-675.

Poh, K. W., Bennetts, I. D. (1995b). "Behaviour of Steel Columns at Elevated Temperatures", Journal of Structural Engineering, American Society of Civil Engineers (ASCE), No. 4, Vol. 121, pp. 676-684.

Quiel, S. E., Garlock, M. E. M.(2008), "A closed-form analysis of perimeter member behavior in a steel building frame subject to fire", Engineering Structures 30 (2008) 3276-3284.

Randriantsara C.(1984) "Etude critique du flambement des poteaux métalliques dans les conditions d'incendie". Ph.D. Thesis, INSA, Rennes.

Real, P., Lopes, N., Silva, L., Piloto, P., Franssen, J. (2004). "Numerical modelling of steel beam-columns in case of fire - comparisons with Eurocode 3". Fire Safety Journal,Vol. 39, pp. 23–39.

Rodrigues, J., Neves, I., Valente, J. (2000a). "Experimental research on the critical temperature of compressed steel elements with restrained thermal elongation". Fire Safety Journal, Vol. 35, pp. 77-98.

Rodrigues J.P.C. (2000b).“Fire Resistance of Steel Columns with Restrained Thermal Elongation”. Ph.D. Thesis, Instituto Superior Técnico, Technical University of Lisbon, Portugal, December.

Rodrigues, J.P.C., Gomes, F.T., Neves, I.C. (2002). “Fire Resistance Tests on Steel Columns – A Summary Review”. XXX IAHS World Congress on Housing, Housing Construction – An Interdisciplinary Task, Coimbra, Portugal, pp. 1639-1651.

Rodrigues, J.P.C. & Correia, A.M.(2004). “Numerical Simulations on the Fire Behaviour of Building Steel Columns”; International Congress “Computational Simulation Models in Fire Engineering and Research”, Universidade de Cantabria, Spain, pp. 107-123.

Rodrigues, J.P.C.; Gomes, F.T. & Correia, A.M. (2004). “Fire Resistance of Steel Columns – Methods of Assessment”; International Congress “New Trends in Statics and Dynamics of Buildings”, Bratislava, pp. 209-218.

Rodrigues, J.P.C., Laím, L., Correia A.M. (2009a). “Behavior of Fiber Reinforced Concrete Columns in Fire”*;* Composite Structures, doi: 10.1016/j.compstruct.2009.10.029.

Rodrigues, J.P.C.; Laím L.; Correia A.M.(2009), “Behaviour of Fiber Reinforced Concrete Columns in Fire”; 15th International Conference on Composite Structures, June, Porto.

Rodrigues, J.P.C.;Laim L.; Correia, A.M. (2010) “Experimental-Numerical Study on the Behaviour of Steel Columns Protected with Expanded Clay Concrete Boards”; International Symposium “SSCS 2010 - Steel Structures: Culture & Sustainability 2010”, Istambul, Turkey.

Rotter, J. M., Usmani, A.S., (2000) “Fundamental Principles of Structural Behaviour under thermal effects” Proceedings of First International Workshop on Structures in Fire, Denmark.

Santiago, A.M.C. (2008). “Behaviour of beam-to-column steel joints under natural fire”, Ph.D. Thesis, Departamento de Engenharia Civil, Faculdade de Ciências e Tecnologia da Universidade de Coimbra, Portugal.

Schaumann, P., Kettner, I., (2004). “BOFIRE – A FEM-programm for non-linear analysis of structural members under fire conditions”, Hannover.

Shepherd P., Burgess I.W., Plank R.J., O’Connor D.J. (1997). “The performance in fire of restrained steel columns in multi-storey constructions”. Fourth Kerensky International Conference, 333-42.

Silva, L. S., Gervásio, H., (2007). "Manual de dimensionamento de estruturas metálicas: métodos avançados", CMM – Associação Portuguesa de Construção Metálica e Mista.

Silva, L. S., Santiago, A., Haremza, C. Rodrigues, J. P., (2009). "ROBUSTFIRE Project - Document 3 – Steel Columns – v2(2).", UC/DEC/ISISE/2009-003.

Silva, V.P. (2005). "Determination of the steel fire protection material thickness by an analytical process – a simple derivation", Engineering Structures, 27, 2036-2043.

Silva, V.P. (2006). "Determination of the Temperature of Thermally unprotected Steel Members under Fire Situations: considerations on the Section Factor", Latin American Journal of Solids and Structures, 3, p 113 – 125, São Paulo.

Silva V.P., Correia A.M., Rodrigues J.P.(2008). "Simulation on fire behavior of steel columns embedded on walls". XXXIII Jornadas Sudamericanas de Ingenieria Estructural, Santiago, Chile.

Silva, V. P., Rodrigues, J. P., Correia, A. M., (2009)."Análise térmica de pilares de aço em contato com alvenaria, em situação de incêndio"; Congresso CMNE CILAMCE – Métodos Numéricos e Computacionais em Engenharia, Búzios, Brasil.

Simões, R.A.D., (2005). "Manual de Dimensionamento de Estruturas Metálicas – Eurocódigo 3: Projecto de Estruturas Metálicas Parte 1-1: Regras gerais e regras para edifícios", CMM – Associação Portuguesa de Construção Metálica e Mista.

Simms WI, O'Connor DJ, Ali F, Randall M. (1995)."An experimental investigation on the structural performance of steel columns subjected to elevated temperatures". Journal of Applied Fire Science 5(4), 269-84.

Takagi J., Deierlein G.G. (2007)."Strength design criteria for steel members at elevated temperatures". Journal of Constructional Steel Research 63, 1036-1050.

Talamona D., Franssen J.M., Schleich J.B., Kruppa J. (1997) "Stability of Steel Columns in case of Fire: Numerical Modelling". Journal of Structural Engineering, Vol. 123, No. 6.

Tan K.H., Ting S.K., Huang Z.F. (2002)."Visco-Elasto-Plastic Analysis of Steel Frames in Fire". Journal of Structural Engineering, Vol. 128 (1).

Tan K.H., Toh W.S., Phng G.H.E. (2004).“Fire Resistance of Steel Columns Subjected To Different Restraint Ratios”. The Second International Conference on Steel & Composite Structures, Seoul, Korea, 625-635, September 2-4.

Tan K.H., Toh W.S., Huang Z.F., Phng G.H. (2007).“Structural responses of restrained steel columns at elevated temperatures. Part 1: Experiments”. Engineering Structures 29, 1641-1652.

Tan, K., Yuan, W. (2008). “Buckling of elastically restrained steel columns under longitudinal non-uniform temperature distribution”. Journal of Constructional Steel Research, Vol. 64, pp. 51–61.

Tan K.H. and Yuan W.F.(2009). “Inelastic buckling of pin-ended steel columns under longitudinal non-uniform temperature distribution”. Journal of Constructional Steel Research 65, 132-141.

Tang C.Y., Tan K.H., Ting S.K. (2001).“Basis and Application of a Simple Interaction Formula for Steel Columns under Fire Conditions”. ASCE Journal of Structural Engineering, Vol. 127, No. 10, 1206-1213, October.

Toh W.S. (2000a).“Stability and strength of steel structures under thermal effects”. Ph.D. Thesis, CSE, Nanyang Technological University, Singapore.

Toh W.S., Tan K.H., Fung T.C. (2000b).“Compressive Resistance of Steel Columns in Fire: Rankine Approach”. Journal of Structural Engineering 126(3), 398-405.

Toh W.S., Tan K.H., Fung T.C. (2001).“Strength and Stability of Steel Frames in Fire: Rankine Approach”. Journal of Structural Engineering, Vol. 127, No. 4.

Toh W.S., Tan K.H., Fung T.C. (2003).“Rankine approach for steel columns in fire: numerical studies”. Journal of Constructional Steel Research 59, 315-334.

Tsalikis, C. T., Koltsakis, E. K., Baniotopoulos, C. C.(2009), “Steel beam-colums under thermal gradient”, Proc. of int. conference Application of Structural Fire Engineering, 2011, Prague, Czech Republic.

Tsalikis, C. T., Koltsakis, E. K., Baniotopoulos, C. C.(2011), “Elastic buckling of steel columns under thermal gradient”, Proc. of 2nd Application of Structural Fire Engineering, 2011, Czech Republic.

Usmani, A.S., Rotter, J. M., Lamont, S., Sanad, A. M., Gilie, M. (2001) "Fundamental principles of structural behaviour under thermal effects" Fire Safety Journal (36), 721-744.

Usmani, A. S., Chung, Y.C., Torero, J.L., (2003). "How did the WTC towers collapse: a new theory" Fire Safety Journal, 38, 501-533.

Valente, J. C. (1988). " Simulação do Comportamento das Estruturas Metálicas Sujeitas a Altas Temperaturas", Tese, Instituto Superior Técnico, Lisboa, Portugal.

Valente, J., Neves, I. (1999). "Fire resistance of steel columns with elastically restrained axial elongation and bending". Journal of Constructional Steel Research, Vol. 52, pp. 319–331.

Vandamme M. and Janss J. (1981) "Buckling of Axially loaded Steel Columns in Fire Conditions". IABSE Proceedings, 43-81.

Vila Real, P., (2003a). "Incêndio em estruturas metálicas", Edições Orion, Portugal.

Vila Real, P.M.M.., Piloto, P., Franssen, J.-M., (2003b) "A new proposal of a simple model for lateral-torsional buckling of unrestrained steel I-beams in case of fire: Experimental and numerical validation", Journal of Constructional Steel Research 59(2), 179-199.

Vila Real, P.M.M., Lopes, N., Simões da Silva, L., Piloto, P., Franssen, J.-M., (2003c) "Towards a consistant safety format of steel beam-columns: application of the new interaction formulae for ambient temperature to elevated temperatures", Steel and Composite Structures 3 (2003), 6.

Vila Real, P.M.M., Lopes, N., Simões da Silva, L., Piloto, P., Franssen, J.-M., (2004) "Numerical modelling of steel beam-columns in case of fire – comparisons with the Eurocode 3", Fire Safety Journal 39, 23-39.

Wald, F., Burgess, I., De la Quintana, J., Vila Real, P., Kwasniewski, L., Horová, K., Jána, T. (2011) "State of the Art Report", COST Action TU0904, Integrated Fire Engineering and Response, Czech Technical University of Prague.

Wainman, D. E., Kirby, B. R. (1988). "Compendium of UK Standard Fire Test Data – Unprotected Structural Steel – 1", Ref. No. RS/RSC/S10328/1/87/B, British Steel Corporation, Swinden Laboratories, Rotherham, UK.

Wainman D.E. and Kirby B.R. (1989).“Compendium of UK Standard Fire Test Data – Unprotected Structural Steel – 2” Ref. No. RS/R/S1199/8/88/B, British Steel Corporation, Swinden Laboratories, Rotherdam, UK.

Wang Y.C. and Moore D.B. (1994a). “The effect of frame continuity on the critical temperature of steel columns”. Proc., 3rd Kenrensky Conf. on Global Trends in Structural Engineering, Singapore, 681-686.

Wang Y.C. and Moore D.B. (1994b). “Effect of thermal restraint on column behaviour in a frame”. Proc., 4th Int. Symp. on Fire Safety Science, T. Kashiwagi, ed., Ottawa, 1055-1066.

Wang Y.C., Lennon T., Moore D.B. (1995a).“The Behaviour of Steel Frames Subject to Fire”. Journal of Constructional Steel Research, vol. 35, pp. 291-322.

Wang, Y., Moore, D. (1995b). “Steel frames in fire: analysis”. Engineering Structures, Vol. 17, No. 6, pp. 462-472.

Wang Y.C. (1997a).“The Effects of Frame Continuity on the Behaviour of Steel Columns Under Fire Conditions and Fire Resistant Design Proposals”. Journal of Constructional Steel Research, vol. 41, No. 1, 93-111.

Wang Y.C.(1997b). “Effects of Structural Continuity on Fire Resistant Design of Steel Columns in Non-sway Multi-storey Frames”. Fire Safety Journal 28, 101-116.

Wang Y.C.(2002). “Steel and composite structures – Behaviour and design for fire safety”, Spon Press.

Wang Y.C. and Davies J.M. (2003a).“An experimental study of non-sway loaded and rotationally restrained steel column assemblies under fire conditions: analysis of test results and design calculations”. Journal of Constructional Steel Research 59, 291-313.

Wang Y.C. and Davies J.M. (2003b).“Fire tests of non-sway loaded and rotationally restrained steel column assemblies”. Journal of Constructional Steel Research 59, 359-383.

Wang Y.C. and Davies J.M. (2003c). “An experimental study of the fire performance of non-sway loaded concrete-filled steel tubular column assemblies with extended end plate connections”, Journal of Constructional Steel Research, 59: 819-838.

Wang Y.C. (2004).“Postbuckling Behavior of Axially Restrained and Axially Loaded Steel Columns under Fire Conditions”. Journal of Structural Engineering, ASCE.

Wang, Z.-H., Tan, K. H., (2006). “Residual Area method for heat transfer analysis of concrete-encased I-sections in fire”, Engineering Structures 28 (2006) 411-422.

Wang, P., Wang. Y., Li, G.-Q., (2010). “Behaviour and design of restrained steel column in fire: part 2. Parameter study”, Journal of Constructional Steel Research 66 (2010) 1148-1154.

Wickström, U. (1979). “TASEF 2 – A computer Program for Temperature Analysis of Structures Exposed to Fire”, Rep. No. 79/2, Department of Structural Mechanics, Lund Institute of Technology, Lund, Sweden.

Wong, M., (2005). “Modelling of axial restraints for limiting temperature calculation of steel members in fire”. Journal of Constructional Steel Research, Vol. 61, pp. 675–687.

Yang K.C., Chen S.J., Lin C.C., Lee H.H. (2005).“Experimental study on local buckling of fire-resisting steel columns under fire load”. Journal of Constructional Steel Research, vol. 61, 553-565.

Yang, K., Lee, H., Chan, O. (2006a). “Performance of steel H columns loaded under uniform temperature”. Journal of Constructional Steel Research, Vol. 62, pp. 262–270.

Yang K. C., Lee H. H., Chan O. (2006b). “Experimental study of fire-resistant steel H columns at elevated temperature”. Journal of Constructional Steel Research, vol. 62, 544-553.

Yang K. C., Hsu, R., (2009). “Structural behaviour of centrally loaded steel columns at elevated temperature”. Journal of Constructional Steel Research, vol. 65, (2009) 2062-2068.

Yu, J., Lu, Z., Xie, K. (2007). “Nonlinear analysis of SRC columns subjected to fire”. Fire Safety Journal, Vol. 42, pp. 1–10.

Yuan W.F. and Tan K.H. (2007). “Analytical inelastic loads of restrained steel columns under longitudinal non-uniform temperature distribution”. Steel and composite Structures – Wang & Choi, Taylor & Francis Group, London, ISBN 978-0-415-45141-3, p661-666.

Wang & Choi (eds), Taylor & Francis Group, London, ISBN 978-0-415-45141-3, p661-666.

Zeng, J., Tan, K., Huang, Z., (2003). "Primary creep buckling of steel columns in fire". Journal of Constructional Steel Research, Vol. 59, pp. 951–970.

APPENDIX A – Mechanical properties of steel

Table A.1– Mechanical properties of steel of the columns embedded on walls

Test Number	Steel Profile	Orientation of web to furnace	σ_{su} (MPa)	σ_{sy} (MPa)	ε_{su} %	Steel specimen
E01	HEA 160	parallel	522.08	389.05	0.26	Specimen 5
E02	HEA 160	perpendicular	534.33	395.26	0.33	Specimen 1
E03	HEA 200	parallel	539.90	364.78	0.31	Specimen 10
E04	HEA 200	perpendicular	538.90	362.28	0.28	Specimen 12
E05	HEA 160	parallel	522.08	389.05	0.26	Specimen 5
E06	HEA 160	perpendicular	529.14	394.43	0.30	Specimen 4
E07	HEA 160	parallel	559.47	394.45	0.25	Specimen 7
E08	HEA 200	parallel	542.74	425.37	0.29	Specimen 6
E09	HEA 200	perpendicular	579.40	412.17	0.30	Specimen 11
E10	HEA 160	parallel	540.80	399.37	0.32	Specimen 3
E11	HEA 160	perpendicular	529.14	394.43	0.30	Specimen 4
E12	HEA 160	parallel	559.47	394.45	0.25	Specimen 7
E13	HEA 160	perpendicular	529.14	394.43	0.30	Specimen 4
E14	HEA 160	parallel	588.7	391.44	0.29	Specimen 9
I16	HEA 160	-	588.7	391.44	0.29	Specimen 9
I20	HEA 200	-	542.74	425.37	0.29	Specimen 6

Table A.2 – Mechanical properties of steel of the bare steel columns

Test Reference	Internal Test Number	σ_{su} (MPa)	σ_{sy} (MPa)	ε_{su} %	Steel specimen
HEA200-K13-L70	E15	539.90	364.78	0.31	Specimen 10
HEA200-K13-L70-E2	E16	544.50	375.35	0.27	Specimen 13
HEA200-K13-L70-E1	E17	579.40	412.17	0.30	Specimen 11
HEA160-K13-L70	E18	540.80	399.37	0.32	Specimen 3
HEA200-K13-L30	E19	544.50	375.35	0.27	Specimen 13
HEA160-K13-L30	E20	540.80	399.37	0.32	Specimen 3
HEA160-K45-L70	E21	540.80	399.37	0.32	Specimen 3
HEA160-K45-L30	E22	522.08	389.05	0.26	Specimen 5
HEA200-K45-L70	E23	532.92	360.36	0.31	Specimen 8
HEA200-K45-L30	E24	539.90	364.78	0.31	Specimen 10
HEA200-K128-L30	E25	579.40	412.17	0.30	Specimen 11
HEA160-K128-L30	E26	534.80	395.82	0.29	Specimen 2
HEA200-K128-L70	E27	579.40	412.17	0.30	Specimen 11
HEA160-K128-L70	E28	581.1	460.54	0.27	Specimen 15

Table A.3 – Mechanical properties of composite steel-concrete columns

TestNumber	Internal Test Number	Steel specimen	σ_{su} (MPa)	σ_{sy} (MPa)	ε_{su} %	Concrete specimen	Compressive strenght of concrete (MPa)
CSC160-K128-L30	E29	Specimen 2	534.80	395.82	0.29	Concrete 1	41.31
CSC160-K128-L70	E30	Specimen 4	529.14	394.43	0.30	Concrete 1	41.31
CSC200-K128-L30	E31	Specimen 13	544.50	375.35	0.27	Concrete 1	41.31
CSC200-K128-L70	E32	Specimen 12	538.90	362.28	0.28	Concrete 1	41.31
CSC160-K45-L30	E33	Specimen 1	534.33	395.26	0.33	Concrete 1	41.31
CSC160-K45-L70	E34	Specimen 4	529.14	394.43	0.30	Concrete 1	41.31
CSC200-K45-L30	E35	Specimen 6	542.74	425.37	0.29	Concrete 2	42.15
CSC200-K45-L70	E36	Specimen 8	532.92	360.36	0.31	Concrete 3	38.59
CSC160-K13-L30	E37	Specimen 2	534.80	395.82	0.29	Concrete 2	42.15
CSC160-K13-L70	E38	Specimen 2	534.80	395.82	0.29	Concrete 2	42.15
CSC200-K13-L30	E39	Specimen 12	538.90	362.28	0.28	Concrete 2	42.15
CSC200-K13-L70	E40	Specimen 8	532.92	360.36	0.31	Concrete 2	42.15

Table A.4 – Mechanical properties of concrete specimen – Concrete 1 – C25/30

Number of specimen	Specimen dimensions (mm)	Specimen mass (kg)	Load (kN)	Compressive strength (MPa)
1	150 x 150	8.10	936.6	41.63
2	150 x 150	8.10	924.8	41.10
3	150 x 150	8.10	927.3	41.21
Mean		8.10	929.6	41.31
Maximum		8.10	936.6	41.63
Minimum		8.10	924.8	41.10

Table A.5 – Mechanical properties of concrete specimen – Concrete 2 – C25/30

Number of specimen	Specimen dimensions (mm)	Specimen mass (kg)	Load (kN)	Compressive strength (MPa)
1	150 x 150	7.75	882.9	39.24
2	150 x 150	7.80	981.4	43.62
3	150 x 150	7.80	949.9	42.22
4	150 x 150	7.90	999.8	44.44
5	150 x 150	7.75	928.2	41.25

Mean	7.80	948.4	42.15
Maximum	7.90	999.8	44.44
Minimum	7.75	882.9	39.24

Table A.6 – Mechanical properties of concrete specimen – Concrete 3 – C25/30

Number of specimen	**Specimen dimensions (mm)**	**Specimen mass (kg)**	**Load (kN)**	**Compressive strength (MPa)**
1	150 x 150	7.75	841.1	37.38
2	150 x 150	7.90	893.7	39.72
3	150 x 150	7.85	870.2	38.68
Mean		7.83	868.3	38.59
Maximum		7.90	893.7	39.72
Minimum		7.75	841.1	37.38

a) b) c)

Figure A.1 – Strength tests on the steel coupons of the steel profiles

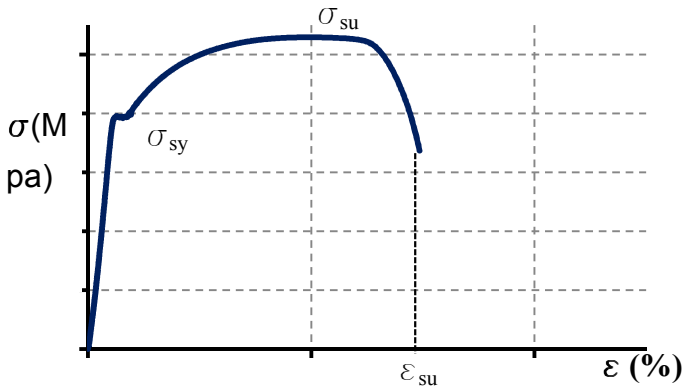

Figure A.2 – Stress-strain relationship of the steel coupons

APPENDIX B – Calculation of the serviceability loads

B. 1 Steel Columns

For compression members with class 1, class 2 or class 3 cross-sections, the design buckling resistance $N_{b,Rd}$of a compression member with class 1, class 2 or class 3 cross-section should be determined from:

$$N_{b,Rd} = \chi A f_y / \gamma_{M1} \tag{B.1}$$

whereχ is the reduction factor for the relevant buckling mode;

For axial compression in members, the value of χ for the appropriate non-dimensional slenderness $\bar{\lambda}$ should be determined from:

$$\chi = \frac{1}{\varphi + \sqrt{\varphi^2 - \bar{\lambda}^2}} \tag{B.2}$$

with

$$\varphi = \frac{1}{2}\left[1 + \alpha\lambda + \lambda^2\right] \tag{B.3}$$

For class 1,2 and 3 cross-sections

$$\bar{\lambda} = \sqrt{\frac{A.f_y}{N_{cr}}} = \frac{L_{cr}}{i}\frac{1}{\lambda_1} \tag{B.4}$$

L_{cr} is the buckling length
i is the radius of gyration about the relevant axis

$$\lambda_1 = \pi\sqrt{\frac{E}{f_y}} = 93.3\varepsilon \tag{B.5}$$

$$\varepsilon = \sqrt{\frac{235}{f_y}} \tag{B.6}$$

In which i is the gyration radius of the cross section, and λ_1 is given by

in which

E – is the Young´s modulus of steel at ambient temperature;

f_y– is the yield strength at ambient temperature.

The buckling length $l_{fi}$of a column for the fire design situation should generally be determined as for normal temperature design. However, in a braced frame the buckling length l_{fi} of a column may be determined by considering it as fixed in direction at continuous or semi-continuous connections to the column lengths in the fire compartments above and below, provided that the fire resistance of the building components that separate these fire compartments is not less than the fire resistance of the column.

In the case of a braced frame in which each storey comprises a separate fire compartment with sufficient fire resistance, in an intermediate storey, the buckling length $l_{fi}$of a continuous column may be taken as $l_{fi} = 0,5\ L$ and in the top storey the buckling length may be taken as $l_{fi} = 0,7\ L$, where L is the system length in the relevant storey.

When design using nominal fire exposure, the design resistance $N_{b,fi,t,Rd}$, at time t, of a compression member with a non-uniform temperature distribution may be taken as equal to the design resistance $N_{b,fi,\theta,Rd}$ of a compression member with a uniform steel temperature $\theta_a$equal to the maximum steel temperature $\theta_{a,max}$reached at time t.

Table B.1 – Applied loads used in the experimental tests for the steel columns

Steel Profile	Load Level (% of $N_{Rd,20}$)	Load (kN)
HEA 160	30%	266
HEA 160	70%	621
HEA 200	30%	428
HEA 200	70%	999.8

B.2 Composite Steel-Concrete Columns

The plastic resistance to compression $N_{Pl,Rd}$ of a composite cross-section should be calculated by adding the plastic resistances of its components:

$$N_{Pl,Rd} = A_a f_{yd} + 0.85 A_c f_{cd} + A_s f_{sd} \tag{B.7}$$

The relative slenderness $\overline{\lambda}$ for the plane of bending being considered is given by:

$$\overline{\lambda} = \sqrt{\frac{N_{pl,Rk}}{N_{cr}}} \tag{B.8}$$

where:
$N_{pl,Rk}$ is the characteristic value of the plastic resistance to compression, if instead of the design strengths, the characteristic values are used;
$N_{cr}$is the elastic critical normal force for the relevant buckling mode, calculated with the effective flexural stiffness $(EI)_{eff}$

$$(EI)eff = E_a I_a + E_s I_s + K_e E_{cm} I_c \tag{B.9}$$

where:
K_e is a correction factor that should be taken as 0.6
I_a, I_c and $I_s$are the second moments of area of the structural steel section, the uncracked concrete section and the reinforcement for the bending plane being considered.

For simplification for members in axial compression, the design value of the normal force N_{Ed} should satisfy:

$$\frac{N_{Ed}}{\chi N_{pl,Rd}} \leq 1.0 \tag{B.10}$$

where:
$N_{Pl,Rd}$ is the plastic resistance of the composite section;
χ is the reduction factor for the relevant buckling mode given in EN 1993-1-1, in terms of the relevant relative slenderness $\overline{\lambda}$

Table B.2 – Applied loads used in the experimental tests for the composite columns

Steel Profile	Load Level (% of $N_{Rd,20}$)	Load (kN)
CSS 160	30%	272.7
CSS 160	70%	636.5
CSS 200	30%	514
CSS 200	70%	1199

APPENDIX C – Temperatures in the columns of experimental tests

C.1 – Columns embedded on walls

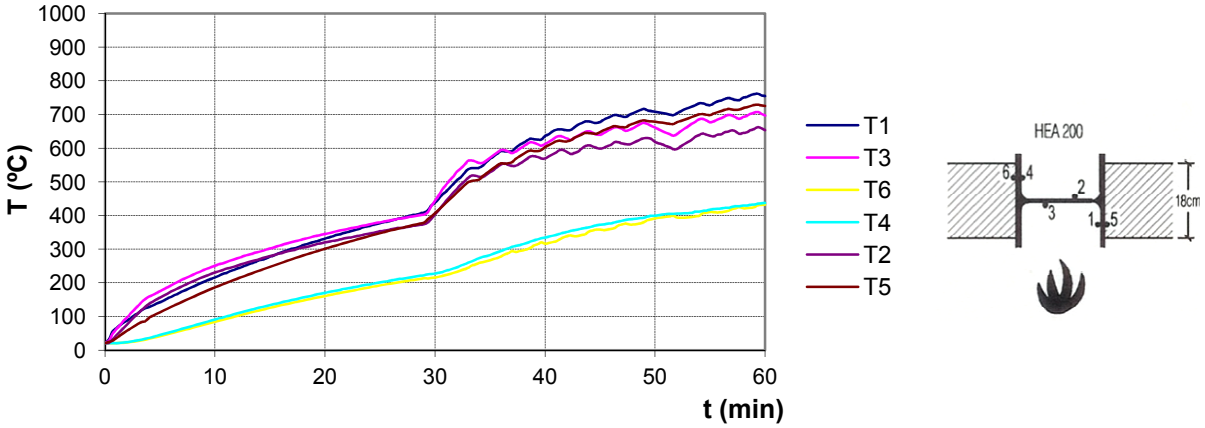

Figure C.1.1 – Evolution of temperatures at mid-height of column of test E03

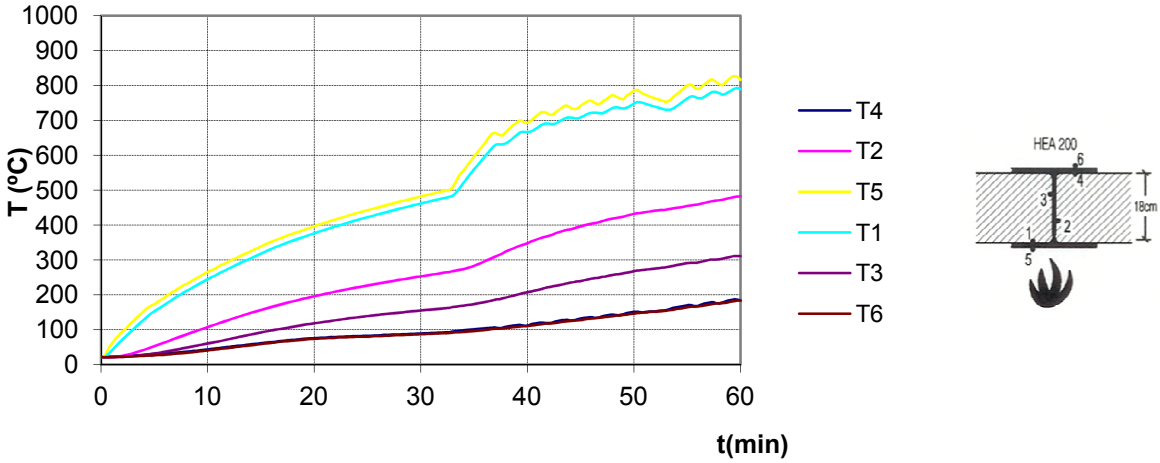

Figure C.1.2 – Evolution of temperatures at mid-height of column of test E04

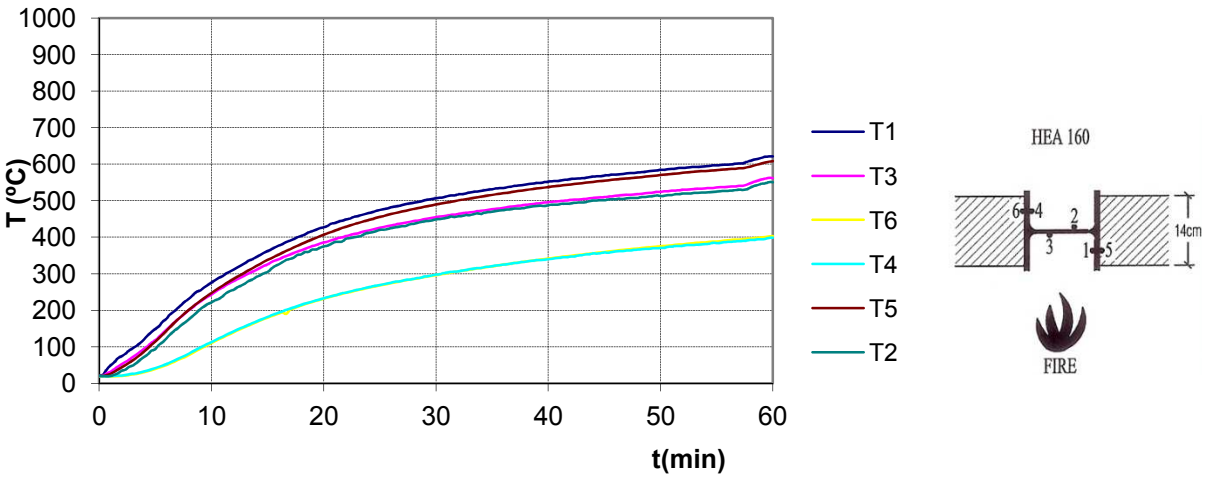

Figure C.1.3 – Evolution of temperatures at mid-height of column of test E05

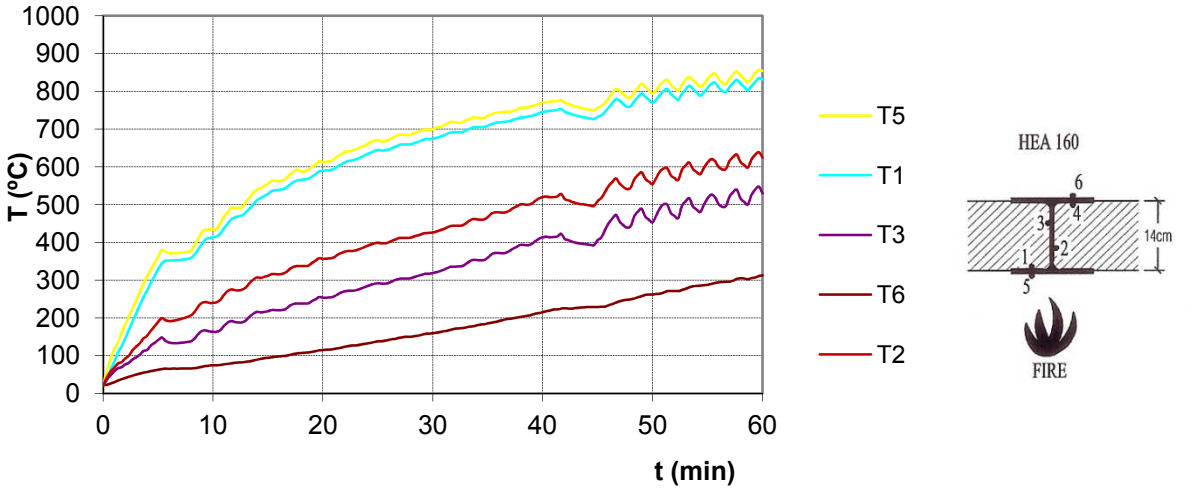

Figure C.1.4 – Evolution of temperatures at mid-height of column of test E06

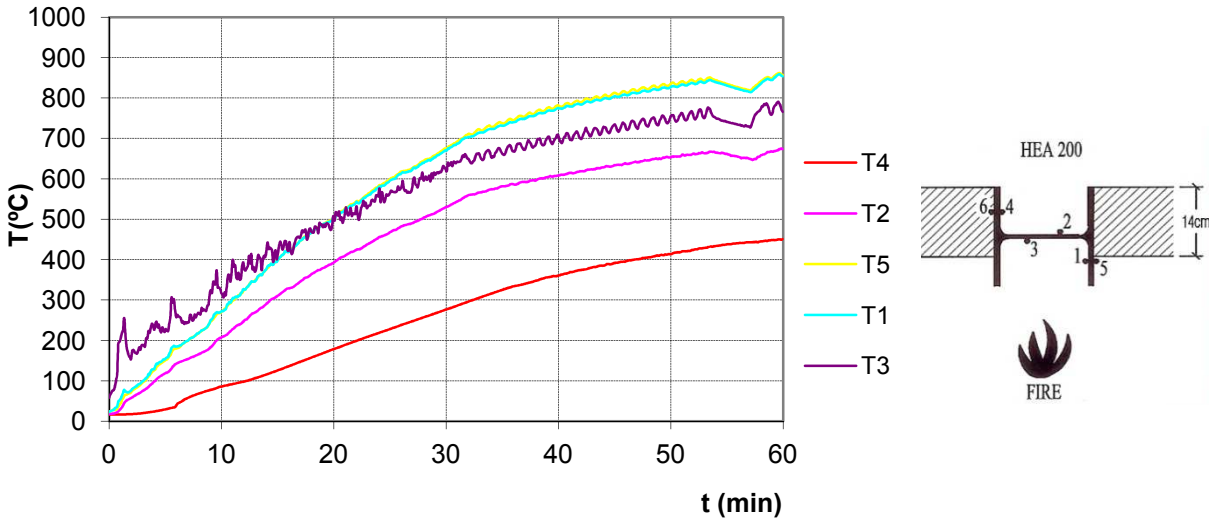

Figure C.1.5 – Evolution of temperatures at mid-height of column of test E08

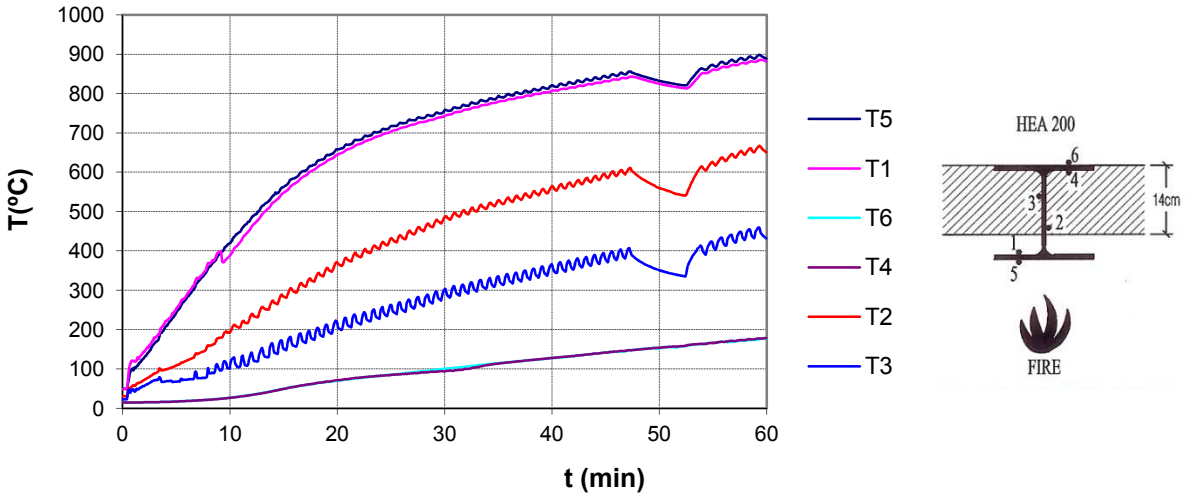

Figure C.1.6 – Evolution of temperatures at mid-height of column of test E09

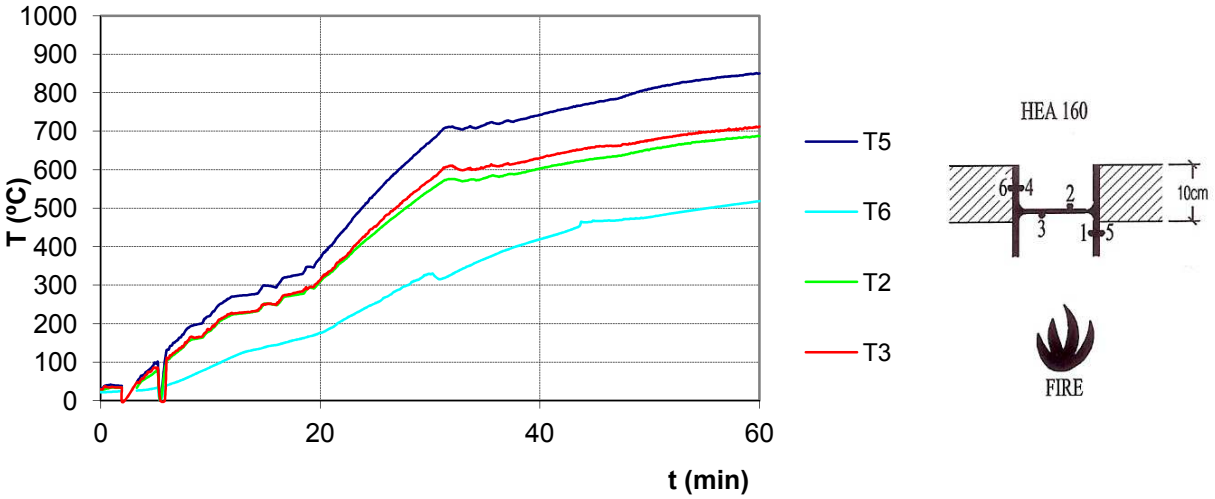

Figure C.1.7 – Evolution of temperatures at mid-height of column of test E10

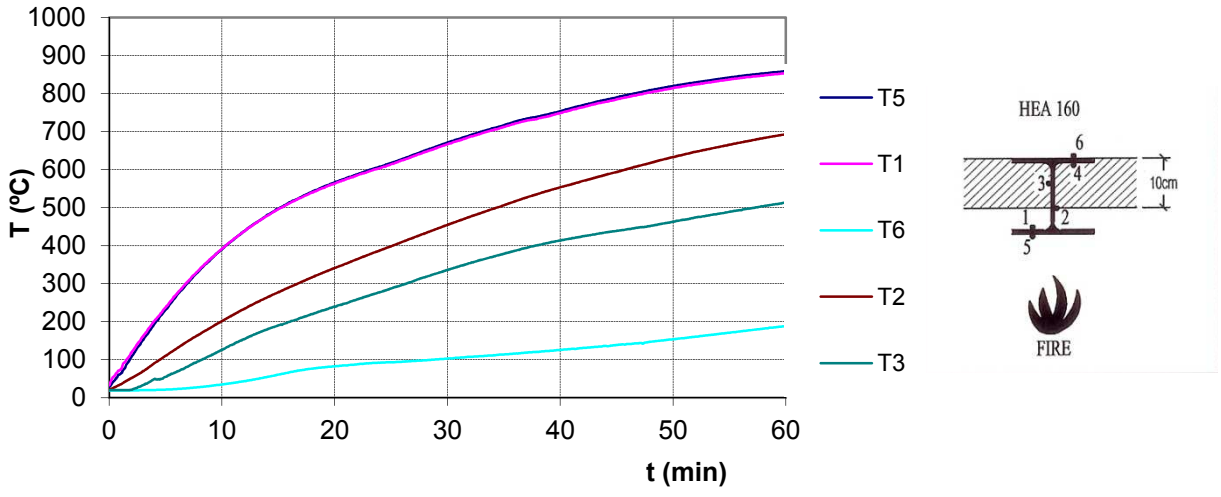

Figure C.1.8 – Evolution of temperatures at mid-height of column of test E11

C.2 – Steel Bare Columns

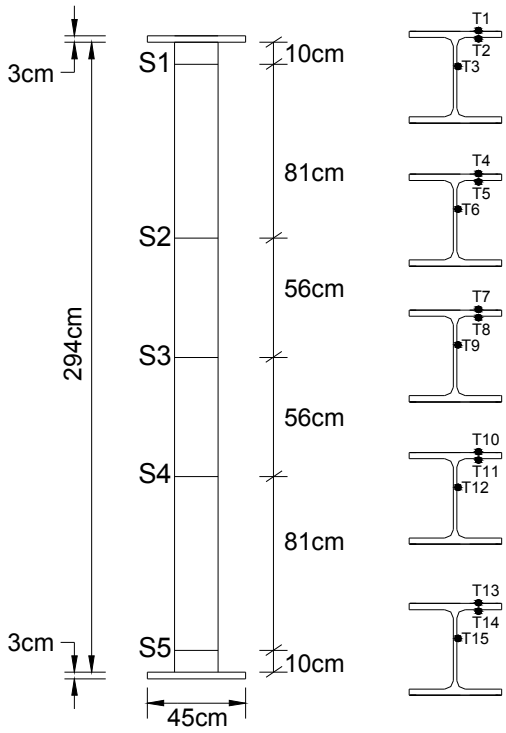

Figure C.2.1 – Steel specimen with position of thermocouples

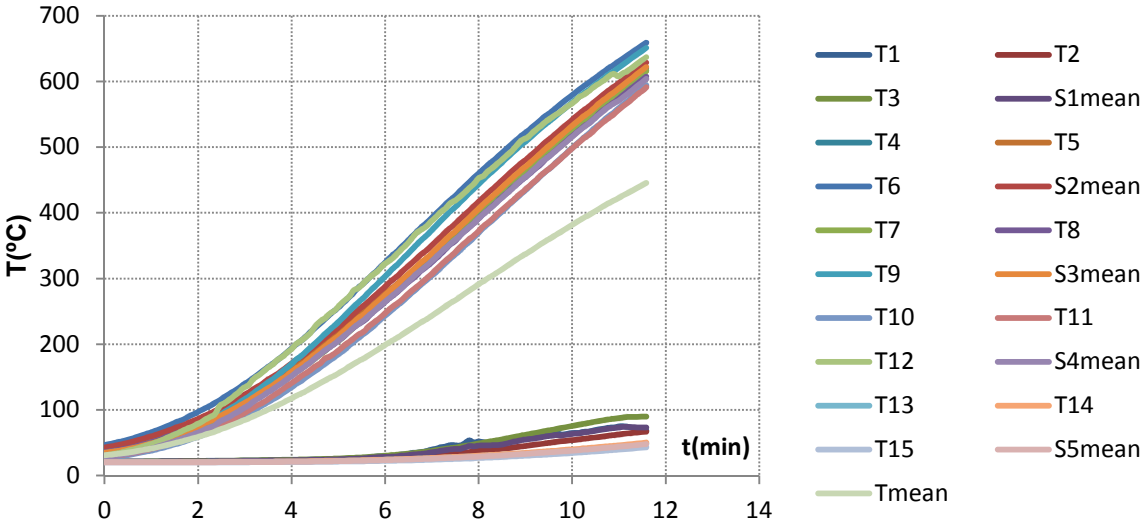

Figure C.2.2 – Evolution of temperatures at mid-height of column of test HEA200-K13-L70

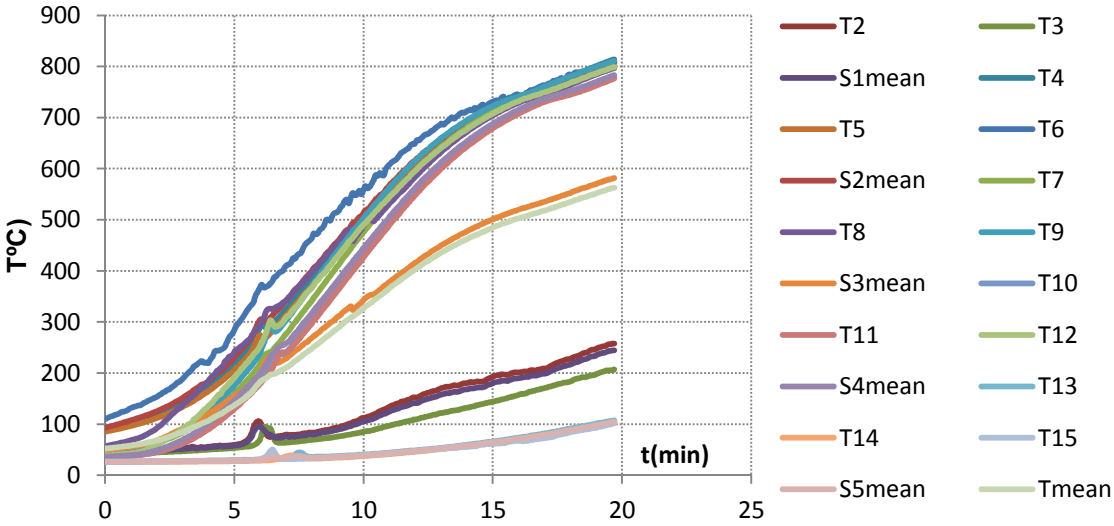

Figure C.2.3 – Evolution of temperatures at mid-height of column of test HEA200-K13-L70-E2

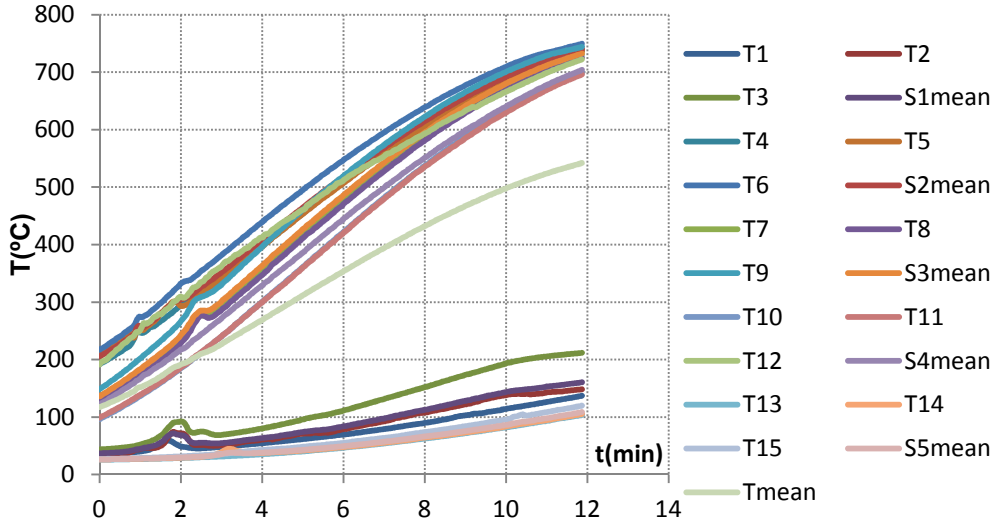

Figure C.2.4 – Evolution of temperatures at mid-height of column of test HEA200-K13-L70-E1

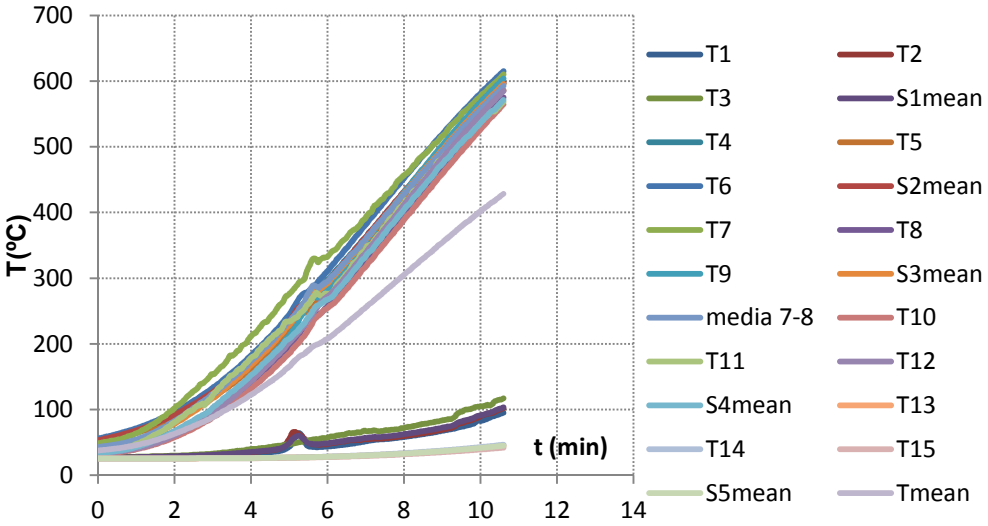

Figure C.2.5 – Evolution of temperatures at mid-height of column of test HEA160-K13-L70

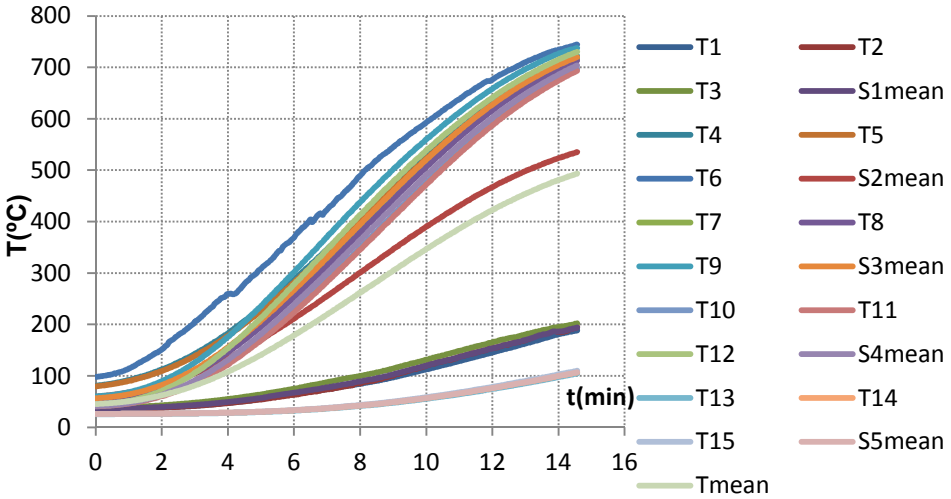

Figure C.2.6 – Evolution of temperatures at mid-height of column of test HEA200-K13-L30

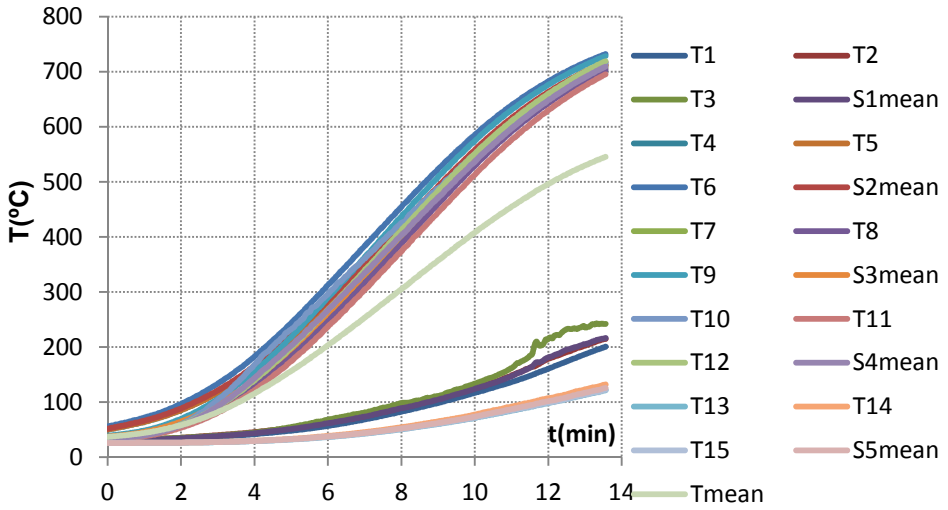

Figure C.2.7 – Evolution of temperatures at mid-height of column of test HEA160-K13-L30

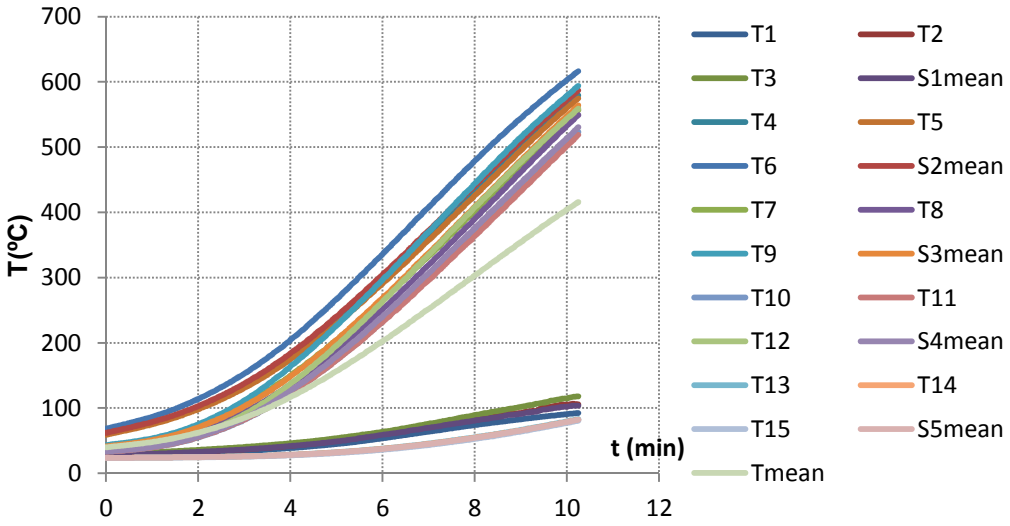

Figure C.2.8 – Evolution of temperatures at mid-height of column of test HEA160-K45-L70

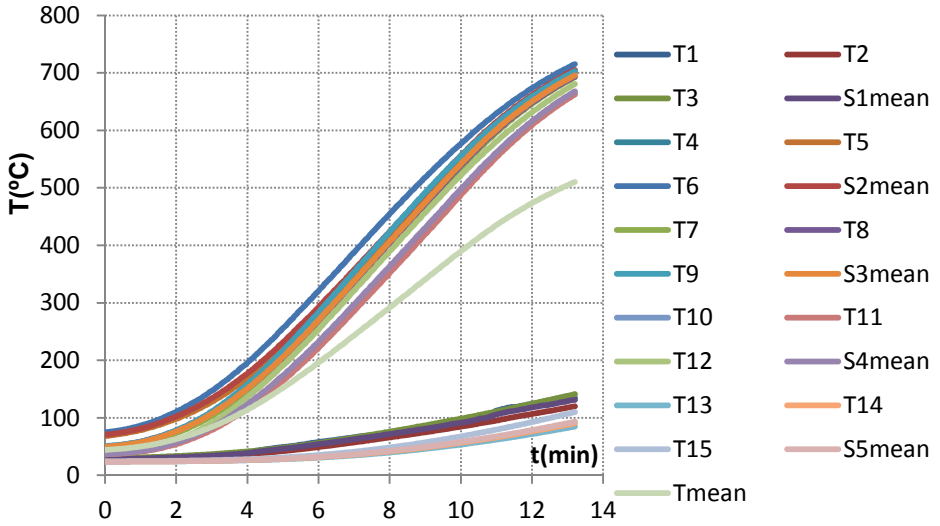

Figure C.2.9 – Evolution of temperatures at mid-height of column of test HEA160-K45-L30

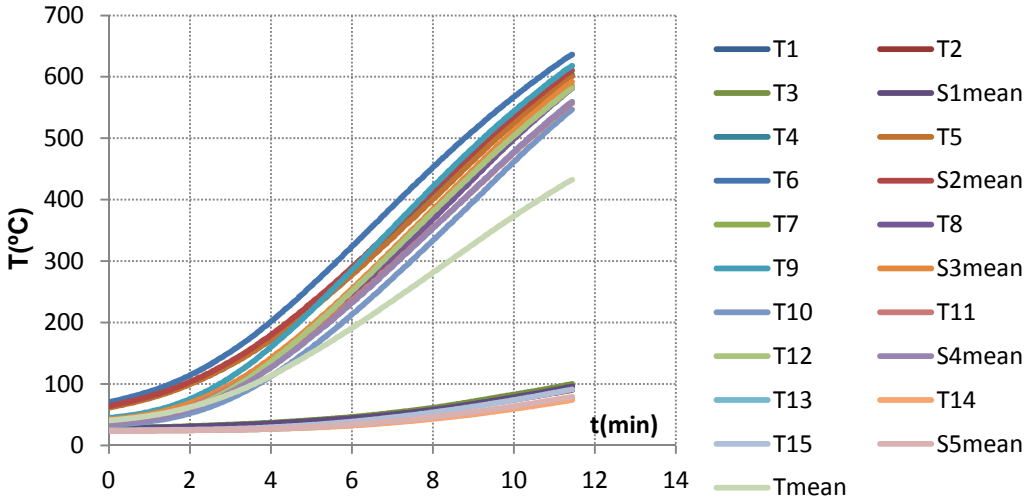

Figure C.2.10 – Evolution of temperatures at mid-height of column of test HEA200-K45-L70

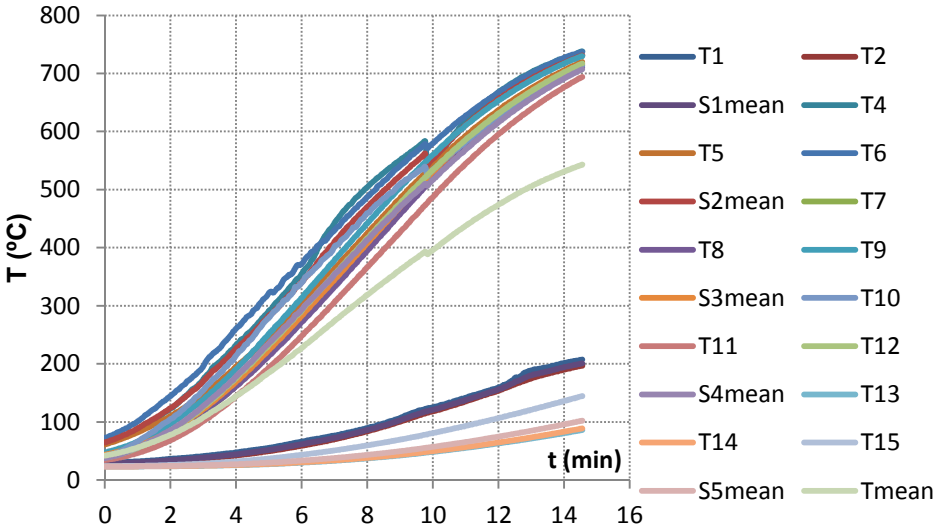

Figure C.2.11 – Evolution of temperatures at mid-height of column of test HEA200-K45-L30

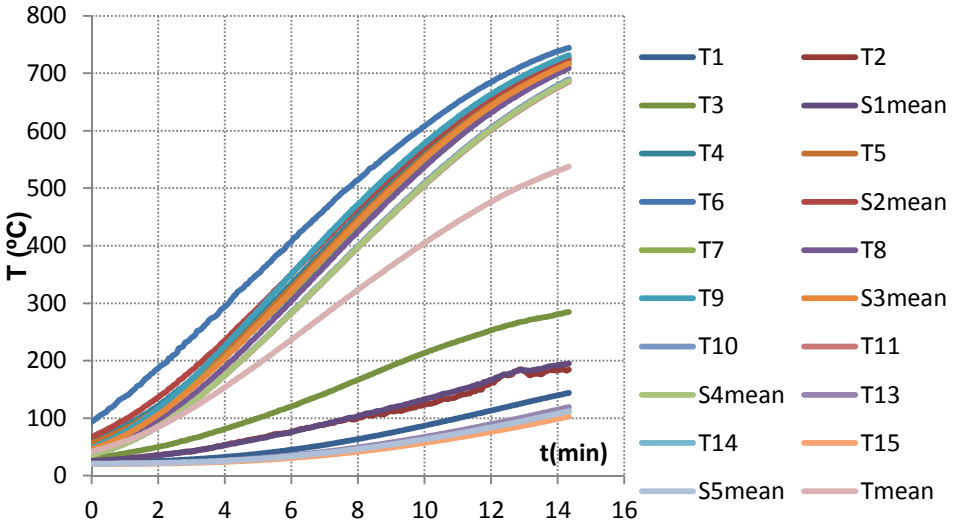

Figure C.2.12 – Evolution of temperatures at mid-height of column of test HEA200-K128-L30

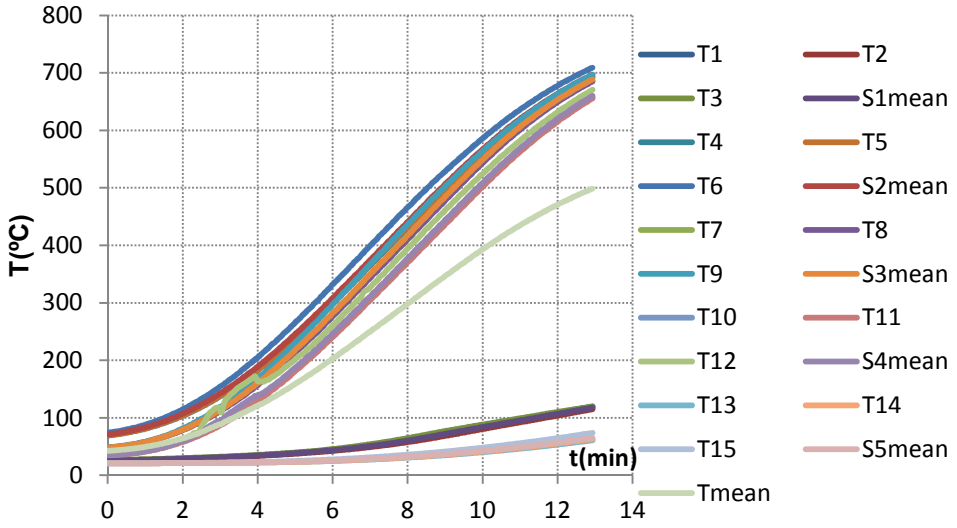

Figure C.2.13 – Evolution of temperatures at mid-height of column of test HEA160-K128-L30

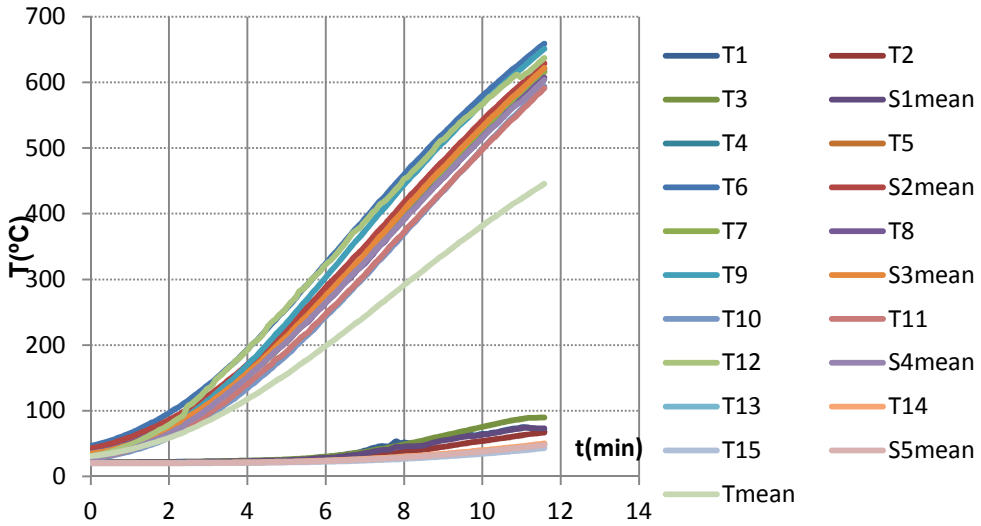

Figure C.2.14 – Evolution of temperatures at mid-height of column of test HEA200-K128-L70

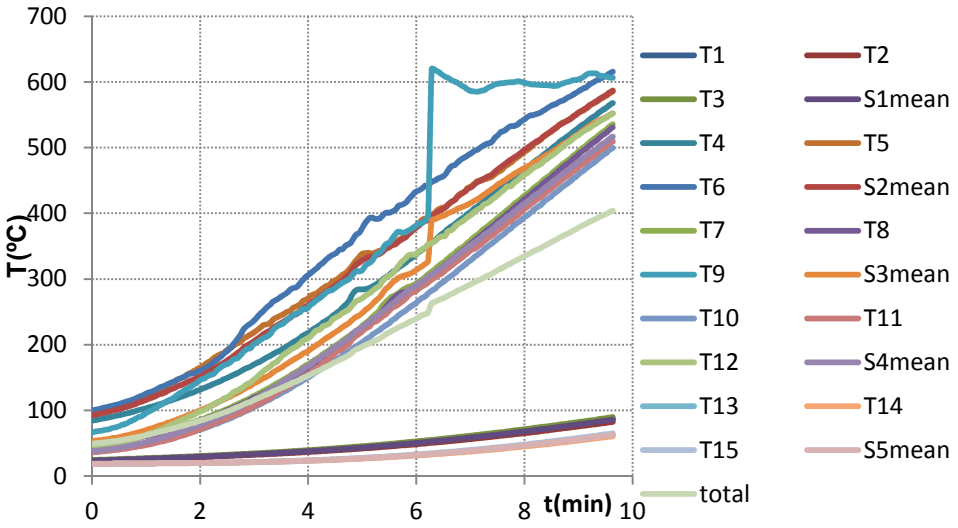

Figure C.2.15 – Evolution of temperatures at mid-height of column of test HEA160-K128-L70

C.3 – Composite steel-concrete columns

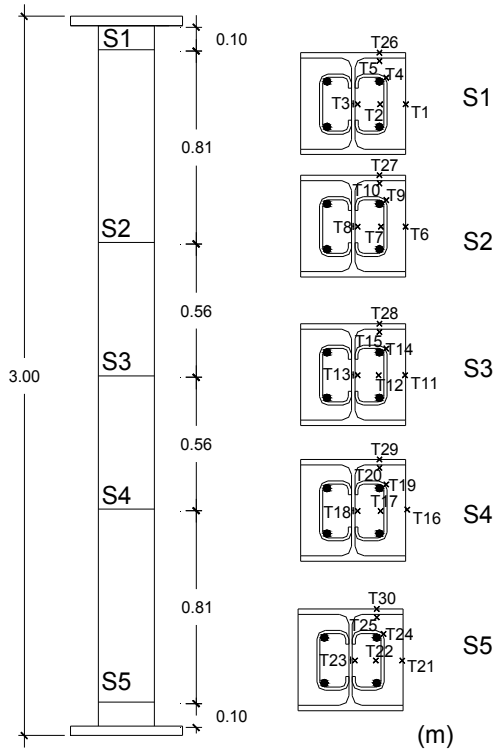

Figure C.3.1 – Composite steel-concrete specimen with position of thermocouples

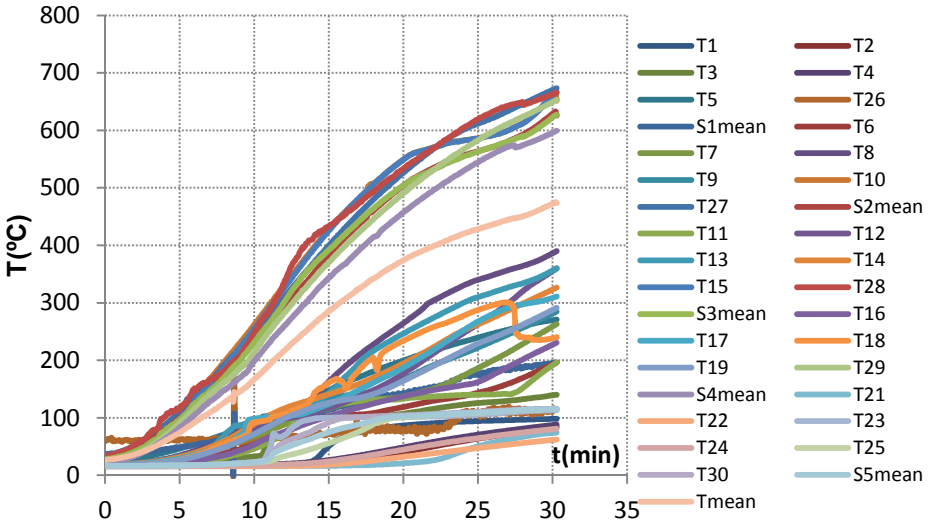

Figure C.3.2 – Evolution of temperatures at mid-height of column of test CSC160-K128-L30

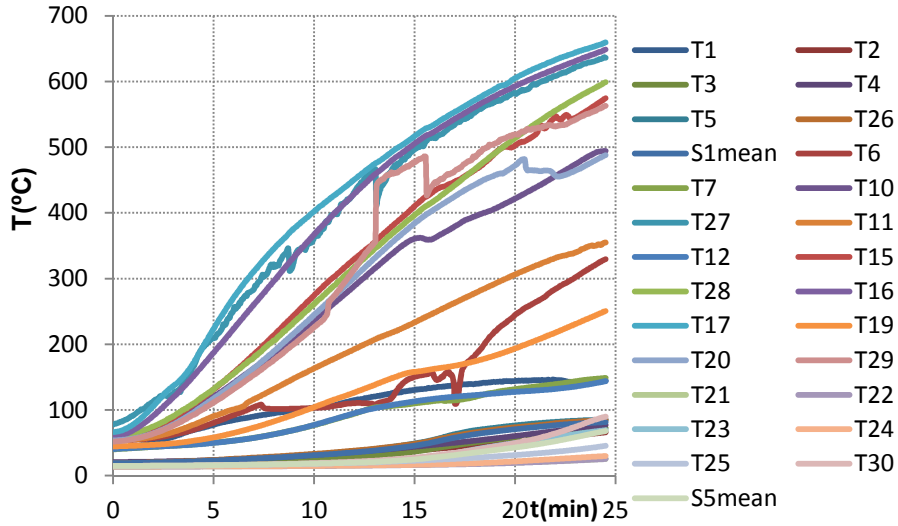

Figure C.3.3 – Evolution of temperatures at mid-height of column of test CSC160-K128-L70

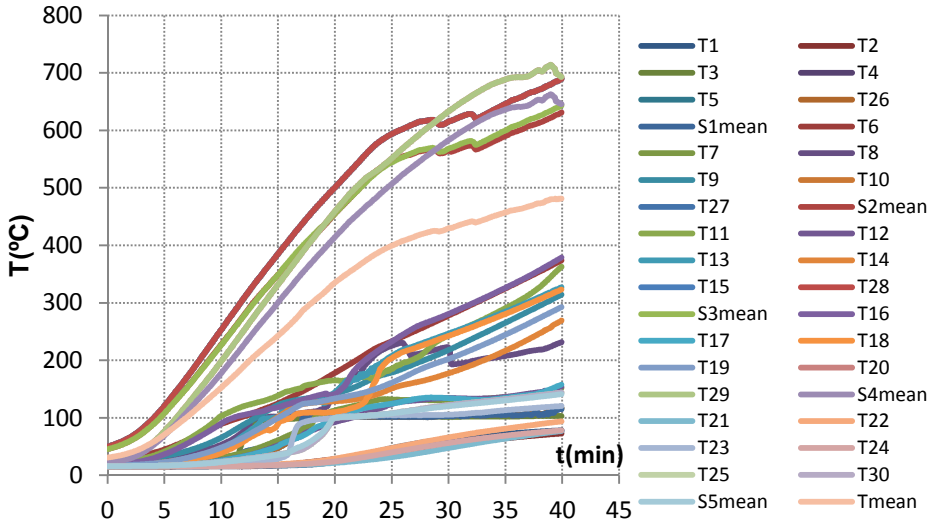

Figure C.3.4 – Evolution of temperatures at mid-height of column of test CSC200-K128-L30

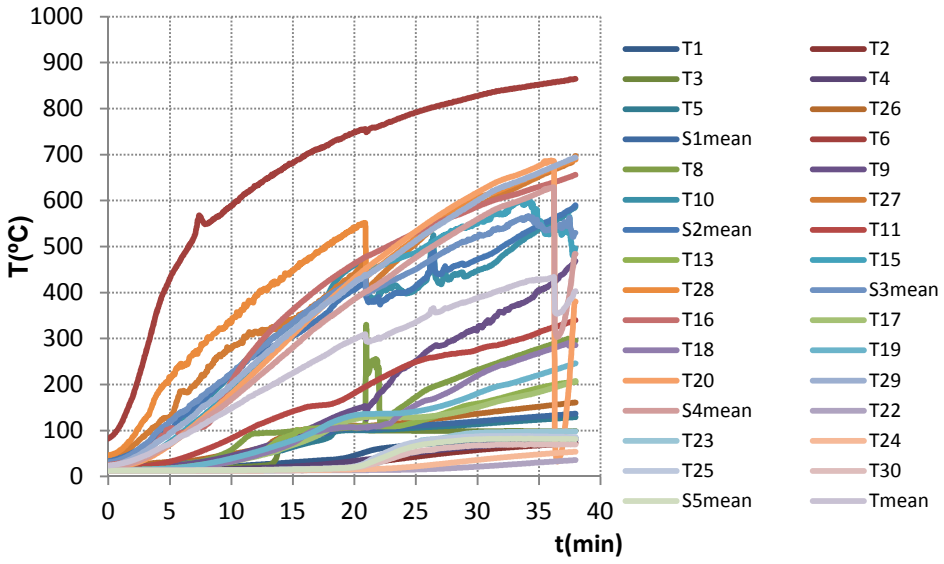

Figure C.3.5 – Evolution of temperatures at mid-height of column of test CSC200-K128-L70

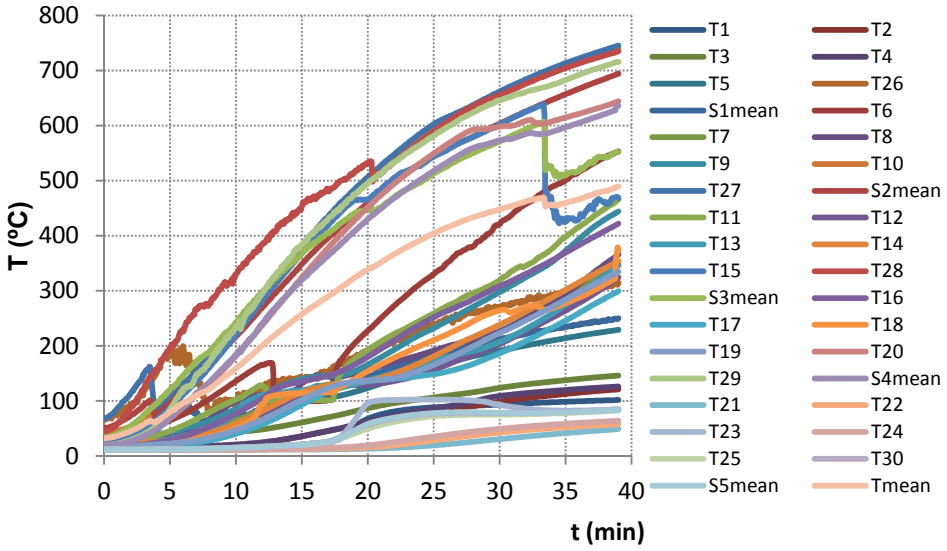

Figure C.3.6 – Evolution of temperatures at mid-height of column of test CSC160-K45-L30

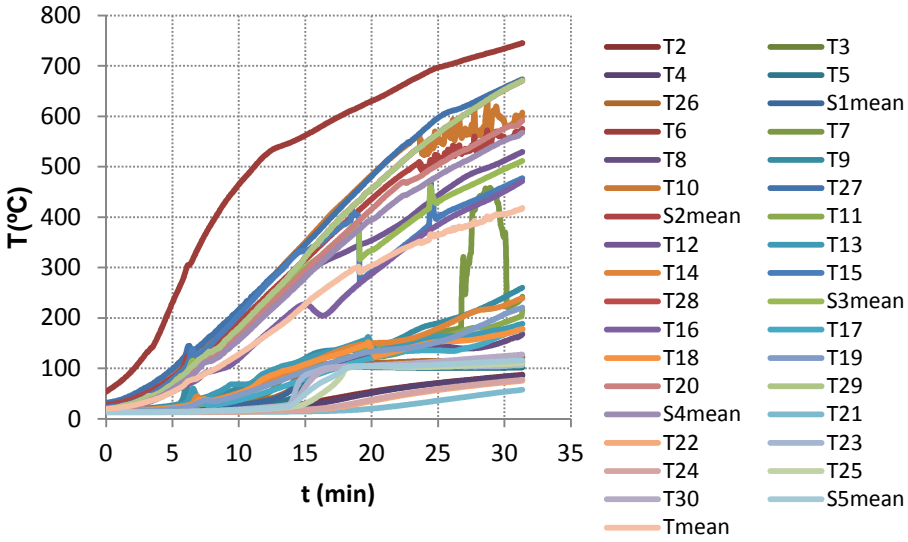

Figure C.3.7 – Evolution of temperatures at mid-height of column of test CSC160-K45-L70

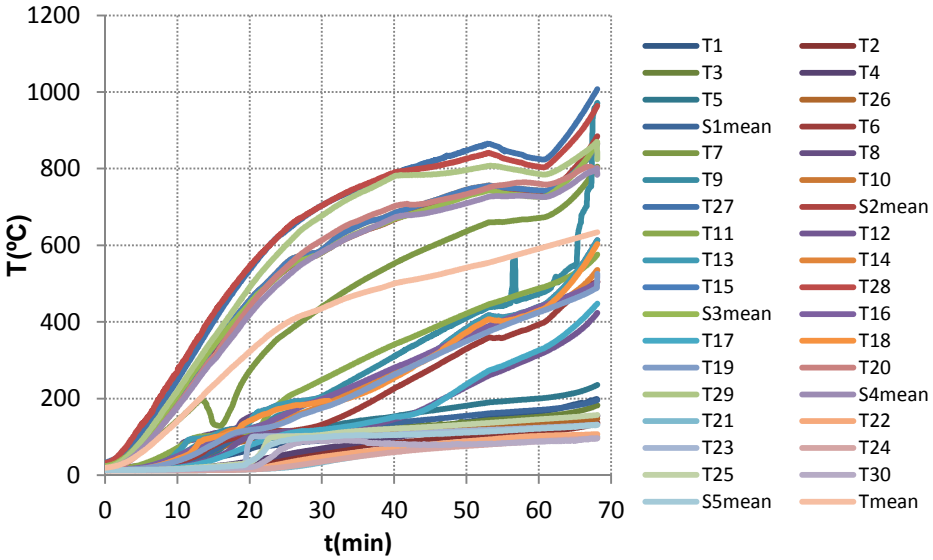

Figure C.3.8 – Evolution of temperatures at mid-height of column of test CSC200-K45-L30

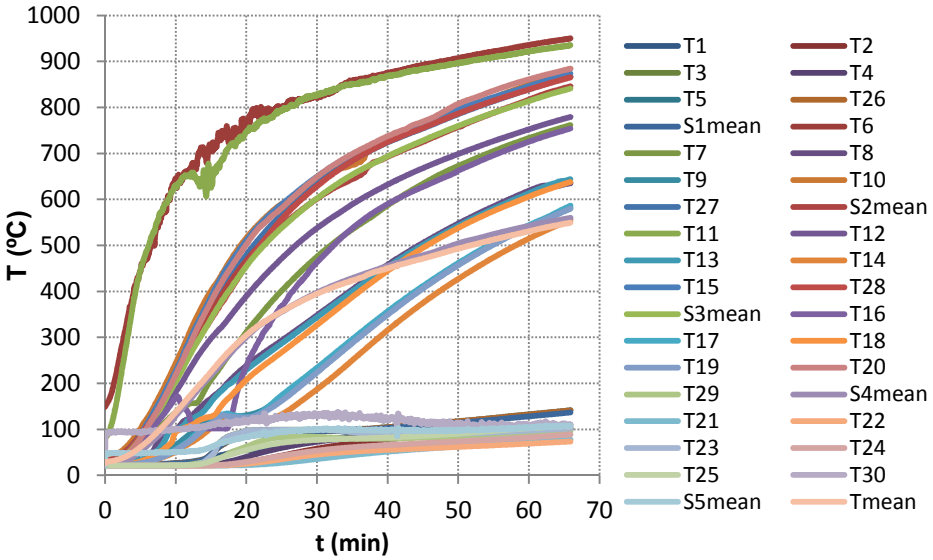

Figure C.3.9 – Evolution of temperatures at mid-height of column of test CSC160-K13-L30

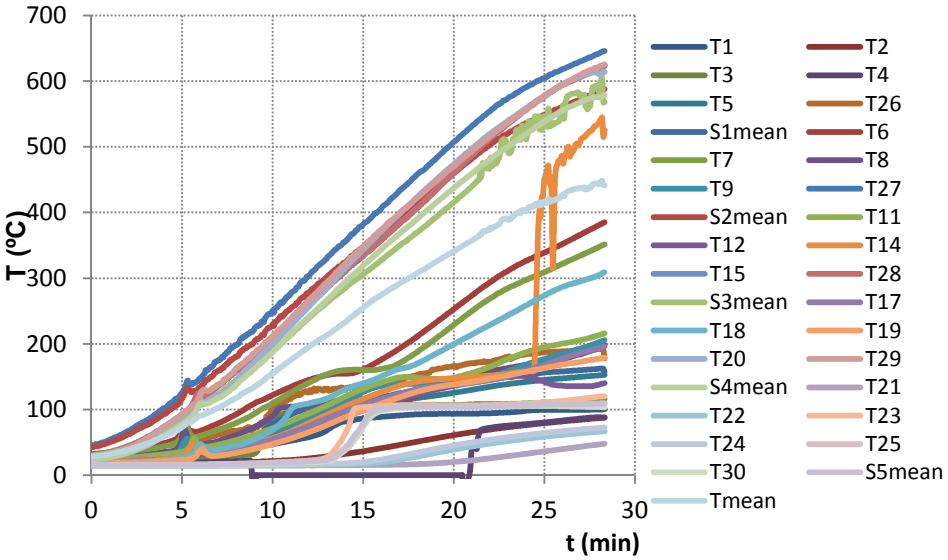

Figure C.3.10 – Evolution of temperatures at mid-height of column of test CSC160-K13-L70

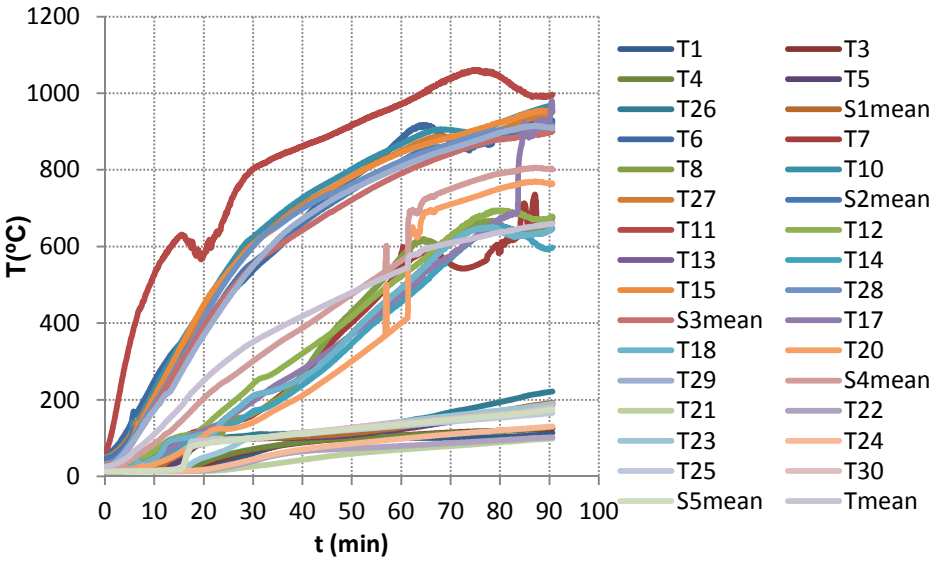

Figure C.3.11 – Evolution of temperatures at mid-height of column of test CSC200-K13-L30

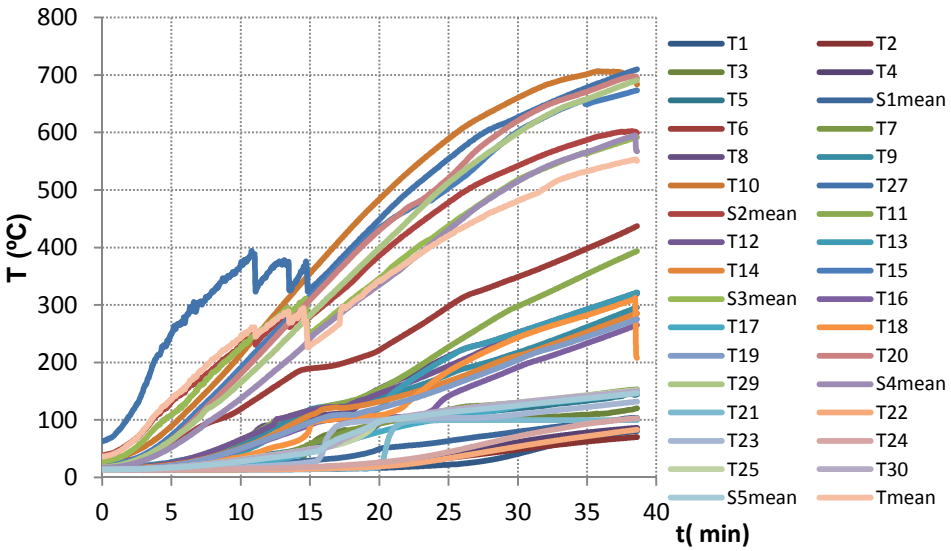

Figure C.3.12 – Evolution of temperatures at mid-height of column of test CSC200-K13-L70

APPENDIX D – Restraining forces in experimental tests

D.1 – Steel bare columns

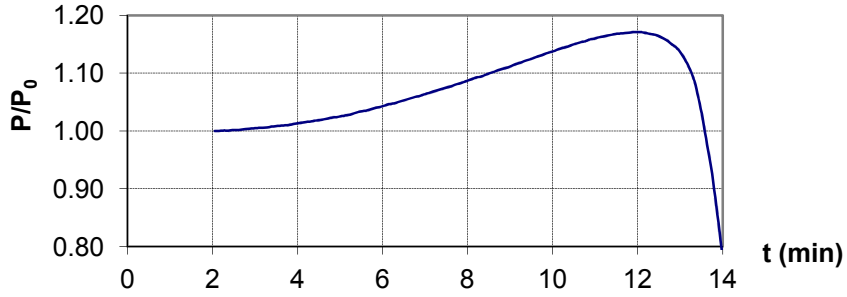

Figure D.1.1 – Evolution of the restraining forces of column HEA200-K13-L70

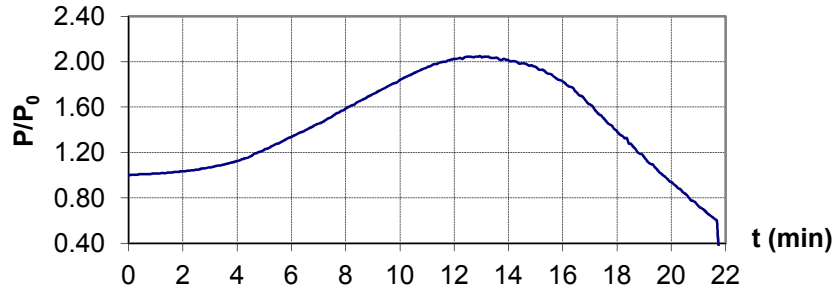

Figure D.1.2 – Evolution of the restraining forces of column HEA200-K13-L70-E2

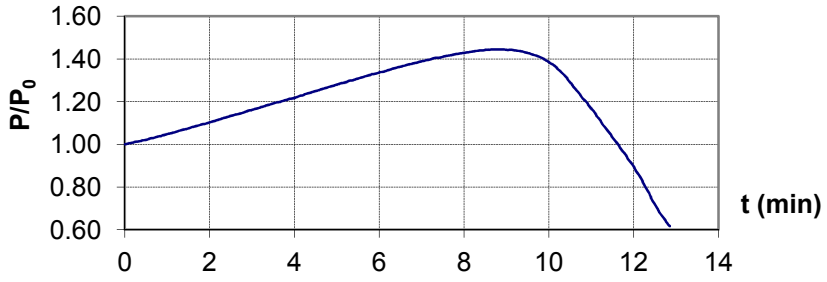

Figure D.1.3 – Evolution of the restraining forces of column HEA200-K13-L70-E2

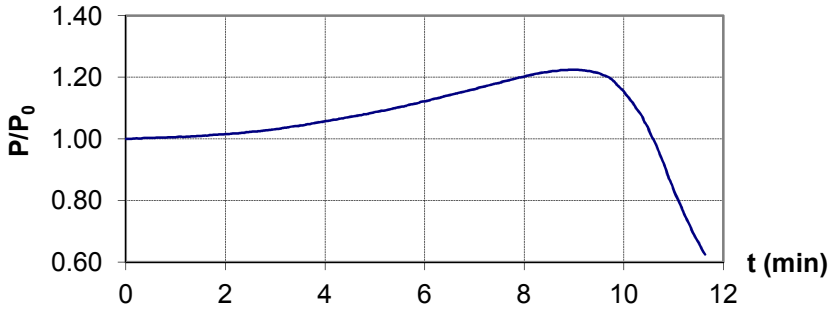

Figure D.1.4 – Evolution of the restraining forces of column HEA160-K13-L70

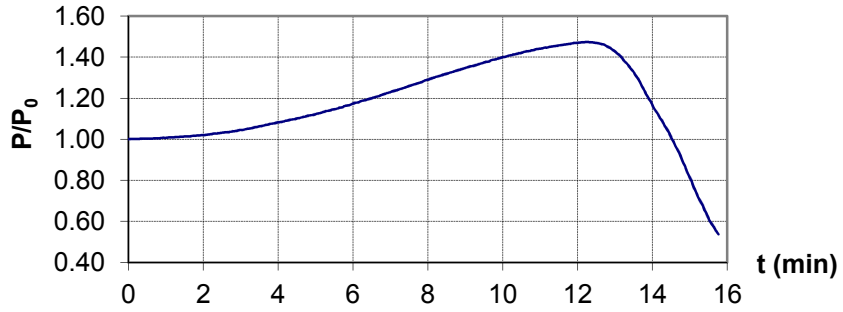

Figure D.1.5 – Evolution of the restraining forces of column HEA200-K13-L30

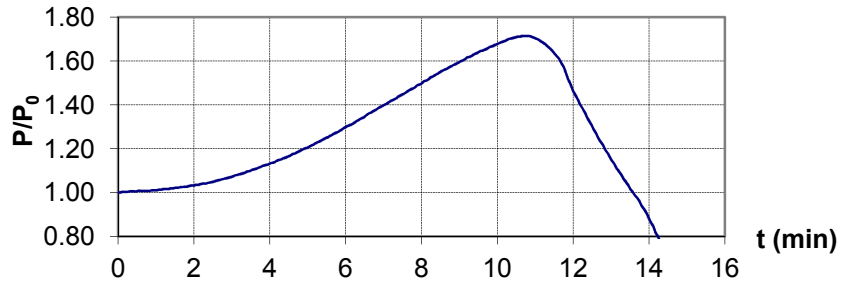

Figure D.1.6 – Evolution of the restraining forces of column HEA160-K13-L30

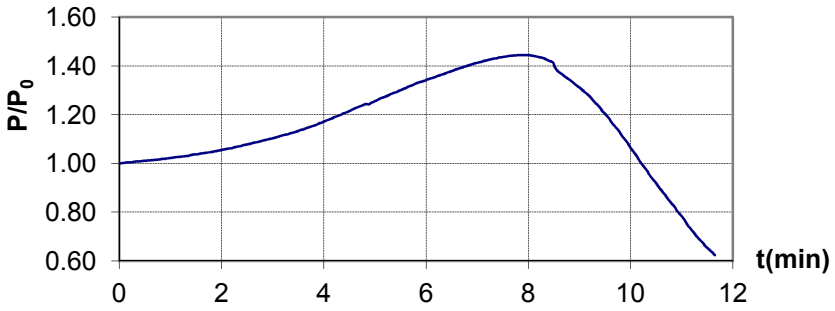

Figure D.1.7 – Evolution of the restraining forces of column HEA160-K45-L70

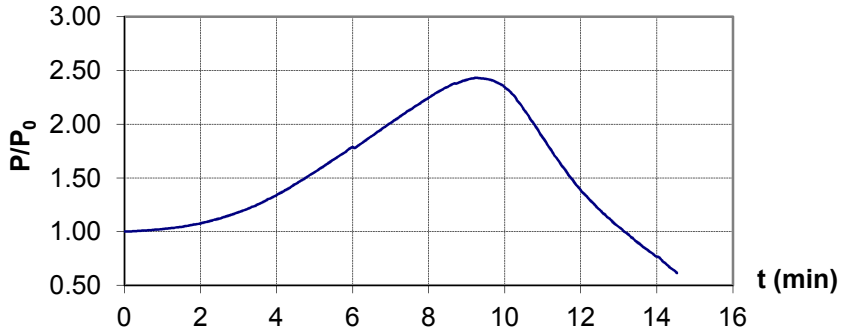

Figure D.1.8 – Evolution of the restraining forces of column HEA160-K45-L30

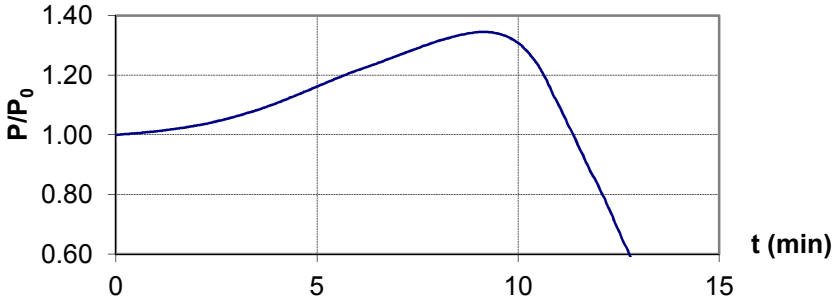

Figure D.1.9 – Evolution of the restraining forces of column HEA200-K45-L70

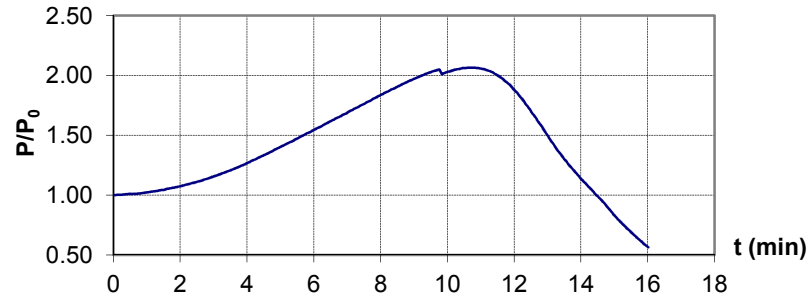

Figure D.1.10 – Evolution of the restraining forces of column HEA200-K45-L30

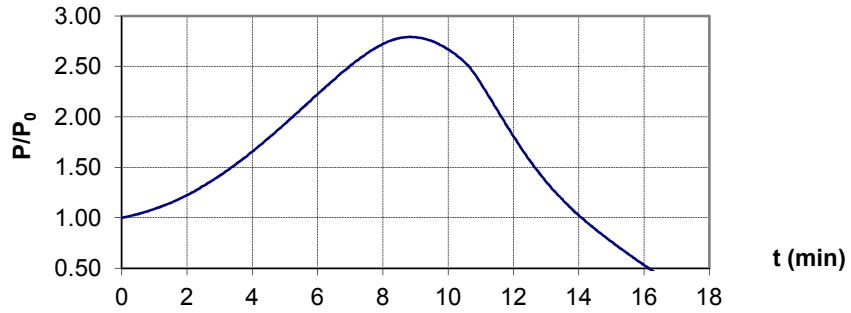

Figure D.1.11 – Evolution of the restraining forces of column HEA200-K128-L30

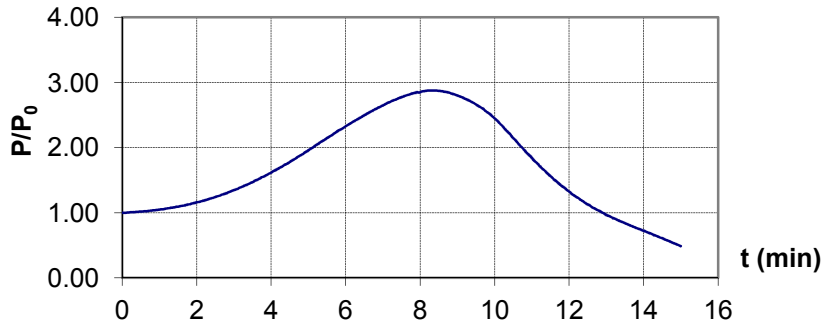

Figure D.1.12 – Evolution of the restraining forces of column HEA160-K128-L30

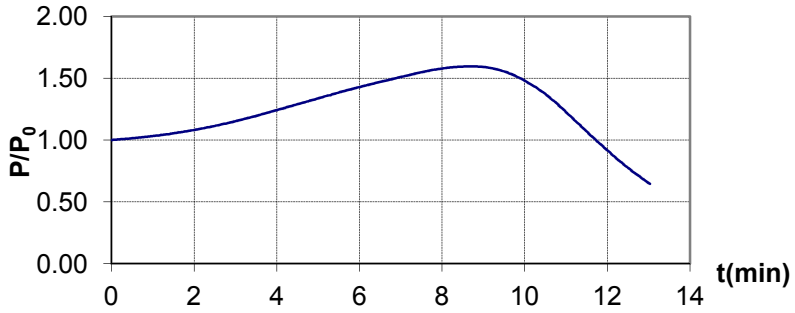

Figure D.1.13 – Evolution of the restraining forces of column HEA200-K128-L70

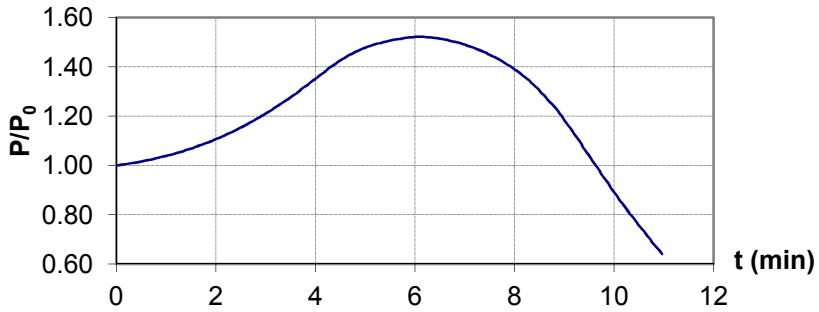

Figure D.1.14 – Evolution of the restraining forces of column HEA160-K128-L70

D.2 – Composite steel-concrete columns

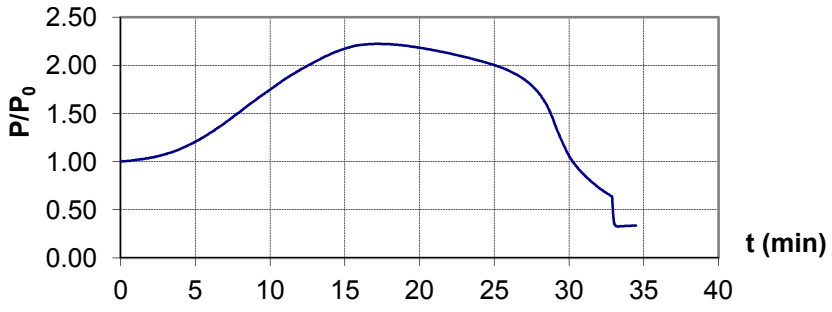

Figure D.2.1 – Evolution of the restraining forces of column CSC160-K128-L30

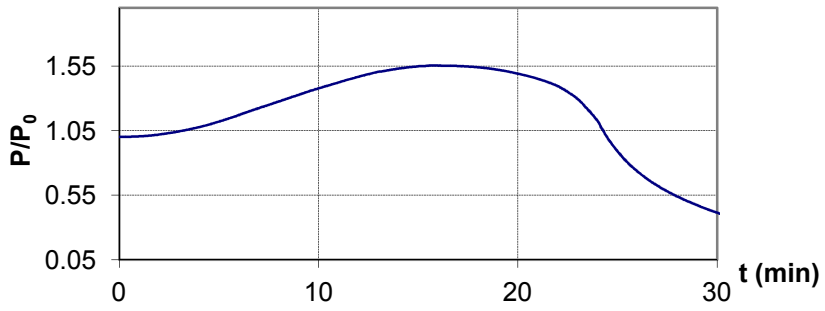

Figure D.2.2 – Evolution of the restraining forces of column CSC160-K128-L70

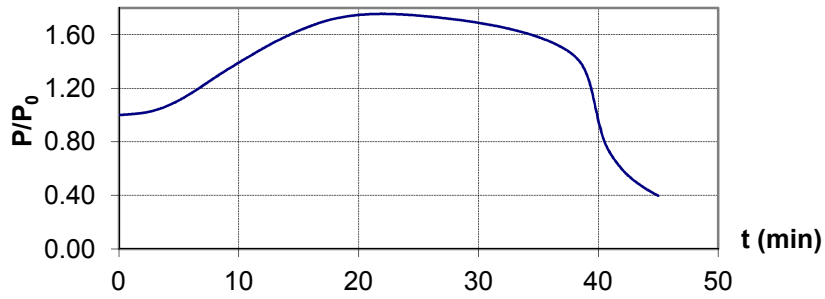

Figure D.2.3 – Evolution of the restraining forces of column CSC200-K128-L30

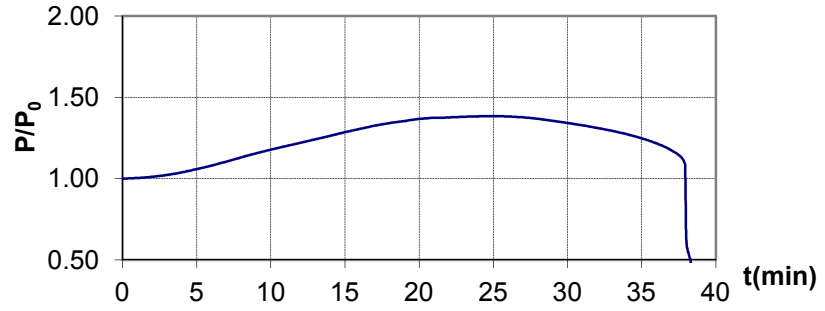

Figure D.2.4 – Evolution of the restraining forces of column CSC200-K128-L70

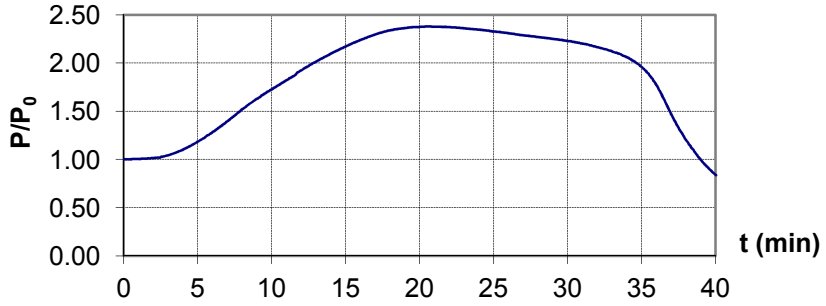

Figure D.2.5 – Evolution of the restraining forces of column CSC160-K45-L30

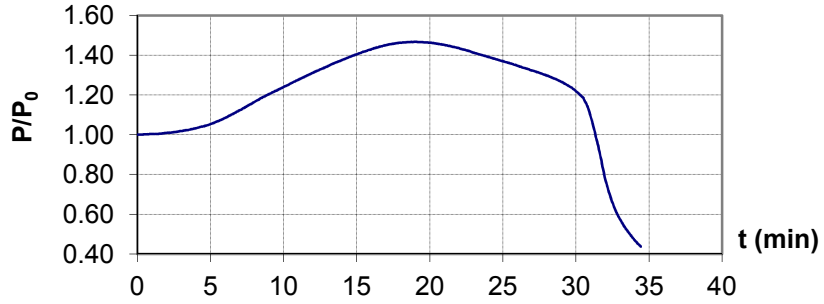

Figure D.2.6 – Evolution of the restraining forces of column CSC160-K45-L70

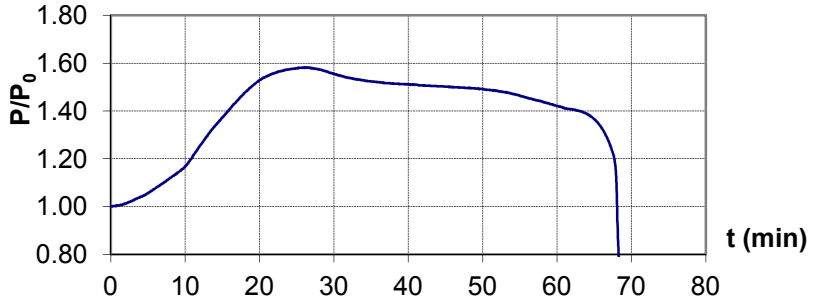

Figure D.2.7 – Evolution of the restraining forces of column CSC200-K45-L30

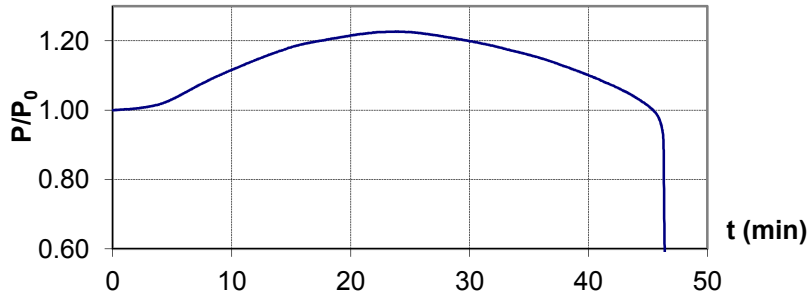

Figure D.2.8 – Evolution of the restraining forces of column CSC200-K45-L70

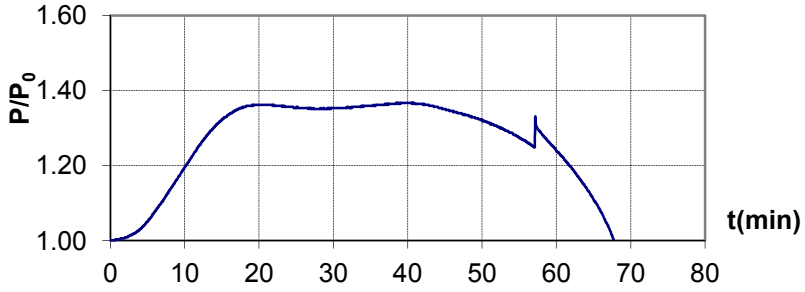

Figure D.2.9 – Evolution of the restraining forces of column CSC160-K13-L30

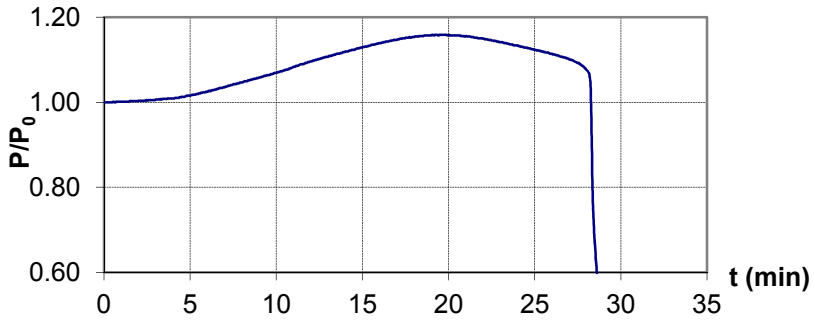

Figure D.2.10 – Evolution of the restraining forces of column CSC160-K13-L70

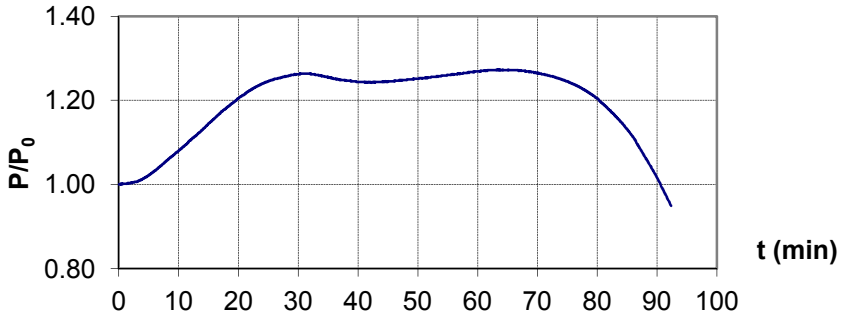

Figure D.2.11 – Evolution of the restraining forces of column CSC200-K13-L30

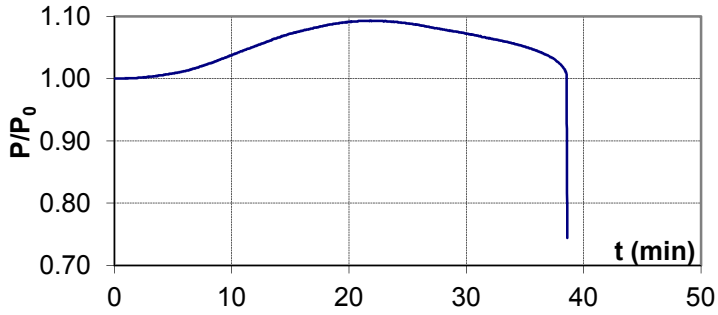

Figure D.2.12 – Evolution of the restraining forces of column CSC200-K13-L70

APPENDIX E – Vertical displacements in the experimental tests

E.1 – Steel bare columns

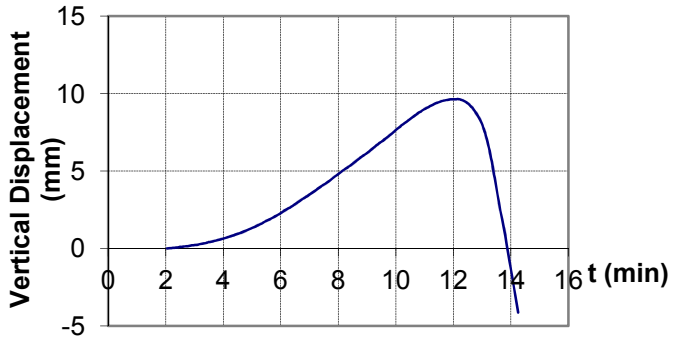

Figure E.1.1 – Evolution of the vertical displacement of column HEA200-K13-L70

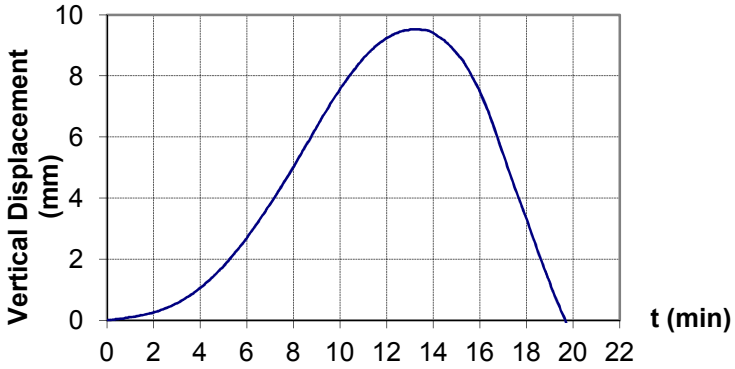

Figure E.1.2 – Evolution of the vertical displacement of column of test HEA200-K13-L70-E2

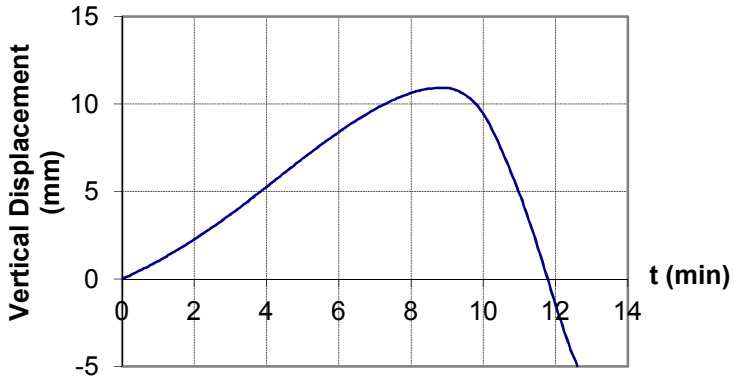

Figure E.1.3 – Evolution of the vertical displacement of column of test HEA200-K13-L70-E1

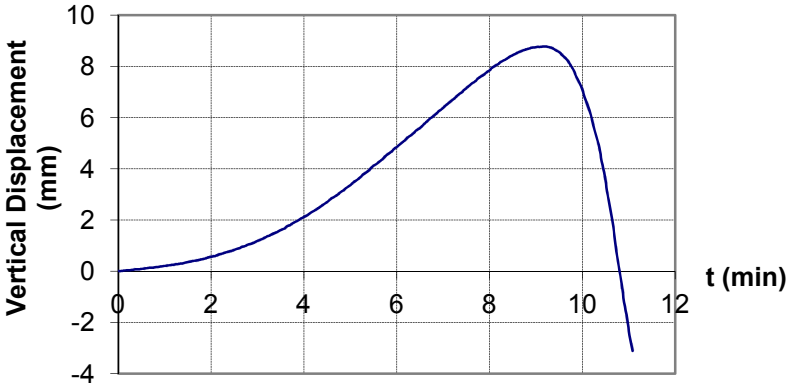

Figure E.1.4 – Evolution of the vertical displacement of column of test HEA160-K13-L70

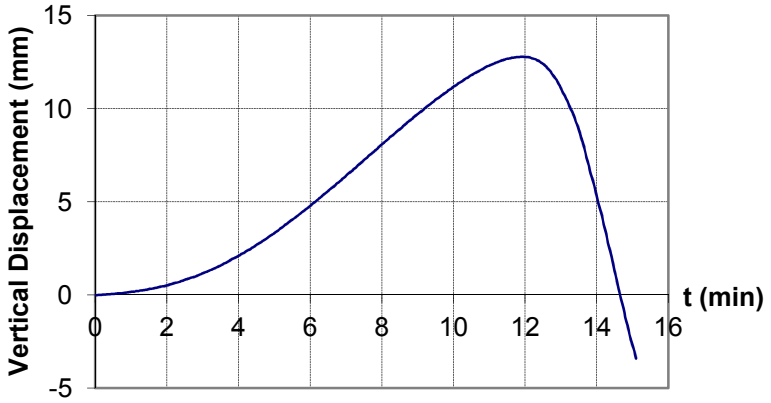

Figure E.1.5 – Evolution of the vertical displacement of column of test HEA200-K13-L30

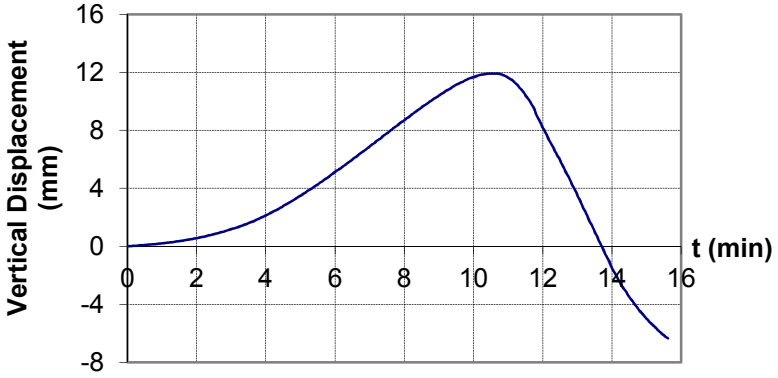

Figure E.1.6 – Evolution of the vertical displacement of column of test HEA160-K13-L30

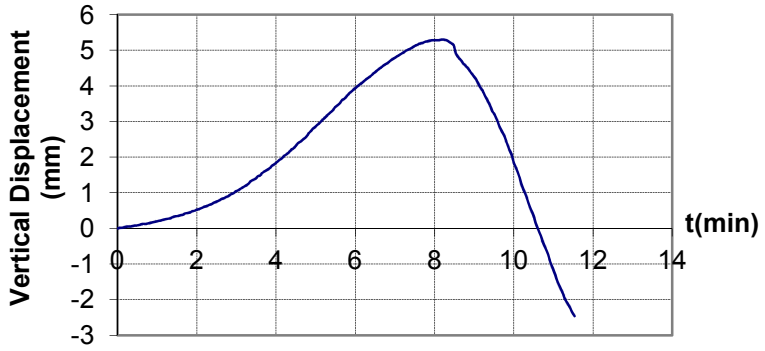

Figure E.1.7 – Evolution of the vertical displacement of column of test HEA160-K13-L70

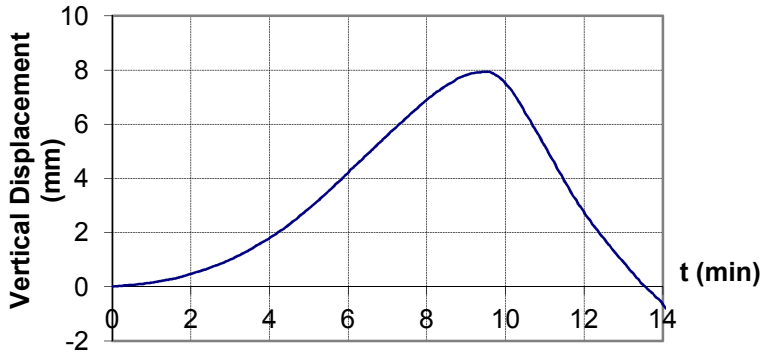

Figure E.1.8 – Evolution of the vertical displacement of column of test HEA160-K13-L30

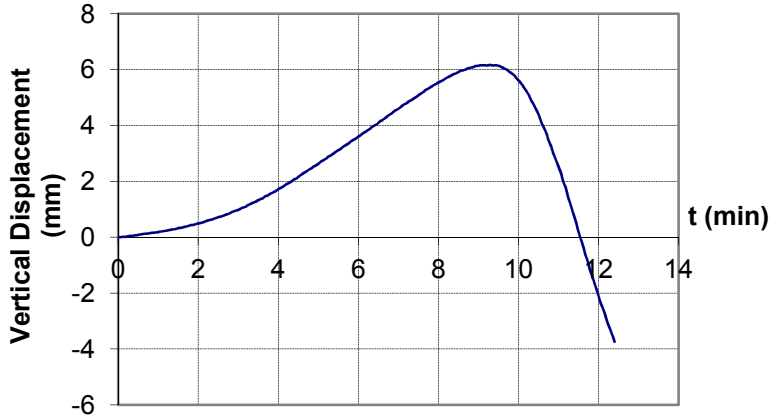

Figure E.1.9 – Evolution of the vertical displacement of column of test HEA200-K13-L70

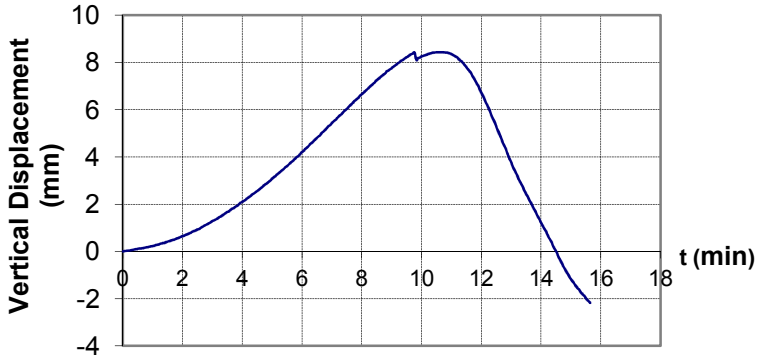

Figure E.1.10 – Evolution of the vertical displacement of column of test HEA200-K45-L30

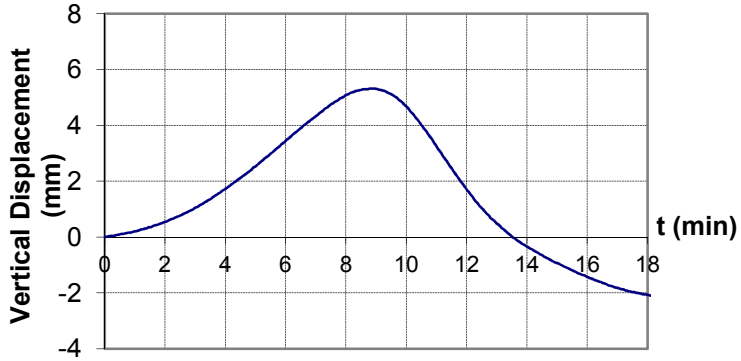

Figure E.1.11 – Evolution of the vertical displacement of column of test HEA200-K128-L30

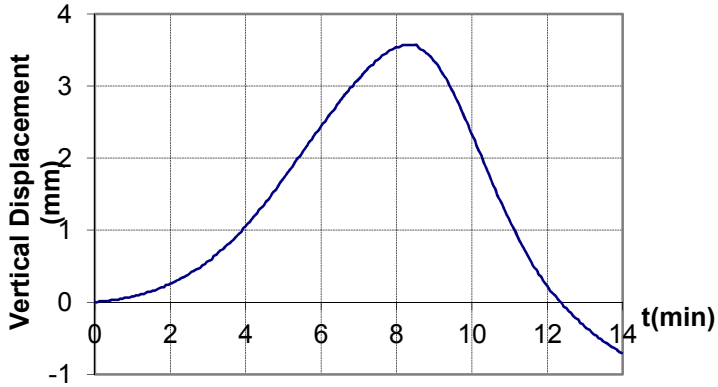

Figure E.1.12 – Evolution of the vertical displacement of column of test HEA160-K128-L30

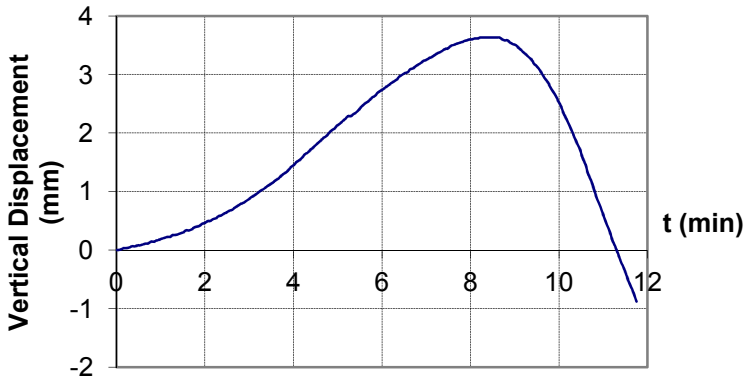

Figure E.1.13 – Evolution of the vertical displacement of column of test HEA200-K128-L70

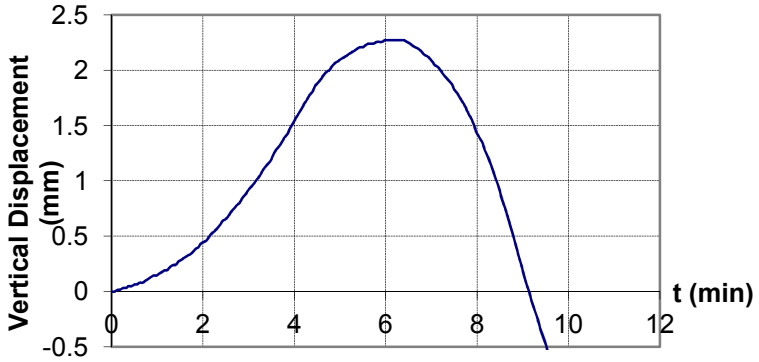

Figure E.1.14 – Evolution of the vertical displacement of column of test HEA160-K128-L70

E.2 – Composite steel-concrete columns

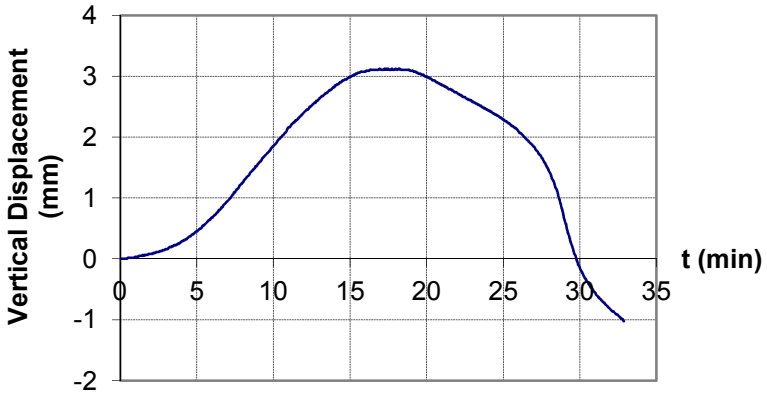

Figure E.2.1 – Evolution of the vertical displacement of column of test CSC160-K128-L30

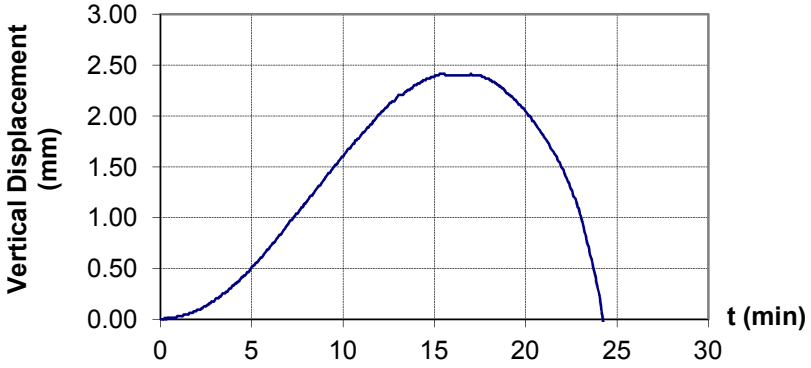

Figure E.2.2 – Evolution of the vertical displacement of column of test CSC160-K128-L70

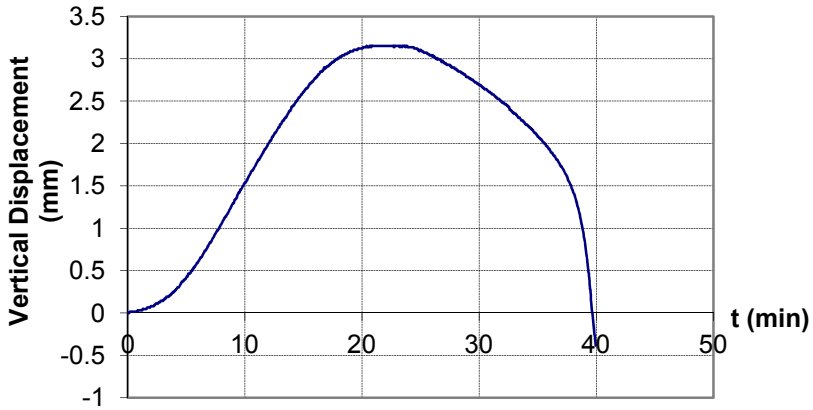

Figure E.2.3 – Evolution of the vertical displacement of column of test CSC200-K128-L30

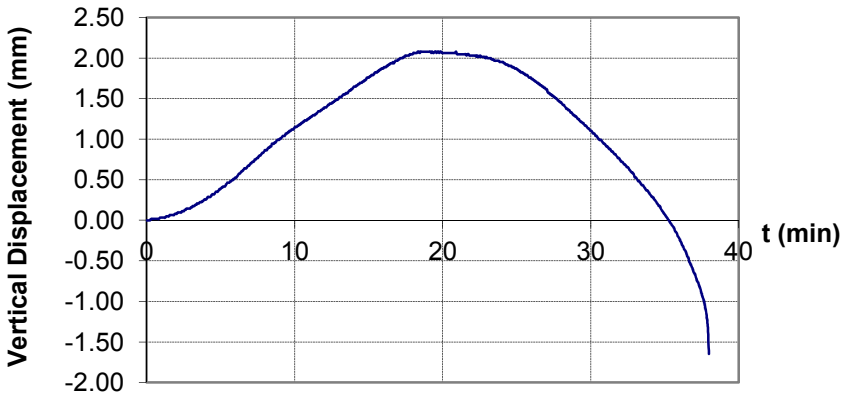

Figure E.2.4 – Evolution of the vertical displacement of column of test CSC200-K128-L70

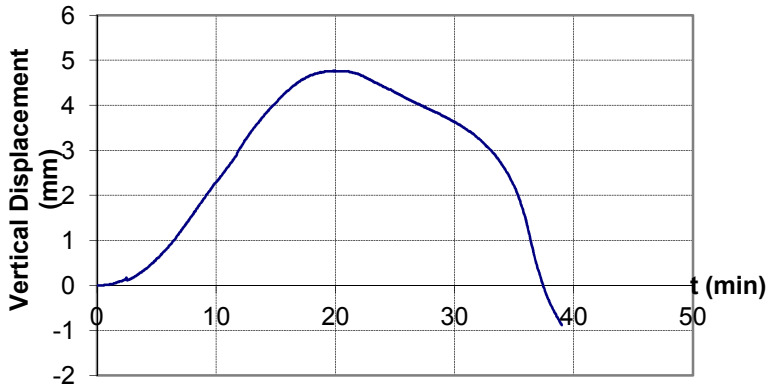

Figure E.2.5 – Evolution of the vertical displacement of column of test CSC160-K45-L30

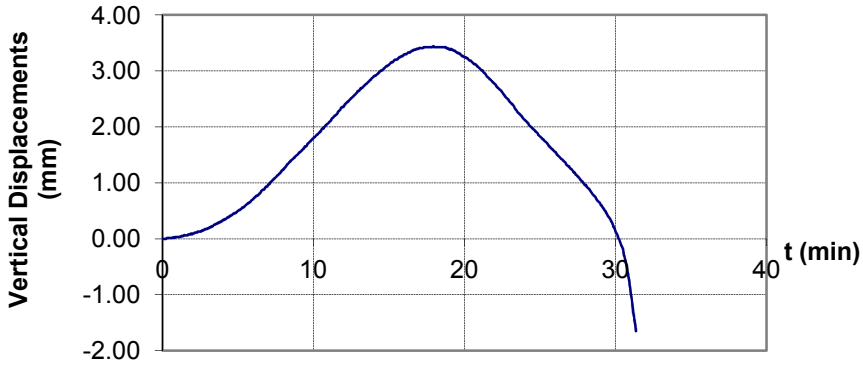

Figure E.2.6 – Evolution of the vertical displacement of column of test CSC160-K45-L70

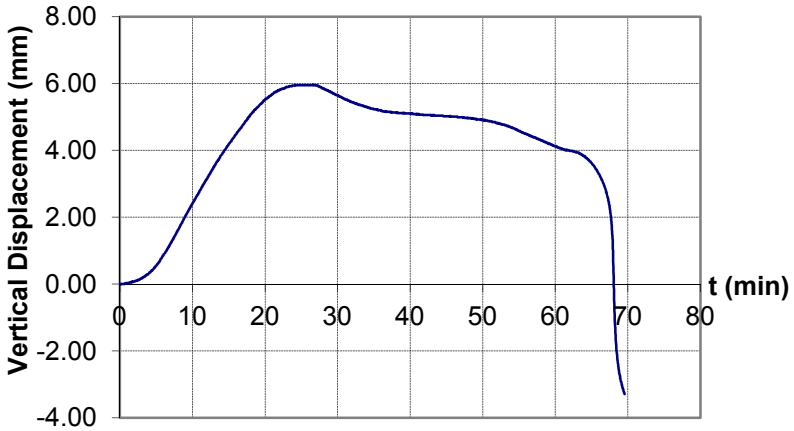

Figure E.2.7 – Evolution of the vertical displacement of column of test CSC200-K45-L30

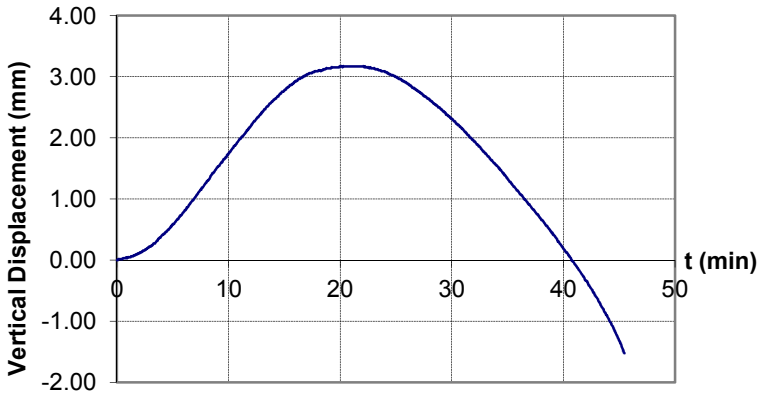

Figure E.2.8 – Evolution of the vertical displacement of column of test CSC200-K45-L70

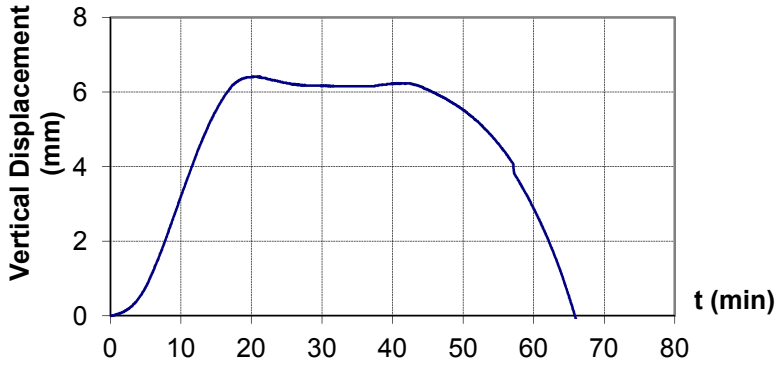

Figure E.2.9 – Evolution of the vertical displacement of column of test CSC160-K13-L30

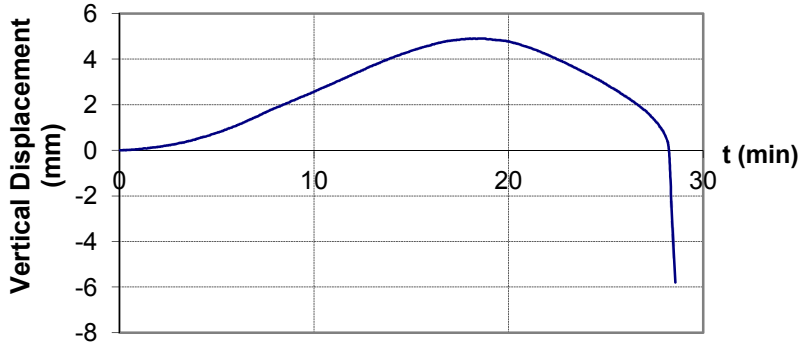

Figure E.2.10 – Evolution of the vertical displacement of column of test CSC160-K13-L70

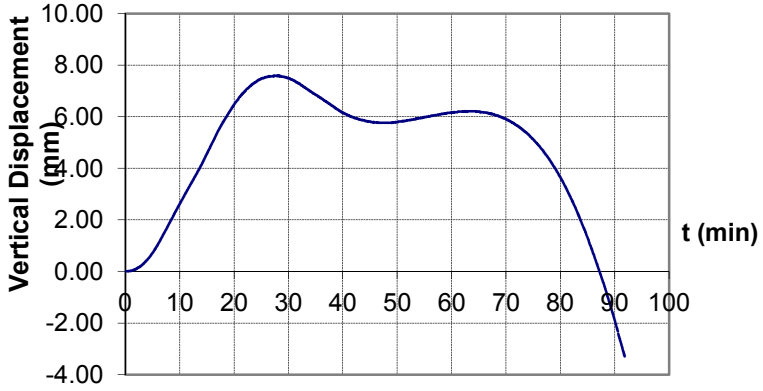

Figure E.2.11 – Evolution of the vertical displacement of column of test CSC200-K13-L30

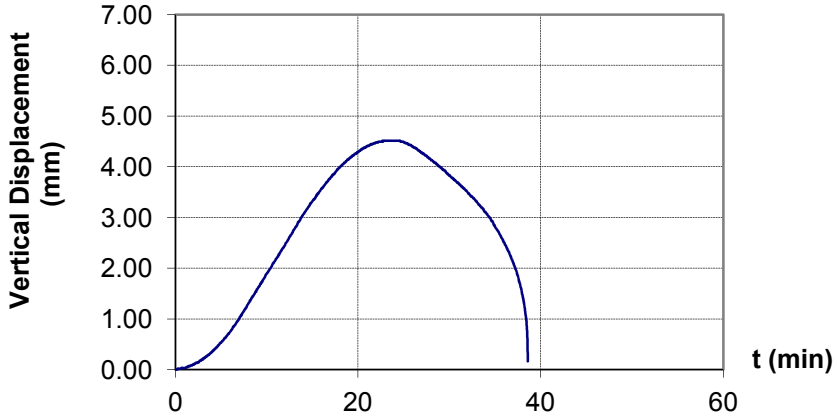

Figure E.2.12 – Evolution of the vertical displacement of column of test CSC200-K13-L70

APPENDIX F – Lateral deflections in the experimental tests

F.1– Steel bare columns

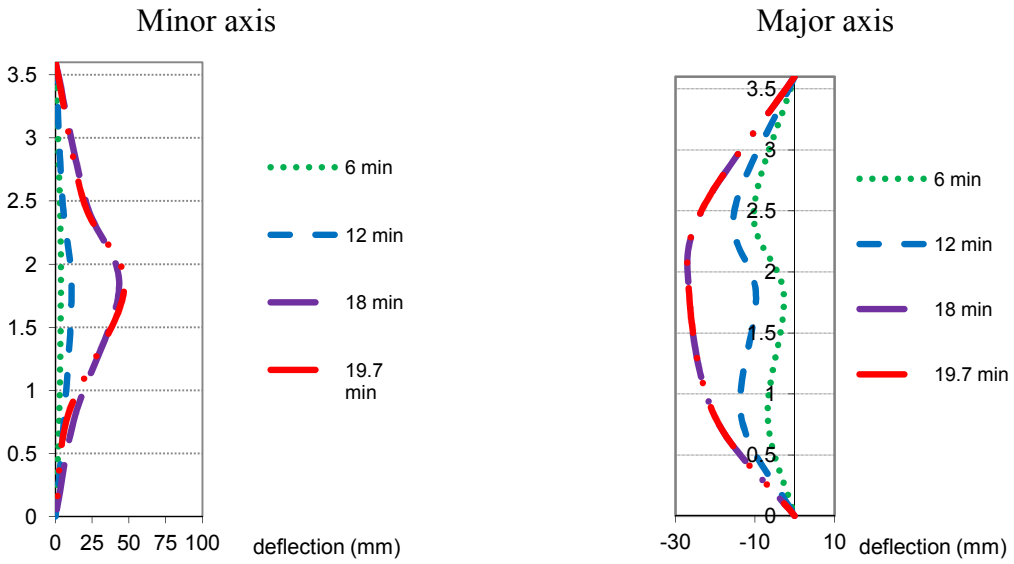

Figure F.1.1 – Evolution of the lateral deflections of column HEA200-K13-L70-E2 around principal axis of inertia.

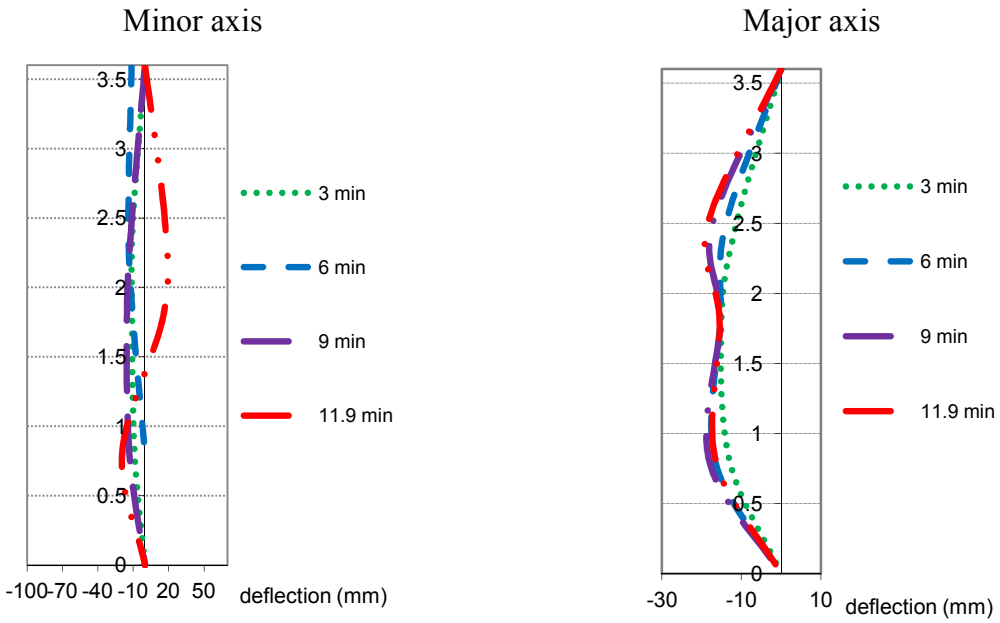

Figure F.1.2 – Evolution of the lateral deflections of column HEA200-K13-L70-E1 around principal axis of inertia

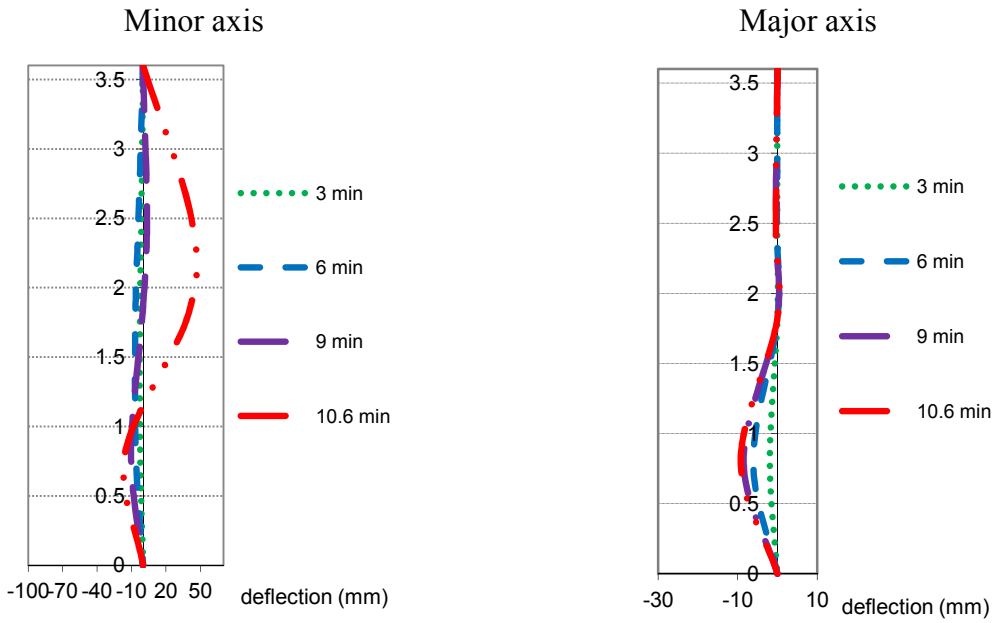

Figure F.1.3 – Evolution of the lateral deflections of column HEA160-K13-L70around principal axis of inertia

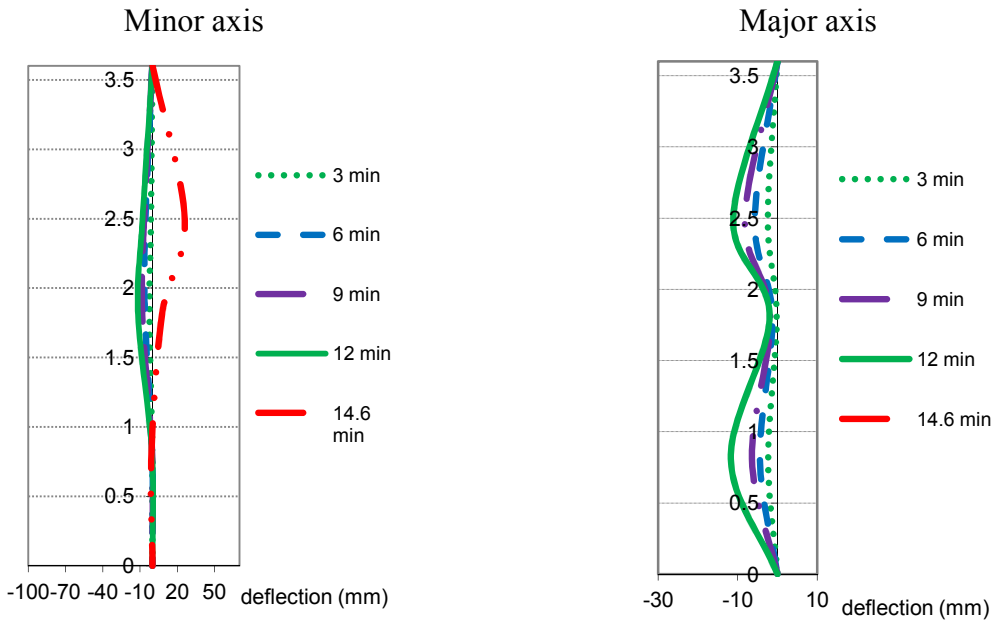

Figure F.1.4 – Evolution of the lateral deflections of column HEA200-K13-L30around principal axis of inertia

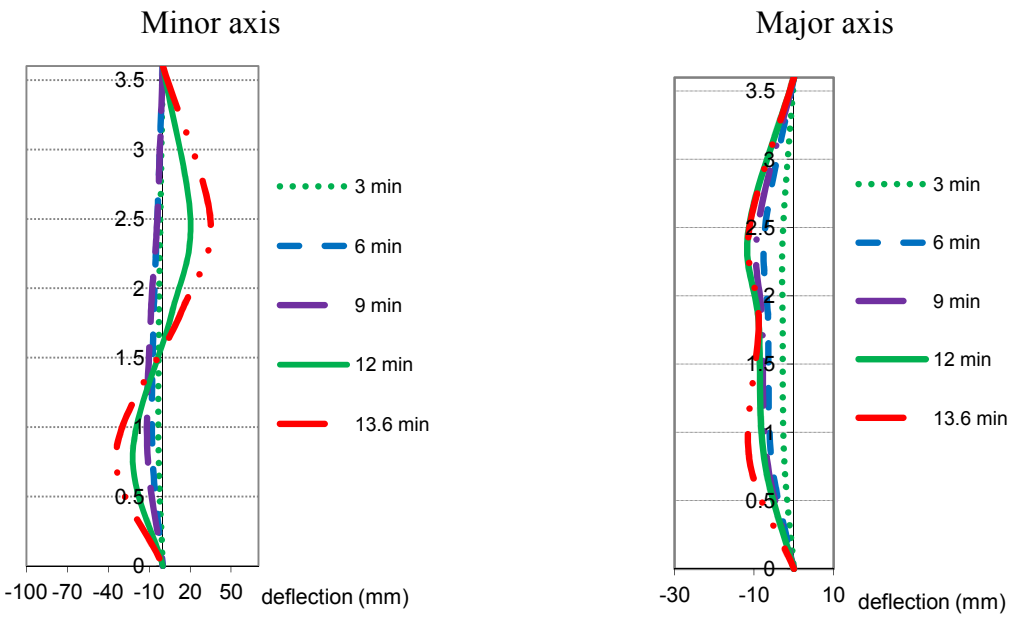

Figure F.1.5 – Evolution of the lateral deflections of column HEA160-K13-L30around principal axis of inertia

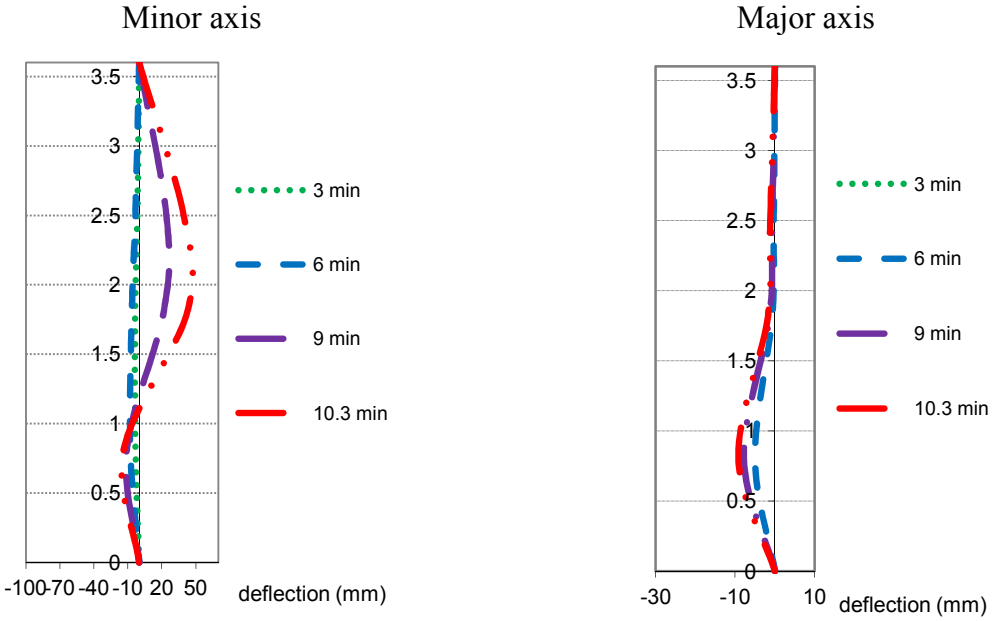

Figure F.1.6 – Evolution of the lateral deflections of column HEA160-K45-L70around principal axis of inertia

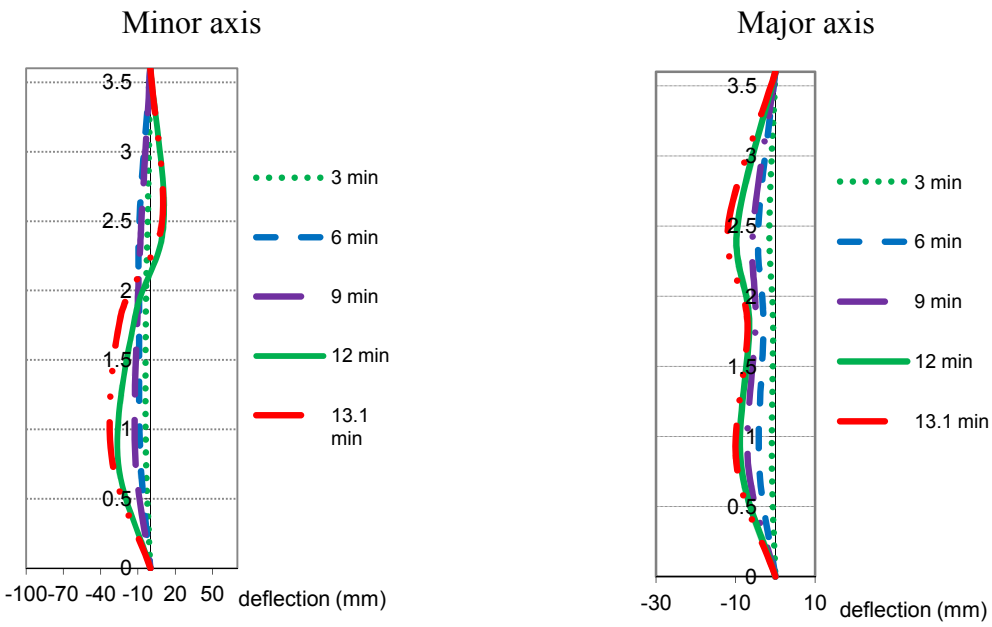

Figure F.1.7 – Evolution of the lateral deflections of column HEA160-K45-L30 around principal axis of inertia

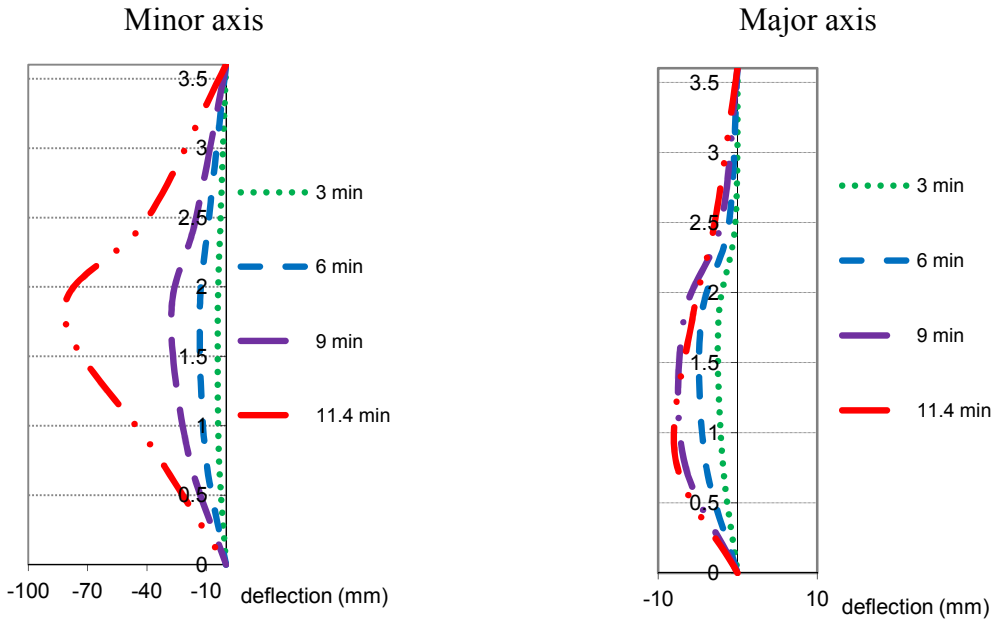

Figure F.1.8 – Evolution of the lateral deflections of column HEA200-K45-L70 around principal axis of inertia

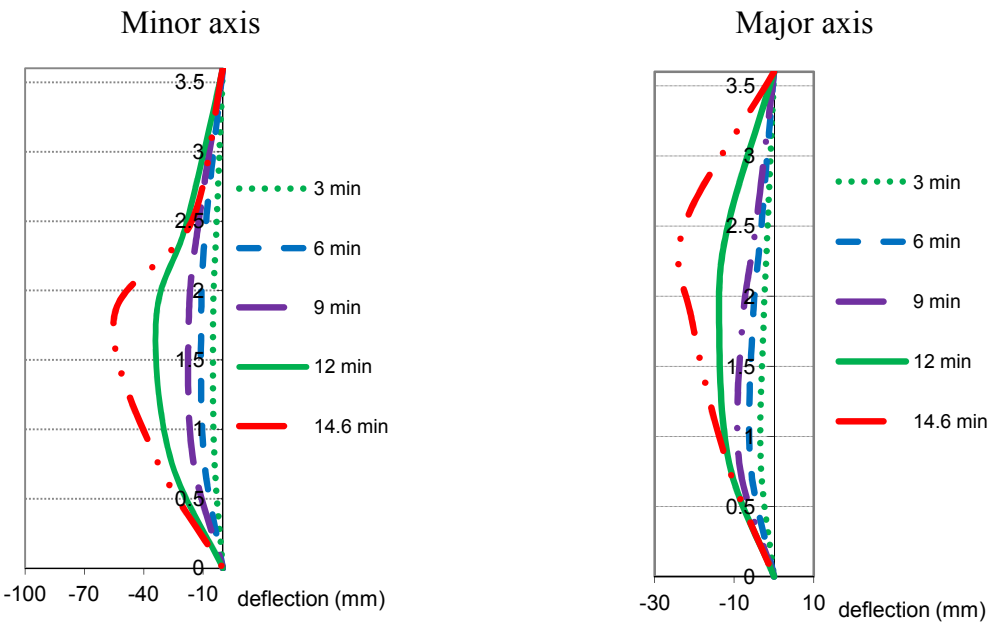

Figure F.1.9 – Evolution of the lateral deflections of column HEA200-K45-L30around principal axis of inertia

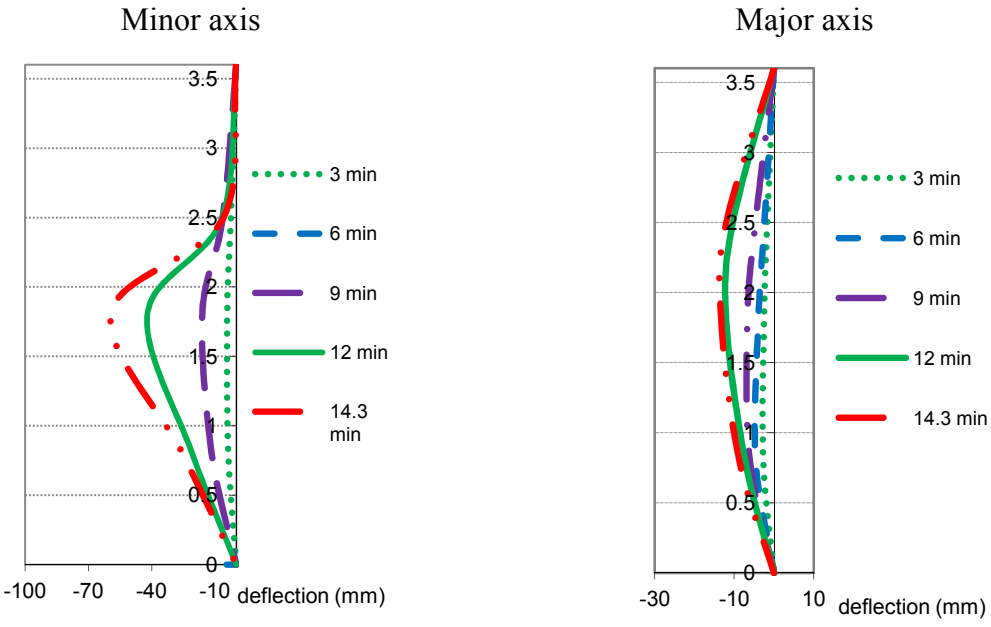

Figure F.1.10 – Evolution of the lateral deflections of column HEA200-K128-L30around principal axis of inertia

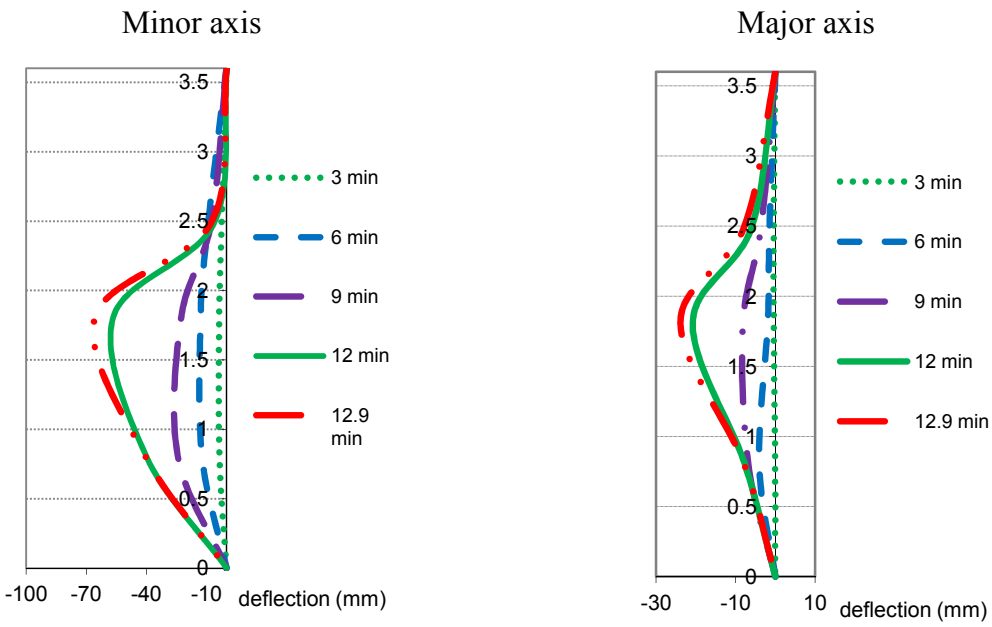

Figure F.1.11 – Evolution of the lateral deflections of column HEA160-K128-L30around principal axis of inertia

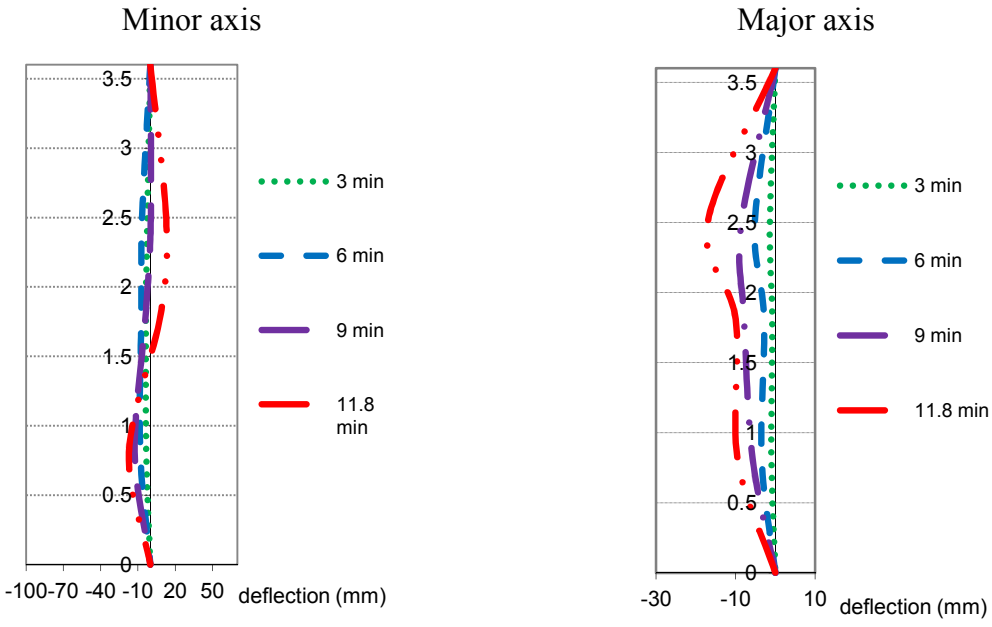

Figure F.1.12 – Evolution of the lateral deflections of column HEA200-K128-L70around principal axis of inertia

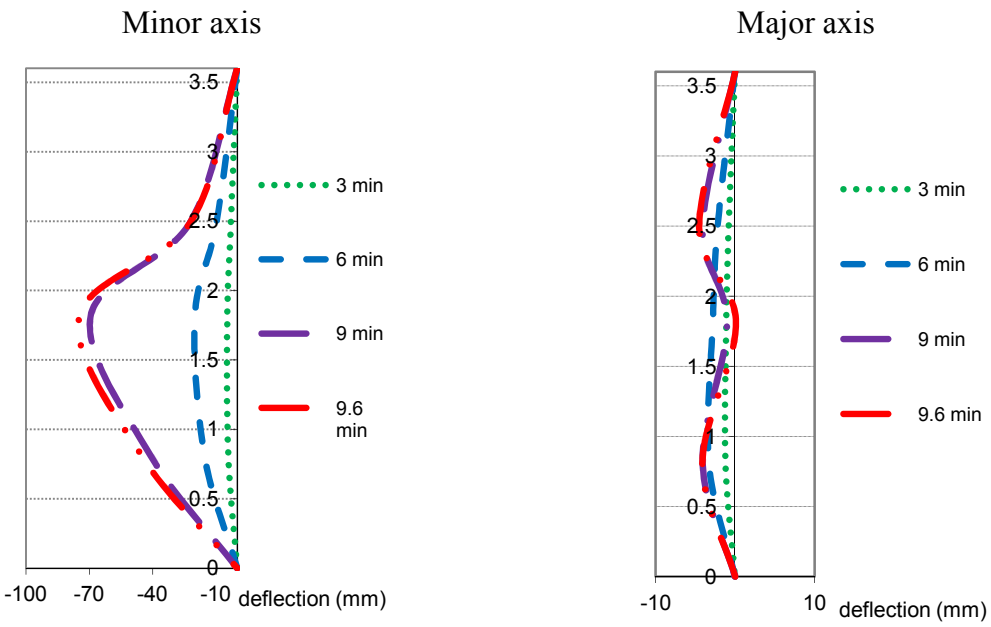

Figure F.1.13 – Evolution of the lateral deflections of column HEA160-K128-L70around principal axis of inertia

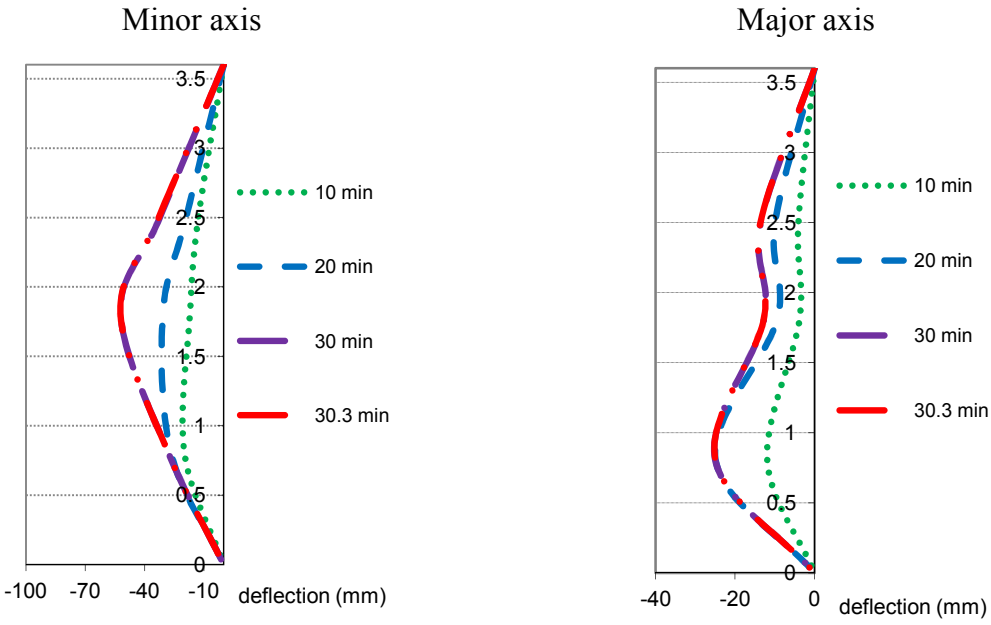

Figure F.1.14 – Evolution of the lateral deflections of column oCSC160-K128-L30 around principal axis of inertia

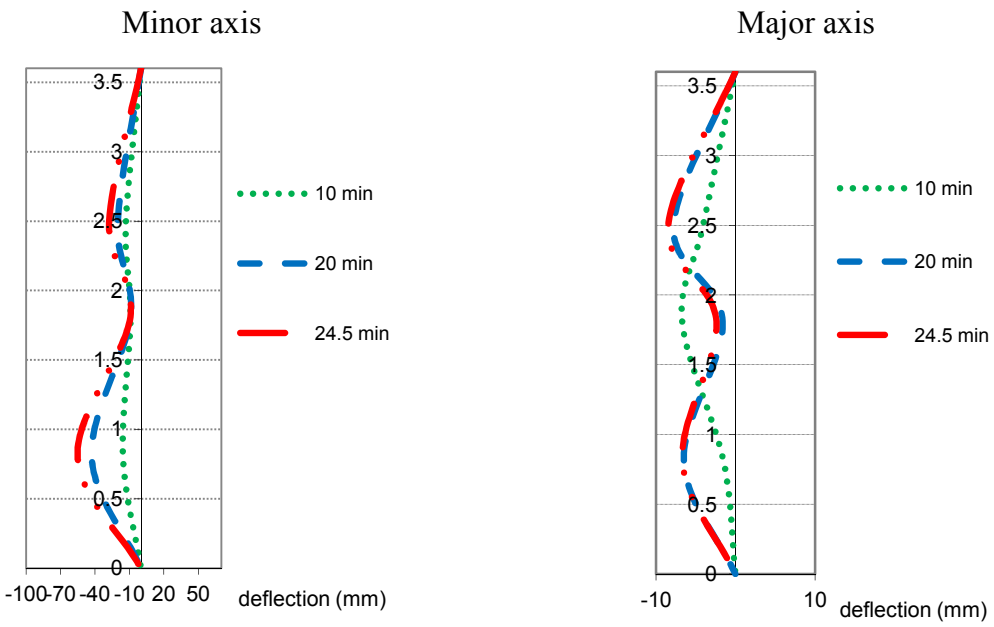

Figure F.15 – Evolution of the lateral deflections of column CSC160-K128-L70around principal axis of inertia

F.2 – Composite steel-concrete columns

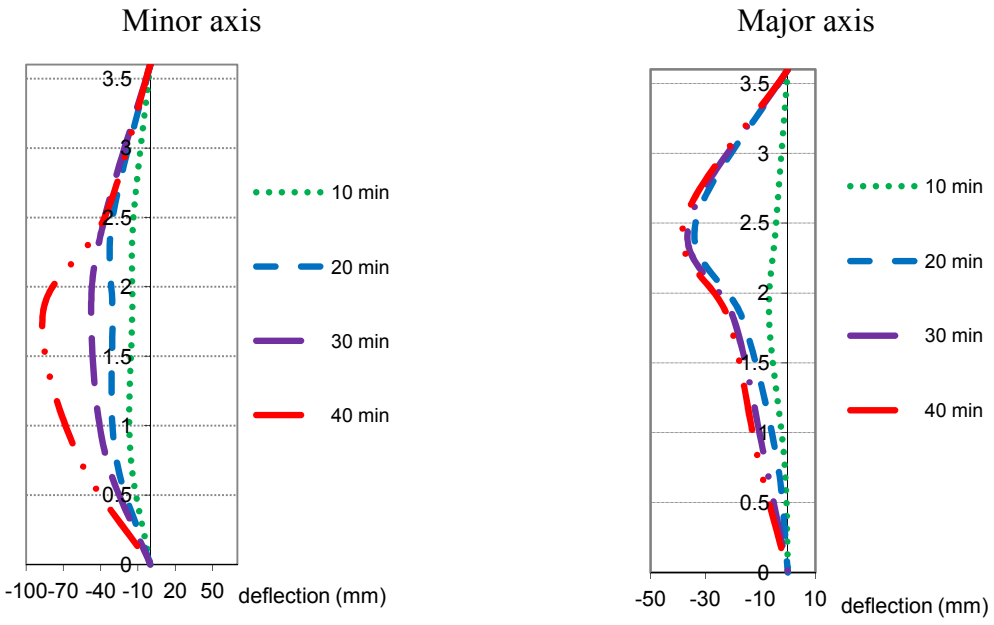

Figure F.2.1 – Evolution of the lateral deflections of column CSC200-K128-L30around principal axis of inertia

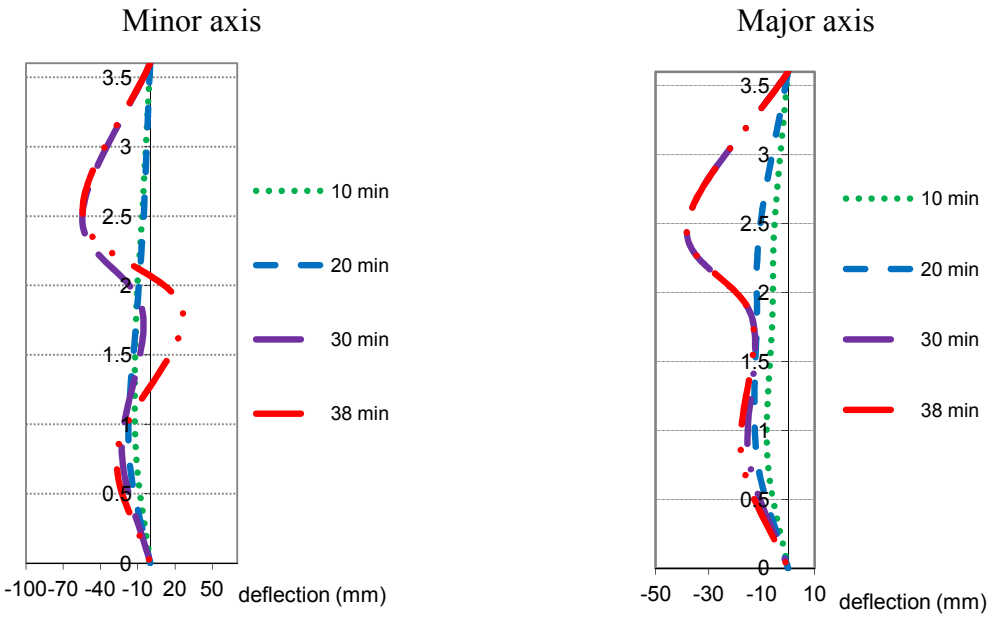

Figure F.2.2 – Evolution of the lateral deflections of column CSC200-K128-L70around principal axis of inertia

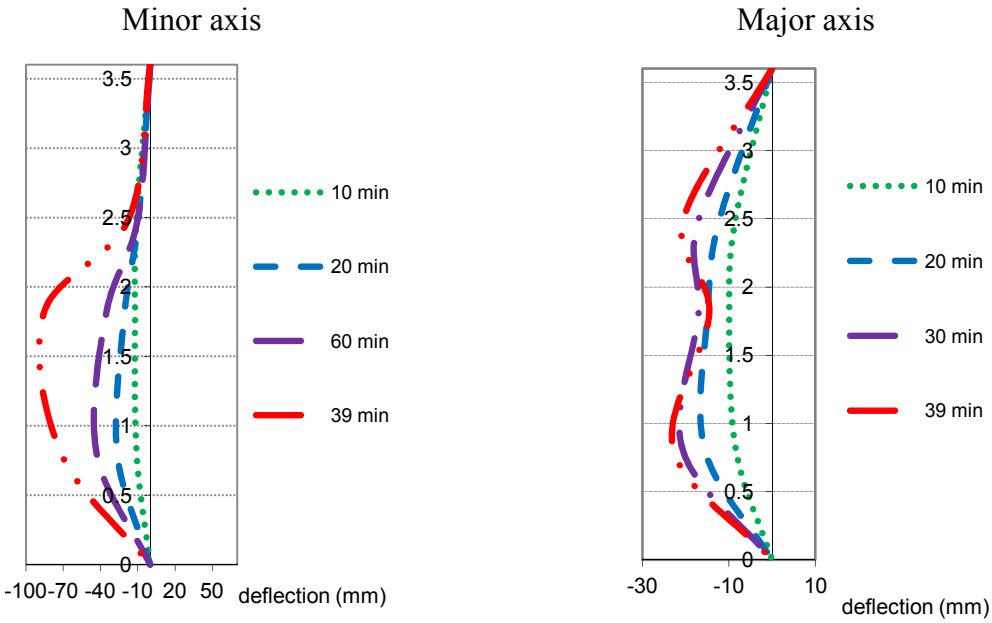

Figure F.2.3 – Evolution of the lateral deflections of column CSC160-K45-L30around principal axis of inertia

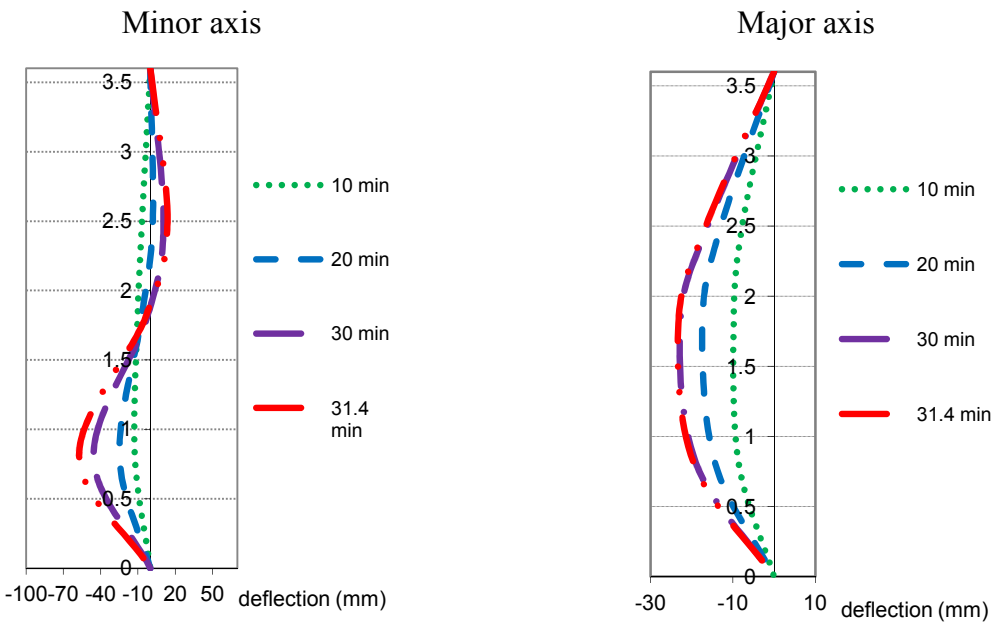

Figure F.2.4 – Evolution of the lateral deflections of column CSC160-K45-L70around principal axis of inertia

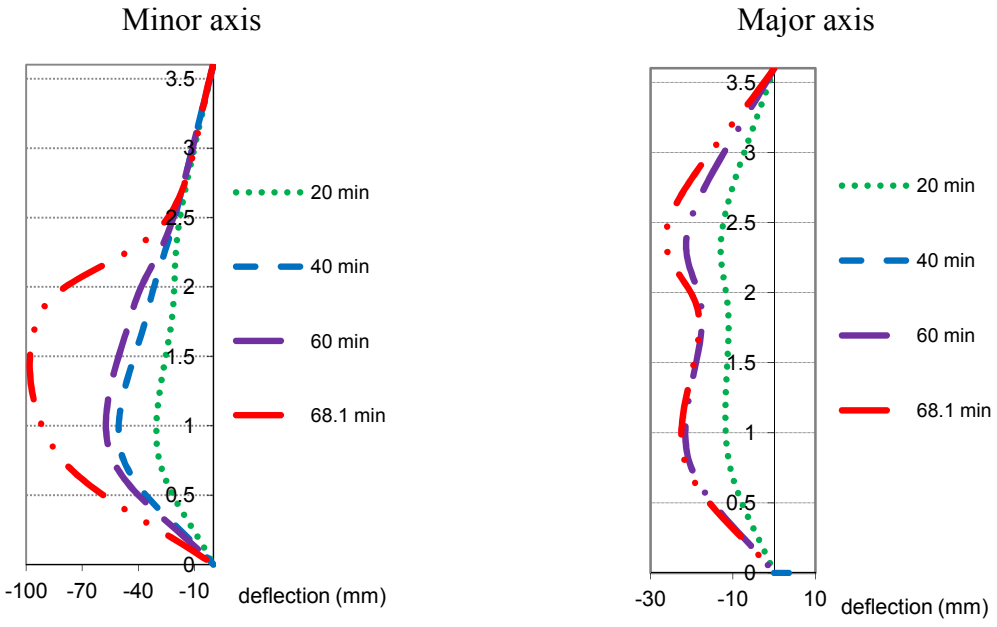

Figure F.2.5 – Evolution of the lateral deflections of column CSC200-K45-L30 around principal axis of inertia

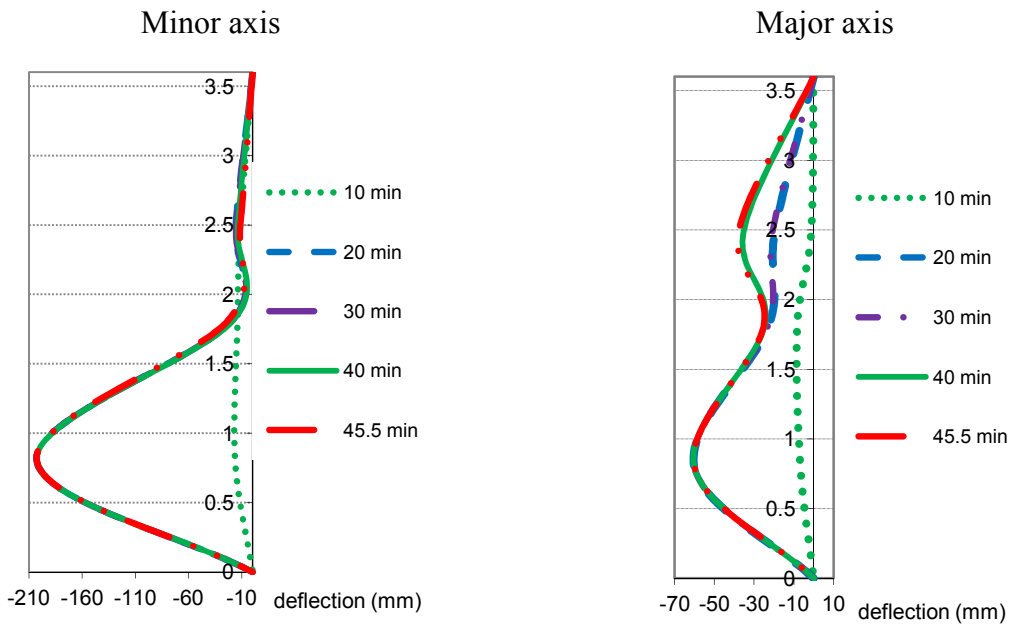

Figure F.2.6 – Evolution of the lateral deflections of column CSC200-K45-L70around principal axis of inertia

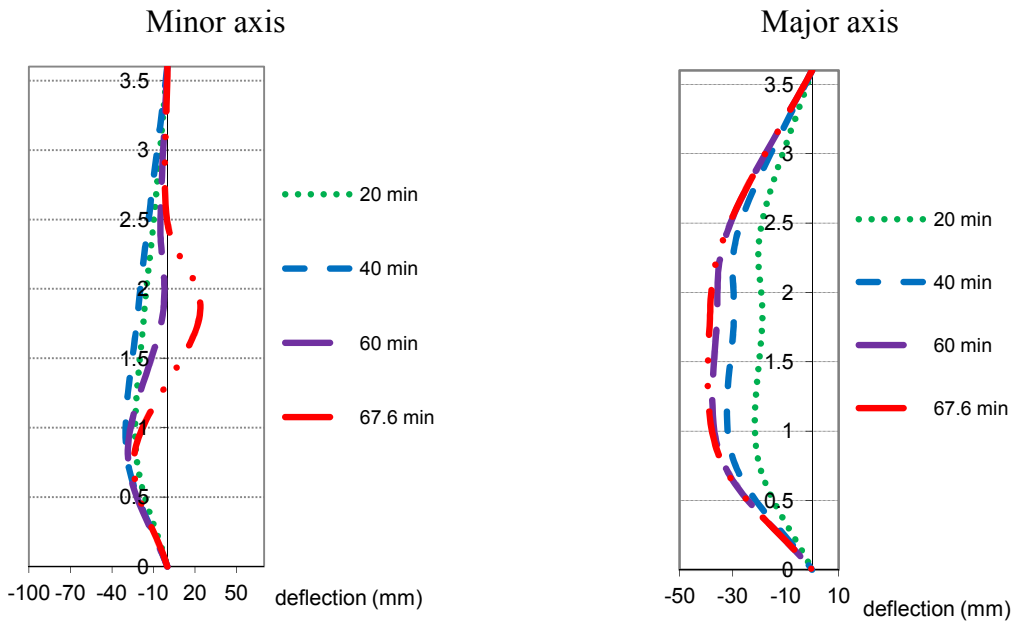

Figure F.2.7 – Evolution of the lateral deflections of column CSC160-K13-L30around principal axis of inertia

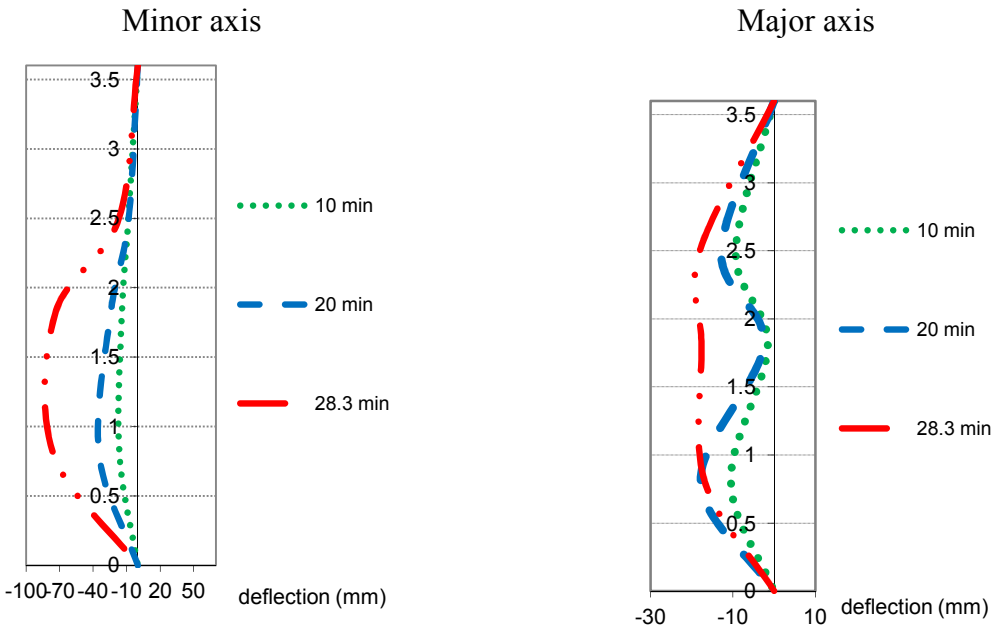

Figure F.2.8 – Evolution of the lateral deflections of column CSC160-K13-L70around principal axis of inertia

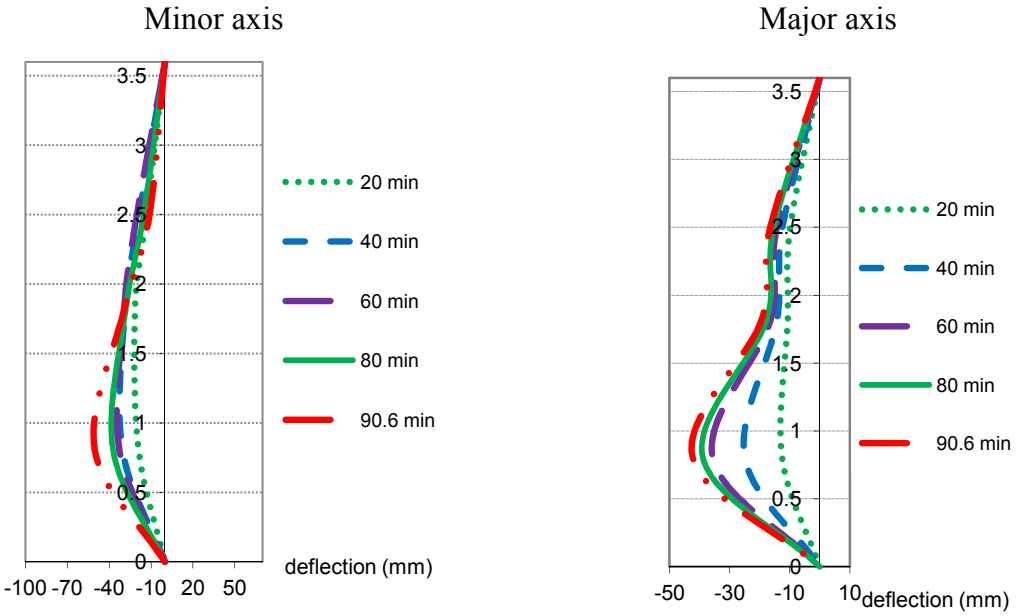

Figure F.2.9 – Evolution of the lateral deflections of column CSC200-K13-L30around minor and major axis

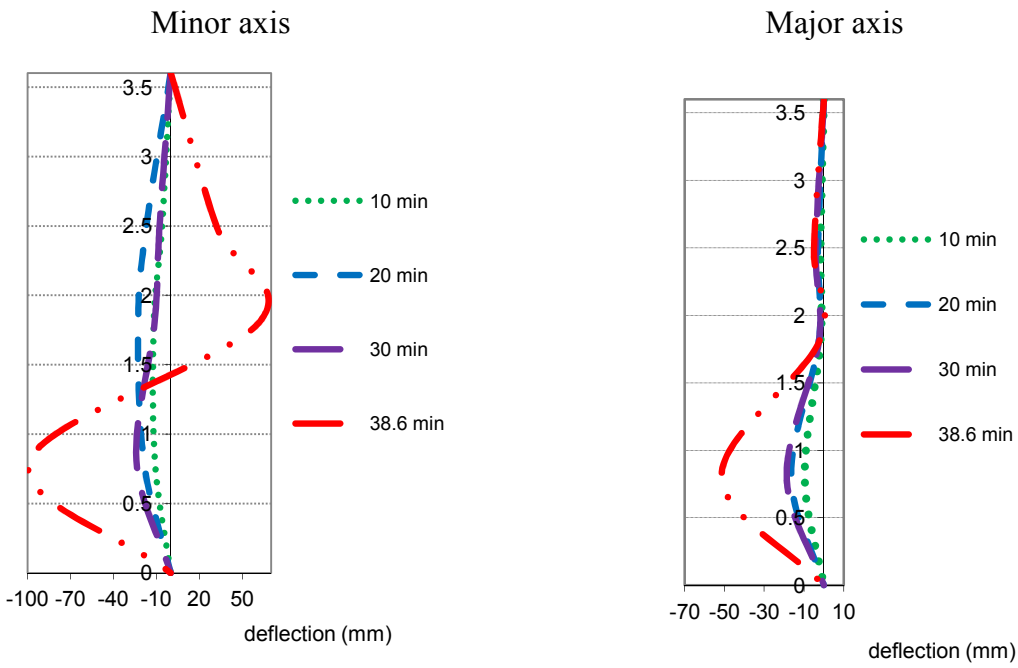

Figure F.2.10 – Evolution of the lateral deflections of column CSC200-K13-L70 around minor and major axis

APPENDIX G – Comparison of the restraining forces between experimental tests and numerical simulations

G.1– Steel bare columns

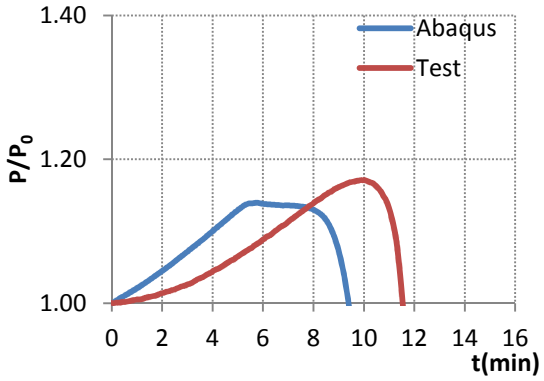

Figure G.1.1 – Comparison of restraining forces betweentests and numerical simulations for column HEA200-K13-L70

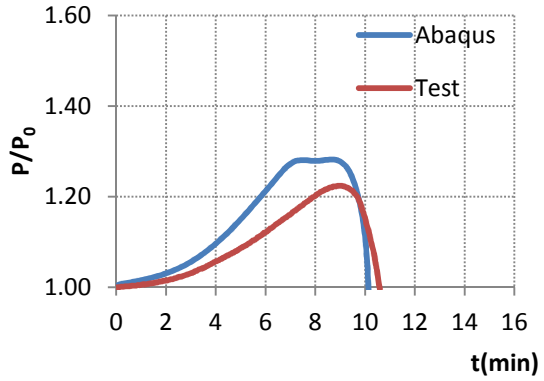

Figure G.1.2 – Comparison of restraining forces between tests and numerical simulations for column HEA160-K13-L70

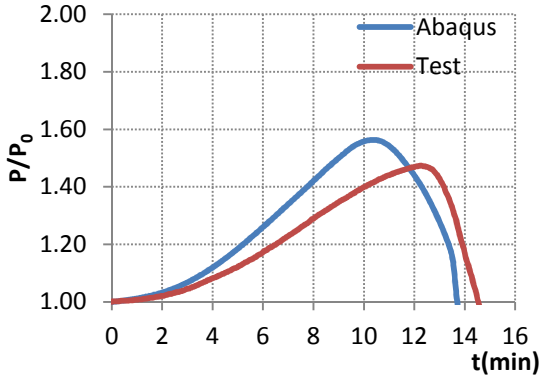

Figure G.1.3 – Comparison of restraining forces betweentests and numerical simulations for column HEA200-K13-L30

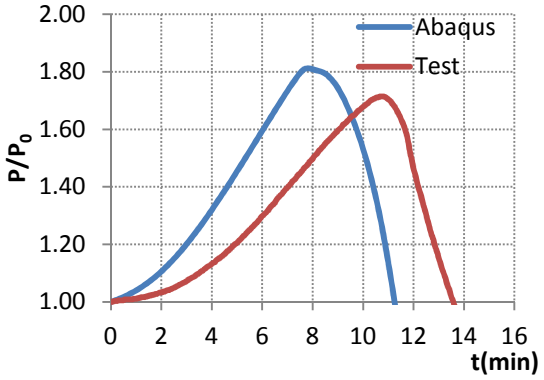

Figure G.1.4 – Comparison of restraining forces between tests and numerical simulations for columnHEA160-K13-L30

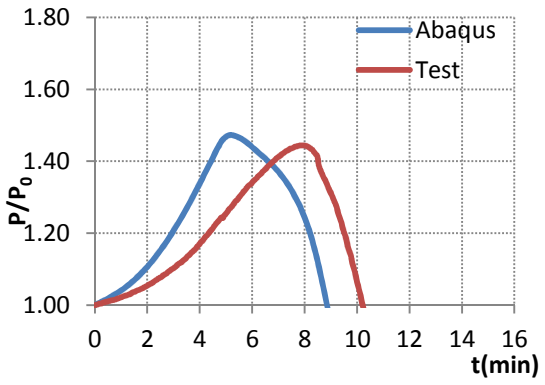

Figure G.1.5 – Comparison of restraining forces between tests and numerical simulations for column HEA160-K45-L70

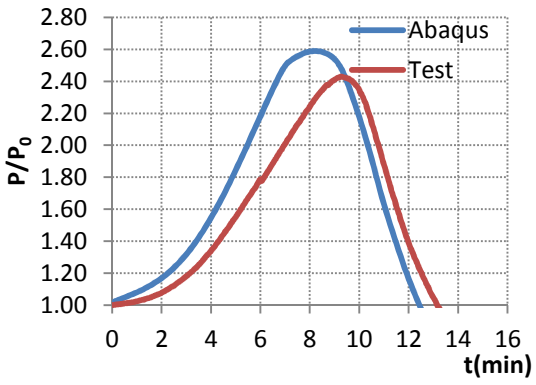

Figure G.1.6 – Comparison of restraining forces between tests and numerical simulations for column HEA160-K45-L30

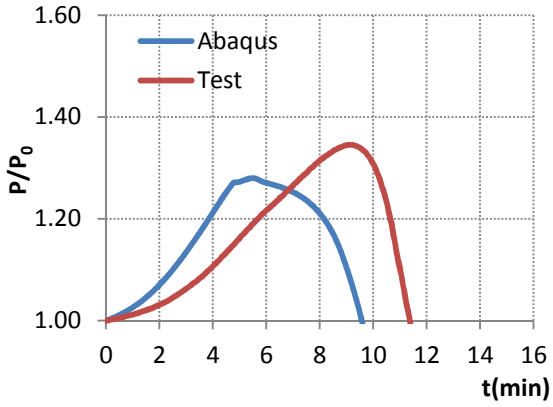

Figure G.1.7 – Comparison of restraining forces between tests and numerical simulations for column HEA200-K45-L70

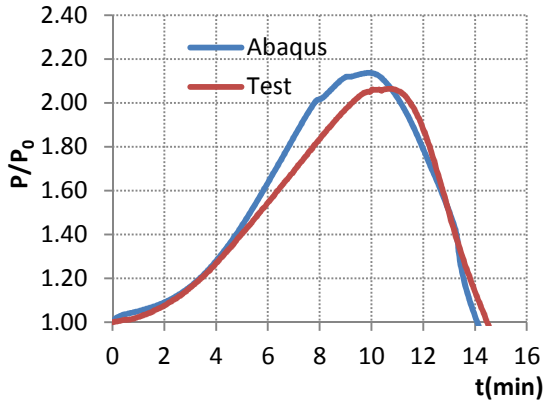

Figure G.1.8 – Comparison of restraining forces between tests and numerical simulations for column HEA200-K45-L30

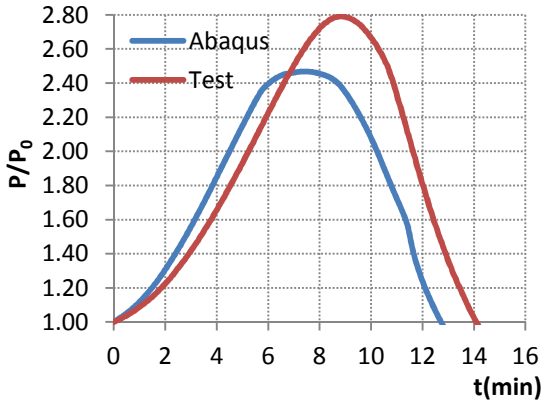

Figure G.1.9 – Comparison of restraining forces between tests and numerical simulations for column HEA200-K128-L30

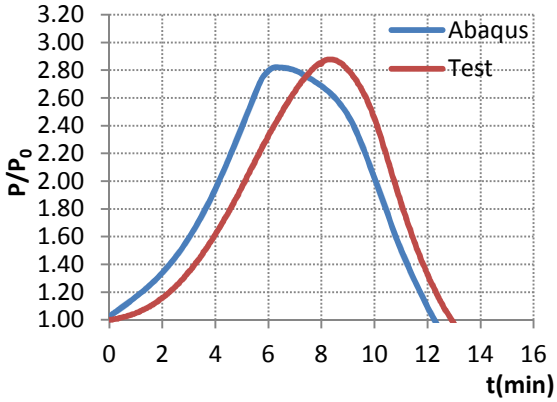

Figure G.1.10 – Comparison of restraining forces between tests and numerical simulations for column HEA160-K128-L30

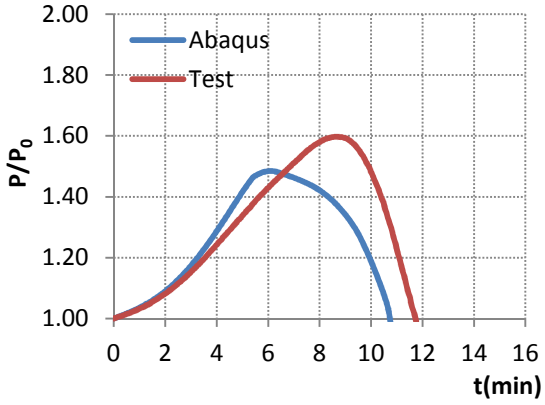

Figure G.1.11 – Comparison of restraining forces between tests and numerical simulations for column HEA200-K128-L70

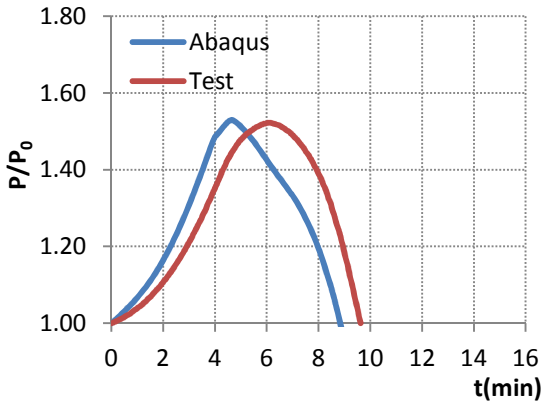

Figure G.1.12 – Comparison of restraining forces between tests and numerical simulations for column HEA160-K128-L70

G.2 – Composite steel-concrete columns

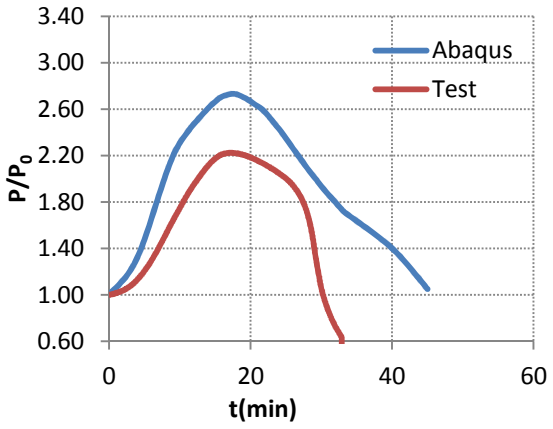

Figure G.2.1 – Comparison of restraining forces between tests and numerical simulations for column CSC160-K128-L30

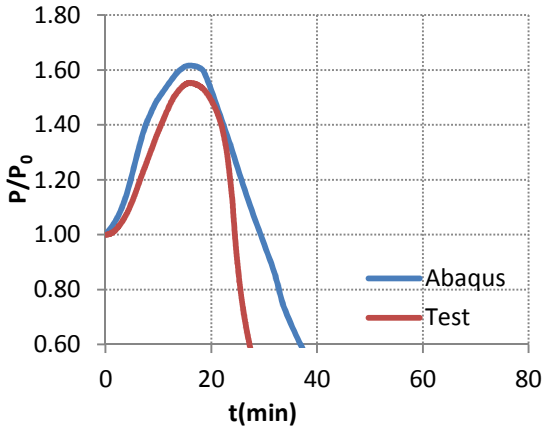

Figure G.2.2 – Comparison of restraining forces between tests and numerical simulations for column CSC160-K128-L70

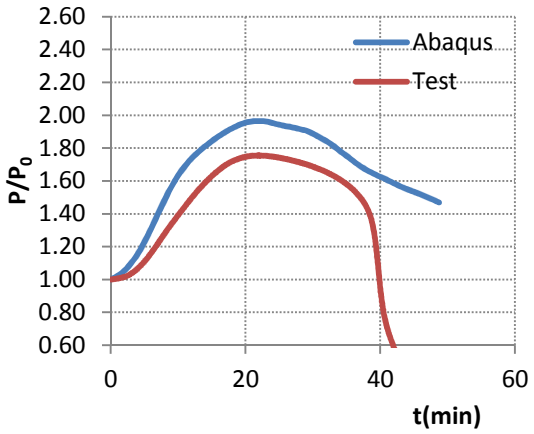

Figure G.2.3 – Comparison of restraining forces between tests and numerical simulations for column CSC200-K128-L30

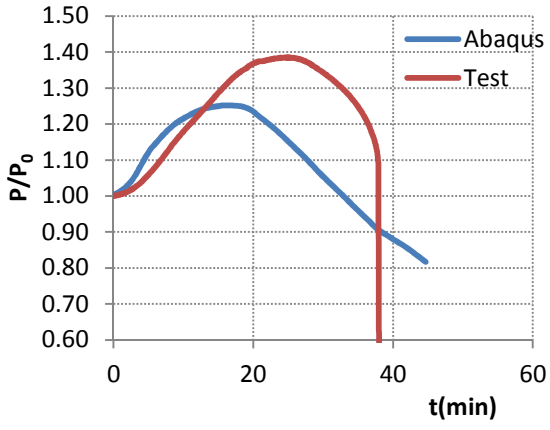

Figure G.2.4 – Comparison of restraining forces between tests and numerical simulations for column CSC200-K128-L70

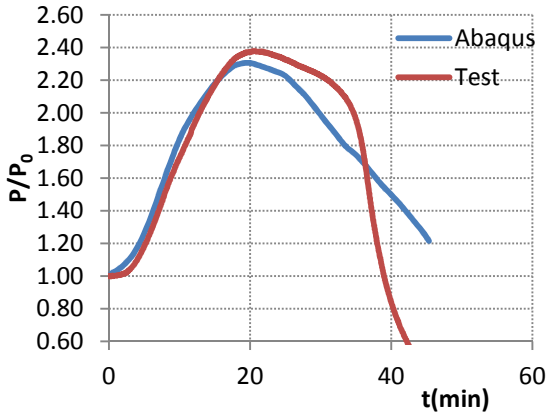

Figure G.2.5 – Comparison of restraining forces between tests and numerical simulations for column CSC160-K45-L30

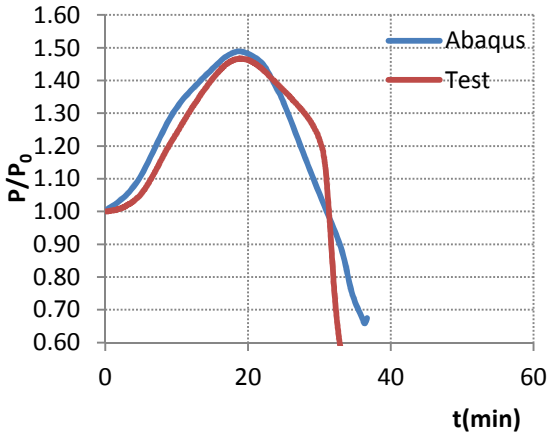

Figure G.2.6 – Comparison of restraining forces between tests and numerical simulations for column CSC160-K45-L70

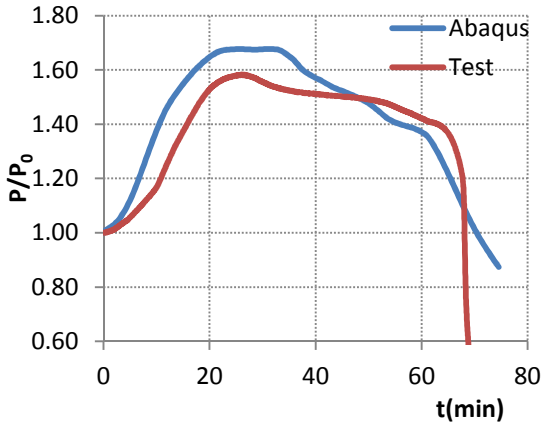

Figure G.2.7 – Comparison of restraining forces between tests and numerical simulations for column CSC200-K45-L30

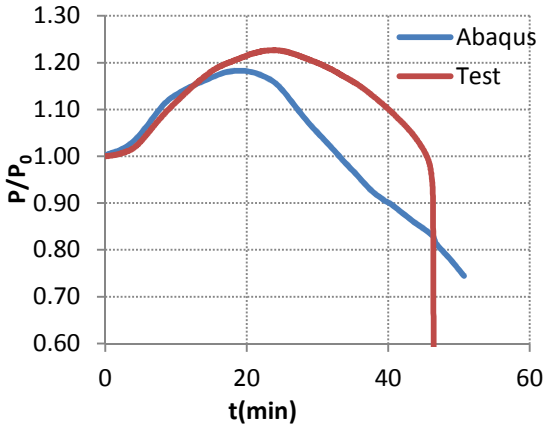

Figure G.2.8 – Comparison of restraining forces between tests and numerical simulations for column CSC200-K45-L70

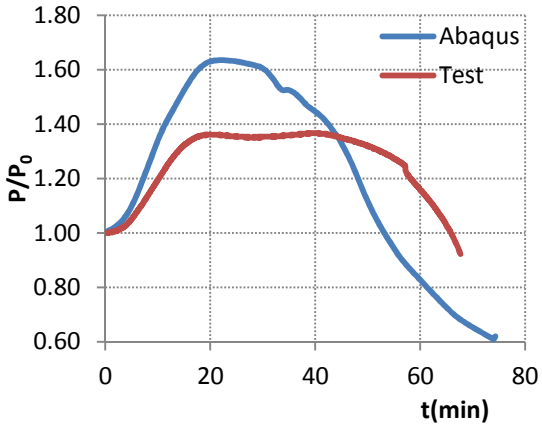

Figure G.2.9 – Comparison of restraining forces between tests and numerical simulations for column CSC160-K13-L30

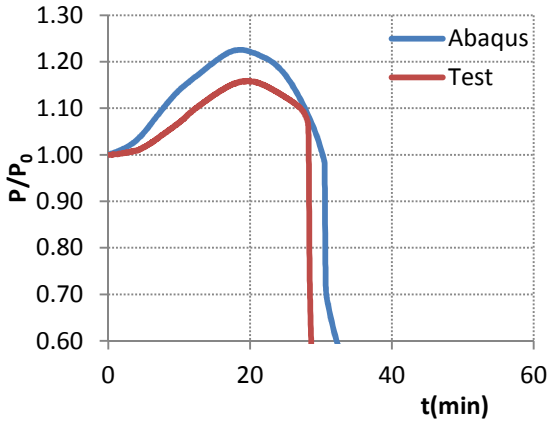

Figure G.2.10 – Comparison of restraining forces between tests and numerical simulations for column CSC160-K13-L70

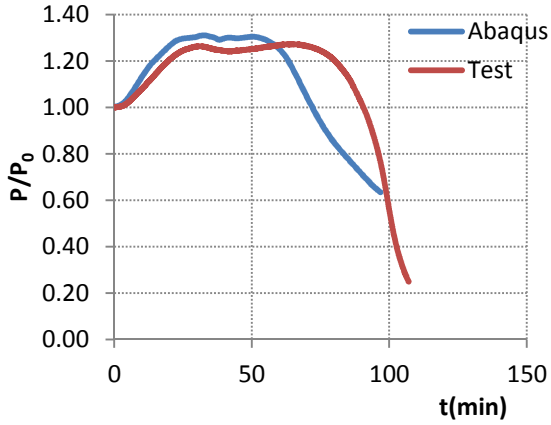

Figure G.2.11 – Comparison of restraining forces between tests and numerical simulations for column CSC200-K13-L30

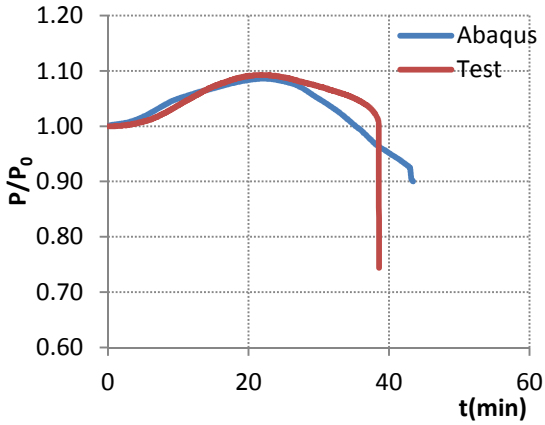

Figure G.2.12 – Comparison of restraining forces between tests and numerical simulations for column CSC200-K13-L70

APPENDIX H – Photos of the experimental tests

H.1 – Columns embedded on walls

Figure H.1.1 – Views of the test E01

Figure H.1.2 – Views of the test E02

Figure H.1.3 – Views of the test E03

Figure H.1.4 – Views of the test E04

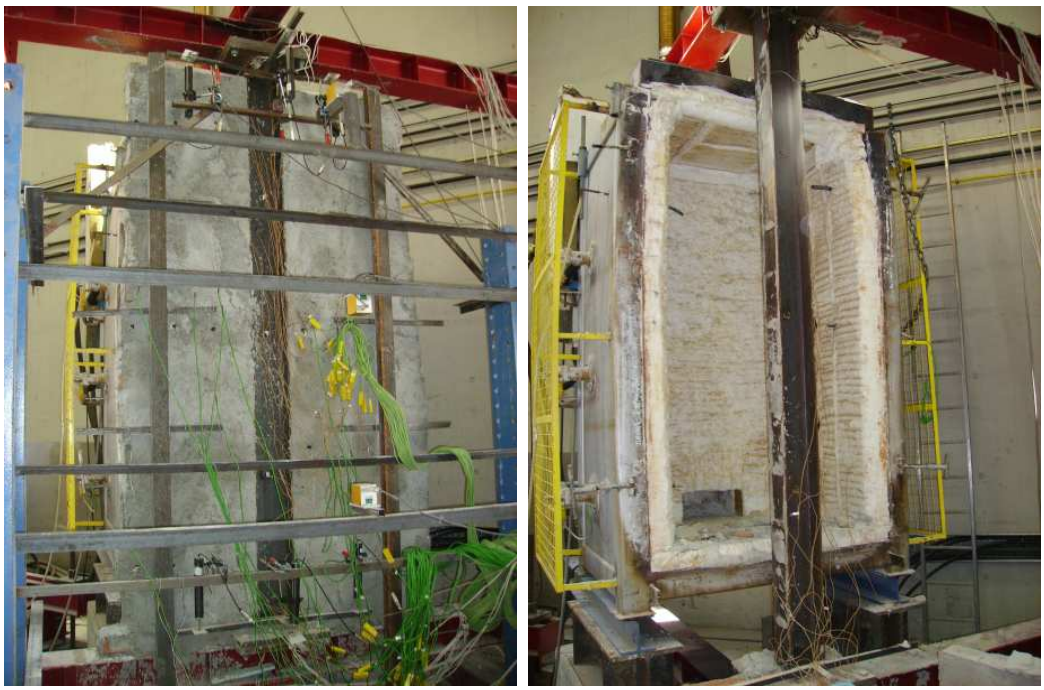

Figure H.1.5 – Views of the test E05

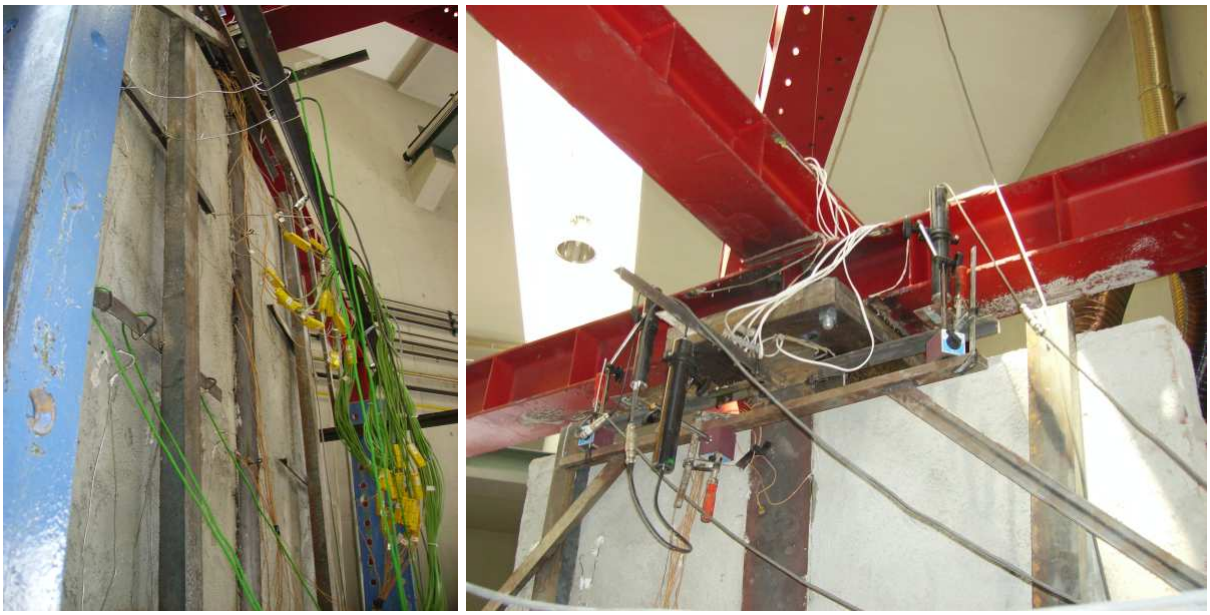

Figure H.1.6 – Views of the test E06

Figure H.1.7 – Views of the test E07

Figure H.1.8 – Views of the test E08

Figure H.1.9 – Views of the test E09

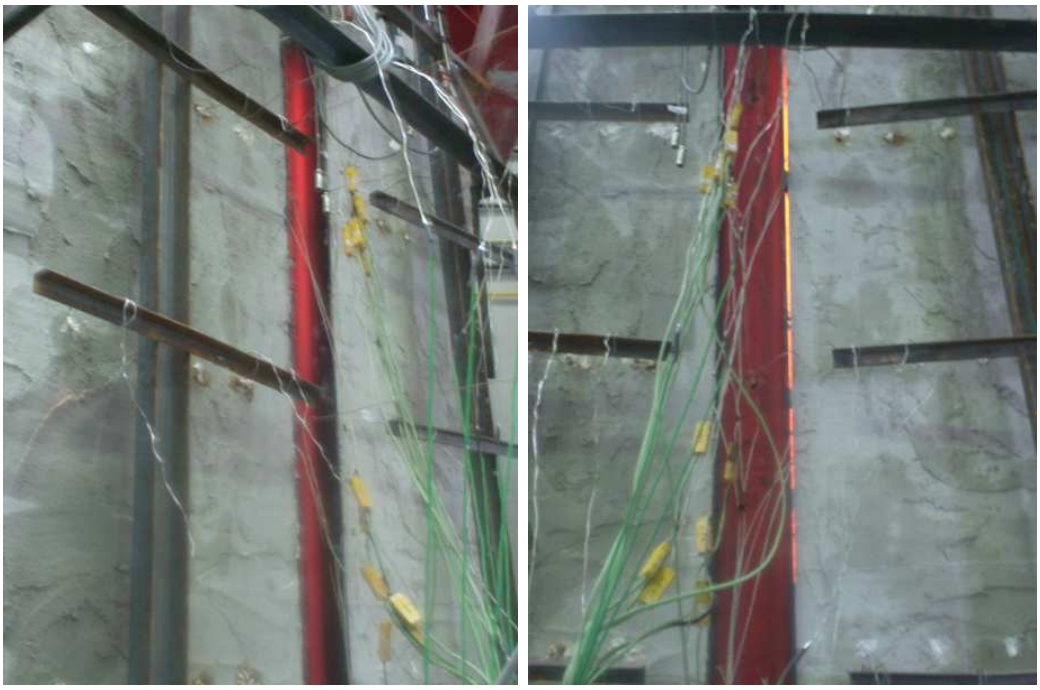

Figure H.1.10 – Views of the test E10

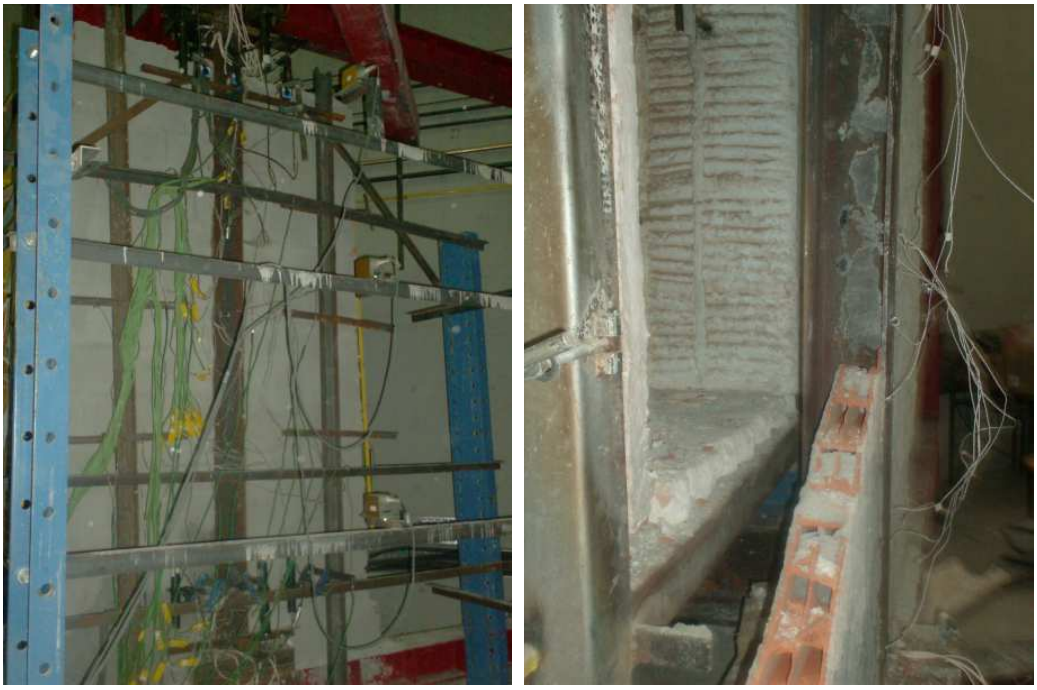

Figure H.1.11 – Views of the test E11

Figure H.1.12 – Views of the test E12

Figure H.1.13 – Views of the test E13

Figure H.1.14 – Views of the test E14

H.2 – Steel bare columns

Figure H.2.1 – Views of the test HEA200-K13-L70

Figure H.2.2 – Views of the test HEA200-K13-L70-E2

Figure H.2.3 – Views of the test HEA200-K13-L70-E1

Figure H.2.4 – Views of the test HEA160-K13-L70

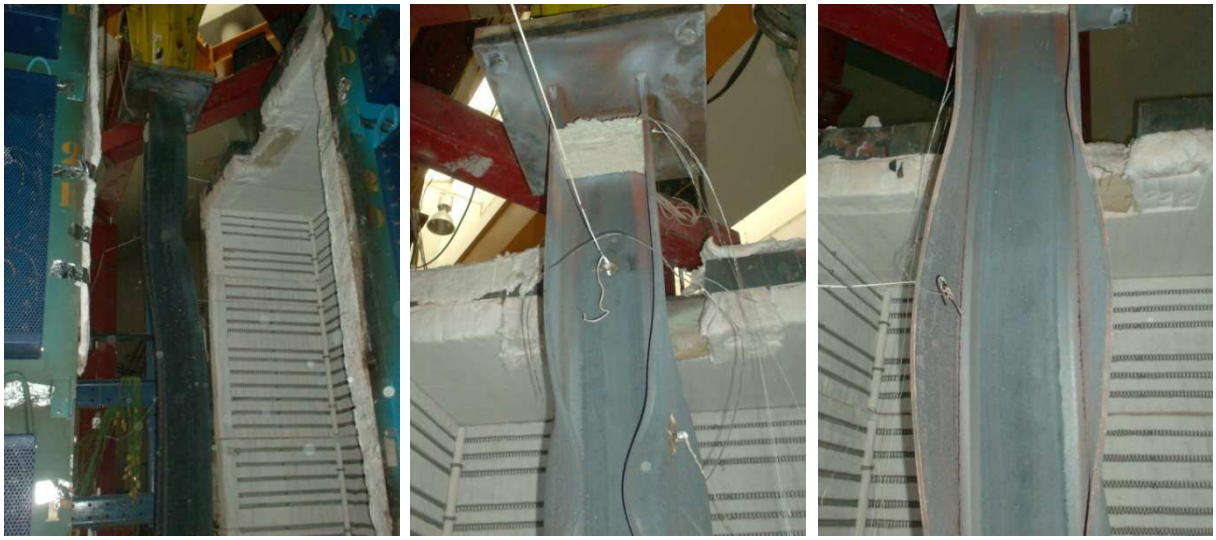

Figure H.2.5 – Views of the test HEA200-K13-L30

Figure H.2.6 – Views of the test HEA160-K13-L30

Figure H.2.7 – Views of the test HEA160-K45-L70

Figure H.2.8 – Views of the test HEA160-K45-L30

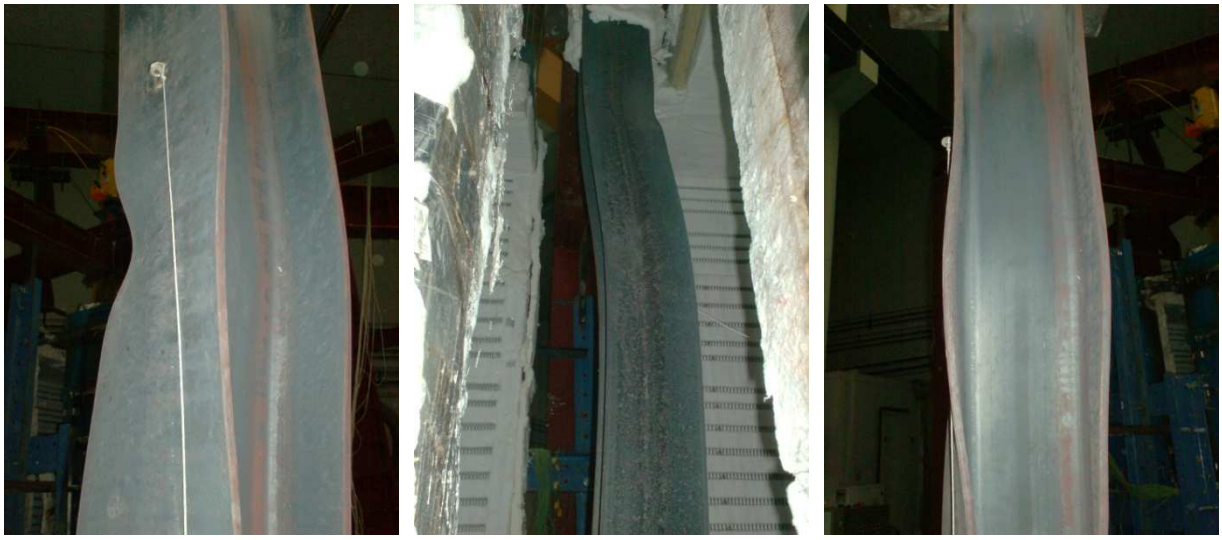

Figure H.2.9 – Views of the test HEA200-K45-L70

Figure H.2.10 – Views of the test HEA200-K45-L30

Figure H.2.11 – Views of the test HEA200-K128-L30

Figure H.2.12 – Views of the test HEA160-K128-L30

Figure H.2.13 – Views of the test HEA200-K128-L70

Figure H.2.14 – Views of the test HEA160-K128-L70

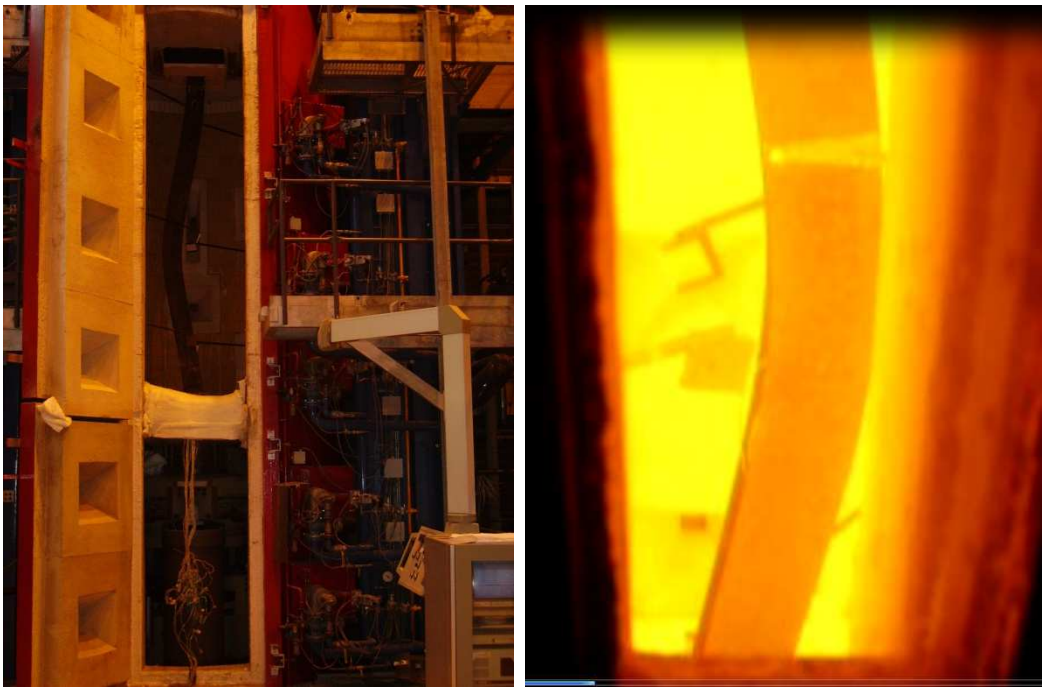

Figure H.2.15 – Views of the test BAM-SC180-K69.5-L70

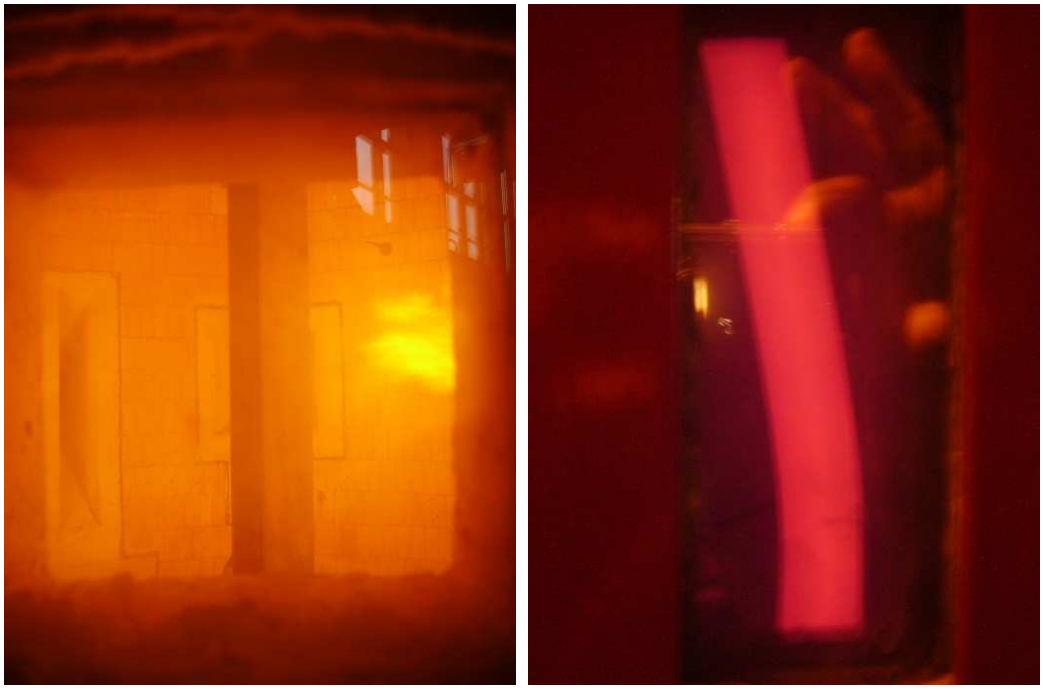

Figure H.2.16 – Views of the test BAM-SC140-K47-L70

H.3 – Composite steel-concrete columns

Figure H.3.1 – Views of the test CSC160-K128-L30

Figure H.3.2 – Views of the test CSC160-K128-L70

Figure H.3.3 – Views of the test CSC200-K128-L30

Figure H.3.4 – Views of the test CSC200-K128-L70

Figure H.3.5 – Views of the test CSC160-K45-L30

Figure H.3.6 – Views of the test CSC160-K45-L70

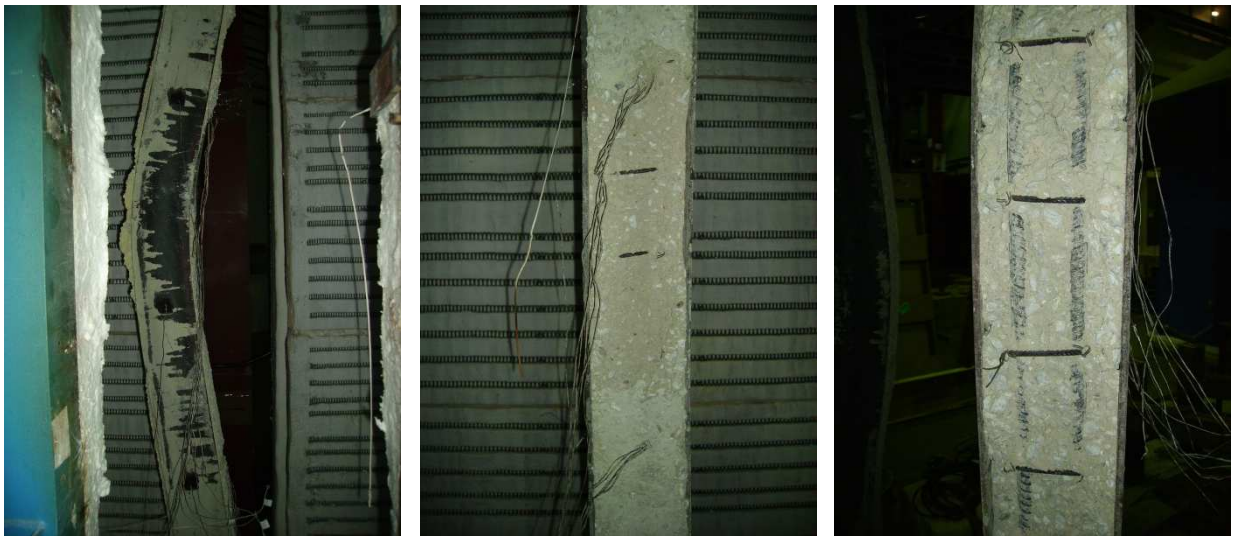

Figure H.3.7 – Views of the test CSC200-K45-L30

Figure H.3.8 – Views of the test CSC200-K45-L70

Figure H.3.9 – Views of the test CSC160-K13-L30

Figure H.3.10 – Views of the test CSC160-K13-L70

Figure H.3.11 – Views of the test CSC200-K13-L30

Figure H.3.12 – Views of the test CSC200-K13-L70

Figure H.3.13 – Views of the test BAM-CSC200-K59-L70

Figure H.3.14 – Views of the test BAM-CSC200-K11-L70